The Marine Environmental Geochemistry of the Southern Baltic Sea

A thesis submitted for the degree of

DOCTOR OF PHILOSOPHY

by

Jason Alistair Christian Smith

(B.Sc. Geology; Edinburgh)

The University of Edinburgh

Faculty of Science and Engineering

September 1999

DECLARATION

I certify that the work presented in this thesis is my own work, except where otherwise stated and has not been presented for a degree at this, or any other, university.

Jason A. C. Smith

Abstract

The initial focus of this research sought to investigate the marine geochemistry of radium and barium in order to elucidate upon the processes governing circulation patterns and residence times in the southern Baltic Sea. The project has since developed and transformed into a detailed study of the spatial and temporal distribution and processes affecting a select group of metals, and in some respects pollutants, in the region north of the river Oder where it discharges into the Baltic Sea.

A transect of progressively deepening water depths, thought to trace the major outflow of the river Oder into a depositional basin, were investigated over a period of 15 months. Four cruises during this time were undertaken to coincide with each season in order to investigate any broad scale seasonalities.

This thesis looks at the main compartments and integrated processes associated with the sediment, nepheloid layer and the water column of this marine environment. This has been achieved by the use of coupled radionuclide and trace metal data followed by the calculation of fluxes and inventories for a select group of elements. Major and trace metals were analysed via ICPMS and XRF; and radionuclides were measured by gamma ray spectrometry. Supporting data in the form of grain size analysis, XRD and carbon and nitrogen measurements were also made. Radium measurements were attempted using the Photo-Electron Rejecting Alpha Liquid Scintillation (PERALS) spectrometer system.

This research challenges the traditional role and concept of the Arkona Basin as the primary repository for the pollutants discharged by the river Oder into the Baltic Sea and instead evaluates the depositional role of the Arkona Basin as principally a sink for atmospherically derived Pb, Cu, Zn and Sn. Likely depositional areas for the Oder pollutant load include the Oderhaff lagoon and transport eastwards along the Polish coast towards the Bornholm deep and Gdansk Bay in response to the forcing generated by the dominant westerly wind direction. Lateral modification and

transport of material is inferred by the use of iron/rubidium ratios and both vertical and lateral modifications are observed for normalised lead, copper, zinc and tin ratios.

The mobile nepheloid layer is proposed as the primary transport medium of metals and is considered to be highly mobile and responsive to wind and wave action especially throughout the Pomeranian Bight. It is likely that throughout the depositional history of the Arkona Basin, the nepheloid layer has been the primary contributor to the sediment pile.

Lead isotope ratios detail a historical picture of increased pollution associated with the rise of the automobile and subsequent decline of lead concentrations with the advent of unleaded petrol in the mid eighties. The main maxima in lead concentrations are found during the mid-twentieth century with peak fluxes some 600% greater than that of the natural background. Temporally varying magnitudes of inputs were found relating to the relative contributions from industrial and combustion engine pollutant sources over the period of study.

Coupled stable lead isotope data and ^{210}Pb and ^{137}Cs dating techniques suggest a period of enhanced sedimentation since the 1970's, followed by a period of non-deposition which is first registered at the shallow water site of ODAS Tonne, and is also found at Arkona, being equivalent to 3 years of sedimentation. The possibility of sediment bypassing this region during these periods of non-deposition, primarily in the mobile nepheloid layer, is proposed followed by entrainment into the main Baltic Sea circulation pattern.

I only wish that someone had shown me this six months ago, and that it were true...

A Rabbit's Thesis

One sunny day a rabbit came out of her hole in the ground to enjoy the fine weather. The day was so nice that she became careless and a fox snuck up behind her and caught her.

"I am going to eat you for lunch!", said the fox.

"Wait!", replied the rabbit, "You should at least wait a few days."

"Oh yeah? Why should I wait?"

"Well, I am just finishing my thesis on 'The Superiority of Rabbits over Foxes and Wolves.'"

"Are you crazy? I should eat you right now! Everybody knows that a fox will always win over a rabbit."

"Not really, not according to my research. If you like, you can come into my hole and read it for yourself. If you are not convinced, you can go ahead and have me for lunch."

"You really are crazy!" But since the fox was curious and had nothing to lose, it went with the rabbit. The fox never came out.

A few days later the rabbit was again taking a break from writing and sure enough, a wolf came out of the bushes and was ready to set upon her.

"Wait!" yelled the rabbit, "you can't eat me right now."

"And why might that be, my furry appetizer?"

"I am almost finished writing my thesis on 'The Superiority of Rabbits over Foxes and Wolves.'"

The wolf laughed so hard that it almost lost its grip on the rabbit.

"Maybe I shouldn't eat you. You really are sick...in the head. You might have something contagious."

"Come and read it for yourself. You can eat me afterward if you disagree with my conclusions."

So the wolf went down into the rabbit's hole...and never came out.

The rabbit finished her thesis and was out celebrating in the local lettuce patch. Another rabbit came along and asked, "What's up? You seem very happy."

"Yup, I just finished my thesis."

"Congratulations. What's it about?"

"'The Superiority of Rabbits over Foxes and Wolves.'"

"Are you sure? That doesn't sound right."

"Oh yes. Come and read it for yourself."

So together they went down into the rabbit's hole. As they entered, the friend saw the typical graduate student abode, albeit a rather messy one after writing a thesis.

The computer with the controversial work was in one corner. To the right there was a pile of fox bones, to the left a pile of wolf bones. And in the middle was a large, well-fed lion.

The moral of the story:

The title of your thesis doesn't matter.
The subject doesn't matter.
The research doesn't matter.

All that matters is who your advisor is.

Anon.

Acknowledgements

At last, its now my turn to write something free from the rigours of scientific prose. To all those words and phrases such as th e mistime dspace ba r, nad my inability to spell occur(r)ing after 70,000 words. I loathe my typing ability.

This could go on forever.....

Well I guess its now my turn to return in a small way the many joy tokens, thanks and favours asked over the last four years, to the many people who have cajoled me on my way, never losing heart. In no particular order the Edinburgh possy, my flatmate Martin with whom many a happy hour have been spent discussing the finer points of Staropramen. Many thanks for your companionship and if you ever need a field assistant let me know! To Gav, Kenny, Bradley and the GBR crew (you all know who you are) - a massive stress relieving thanks.

To Jim Smith for introducing me to pipetting, the compressor and beer (en mass), Gordon the department god (i.e. purse sting holder), his beautiful assistants Nikki, Helena, and Lisa. To Margaret and Ann the librarians, many many thanks, only you know just how many references I've requested and just how appalling my handwriting is. Dodie, Ann and Geoff for their analytical expertise and guidance through the experimental minefields and to my other colleagues in the Geology and Geophysics department, particularly Amanda, Sandy, Clare and the post-grads past.

Tim, I'm not sure where to put you having transcended the boundaries of Edinburgh and Oban but thanks for keeping me on the straight and narrow with all your knowledge, foresight and training tips.

A big thank you, although I didn't think so at the time, must go to Bob Allison for his inspiration and for his repeated chants of don't pack it in, it'll all be worth it in the end (and for numerous other supporters, I'll just have to wait and see as to whether I manage to reap the so called benefits).

Leaving Edinburgh aside, my journeys in the later half took me to the hallowed mecca of Oban which depsite my best attempts and continual self denial I actually quite like (for a hicksville). Thanks to the DML community for accepting my glancing tackles on the footy pitch. In particular thanks must go to Steve Craig (aka Wad) for being a good mate through some pretty shady times. Tom N. for his frankness and advice on the pitch, Eric 'Bruiser' Breuer for introducing me to the joy of H_2S sniffing and some good times close to Oil Rigs (and Macy Gray). The companionship and good-natured banter and blame dealt out from Jane F. and the instantaneous disclaimer on my behalf. Although they perhaps didn't realise it thanks must also go to Oli, Paulie P, Paula, Terrie, Kenny, Jim, Alison, Fiona and the rest of the DML community for keeping me going throughout the last two years.

Finally this project would not have been possible without the instigation, guidance and help of Graham Shimmield, my supervisor, with which a very large, loch sized thanks goes to. To Gus Mackenzie, sorry SURRC was just too much to take!, you were more of an inspiration than perhaps you realised, many thanks for the important 'ups' that occurred whenever I saw you. To Tracy who has borne the brunt of the pain via both the constant barrage of questions and for her remarkable patience when it came to fixing the bain of my life (ICPMS).

I would also like to express my gratitude to the crew and scientific party involved in the BASYS, 3A subgroup, in particular Kay Emeis, Thomas Leipe and Sabine Jahmlich for their good natured camaraderie and their introduction to all things Baltic. Additionally thanks must go to the Natural Environment Research Council for providing the funding that allowed me to complete this work under grant number GT4/95/90/E.

Penultimately, to the folks, many thanks for your continued support and belief over the last 4 and 26 years!. Finally, the girl with the secret smile, Elise, without whom this thesis wouldn't have been nearly so much fun?!, I am indebted to you for your support and ability to brighten up even the darkest day. Many Thanks.

Table of Contents

List of Figures

List of Tables

1.0 Introduction and Rationale

1.1 INTRODUCTION

The coastal marine environment represents one of the most dynamic zones of the hydrosphere and lies at the interface between the open sea and the terrestrially dominated system. This coastal zone delineates an important region in which there is intense usage by man and thus has important socio-economic interests and is of concern to the population as a whole.

Due to the transitory nature and the complex geochemical interactions that take place within this zone it is still not fully understood, despite much scientific study, especially, in terms of the mixing, modification and turnover processes that affect the distribution of trace metals. Our knowledge of the interactions between physical and biological processes and their interaction and influences on the (re)cycling of metals in coastal environments is still inadequate and provides a fundamental stumbling block in the eyes of policy makers for this zone.

This project is based, principally, upon the inorganic geochemical variations of the southern Baltic Sea studied on both a spatial and temporal scale. This region of investigation offers an unparalleled opportunity to study the geochemical changes that occur from a shallow, high energy site to that of a deeper, low energy depositional zone and to evaluate the anthropogenic impact upon this part of the Baltic Sea system. The environmental condition of this heavily used stretch of sea has important implications, which span not only the aesthetic pleasures of this rich and varied coastline but also of health issues and employment for the local and visiting population. Thus in investigating the transitional and resultant geochemical zones of deposition of the river Oder and its passage into the southern Baltic Sea the nature of the transitional boundaries that the metals have to surpass will be elucidated in the form of resultant conditions of deposition. These boundaries include the riverine environment being the Oder itself with its own set of inorganic geochemical processes. The extensive OderHaff lagoon / estuarine type environment where much

filtering and exchange of metals occurs both in a physical and biological sense. The resultant inorganic geochemistry then has to transgress the region of study in which there is a pronounced salinity gradient and an energy gradient to the assumed final resting place in the Arkona Basin. This study investigates a selection of trace metals in different but connected compartments of the coastal environment and aims to marry them in order to define the critical processes that govern the inorganic geochemistry of this region. This project 'piggy backed' upon the BAltic sea SYstems Study (BASYS), Coast to Basin Fluxes Group co-ordinated by Prof. Kay Christian Emeis of the Baltic Sea Research Institute, Warnemunde and hence was governed by timings and stations deemed appropriate to this study of the dynamics of the coast to basin interactions.

While the Baltic Sea is one of the most intensively studied seas in the world due to its proximity to scientific expertise and its multi-national seaboard, many with strong environmental credentials, there are still a great many scientific questions that lie unanswered. In the field of environmental pollution, recent initiatives such as TRUMP, GOBEX, HELCOM and most recently the BASYS project have set out in an endeavour to provide a multidisciplinary approach to the environmental condition of this sea. However, inherent to science is a seemingly disparate approach to communication both between scientists and to the public at large. Communication within the same field of work, not to mention with those in other disciplines, is often sadly lacking. However to enable a full and complete understanding of the marine environment a multi-faceted approach is a necessity.

From an inorganic geochemical approach, fundamental to the study of the sedimentary and water column metal distributions is the variability in the spatial and temporal distributions of the natural system. Superimposed on these fundamentals are the influences in the form of both biological and physical processes. In general terms the inorganic geochemistry of the marine environment is a product of a wide variety of processes. The most important of which are the inputs to the system be it by the hydro or atmosphere, the erosion of in situ material and the transport and modification that occurs due to physical, biological and diagenetic processes.

The introduction of suspended material into the marine environment and the path to its final deposition in the marine sediments is one of complex interactions with many phases of re(cycling) throughout the whole of the marine ecosystem. Particulate material introduced into the marine environment will primarily be governed by gravity and will differentiate according to grain size with large particles deposited in the highest energy environment while finer particles will be transported further. In addition to this basic premise many other processes such as wind and current induced resuspension plus transport will act to modify the distribution of material. The incorporation of matter into the biological cycle and the association with organic matter from both the dissolved and particulate phase significantly alter a particles pathway. Furthermore, redox conditions, flocculation across the steep salinity gradient and associations with Fe and Mn oxyhydroxides along with later diagenetic change can influence the redistribution of elements and lead to their recycling in the marine environment.

1.2 THE STUDY AREA

1.2.1 Introduction to the Baltic Sea

The Baltic Sea is the largest body of brackish water in the world and has a surface area of approximately 393,000 km^2, a drainage basin some four times this area, a total volume of 21,200 km^3, a mean depth of 52m and is located as shown in Figure 1-1. This shallow, land-locked sea is situated in the centre of one of the most intensively utilised regions of the world, with large, intensively cultivated, agricultural swathes of land, locally concentrated, heavily populated regions and comes under the influence of a great many industries be it by direct input or by indirect atmospheric input. Some 20 million people live permanently at the coast with a further 70 million within the catchment area (RHEINHEIMER, 1995), 45 % of these within Poland.

During the twentieth century the Baltic sea has been transformed from a clear oligotrophic sea into one of the most contaminated sea areas in the world

(MELVASALO, 1981; NEHRING *et al.*, 1987). In addition to a substantial increase in the trace metal load, LARSSON *et al*, 1985 showed that since the period before 1900 there has been a four-fold increase in nitrogen and an eight fold increase in phosphorus up to current times. As a consequence the oxygen conditions below the halocline have declined steadily throughout the twentieth century and at present one third of the Baltic periodically shows low bottom water concentrations of 2-3ml l^{-1}. This has important implications for eutrophication, which is well documented, and this can in turn have important controls on the inorganic geochemistry in the form of changing redox processes and the controls on the biology including the benthos and bioturbation in respect to sediment core interpretation.

Location Map of the Study Area

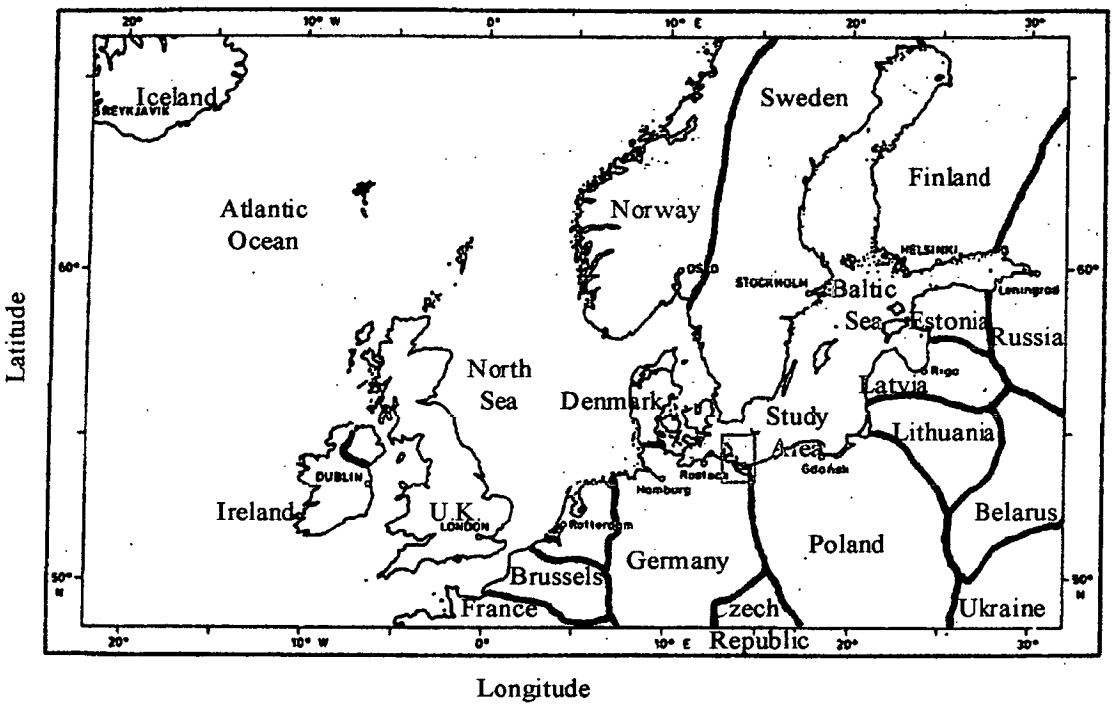

Figure 1-1 Location map of the study area and Baltic Sea.

Geopolitically there are fourteen independent states which border the Baltic sea each with there own agenda, interests and politics. However, efforts have been made in recent times to combat the growing threat of damaging and lasting pollution in this international waterway with the ratification of the Helsinki convention in 1980 and the implementation of the Helsinki Commission (HELCOM) taskforce which has provided a series of state of the environment reports since the mid eighties.

Geologically, the Baltic Sea is a sea of contrasts being both old and young; formed in a depression some three billion years old with lithologies of Pre-Cambrian age forming the northern terrestrial border. In contrast, the geology of the sea floor is composed of remnants of the last glaciation only 14, 000 to 12, 000 years old which line a number of basins, separated by sills, the shallowest of which is the Arkona Basin and to the south are the Phanerozoic sedimentary units of the East European sedimentary complex. Superimposed on this entire region are the recent processes of weathering and erosion which all add up to a varied geological history for the area. Ecologically, the Baltic Sea is relatively immature when compared to the likes of the Mediterranean Sea where the ecosystem there has had millions of years to adapt. Hence the Baltic Sea seems to harbour tough resilient species or those that are quick to adapt to changes in the environment. While the diversity may not be on a par with the North Sea or similar inland seas those species that do flourish often do so in high numbers.

1.2.2 Hydrography of the Baltic Sea

The main controls on the hydrography of the Baltic sea are the restricted, two layer flow with the North Sea through the Skagerrak and Kattegat, the large proportion of freshwater input from rivers, totalling some 430km^3/a and the surplus of precipitation over evaporation which operationally separates it from its close neighbour, the Mediterranean Sea. Thus the Baltic Sea has a positive water balance, i.e. more water is lost to, than added from, the North Sea (mainly through surficial flows), of (475km^3/a comprised of a river runoff component (430km^3/a) and a precipitation component of 230km^3/a which exceeds evaporation (185km^3/a)). As a result the water in the Baltic Sea has a mean residence time of approximately 25 years (VOIPIO, 1981).

There is a permanent halocline at 40-70m depth which separates the low salinity, oxygenated surface waters from the more saline but oxygen deficient waters of the deep Baltic. The deep water is periodically refreshed by inflow events from the

North Sea which result in large inflows of saline water, the last one of which occurred in January 1993 after a period of 16 years stagnation which was extensively studied by MATTHAUS and LASS, 1994 and NEHRING *et al.*, 1996. In addition the salinity difference between the two layers is sufficiently small so as to allow the periodic renewal of deep water in the basins. Hence, unlike the Black Sea, permanent stagnant water is not found but prolonged periods of stagnation have occurred leading to considerable stress on the ecosystem.

The region of study is found in the Southern Baltic Sea which is bounded to the south by Poland and Germany with the river Oder defining the border between these two countries.

1.2.3 The Southern Baltic Sea and the Pomeranian Bight

The southern Baltic Sea (92,795 km^2) divides into the Arkona Basin with a maximum depth of 53m, Pomeranian Bight (20m), Bornholm Basin (105m), Slupsk Furrow (95m), Gdansk Basin (118m) and other smaller bays. This study is primarily centred around the transport and transitional zone from the Pomeranian Bight and into the Arkona Basin although exchanges between other basins and in particular the Bornholm Basin will be considered.

The river Oder and to a lesser extent the Peene drain into the shallow Pomeranian Bight and then onwards into the Baltic proper as shown in Figure 1-2 which details the study area and the four main stations. The Bight is predominately characterised by the fresh water outputs from the near shore 'boddens' and 'haffs' or lagoonal areas which act as an interface between the river Oder and the southern Baltic Sea and trap much of the mud and silt. These lagoonal areas enclose an area of some 683km^2 with a mean depth of 3.8m and often have residence times of several weeks in which much modification of the pollutant load may occur. The HELCOM report of 1993 showed that the decomposition and accumulation of pollutants within these shallow water regions does lead to a substantial decrease in the pollution loads carried to the sea. Conversely, nutrients and associated metals in the lagoonal areas

are transformed into particulate organic matter during the phytoplankton growth season and these may readily be transported into the Bight during periods of outflow.

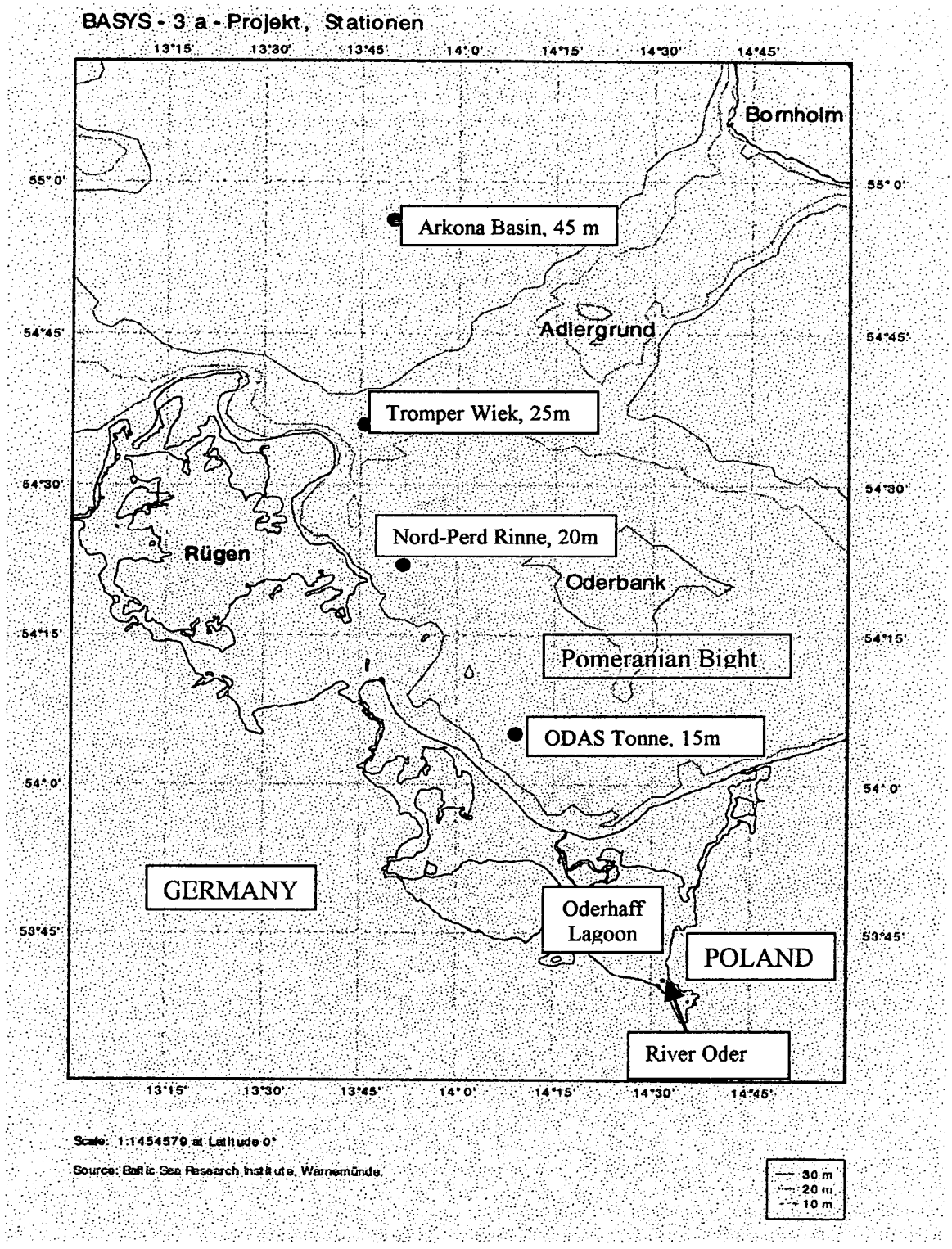

Figure 1-2 Locations of the survey stations and southern Baltic Sea, Courtesy of Dr T. Leipe, Baltic Sea Research Institute, Warnemunde.

The Pomeranian Bight itself is a shallow sea area covering some 5580km^2 and has a volume of approximately 74km^3 within the 20m isobath, which is regarded as the northern border to the open Baltic. Three different outlets connect the lagoon to the Pomeranian Bight with about 60-70% of the water being discharged through the Swine Outlet, 15-20% from the Dziwna and 15-20% through the Peenestrom located as shown in Figure 1-3. The discharge through these outlets is not continuous and is thought to be of a pulsed nature depending upon wind duration, direction, strength and also on the sea level differences between the Oder lagoon and the Pomeranian Bight (SIEGEL *et al.*, 1996).

Outflow sites from the Oderhaff Lagoon into the Pomeranian Bight

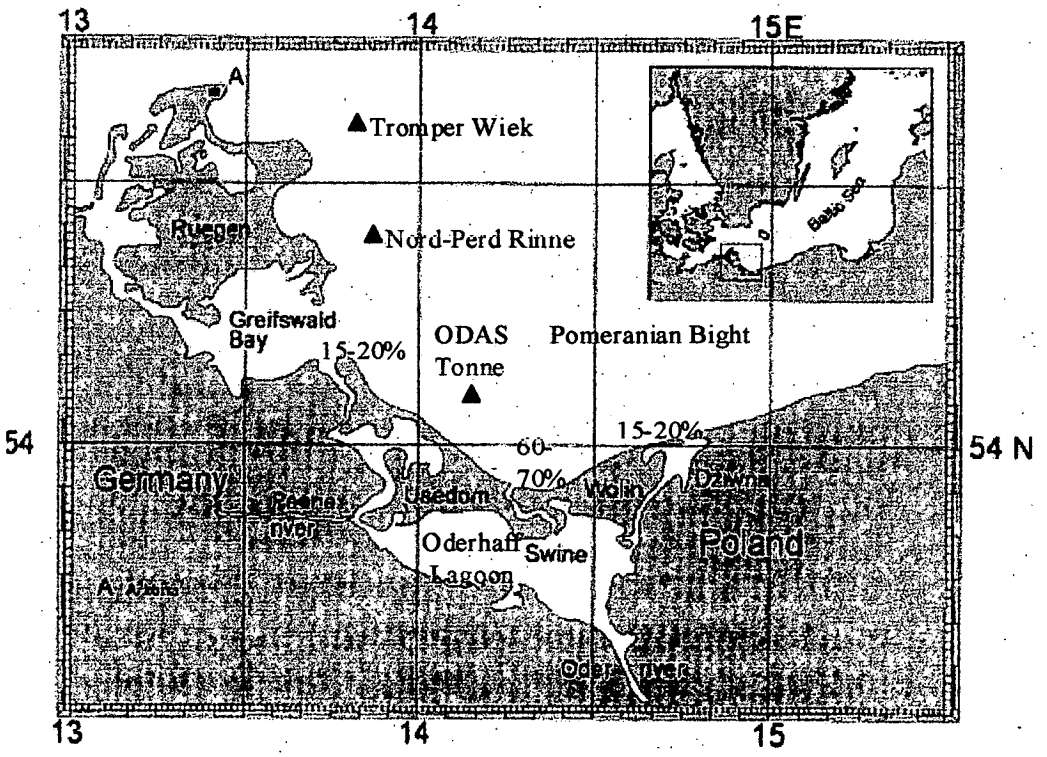

Figure 1-3 The Oderhaff lagoon and outflow sites into the Pomeranian Bight, after SIEGEL *et al., 1996.*

Hence depending upon the sea level differences between the lagoon and the Bight both in and outflow of waters can occur with occasional incursions of Baltic seawater leading to a salinity in the range of 0.5 to 3‰ for the Oderhaff lagoon. SIEGEL *et al.*, 1996 showed that these episodic outflows form lenses of water with diameters of

a few hundred metres and estimated that they become mixed with waters of the Pomeranian Bight on a time scale of hours to days.

The BASYS project was initially proposed so as to investigate what was thought to be the role and the natural path of the particulate load from the river Oder down the Oderinne, a drowned Pleistocene channel from the coast and out to the Arkona Basin. This was based upon knowledge of the topography of the region but recent work using satellite images and knowledge of the wind direction by SIEGEL *et al.*, 1996 has shown that for the surface currents at least there are two main pathways. Sea surface temperature (SST) maps showed that during the dominantly westerly winds in summer, autumn and winter surface currents were found to be transported either parallel to the Polish coast or out towards the Bornholm Basin and further on to the Gdansk Bay. In the period of main freshwater inflow in spring, when easterly winds prevail, and during calm periods throughout the year transport was observed along the German coast and into the Arkona Sea. These conditions are illustrated in Figure 1-4.

The relative importance and contribution of topographically driven currents and the effect of wind-induced surface currents to the resultant flow of particulate matter and particularly the mobile nepheloid layer is as yet unresolved but could prove vital in interpreting the environmental state of this region of the Baltic Sea.

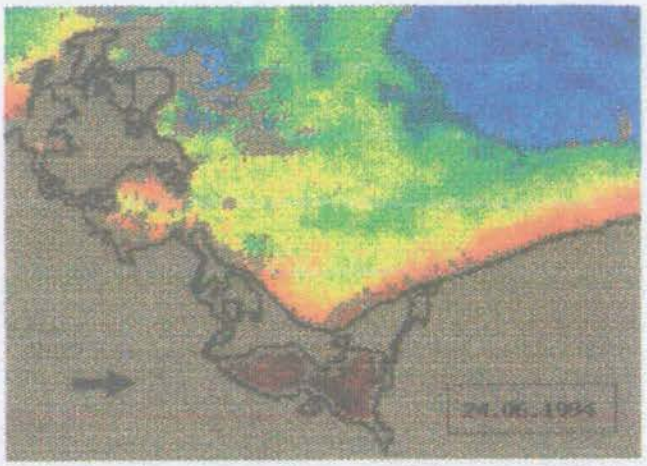

A) Westerly winds blowing the outflow parallel to the Polish Coast

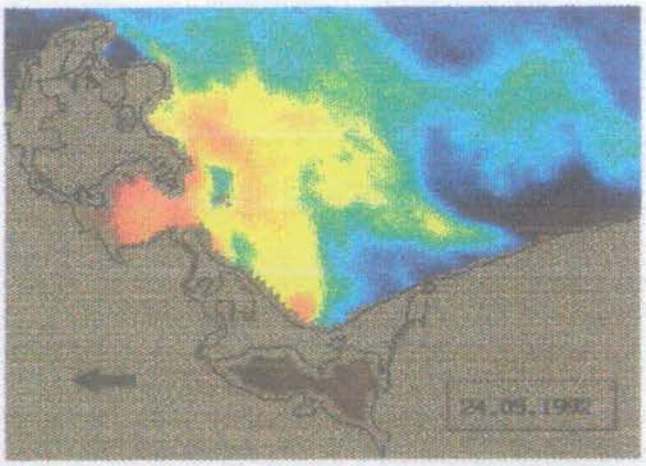

B) Easterly winds blowing the outflow north and towards the Arkona Basin

Figure 1-4 Sea surface temperature diagram illustrating the effects of wind direction on the Oder outflow direction, taken from SIEGEL *et al., 1996.*

1.2.4 The River Oder

The river Oder is the fifth largest river by runoff draining into the Baltic Sea and has a catchment area of approximately 130,000 km^2 with a fresh water input into the Pomeranian Bight in the order of 15-17 km^3 per year.

The river Oder originates in the Oder mountains (640m) of the Hruby Jesenik range in the Czech Republic and flows some 855 km north-westward to the Baltic Sea. Its passage takes it through some of the most heavily industrialised regions of central Europe, passing through the Polish Silesia region where intensive coal mining has occurred for much of this century. In addition to coal, lead, tin, copper and zinc are also mined in this region along with associated heavy industries and power generation facilities. The Oder then passes along a heavily canalised passage through numerous locks along the canal sections and crosses the sedimentary strata and glacial quaternary tills of western Poland. In addition to the locks associated with the canals, the Oder is also extensively dammed in its upper reaches and reservoirs are used to control the flow of water during the summer months. The Oder is an important waterway and carries about 10% of the total tonnage from the highly industrialised regions in the south to the northern port of Szczecin.

The peak discharge of the Oder typically occurs during spring when maximum loads of dissolved and suspended material are carried to the Baltic Sea. Typically, in the period between December and May as much as two thirds of the entire volume of fresh water enters the sea. In addition to the 'normal' flow characteristics of the river, extreme events do occur and one such flood event took place in the summer of 1997. Two cyclones associated with strong precipitation (up to 500% of monthly mean) crossed the Oder catchment region between the 4^{th} to 7^{th} and 18^{th} to 21^{st} July 1997. In order to put this flood in context MOHRHOLZ *et al., (In Press)* states that the mean annual discharge of the Oder amounts to 545 m^3/s with an annual spring maximum of 1274 m^3/s and a corresponding minimum in summer and autumn of 261m^3s. The flood event was not only exceptional due to the presence of flows up to 3000m^3s in pure volume terms but was also remarkable due to the season in which it occurred. The flood reached Eisenhuttenstadt in the German Oder river area on 11^{th}

July and registered an initial 2m depth increase with an additional 2m increase on 17th July. This elevated water level was then observed through to 5th August. The flood reached the Oderhaff lagoon on the 24th July (ROSENTHAL *et al.*, *(In Press)*) and was measured in the Pomeranian Bight on the 28th July (MOHRHOLZ *et al.*, *(In Press)*). The characteristics of the Oder discharge along with variations in sea level are shown in Figure 1-5.

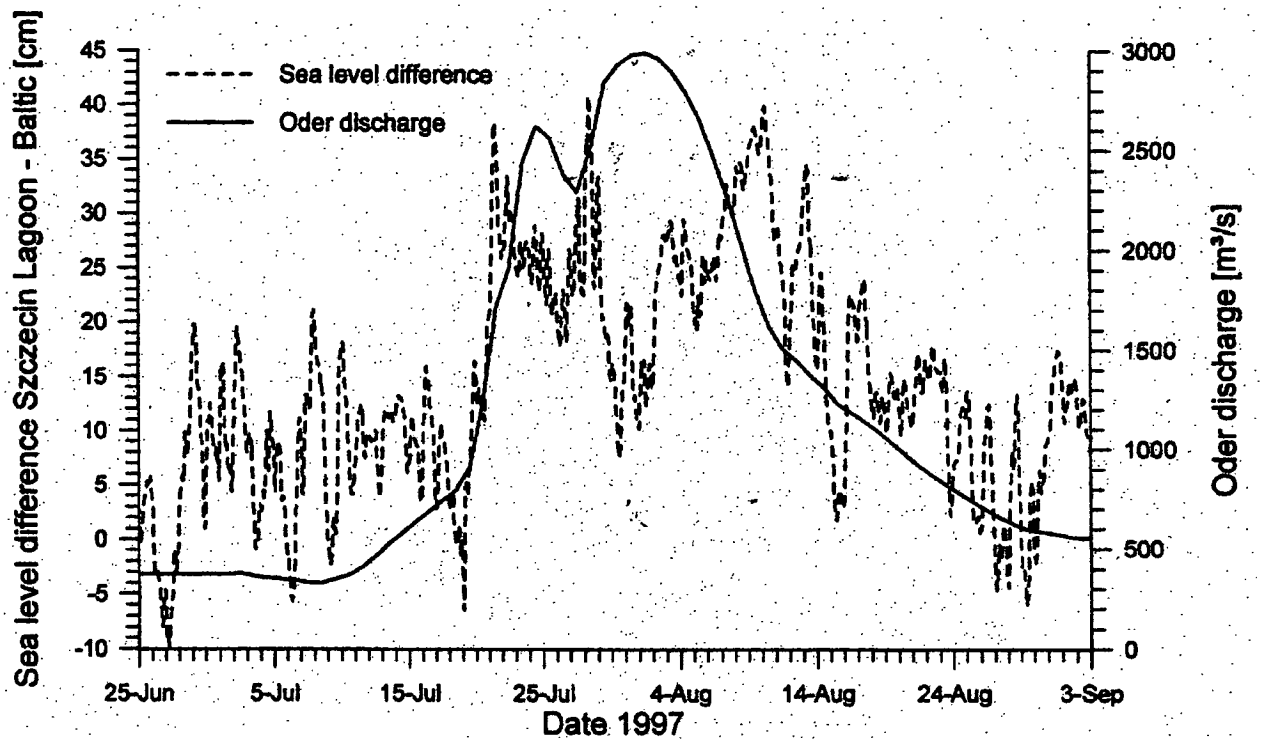

Figure 1-5 The Oder flood in terms of discharge pattern and sea level difference, Taken from MOHRHOLZ *et al.*, *(In Press)*.

1.2.5 Location of Sampling Stations

Four sampling stations were selected to meet the objectives of the Baltic Sea Systems Study (BASYS) Sub Group 3a studying coast to basin fluxes. The sites were chosen so as to investigate a continuum of environmental conditions from the shallow water station of Tonne in the Pomeranian Bight to the deeper, adjacent region of the Arkona Basin. This transect was chosen so as to follow the most likely path of the Oder river particulate load along a glacial valley and its transition through various

environmental depths to its assumed deposition in the Arkona Basin. On one side of the transect lies ODAS Tonne where shallow water depths and proximity to the main outflow of the river Oder lead to rapid bottom currents which is in stark contrast to the Arkona Basin at 45m depth where fine grained material accumulates in a low energy environment. The two sites located between these two end-members are Nord-Perd Rinne (20m) and Tromper Wiek (25m) as shown in Figure 1-2 and these are thought to represent regions where intermediate storage and modification of the material occurs.

The official positions of these stations are shown in Table 1-1

Table 1-1 Latitude and Longitude of the Survey Sites

Station	*Latitude Degree*	*Longitude Degree*
ODAS Tonne	54°04.85'N	14°09.52'E
Nord-Perd Rinne	54°21.94'N	13°51.72'E
Tromper Wiek	54°36.06'N	13°45.64'E
Arkona Basin	54°56.14'N	13°49.95'E

1.3 RADIUM AND BARIUM GEOCHEMISTRY OF THE BALTIC SEA

This thesis was originally conceived as an investigation into the marine environmental geochemistry of radium and barium and hence after two years of work there is one chapter devoted to this subject. Subsequently the focus of this project moved to the inorganic geochemistry of the southern Baltic Sea but the following serves as a brief introduction to radium and the chapter on radium analysis focusing on the problems associated with the Photo-Electron Rejecting Alpha Liquid Scintillation (PERALS) spectrometer system.

1.3.1 Radium the Element .

Radium belongs to the Group IIA, alkaline Earth Metals and is its heaviest member being the 88th Element in the periodic table. Thirty isotopes of radium have been discovered to date, each with a different number of neutrons within the nucleus from mass number 206 through to 230. All are radioactive, unstable and only four are found naturally, the most important and abundant of which are ^{226}Ra with a half life of just over 1600yrs which decays by alpha emission, and ^{228}Ra (mesothorium), a beta emitter with a half life of 5.8 years. These radium isotopes are the daughters of uranium ^{238}U and Thorium ^{232}Th respectively shown in the decay chains, decay modes and energies of Figure 1-6. The other two isotopes ^{224}Ra and ^{223}Ra are daughter products of the ^{232}Th and ^{235}U decay series respectively. The remaining 26 isotopes are not found naturally because their half-lives are shorter, or much shorter than an hour and therefore are not compatible with environmental processes.

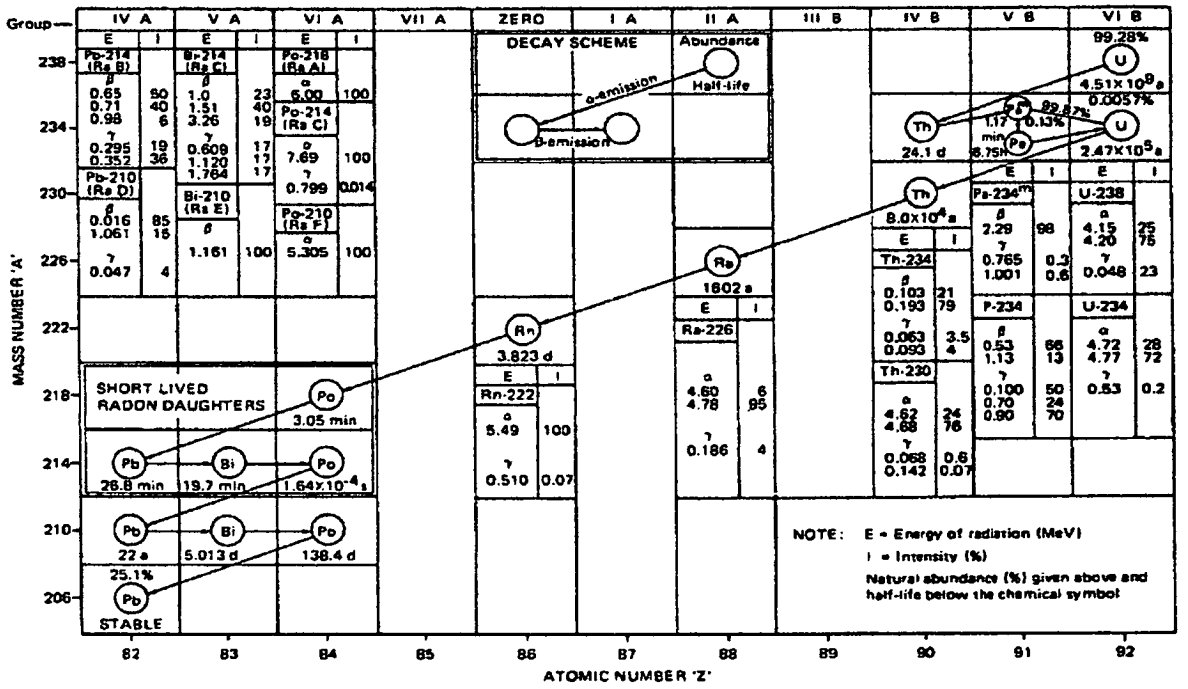

A) Decay scheme of Radium-226

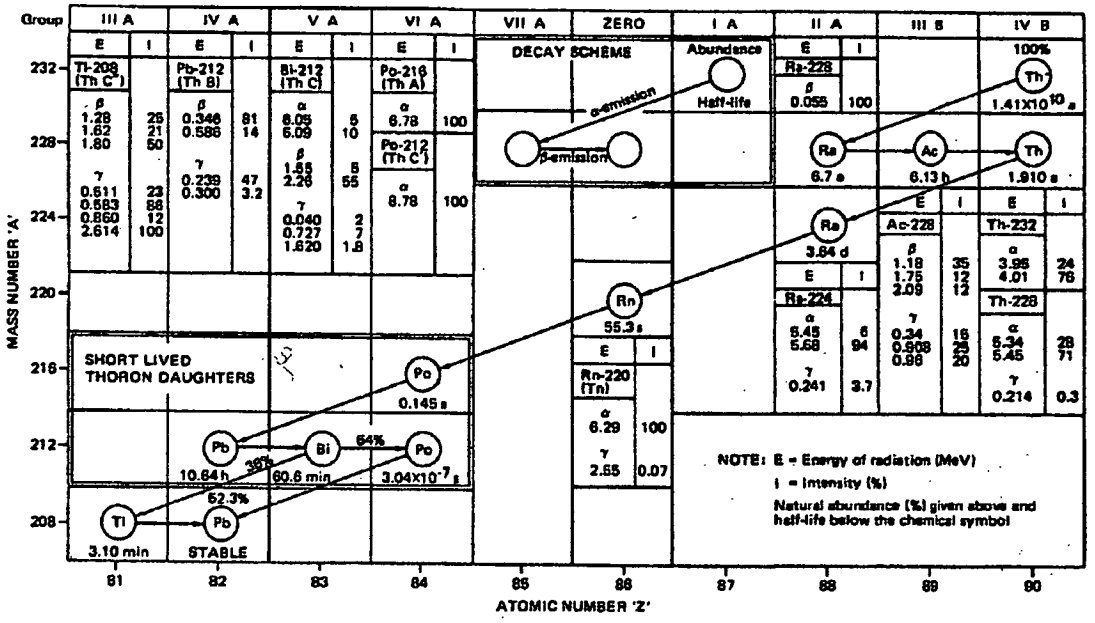

B) Decay scheme of Radium-228

Figure 1-6 The two main decay schemes of radium for ^{226}Ra and ^{228}Ra , Taken from IAEA report on The Environmental Behaviour of Radium, No. 310.

Pure radium is a lustrous, highly reactive, radioactive, metal of group IIA with an atomic weight of 226.05 and atomic number of 88. It has a melting point of 700°C and a boiling point of 1150°C and is highly radiotoxic. A summary of its principal properties is given in Table 1-2

Table 1-2 The main properties of the naturally occurring isotopes of Radium

Mass	Common Name	Decay Series	Half Life	Nature and Energy (MeV) of Decay
226	Radium	U-238	1622a	α, 4.79
228	Mesothorium	Th-232	6.7a	β^-, 0.012
224	Thorium-X	Th-232	3.64d	α, 5.68, 5.45
223	Actinium-X	U-235	11.2d	α, several, 5.4-5.7

1.3.2 Radium in the Environment

The cycling of radium in the environment is adequately addressed in Figure 1-7 in which details of the primary pools are given. As can be seen the distribution of radium is wide spread but especially high concentrations can be found associated with mining operations. It was on this basis that this study was initially proposed to capitalise on what potentially could be the elevated radium levels in the Baltic Sea due to the presence of extensive mining operations in the upland stretches of the river Oder. However radium analyses were never obtained for reasons detailed in Chapter 3 but work by KOWALEWSKA, 1986 in the southern Baltic Sea showed unexpectedly low levels of radium in both the water column and sediment core of 1.8mBq dm^{-3} and 3.6 to 47mBq dm^{-3} respectively. This may be due to the precipitation of a radium salt in the sulphide rich mine waters close to its release in the Silesia district of Poland although no direct literature can be found to substantiate this speculative claim.

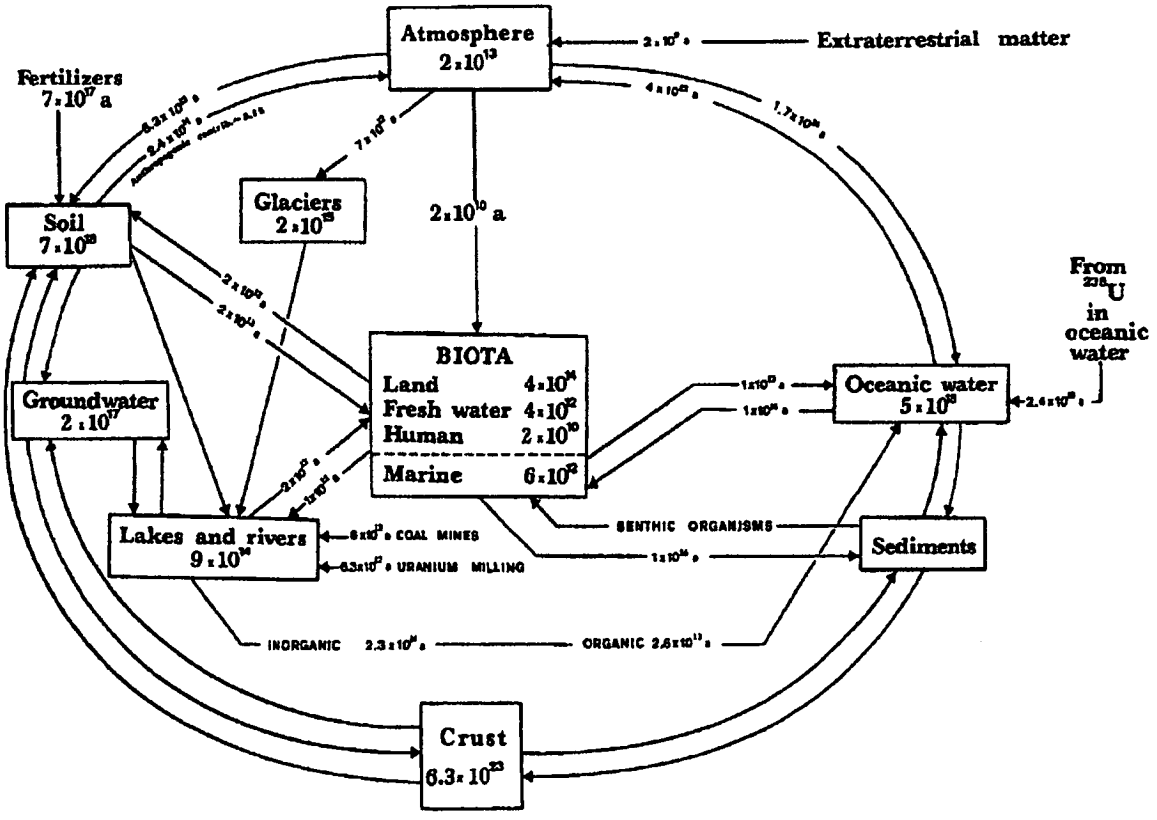

Figure 1-7 Global cycle of ^{226}Ra (Content in pools and annual flows given in Bq), after Jaworowski, 1990.

1.4 RATIONALE

The initial rationale behind this project involved the use of radioisotopes in order to determine the residence time of water within the Pomeranian Bight and the Arkona Basin. In achieving this a further aim was to then form a predictive tool by which inferences could be made on the residence time of heavy metals and pollutants in this region of the Baltic Sea. The final goal was then to assess the environmental stress on the system, paying particular attention to the role of the river Oder and its pollutant load in the Southern Baltic Sea.

While problems were incurred with the basic analysis of the fundamental element, radium, due to the failure of a novel method of determination, the project then moved on to achieve its further objectives and was refined with a further set of objectives as is shown below:

- To establish a spatial and temporal investigation into the magnitude and processes of trace metal distribution within the region of interest.

- By the use of normalised elemental ratios to compare the distributions and modification of metals and their transfer through and across the dissolved, particulate, mobile nepheloid layer and sediment core phases and assess the importance of each phase

- To obtain an historical record by the use of radionuclide dating techniques (^{210}Pb and ^{137}Cs) so as to enable a historical reconstruction of pollution input to the Southern Baltic Sea.

- To investigate by means of stable lead isotopes the relative magnitude of lead input from natural and anthropogenic sources and to attempt to rationalise the source regions of this input.

- Additionally associations between metals will be sought along with knowledge of the geographical history of the region and used to try and infer the source activities of these metals that are the main contributors to the concentrations found.

- This study will also attempt to investigate any seasonal changes in the input and transport of metals to this environment from the main source of the Oder.

- The main aim will then be to combine all of the above information and in doing so interpret the environmental state and the primary processes that occur in this heavily populated region of the Baltic Sea.

2.0 Sample Collection and Methodology

2.1 INTRODUCTION

The sampling strategy in the Southern Baltic Sea aimed to produce a detailed data set regarding the water column, the sediment/water interface and the underlying sediment. Analysis of this data, in particular, for radium and barium would then lead to a greater understanding of the biogeochemistry of the two elements and would also give valuable information regarding the residence times, fluxes and inventories for this region of the Baltic Sea.

An integrated sampling strategy was conducted on a seasonal basis for 24 months in order to determine the quarterly variations and perturbations to the dynamic environment of the Oder river path and its transition from a coastal environment into that of the deeper Arkona Basin (SHIMMIELD, 1995). The sampling cruises were undertaken as part of the BAltic sea SYstems Study (BASYS) and the research vessels Professor Albrect Penck and Alexander Von Humboldt from the Warnemünde Institute of Oceanography were used.

As this work is in part experimental and part fieldwork based, the following chapter shows in detail the main avenues of methodological development while leaving those methods used, but already well characterised, to short paragraphs and the appendices. The main thrust of experimental development concerned the measurement of radium and hence a detailed account of the principal method developed follows along with short descriptions of the main alternative methods along with some basic sampling strategies.

2.1.1 Water Column Sampling

Routine temperature, oxygen and salinity measurements were taken every metre on the downward cast of a rosette CTD (Conductivity-Temperature-Depth) sampler (CTD Sea Bird 911). Density was calculated from the CTD temperature and salinity

measurements according to the polynomial equations given in UNESCO (1983) (see A.1.1). Water column samples for radium, barium, cesium and lead were taken at 5m intervals from the surface at all but the deepest station where samples were taken at 1m, 5m, 10m, 20m, 30m, 35m, 40m and 45m depths. At each depth three 25l samples were taken in pre-cleaned and sample rinsed high-grade polyethylene carboys and a further 5l water sample was collected in a similarly cleaned polyethylene jerrycan. Upon collection the 25l water samples were acidified with 50mls of Analar grade conc. HCl and filtered through a 0.45μm Asypor filter so as to distinguish between the dissolved and particulate phase (MCKEE *et al.* 1986, SHIMMIELD *et al.* 1995). In addition, 5l samples were taken by way of the GEOMAR BIOPROBE II bottom lander at 5cm, 10cm, 20cm and 40 cm above the sediment-water interface and acidified to pH 0-1 so as to study in detail the fluxes and biogeochemistry of this increasingly important fluff/transition.

2.1.2 Sediment Sampling

Sediment cores were taken at each of the four stations on the October 1996 cruise. A Rhumohrlot gravity corer device was used for Nord-Perd and the deeper Arkona station. Experienced research divers obtained cores from Tonne and Wiek, as the nature of the sediment did not allow cores of sufficient length to be brought to the surface. It was essential that the retained cores represented the existing conditions of the sub surface and the sediment/water interface as closely as possible so that undisturbed and accurate geochemical analysis could be undertaken. Therefore upon collection, the cores were studied to detect any sign of disturbances be they obvious hiatuses in the sediment record, evidence of bioturbation or trawling.

The cores were then photographed, annotated, sketched and then sliced in air at 10mm intervals for the first 100mm and then at 20mm for the remainder of the core using a plastic slicer and dividers. The individual samples were then bagged, labelled and stored at 4°C until analysis. Further details on the subsequent sediment sampling and processing can be found in A.2.1.

Specific 'fluff' layer samples (the region of high density suspended sediment above the sediment/water interface) were taken using a pump and hose in parallel with real time video images so that the nozzle could be directed to zones of high particulate concentration. These samples were then centrifuged using a flow through centrifuge so that a particulate concentrate could be obtained and stored at 4°C until analysis.

2.2 RADIUM ANALYTICAL METHODS

2.2.1 Introduction

Radium and its isotopes have been notoriously difficult to analyse since the days of its discovery in 1898. The most problematic characteristics are that it is usually present in exceedingly small quantities, it requires labour intensive and complex pre-concentration and sample preparation steps and measurement accuracy is generally low. The amount of radium present in an environmental sample has traditionally been determined by measuring the radioactivity of radium isotopes. This can be done via a number of methods such as measuring the radioactivity of radium decay products (via emanation or active precipitate), by measuring the gamma activity of equilibrated radium samples and also by direct alpha and gamma spectroscopy. There are many permutations and combinations of both sample preparation and detector types and the following paragraphs give a brief overview of the main methods currently available.

2.2.2 Emanometry

Radon emanation is by far the most widely used method and has been extensively described in the literature by such authors as MACKENZIE *et al.* (1979) SCHLOSSER *et al.* (1984), HUNTLEY *et al.* (1985), BUTTS *et al.* (1988), MATHIEU *et al.* (1988) and with a detailed overview by LUCAS & MARKUN (1990). Briefly, the analysis of radium involves the measurement of the ingrown ^{222}Radon from the water sample, sealed for a prescribed period of time in a radon bubbler. The radium activity is then inferred from that of the radon activity measured in either an ionisation chamber, FIRSENNE & KELLER. (1985), a

scintillation cell, KEY *et al.* (1979) or a proportional counter ZIKOVSKY (1991) according to the general Equation 2-1 below:

Equation 2-1

$$^{226}Ra = \frac{R}{3 \times E} \times \frac{1}{(1 - e^{\lambda t_1})} \times \frac{e^{-\lambda t_3}}{e^{-\lambda t_2}(1 - e^{-\lambda t_3})}$$

Where:

R = The net count rate in the scintillation cell (cpm);

E = The efficiency of the whole system (including radon stripping, radon transfer and counting cell efficiency) expressed as a fraction;

λ = The radioactive decay constant of the measured radium daughter, ^{222}Rn (1.235×10^{-4} min^{-1}.

T_1 = Radon ingrowth time. The time from the initial degassing of sample to the end of sample emanation (min);

T_2 = Time from the end of sample flushing to the start of counting (min); and

T_3 = Counting time (min)

The method is generally both sensitive and reliable especially when dealing with large volumes of water or when the activity is collected on manganese or ferric oxyhydroxide impregnated fibres (KRISHNASWAMI *et al.* (1972), MOORE and REID (1973), AMES *et al.* (1983) and MOORE *et al.* (1995). However, it is time consuming by way of a 23 day ingrowth period (^{222}Rn $t_{1/2}$ = 3.824 days), suffers from a low energy resolution and requires complicated operations for handling radon gas where large numbers of samples need to be assayed.

2.2.3 Alpha Particle Spectrometry

With alpha particle spectrometry silicon surface barriers are commonly used to detect alpha particles generated by radioactive decay of radium deposited on a planchet. A detailed summary of the various types and configurations of alpha particle spectrometers is given by BLAND, (1990). The main advantages of this method are

very low background levels, excellent stability within the required bias voltage range, insensitivity to magnetic fields, gamma and beta rays and high resolution relating to the fast output pulses and hence high counting rates. Disadvantages relate to excessive electrical noise due to keeping the detector in a vacuum without bias and also due to the fragility of silicon and its tendency to shatter easily. Care should therefore be taken to avoid shock or any sudden changes in temperature. The main drawback, however, is the reliance and importance placed upon obtaining a uniform geometry on the planchet during deposition. Typical depositional procedures include the precipitation of $Ra/BaSO_4$ on a filter that is then attached to a planchet, GOLDIN, (1961), LOYD and DRAKE, (1989) and electrodeposition after cation exchange to remove extraneous alpha emitters, BENOIT and HEMOND, (1988), ALVARADO *et al.* (1995) and BAYES *et al.* (1996). A detailed comparison of other depositional methods is given in LALLY & GLOVER (1984).

Initially, in this project, much work was devoted to developing the experimental method of ALVARADO *et al.* (1984) in parallel to the development of alpha liquid scintillation spectrometry. Alpha particle spectrometry offered an ideal method for analysing small amounts of low activity radium but the time and effort in preparation for the large numbers of samples was too great and was abandoned after the first year when developments in alpha liquid scintillation and gamma spectrometry showed much promise.

2.2.4 Gamma Spectrometry

The principles and considerations when undertaking gamma spectrometry are well established and described by many authors (FRIEDLANDER *et al.* 1981, CANET and JACQUEMIN 1990, MACKENZIE 1991, LUCAS and MARKUN 1992 and CHOPPIN *et al.* 1995). The main advantage with gamma spectrometry for relatively high activity sediment is the ease of sample preparation although long ingrowth times are required. JOHNSTON and MARTIN (1997) detail measurement methods with a time span of less than three days relating to the subtraction of the uranium interference at 186KeV and also by the double count ^{222}Radon progeny method.

Problems still arise, however, as the detection limit for ^{226}Ra is approximately 2Bq/L for a 1000ml sample and hence it cannot detect low radium activities commonly found in the natural environment and gamma spectrometry still requires relatively expensive hardware and software. Problems also arise when measurements of water samples are attempted due to the wet plastic wall radon permeation phenomenon and/or vessel background radiation in glass or stainless steel, especially when low activities are expected (MICHEL *et al.* 1981). These problems with water samples can be overcome by barium sulphate co-precipitation procedures (JIANG and HOLTZMAN, 1989 and NIESE, 1994) or by pre-concentration on manganese-impregnated fibres and then counting by gamma spectrometry (CLIFFORD and HIGGINS, 1992 and BASKARAN *et al.* 1993).

2.2.5 Liquid Scintillation

Liquid scintillation counting for beta emissions has been used since the early 1940s but it was not until the early 1980s that suitable improvements in machine and method design enabled the development of a reliable alpha liquid scintillation method for radium analysis (THORNGATE and CHRISTIAN 1977, MCDOWELL 1971, HORROCKS and ALPEN 1980, MCDOWELL and MCDOWELL 1992 and CHAU *et al* 1997). Essentially, alpha liquid scintillation source preparation requires the dispersion or dissolving of the activity in a scintillation cocktail containing an aromatic hydrocarbon solvent. This cocktail is designed to homogenise the sample and scintillator, absorb the kinetic energy of the alpha particle and to convert this to visible light (photons) which can then be detected by the photomultiplier tube.

Alpha liquid scintillation counting has the advantages of ease of sample preparation, essentially a 100% counting efficiency via 4π counting reproducibility (no counting geometry problems) and the elimination of self absorption effects which plague traditional alpha particle spectrometric methods. Conversely problems were initially encountered with variable quenching (an inhibition of the energy transfer between kinetic energy and light energy) relating to the presence of quenching chemical complexes and sample colour, interference from beta and gamma radiation and low

energy resolution. The main developments since the 1950s in making alpha liquid scintillation viable have been the attempts at applying pulse shape analysis so as to discriminate against beta and gamma radioactive interference (BURNETT and TAI, 1992, SAARINEN and SUSKI 1992 and BLACKBURN and AL-MASRI 1994), improvements in the energy resolution relating mainly to quenching and the photomultiplier design (HANSHCKE 1971, and MCDOWELL, 1994), and finally, the development of element specific extractive scintillators (MCDOWELL *et al.* 1989 and MCDOWELL 1994).

Improvements in pulse shape analysis have led to the eradication of beta/gamma interference due to the nature of a scintillation event which consists of a fast component and a delayed component. The relative amounts of light in each component is dependant on the specific ionisation in which beta and gamma radiation produce 10 times as much light per unit of radiation energy as does alpha radiation (HORROCKS, 1974). However, the delayed component of an alpha induced pulse is longer (30-40 nsec) than that of a beta/gamma pulse and this slight time difference enables electronic discrimination and separation of the alpha pulses from the beta/gamma counts as shown in Figure 2-1.

Energy resolution has been improved by optimising detector geometry to a more efficient spherical cavity design with an efficient diffuse reflector arrangement and light coupling optics to transmit the maximum amount of light to the photocathode of the photomultiplier tube. In parallel to this significant advances were made with extractive scintillators that enabled complexes of constant composition, high light producing efficiency and devoid of quenching agents to be manufactured. Extractive scintillators generally combine, in solution, an organophilic metal-ion-complexing agent (extraction agent) with a relatively inert organic solvent or dilutent. The extraction occurs when a metal-organophilic-extraction-reagent salt complex forms at the aqueous / organic interface which is subsequently drawn into the bulk of the organic phase.

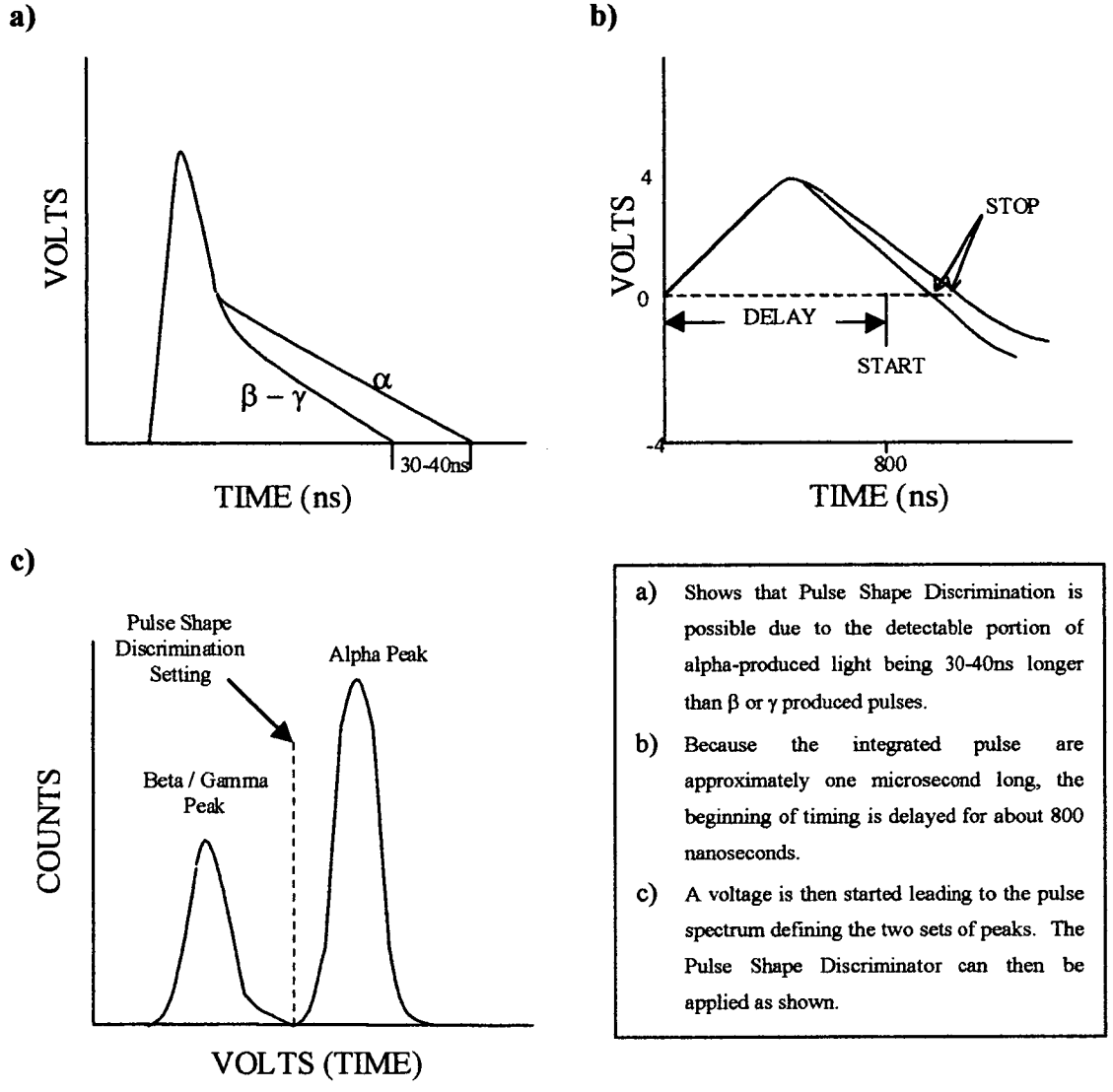

Figure 2-1 A schematic illustration of Pulse Shape Discrimination. Adapted from MCDOWELL 1986.

Size selective synergism has allowed metal specific extractions to occur and in the case of radium, MCDOWELL *et al* (1989), showed that a neo-carboxylic acid, 2-methyl-2-heptylnonanoic acid (HMHN) and the crown ether dicyclohexano-21-crown-7 (DC21C7) when used in a mole ratio of 2:1 in toluene proved to be an efficient extractant. The selectivity of element specific extractants inhibits potential interference from other elements and original sample matrices in the scintillator thus limiting quenching effects and ensures constant response characteristics of the

scintillator. Table 2-1 shows separation factors (= D_{Ra}/D_M) from the potentially troublesome neighbouring and related elements of the periodic table.

With an appropriate aromatic dilutent (toluene), a fluor, 2-(4'-biphenylyl-6-phenylbenzoxazole) (PBBO), (MCDOWELL *et al.* 1974) and an energy transfer agent, naphthalene, an extractive scintillator known as RADAEX was developed by the Oak Ridge National Laboratory group headed by G.N. Case and W.J. McDowell.

Table 2-1 Radium Separation Factors (Taken from McDowell, 1986)

Radium from	Separation Factor	Radium from	Separation Factor
Barium	9.3	Zinc	7×10^6
Strontium	12.3	Lithium	8×10^3
Calcium	58.2 (Approx)	Cesium	1.9×10^5
Magnesium	564 (Approx)	Thorium	3.7×10^6
Beryllium	2×10^6 (Approx)	Uranium	6.2×10^6

Conditions for extraction:

Organic Phase: HMHN, 0.1 M; DC21C7, 0.05M.

Aqueous Phase: $NaNO_3$, NaOH, 0.5M with each of the metals above present as the nitrate at 0.001M and pH at 11-12.

In summary, alpha liquid scintillation offers the opportunity for a highly accurate determinative method for radium analysis via its key characteristics of:

- 4π counting and hence minimal counting geometry problems;
- Effective, element specific, extractive scintillation cocktails;
- No self absorption of the activity as with plates;
- The ability to discriminate against interference from β and γ radiation and other 'unwanted' alphas and hence low backgrounds;
- A high counting efficiency (>99%), and
- Relatively rapid sample preparation and counting times

The specific developments in alpha liquid scintillation outlined above have been combined into an analytical operational package called PERALS®, Photon-Electron Rejecting Alpha Liquid Scintillation spectrometer by the Oak Ridge Detector Laboratory. It is this method that much development work was based around owing to its novelty as a new method for radium analysis and the attributes of alpha liquid scintillation spectrometry (see Chapter 6).

2.2.6 Other Analytical Methods

There remain a number of alternative methods of radium analysis which are not commonly used or are still in their infancy but are worth mentioning for completion. Further details can be found via the stated references, the alternative methods are Gross Alpha and Beta Counting (GODOY 1990 and GODOY *et al.* 1994), Track Detection (SOMOGYI 1990), Coincidence Methods (α-γ or β-γ) (MCCURDY and MELLOR 1981 and GODOY 1990), Magnetic Recovery (TOWLER *et al.* 1996) and Electrothermal Vaporisation Inductively Coupled Plasma Mass Spectrometry (ETV-ICP-MS) (MCINTYRE *et al.* 1997).

2.3 DEVELOPMENTAL RADIUM METHODS

2.3.1 Radium by PERALS Analysis

The PERALS method of analysis was chosen as the main route for methodological development due to the attributes described in 2.2.5 and the lack of a current rapid, precise method of radium analysis. The methodological details and findings are shown in detail throughout Chapter 3.

2.3.2 Radium by Amberlite Columns

In tandem with the development of the PERALS methodology a separate method of radium analysis was being developed. This originated from the purchase of two insitu Seastar water samplers that were later abandoned due to technical problems. However, the mechanism by which these samplers worked relied on a pumping

system that firstly filtered the water and then pumped it through an extractive column. In the case of radium this column was filled with 45g of Amberlite XAD-7 macroreticular resin coated with manganese dioxide. In light of the technical problems it was decided that the use of similar columns could provide an interesting alternative to the PERALS method and provide a means of comparison between the two methods.

The principals by which the column worked can be traced back to the early days of MOORE, 1969 and KRISHNASWAMI *et al.* 1972 who were the first to load a synthetic fibre with ferric hydroxide. MOORE and REID, 1973 first pioneered the use of manganese impregnated acrylic fibres for the measurement of radium. A subsequent improvement on the method was achieved by MOORE, 1976 and thereafter the method has formed a common base for the extraction of radium from water (KEY *et al.* 1979, MACKENZIE *et al.* 1979, KOULOURIS, 1996 and TOWLER *et al.* 1996). Problems existed, however, with the acrylic fibre in that flow was not uniform through the cartridge (MOORE and COOK, 1974) and there was a significant amount of 'washout' of MnO_2 particles that were not firmly bonded to the fibre. GERSHEY and GREEN, 1988 carried out a series of experiments using Amberlite XAD resins with the result that XAD-7 resin coated easily with a consistent amount of MnO_2 (5% by weight) and that uniform packing and flow characteristics were attained. It was these findings that the following method was developed upon. The actual nature of the bonding between the MnO_2 and the resin is not clearly understood but GERSHEY and BOYLE, 1987 postulate that the MnO_2 and resin form a complex of the oxygen atoms in the acrylic ester groups on the resin and the manganese atom. The manganese-oxygen bonds in MnO_2 are highly polarised, with the oxygen atoms having a substantial negative charge and the manganese bearing a large positive charge. The Mn-O bond therefore constitutes an electrical dipole and if the resins oxygen atoms donate electrons to the positive manganese a cyclic complex is formed as shown in Figure 2-2.

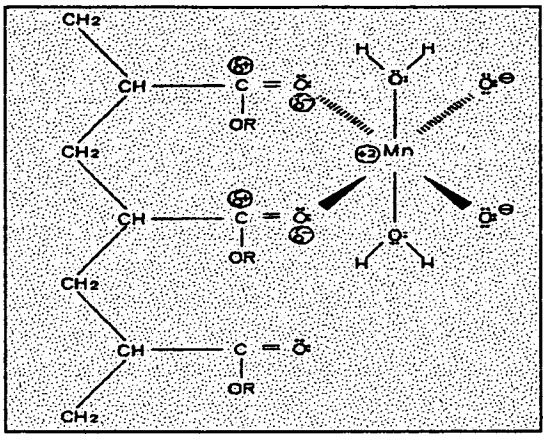

Figure 2-2 Proposed bonding of the Manganese to the XAD-7 Acrylic Resin (Gershey and Boyle, 1987).

The oxygen atoms of the MnO_2 would then be capable of attracting radium and other ions of similar charge and diameter by either forming ion-dipole attractions, as shown in Figure 2-3a or by donating electrons to the radium ion and forming a complex as shown in Figure 2-3b.

a) b)

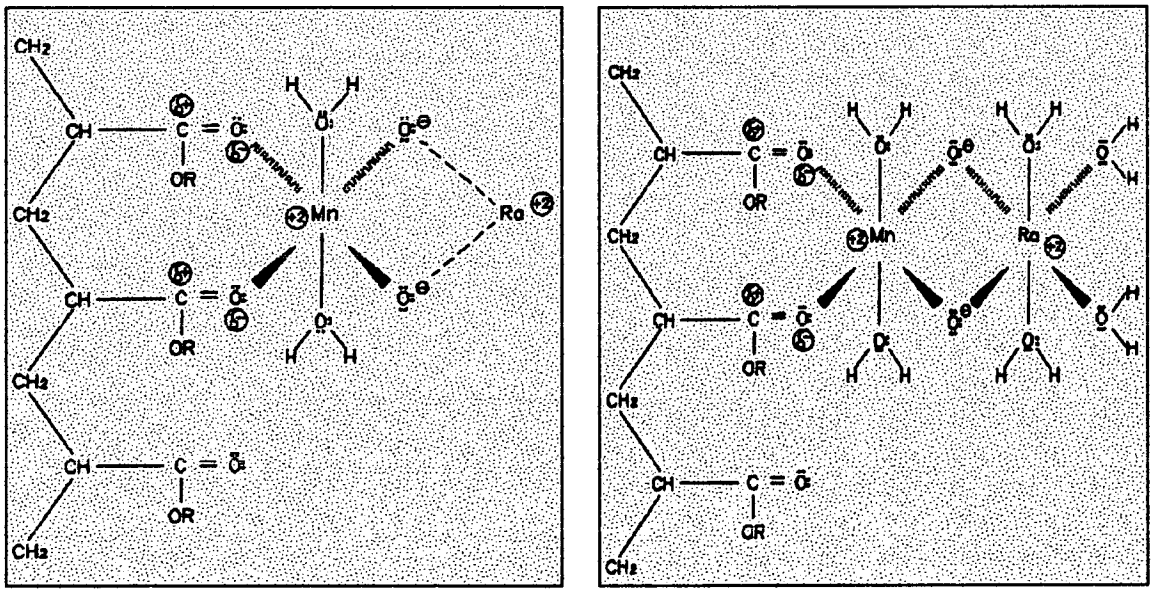

Figure 2-3 Proposed bonding of the Radium to MnO_2 and hence the resin (Taken from Gershey and Boyle, 1987).

The procedural details of the amberlite methodology are given in the appendix A3.

2.4 SEDIMENTARY RADIONUCLIDES BY GAMMA SPECTROSCOPY

Sediment core samples were analysed on an EG&G Ortec High Purity Germanium (HPGe) semiconductor detector for both natural and manmade radionuclides according to the method outlined in A4.

The principles, operational procedures and use of gamma detectors is well known and is thoroughly documented as given in section 2.2.4. Therefore only a limited description is presented below of the principles of gamma ray spectroscopy, interferences, sources of error and calibration procedures.

2.4.1 Interactions of Photons with Matter

Gamma photons interact with matter (electrons) via three main mechanisms:

The photoelectric effect, The total energy of the photon is given up to a bound electron in the 'K-layer' which thereby becomes a 'photoelectron' or essentially a β^- particle which leads to further ionisation.
Compton Scattering, The photon gives up part of its energy to a weakly bound electron with the remainder of the energy carried off by a new photon.
The Creation of Electron-Positron Pairs, Photons that have an energy greater than 1.022 MeV can spontaneously produce two photons (β^+ and β^-) by annihilation of the positron with an electron when it has lost its kinetic energy giving rise to the observed annihilation peak at 609KeV for radium.

The photoelectric effect is the most significant in gamma spectroscopy with its efficiency decreasing with increasing gamma photon energy and conversely increasing approximately in proportion to Z^5 of the absorber, where Z is the average atomic mass.

The ionisation or electron excitation induced by the interaction of gamma photons with the semiconductor material gives rise to a series of voltage pulses which are the amplified and detected electronically. The spectra are then analysed using Omnigam® software which calculates the energy, shape, area of peaks and constructs a report detailing the energies in KeV, counts per second (cps) and % counting error at each of the detected energies. The specifications of the EG & G Ortec Gamma-X detector are given in Table 2-2.

Table 2-2 Gamma Spectrometer specifications

Detector	EG & G Ortec HpGe Gamma-X
Relative Efficiency @ 1.33 MeV	38%
Resolution @ 1.33 MeV	1.86 KeV
Hardware	EG & G Ortec NOMAD 92X-P processor Locland 486 SX/PX computer
Software	Omnigam version 3.5, 1991

2.4.2 Factors Affecting the Detector Response

The main factors that affect the accuracy and precision of the detector are the, background, counting geometry, counting statistics and self-adsorption. The main source of background comes from both natural cosmic radiation and the natural radiation found in buildings and from man-made materials including those used in the detector construction. In order to minimise the background from the main source of cosmic radiation, a 4" lead shield encompasses the detector along with a Cu/Cd lining to minimise interference from secondary lead X-rays emitted from the shielding. The counting geometry and the effect on detection efficiency can be defined as,

Equation 2-2

$$\textbf{\% Detection Efficiency} = \left(\frac{\textbf{Observed Counting Rate}}{\textbf{Source Disintegration Rate}}\right) \textbf{x } 100$$

This varies in proportion to $1/d^2$ where d is the distance of a point source from the detector and hence it is essential for comparative work that geometries should be reproducible and accurate. Self-adsorption of gamma photons is related to the atomic mass and sample density and is of particular importance for low energy photons, hence differences in sample type and matrix can introduce an error. Finally there is a statistical uncertainty associated with the number of counts, N. This is usually given as the standard deviation (σ) which is equal to the $\sqrt{N}$. This uncertainty applies to the counts in the peak and the associated near peak background and ultimately determines the detection limit. It was therefore essential to keep background radiation to a minimum and counting error statistics to the lowest practical value so as to give the best signal to noise ratio.

2.4.3 Detector Calibration

An energy peak calibration of the detector was carried out using a Eu-152 source so as to ensure that peak identification was correct. In addition spiked reference sediment samples at 5, 10, 15 and 20g were used to determine counting efficiencies for the respective weights in order to account for variations in the counting geometries for different sized samples.

The radionuclides capable of detection by gamma spectroscopy and of primary concern to this project are shown along with their primary detection energies and half lives ($t_{½}$) in Table 2-3. The energies shown give the best overall count rate and the least interference from other radioactive decay products.

Table 2-3 The main radionuclides of interest with their half-lives and energies of measurement.

Radionuclide	$t_{½}$ (y)	Energy (KeV)
Radium 226	1600	609
Lead 210	22.3	46
Caesium 137	30.2	661

The precision along with the accuracy for the gamma counting procedure relative to the IAEA-300 Baltic Sea sediment standard is given in Table 2-4 with the actual precision data for a Baltic Sea sample shown in Table 2-5 for 11 repeat counts.

Table 2-4 Accuracy and precision measurements for both the IAEA standard and sediment samples.

Nuclide	IAEA 300 Certified Value (Range)	Mean IAEA Count Bq/Kg	IAEA Precision (1σ, n = 15)	Sed. sample Mean Bq/Kg	Sed. Sample Precision (1σ, n = 11)
^{137}Cs	1066.6 (1046-1080)	1048	± 2.2%	80	± 1.5 %
^{226}Ra	56.5 (not given)	49.9	± 12%	23	± 11.7 %
^{210}Pb	360 (339-395)	340	± 4.3%	174	± 6.8 %

From the above details it was concluded that the accuracy of the analytical procedure was satisfactory and that the results would give an answer within error of the true value.

Table 2-5 Precision data for 11 repeat counts of a sediment sample.

Sample	^{137}Cs	^{226}Ra	^{210}Pb
1	79.8 ± 3.1	20.3 ± 2.4	154.9 ± 10
2	78.3 ± 3.2	19.6 ± 1.5	166.5 ± 9.5
3	81.7 ± 3.3	22.3 ± 2.3	168.7 ± 10.1
4	79.1 ± 2.8	24.9 ± 2.6	177.2 ± 10.6
5	80.3 ± 2.8	26.9 ± 2.8	194.4 ± 12.5
6	79.7 ± 3.4	23.4 ± 2.0	181.5 ± 10.9
7	82.0 ± 3.1	23.7 ± 2.3	182.3 ± 11
8	78.6 ± 3.1	28.2 ± 3.3	182.8 ± 11.9
9	81.0 ± 3.0	22.7 ± 2.4	155.7 ± 10.2
10	80.7 ± 2.1	19.9 ± 1.5	175.7 ± 8.9
11	80.6 ± 2.3	23.7 ± 1.8	175.8 ± 9.4
$\bar{X}$ (11)	80	23	174

2.5 INDUCTIVELY COUPLED PLASMA MASS SPECTROMETER (ICP-MS)

A VG Elemental Plasmaquad PQ3 Inductively Coupled Plasma-Mass Spectrometer (ICP-MS) was used to determine elemental concentrations (Li, Ti, V, Mn, Fe, Co, Ni, Zn, Cu, As, Rb, Sr, Y, Zr, Mo, Cd, Sn, Sb, Cs, Ba, Ce, Pb, Th and U) for both the water column dissolved and particulate phase and also the sediment traps, cores and 'fluff' layers samples collected over a 24 month period in the Southern Baltic Sea.

2.5.1 Principles of ICP-MS

The ICP-MS provides a relatively sensitive method of analysis with very low detection limits, rapid sample analysis time, good accuracy and precision. In this particular project the ICP-MS was used to measure both the concentration and isotopic ratios of elements to a parts per billion level. Figure 2-4 shows the ICP-MS present at Dunstaffnage Marine Laboratory, Oban.

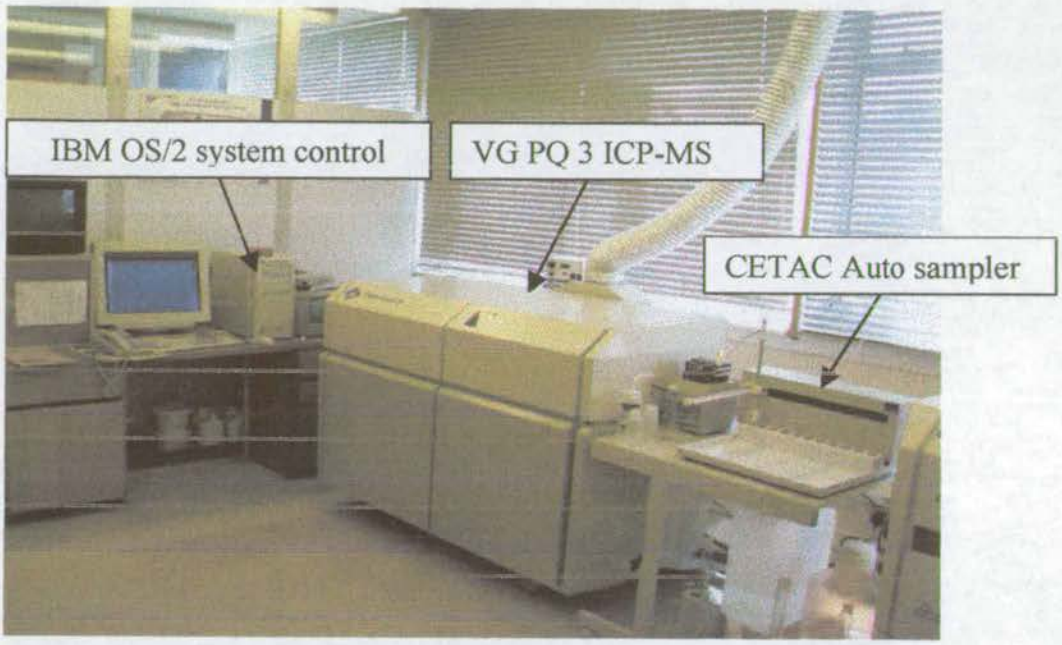

Figure 2-4 VG Plasmaquad 3 at Dunstaffnage Marine Laboratory, Oban.

The ICP-MS is a comparatively simple technique which can be used to analyse a wide range of sample types and is described in numerous publications including DATE and GREY, 1987, RIDDLE *et al.* 1988, GARBE-SCHÖNBERG, 1993, HOLLLAND and EATON, 1993 and POPPITI, 1994. Essentially the operation of the ICP-MS can be broken down into five basic entities. Figure 2-5 shows the main hardware components that comprise these basic processes.

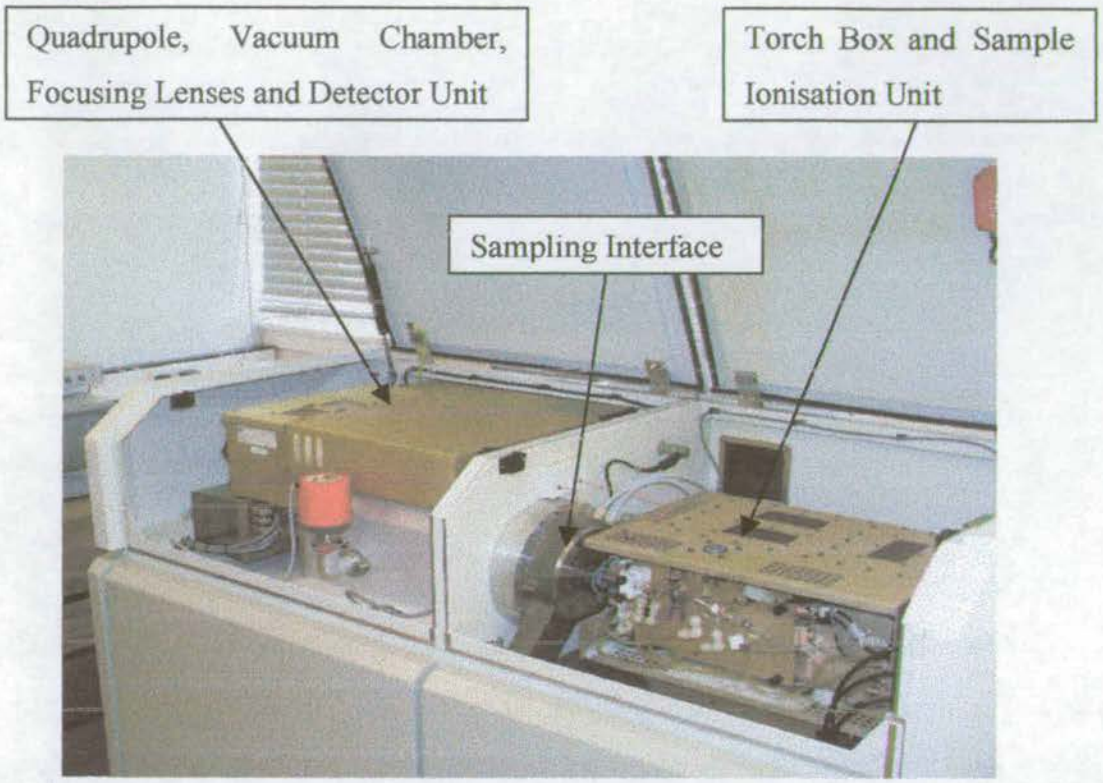

Figure 2-5 Main hardware components of the VG PQ 3 ICP-MS

2.5.1.1 Detection

The detection unit is sensitive to charged species and operates as a cascading unit in that when one ion hits the detector surface, more electrons are released from the barrier and so on until a relatively large number of electrons are released at the bottom in the form of a pulse. These pulses of electrons can then be counted individually (as pulse counting mode) or integrated as a flow against a function of time (analogue).

2.5.1.2 Filtering

Positively charged ions are transported as an ion beam into the quadrupole mass filter which consists of four charged rods across which the current is varied. This acts as a type of electromagnet which causes the ions to oscillate about their central travel

path, dependant upon their masses. Only ions with a certain mass to charge ratio can pass through the quadrupole without colliding with one of the rods. Hence, only specific ion masses are transmitted to the detector, in which the number of ions registered are proportional to the concentration of the element in the sample.

2.5.1.3 Focusing

Within the mass spectrometer the sampled ions, under high vacuum, are accelerated and focused into a mass filter by a set of electrostatic lenses. These lenses consist of stainless steel plates or tubes with precise and controllable DC voltages, which attract or repel the sampled ion beam.

2.5.1.4 Sampling and Ionisation

Figure 2-6 shows the unit responsible for the creation and introduction of the ion beam into the mass spectrometer.

The samples in 2% HNO_3 are introduced into the ICP-MS using a peristaltic pump which injects the sample into an argon gas stream which takes place within a water cooled nebuliser and leads to the formation of an aerosol. The aerosol is then introduced through a borosilicate torch into the core of a high temperature plasma, maintained at 10000° K by a radiofrequency field. The energy transfer from the plasma to the sample leads to the sample dissociating, atomising and finally ionising. The plasma core containing the sample ions is extracted into a reduced pressure region maintained by a mechanical rotary pump and water cooled to prevent high temperature damage to the components. The sample ions travel through a nickel sampling cone with a 1mm orifice and then onto a nickel micro skimmer (0.75mm orifice) before introduction to the mass spectrometer unit.

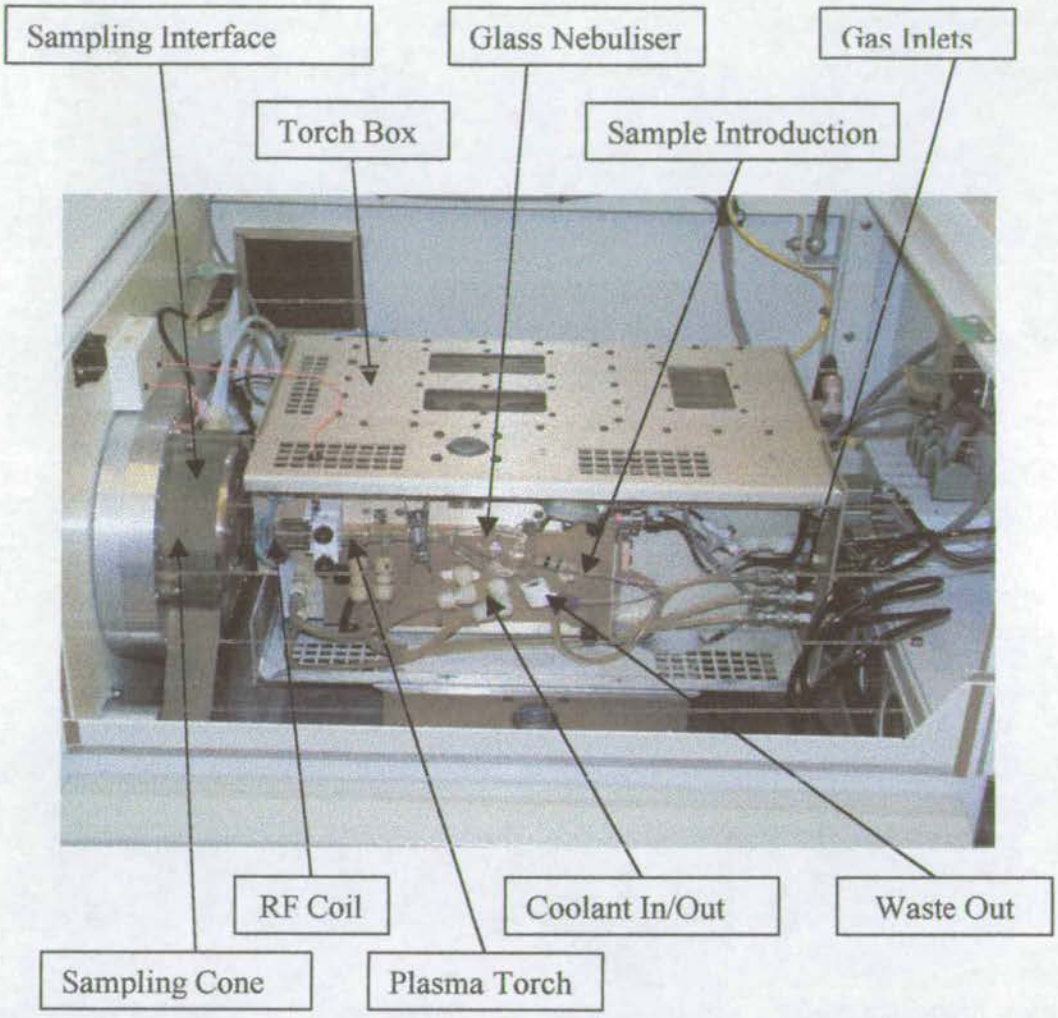

Figure 2-6 Main features of the ICP-MS Torch box and Ionisation Unit

Typical Operating Parameters

Plasma

R.f. power		
	Forward	1.35kW
	Reflected	< 10 W
Gas Controls		
	Auxiliary	0.55 l min^{-1}
	Coolant	14 l min^{-1}
	Nebuliser	0.88 l min^{-1}
Nebuliser		
	Glass expansion type	
Spray Chamber		
	Impact bead spray chamber, water cooled (5°C)	

Ion Sampling

Sampling Cone	Nickel with 1.0 mm orifice
Micro skimmer Cone	Nickel with 0.75mm orifice
Sampling distance	10mm from load coil

Optimisation

Lenses are adjusted to maximise the ^{115}In signal

Vacuum

Expansion stage	< 2.0mbar
Intermediate	< 1 x 10^{-4} mbar
Analyser	3.8 x 10^{-6} mbar

Data acquisition

Dwell time	320μs
Dead time	20ns

2.5.2 ICP-MS Sample Preparation: Bulk Sediment Digestion

Samples were collected as outlined in section 2.1 and were introduced into the ICP-MS in a 2% HNO_3 solution. The particulate phases filters and the sediment trap and core samples first required digesting. Two methods were employed to achieve this, the first used a CEM corp. microwave accelerated reaction system (MARS 5) unit to digest the sediments and the second used a more basic but equally effective hotplate / teflon beaker set up.

2.5.2.1 CEM corp. microwave accelerated reaction system (MARS 5)

This system has been reviewed and validated by a number of authors amongst which KINGSTON and JASSIE, 1988, STURQEON, 1988, GILMAN and ENGELHART, 1989, CORL, 1991, TOTLAND et al, 1992 are but a few with HEWITT and REYNOLDS , 1990 concluding that over traditional dissolution techniques there was no compromise in efficiency or precision for the reduced sample dissolution time involved with microwave digestion techniques.
The digestion procedure used was similar to that outlined in KINGSTON et al, 1992 and a summary can be found in appendix A.5.

2.5.2.2 Filter Digestions

The filters that had been used to collect the water particulate phase as differentiated by the 0.45μm filter were digested using the traditional method of an acid-teflon beaker-hot plate combination and is summarised in appendix A.5.

2.5.3 ICPMS Sample Preparation for Quantitative Analysis

The ICP-MS like any analytical machine suffers from drifts in sensitivity over a prolonged period of time but this can be accounted for by careful use of internal standards. Commonly, depending on the elements under investigation, indium and bismuth are used to provide an internal corrective factor to account for such drift. Another common problem with ICP-MS are the polyatomic interferences (GILSON *et al.*, 1988, JARVIS *et al.*, 1992, EVANS and GIGLIO, 1993) but these can be

readily accounted for by the use of interference equations and for the majority of elements there is at least one isotope that is not overlapped by isotopes of other elements. Care should also be taken to ensure that the solid or salt content of the dissolved phase samples does not exceed 0.2 %. Hence, with the highest salinity being 22‰ a dilution factor of twenty times accounted for this requirement.

Analysis times per sample are short with a typical quantitative analysis of 3 repetitions for multi-element analysis and 5 repetitions for isotope ratios taking 10 and 15 minutes respectively. A standard sample volume of 10ml is usually prepared for either type of analysis. The two sections below provide greater detail on the techniques used for the two main types of analysis.

2.5.3.1 Multi-element Analysis

A typical quantitative multi-element run would consist of a wash followed by 6-8 standards that are used to define the calibration line for the elements of interest. The actual samples were diluted sufficiently to not only lie within this concentration line but also to lie comfortably within the machine pulse counting detection threshold. The standards used were prepared from the CLARITAS PPT certified reference solution range. Following the standards would then be another wash followed by 6 samples, a wash, and then two 'check' standards, one low and one high concentration, followed by another wash and 6 samples and finally another complete set of standards. During dilution of the samples an internal standard solution of indium and bismuth was also added to every sample so as to account for machine drift.

2.5.3.2 Stable Lead Isotope Ratios

Lead isotope ratios were determined using more 'reference standards' than the multi-element method previously described. The 'standards' used here took the form of mass bias solutions, in which the ratio of the various lead isotopes are accurately known, hence the deviation from this standard to a 'sample' mass bias can be used to determine the drift of the machine and help to decide as to whether the data is of high

quality. A typical cycle would therefore consist of a mass bias, wash, three samples, mass bias, wash etc with each sample repeated five times to ensure good counting statistics.

2.5.3.3 Uranium Isotope Ratios

Uranium isotope ratios were essentially carried out in the same manner as the lead isotope ratios except that a spike was added in order that an absolute value of uranium could be determined. A U-236 spike was added in a calculated 1:1 ratio with the U-238 peak thus massively overspiking and negating the natural U-236 present.

2.5.4 ICPMS Calibration and Acceptance Criteria

The accuracy of the machine was measured relative to four standards, two of which and a selection of metals are shown in Table 2-6

Table 2-6 Accuracy of the ICP-MS relative to IAEA 356 and Mag-1.

Element	IAEA 356 Certified Value ppm	Measured Value ppm ± (1σ, n=9)	MAG-1 Certified Value ppm	Measured Value ppm ± (1σ, n=9)
Ti	2190	2163 ± 3.4%	4501	4432 ± 2.7%
V	55.5	61 ± 2.54%	140	148 ± 4.26%
Mn	312	336 ± 1.27%	759	751 ± 2.1%
Fe	24100	24638 ± 1%	24410	25127± 2.2%
Ni	36.9	37.9 ± 1.64%	53	51.6 ± 2.3%
Zn	977	918 ± 8.45%	130	144 ± 2.64%
Rb	71	69.8 ± 1.7%	149	156 ± 2.76%
Sr	170	184 ± 2.5%	146	151 ± 3.33%
Cs	Not given	4.4 ± 1.5%	8.6	8.75 ± 2.85%
Ba	548	529 ± 0.75%	479	483 ± 2.0%
Pb	347	347 ± 2.3%	24	30.4 ± 3.78%
U	3.2	2.9 ± 3.05%	2.7	3.04 ± 1.7%

Table 2-7 Precision of the ICPMS for ten repeats of a sediment sample.

Element	Value (ppm ± (1σ, n=10))
Li	644 ± 3.2%
Ti	22726 ± 3.8%
V	42.2 ± 3.7%
Mn	1101 ± 2.6%
Fe	1036 ± 1.9%
Co	8.13 ± 2.7%
Ni	32.8 ± 3.0%
Cu	47.6 ± 3.1%
Zn	182 ± 2.5%
As	15.1 ± 2.6%
Rb	503 ± 1.7%
Sr	217 ± 3.2%
Y	134 ± 1.8%
Zr	768 ± 1.7%
Sn	31 ± 1.9%
Sb	2.37 ± 2.4%
Cs	13.8 ± 1.2%
Ba	1045 ± 3.8%
Pb	58.0 ± 1.1%
Th	4.77 ± 2.0%
U	1.02 ± 2.7%

The accuracy for the standards analysed and the precision for the sample repeats was judged to be satisfactory for this set of analyses. In support of this an acceptance criteria was developed in order to act as a quality control on the data whereby results were rejected if the sample errors were greater than 10%, if the calibration regression line fell below 99.5 and the standard values were outwith 10% of the certified value.

2.6 CARBON AND NITROGEN ANALYSIS

A Carlo Erba (NA 1500) Elemental Analyser, based at the Geology and Geophysics institute, Edinburgh Univeristy, was used to determine both the organic and inorganic carbon fractions along with the total nitrogen content of the sediment cores collected. The method used was similar to that described by VERARDO *et al.* 1990 with the exception that silver capsules were used instead of the published aluminium capsules which were found to split upon the addition of sulphurous acid.

In summary, two dried sediment samples each of approximately 20mg in weight were placed in a tin capsule for total carbon analysis and in a silver capsule for organic carbon analysis. The tin capsule was then compressed into a sphere and loaded into a carousel from which they dropped into the machine for analysis. To the silver capsules and sediment 75ul of sulphurous acid (0.6ml, 6% w/v SO_2 AnalaR) was then added. The sample was then left overnight in vacuum oven to effervesce and dry before being compressed into a sphere and loaded into the carousel. A standard calibration line was generated using the method outlined above using acetanilide ($C_6H_5.NH.CO.CH_3$) instead of sediment.

As the sample is introduced into the machine it enters the combustion chamber which is maintained at 1050°C and the gases generated (with a helium carrier) then pass through an oxidation column containing chromium trioxide and silvered cobaltous oxide and then through a reduction column containing copper wire. The nitrogen and carbon dioxide gases are separated in a gas chromatograph column and measured by a thermal conductivity detector.

The precision of the analysis as determined on replicate samples was found to be ±0.56 % (1σ, n=9) for carbon and ± 0.54 % (1σ, n=9) for nitrogen. In addition the above method was recently compared using a standardised marine sediment sample with those of nine other laboratories (KING *et al.* 1998). The results obtained from Edinburgh showed good agreement with the mean values generated from the study as shown in Table 2-8.

Table 2-8 Summary of the Interlaboratory comparison (KING *et al. 1998)* for marine sediment.

% Total Carbon	Acetanilide Mean	Variance	Marine Sediment Mean	Variance
Study Range	69-72.31		5.34-5.83	
Edinburgh	70.76	0.12	5.43	0.003
All Means	69.58	8.52	5.54	0.022
% Total Nitrogen				
Study range	9.97-10.51		0.17-0.18	
Edinburgh	10.27	0.01	0.17	0.000136
All Means	10.38	0.15	0.17	0.0000072
% Organic Carbon				
Study Range			1.30-1.71	
Edinburgh			1.38	0.007
All Means			1.49	0.35

2.7 X-RAY FLUORESENCE

Bulk sediment geochemistry for a wide range of both major and trace elements was determined by a Philips PW 1480 sequential wavelength dispersive X-ray spectrometer equipped with a PW 1510 sample changer, located in the Geology and Geophysics institute, Edinburgh Univeristy,. The principles and methodology used have been extensively described by DZIUNIKOWSKI, 1989 and CHOPPIN *et al.*, 1996. A detailed preparation procedure along with corrective procedures can be found in appendix A.6.

2.7.1 Accuracy and Precision of the XRF analyses.

Table 2-9 shows analytical precision and accuracy measurements for the XRF analysis. Precision calculations are based upon 10 repeats of a Baltic sea sediment sample and analytical calculations are taken from MATTHEWSON, 1995. Typical

errors in XRF analysis occur due to machine related analytical error and errors due to the manufacturing process of the glass disc or pressed pellet. For major element analysis machine precision is generally high but the manufacturing error is likely to be of greatest concern. Conversely, in minor element analysis precision in the manufacturing process is high but machine analytical error provides the largest error. Despite this the errors generated on the main elements of interest were not considered significant enough to affect data interpretation.

Table 2-9 Accuracy and Precision of the XRF analyses.

Oxide (wt. %)	Mean (n=10)	S.D.	Precision (% S.D.)	Accuracy	Oxide (wt. %)	Mean (n=10)	S.D.	Precision (% S.D.)	Accuracy
SiO_2	39	1.01	2.5	0.147	Ba	276	9.9	3.6	27.66
Al_2O_3	2.8	0.13	4.6	0.124	Br	9.38	0.68	7.2	2.40
Fe_2O_3	1.4	0.05	3.4	0.157	Ce	51.3	5.31	10.3	7.89
MgO	0.25	0.02	9.2	0.037	Cr	31.5	3.87	12.3	55.48
CaO	0.45	0.02	3.4	0.086	Cu	5.61	0.61	10.8	5.69
K_2O	1.61	0.05	2.8	0.017	I	12.6	4.58	36.3	3.70
TiO_2	0.26	0.001	2.1	0.017	La	12.4	2.90	23.3	4.30
MnO	0.019	0.001	8.6	0.010	Mo	1.97	0.11	9.1	0.60
P_2O_5	0.041	0.002	3.8	0.014	Nb	8.08	0.58	7.1	2.42
					Nd	10.8	1.95	18.1	3.14
					Ni	8.25	0.51	6.1	4.45
					Pb	9.79	1.13	11.5	2.02
					Rb	55.2	0.72	1.3	3.08
					Sc	81.9	0.65	0.8	3.19
					Sr	81.8	0.64	0.8	8.46
					Th	4.84	0.48	9.9	1.77
					U	4.16	0.71	16.9	4.73
					V	24.7	2.58	10.4	6.37
					Y	18.20	0.39	2.1	1.28
					Zn	23.96	0.93	3.8	3.27
					Zr	432	10.3	2.3	10.49

Precision includes counting error, disc reproducibility, error in regression line and error in matrix mass absorption determinations

Accuracy is determined from r.m.s.d. of international standards about the regression line, after MATTHEWSON, 1995.

2.8 X-RAY DIFFRACTION

A Phillips PW 1011/1050 diffractometer was used to determine the mineralogical composition of the sediment samples using the analytical conditions shown in Table 2-10. Sample preparation, simply involved the gentle grinding of the dried sediment in acetone and the dispersal of this mixture using a pipette onto a glass plate where it was then left to dry as a thin, even coating.

Table 2-10 Typical X-ray diffraction operating settings

Generator Settings	40 kV, 50mA
Cu kα 1,2 wavelengths	1.54060, 1.554439
Step size, sample time	15 sec/°
Monochromator used	Yes
Divergence slit	Automatic
Analysis program number	8
Peak angle range	2° to 60° (2θ°)
Range in D-spacing	2.25221 to 44.1372 Å
Crystal peak width range	0 to 2°
Minimum peak significance	0.75

2.9 PARTICLE SIZE ANALYSIS

Grain size analysis was carried out using a Coulter LS100 grain size analyser which utilises laser diffraction technology to measure the proportion of grains within specific grain size boundaries. The particles in suspension are passed through a laser beam leading to the diffraction of the beam in which the angle of diffraction is inversely proportional to the grain size. The diffracted beams are then picked up by a series of photodiode detectors which together form a composite diffraction pattern which can then be used to determine the quantity of particles in a particular grain size.

3.0 Photon-Electron Rejecting Alpha Liquid Scintillation Spectrometer

3.1 THE PERALS SPECTROMETER

The Photon-Electron Rejecting Alpha Liquid Scintillation (PERALS) spectrometer was chosen as the main avenue of research into radium analysis because of the presence of a radium-specific extractant in *ETRAC* RADAEX which allows instant analysis (no ingrowth period), a relatively simple and rapid chemical preparation, the ability to concentrate low activities via the extractive scintillant into the sample and the novelty of this new method. The manufacturers claim that PERALS is the most rapid and sensitive alpha spectrometric method available with backgrounds as low as 0.001dpm, a constant 99.7% counting efficiency (the 0.3% represent the alphas that collide with the culture tube), energy resolution of 4.2%, a 99.99% rejection of ambient and sample induced β and γ counts and a lower limit of detection better than 0.01dpm also bode well in the adaptation of this method.

Early trials of the PERALS system for ^{232}Th, ^{228}Th, ^{238}U, ^{241}Am and ^{239}Pu were carried out by CADIEUX, 1990 and CADIEUX *et al.* 1994 who focussed their work on complex samples (caustic sludge samples from the dissolution and neutralisation of irradiated fuel and target elements). These samples had presented difficulties in analysis by traditional alpha spectrometric methods due to the nature of the sample and the high concentrations of beta and gamma emitting fission products. Their results sparked interest in the PERALS methodology and reinforced the manufacturers claims about its specification.

3.1.1 Key technical developments regarding the PERALS spectrometer

The main improvements over commercial liquid scintillation spectrometers relate to the hemispherical design of the counting tube and its positioning relative to the photomultiplier tube along with the incorporation of the pulse shape discrimination facility. Figure 3-1 shows the photomultplier tube design and Figure 3-2 shows a same scale comparison between traditional beta liquid scintillation and PERALS Spectrometry of two alpha peaks (^{239}Pu and ^{232}Th) approximately 1 MeV apart.

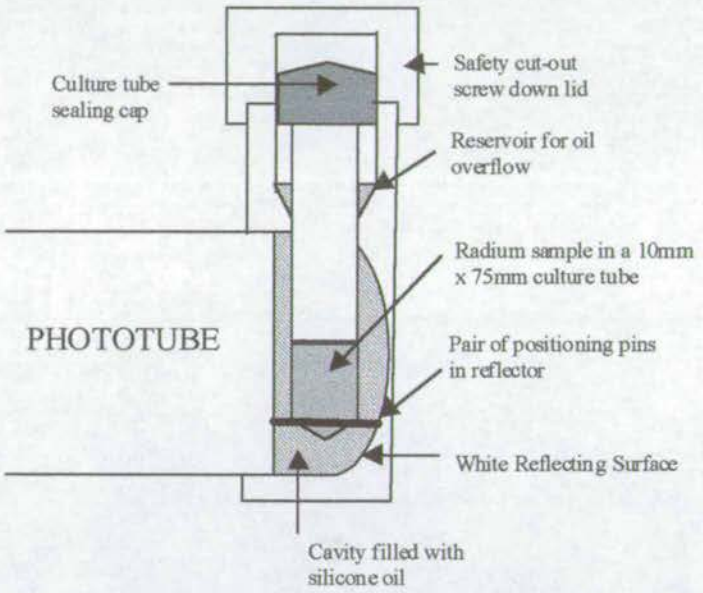

Figure 3-1 The PERALS phototube assembly illustrating the unique hemispherical, single phototube design. (McDowell, 1981)

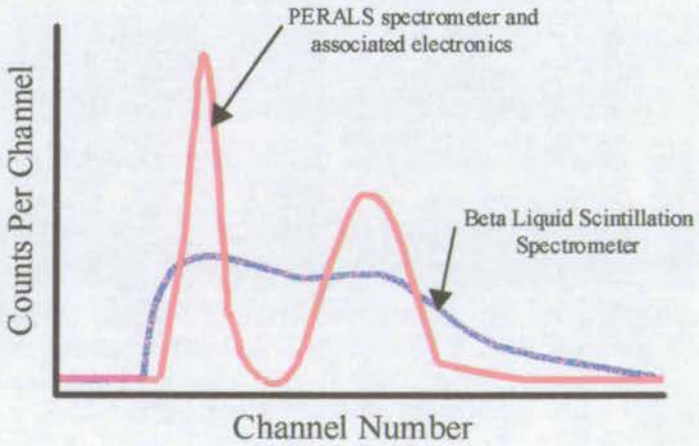

Figure 3-2 A direct, same scale comparison of the resolution of two alpha peaks approximately 1 MeV apart by PERALS and a beta liquid scintillation spectrometer (after McDowell, 1981).

Figure 3-2 clearly shows the advantages of the PERALS system in peak analysis, combining the pulse shape rejection facility, the advanced photomultiplier design and the advantages of an extractive scintillator. The resolution of the beta liquid scintillation spectrometer would have been worse if the extractive scintillator used with the PERALS system had not been used.

The design of the photomultiplier tube and associated electronics optimises the reflectivity and reception of the light generated from the interaction of the fluor and alpha particles to the detector itself. The light is generated by the ionising radiation, given off by the passage of alpha particles, which causes the excitation of molecules in its path with the light corresponding to the de-excitation of these photons. The specific luminescence is a function of the specific energy loss for the particle or photon (VOLTZ *et al.* 1966) and, hence the intensity of the pulse is proportional to the energy of the event.

If a photon has sufficient energy upon colliding with the photocathode then a number of photoelectrons are produced, proportional to the energy of the photon. These photoelectrons are then accelerated and multiplied by a series of dynodes. The dynodes consist of electron releasing materials which when struck on the front face by an electron release a number of incident electrons hence multiplying the signal by a factor of M given by Equation 3-1 (ADAMS and DAMS, 1970):

Equation 3-1

$$\mathbf{M = \delta g}$$

Where δ is the mean number of emitted secondary electrons per incident electron and g is the probability of their capture by the next dynode. The electrons are progressively accelerated and multiplied through fields of increasing voltage until the number of electrons has been increased by a factor of 10^6-10^8 (ADAMS and DAMS 1970). Ultimately the electrons reach the anode and an electrical pulse is generated proportional to the initial event energy.

3.1.2 Radium Pre-Concentration and Extraction

The first application of PERALS to radium analysis was carried out by CASE and MCDOWELL, 1990 who developed a methodology for the sample preparation and analysis using the *ETRAC* RADAEX scintillation cocktail. Building upon the work by MCDOWELL, 1986 and CASE and MCDOWELL, 1990 a second round of papers with specific methodologies for radium in natural waters by TAI, 1991 and BURNETT and TAI, 1992 then followed. It was these papers along with an application note by HERITAGE LABORATORIES INCORPORATED, 1994 that formed the basis for my radium analytical work. Common to all the methods is the use of a barium/radium sulphate co-precipitation followed by a dissolution conversion to the more soluble carbonate form and finally an extractive phase using *ETRAC* RADAEX. As described previously RADAEX consists of an extractant neo-carboxylic acid, 2-methyl-2-heptylnonanoic acid (HMHN) and the crown ether dicyclohexano-21-crown-7 (DC21C7) in a toluene base along with the scintillator, PBBO and an energy-transfer agent, naphthalene. A Ba-133 tracer is used in both methods to determine the chemical recovery of the procedure. Figure 3-3 illustrates by way of a flow chart the method of BURNETT and TAI, 1992.

During my early investigations the method devised by Heritage Laboratories, as shown in Figure 3-4, was the principal route used for radium analysis as this method was the latest version and was quicker for the large number of samples collected. As the research continued further modifications were made to try and overcome particular problem areas and these along, with the primary method, are detailed below.

The following sections show in detail the methods and equipment required for radium analysis using the PERALS methodology.

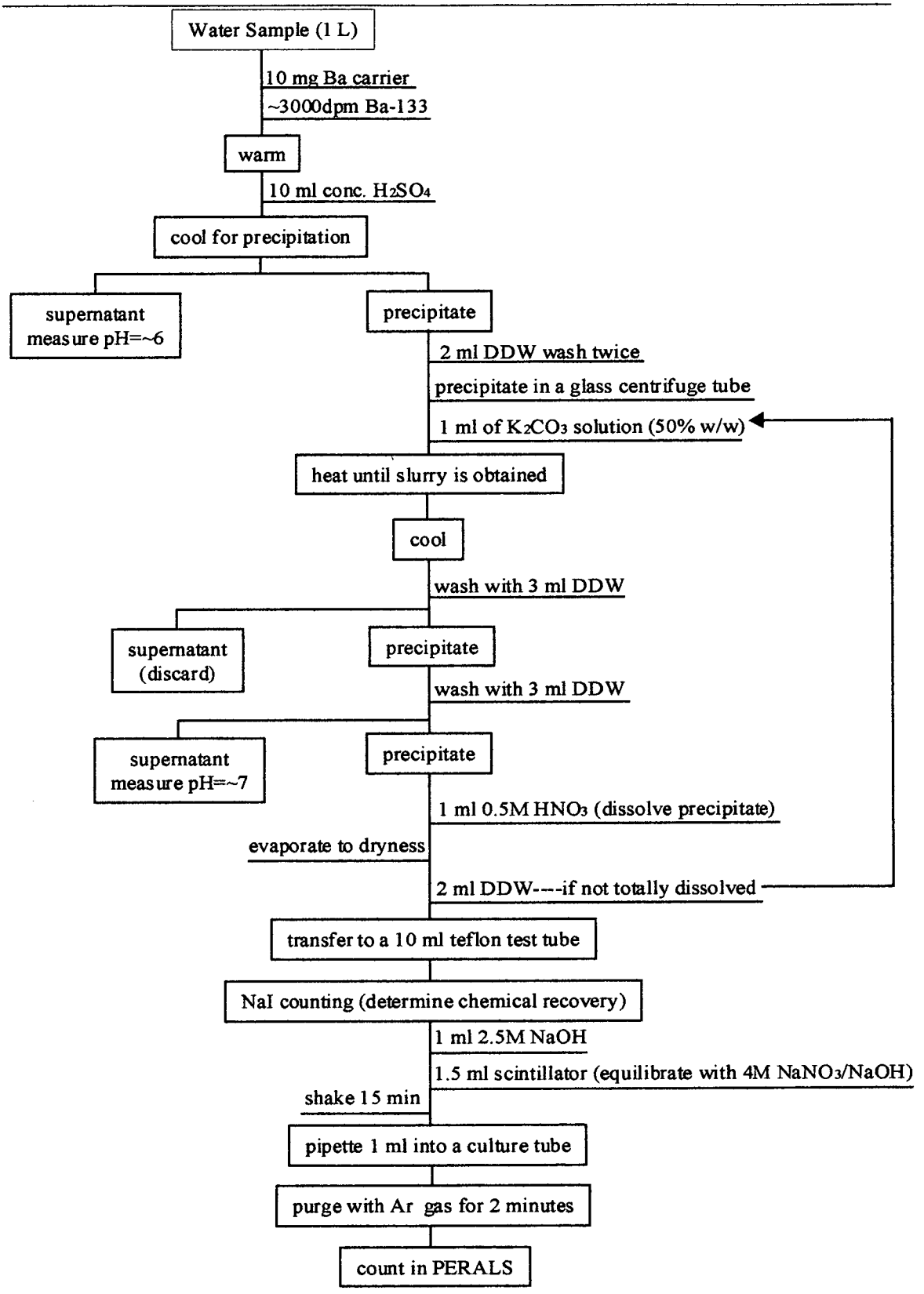

Figure 3-3 Flow diagram illustrating radium pre-concentration and extraction steps according to Burnett and Tai, 1992.

3.2 THE PERALS METHODOLOGY

3.2.1 Equipment Requirements

1) The self-contained PERALS® spectrometer housed in a triple width nuclear instrument module (NIM). The PERALS spectrometer contains the following functional circuits and sub-systems:

An integrated photomultiplier tube (PMT) detector and sample chamber;
Preamplifier;
High-voltage filter and bias interlock circuit;
Shaping amplifiers/stretchers;
Time-to-pulse-height converter;
Pulse-shape discriminator (PSD) and coincidence gate;
PSD level indication, and
Pulse pile-up rejection

2) A NIM bin power supply capable of providing ±12 and ±24V, direct current (dc);

3) A stable high voltage power supply for the phototube capable of delivering up to 1000 V positive bias;

4) A Multi-Channel analyser for spectral analysis,

5) An in-line computer for data storage, display and analysis, and

6) A Gamma Spectroscopy unit with software and computer.

3.2.2 Apparatus and Reagents Required

A. Apparatus

(a) Glassware- 250ml Beakers, Pasteur pipettes, Centrifuge Vials (MSE Heat Resistant), Glass rods, Culture Tubes (VWR Borosilicate glass, 10x75mm) and Side Arm Conical flask;

(b) Volumetric pipettes (200-1000µl and 1-5ml);

(c) Polypropylene Vials (Kartell 5ml and Simport 20ml Snaptwist);

(d) pH meter, 0.1 pH resolution;

(e) Hot plate, Bunsen Burner and Tongs;

(f) Centrifuge capable of 3000 r.p.m. and,

(g) Thermometer, Bung, tubing, wash bottles and weighing scales

B. Chemicals, Reagents and Standards. All reagents are Analar grade unless otherwise stated.

(a) *Double Distilled Water (DDW).* Radon Free;

(b) *Sodium Hydroxide Solution (0.3M):* Dissolve 12g of sodium hydroxide in DDW and dilute to 1L;

(c) *Barium Nitrate Solution (20mg/ml barium):* Dissolve 38.1g $Ba(NO_3)_2$ per litre of DDW;

(d) *Barium-133 tracer*: Less than 400Bq (245.8Bq/ml Nycomed Amersham Solution;

(e) *Sulphuric Acid (18M)*: Concentrated analytical grade;

(f) *Sulphuric Acid (1M)*: Add 55.5ml of concentrated sulphuric acid to 900ml of DDW and dilute to 1 L;

(g) *Potassium Carbonate Solution (Saturated)*: Dissolve 115g of K_2CO_3 in 100ml of DDW;

(h) *Ammonium Carbonate Solution (1M)*: Dissolve 96g of $(NH_4)_2CO_3$ in water and dilute to 1 L;

(i) *Nitric Acid Solution (0.*5M): Dilute 32ml of concentrated nitric acid to 1 L;

(j) *Sodium Nitrate (F.*W. 84.99): Powder/granular form;

(k) *Radium extractive scintillator, RADAEX® and,*

(l) *High Purity Argon Gas.*

C. Chemicals and Reagents for the later procedural adaptations

(a) *Barium Chloride carrier (10mg/ml)*: Prepare solution by dissolving 4.44g $BaCl_2$ in 250ml of DDW;

(b) *Sodium Nitrate (4M) and Sodium Hydroxide (2.*5M) *mixture*: Dissolve 34g of $NaNO_3$ and 0.8g of NaOH in 100mls of DDW;

(c) *Sodium Hydroxide (2.*5M): Dissolve 10g of NaOH in 100mls of DDW and,

(d) *Potassium Carbonate (50% w/w)*: Dissolve 1g of K_2CO_3 per milliliter of DDW.

3.2.3 Procedure

The following is a step by step guide to the method used and this is summarised in Figure 3-4.

1. Filter and acidify the water directly after sampling until the pH is in the range 0-1
2. Back in the laboratory measure 200ml of the sample into a 250ml beaker (a larger sample can be pre-concentrated by evaporation);
3. Add 1ml of the 245.8Bq/ml Barium yield tracer;
4. Add 0.75ml of the barium nitrate carrier solution;
5. Warm the sample to approximately 38°C;
6. Remove from the heat and leave to cool in an ice bath in order that the precipitate may cure and collect;
7. Carefully decant the largest portion of the clear supernate and quantitatively transfer all the precipitate into labelled centrifuge vials using 1M sulphuric acid;
8. Centrifuge at 3000r.p.m. for 4 minutes;
9. Decant the supernate and wash the precipitate twice to remove excess H_2SO_4 with 10ml of DDW, centrifuging each time for 4mins. The pH should be approximately 6.
10. Add 10ml of the potassium carbonate solution and heat the centrifuge tube over a Bunsen burner on low heat, mixing the solution constantly with a glass rod until a thick slurry is formed in approximately 7-10 minutes and leave briefly to cool;
11. Add just enough water (<8ml) to dissolve the K_2CO_3 slurry. Do not add excess water because the differential solubility of barium and radium carbonate can cause errors in evaluating the chemical losses in the metathesis step. Centrifuge and discard the supernate.
12. Wash the solids and centrifuge twice with 2-3ml of 1M $(NH_4)_2CO_3$ and then wash once with 3-5ml of DDW. The inside of the centrifuge tube should be washed each time with the clear supernate using a pasteur pipette and then discarded.
13. Add 1ml of 0.5M HNO_3 and warm gently. At this point all the solids should dissolve. If they do not then there is still some calcium sulphate present and the metathesis steps from 10 onwards should be repeated until all the solids dissolve easily.

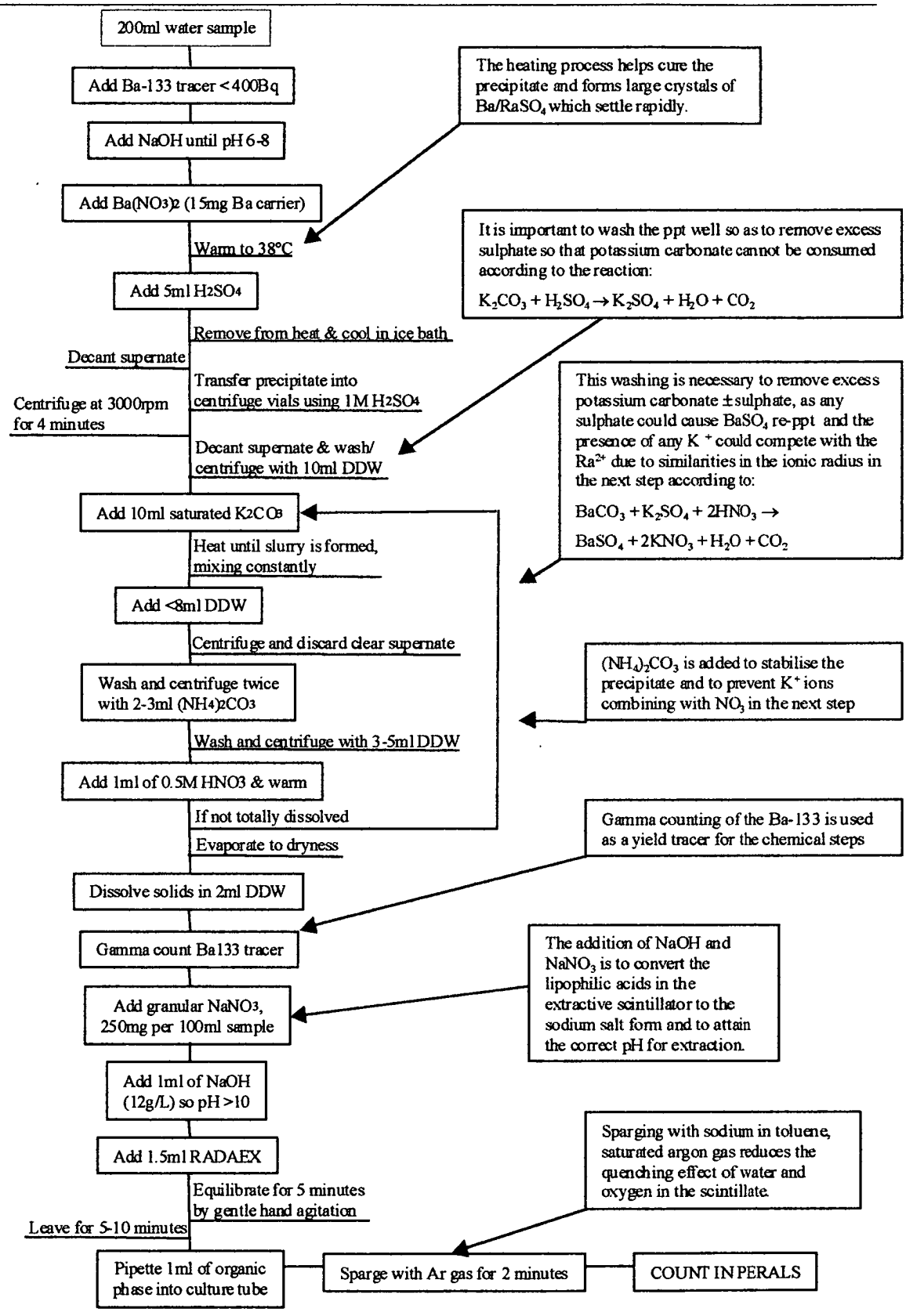

Figure 3-4 Flowchart of PERALS pre-concentration and extraction phase of the methodology

14. Carefully evaporate the sample to dryness over a low flame and then dissolve the remaining solids $Ba/Ra(NO_3)_2$ in 2ml of DDW. All the solids should dissolve.

15. Using a minimum of DDW transfer the solution to a 20ml polypropylene vial. The sample volume at this stage is usually 10ml.

16. The sample is then counted for 5 minutes on an EG&G Ortec HPGe gamma ray detector followed by an identical, with respect to sample volume and geometry, Ba-133 standard solution. The two results can then be used to determine the barium (radium) recovery via Equation 3-2:

Equation 3-2

$$\mathbf{R} = \frac{\gamma_{303(Sa)} + \gamma_{356(Sa)} + \gamma_{384(Sa)}}{\gamma_{303(Std)} + \gamma_{356(Std)} + \gamma_{384(Std)}} \times \frac{100}{1}$$

Where R is the radium recovery, $\gamma_{303(Sa)/356(Sa)/384(Sa)}$ are the actual sample counts from the photopeaks 303, 356 and 384 KeV and $\gamma_{303(Std)/356(Std)/384(Std)}$ are the same counts but for the standard solution.

17 Add granular $NaNO_3$ at the rate of 250mg of sodium nitrate for every 10ml of sample volume (typically 10ml).

18 Add 1ml of the NaOH solution and check that the pH is greater the 10. Add additional NaOH as needed to reach the required pH.

19 Using a volumetric pipette add 1.5ml of the radium extractive scintillator and equilibrate by gentle hand agitation for 5 minutes.

20 Allow the sample to sit undisturbed for 5 to 10 minutes so as to let the phases separate. If a clean phase separation is not evident then the vial should be centrifuged for two minutes.

21 Using a long form Pasteur pipette remove the bottom aqueous layer and discard as aqueous radioactive waste.

22 Transfer the organic sample ± aqueous remains into a tall, slim 5ml polypropylene vial so as to make the final extraction more precise

23 Carefully, using a volumetric pipette, transfer 1ml of the organic phase to the Borosilicate culture tubes.

24 Sparge the sample for two minutes with dry, oxygen-free, toluene saturated argon gas. Seal the culture tube tightly immediately following the withdrawal of the sparging lance.

25 The sample is now ready for counting in the PERALS spectrometer.

3.2.4 Counting Procedure using the PERALS spectrometer

1 After initial calibrations with the ORDELA ^{226}Ra counting standard to determine the counting efficiency the sample would be placed in the counting well with sufficient silicon oil to cover the recessed ring.

2 With the coaxial cable from the MCA attached to the pulse shape connector the acquisition should be commenced. This first step needs to be repeated for every sample as it is of critical importance to set the pulse shape discriminator correctly as each change of scintillation cocktail will have a slightly different light output. Two peaks should appear on the screen representing a beta/gamma peak and an alpha peak as shown in Figure 3-5.

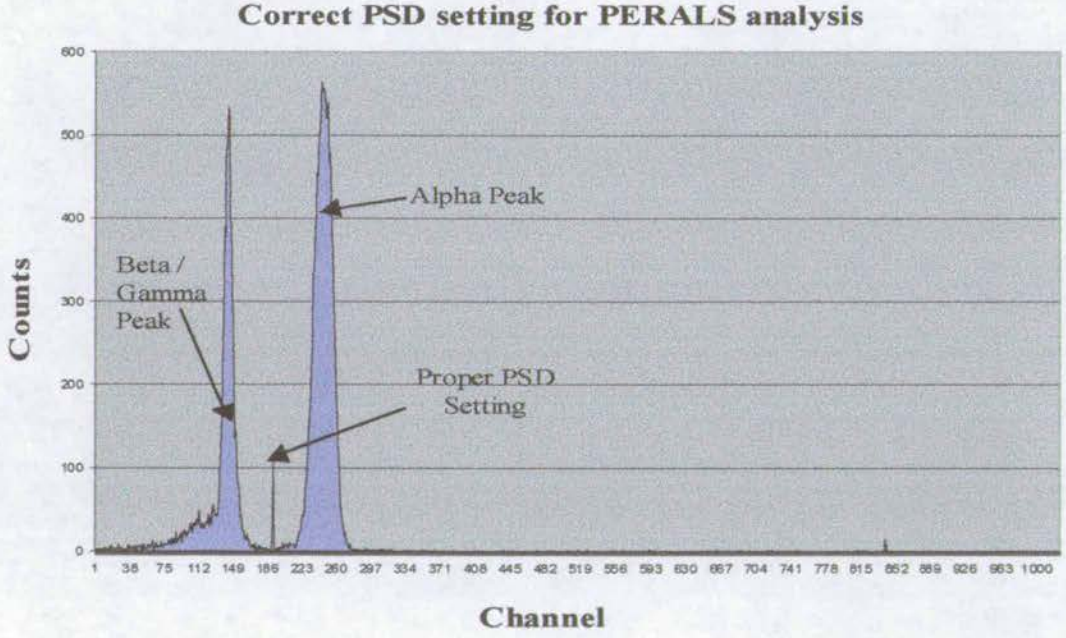

Figure 3-5 Multichannel analyser (MCA) spectrum obtained from the Pulse Shape Output on the PERALS spectrometer showing the correct PSD setting.

3 While acquiring the pulse shape spectrum the DSP switch should be depressed momentarily giving rise to a rising set of dots which should appear in the valley between the two peaks. The correct setting is illustrated Figure 3-5 with the PSD setting just to the right of the beta/gamma peak, if adjustments are required then the PSD front panel setting should be adjusted so as to position the PSD correctly.

4 Once the PSD has been set correctly then the coaxial cable should be moved to the Pulse Height port whereby a spectrum such as that shown in Figure 3-6 will be obtained for the radium standard along with its ingrown daughters as illustrated.

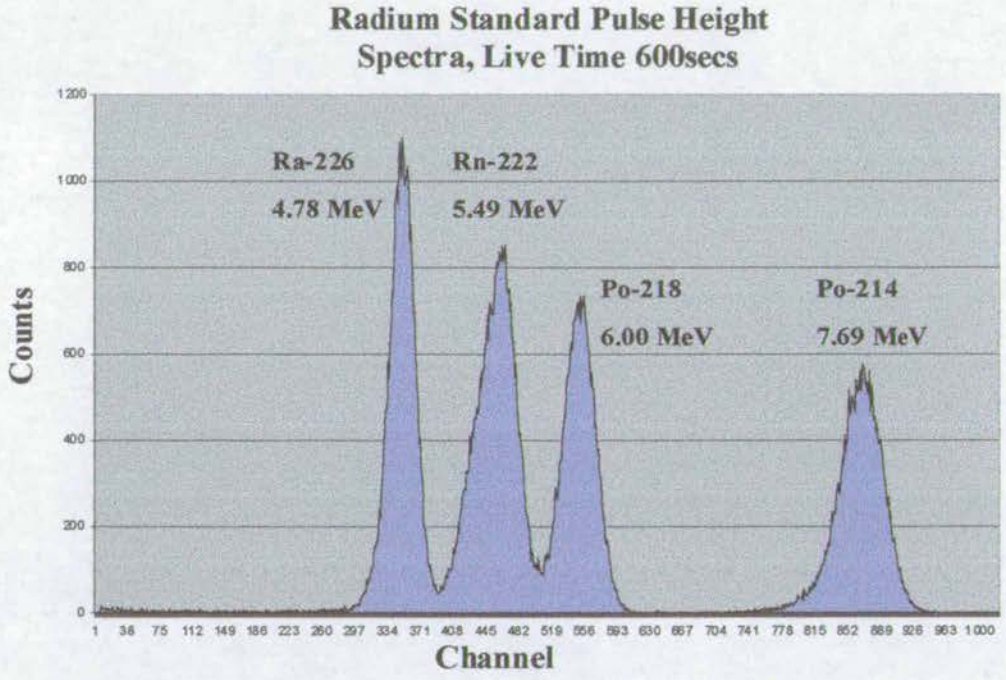

Figure 3-6 PERALS pulse height spectrum using the Ra-226 counting reference standard.

5 Finally the ^{226}Ra activity can be calculated from the net count rate (dpm) in the ^{226}Ra peak and multiplying by 1.5 to compensate for only using 1ml of the 1.5ml of scintillator added and then dividing by the sample volume as shown in Equation 3-3:

Equation 3-3

$$^{226}\text{Ra (dpm / L)} = \frac{\left(\frac{\text{Counts in } ^{226}\text{Ra peak}}{\text{Time in Minutes}}\right) \times 1.5}{\text{Volume in Litres}}$$

3.3 PERALS SYSTEM RESULTS

Eighteen months were spent developing and trying to perfect this method of radium analysis with little reward. Essentially, no consistent reproducible results were found even when using the most basic method of a spiked ^{226}Ra solution in distilled water. Therefore with approximately £8000 of costs incurred (not including the actual cost of the PERALS system) and a visit to the actual laboratory (where the machine and methods were developed) where samples were run and the results of which corroborated my own findings, a decision was made to cease any further developmental work.

The following section thus gives a brief summary of the 16Mb of data generated in the form of ways, means and outcomes of my efforts to try and develop the methodology for a quick, efficient and reliable method of analysing for the elusive radium. Due to the amount of permutations and combinations of the variables tried the following section outlines what these variables were and only goes into detail on some of the key experiments carried out.

3.3.1 Basic Operational Parameters

During the 18-month period a series of blanks and calibration checks with the Ordela Ra-226 Standard were performed to establish the standard conditions and thresholds of the machine.

Background measurements using a borosilicate culture tube containing 1.5ml of *ETRAC* RADAEX were run regularly throughout this period with a mean of only 2 counts per 24hr period in the ^{226}Ra region (Channel No. 316-421). The precision of these blank runs was of the order ±0.162 % (1σ, n = 8). Using Equation 3-4 a theoretical Lower Limit of Detection (LLD) as defined by CURRIE, 1968 can be calculated for the PERALS system.

Equation 3-4

$$LLD = \frac{4.66\sqrt{\text{Background Counts}}}{\text{Counting Time}}$$

Where 4.66 is a statistical factor accounting for the one-tailed distribution required for consideration at the 95% confidence level.

This calculation gives a LLD value of approximately 0.0045cpm for a one day counting period. This is an order of magnitude lower (0.025cpm for a one day count, KEY *et al.* 1979) than that of alpha scintillation cell method for radon emanation. Similarly the Ordela ^{226}Ra standard was run eight times over the experimental period so as to give a measure of the long term precision and to check that there had been no loss in efficiency of the PERALS system. A typical spectrum generated for a 600 second count along with a typical blank for the same time period is shown in b)

Figure 3-7 a) and b) respectively. The long term precision using the Ordela standard over an 18-month period had a mean count of 38154 ±0.023 % (1σ, n=8) and the short term precision of 11 repeats can be seen in Table 3-1 and gives a mean count of 38053 ±0.00631 % (1σ, n=11).

a)

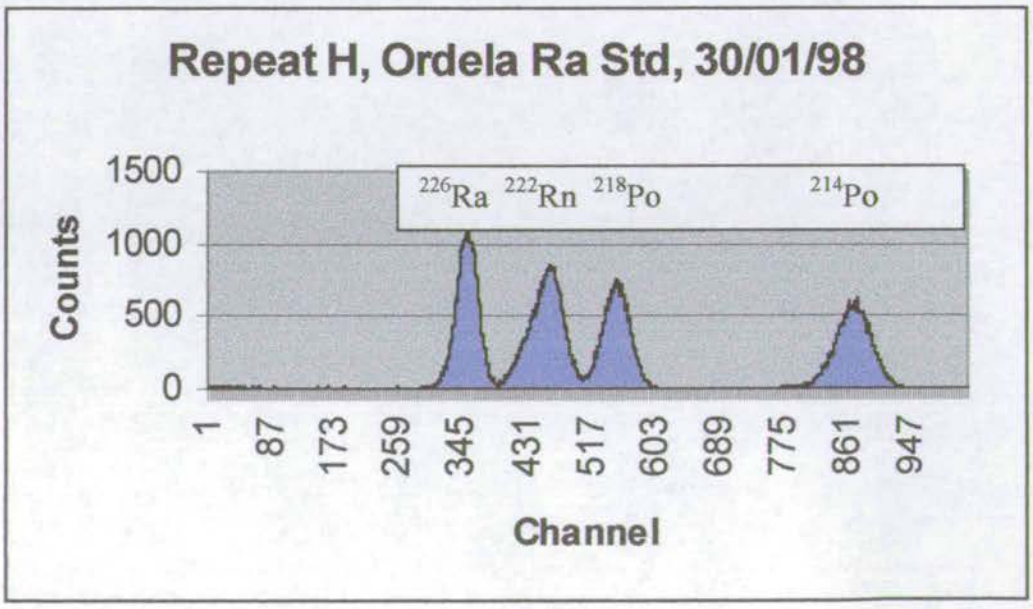

b)

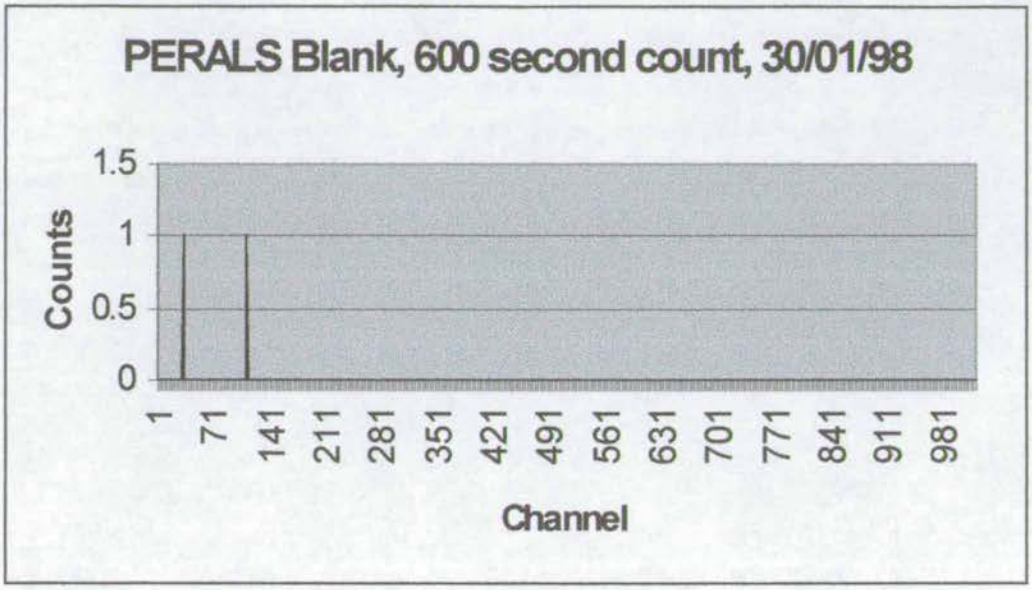

Figure 3-7 a) Typical spectra generated by a 600 second count of the Ordela ^{226}Ra standard (1.76nCi) and b) a typical blank spectra generated over the same time period (typical ^{226}Ra channels are in the region of 316-421)

Table 3-1 Short term precision of the Ordela Ra-226 standard

Standard	Live Time	Computer Integrated Counts	Spreadsheet based Count Integration
A	598.6	37676	37837
B	598.7	38119	38233
C	598.6	37834	37952
D	598.9	37997	38151
E	599.0	38509	38654
F	598.6	37775	37854
G	598.6	38014	38107
H	598.9	38133	38230
I	598.5	38107	38228
J	599.0	38048	38169
K	598.9	37721	37829
Mean LT =	598.8	Mean = 37993.91	Mean = 38113.09

The efficiency of the PERALS system can then be worked out by first decay-correcting the standard using Equation 3-5.

Equation 3-5

$$A_t = A_0 e^{-\lambda t}$$

Where A_t is the Activity at time t (current), A_0 is the original activity at time zero, λ is the decay constant ($\ln 2/t_{½}$) and t is the time elapsed.

Therefore converting the standard activity of 1.76nCi into disintegrations per second (dps) giving a value of 65.12 dps and with a time elapsed of 4.33217×10^{-4} yr a decay-corrected activity of 65.07 is calculated.

As the background was essentially zero over a 600-second counting period the efficiency can be calculated from Equation 3-6

Equation 3-6

$$\% \text{ Efficiency} = \frac{\text{Counts per second (Std Samples)}}{\text{Disintegration per second (Calculated)}} = \left(\frac{\left(\frac{\text{Total Std sample counts}}{\text{Live Time}} \right)}{\text{Dps (Calculated)}} \right)$$

This therefore gives a calculated practical average PERALS spectrometer efficiency of 97.6%.

From the data and statistics presented here using the counting reference and blank counts a close agreement can be found with that of the manufactures claims as stipulated in 3.1 in that the PERALS system offers a low background method of radium analysis which is precise in both the long and short term.

A further procedural check, this time relating to the actual analytical method used, is the use of ^{133}Barium as an internal standard, which, because of its close chemical similarities to radium (LI *et al.* 1973; BROECKER and PENG, 1982; RHEIN *et al.* 1987 and MOORE and DYMOND, 1991) can be used as a tracer throughout the

initial methodological steps (see Figure 3-4) to determine the chemical recovery of the method.

Typical ^{133}Ba gamma count values and recoveries as defined in Equation 3-2 are given in Table 3-2 in which chemical recoveries were generally high and in the 90-95% range.

Table 3-2 Ba-133 chemical recoveries as determined by gamma counting for 600 seconds.

Sample	Peak Area 303 keV	Peak Area 356 keV	Peak Area 384 keV	Total Counts	% Recovery
Std	309 ± 20	1120 ± 34	162 ± 14	1591	
A	301 ± 20	1086 ± 34	155 ± 14	1542	97
Std	324 ± 20	1107 ± 35	170 ± 14	1601	
B	302 ± 19	1022 ± 34	168 ± 15	1492	93
Std	331 ± 20	1075 ± 35	188 ± 15	1594	
C	287 ± 19	1049 ± 34	186 ± 15	1522	95
Std	343 ± 21	1123 ± 36	179 ± 16	1645	
D	312 ± 19	1043 ± 34	172 ± 15	1527	93
Std	317 ± 20	1107 ± 34	167 ± 14	1591	
E	292 ± 19	1001 ± 32	159 ± 13	1452	91

Therefore from these basic tests it was apparent that the PERALS system was highly efficient with a low background and that the internal tracer yielded high recovery rates.

From the above results it was then possible to work out what the minimum expected count rate would be for 0.2ml of a 22.7Bq/ml ^{226}Ra spike added to the sample using a chemical tracer recovery of 90%, a machine efficiency of 97%, a 66% scintillant recovery through the use of only 1ml out of the 1.5ml of organic scintillant added and a notional 5000 second count time. This leads to a minimum value, even using

ultra pure water as the sample, of an expected 13,361 counts over a 5000 second counting period.

From this simple calculation it became immediately apparent that when compared to the results obtained from running a number of analysis's that there was a fundamental flaw in the analytical process.

Every permutation and combination of the following basic variables were run during the 18-month period, repeated on numerous occasions and on each occasion using paired sample runs and all yielding inconsistent and wide-ranging results. Hence it was impractical to even try and attempt to analyse dissolved phase radium when the published levels of 1.8mBq dm^{-3} ^{226}Ra in the Southern Baltic Sea (KOWALEWSKA, 1986) were some four times lower than the spike added.

The basic parameters that were interchanged were:

Sample Solution

Double Distilled Water
Loch Etive Deep Water
Sampled Baltic Sea Water

Initial Sample Volume

Two Litre
One litre and one litre reduced by evaporation to 500ml
500ml
200ml

Standards

Non-spiked solution
Spiked solution with ^{226}Ra (22.7Bq/ml), 1ml, 0.5ml and 0.2ml
With and without ^{133}Ba tracer

Duration of time for (Ra/Ba)SO_4 precipitation and amount of H_2SO_4 added.

3-5 hours

24 hours

48 hours

Amount of H_2SO_4 added: 2ml, 5ml, 10ml to a 200ml sample or equivalent ratio

Nature of post gamma counting Nitrate / Hydroxide addition

Granular addition of $NaNO_3$, @250mg upto 500mg per 100ml of sample followed by the addition of hydroxide until pH > 10.

Addition of a 4M $NaNO_3$/NaOH solution

Pre-equilibration of the RADAEX in the 4M $NaNO_3$/NaOH solution.

Level of Agitation after addition of RADAEX and standing time

None

Gentle Agitation

Vigorous Shaking

Standing time: from the recommended 5 minutes upto 2 hours.

Duration of Sparging

2 minutes to 30 minutes in duration

One of the best indicators of the quality of results achieved is shown graphically in Figure 3-8 and summarised in Table 3-4 where % recoveries from the minimum estimated counts are also given. Eight samples, as duplicates, were run as part of the same experiment and the control conditions and chemical recoveries achieved are given in Table 3-3.

Table 3-3 Experimental conditions for a set of methodological trials

Sample	Experimental Details	Chem. Recovery
A	200ml, 0.2ml spike, Baltic Sea Water, Method as procedure, pH taken to 11, Sparge for 300secs	93%
B	200ml, 0.2ml spike, Baltic Sea Water, Method as procedure, pH taken to 11, Sparge for 300secs	90%
C	200ml, *No spike*. Baltic Sea Water, Methods as procedure, pH taken to 11, Sparge for 300secs	92%
D	200ml, *No spike*, Baltic Sea Water, Methods as procedure, pH taken to 11, Sparge for 300secs	87%
E	200ml, 0.2ml spike, Baltic Sea Water, Method as procedure, pH 11, *Sparge for 120 seconds.*	95%
F	200ml, 0.2ml spike, Baltic Sea Water, Method as procedure, pH 11, *Sparge for 120 seconds.*	93%
G	200ml, 0.2ml spike, Baltic Sea Water, Method as procedure, pH 11, *Sparge for 600 seconds.*	92%
H	200ml, 0.2ml spike, Baltic Sea Water, Method as procedure, pH 11, *Sparge for 600 seconds.*	94%

Table 3-4 gives a summary of the experimental replicate sample variations as shown in Figure 3-8 and a calculated % efficiency from the minimum expected counts (13,361) and the counts from the two samples.

Table 3-4 Summary of experimental results

Replicate Set	Replicate Sample Variation (1σ, n=2)	% efficiency from the minimum estimated counts per sample	
1	Mean 5689 ± 22%	A = 36%	B = 49%
2	Mean 193 ± 107%	C = n/a	D = n/a
3	Mean 3936 ± 28%	E = 35%	F = 24%
4	Mean 6230 ± 9%	G = 50%	H = 43%

Replicate Set 1

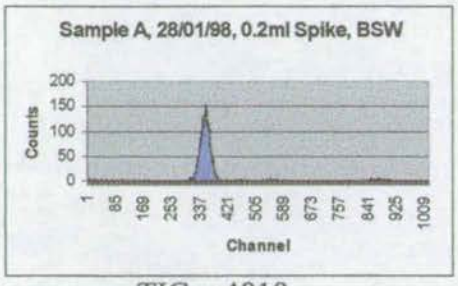

TIC = 4818

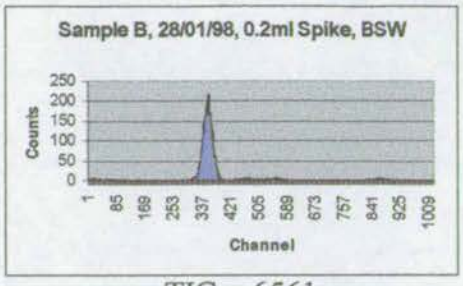

TIC = 6561

Replicate Set 2

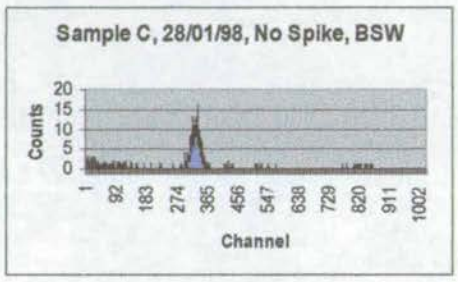

TIC = 339

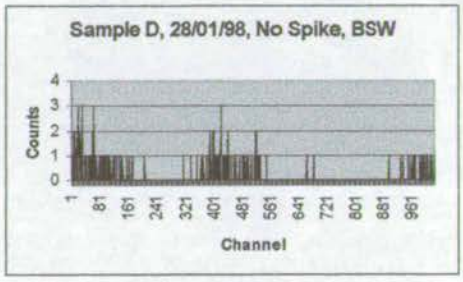

TIC = 46

Replicate Set 3

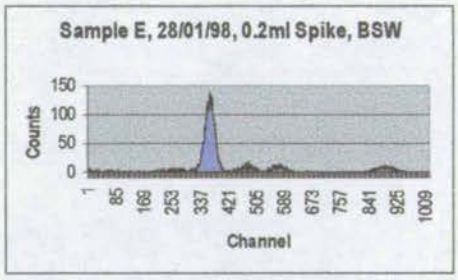

TIC = 4709

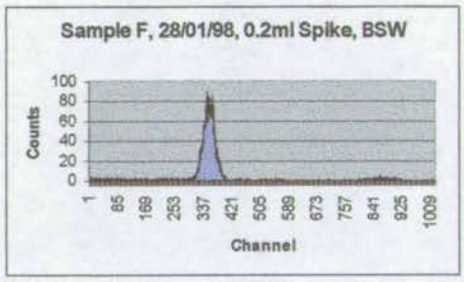

TIC = 3162

Replicate Set 4

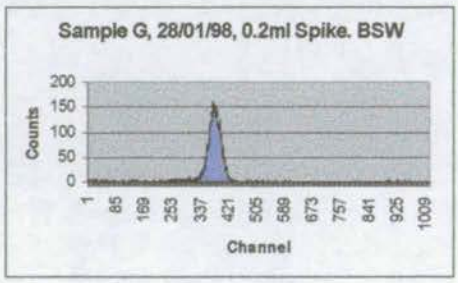

TIC = 6620

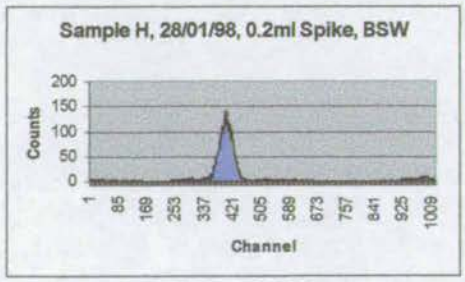

TIC = 5839

Figure 3-8 Experimental results with total integrated counts (TIC) for a live time of 5000 seconds for the ^{226}Ra peak, BSW = Baltic Sea Water. (N.B. Scale)

3.4 DISCUSSION

The results shown here were by no means unique and do not provide a firm basis for the detailed analysis of low activity samples primarily because the results obtained had such a large standard deviation and the amount of counts relative to the minimum expected were of such a low and variable percentage. This was despite having a relatively constant ^{133}Ba recovery yield throughout the experiments and the complete renewal of all the reagents including a new batch of *ETRAC* RADAEX. Replicates of some of the more promising experimental combinations also gave results that were outwith an acceptable standard deviation to such an extent that a run of 8 samples with identical experimental parameters would give a typical standard deviation of 50-60%.

3.4.1 Possible discrepancy theories

The most basic presumption of this method is that the synergy between radium and barium is complete and hence the recovery yields from ^{133}Ba are indicative of the percentage of radium present at the gamma counting stage.

There is a slight possibility that the two could become uncoupled, most likely as a form of complexion, due to the presence of humic substances or complexing ligands present in the seawater (BENEŠ, P. *et al.* 1982). Due to the relatively large cation size of radium and the decreasing tendency to form complexes with an increasing cation size it is doubtful whether any significant complexes would form even with strong organic acids. However, as similarly variable results were found when using double-distilled water as seawater this is not thought to be a probable cause of the inconsistency.

As radium salts are less soluble than the corresponding barium salts (MOORE, W. S., 1972) there is also a possibility that through the Sulphate-Carbonate-Nitrate transition that there could be a loss of radium with respect to barium. Although speculative, the probable loss of radium via this transition would be negligible and

would most likely be a constant deductive factor rather than that of the wide-ranging results attained.

From a purely methodological perspective the remaining possibilities in explaining the broad standard deviations laid with the post gamma counting methodology. An exhaustive range of experiments was carried out to try and remedy the problem of erratic results.

As *ETRAC* RADAEX is transported in its most stable form containing lipophilic acids it is necessary to convert the acid to the salt prior to the extraction phase where the pH must be maintained greater than 10 for the most effective extraction. Both PATES, J., 1998 pers. comm. and KOPP, D., 1998 pers. comm. reinforced the criticality of maintaining the pH > 10 and great care was taken in monitoring and maintaining this throughout the final steps. Tests were also run to determine the effective thresholds of pH control and the nature of addition of the hydroxide and nitrate but, again due to the nature of the results obtained, no effective conclusions could be reached.

Consideration then moved to the possible complications in the materials used in the method itself. The pioneering work of HORROCKS, D. L., 1964 into the effect of vial size and shape had already been incorporated into the PERALS design but in order to extract 1ml of the RADAEX from the 1.5ml added, the sample was transferred from the gamma counting vessel into a slim plastic vial. ELLIOT, J. C., 1984 and YANG, 1991 concluded that glass vials were superior over plastic vials for event separation but worryingly PATES, J., 1995 suggested that the decrease in event separation was possibly due to a reaction with the plastic vessel and the extractive scintillate. Tests were carried out but no conclusive results were found on the differential use of plastic and glass vials. The lack of a conclusive outcome probably related to the very short length of time that the RADAEX was in contact with the vial and as the results obtained were no less erratic than before then this factor presumably could not have been a major contributor to the irregular results found.

According to PATES, J., 1995 and HORROCKS, D. L., 1970 even small changes in the composition of the cocktail can bring about large changes in the separation efficiency and hence if the RADAEX was even slightly off then this could have significant affects on the outcome of the extraction. The possibility that there was a default with the RADAEX was considered at a relatively early stage and a new bottle was purchased but no improvement in the results were found when the whole method was run. However, a series of experiments were run whereby the radium spike was added straight to the RADAEX pre-converted into the salt form. The results from which gave relatively good and with an efficiency approaching 85% against the calculated count rate expected but more importantly showed some sign of consistency (within 10%, n=6). Therefore, this seemed to validate the post gamma counting procedure which was the main avenue of investigation having found consistency from the Ba-133 gamma counting chemical recoveries.

Having found that the two possible checks of the procedure gave relatively good results when compared to the whole procedural method, and that all the alternative experimental combinations had been exhausted, the decision was made on the basis of a lack of available options and from a financial perspective to cease the investigation into radium by the PERALS method. However, in parallel to the radium investigations using the PERALS system, experiments with 25l Baltic Sea Water samples involving extraction on amberlite columns as described in 3.3.1 and appendix A.3 had been carried out. In summary, the results from these were equally disappointing. The manganese impregnated amberlite having been ashed and sealed were counted on a gamma detector but the results of which had error statistics ranging from 18-45% and were therefore not practical for detailed radium analysis. Hence both avenues of radium analysis proved to be fruitless, at the expense of a large expenditure of both time and money.

It was at this point that the decision was taken to

the investigation into the elusive radium and instead to go and enjoy a drink having joined the exclusive.....

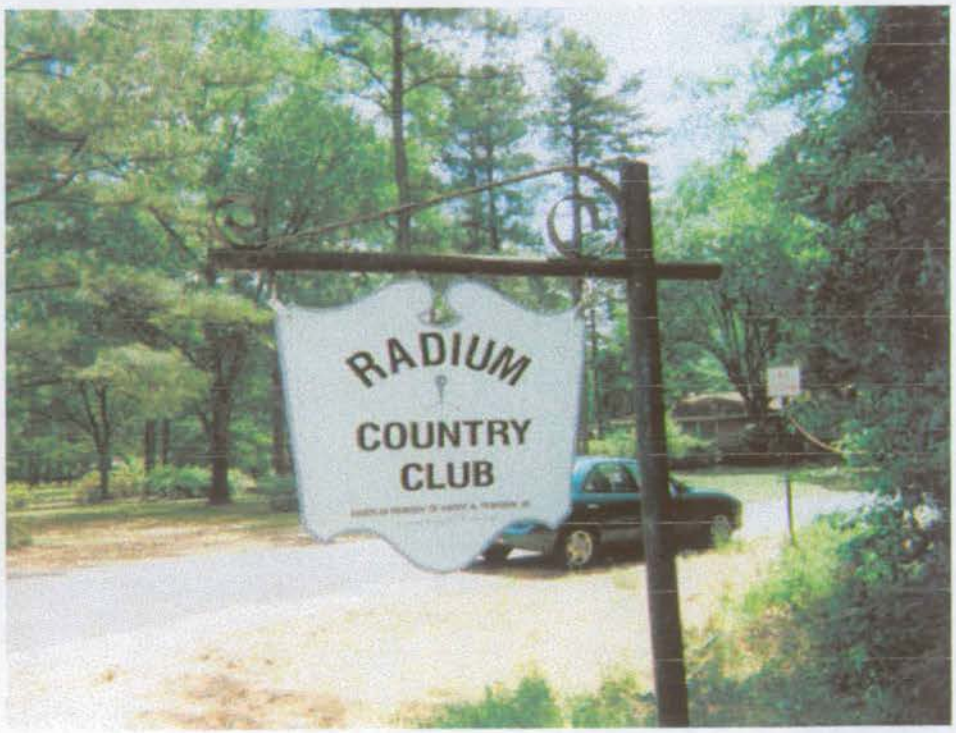

And to ponder over what possibilities the future held without radium.

It was not until sometime after the decision was taken to stop the radium methodological development that I came across a significant set of papers by BENES, P., 1990 that described what could quite possibly be the solution to the erratic results obtained throughout the period of investigation. The article followed earlier investigations (STARIK I. E. and GUREVICH, A. M., 1937, BENES, P. *et al.*, 1986) into the adsorption of radium onto membrane filters, glass and polyethylene in which preliminary findings indicated that there could be strong adsorption of radium onto glass depending upon the aqueous composition and the pH range. Figure 3-9 taken from BENES, P. 1990 shows that adsorption on glass from chloride solutions is negligible at pH < 3 but passes through a maximum at pH 6-9.5. However the conditions most conducive to adsorption follow the addition of sulphates to the solution and that strong adsorption of close to 50% exists even in the acidic region of pH 2-3.

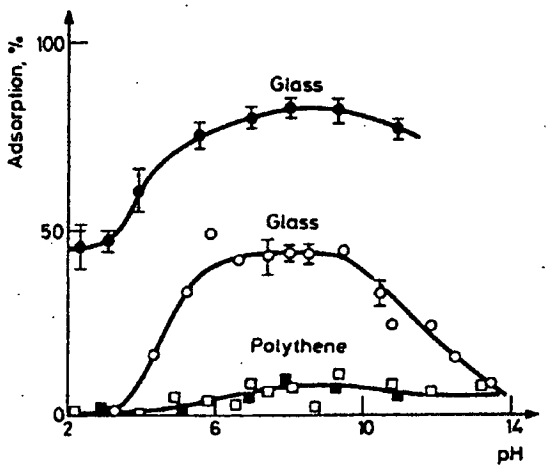

Figure 3-9 Adsorption of radium (in %) from 10ml of aqueous solution on the walls of 30mL polyethylene bottles and 20mL glass ampoules as a function of the sample composition and pH. Open points: 0.01M (HCl + NaCl); filled points: H_2SO_4 + Na_2SO_4). Taken from BENEŠ *et al.*, 1986.

From this figure it is clear that the composition of the aqueous solution has little effect on the adsorption of radium on polythene vessels. As the method relies on the precipitation of barium sulphate and the co-precipitation of radium sulphate then

there is a possibility that even under strongly acidic conditions that a substantial amount of radium could be adsorbed to the glassware used in the methodology. Micro-scale changes in the 'environmental' conditions could then lead to wide ranging degrees of adsorption leading to the inconsistencies found. Although this is highly speculative it does at least offer a potential explanation to the disappointing results obtained.

In light of this new evidence of radium adsorbing onto a glass substrate it would be possible to modify the methodology so as to use Teflon beakers in the initial stages rather than glassware. This, again is speculative as no research effort or literature has been found to support this but a possible future work plan could involve the use of Teflon ware rather than glass. However, Pyrex, glass centrifuge tubes or a transparent alternative would still have to be used in the addition of K_2CO_3 and borosilicate culture tubes still have to be used in the final analytical step so as to reduce quenching, as any substance that inhibits the fluors transition to the photomultiplier will lead to a reduced count rate.

3.5 CONCLUSION

Therefore, in summary, the reason why the development of the radium methodology, primarily by way of PERALS, was suspended was due to the inconsistent nature of the results obtained despite continually consistent chemical recovery yields. There was no substantial or reliable basis for the precise and detailed analysis of radium in the Southern Baltic Sea where concentrations were not expected to vary on an order of magnitude scale. Thus after two years of hard work, major financial investment and a validation trip to the manufacturers facility in Tennessee, USA which reinforced the instability and inconsistencies of my results, the methodological work ceased.

The failure of this method caused a major re-assessment of the direction of the research programme. A decision was made to investigate the temporal and spatial

distribution of trace metals in the Southern Baltic Sea as water samples had been collected and stored ready for radium analysis. However, due to the nature in which the original samples were collected not all the methodological prerequisites for a complete trace metal analysis were met as the original methodology did not demand such preparation. Most importantly there was no scope for sequential extraction or speciation experiments. Similarly, detailed grain size work was not carried out which is important in determining the mechanisms of metal concentration, transport and deposition. Hence, total metal concentrations were determined throughout the water column for dissolved and particulate phase material, sediment trap, fluff layer and sediment core samples. This new collection of data therefore forms the basis of the rest of the research programme and is discussed in detail in the following chapters.

4.0 Sediment Composition and Distribution

To aid the interpretation of geochemical variations both spatially and temporally (down core variations) it is important to conduct investigations into geotechnical and lithogenic compositions in order to provide the fundamental parameters for the assessment of potential flux rates and inventory calculations (SEUSS and ERLENKEUSER, 1975, BOSTRÖM *et al.*, 1983 SZEFER, P., 1990, HUNG, J., 1995 and YOUNG, S. A., 1996). The basic parameters assessed are given in 4.1 allowing a primary line of investigation into major and trace metal geochemistry, stable lead isotopes and radioisotope signatures in terms of fluxes and inventories.

4.1 FUNDAMENTAL PARAMETERS

The fundamental parameters investigated were geotechnical properties such as wet weight, porosity and dry bulk density. Variations in grain size were measured using the laser-diffaction Coulter Counter™ and mineralogy was briefly investigated using X-ray diffraction all of which are described in chapter 3. In addition carbon and nitrogen measurements were made and are presented here.

4.1.1 Sediment Core Descriptions

The following is a description of the sediment cores retrieved on the October 1996 BASYS cruise; an in depth description of the sediments and mineralogy of the Southern Baltic Sea can be found in BRUGMANN *et al.* 1992, BELMANS *et al.* 1993, SHIMMIELD G. B., 1995, DAVIS *et al.* 1996 and GINGELE and LEIPE, 1997.

4.1.1.1 Core 204324; ODAS Tonne

A short core only 14cm in length was retrieved by divers as the nature of the sandy sediment prohibited greater penetration and retention within the core tube. On inspection the majority of the core represented a well sorted, medium-fine sandy mudstone with a bioturbated surface layer. Two reasonably distinct regions could be

seen the first comprised a top region of 10 cm of sandy/beige colouring which darkened with depth and few shells were present. This laid on top of a similarly coloured 4 cm of bio-supported, fine sandy mudstone with a thin dark black organic stained undulose boundary between the two. The bottom 4 cm had a much greater abundance of shells lying in a death assemblage formation.

4.1.1.2 Core 204322; Nord-Perd Rinne

A 36cm long core was collected from Nord-Perd Rinne again by divers. The sedimentary composition was fairly uniform throughout the core and consisted of a sorted fine sandy / coarse mudstone grain size. The top 4cm of this core consisted mainly of mussel shells with a brown-beige coloured fluffy soup found interstitially between the shells. Broken, rather than whole, shells made up a highly erratic boundary beneath which the core took on a much darker and greyer colour for approximately 5cm and then for the remainder of the core a lighter grey was found with a transition to mid grey with depth. No significant variations in grain size were found down core although there were two prominent shell layers at 17cm and 33cm and some patchy sands.

4.1.1.3 Core 204320; Tromper Wiek

Divers collected a pristine 18cm long core from 26m depth, which appeared homogeneous down core with respect to grain size and sorting however variations in colour could be detected. Few shelly fragments could be detected throughout the core which consisted of a well sorted coarse mudstone, the top 3cm of which was a fluffy light brown colour underlain by a darker grey layer for 7cm. Beneath this for the remainder of the core was a olive-grey layer with few sedimentary structures but there were some signs of bioturbation on the upper most layer.

4.1.1.4 Core 204310, Arkona Basin

The longest core of 50cm was obtained using the 'Rumohrlot' coring device which extracted a relatively homogeneous core of a moderately well sorted silty mudstone

with a light-medium grey upper 1cm underlain by quite a dark grey / black homogeneous body of mudstone. No distinctive features could be found apart from the relatively sharp boundary between the surface layer and the majority of the core and the strong smell of sulphides which evolved as the core was extruded.

4.1.2 Geotechnical Properties

There are a number of important physical parameters such as wet weight, porosity and dry bulk density (as described in **A.2.**) that can have a significant effect on the biogeochemical cycling that occurs both within the sediment and across the sediment-water boundary (BERNER, 1980, SANTSCHI *et al.* 1990, VAN CAPPELLEN and WANG, 1996, CARMAN and RAHM, 1997 and SLOMP *et al.* 1997). These parameters are shown comparatively in Figure 4-1 to Figure 4-4 and summarised in Figure 4-5, in which there can be seen a progressional transition from the shallow, high energy station of ODAS Tonne to the deep, basinal, low energy station of Arkona in all of the parameters. The greatest water content and correspondingly the greatest porosity and the only significant salt content can be found at the Arkona Basin site which has a general trend of decreasing values with depth. Conversely, ODAS Tonne has a negligible salt content and a low porosity and water content. The two intermediate sites of Nord-Perd and Wiek show reasonably close values, as expected from their similar localised environments with the only discrepancy being the top of the Nord-Perd core in which the profiles were altered due to the presence of a *Mytilus edulis* (L.) shell band. The dry bulk density profiles show, as expected, an exact inverse relationship to the other geotechnical properties from both a spatial and core depth perspective.

The wide range in these basic parameters and associated mineralogical associations between the two end member stations manifest themselves in two sharply contrasting environments.

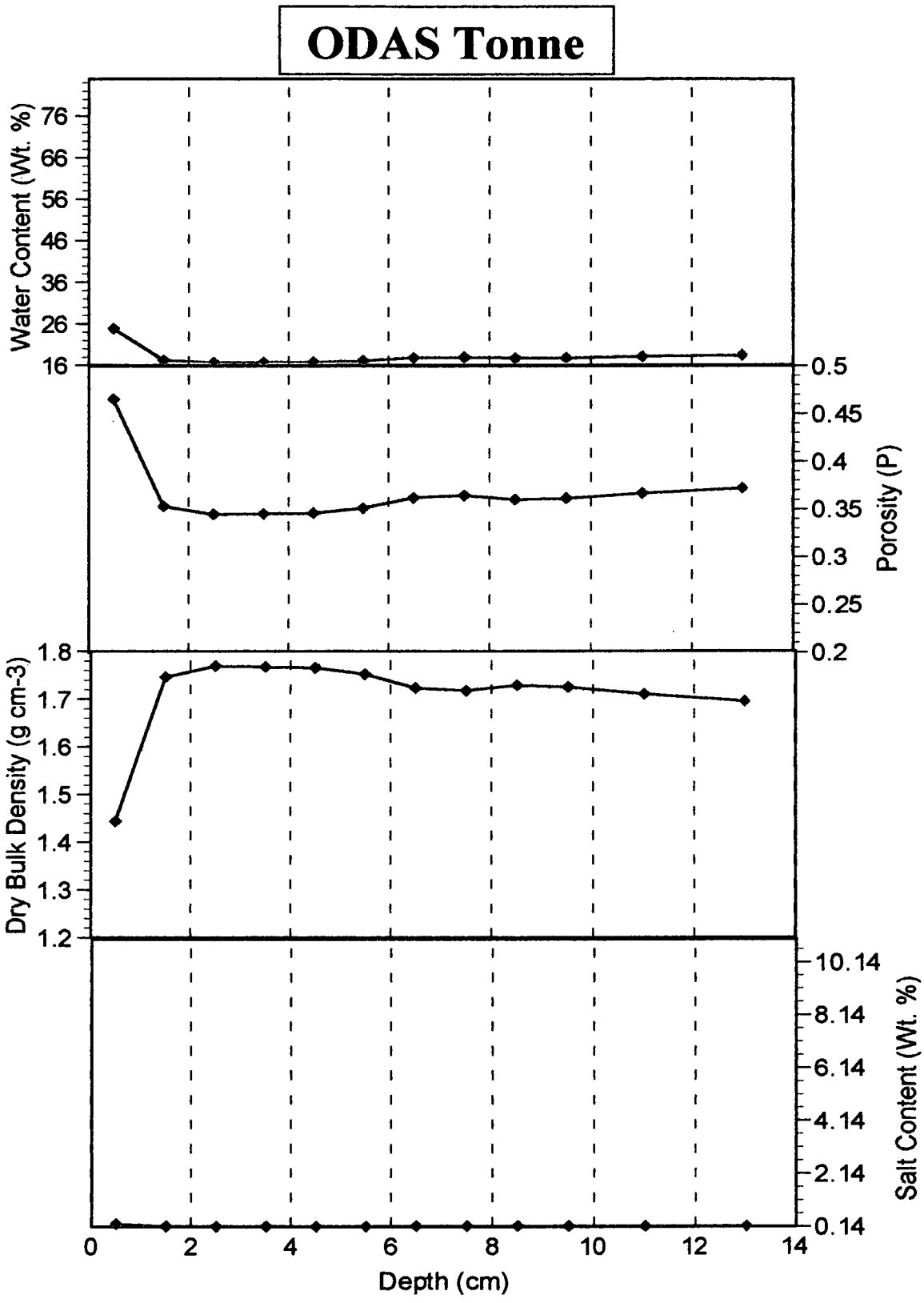

Figure 4-1 Water content, porosity, dry bulk density and salt content plotted against depth for the ODAS Tonne core

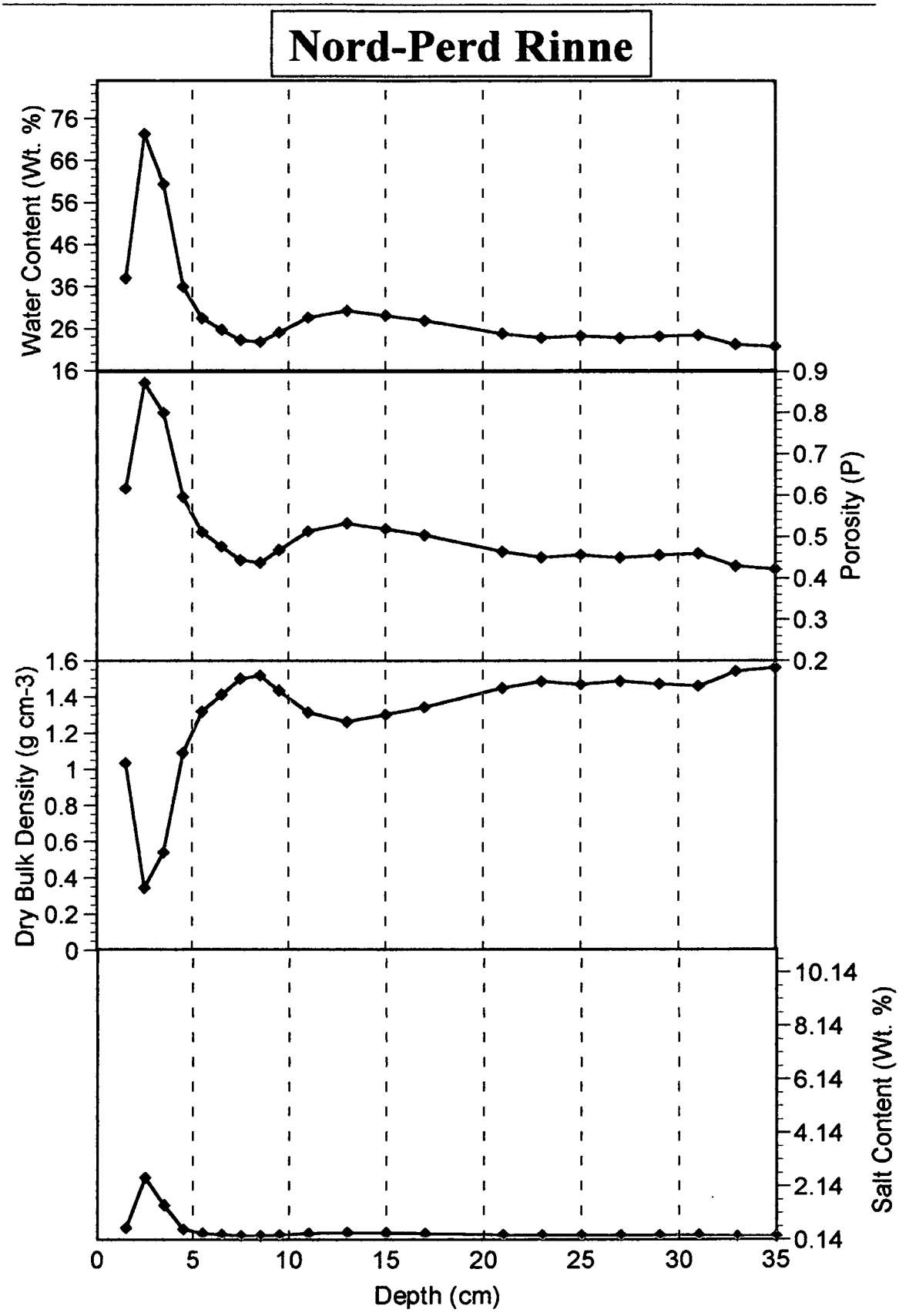

Figure 4-2 Water content, porosity, dry bulk density and salt content plotted against depth for the Nord-Perd Rinne core

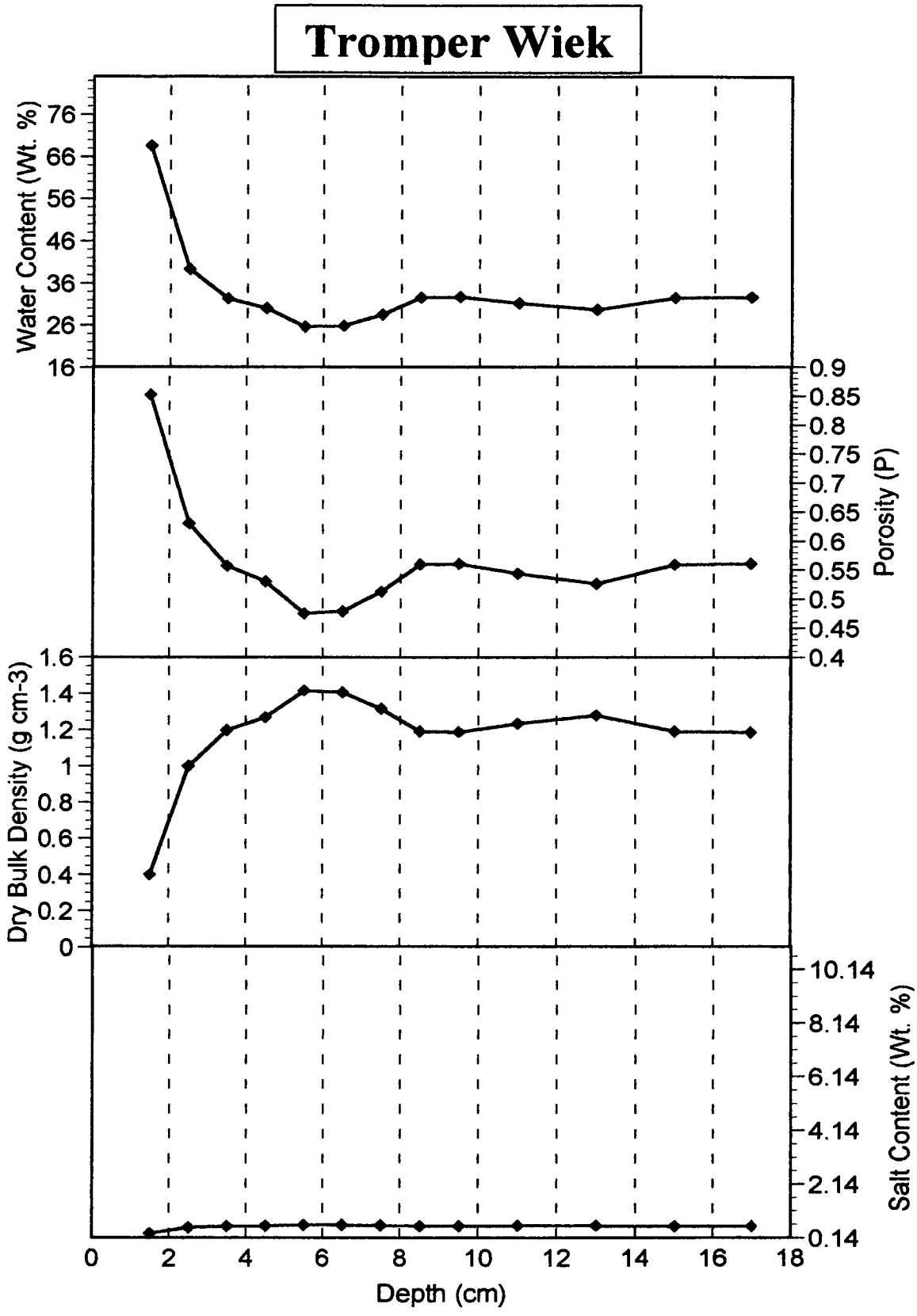

Figure 4-3 Water content, porosity, dry bulk density and salt content plotted against depth for the Tromper Wiek core

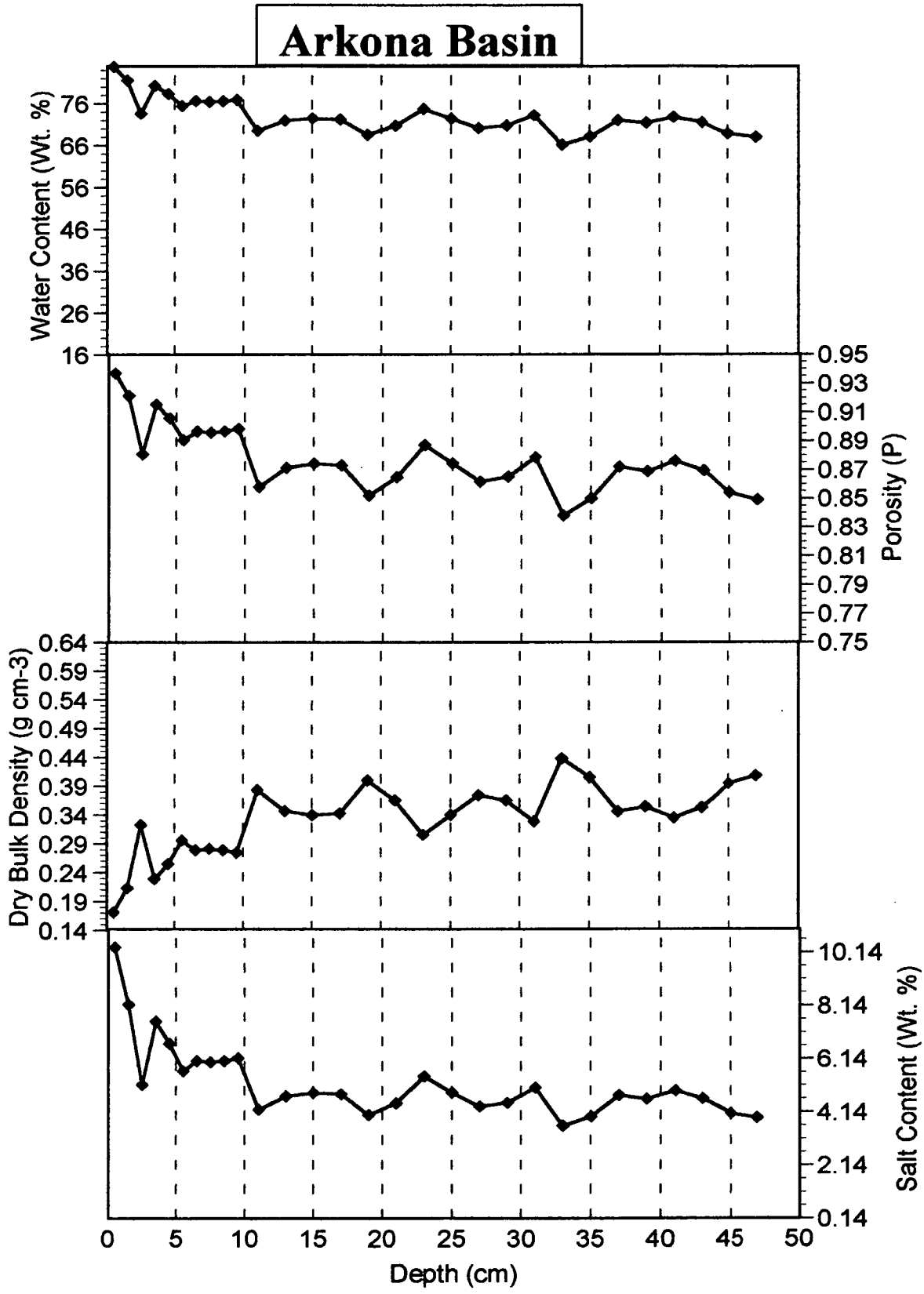

Figure 4-4 Water content, porosity, dry bulk density and salt content plotted against depth for the Arkona Basin core.

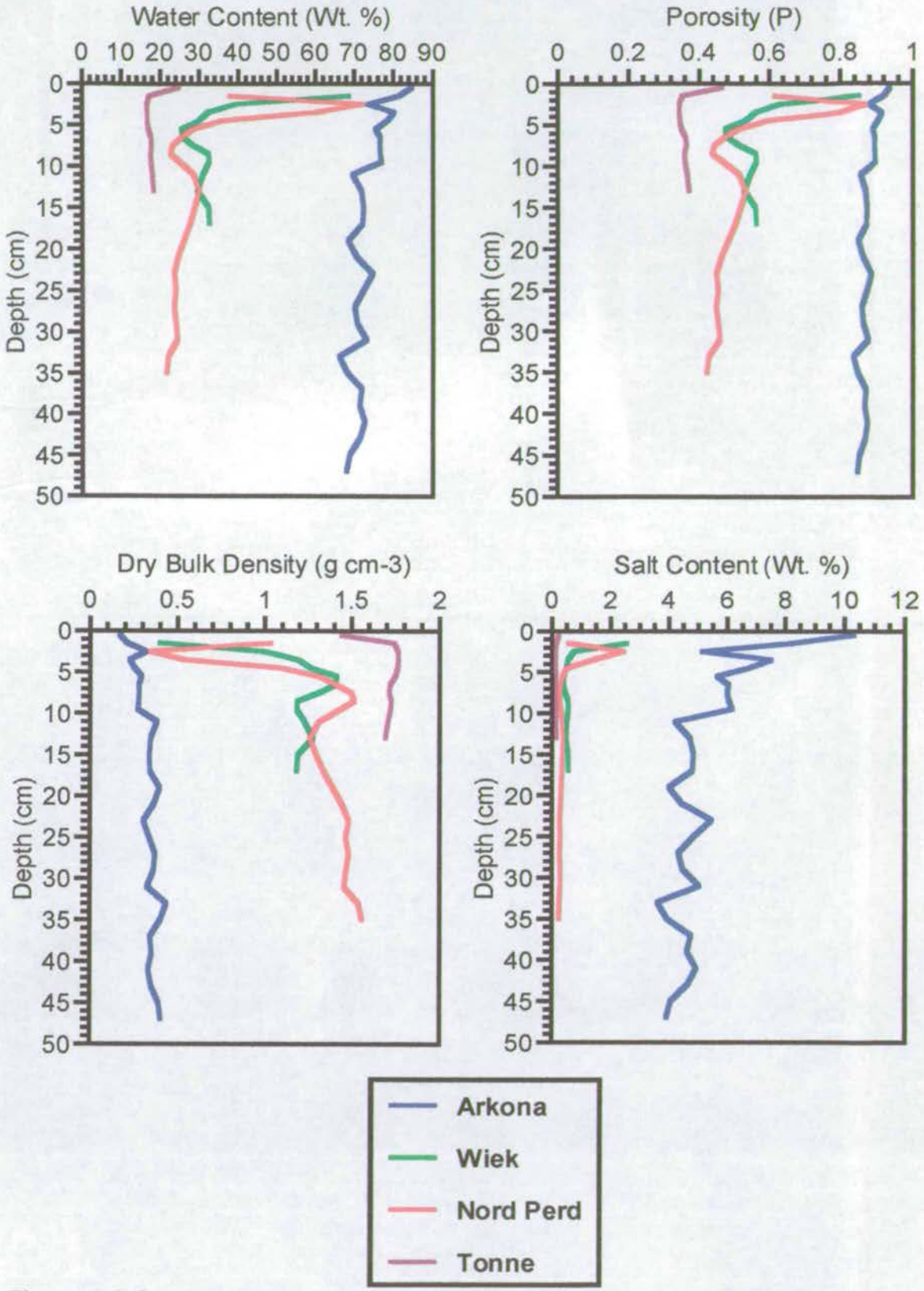

Figure 4-5 Geotechnical parameter summary for Tonne, Nord Perd, Wiek and Arkona in the Southern Baltic Sea.

4.1.3 Grain Size Distribution

An extensive study of the grain size distribution in the Southern Baltic Sea has been carried out by BOBERTZ, B., 1996 whose findings are shown in Figure 4-6. It can be clearly seen that the location of the sampling stations was deliberately chosen so as to encompass the wide sediment distributional range found and also to incorporate the main direction of sediment transport into the Arkona Basin from the Oder River outlets.

Grain size analysis was determined in order that quantitative interpretations of the sediment geochemistry could be made. These results are summarised in Figure 4-7 with individual down-core distribution shown in .

It is evident that there is a marked and definable transition from a shallow, sandy station (ODAS Tonne) through a range of fining grain sizes to the Arkona Basin where fine silt and clays are the dominant sediment type. This has significant implications for the interpretation of trace metal concentrations and creates a situation in which a normalising element has to be used to compensate for these effects which is detailed in the following section 4.1.5

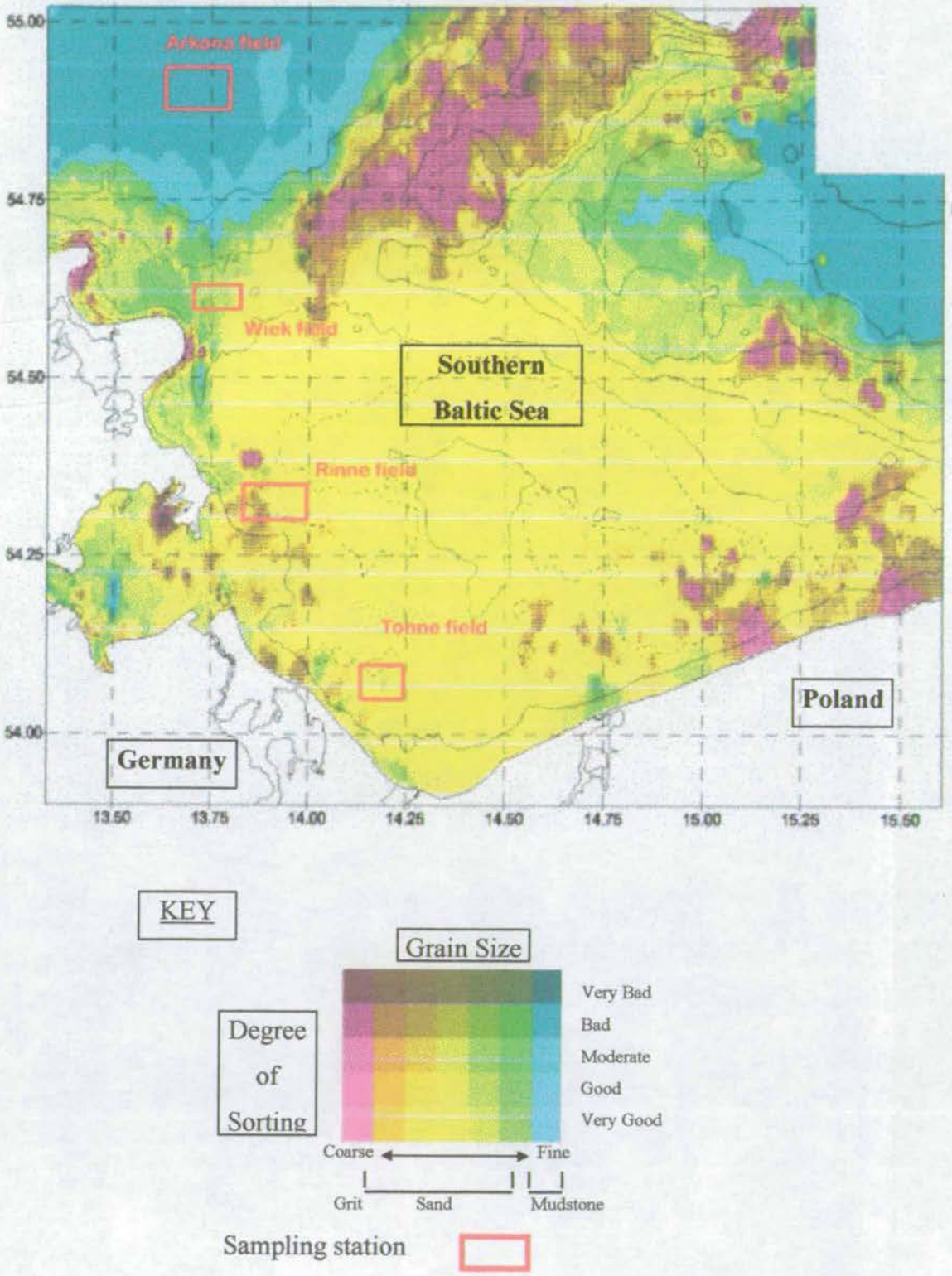

Figure 4-6 Sediment distribution and grain size in the Southern Baltic Sea. After BOBERTZ, B. 1996.

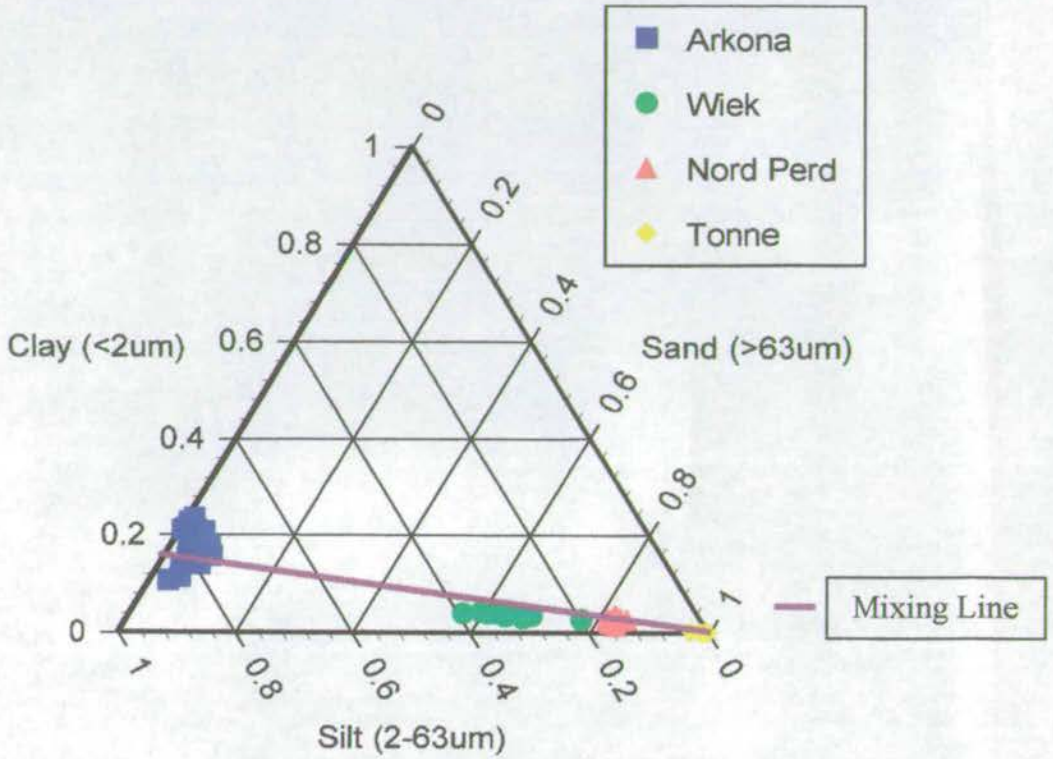

Figure 4-7 Sediment core granulometric summary for the Southern Baltic Sea.

From both a composition and spatial perspective the distribution of sediment grain size is an important controlling factor as it is the fine sedimentary fraction and the associated contaminant phase that determines the potential metal accumulation in a given area (ACKERMANN, 1980, LOHRING, 1991 and BRUGMANN, 1992. Thus, from figures 4-8 and 4-9 it is quite apparent that Arkona and Tonne stand at opposite ends of the grain size spectrum. Superimposed on Figure 4-7 is a mixing line with Tonne and Arkona as the sand and clay end members respectively with Nord Perd at only 18% and Wiek at 38% of the clay end member. Thus from a first, total metal environmental concentration, perspective it would be expected that Tonne would be the least contaminated and that Arkona would be the main repository due to the presence of fine grain clays and silts which could act as a carrier phase and repository for the contaminants.

In addition it should also be noted that in all the cores there are only minimal changes in the relative grain size distribution downcore and hence can be regarded as having a constant granulometric input through time.

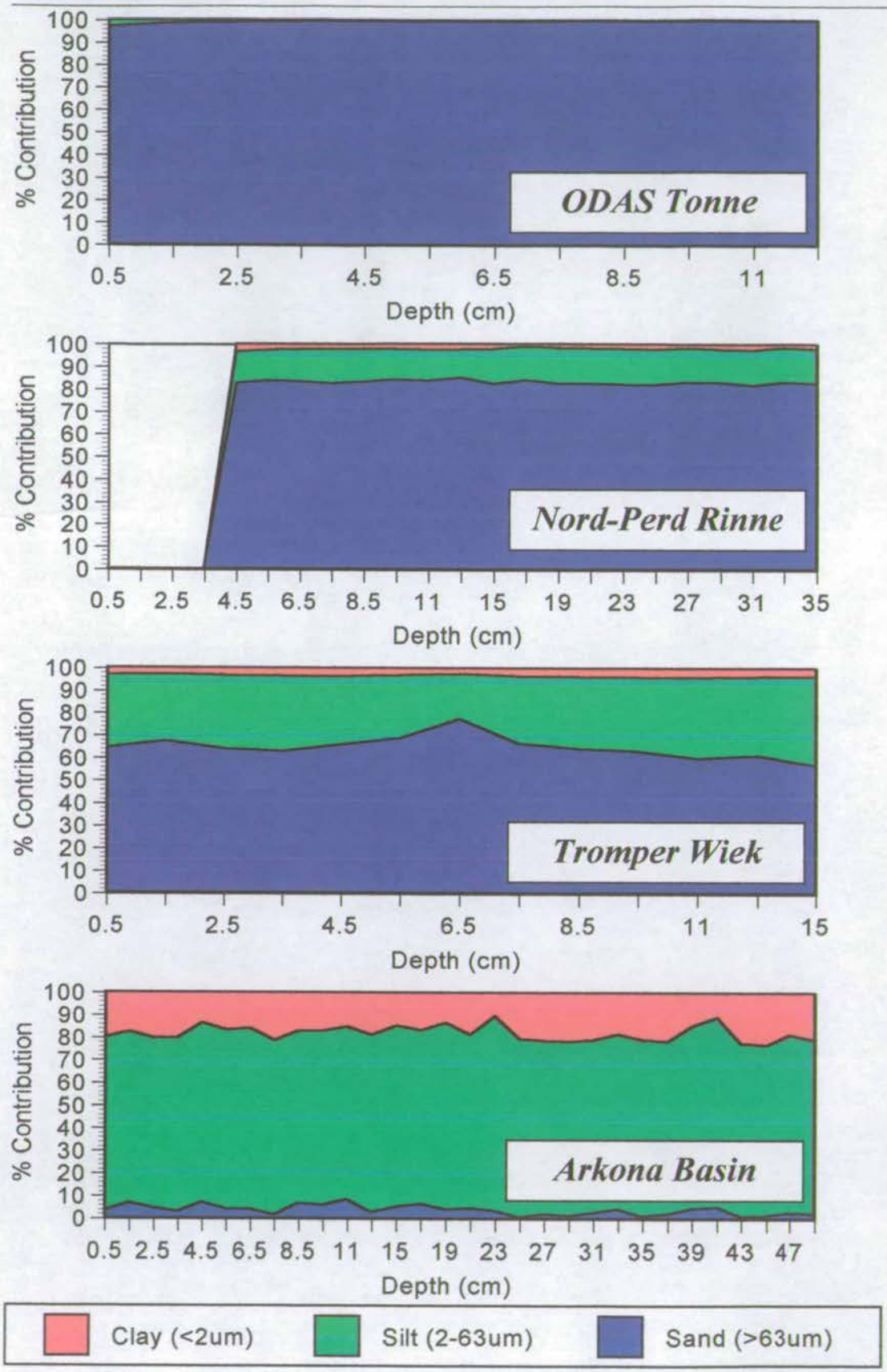

Figure 4-8 Down core grain size distribution for stations in the Baltic Sea.

4.1.4 X-ray Diffraction

X-ray diffraction (XRD) was used to investigate the mineralogy of the sediment cores in order to determine whether there were any significant variations in the nature and composition of the sediment from the shallow, high energy environment to that of the deep basinal repository. The results of which are shown in Figure 4-9.

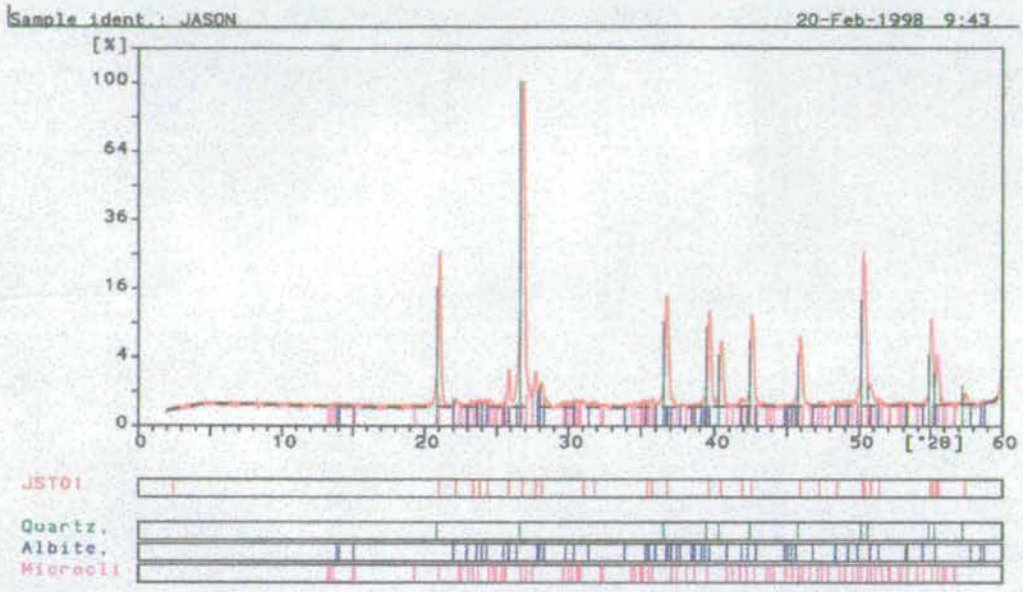

a) A typical XRD trace for ODAS Tonne (1cm depth)

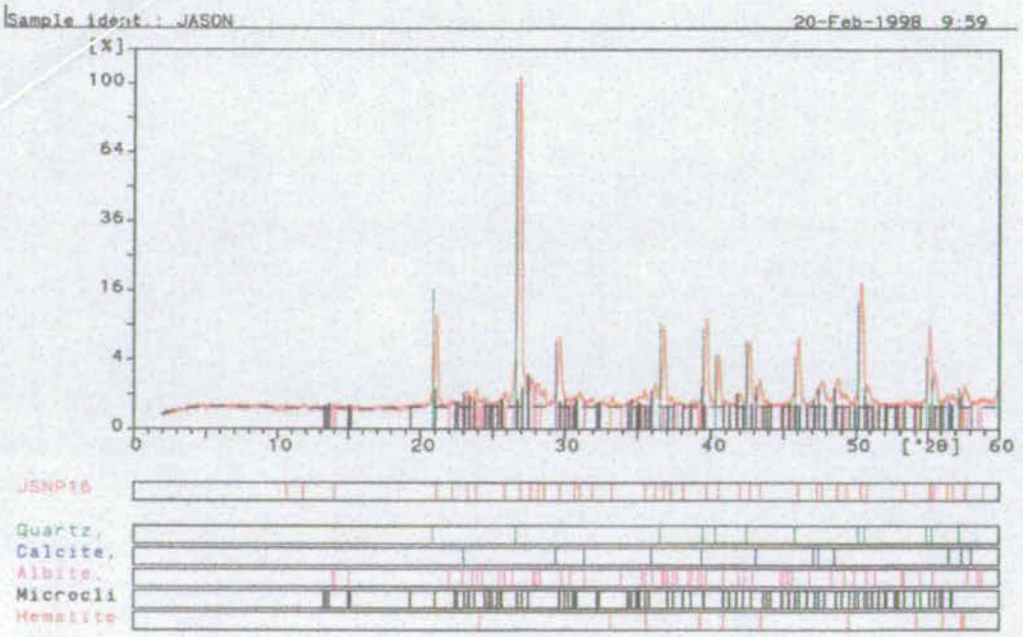

b) A typical XRD trace for Nord Perd Rinne (16cm depth)

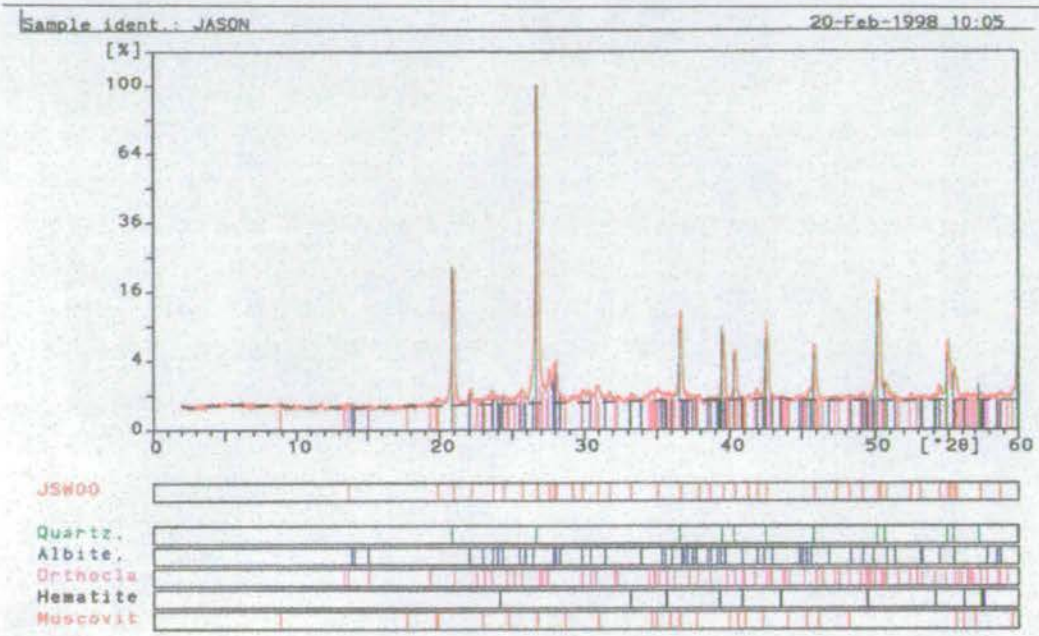

c) A typical XRD Trace for Tromper Wiek (1cm depth)

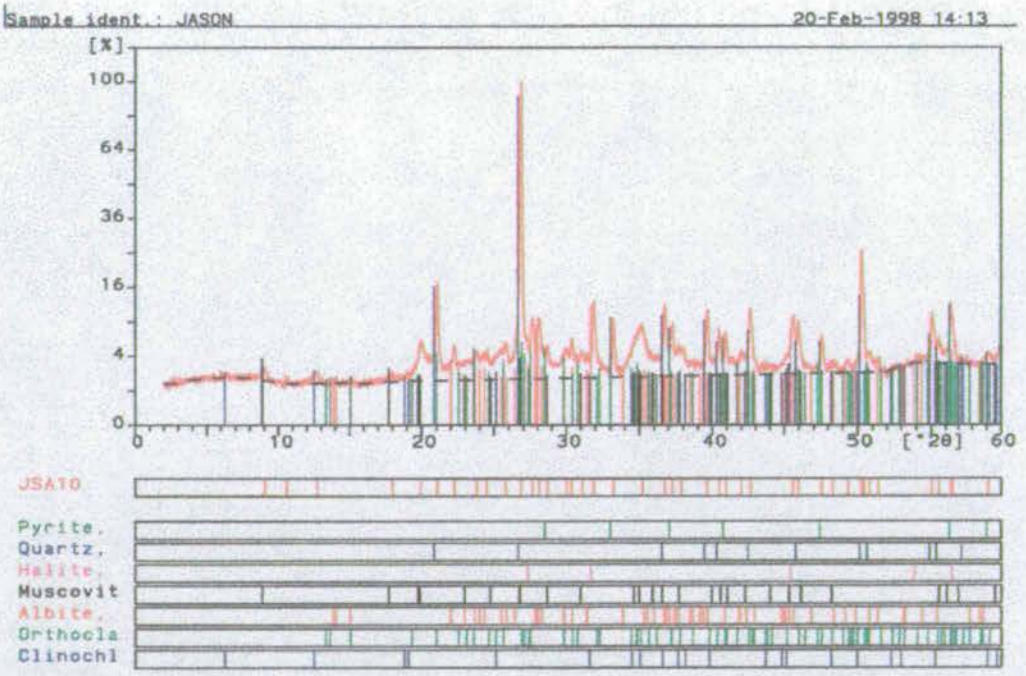

d) A typical XRD Trace for the Arkona Basin (10cm depth)

Figure 4-9 Spatial mineralogical variations as denoted by XRD analysis

The XRD traces above show the increasing mineralogical variation found with an increase in station water depth. Of particular interest is the transition in iron bearing

minerals as seen from Tonne to Arkona with the absence of heamatite at Tonne, the presence of heamatite at Nord-Perd and finally the occurrence of pyrite at Arkona. This could be related to the changing redox conditions of the sediment component with the reduction of hematite Fe_2O_3 to pyrite FeS_2 as shown in Figure 4-10 or there could be no change in Eh and the transition could be as a result of an increase in the elemental sulphur availability due to the associated increase in sulphate with salinity.

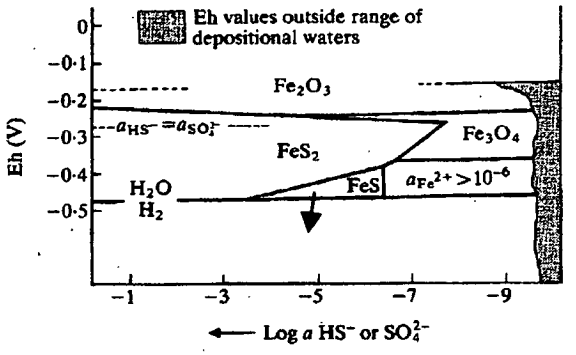

Figure 4-10 Mineral stability fields as a function of Eh and HS^- activity in conditions of pH, α_{HCO3} and $\alpha_{Fe2=}$ comparable with marine depositional waters (after Curtis, C. D. and Spears, D. A., 1968)

The mineralogical compositions as determined by X-ray diffraction are of a semi-quantitative nature with the interpretation based on a peak height comparison relative to the quartz 26.8 peak. The XRD traces show a quartz and feldspar dominated system for Tonne with the additional presence of calcite and hematite at Nord-Perd. Wiek has a very similar mineralogy to Nord-Perd with the added presence of muscovite mica whereas Arkona shows the additional mineral assemblages of pyrite, halite and chlorite in addition to the presence of quartz, feldspar and muscovite. These transitional assemblages are shown in Figure 4-11 and provide further evidence that the Arkona Basin is an area of accumulation and deposition and is a key repository of the clay fraction commonly associated with contaminants.

A representative down core XRD trace is given in Figure 4-12 for Tromper Wiek with analyses at 0, 4, 10 and 16cm which shows the great mineralogical consistency of the assemblages. In all the cores little mineralogical variation was found down

core with the exception of calcite in Nord-Perd which coincided with the presence of shell bands.

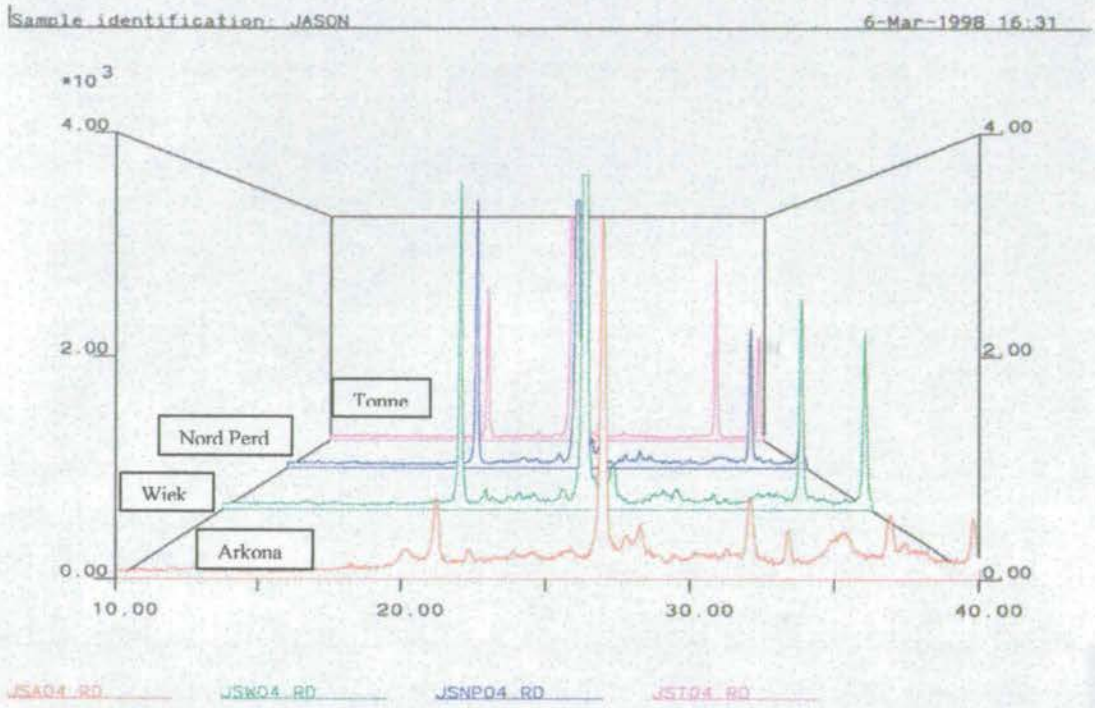

Figure 4-11 XRD comparative trace at 4cm depth for all Stations illustrating the increased mineralogical variations with an increase in station depth.

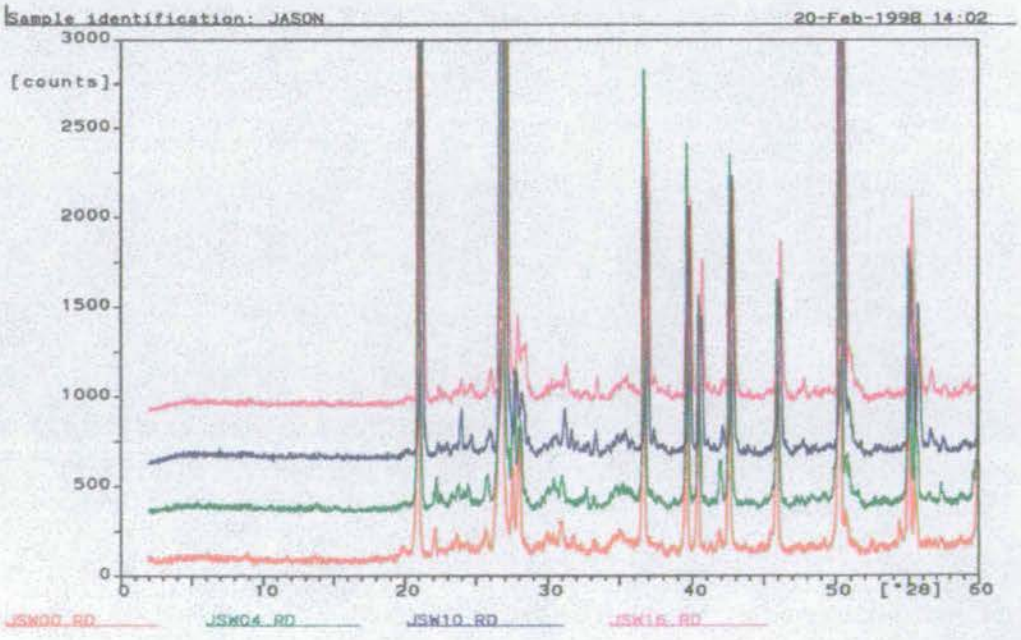

Figure 4-12 A down core series of analyses for Tromper Wiek illustrating the mineralogical consistencies throughout the whole core.

As XRD is a relative measure of the components in a given analytical sample then it is not possible to determine the absolute mineralogical concentrations without the use of a standard. The analysis run on the Baltic Sea samples can only therefore be used semi-quantitatively and care should be taken in its interpretation as it is possible if there is an extreme dominance by any one particular mineral that it could mask the presence of other minerals at low concentrations.

In addition to the XRD analysis BELMANS *et al.* 1993 concluded that the bulk material of the silty and clayey Baltic Sea recent sediments consisted mainly of quartz and hydrous aluminosilicates with other sedimentary species (oxyhydroxides, sulphides and heavy minerals) being related to geographical location. GINGELE and LEIPE, 1997 also showed that the predominant clayey components in the Baltic Sea system could be found lying on a dilution line between illite and kaolinite as shown in Figure 4-13.

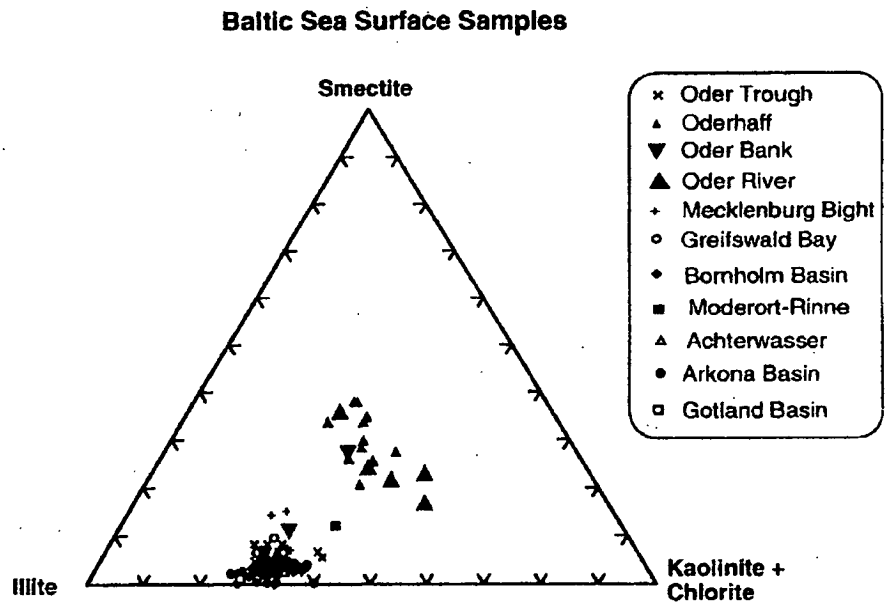

Figure 4-13 Clay mineralogy of surface sediment samples from the Baltic Sea (after Gingele and Leipe, 1997)

4.1.5 Normalisation Procedures

Extensive work has been carried out on the effect of grain size and its control on metal concentration by such authors as ACKERMANN, F., 1980, DE GROOT *et al.* 1982, HELLMAN, H., 1983, SCHNEIDER and WEILER, 1984, BELZUNCE *et al.* 1988, BRUGMANN and LANGE, 1990, DIN, Z. B., 1992 and BRUGMANN 1992. Their work has reinforced the basic conclusion that the majority of metals are incorporated mainly in a limited number of aluminosilicates such as micas, pyroxenes, amphiboles and the secondary clay minerals. Consequently, this conclusion can be extrapolated, in that the coarse sediments with sandy grain size distributions, normally with very low metal concentrations, will tend to 'dilute' the contaminant concentration in more clay rich sediment samples. Hence, if there are different grain size abundances across the spatial scope of the area under investigation then it is important to compensate for this by the use of a grain size correction factor or 'normalisation' factor. LORING, 1991 compared the two main approaches to normalisation; namely, the granulometric (analysing specific size fractionations) and geochemical methods (relating the 'total' concentration to that of a 'conservative, non anthropogenically influenced' element) and concluded that the geochemical normalisation process was superior as this compensated for the mineralogical as well as the natural granular variability of the metal concentration in the sediment.

In order to find a suitable normalising agent a number of requirements have to be met. The element of choice should ideally be conservative, refractory, anthropogenically inert, covary with the grain size variations and be able to be analysed with good accuracy and precision.

There are a number of elements that have been suggested as potential normalising agents for metals in the marine sedimentary environment amongst which Al, C-org, Cs, Fe, Li, Rb, Sc, Si, Ti, and Th are the main suitors. Traditionally, aluminium has been the normalising element of choice due to aluminium being a major constituent in aluminosilicates with which the bulk of trace metals are associated (SCHROPP and WINDOM, 1988). However, in some high latitude environments aluminium

does not always vary significantly with changes in grain size. This is due to the incorporation of aluminium into the feldspar lattice during crystallisation of igneous rocks and because weathering in high latitudes typically has a greater physical component relative to that of chemical breakdown commonly found in low latitudes. Consequently, weathering tends to comprise more of physically-comminuted breakdown products. On weathering, aluminium is not released by chemical weathering into a secondary clay structure but instead resides in feldspars of various sizes. In doing so aluminium can become decoupled from its usual 'normalising' role because as a component in the feldspar it is possible to have a relatively high aluminium component in a relatively metal-poor feldspar phase even in the fine grain size fraction (LORING, 1978, 1979 and BOSTROM *et al.* 1978). In a similar respect care should be taken to ensure that the normalising element of choice is not preferentially partitioned into a phase that does not constitute the fine grain size fraction and hence distort the interpretation of the data set. From the above it is obvious that detailed attention should be paid to the mineralogy of the sediment and possible substitutions in order to determine the most suitable normalising element.

The Baltic has a varied geological history; to the north lies the Scandinavian Precambrian crystalline basement of the Baltic shield, while to the south lies the Phanerozoic sedimentary units of the East European sedimentary complex. Superimposed on the solid geology are the extensive glacial tills and subsequent weathering deposits of the Pleistocene and Holocene. The relative importance of each of these groups in weathering, and hence the mineralogical characteristics of recent sediments and the predominance of a region of provenance, is disputed although undoubtedly the erosion of glacial till and its provenance is of major importance. Before determining which normalising element can be used detailed, mineralogical studies should be initiated such as XRD analysis to determine the relative magnitude of any 'problematic' substitution phases.

The XRD traces show a transitional increment in the amount of minerals found in the sediment samples from ODAS Tonne to the Arkona Basin, with Tonne being chiefly composed of quartz with a very small proportion of sodic feldspar to the decreasing

dominance of quartz in Arkona with the addition of increasingly significant proportions of pyrite, sodic and potassic feldspar, halite, muscovite, and chlorite. On the data acquired here there does not seem to be a significant feldspar component in the Southern Baltic Sea and thus aluminium may be considered a potentially suitable element of normalisation

In order to assess the suitability of the four main potential normalising elements (Li, Al, Rb and Sc) it is necessary to plot grain size against potential normaliser to see as to whether there is a strong covariance between the two as shown in Figure 4-14.

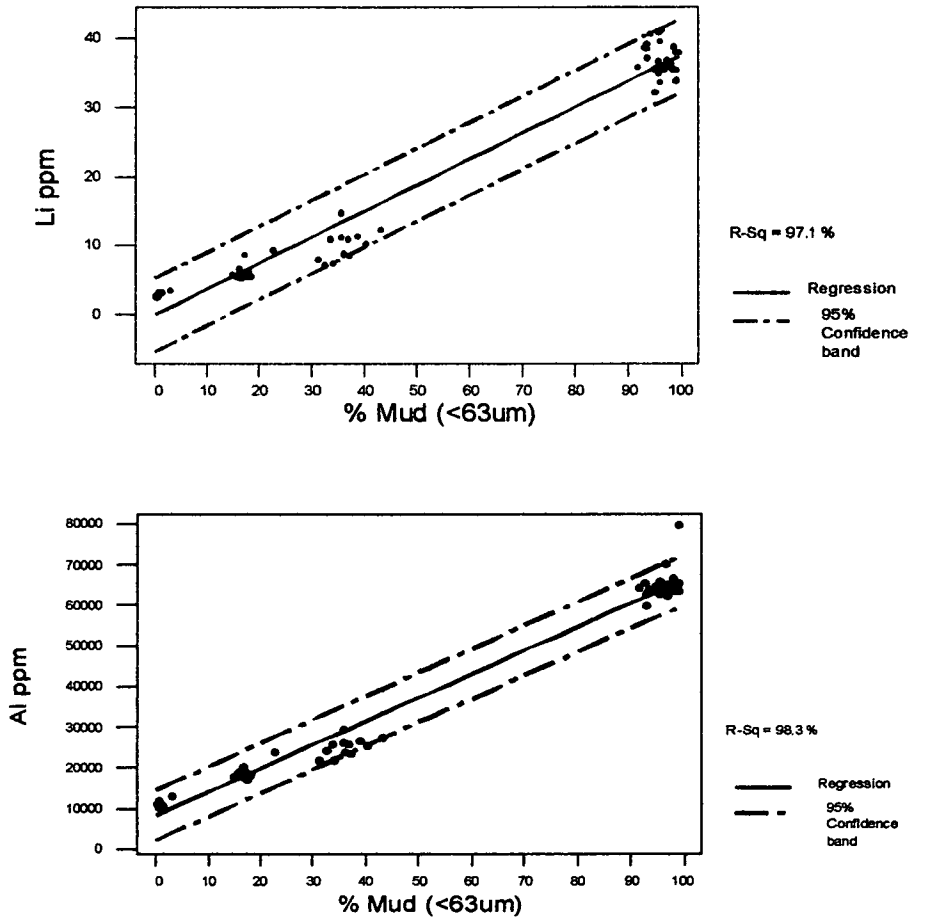

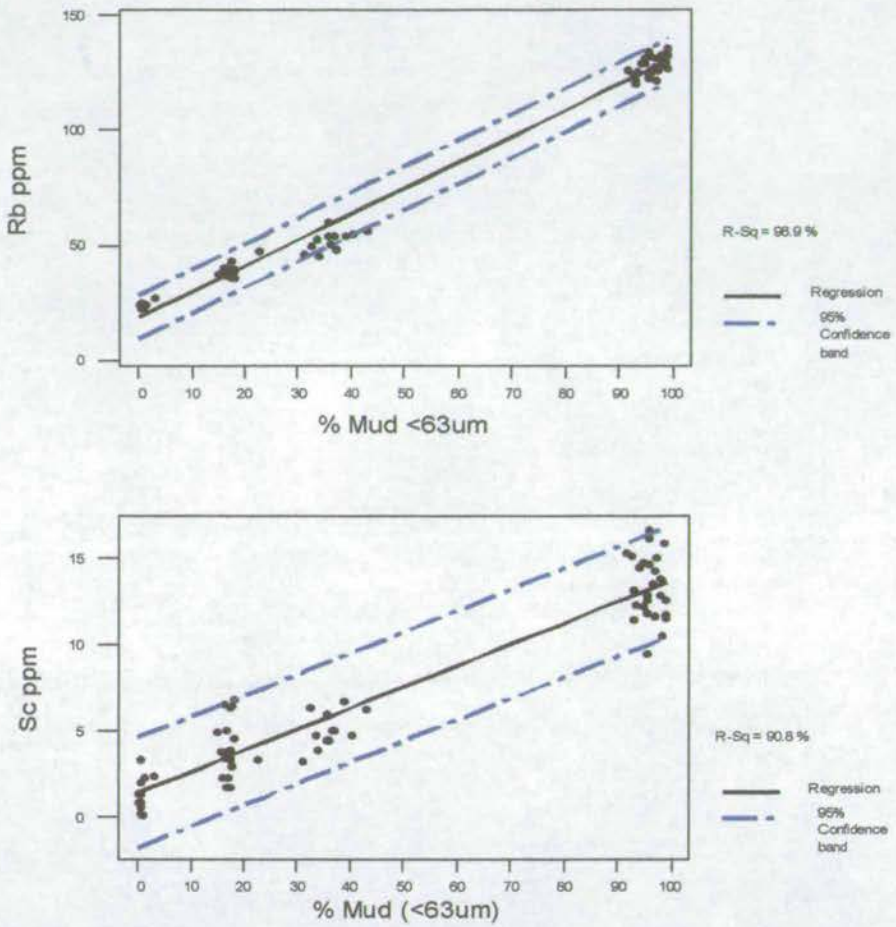

Figure 4-14 Regression lines of normalising elements against % Mud plots.

From Figure 4-14 rubidium displays the closest correlation with % mud, with lithium and, in particularly scandium, having a weaker correlation which probably relates to the lower analytical precision of these low concentration elements. In addition to this, rubidium shows the most significant variation in grain size and concentration, as shown in Figure 4-15.

To meet the final criteria for a normalising agent there must be a significant correlation between the lithogenic metal content and the normalising element. To illustrate the strong correlation of rubidium, as a summary, with these metals Figure 4-16 shows two regression lines of rubidium against the lithogenic elements of Ti, and Al.

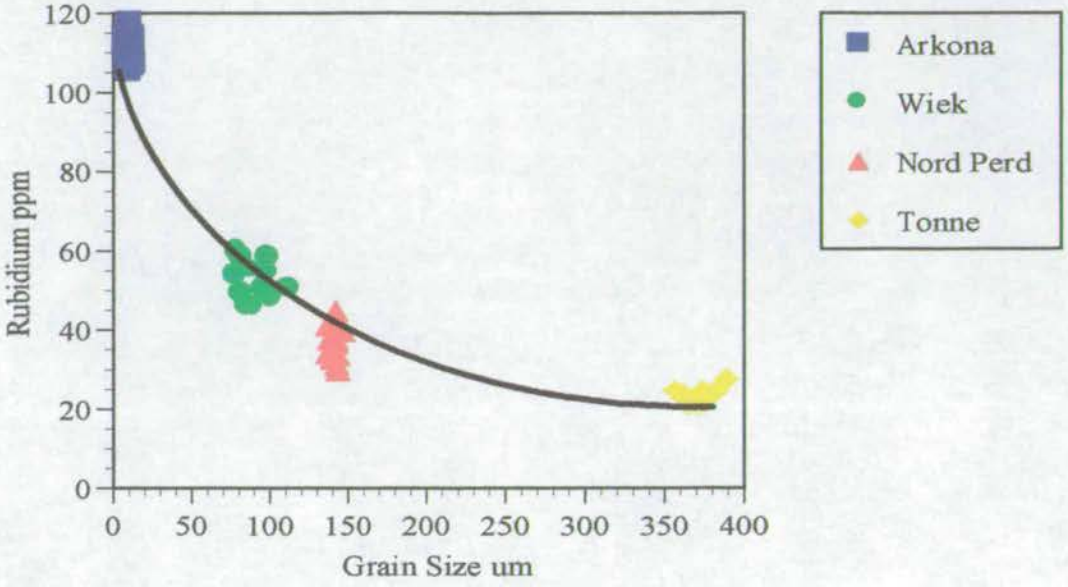

Figure 4-15 Plot of rubidium (ppm) concentration against grain size (um) showing a significant variation with changes in grain size.

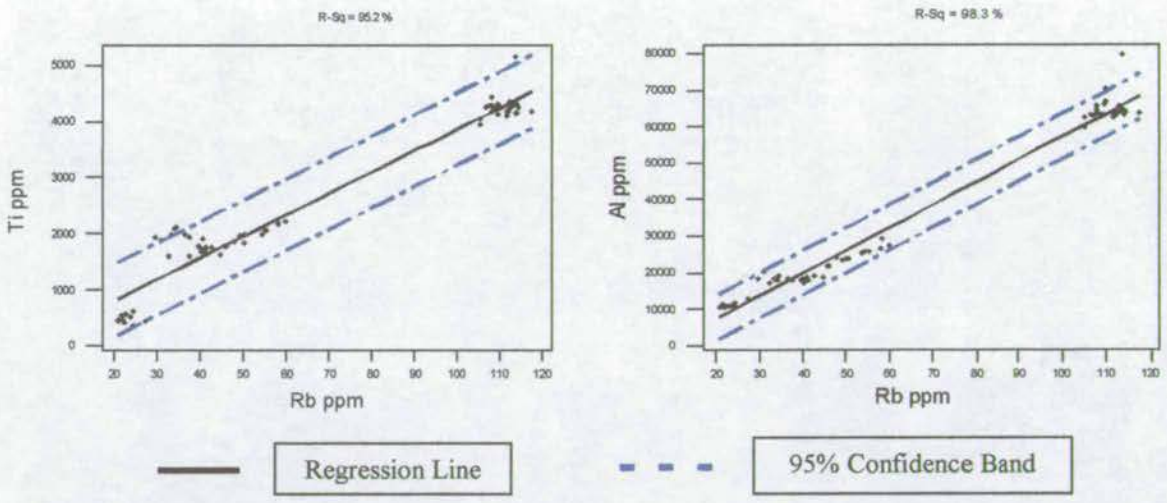

Figure 4-16 Regression lines for Rb against the lithogenic elements of Titanium and Aluminium.

Hence, in summary, as rubidium has no independent host minerals, is a lattice component of fine grained minerals, reflects the granular variability of it host mineral component, is not usually influenced by anthropogenic inputs, shows good correlation with the lithogenic elements and has good analytical precision and accuracy then rubidium was chosen as the element of choice for normalisation of both the sediment core and mobile nepheloid layer.

4.1.6 Carbon and Nitrogen Data

There are two principle types of carbon found in the marine environment, organic and carbonate carbon. Organic carbon is primarily derived from the remains of plants, excretion products and animal body tissue. Carbonate carbon, is chiefly derived from the preserved tests of plankton in the water column but can also be found in the lithogenic and authigenic phases. The simultaneous measurement of nitrogen enables the use of C/N ratios and the weight percent of these fractions to be used as an aid in identifying potential sources and post depositional diagenesis of carbon and nitrogen in the marine sedimentary environment (MULLER and MATHESIUS, 1999). This is possible due to the relatively constant values of carbon, nitrogen and phosphorus found in living marine organisms. This 'normal' ratio of 106 atoms of carbon, 16 atoms of nitrogen for every one phosphorus atom is known as the Redfield Ratio (REDFIELD *et al.* 1963) and constitutes a molar C/N value of approximately 7 for marine organic carbon. As protein has an atomic C/N ratio of approximately 3 then animals' rich in protein will have low C/N ratios and conversely land plants with low protein contents will have a high ratio (MULLER, 1975). Table 4-1 shows literature derived molar C/N values for a range of organisms, sediments and plants and Figure 4-17 shows the results obtained from the sediment cores analysed in the Southern Baltic Sea. Further C/N ratios for aquatic macrophytes and selected plant species in the southern Baltic Sea region are given in MULLER and MATHESIUS, 1999.

Preliminary results from Figure 4-17 show that the molar C/N ratio for all the cores is relatively constant and lies in the 7-13 range for most of the cores. The main exceptions being Nord-Perd where elevated C/N ratios are found relating to the presence of shell bands as depicted by the inorganic carbon results. The upper C/N ratio values of 13 are consistent with those given by MACKENZIE, 1981 for organic matter accumulation in sediment. A slight increase in the C/N ratio can be seen in most of the cores with depth which probably reflects the limited extent of preferential bacterial degradation of sedimentary organic nitrogen (BORDOVSKIY, 1965 and SEKI *et al.* 1968, PATIENCE *et al.*, 1990).

Table 4-1 C/N ratios of some components in the marine system.

Organism / Plant / Sediment	Author	Molar C/N Ratio
Diatoms	Bordovskiy, 1965a	8.75
Benthos	Bordovskiy, 1965a	4.88
Zooplankton	Redfield *et al.* 1963	6.24
Phytoplankton	Slawyk *et al.* 1978	6.5
Land Plants	Nakai, 1986	>30
Land Plants	Deevy, 1973	98
Land Plants	Delwiche and Lyons, 1977	128
Land Plants	Muller, 1977	25-30
SPM Southern Baltic Sea	Shimmield, 1995	4
Accumulating Organic Matter	Mackenzie, 1981	13
Kiel Bight Sediment	Balzer, 1984	9-13
Southern Baltic Sea Sediment	Blazhchishin, 1982c	6-8

It is quite apparent that only the Arkona Basin has the most significant quantities of organic carbon fluctuating between 5-6 dry wt. %. The other cores tend to have a slight increase in organic carbon towards the surface layer but remain at a much lower value and are constant down core thereafter. These spatial differences in organic carbon content could arise for a variety of different reasons and are most likely to be function of the following factors:

- As a function of the biogenic production and settling conditions at the stations.
- As a function of the preservation potential (redox and bottom water conditions) of the station.
- As a function of lithogenic dilution of the carbon content.

However it would seem that the Arkona Basin with the lower energy and periodically reducing setting (i.e. low dissolved oxygen) of Arkona being conducive to deposition and incorporation of organic carbon into the sediment record.

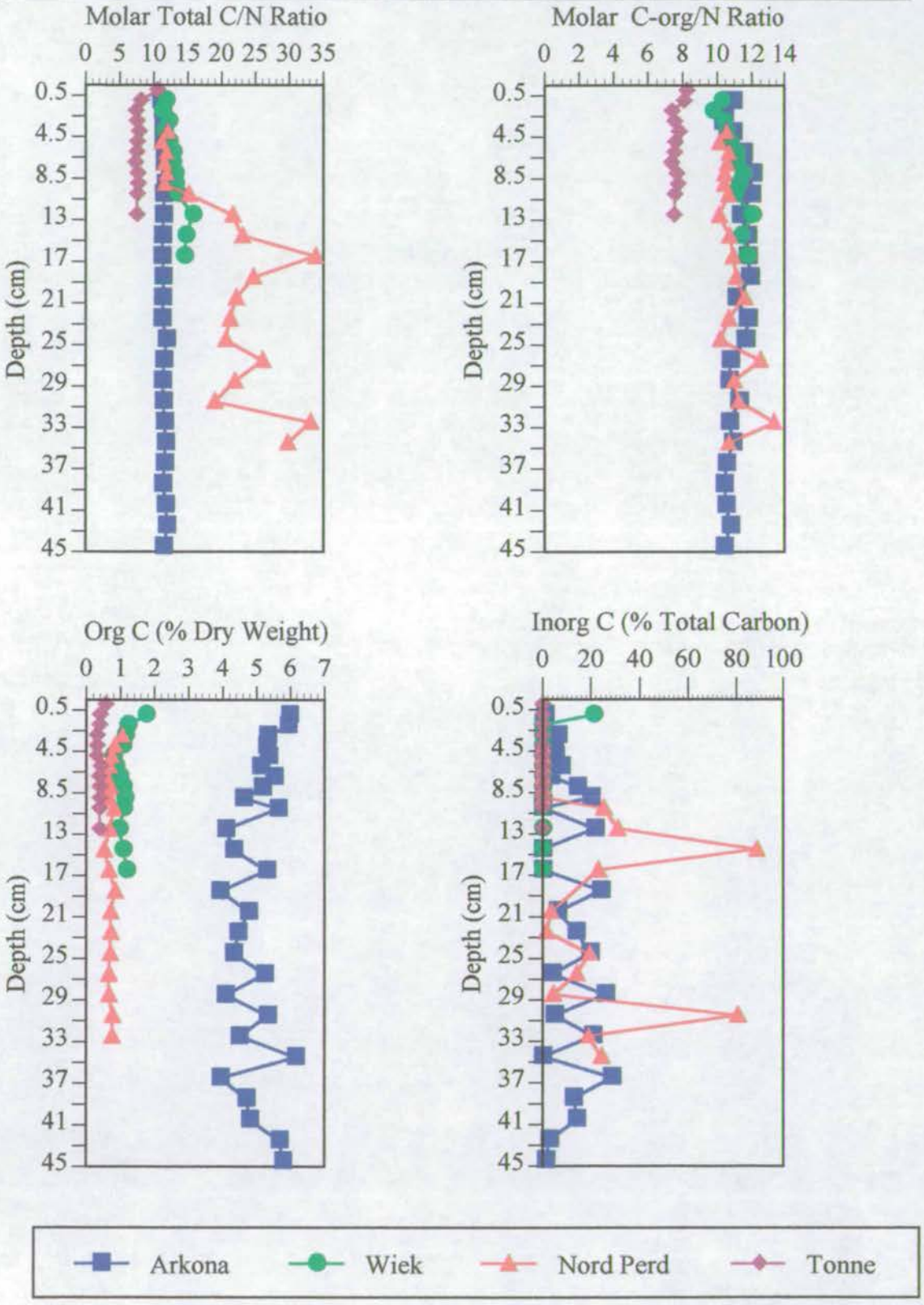

Figure 4-17 Down core variations in carbon and nitrogen for Tonne, Nord Perd, Wiek and Arkona.

Inorganic carbon is negligible in all the cores apart from the shell bands in Nord-Perd where sharp peaks in inorganic carbon are displayed. The small variations of around 10% of total carbon for Arkona probably relate to that of either a detrital or authigenic origin. The small deviations found in the organic and inorganic dry weight figures are probably related to analytical uncertainty.

The consistency of both the total molar C/N and molar C-org/N ratios indicates that the controls on the C/N ratio are similar throughout the study area. Comparisons to the data in Table 4-1 suggest that the C/N ratio is essentially controlled by the organic marine sources as opposed to a terrestrial higher land plant input.

5.0 Sediment Core Metal Geochemistry

This section will deal with the distribution and concentration of metal contents within the sediment cores analysed on both a normalised and total metal content basis. Initially, statistical analysis will be applied to the data set to determine groups of co-varying elements and then a detailed investigation of the four main categories of input into the sedimentary system, those of lithogenic, biogenic, diagenetic and anthropogenic will be instigated.

The study of sediment core geochemistry is of great importance in the natural environment as the sediments represent one of the ultimate sinks of metals discharged into the marine environment (LOUMA and BRYAN, 1981; BRÜGMANN and LANGE, 1990) and hence give a historical record of metal accumulation. This historical record should be quite apparent in the Baltic Sea because, during the twentieth century, the Baltic Sea has changed from being a clean, oligotrophic water body into one of the most contaminated sea areas in the world (MELVASALO, 1981). There have been numerous studies of the metal distribution in sediments for various regions of the Baltic Sea since the 1970s (HASSELROT, 1972, SUESS and ERLENKEUSER, 1975, HALLBERG, 1979, MÜLLER *et al.* 1980, SZEFER and SKWARZEC, 1988, NEUMANN *et al.* 1996, BORG and JONSSON, 1996, SZEFER *et al.* 1998) all of which have shown substantially increased metal contents in the surface layer when compared with that of the pre-industrial era. The distribution of these metals is not solely dependant upon input and accumulation rates but is also influenced by diagenetic processes occurring in the sediment column and the binding phase to which the metal is attached, be it to clay minerals, carbonates, sulphides, Fe and Mn hydroxides or organic material (LU and CHEN, 1977, SALOMONS and FÖRSTNER, 1980, LI, 1981, BELZUNCE, 1989, SANTSCHI, 1990, HELIOS RYBICKA, 1993, SZEFER *et al.* 1995.).

The samples collected were analysed using a bulk geochemical approach together with normalisation techniques in order that comparative work could be achieved.

5.1 SEDIMENT CORE STATISTICAL ANALYSIS

In order to constrain and group the data generated by both the XRF and ICPMS, statistical analysis was employed and used as an aid in the interpretation of the large data set. Initially the two data sets were combined and where there was elemental duplication the element that had the lowest standard deviation and greatest accuracy to a known standard was chosen as representative. Two statistical tests were used to investigate inter-element variations; the first was by way of the Pearson product-moment coefficient of linear correlation which results in a correlation matrix which can then be compared to statistical tables in order to establish a degree of significance for the correlation found. The second technique used was principle component analysis which defines a user controlled number of perpendicular axes in an attempt to group the data sets according to similarity. These axes are called eigenvectors and the first eigenvector will define a line of 'best fit' through the data set in *n*-dimensional space and will give values for principal component 1. The second principle component is defined by the eigenvector that gives the 'best fit' at right angles to the first. These principle components can then be plotted to produce variation diagrams that are independent of each other and in which, each diagram shows the metals plotted relative to one another. Figures 5-1 to 5-5 show the correlation matrices for the total data set, Tonne, Nord Perd, Wiek and Arkona respectively. Unsurprisingly, because of the large, consistent environmental differences between stations, the total data set correlation matrix shows very high degrees of correlation for the data set as a whole. In addition to this there is an increase in the statistically significant correlations from Tonne to Arkona. Greater detail of the significant correlations will be detailed in the summary section of this section.

Figures 5-6 to 5-9 show the variation diagrams derived from the principle component analyses and in addition on each page are short summaries of the initial findings.

Total	Li	Ti	V	Mn	Fe	Co	Ni	Cu	Zn	As	Rb	Sr	Y	Zr	Sn	Sb	Cs	Ba	Ce	Pb	Th	U	Si	Al	Mg	Ca	K	P	Sc	La	Nd	Cr	Nb	Mo	C-org
Li	1																																	
Ti	0.96	1.00																																
V	1.00	0.97	1.00																															
Mn	0.88	0.92	0.89	1.00																														
Fe	0.98	0.97	0.98	0.94	1.00																													
Co						1.00																												
Ni	0.97	0.95	0.97	0.90	0.97		1.00																											
Cu	0.98	0.94	0.98	0.81	0.94		0.94	1.00																										
Zn	0.83	0.74	0.82	0.51	0.72		0.78	0.88	1.00																									
As	0.97	0.93	0.97	0.84	0.95		0.94	0.97	0.82	1.00																								
Rb	0.99	0.98	0.99	0.91	0.98		0.96	0.96	0.78	0.96	1.00																							
Sr	0.79	0.88	0.81	0.79	0.80		0.80	0.81	0.63	0.78	0.81	1.00																						
Y	0.98	0.99	0.99	0.91	0.98		0.97	0.96	0.78	0.95	0.99	0.85	1.00																					
Zr														1.00																				
Sn	0.89	0.79	0.88	0.59	0.80		0.82	0.93	0.97	0.89	0.85	0.65	0.84	-0.33	1.00																		
Sb																1.00																		
Cs	0.99	0.96	0.99	0.92	0.99		0.97	0.96	0.77	0.96	0.99	0.78	0.98	-0.33	0.84		1.00																	
Ba	0.88	0.94	0.89	0.79	0.87		0.88	0.88	0.73	0.85	0.92	0.84	0.92		0.77		0.85	1.00																
Ce	0.98	0.99	0.98	0.91	0.98		0.96	0.96	0.77	0.95	0.99	0.86	1.00		0.83		0.97	0.93	1.00															
Pb	0.87	0.77	0.85	0.55	0.76		0.80	0.92	0.97	0.88	0.82	0.64	0.81		0.99		0.81	0.75	0.80	1.00														
Th	0.96	0.99	0.97	0.95	0.98		0.96	0.93	0.71	0.92	0.97	0.86	0.99		0.77		0.97	0.90	0.99	0.73	1.00													
U	0.97	0.98	0.98	0.92	0.98		0.95	0.95	0.75	0.94	0.98	0.87	0.99		0.81		0.97	0.91	0.99	0.78	0.99	1.00												
Si	-0.98	-0.95	-0.98	-0.88	-0.97		-0.95	-0.97	-0.79	-0.96	-0.98	-0.80	-0.98		-0.87		-0.98	-0.88	-0.97	-0.84	-0.96	-0.96	1.00											
Al	0.99	0.98	0.99	0.92	0.99		0.97	0.96	0.76	0.95	0.99	0.80	0.99		0.84		0.99	0.89	0.98	0.81	0.97	0.98	-0.97	1.00										
Mg	0.99	0.97	0.99	0.92	0.99		0.97	0.95	0.77	0.95	0.98	0.80	0.98		0.84		0.99	0.87	0.97	0.81	0.97	0.97	-0.96	1.00	1.00									
Ca												0.64		0.45												1.00								
K	0.97	0.99	0.97	0.92	0.97		0.95	0.93	0.74	0.93	0.99	0.83	0.98		0.80		0.96	0.94	0.98	0.77	0.97	0.97	-0.95	0.99	0.97		1.00							
P	0.98	0.95	0.98	0.86	0.96		0.95	0.97	0.82	0.94	0.97	0.80	0.96		0.88		0.97	0.88	0.96	0.85	0.94	0.95	-0.96	0.98	0.98		0.96	1.00						
Sc	0.94	0.95	0.94	0.87	0.94		0.93	0.92	0.74	0.92	0.95	0.82	0.95		0.80		0.94	0.88	0.95	0.78	0.94	0.94	-0.94	0.94	0.93		0.94	0.91	1.00					
La	0.81	0.87	0.82	0.80	0.82		0.80	0.79	0.60	0.78	0.84	0.83	0.86		0.65		0.80	0.86	0.87	0.62	0.86	0.85	-0.82	0.83	0.81		0.86	0.80	0.80	1.00				
Nd	0.73	0.84	0.75	0.76	0.77		0.76	0.68	0.54	0.68	0.78	0.79	0.81		0.56		0.72	0.84	0.83	0.52	0.84	0.81	-0.74	0.76	0.74		0.82	0.72	0.77	0.83	1.00			
Cr	0.98	0.98	0.99	0.92	0.98		0.96	0.97	0.77	0.95	0.99	0.86	0.99		0.84		0.98	0.91	0.99	0.81	0.98	0.98	-0.98	0.98	0.98		0.98	0.97	0.95	0.85	0.80	1.00		
Nb	0.97	0.99	0.98	0.92	0.98		0.96	0.94	0.74	0.94	0.98	0.86	0.99		0.81		0.97	0.93	0.99	0.78	0.99	0.98	-0.97	0.98	0.97		0.98	0.96	0.95	0.87	0.83	0.99	1.00	
Mo	0.76	0.87	0.79	0.85	0.81		0.79	0.75	0.49	0.80	0.80	0.83	0.84		0.55		0.78	0.81	0.84	0.53	0.85	0.87	-0.76	0.81	0.79	0.38	0.84	0.75	0.84	0.80	0.76	0.83	0.85	1.00
C-org	0.98	0.94	0.98	0.87	0.97		0.95	0.96	0.81	0.95	0.97	0.77	0.96	-0.32	0.88		0.98	0.85	0.95	0.85	0.94	0.95	-0.96	0.97	0.98		0.95	0.98	0.91	0.78	0.70	0.96	0.95	0.73
% < 63um	0.99	0.98	0.99	0.91	0.98		0.96	0.95	0.77	0.95	1.00	0.82	0.99		0.84		0.98	0.92	0.99	0.81	0.98	0.98	-0.97	0.99	0.98		0.99	0.97	0.95	0.85	0.79	0.99	0.99	0.81

n=70, significance at p = 0.01 (> 0.31)

Figure 5-1 Correlation matrix for the total metal data set detailing significant correlation at 99% confidence, r = 0.31.

Tonne	Li	Ti	V	Mn	Fe	Co	Ni	Cu	Zn	As	Rb	Sr	Y	Zr	Sn	Sb	Cs	Ba	Ce	Pb	Th	U	Si	Al	Mg	Ca	K	P	Sc	La	Nd	Cr	Nb	Mo	C-org
Li	1																																	
Ti		1.00																																
V			1.00																															
Mn				1.00																														
Fe		0.80	0.93		1.00																													
Co	0.78			0.94		1.00																												
Ni							1.00																											
Cu								1.00																										
Zn	0.74		0.82	0.80	0.83	0.82	0.82		1.00																									
As			0.77	0.85		0.86			0.77	1.00																								
Rb	0.74	0.83	0.86		0.93				0.87		1.00																							
Sr		0.82	0.86		0.94				0.82		0.97	1.00																						
Y		0.92	0.86		0.93				0.78		0.95	0.97	1.00																					
Zr		0.96	0.72								0.77	0.74	0.87	1.00																				
Sn		-0.87			-0.75						-0.87	-0.89	-0.91	-0.77	1.00																			
Sb																1.00																		
Cs		-0.92	-0.78		-0.83				-0.77		-0.93	-0.91	-0.94	-0.87	-0.83		1.00																	
Ba		0.85	0.91		0.93				0.84	0.92	1.00	0.98	0.97	0.80	0.97		0.83	1.00																
Ce		0.88	0.81		0.87				0.83		0.91	0.90	0.92	0.83	-0.77		-0.89	0.92	1.00															
Pb			0.92		0.84				0.78	0.81	0.76	0.80						0.75		1.00														
Th																					1.00													
U		-0.75	-0.77		-0.84						-0.88	-0.95	-0.90		-0.78			-0.90	-0.79		-0.76	1.00												
Si		0.86	0.89		0.90				0.75	0.88	0.96	0.99	0.98	0.78	0.98		0.88	0.97	0.93	0.82	0.95	0.99	1.00											
Al		0.79	0.85		0.95				0.85		0.98	0.99	0.96		-0.77		-0.79	0.98	0.87	0.82		-0.92	0.97	1.00										
Mg			0.87		0.88		0.81		0.84	0.81	0.79	0.80	0.76					0.77	0.81	0.83	0.68			0.80	1.00									
Ca			0.89		0.92				0.81		0.92	0.97	0.90					0.93	0.83	0.86		-0.76	0.92	0.95	0.84	1.00								
K		0.80	0.84		0.93				0.80		0.97	0.99	0.96					0.98	0.87	0.80			0.98	0.99	0.78	0.96	1.00							
P		0.80	0.91		0.97		0.78		0.91	0.76	0.96	0.94	0.93	0.76			-0.74	0.94	0.91	0.84			0.90	0.96	0.90	0.91	0.93	1.00						
Sc																													1.00					
La																														1.00				
Nd																															1.00			
Cr																																1.00		
Nb								-0.82																									1.00	
Mo											-0.70	-0.79	-0.79		0.84		-0.76	-0.74	-0.74		-0.81		-0.82			-0.74	-0.78						-0.77	1.00	
C-org		-0.86									-0.83	-0.87	-0.90	-0.75	-0.85		-0.77	-0.85	-0.83		-0.83	-0.91	-0.93	-0.84		-0.77	-0.87						-0.86	-0.79	1.00
% < 63um	0.74			0.81		0.88		0.80																										

n= 12, significant at p = 0.01 (> 0.735)

Figure 5-2 Correlation matrix for the ODAS Tonne metal data set detailing significant correlation at 99% confidence, r = 0.735.

NordPerd	Li	Ti	V	Mn	Fe	Co	Ni	Cu	Zn	As	Rb	Sr	Y	Zr	Sn	Sb	Cs	Ba	Ce	Pb	Th	U	Si	Al	Mg	Ca	K	P	Sc	La	Nd	Cr	Nb	Mo	C-org
Li	1																																	
Ti		1.00																																
V		0.92	1.00																															
Mn		0.84	0.77	1.00																														
Fe		0.89	0.94	0.72	1.00																													
Co						1.00																												
Ni							1.00																											
Cu								1.00																										
Zn							0.96		1.00																									
As			0.81		0.72					1.00																								
Rb		0.75	0.80		0.92						1.00																							
Sr		0.67	0.68	0.85								1.00																						
Y		0.95	0.85	0.80	0.84					0.63	0.73	0.64	1.00																					
Zr		0.91	0.80	0.69	0.81						0.72		0.97	1.00																				
Sn	0.85	-0.67		-0.69								-0.73	-0.73	-0.61	1.00																			
Sb							0.97		0.92							1.00																		
Cs	0.74	-0.61											-0.71	-0.68			1.00																	
Ba		0.91	0.91	0.76	0.94					0.71	0.94		0.90	0.85	0.87		0.75	1.00																
Ce		0.97	0.94	0.83	0.87					0.72	0.71	0.69	0.95	0.92			0.65	0.87	1.00															
Pb	0.84																0.63			1.00														
Th		0.91	0.88	0.76	0.79					0.69		0.61	0.90	0.89			0.64	0.75	0.96		1.00													
U		0.66	0.69	0.76								0.87	0.62		-0.62				0.73		0.71	1.00												
Si		0.92	0.85	0.77	0.87					0.67	0.84	0.64	0.88	0.83				0.95	0.84		0.81	0.64	1.00											
Al		0.94	0.89	0.77	0.91					0.66	0.87	0.63	0.89	0.85				0.97	0.87		0.81	0.61	0.98	1.00										
Mg		0.85	0.83	0.86	0.70					0.74		0.84	0.76	0.65			0.64	0.68	0.84		0.81	0.89	0.77	0.77	1.00									
Ca				0.67								0.90										0.81			0.70	1.00								
K		0.93	0.88	0.77	0.91					0.69	0.89	0.61	0.87	0.83			0.68	0.97	0.86		0.82	0.75	0.99	1.00	0.75		1.00							
P		0.76	0.74	0.75	0.66					0.61		0.81	0.65					0.69	0.68		0.61	0.76	0.80	0.80	0.90	0.67	0.79	1.00						
Sc																												1.00						
La																													1.00					
Nd		0.73											0.80	0.84				0.61	0.75		0.80		0.64	0.62			0.61			1.00				
Cr		0.80	0.82	0.74	0.83			0.65			0.74	0.76	0.85	0.80				0.82	0.84		0.80	0.78	0.75	0.79	0.69		0.77	0.64				1.00		
Nb		0.91	0.83	0.76	0.76						0.64		0.92	0.91				0.81	0.91		0.89	0.69	0.82	0.83	0.75		0.82	0.63			0.80	0.77	1.00	
Mo												0.74			-0.75							0.73			0.69	0.71		0.62					1.00	
C-org	0.77																																	1.00
% < 63um		0.94	0.92	0.81	0.90					0.71	0.84	0.71	0.93	0.86	0.72		0.75	0.95	0.92		0.85	0.92	0.95	0.95	0.80		0.95	0.75	0.61		0.67	0.85	0.92	0.77	0.90

n = 17, significant at p = 0.01(>0.61)

Figure 5-3 Correlation matrix for the Nord-Perd metal data set detailing significant correlation at 99% confidence, r = 0.61

Wiek	Li	Ti	V	Mn	Fe	Co	Ni	Cu	Zn	As	Rb	Sr	Y	Zr	Sn	Sb	Cs	Ba	Ce	Pb	Th	U	Si	Al	Mg	Ca	K	P	Sc	La	Nd	Cr	Nb	Mo	C-org
Li	1																																	
Ti	0.85	1.00																																
V	0.99	0.90	1.00																															
Mn	0.83	0.79	0.89	1.00																														
Fe	0.97	0.89	0.98	0.91	1.00																													
Co						1.00																												
Ni	0.87	0.78	0.93	0.72	0.89		1.00																											
Cu	0.70		0.75				0.87	1.00																										
Zn									1.00																									
As	0.80	0.81	0.91	0.74	0.91		0.92	0.77		1.00																								
Rb	0.92	0.99	0.92	0.84	0.92		0.81			0.85	1.00																							
Sr		0.95	0.88		0.83		0.87			0.84	0.93	1.00																						
Y	0.79	0.98	0.90	0.85	0.91		0.77			0.83	0.99	0.90	1.00																					
Zr		0.81									0.77		0.81	1.00																				
Sn								0.71							1.00																				
Sb																1.00																		
Cs	0.86																1.00																	
Ba		0.98	0.82		0.79		0.75			0.81	0.96	0.95	0.95	0.86	0.78	0.83		1.00																
Ce	0.81	0.96	0.92	0.87	0.92		0.78			0.89	0.97	0.87	0.98	0.81				0.92	1.00															
Pb							0.65								0.85					1.00														
Th	0.79	0.89	0.91	0.87	0.93		0.79			0.91	0.91	0.78	0.92	0.74				0.82	0.97		1.00													
U	0.71			0.83	0.74												0.77				0.73	1.00												
Si	-0.91	0.93	0.71		0.71					0.75	0.91	0.87	0.91	0.93		0.81		0.97	0.88		0.85		1.00											
Al	0.94	0.99	0.92	0.81	0.91		0.84			0.87	0.99	0.96	0.97	0.76		0.81		0.96	0.95		0.91		0.92	1.00										
Mg	0.95	0.85	0.97	0.88	0.96		0.90	0.74		0.83	0.87	0.81	0.86			0.72	0.72	0.73	0.84		0.84	0.76		0.87	1.00									
Ca		0.79	0.86	0.63	0.79		0.88	0.83		0.72	0.78	0.88	0.73			0.73		0.74						0.81	0.88	1.00								
K	0.76	0.99	0.87	0.77	0.85		0.77			0.81	0.99	0.95	0.97	0.82		0.71		0.98	0.94		0.88		0.96	0.99	0.80	0.75	1.00							
P	0.73	0.79	0.89		0.83		0.97	0.87		0.89	0.79	0.90	0.74		0.73	0.69		0.75	0.74	0.74	0.73			0.83	0.83	0.88	0.76	1.00						
Sc		0.79	0.69		0.68						0.79	0.74	0.77					0.75						0.78	0.75	0.76	0.79		1.00					
La																														1.00				
Nd		0.89	0.86	0.85	0.90					0.84	0.91	0.74	0.94	0.77				0.82	0.95		0.96	0.92	0.80	0.88	0.82		0.87		0.72		1.00				
Cr	0.70	0.92	0.92		0.89		0.90	0.80		0.89	0.91	0.94	0.88			0.85		0.89	0.87		0.85		0.77	0.93	0.88	0.90	0.89	0.89	0.80		0.80	1.00			
Nb		0.95	0.90	0.79	0.87		0.81			0.80	0.94	0.90	0.95	0.73		0.78		0.90	0.91		0.87		0.83	0.94	0.88	0.81	0.93	0.77	0.78		0.85	0.88	1.00		
Mo																																		1.00	
C-org	0.72						0.76	0.85							0.79													0.77							1.00
% < 63um		0.95	0.83		0.80		0.73			0.76	0.92	0.88	0.93	0.81	0.73			0.92	0.90		0.86	0.75	0.86	0.91	0.79	0.75	0.93		0.83		0.87	0.88	0.96		0.81

n= 12, significant at p = 0.01 (>0.708)

Figure 5-4 Correlation matrix for the Wiek metal data set detailing significant correlation at 99% confidence, r = 0.708.

Arkona	Li	Ti	V	Mn	Fe	Co	Ni	Cu	Zn	As	Rb	Sr	Y	Zr	Sn	Sb	Cs	Ba	Ce	Pb	Th	U	Si	Al	Mg	Ca	K	P	Sc	La	Nd	Cr	Nb	Mo	C-org
Li	1																																	
Ti	-0.33	1.00																																
V	0.78	0.93	1.00																															
Mn	-0.75	0.71	0.46	1.00																														
Fe	-0.66	0.91	0.81	0.80	1.00																													
Co	0.50	0.62	0.76		0.54	1.00																												
Ni		0.96	0.94	0.66	0.92	0.66	1.00																											
Cu	0.74	0.66	0.85		0.48	0.82	0.68	1.00																										
Zn	0.80		0.53	-0.47		0.70		0.83	1.00																									
As		0.65	0.75		0.58	0.63	0.70	0.78	0.53	1.00																								
Rb	0.36	0.97	0.97	0.60	0.90	0.71	0.97	0.76	0.37	0.74	1.00																							
Sr		0.97	0.97	0.58	0.89	0.73	0.97	0.76	0.39	0.73	0.98	1.00																						
Y		0.97	0.97	0.59	0.88	0.69	0.97	0.76	0.38	0.74	0.99	0.99	1.00																					
Zr	-0.53	0.96	0.91	0.72	0.91	0.58	0.96	0.62		0.66	0.96	0.96	0.97	1.00																				
Sn	0.78		0.50	-0.51		0.64		0.81	0.99	0.53	0.34	0.36	0.35		1.00																			
Sb	0.35		0.35	-0.33				0.57	0.56	0.36					0.58	1.00																		
Cs	-0.38	0.98	0.93	0.69	0.94	0.68	0.98	0.67		0.69	0.98	0.97	0.97	0.97			1.00																	
Ba	0.33	0.94	0.96	0.49	0.84	0.79	0.94	0.83	0.47	0.78	0.96	0.97	0.96	0.91	0.45	0.51	0.95	1.00																
Ce		0.97	0.97	0.61	0.91	0.70	0.98	0.75	0.36	0.72	0.99	0.99	0.99	0.97	0.34	0.38	0.98	0.96	1.00															
Pb	0.77		0.54	-0.47		0.64		0.85	0.98	0.61	0.39	0.40	0.40		0.99	0.65		0.48	0.38	1.00														
Th	-0.59	0.94	0.83	0.81	0.95	0.57	0.93	0.50		0.51	0.91	0.91	0.90	0.94			0.96	0.86	0.92		1.00													
U		0.93	0.88	0.62	0.88	0.66	0.93	0.66		0.68	0.92	0.92	0.91	0.90		0.45	0.94	0.94	0.92		0.91	1.00												
Si	-0.28	0.99	0.93	0.69	0.89	0.62	0.95	0.66		0.65	0.96	0.96	0.96	0.96		0.33	0.97	0.93	0.96		0.93	0.92	1.00											
Al		0.99	0.93	0.69	0.90	0.63	0.95	0.66		0.66	0.96	0.96	0.96	0.95		0.33	0.97	0.93	0.96		0.93	0.92	1.00	1.00										
Mg		0.96	0.89	0.68	0.86	0.64	0.90	0.63		0.57	0.92	0.93	0.92	0.91			0.93	0.90	0.92		0.90	0.90	0.98	0.98	1.00									
Ca	-0.34	0.98	0.90	0.74	0.88	0.59	0.93	0.60		0.58	0.93	0.94	0.94	0.95		0.26	0.95	0.90	0.94		0.93	0.90	0.99	0.98	0.97	1.00								
K	-0.32	1.00	0.92	0.71	0.91	0.62	0.96	0.65		0.67	0.96	0.96	0.96	0.96		0.32	0.98	0.93	0.97		0.94	0.93	0.99	0.99	0.97	0.98	1.00							
P	0.43	0.85	0.88	0.37	0.73	0.82	0.81	0.79	0.52	0.63	0.86	0.90	0.86	0.79	0.50	0.42	0.83	0.90	0.86	0.52	0.75	0.79	0.86	0.86	0.87	0.83	0.84	1.00						
Sc		0.77	0.76	0.47	0.71	0.41	0.78	0.61		0.69	0.80	0.78	0.80	0.79		0.50	0.81	0.78	0.80	0.33	0.72	0.76	0.76	0.76	0.69	0.71	0.77	0.61	1.00					
La		0.91	0.86	0.69	0.88	0.54	0.90	0.55		0.60	0.92	0.90	0.90	0.93			0.92	0.82	0.92		0.90	0.81	0.89	0.89	0.85	0.87	0.90	0.73	0.73	1.00				
Nd		0.61	0.55	0.56	0.67		0.64				0.60	0.62	0.60	0.63			0.63	0.50	0.61		0.65	0.59	0.59	0.61	0.62	0.62	0.62	0.46	0.46	0.70	1.00			
Cr		0.95	0.96	0.62	0.90	0.71	0.97	0.74	0.35	0.75	0.98	0.98	0.98	0.96	0.35	0.41	0.97	0.95	0.98	0.36	0.92	0.91	0.94	0.94	0.91	0.92	0.95	0.85	0.78	0.92	0.60	1.00		
Nb		0.97	0.93	0.68	0.92	0.62	0.96	0.67		0.71	0.98	0.97	0.97	0.97		0.37	0.97	0.93	0.97		0.93	0.91	0.96	0.96	0.92	0.93	0.96	0.83	0.81	0.91	0.59	0.97	1.00		
Mo	-0.44	0.53	0.37	0.60	0.55		0.51			0.52	0.47	0.42	0.45	0.52			0.51	0.46	0.44		0.50	0.58	0.51	0.50	0.42	0.49	0.53		0.55	0.40		0.42	0.51	1.00	
C-org		0.73	0.79	0.32	0.68	0.76	0.71	0.72	0.50	0.62	0.76	0.78	0.75	0.68	0.50	0.43	0.71	0.78	0.74	0.49	0.63	0.70	0.74	0.74	0.75	0.70	0.73	0.83	0.47	0.64	0.45	0.75	0.71		1.00
% < 63um		0.97	0.96	0.65	0.92	0.71	0.97	0.72	0.32	0.70	0.99	0.99	0.99	0.97	0.32	0.33	0.99	0.96	0.99	0.33	0.94	0.94	0.97	0.97	0.94	0.95	0.97	0.86	0.79	0.92	0.63	0.98	0.98	0.50	0.80

n = 27, significant at p = 0.01 (>0.487)

Figure 5-5 Correlation matrix for the Arkona Basin metal data set detailing significant correlation at 99% confidence, r = 0.487

The following Figures 5-6 to 5-9 show plots of both principle component 1 versus principle component 2 and also pc1 versus pc3 which together account for the majority of the variations. Following the figures are short bullet point summaries of the plots and associations.

ODAS Tonne

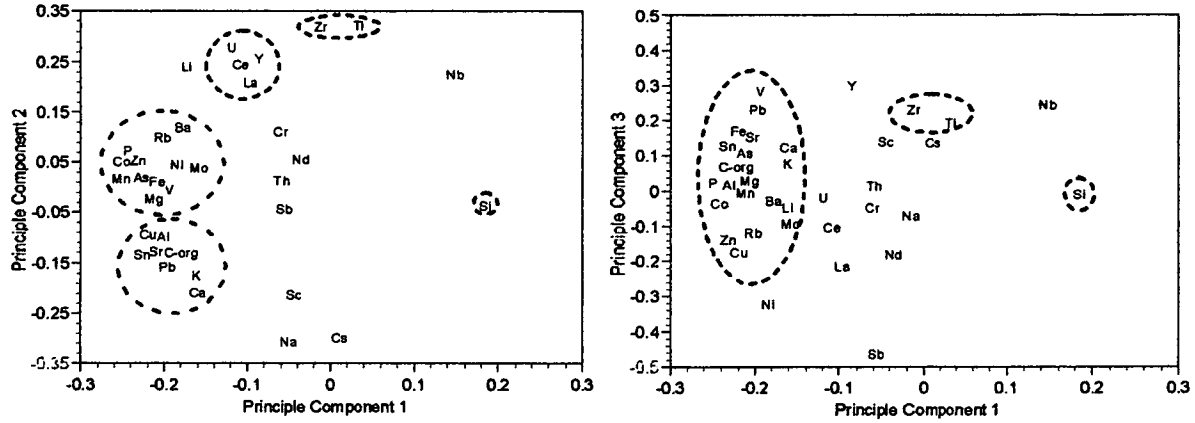

Figure 5-6 Principle Component Analyses for ODAS Tonne (3 components account for 72% of the variation).

- PC1 versus PC2 accounts for 62% of the variation.
- PC1 versus PC3 accounts for 51% of the variation.
- In total PC1 to PC3 accounts for 72% of the variation.
- Zr and Ti are found in close proximity in both plots relating to placer-type deposits.
- A rare earth element cluster can be seen in PC1 Vs PC2 comprising U, Ce. Y and La.
- Two groups of heavy metals are shown in PC1 Vs PC2, one associated with C-org, and the other in the vicinity of the redox sensitive elements of Fe, Mn and Mo.
- However, these two groups amalgamate in the second plot into one large group showing a degree of similarity between the heavy metals.
- In both plots silica has a unique position, separate from the main bulk of the elements possibly relating to its chief role as a dilutant within quartz and its disassociation from the other elements

Nord-Perd Rinne

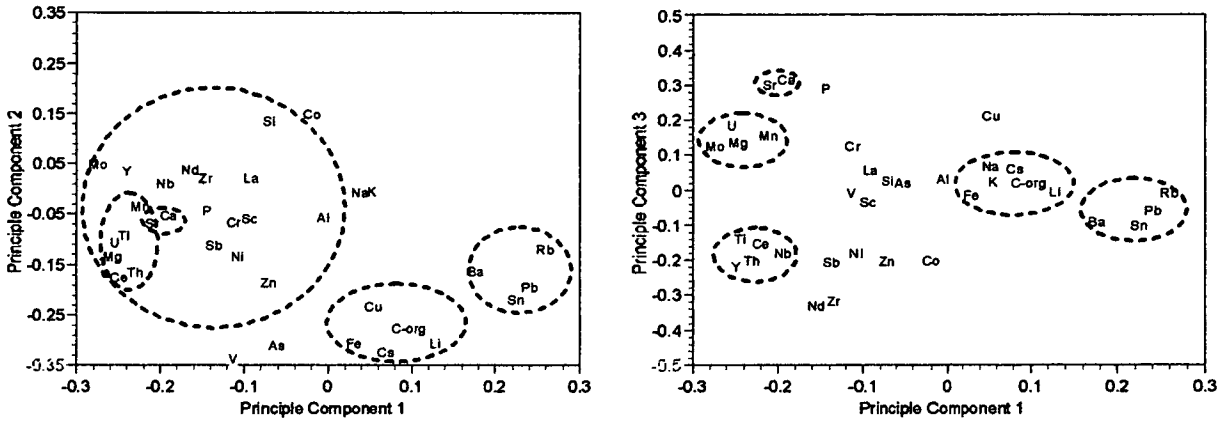

Figure 5-7 Principle Component Analyses for Nord-Perd Rinne (3 components account for 60% of the variation).

- PC1 versus PC2 accounts for 46% of the variation.
- PC1 versus PC3 accounts for 41% of the variation.
- In total PC1 to PC3 accounts for 60% of the variation.
- Nord Perd has the broadest distribution of elements with the lowest degree of correlation of all the stations, therefore a general approach has to be utilised.
- PC1 Vs PC2 shows only two distinct groupings with one further large agglomeration of metals, PC1 Vs PC3 then help to separate out the variations in this group.
- Redox sensitive Mn appears to be related to Mo, U and Mg.
- Ca and Sr show very similar relative positions.
- Pb, Sn, Rb and Ba plot in similar positions on both graphs.
- Organic carbon is associated with Fe, Cs and Li
- Unlike Tonne, silica does not show a distinct position from the rest of the metals.
- Ni and Zn are found in close proximity for both plots.

Tromper Wiek

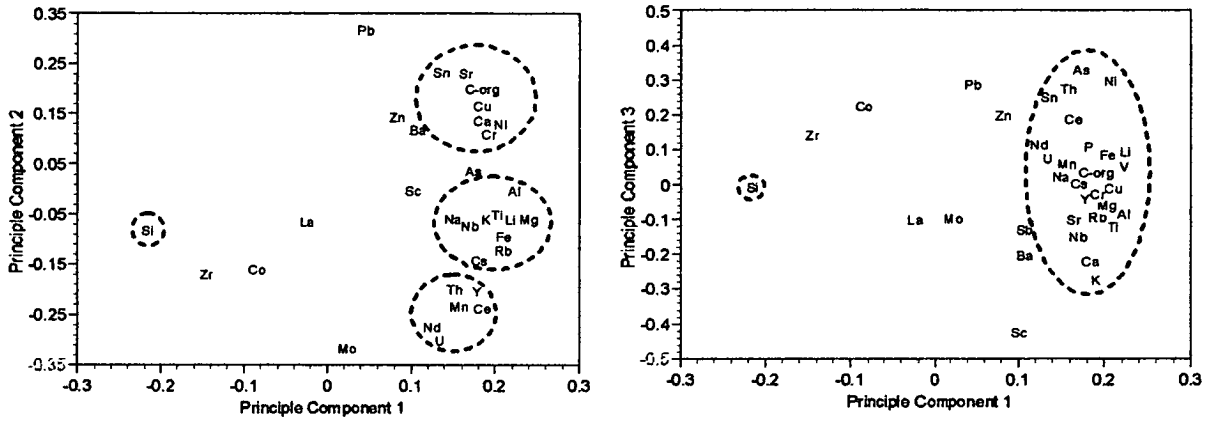

Figure 5-8 Principle Component Analyses for Tromper Wiek (3 components account for 81% of the variation).

- PC1 versus PC2 accounts for 72% of the variation.
- PC1 versus PC3 accounts for 62% of the variation.
- In total PC1 versus PC3 accounts for 81% of the variation.
- The two plots are remarkably similar especially in the heavy metal region which indicates that the data plot in the same eigenvector space around the three axes. The differentiating axes in the groupings is that of the PC1 versus PC2 plot.
- PC1 versus PC2 illustrates three possible groupings, the first of which shows the association between C-Org, Ca, Sr, Cu and Ni.
- The second consists of major and lithogenic elements, Al, Ti, Li, Rb, Cs, Mg, K and redox sensitive Fe.
- Mn then plots in the third group along with U, Th, Y and Ce.
- Silica plots once again as an outlier to the rest of the data set.
- There is a possible tentative correlation between Pb and Zn plotting just outwith the main group of metals.

Arkona Basin

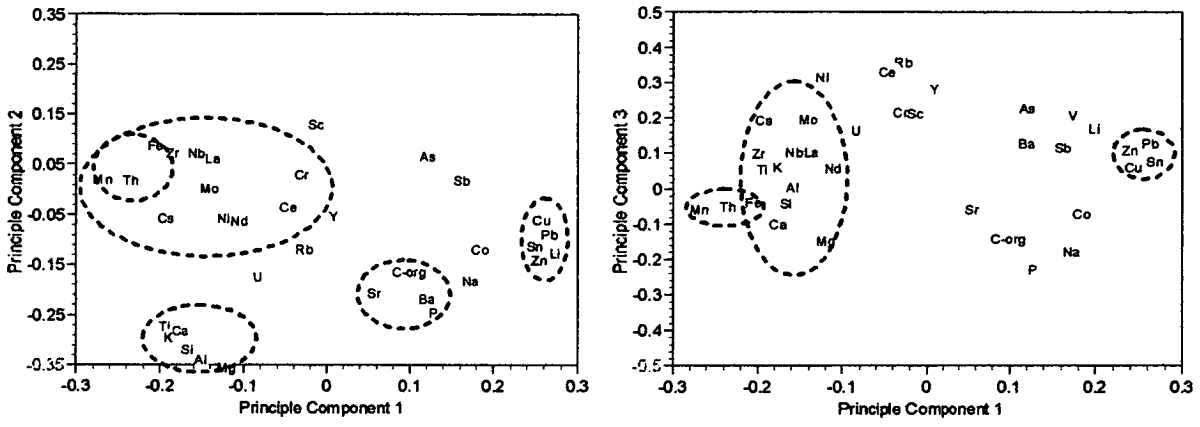

Figure 5-9 Principle Component Analyses for Arkona Basin (3 components account for 60% of the variation).

- PC1 versus PC2 accounts for 50% of the variation.
- PC1 versus PC3 accounts for 46% of the variation.
- In total PC1 to PC3 accounts for 60% of the variation.
- The two plots show a number of discernible groups of elements with each plot having almost equal weighting.
- Both plots show a grouping of the redox sensitive metals Mn and Fe along with Th.
- PC1 versus PC2 show a grouping of Ti, Ca, Si, Al, Mg and K which are the main elemental components in aluminosilicates which are the main constituents of the Arkona Basin.
- PC1 versus PC2 shows C-Org plotting along with Ba, Sr and P but this is not as clear in PC1 versus PC3.
- The heavy metal contaminants of Pb, Zn, Cu and Sn plot very clearly as a group in both plots.

Therefore, in summary the main findings of the initial investigations using statistical analyses show the main following generalisations:

- Three principle components account for a significant amount of the elemental variation for all of the stations
- Heavy mineral geochemistry is only significant at the near-shore station of Tonne.
- In contrast to this aluminosilicate assemblages are only clearly significant at the deepest station of Arkona.
- Associations with redox sensitive metals are common throughout the station transect with Mn dominating at the shallower stations but only at Arkona is there a close correlation between Mn and Fe.
- The heavy metals Pb and Sn often show close similarities and at the Arkona station an association with Cu and Zn is found.
- U and Ce are generally found in close proximity across all stations.
- C-org is often found in close association with Sr and Ba ±Ca.
- Silica generally plots apart from the rest of the metals and this probably relates to its ubiquitous, inert presence as quartz in terms of biogeochemical processes.

5.2 SEDIMENT CORE INORGANIC GEOCHEMISTRY

The following section examines the elemental distributions in terms of total bulk metal geochemistry and total bulk normalised metal geochemistry. The sediment core geochemistry is divided into four groups; those of lithogenic (aluminosilicate and clay geochemistry), diagenetic geochemistry, anthropogenic geochemistry and finally biogenic geochemistry.

5.2.1 Lithogenic Geochemistry

According to GOLDBERG, 1954 the lithogeneous components are defined as those that originate from land erosion, from submarine volcanoes or from underwater weathering in which the solid phase does not undergo any major change on release into the water column. While this definition allows for wide range of solid products

perhaps quantitatively the most important are clay minerals, quartz and feldspars and in turn the most important elemental contributors are Si, Al, Fe, Mg, K. In addition there are a group of elements differentiated by physical hydrodynamic processes that are collectively known as placer deposits and these primarily include ilmenite, rutile and zircon containing Zr and Ti. It has been shown previously in 4.1.5 that Rubidium can be used as a suitable normalising agent and that it has a strong covariance with the lithogenic elements and hence will be used here to exclude dilution effects. The following section will consider this detrital geochemistry by first investigating the distribution of the heavy minerals and then proceeding with aluminosilicate and clay geochemistry.

5.2.1.1 Heavy Mineral Geochemistry

Titanium and Zirconium

Both titanium and zirconium are considered to reside exclusively within terrigeneous phases with titanium usually in the oxide form of ilmenite, rutile or anatase (RANKAMA and SAHAMA, 1950; CHESTER and ASTON, 1976; MURRAY and LEINEN, 1996). In addition titanium can also be found outwith the lithogenic phases in the form of hydrogenous precipitates and also in a biogenic form. However, as average shale values for titanium and zirconium are approximately 4,500ppm (Ti/Rb = 32.1) and 180ppm (Zr/Rb = 1.29), respectively, and as there are a lack of abnormal ratios and a large lithogenic load into the Baltic Sea, then these other phases can be considered negligible.

The total and normalised ratios for both elements are shown in Figure 5-10 which illustrate two contrasting elemental roles. Titanium shows a concentration range from 414 ppm to 5136 ppm that is relatively constant down core and increases markedly from Tonne to Arkona. Hence, titanium does not show an increase in concentration at the shallower sites as might be expected if there was a heavy mineral accumulation. In contrast to this, zirconium concentrations range from 41 ppm to 658 ppm with the highest concentrations found at the intermediate water depth sites. While Tonne and Arkona have relatively constant variations down core

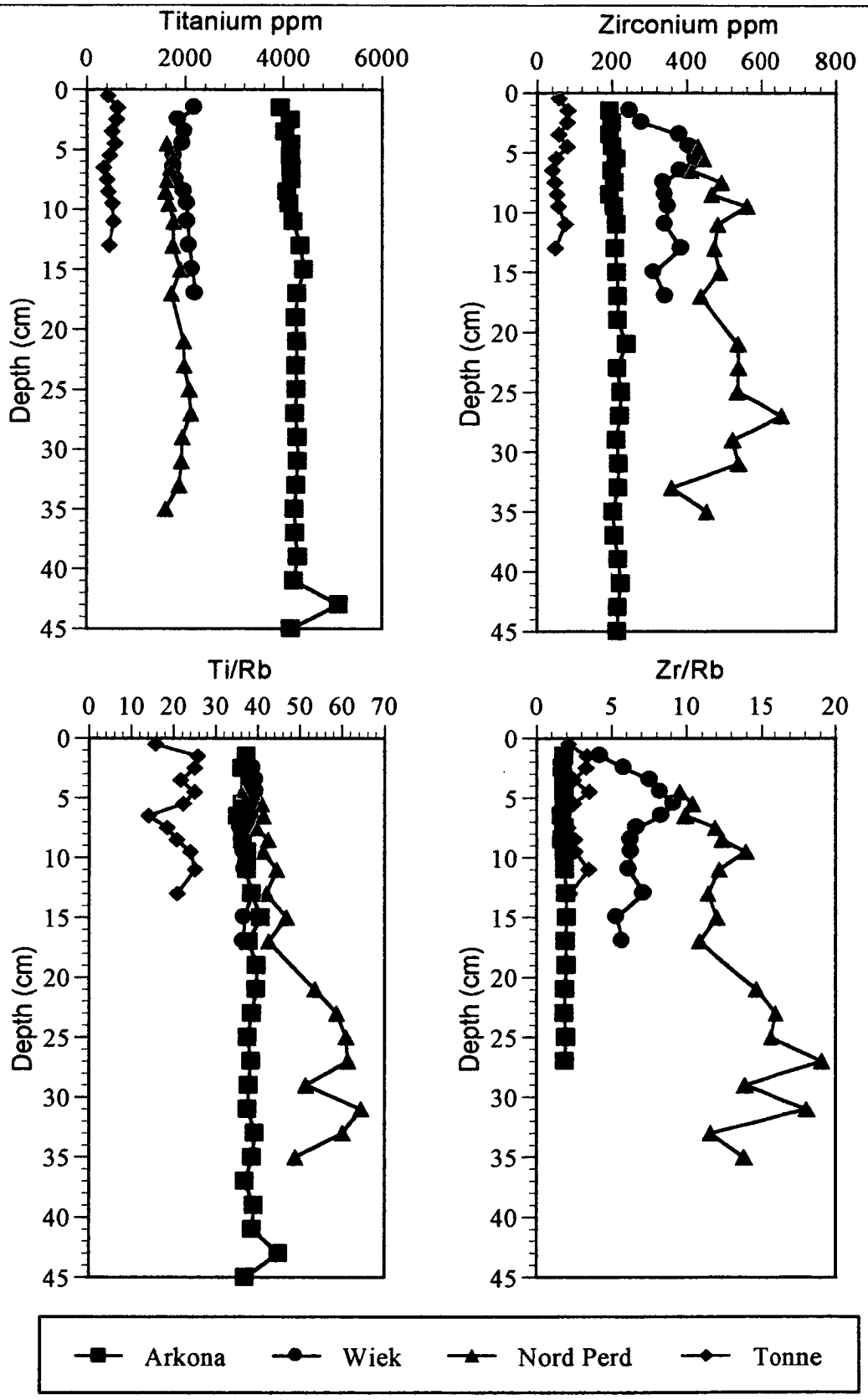

Figure 5-10 Total and Normalised Ti and Zr values for the four BASYS stations

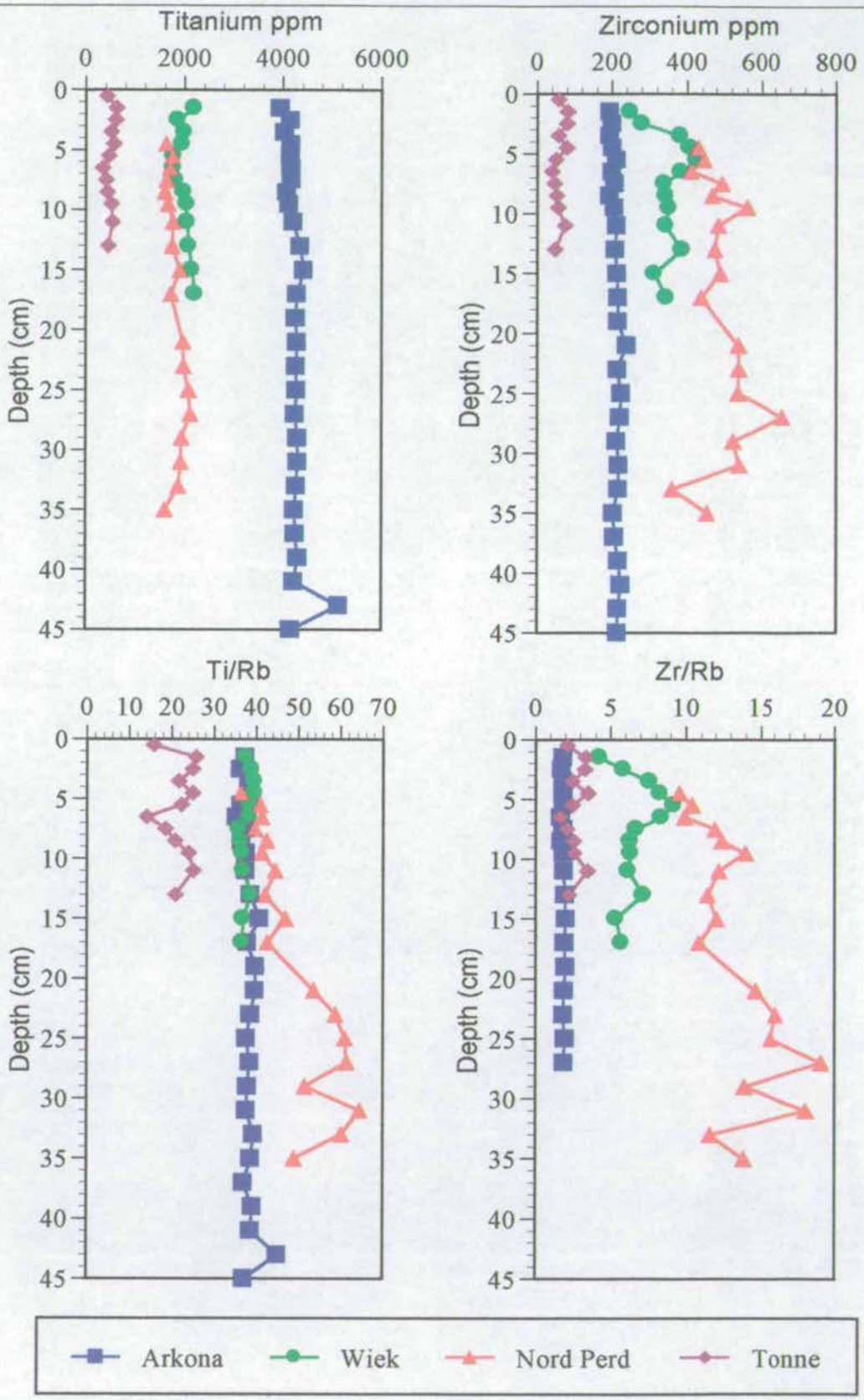

Figure 5-10 Total and Normalised Ti and Zr values for the four BASYS stations

the elevated concentrations found at Nord-Perd and Wiek vary down core. The titanium ratio values show the effect of dilution by quartz as the ratios of the three deepest sites approach a uniform ratio value of 39, at least over the top 17cm. Meanwhile Tonne has a lower, variable ratio which mirrors that of the total titanium concentration and therefore probably relates to a variable titanium input. The deficiency in titanium at Tonne may relate in part to the non-occurrence of heamatite at Tonne in that the titanium may be transported through the Tonne site and onward where the occurrence of heamatite (Fe_2O_3) and its common association with ilmenite ($FeTiO_3$) at Nord-Perd and Wiek allows its preservation. In addition the lack of a typical titanium profile may also relate to the predominantly sedimentary strata of the southern Baltic Sea, which does not contain the igneous bodies that titanium oxides are commonly associated with. The titanium would probably therefore be primarily lattice bound and/or of an authigenic origin which would additionally be subjected to hydrodynamic sorting.

The zirconium to rubidium ratio shows the near constant ratio values of approximately 2 (Av. Shale = 1.29) for the shallowest and deepest sites but the significantly higher ratios (an order of magnitude higher at 20) at Nord-Perd and Wiek. The zirconium data probably relates to a true heavy mineral deposit at these sites of intermediate energy (wind, wave and current) as both the concentrations of the total and the metal ratios are consistently higher.

The lower values of both titanium and zirconium and the statistically derived close correlation of the two at Tonne may be a result of the high-energy environment and the strong wind-induced bottom water currents that develop at this site leading to the progressive movement distal of the heavy minerals. Both titanium and zirconium show a down core increase in their respective ratios at Nord-Perd, which as the rubidium profile is constant down core, has to relate to an increase in titanium and zirconium and may in turn relate to changes, over time, in the terrigeneous input to this site. Given that both zirconium and rubidium show little change under variable redox conditions then this corroborates the idea of a change in terrestrial input over time.

The amount of excess zirconium that is unsupported by the structurally bound detrital terrigenous fraction can be calculated by reference to Equation 5-1.

Equation 5-1

$$Zr_{excess} = Zr_{total} - (Rb_{sample} \times (Zr/Rb_{Av.\ Shale}))$$

This gives a maximum value of excess for the Nord-Perd site of 614 ppm or 93% at 27cm depth.

5.2.1.2 Aluminosilicate and Clay Geochemistry

Silicon

Silicon is partitioned between two phases, that of a terrigenous origin and that involved in the biogenic phase as opaline silica. The silica in the terrigenous phase primarily consists of that combined in the mineral lattice sites of clay minerals and feldspars as well as free quartz. The distribution of silica and aluminium in all the sediment samples is shown in Figure 5-11 in which a strong negative correlation is found detailing a dominantly quartz (proximal) to clay (distal) rich system.

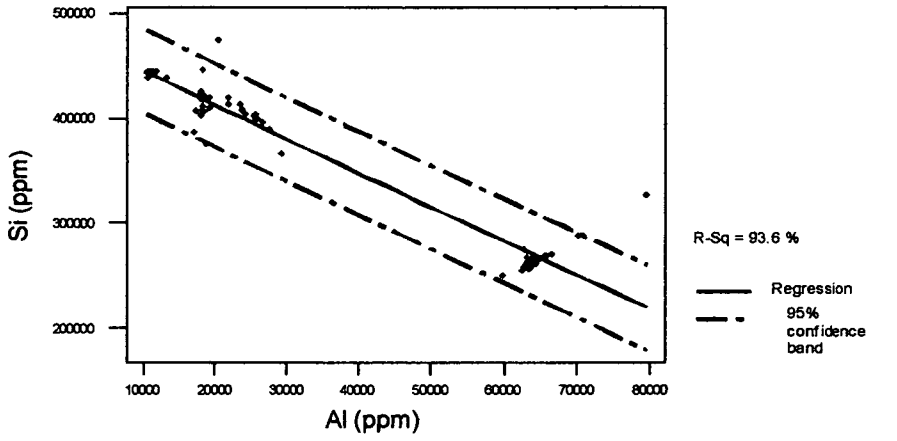

Figure 5-11 The correlation between silica and aluminium for the four Baltic stations

In addition if the data from Arkona is plotted as shown in Figure 5-12 then this can help in determining the relative importance of the respective phases.

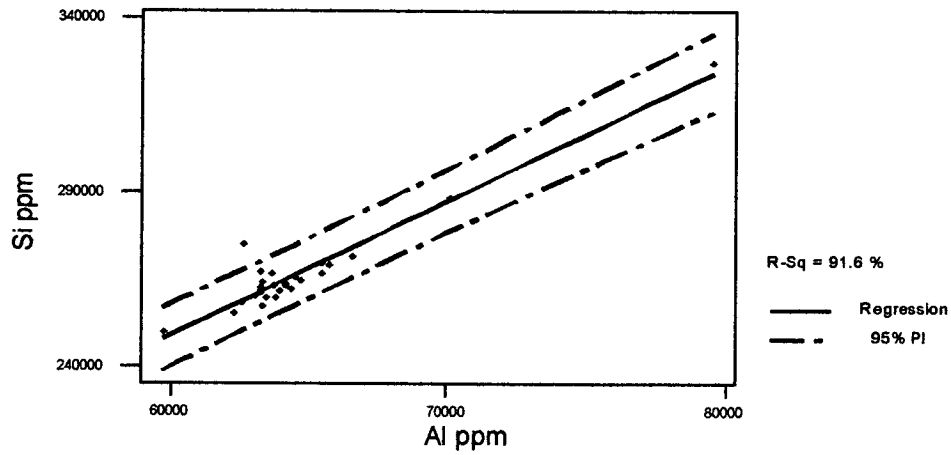

Figure 5-12 Correlation between silica and aluminium for the Arkona Basin

In order to determine the relative magnitude of the terrigenous and biogenic phases, smear slides were examined at all four stations. It soon became apparent that there was very little evidence of siliceous organisms such as diatoms in the sediment and instead they where chiefly found to be composed of glacial detrital material. As expected high quartz contents were found at Tonne with an increase in the percentage of silt and clay in Arkona. In addition to this the Si/Al ratio at Arkona was approximately 1:4 which is consistent with the Si/Al ratio found in clays and feldspars.

As there is a negligible source of silica of biogenic origin then, as has been shown by the XRD traces and Figure 5-11, the high silica, low aluminium values found at Tonne must be present as free quartz and this is evident from the smear slides. In contrast Figure 5-12 shows a typical silica/aluminium plot for Arkona which is characteristic of a fine grained sediment and here the clays may be diluted by a third component (organic matter and diagenetic phases).

The normalised silica plot against rubidium in Figure 5-13 shows a general increase in the ratio down core, particularly at Tonne which could either be a function of an increase in free quartz or an increase in the relative proportion of the silicate minerals present.

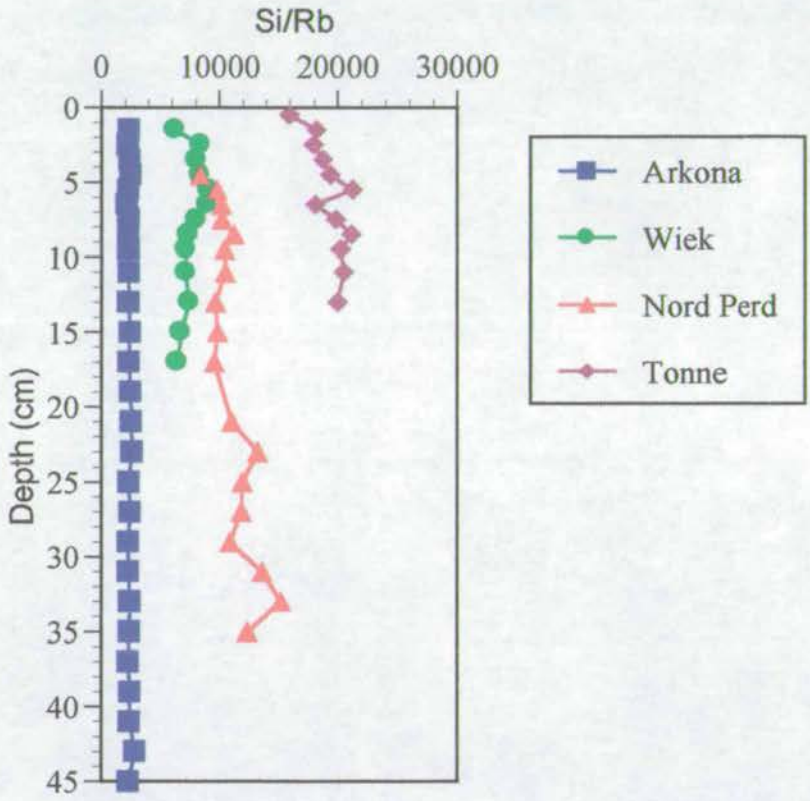

Figure 5-13 Normalised Silica plot for Tonne, Nord Perd, Wiek and Arkona.

Aluminium, Potassium and Rubidium

Aluminium, potassium and rubidium show similar concentration profile characteristics and hence normalised profiles relative to rubidium as shown in Figure 5-14. The concentrations for aluminium range from around 10,000 ppm for Tonne upto 62,000 ppm for Arkona, potassium ranges from 7000 ppm to 25,000 ppm and rubidium ranges from 25 ppm to 110 ppm for Tonne to Arkona respectively. The ratio values are relatively constant down core and cluster in a narrow range with only Nord-Perd showing a variation which is a function of a change in rubidium concentration.

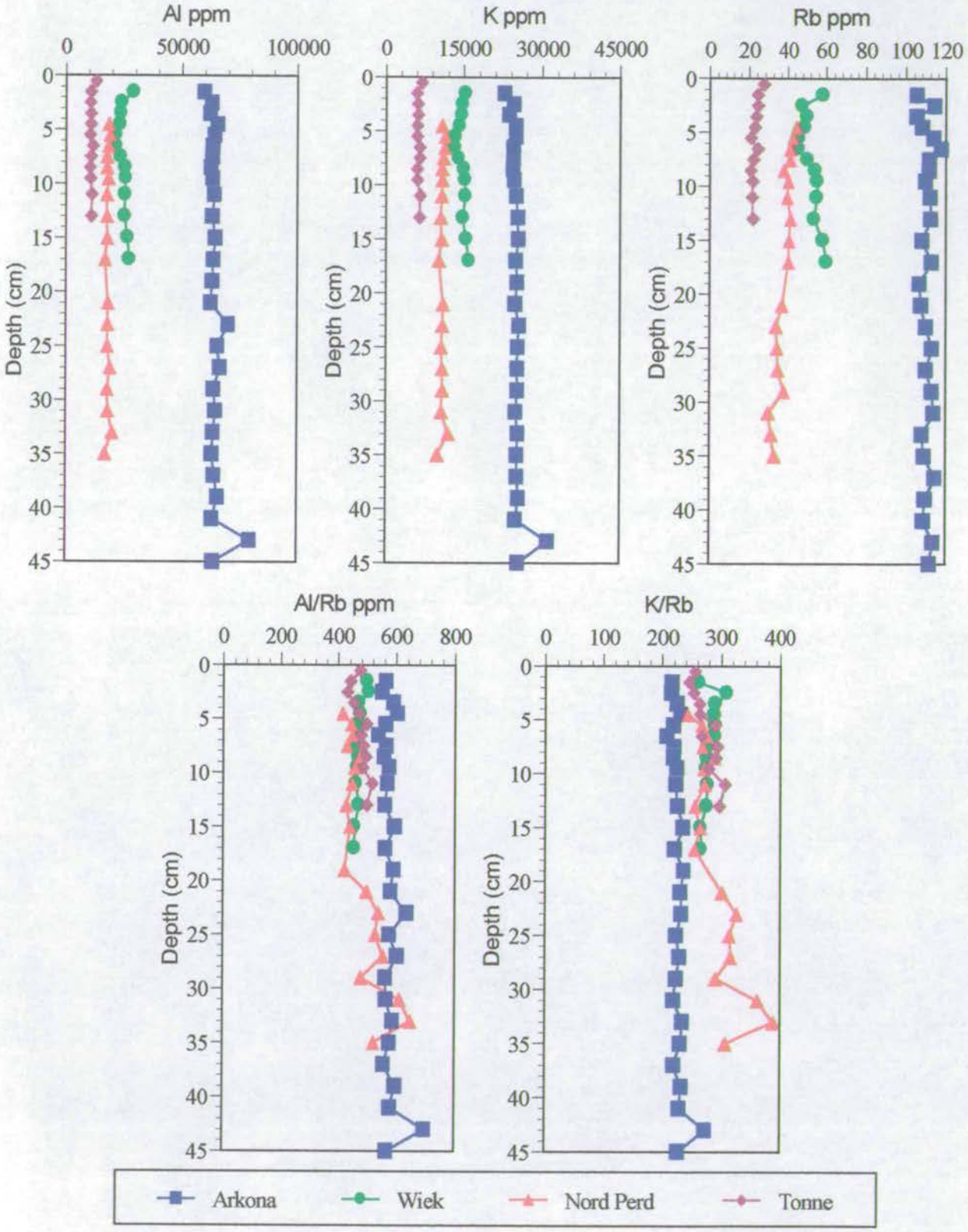

Figure 5-14 Total concentration and normalised elemental ratios for the four Baltic stations.

The ratio for all the major elements are shown in Table 5-1 in which they are compared to values for average shale. As expected the Arkona Basin shows the closest correlation to average shale but with a greater silica contribution. The close correlation between these three elements is predominantly due to their incorporation with relatively fixed ratios into mineral lattice sites, aluminium as an integral part of the aluminosilicate structure and potassium as a common component in certain clay minerals and feldspars such as illite, chlorite, and the alkali group of feldspars. The narrow range of ratio values may be taken as an indication of the consistency between stations in the amount of alkali feldspars present within the sediment cores.

Table 5-1 Station elemental ratio comparison with average shale values (taken from Turekian and Wedepohl, 1961.

Station		Si/Rb	K/Rb	Mg/Rb	Fe/Rb	Al/Rb
Tonne	Min.	15999	246	10	62	432
	Av.	*19314*	*276*	*14*	*80*	*478*
	Max.	21276	307	19	94	518
Nord-Perd	Min.	8410	243	26	147	416
	Av.	*11163*	*293*	*43*	*179*	*490*
	Max.	15272	389	75	219	650
Wiek	Min.	6272	263	38	131	457
	Av.	*7690*	*281*	*56*	*175*	*473*
	Max.	9106	309	78	231	507
Arkona	Min	2208	209	112	275	539
	Av.	*2403*	*227*	*125*	*327*	*582*
	Max.	2873	274	160	384	699
Turekian & Wedepohl (1961)		*1700*	*178*	*100*	*335*	*657*

Iron and Magnesium

The major elements of iron and magnesium also show marked similarities in their normalised ratios with the highest ratios in the organic and clay rich sediments of the deep water station of Arkona. The profiles are displayed in Figure 5-15 and show down core Mg/Rb and Fe/Rb ratio increases for all stations as well as generally elevated surface layers ratios. On average the Mg/Rb ratio ranges from 14 at the shallow station increasing to 125 for the deepest Arkona Basin station, likewise the Fe/Rb ratio increases on average from 80 at Tonne to 327 in Arkona. Unlike the K/Rb and Al/Rb ratios there is a progressive increase in the normalised Fe and Mg values from Tonne to Arkona which probably represents the incorporation of Fe and Mg into the chlorite clay mineral lattice.

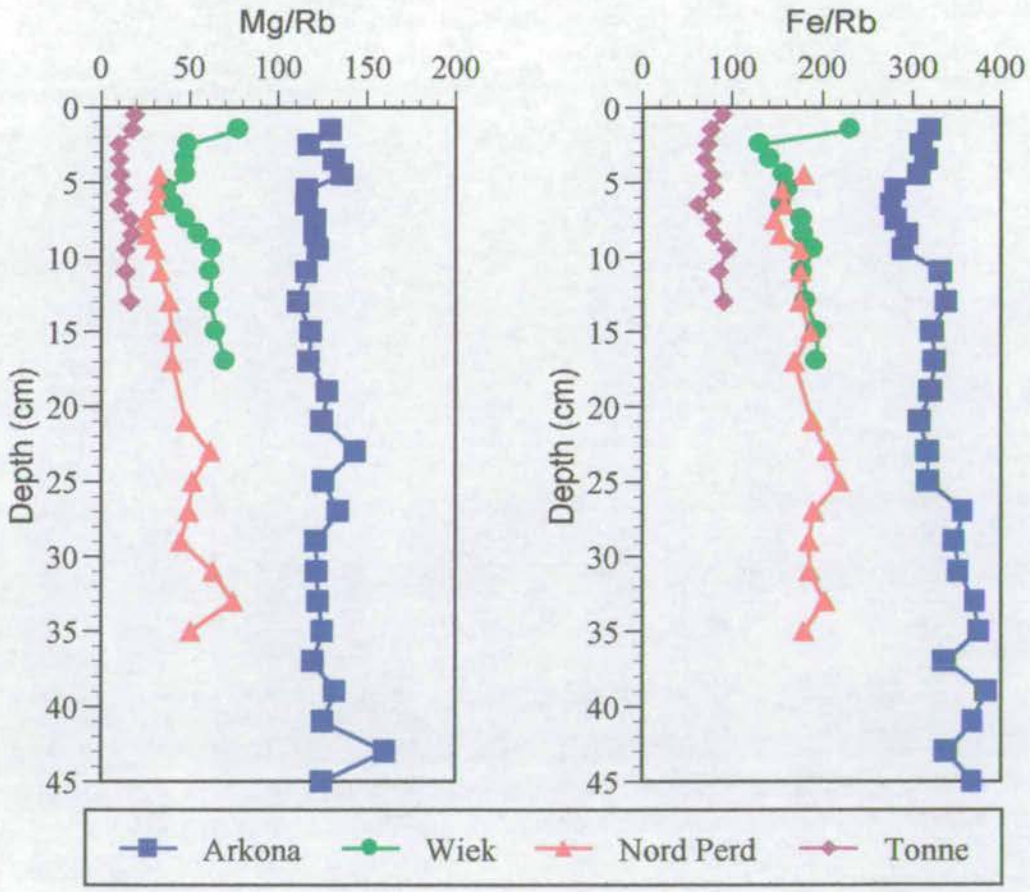

Figure 5-15 Iron and magnesium down core profiles for Arkona, Wiek, Nord-Perd and Tonne

The elevated surface layer ratios found especially in the Fe/Rb profile may represent a significant presence of oxyhydroxides thus increasing the iron concentration at the surface, but due to diagenetic recycling, showing a lower ratio in the sub-surface layers. In addition as Si/Rb as well as Mg/Rb and Fe/Rb show an increase in ratio with depth and organic carbon remains constant over the majority of the core (Figure 4-17) then this may be interpreted as an increase in the clay component down core. As many studies have shown that clay minerals are mainly of a detrital origin and that they reflect the composition of the source area, then variations in the ratios down core may reflect changes in the rate of supply of these clays to the basinal environment. In addition to the role of iron in the clay lattice there is the contribution related to its presence in both oxyhydroxide (especially hematite) and pyrite depending on the redox conditions and hence location. While there is no hematite at Tonne, it is found at Nord Perd and Wiek albeit in small concentrations with an increasing relative abundance of pyrite at Arkona. However, because the distribution of both pyrite and heamatite down core is unlikely to be uniform due to diagenetic processes and in view of the relative consistency of the ratio profiles then the majority of iron seems to be incorporated into the clay mineral structure.

5.2.1.3 Clay and Aluminosilicate Summary

- Silica distribution in the Southern Baltic Sea is primarily controlled by the distribution of free quartz and to a lesser extent by the silica locked away in the aluminosilicate and mineral lattices.
- While a few siliceous organisms were observed the overwhelming majority of the silica is of a detrital nature and acts significantly as a dilutant element.
- As expected aluminium is exclusively found in the lithogenic fraction along with rubidium which in this thesis is used as the normalising agent.
- XRD, published literature and corroborative evidence from this chapter point to three main mineral hosts for potassium; the alkali feldspars, illite and muscovite in order of decreasing importance.
- While potassium is mainly enriched in the alkali feldspars, magnesium and iron seem to be associated to a greater extent in the clay fraction, particularly

associated with chlorite and to a lesser extent with heamatite and pyrite depending upon the redox conditions.

- The presence of oxyhydroxides at the surface of the sediment cores could contribute to the increased ratios found particularly for Fe/Rb.
- The majority of the concentration and normalised elemental ratio profiles are constant down core and thereby reflect a stable and constant supply to this region of the Baltic Sea.

5.2.2 Diagenetic Redox Geochemistry

The restricted exchange environment of the Baltic Sea with the North Sea ensures that the majority of the particle reactive and sedimenting species are contained within the boundaries of the sea. Therefore large amounts of anthropogenic metals (Cu, Pb, and Zn) and organics (agricultural runoff, in-situ biological production and sewage products) have the potential to accumulate in the Baltic Sea sedimentary record. It is not, however, solely the concentration of these contaminants and their accumulation rates which dictate the state of the environment. Perhaps the most important of which, aside from bioturbation and trawling, are those processes collectively grouped under the umbrella of post-depositional diagenetic processes. These include a variety of chemical, physical and biological processes that operate at the interface between the sediment and pore water which lead to the formation of new and altered mineral phases and may lead to changes in the composition of the water, especially the pore waters.

The key determining factor in diagenetic processes is that of reduction and oxidation (redox) reactions related to the degradation of organic matter. As the Baltic Sea has a restricted environment in terms of in and outflow to the North Sea, and as there is a large input of nutrients to this environment, then there is a tendency towards eutrophic waters and locally sub- or anoxic sediments in the basinal regions. This has important consequences for biogeochemical recycling as the oxidation state and speciation of the elemental components change; these processes are discussed later in this section. A number of workers including BOSTROM *et al., 1983;* HELCOM,

1988; NEHRING, 1992; HELCOM, 1993; JONSSON and CARMAN, 1994; HELCOM, 1996; have shown a progressive decrease in the water quality of the Baltic Sea over the last century associated with increasingly common periods of anoxia especially in the deeper depositional basins. MATTHAUS, 1995; MATTHAUS *et al,* 1996 have also shown that there has been a decrease in the occurrence of major inflow events to the Baltic from the North Sea which have served to re-oxygenate the water column over recent times. The combined effect of infrequent inflow events and an increase in the nutrient and anthropogenic load to the Baltic Sea has had, and continues to have, important consequences for the water quality and the biota, particularly the benthos of this environment.

As stated previously, sediment core diagenesis is primarily controlled and is a function of the degradation of organic matter, the burial of which and the ensuing microbially-mediated decomposition uses up dissolved oxygen in the water column and pore waters. Upon exhaustion of this supply other oxidants are utilised in a well established order which is dependant upon the thermodynamic free energy released per unit of reactive organic matter (FROELICH *et al.*, 1979, BERNER, 1980; STUMM and MORGAN, 1981; WILSON *et al.*, 1985, SALONEN *et al.* 1995; VAN CAPPELLEN and WANG, 1996). This progressive sequence of reduction is shown in Table 5-2 and typically leads to a depth zonation of electron acceptors and associated reactions in the sediment. It is the disappearance of dissolved oxygen and the onset of sulphate reduction that is generally taken as the boundary between the oxic and anoxic regions and this is termed the redoxcline. The depths to which the oxic zone extends in the sediment is highly variable, ranging from non-existent in some sediments underlying productive continental margins and deep restricted exchange environments to extending tens of metres in slowly accumulating organic poor pelagic sediments (SHIMMIELD and PEDERSEN, 1990).

The sediment cores sampled were of a relatively short depth and the only predominant redox sensitive element profile identified was that of the reduction of manganese (Mn^{4+} to Mn^{2+}) with a smaller signature in the Fe^{3+} to Fe^{2+} transition. The presence of pyrite in the deep water station of Arkona as shown by XRD

indicates that there must be in addition some sulphate reduction and hence a sulphidic environment at least in the deeper regions of the core.

Table 5-2 Oxidation reactions of sedimentary organic matter (adapted from FROELICH *et al.* 1979)

* depending on the mineral form of the oxyhydroxide

Oxidation Reaction	Gibbs Free Energy (ΔG^o) (kJ per mole of glucose)	
Aerobic respiration $(CH_2O)_{106}(NH_3)_{16}(H_3PO_4) + 138\ O_2 \rightarrow 106\ CO_2 + 16\ HNO_3 + H_3PO_4 + 122\ H_2O$	*Oxic*	-3190
Denitrification $(CH_2O)_{106}(NH_3)_{16}(H_3PO_4) + 94.4\ HNO_3 \rightarrow 106\ CO_2 + 55.2\ N_2 + H_3PO_4 + 177.2\ H_2O$	*Sub-Oxic*	-3030
Manganese Reduction $(CH_2O)_{106}(NH_3)_{16}(H_3PO_4) + 236\ MnO_2 + 472\ H^+ \rightarrow 236\ Mn^{2+} + 106\ CO_2 + 8\ N_2 + H_3PO_4 + 366\ H_2O$		-2920 to -3090*
Iron Reduction $(CH_2O)_{106}(NH_3)_{16}(H_3PO_4) + 212\ Fe_2O_3$ (or 424 FeOOH) $+ 848\ H^+ \rightarrow 424\ Fe^{2+} + 106\ CO_2 + 16\ NH_3 + H_3PO_4 + 530\ H_2O$ (or 724 H_2O)		-1330 to -1410*
Sulphate Reduction $(CH_2O)_{106}(NH_3)_{16}(H_3PO_4) + 53\ SO_4^{2-} \rightarrow 106\ CO_2 + 16\ NH_3 + 53\ S^{2-} + H_3PO_4 + 106\ H_2O$	*Anoxic*	-380
Anaerobic Respiration $(CH_2O)_{106}(NH_3)_{16}(H_3PO_4) \rightarrow 53\ CO_2 + 53\ CH_4 + 16\ NH_3 + H_3PO_4$		-350

While the reductive steps in Table 5-2 represent specific reactions the boundaries between the reductive steps do overlap, for instance depending on the lowest redox potential of the reaction and the form of nitrate reduction the coexistence of manganese reduction can also occur (JAHNKE *et al.*, 1982b). As manganese and iron are readily measured using geochemical techniques then these are the two redox indicators have been used for this particular study. The cycling of Mn and Fe in the sediment and overlying water column and their role in controlling trace metal distribution has been extensively described by a number of authors (RIDGEWAY and PRICE, 1987; SHIMMIELD and PEDERSEN, 1990; LAPP and BALZER, 1993; THAMDRUP *et al.*, 1994; SALONEN *et al.*, 1995; BRUGMANN *et al.*, 1997; GLASBY *et al.*, 1997; SLOMP *et al.*, 1997).

The transition metal characteristics of Mn and Fe allow a number of different oxidation states to exist, (2^+, 3^+, 4^+, 6^+ and 7^+) and (2^+ and 3^+) respectively. For simplification, only soluble Mn^{2+}, insoluble Mn^{4+}, soluble ferrous Fe^{2+} and insoluble ferrous Fe^{3+} will be considered here as these are the commonest forms found in the aquatic environment.

As the majority of the Mn and Fe that falls through the southern Baltic Sea water column to ultimately form the sedimentary record is in the particulate oxyhydroxide form then upon burial below the redoxcline, the Mn^{4+} is reduced to Mn^{2+} according to Equation 5-2.

Equation 5-2

Oxidation

$$\mathbf{MnO_x\ (solid\ hydrous\ oxide) \leftrightarrow Mn^{2+}\ (soluble) + O_x}$$

Reduction

In this form Mn^{2+} is soluble and is diffused into the pore water and recycled along a concentration gradient. A fraction of the Mn^{2+} may diffuse downwards while the rest will diffuse up towards the surface whereby the presence of dissolved oxygen will lead to the precipitation of secondary Mn oxyhydroxides and their re-deposition and possible enrichment in the surface sediments. As sedimentation proceeds this second generation of Mn is again buried and the cycle continues. This general scheme of Mn recycling was refined by FROELICH *et al*, 1979 and remains widely cited today. They proposed that the depth of the maximum Mn solid phase concentration was controlled by the limit of downward diffusion of oxygen. In a steady state system the concentration of the solid phase Mn peak will increase until the sedimentary input of reactive Mn is equivalent to the amount being reduced and released into the pore water. Hence this steady state system would show a solid phase peak concentration just above the redox boundary and just above the top of the dissolved Mn^{2+} boundary (DAVISON, 1985) as shown in Figure 5-16. Iron exhibits very similar dissolution and precipitation reactions as manganese but these reactions take

place at lower redox potentials and consequently occur further down the diagenetic sequence.

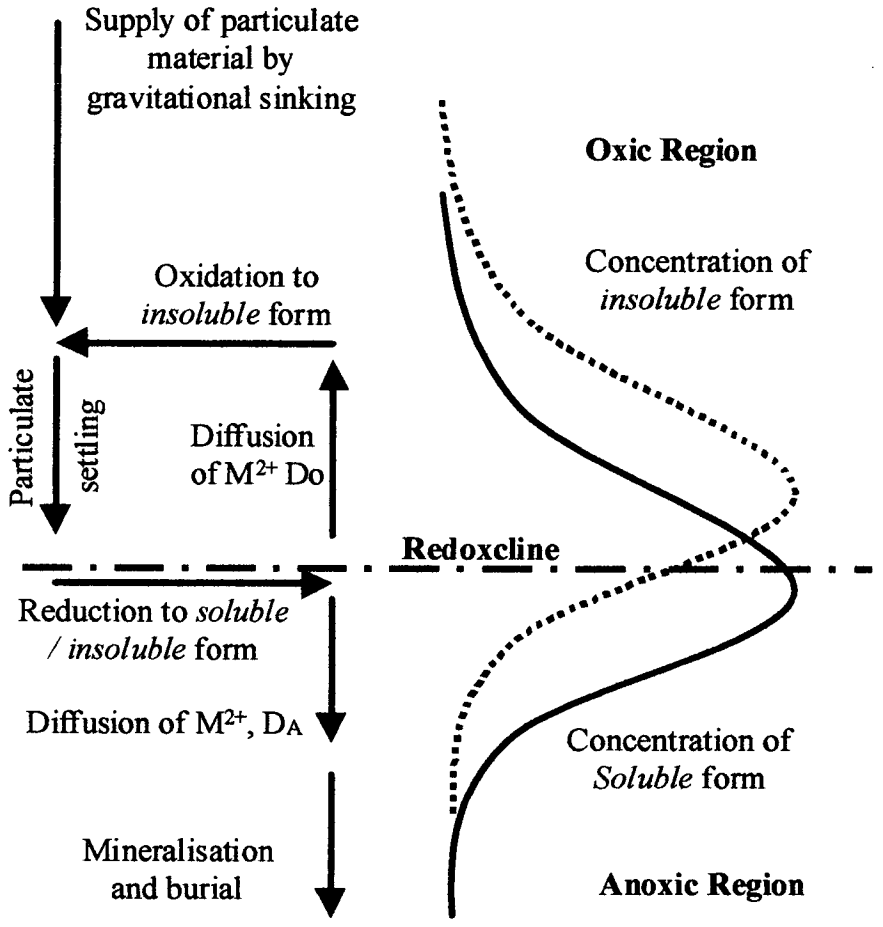

Figure 5-16 A model for Mn or Fe diagenetic cycling at a redox boundary, Do and D_A are diffusion constants, (adapted from DAVISON, 1985).

The position of the redoxcline is migratory in nature and is primarily controlled by the magnitude of the balance between the down column carbon flux, the oxygen consumption and the sediment accumulation rate. Hence in summer after the spring bloom there is a significant increase in the organic carbon flux and the redoxcline moves upwards; conversely in winter when there is little productivity there is a downwards shift.

As Mn and Fe hydroxides are effective scavengers of heavy metals and radionuclides and the sediments act as a repository for trace metals and pollutants then the

sediments themselves could become a potential source of pollutants if there is a change in environmental conditions. Through the natural processes of resuspension or bioturbation and via mans influence in the form of trawling there is the potential for these elements to be released on dissolution of the oxides in the sediment column as shown in Figure 5-17. Hence these events have the ability to redistribute the scavenged elements in a potentially catastrophic release into the sediment pore-water / water column system (BALZER, 1982; FRANCOIS, 1988; SHIMMIELD and PEDERSEN, 1990; PAALMANN *et al.*, 1991; SHIMMIELD, 1991; BRASSARD *et al.*,1994; CHRISTIANSEN and EMELYANOV, 1995; POHL and HENNINGS, 1999).

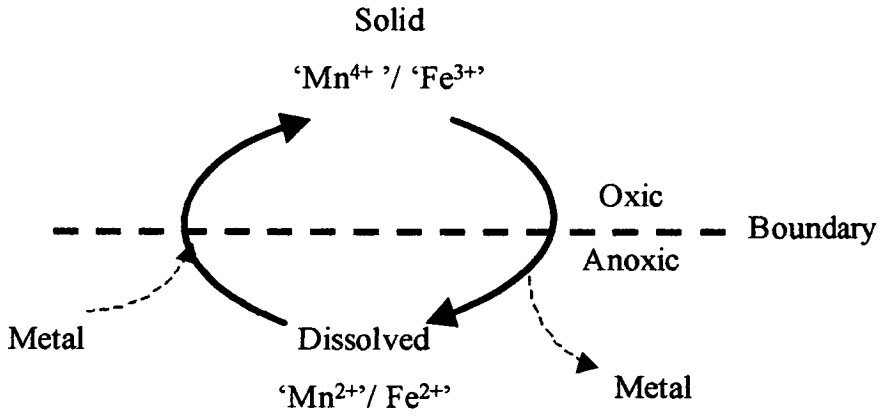

Figure 5-17 Schematic representation of the Mn and Fe redox pathways with metal uptake and release.

While no sediment core nitrate or sulphate measurements were taken on this project and as no pore water measurements were made then inferences on the redox related diagenetic processes have to obtained solely on the basis of the solid sediment metal profiles of iron and manganese. The profiles obtained are shown in Figure 5-18 with the manganese recycling described previously occurring within the upper 9cm of the Arkona Basin core. It is evident that the other stations have a much lower manganese concentration and that Wiek and possibly Nord-Perd shows a similar profile to Arkona. The main components to the Arkona Basin manganese profile are shown on Figure 5-18 with the exhaustion of dissolved oxygen at 1cm thus defining the Mn redoxcline. This is followed by the dissolution of Mn^{4+} and the release of Mn^{2+} into the pore waters. The conversion of sulphate to sulphide at 8cm with a

corresponding increase in sulphide in the pore waters and the combination of this with available iron to initially form monosulphides (BERNER, 1970; LUTHER, 1991; MIDDLEBURG, 1991) and then onwards to the formation of pyrite.

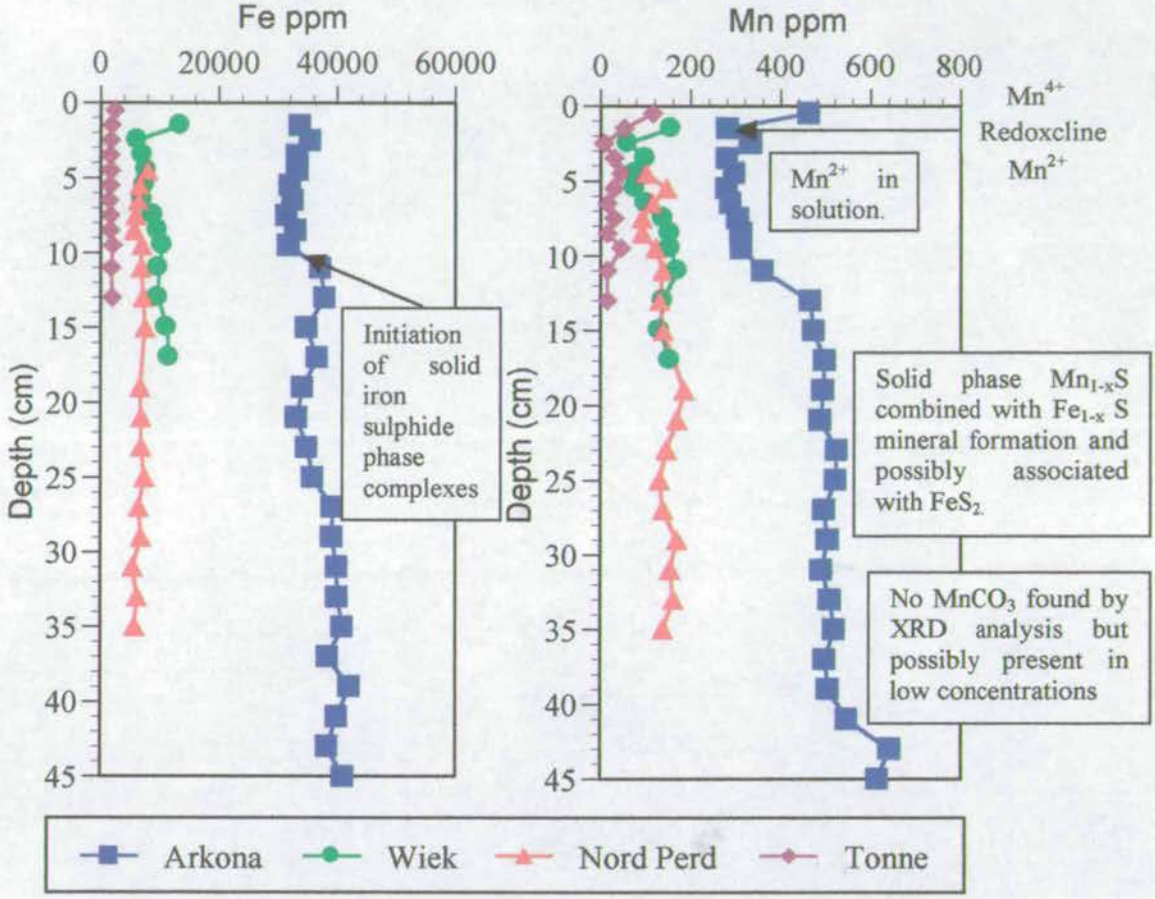

Figure 5-18 Down core profiles of the redox sensitive elements of manganese and iron for Tonne, Nord-Perd, Wiek and Arkona.

Hence the redox cycling previously described is compressed in Arkona into the top 8cm of the core and below this other processes related to sulphate reduction are taking place. There has been extensive work carried out on the forms of iron sulphide, manganese and associated trace metal cycling in the sediment column amongst which GORLICH *et al.*, 1978; KREMLING, 1983; DYRSSEN, 1985; HUERTA-DIAZ and MORSE, 1992; GAGNON *et al.*, 1995; ALONGI *et al.*, 1996; CRUSIUS *et al.*, 1996 are but a few. On dissolution of both Mn^{4+} and Fe^{3+} the

portion that diffuses down core may combine to form monosulphides such as alabandite (MnS), mackinawite (FeS) or amorphous FeS and then onwards to form Hauerite (MnS_2) which is isostructural with pyrite (FeS_2), or depending on the carbonate content of the sediment, to form rhodochrosite ($MnCO_3$). Hence metals that were associated with the oxide forms of iron and manganese have the potential on dissolution to be incorporated in the sulphide phases depending on their sediment core geochemistry. Molybdenum is often cited as a redox sensitive element (MALCOLM, 1985; SHIMMIELD and PEDERSEN, 1990; HELZ *et al.*, 1996) and is shown along with As as they both have a similar profile for Arkona as shown in Figure 5-19.

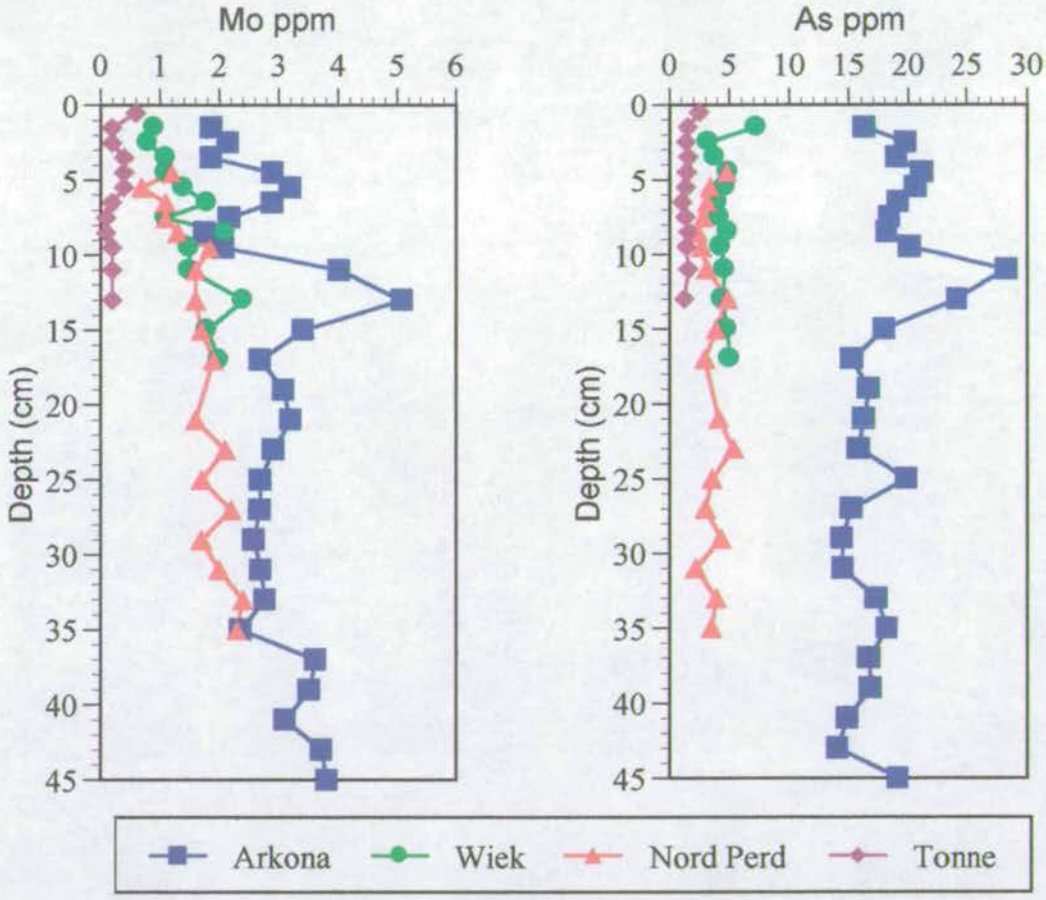

Figure 5-19 Mo and As concentration profiles for Tonne, Nord-Perd, Wiek and Arkona

The main exception to the similarity between the two elements is that for Nord-Perd, Wiek and Arkona there is a definite increase down core in Mo concentrations. As only solid phase data has been obtained then the following inferences are at best

tentative and are solely derived from the solid phase profile and from literature rather than quantitative solid, pore water and speciation evidence.

The two main Mo and As peaks coincide with the onset of Mn and Fe sulphide complexes. There have been several mechanisms proposed to explain Mo distributions in anoxic sediments including the association with iron and manganese oxides (BERTINE, 1972; PEDERSEN, 1979; SHIMMIELD and PRICE, 1986; ALONGI *et al.*, 1996), complexation with organic matter (BRUMSACK and GIESKES, 1983) and remobilization / uptake during organic matter decomposition (CONTRERAS *et al.*, 1978; MALCOLM, 1985; EMERSON and HUESTED, 1991, MCNEILL and SHIMMIELD, 1991). The constancy of the organic carbon profile in Figure 4-17 indicates that in this particular instance, the initial uptake and remobilization of both Mo and As near the sediment-water interface is associated with manganese and iron redox processes. According to MANHEIM, 1961; EDENBORN *et al.*, 1986; HUERTA-DIAZ and MORSE, 1992 sedimentary pyrite is an important sink for both As and Mo. However, as only Mo increases with depth then it would seem from these findings that only Mo is incorporated to a significant extent within the pyrite structure. The main peak at 12-14cm depth may be explained, in contrast to previous ideas pertaining to the emphasis on scavenging related to the reduction of Mn^{4+} to Mn^{2+}, to the role of covalent bonds formed between Mo and transition metals via S bridges as described by HELZ *et al.*, 1996. Furthermore, while the initial uptake of Mo and As is by manganese and iron monosulphides, the major peak at 12-14 cm depth could relate to the expulsion of Mo and As from the $Mn_{1-x}S$ / $Fe_{1-x}S$ sites as a precursor to MnS_2 / FeS_2 development as proposed by MORSE and ARAKAKI, 1993 for the incorporation of Cu, Ni and Co into mackinawite.

Thus the sampling stations described here in the southern Baltic Sea represent a wide range of environments in terms of redox processes. These in part relate to the energetics, organic matter content, sediment accumulation rate and the increasing salinity and associated sulphate levels with water depth. As the above profiles are a 'snap shot' in time it is important to recognise that not only will the redoxcline

migrate with changes in organic carbon content but it will also move due to inflow events which may replenish and re-oxygenate the bottom water altering the redox equilibrium in the sediment core and potentially leading to the release of trace metals into the bottom waters.

5.2.3 Metal Geochemistry

A great deal of work has been carried out on anthropogenic metals and their role in the southern Baltic Sea ecosystem amongst which SUESS and ERLENKEUSER, 1975; SZEFER and SKWARZEC, 1988; SZEFER, 1990; HELIOS-RYBICKA, 1992; BORG and JONSSON, 1996; NEUMANN *et al.*, 1996; SZEFER *et al.*, 1996; SZEFER *et al.*, 1998 are but a few.

The most commonly cited anthropogenic metals within the literature are Pb, Cu, and Zn which in part relate to the large scale mining and metallurgical industries of these elements in the upper regions of the river Oder. In addition there is a substantial coal mining industry in the western part of Poland which could release radioactive elements such as uranium and radium into the aquatic environment. These economic industries are shown in Figure 5-20 which is taken from HELIOS RYBICKA, 1996. From Figure 5-20 it is obvious that there is substantial industrial activity within the watershed of the River Oder and hence any pollutants that are released into the aquatic environment have the potential to reach the southern Baltic Sea providing that they pass the large number of natural 'filters' in the way including the Bodden and Haffs of the Oderhaff lagoon.

The following section is split into three parts defined as follows:

1) Those elements that show a marked increase in near surface concentrations and a marked increase in normalised ratio near surface values.
2) Those elements that show elevated but constant down core concentrations at Arkona compared to Tonne and similar profiles when normalised.
3) Those elements that show relatively constant ratios for all stations when normalised.

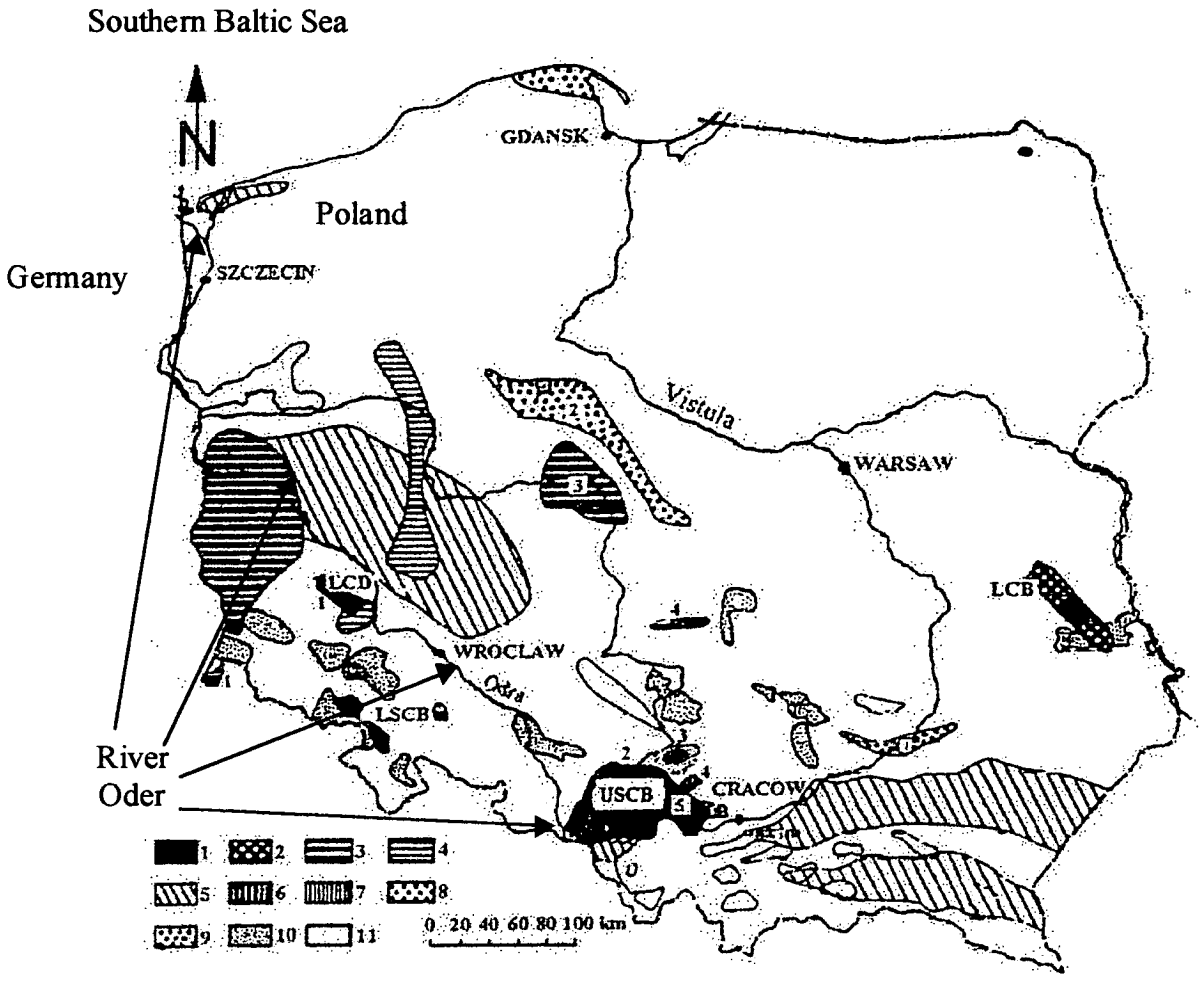

Fig. 1. Occurrence of principal mineral raw-materials in Poland (Kozłowski, 1983). Hard coal districts: 1, operating; 2, designed. Brown coal districts: 3, operating; 4, designed (1, Turoszów; 3, Konin; 4, Bełchatów). 5, petroleum and gas districts. Metallic ore districts: 6, operating; 7, designed (1, copper; 2, 3, 4, 5, Pb–Zn). Chemical raw material districts: 8, operating; 9, designed (1, sulphur; 2, 3, rock-salt). Industrial stones: 10, operating; 11, designed.

Figure 5-20 Occurrence of mineral raw materials and related industries in Poland, taken from HELIOS RYBICKA, 1996.

1) Elevated near surface concentrations and normalised ratio values:

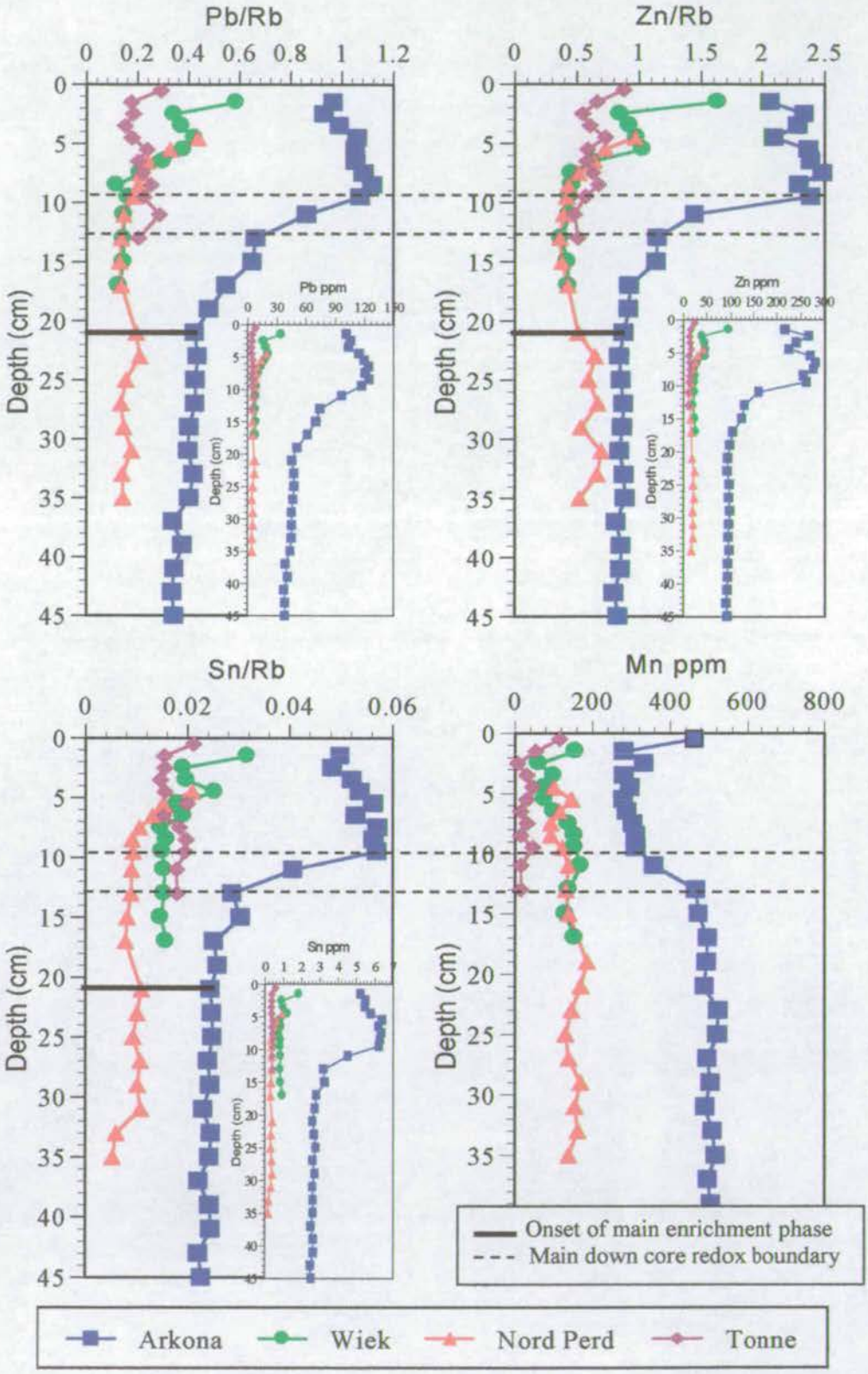

Figure 5-21 Elevated near surface concentrations shown by Pb, Zn and Sn for the four Baltic Sea stations with Mn as a reference profile.

2) Elevated concentrations at Arkona compared to Tonne and similar profiles when normalised.

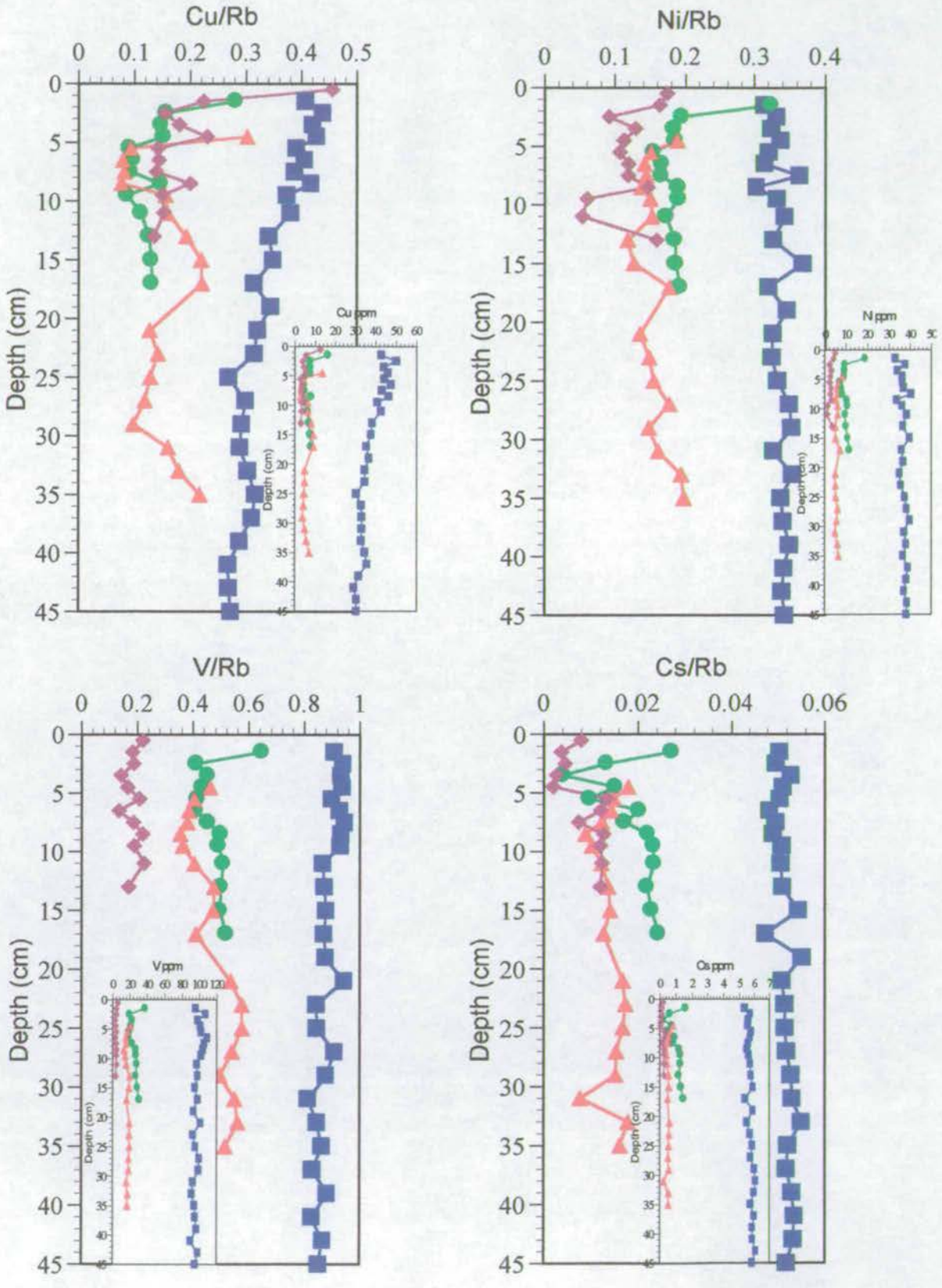

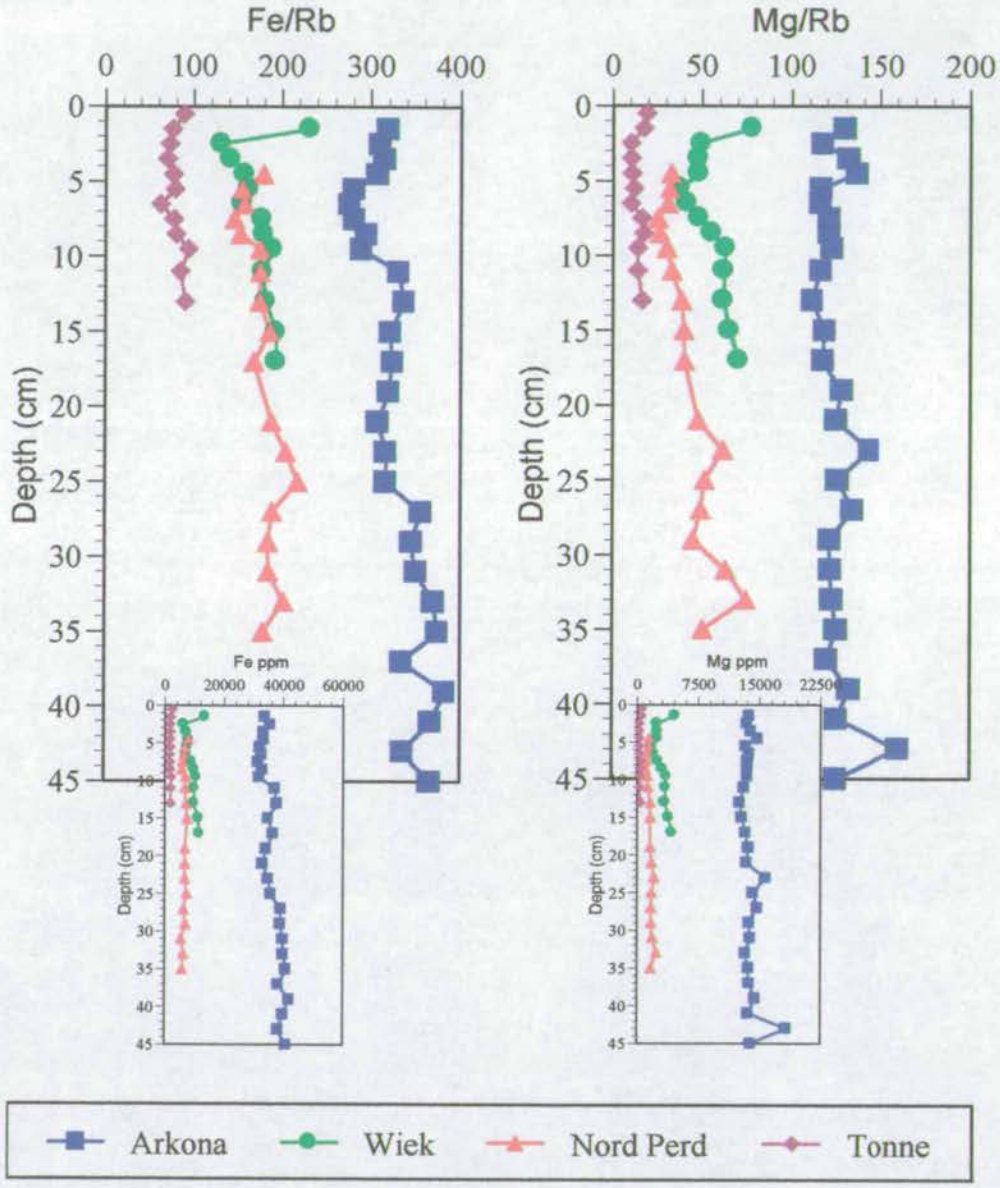

Figure 5-22 Elemental ratio and concentration profiles for Cu, Ni, V, Cs, Fe and Mg showing the elevated levels at Arkona with respect to Tonne for both types of profile.

3) Relatively constant ratio profiles for all stations when normalised to rubidium.

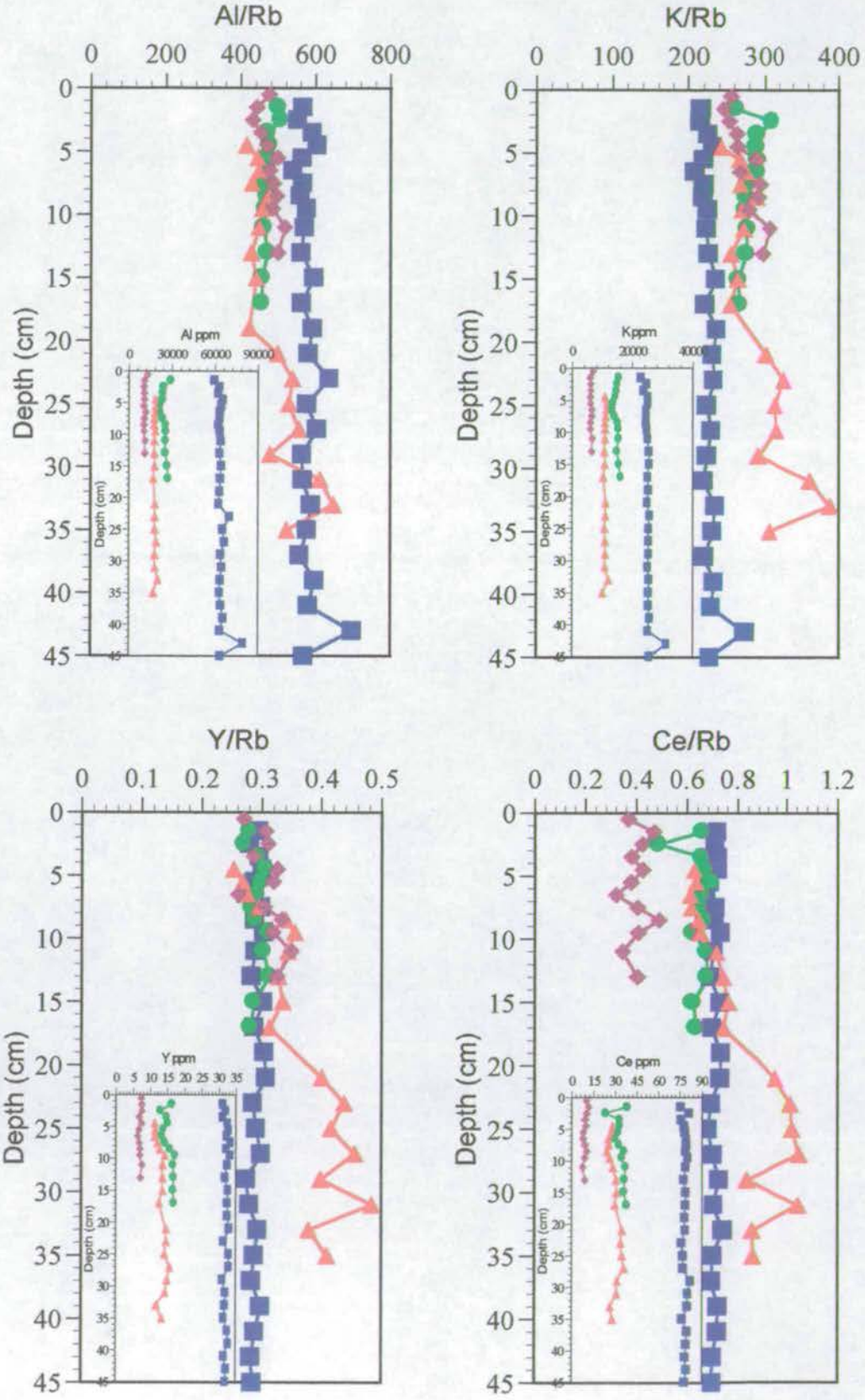

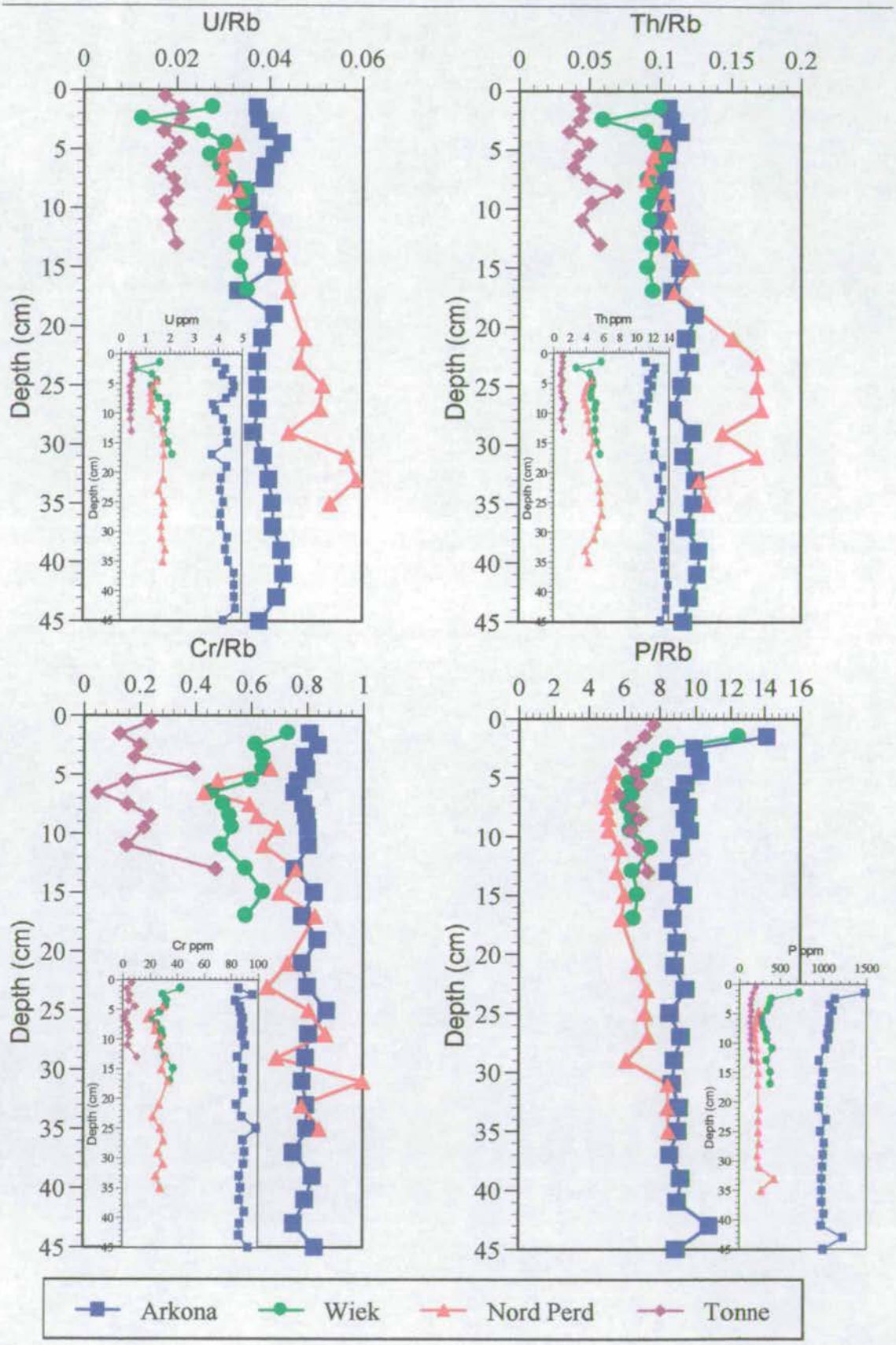

Figure 5-23 Normalised ratio and concentration profiles for Al, K, Y, Ce, U, Th, Cr and P which show a relatively constant ratio value for all stations.

The only elements to show any major enrichment within the sediment cores were Pb, Zn and Sn. To quantify this it is possible to first calculate an enrichment factor as given in Equation 5-3 which generates a ratio to average values; these are shown in Table 5-3.

Equation 5-3

$$\text{Enrichment Factor (E.F.)} = \frac{\left(\frac{\text{Metal (sed core av.)}}{\text{Rb (sed core av.)}}\right)}{\left(\frac{\text{Metal (av. crust or shale)}}{\text{Rb (av. crust or shale)}}\right)}$$

Table 5-3 Enrichment factors for selected elements for an averaged sediment core (Tonne or Arkona) against average crust and average shale (Turekian and Wedepohl, 1961)

Element	E.F. Av. Crust ODAS Tonne	E.F. Av. Crust Arkona Basin	E.F. Av. Shale ODAS Tonne	E.F. Av. Shale Arkona Basin
Al	0.53	0.65	0.73	0.89
K	1.18	0.97	1.55	1.28
Mg	0.05	0.48	0.14	1.25
Fe	0.13	0.56	0.24	0.98
Mn	0.13	0.36	0.21	0.55
Pb	1.56	4.66	1.56	4.66
Zn	0.80	1.78	0.97	2.17
Sn	0.57	1.25	0.4	0.875
Cu	0.34	0.61	0.54	0.95
Ni	0.14	0.40	0.21	0.60
V	0.15	0.73	0.2	0.95
Cs	0.27	1.58	1.8	1.04
Y	0.79	0.75	1.24	1.164
Ba	1.15	0.59	1.49	0.76
Th	0.52	1.26	0.55	1.31
U	0.63	1.3	0.76	1.56

XXX = Enrichment Factor XXX = Closest fit to average value

Table 5-3 shows that the majority of elements determined at Arkona fit closest to the average shale values as determined by TUREKIAN and WEDEPOHL, 1961 and four elements, those of Pb, Zn, Th and U, show enrichments over both average crust and shale. While Pb and Zn show pronounced near surface increases the profiles obtained for U and Th are relatively constant and hence most probably relate to naturally high rates of input over the time period dictated by the core depth. Most of the elements determined at ODAS Tonne are deficient in concentration with respect to average shale and crust with the exception of barium. While most elements show a close correlation to average shale, both K and Ce approximate closely to average crust. In addition to an enrichment factor it is also possible to calculate an 'anthropogenic' factor according to Equation 5-4 which relates the natural background to that of the peak contaminant concentration.

Equation 5-4

$$\text{Anthropogenic Factor (A.F.)} = \frac{\left(\frac{\text{Metal peak concentration}}{\text{Rb concentration at metal peak}}\right)}{\left(\frac{\text{Metal av. natural background}}{\text{Rb av. natural background}}\right)}$$

Although Sn does not show any major enrichments with respect to average shale and crust it can be seen from Figure 5-21 that there is a definite near surface enrichment and hence Table 5-4 shows Sn along with both Pb and Zn in terms of sediment core anthropogenic factors. In addition to the ratio against peak metal concentration the current levels are also given for comparison.

Table 5-4 Anthropogenic factors for Pb, Zn and Sn.

Element	Anthropogenic Factor Peak Metal Conc.	Anthropogenic factor Current Metal Conc.	Published Anthropogenic Values
Pb	2.85	2.42	2.2*, 2.84§, 3.1‡, 2.4†
Zn	2.91	2.42	1.5*, 3.0§, 1.9‡, 2.4†
Sn	2.38	2.08	

* = SZEFER and SKWARZEC, 1988 (Southern Baltic Sea), ‡ = BORG and JONSSON, 1996 (Baltic proper), § = SUESS and ERLENKEUSER, 1975, (Western Baltic) and † = NEUMANN *et al.*, 1996.

While the anthropogenic factors are large for Pb, Zn and Sn at their peak concentrations, with respect to the current levels they show a drop of 15%, 17% and 13% respectively.

The following paragraphs summarise the three categories and graphics depicted by Figures 5-21 to 5-23

Figure 5-21 Elevated near surface concentrations shown by Pb, Zn and Sn for the four Baltic Sea stations with Mn as a reference profile.

Three metals, Pb, Zn and Sn show significant sub-sediment surface concentration maxima for the Arkona Basin with the onset of enrichment at 21cm depth which could be used as a date approximately coincident with the onset of industrialisation. It is not however only Arkona that shows enrichments, both Nord-Perd and Wiek show similar profiles but both the concentration and anthropogenic factors are significantly less than that of Arkona.

All the profiles for Arkona show a post-peak decrease towards the sediment surface whereas in the other stations a decrease is observed close to the surface but surface maxima complicate the picture. The onset of enrichment also takes place at shallower depths for Nord-Perd (11cm) and Wiek (13cm) which may indicate a difference in sedimentation rate between the three stations or the affects of bioturbation as shells were observed at these two intermediate stations.

It is unlikely that the remarkable similarity in the lower redox boundary as depicted by the Mn profile with the exponential increase in the metal concentration is coincidental and this is probably related to the redox cycling in the sediment column.

In addition to these generalisations, the lead profile, unlike the constancy of Zn and Sn, shows a gradual increase in concentration even below 21cm, which may be suggestive of a different mode of input.

Figure 5-22 Elemental ratio and concentration profiles for Cu, Ni, V, Cs, Fe and Mg showing the elevated levels at Arkona with respect to Tonne for both types of profile.

The distribution profiles for Cu, Ni, V, Cs, Fe and Mg are given in Figure 5-22. The concentration and ratio profiles are characterised by significant differences between Arkona and the other stations. This indicates an enrichment of these elements in the sediments of the Arkona Basin together with similar profiles for Fe and Mg which could be interpreted as the association of these elements with the fine silt / clay fraction.

The majority of profiles are constant down core for all stations with the exception of some surface maxima. The main discrepancy from this generalisation is the Cu profile for Arkona which shows a gradually increasing concentration profile becoming steeper in gradient with a shallowing in depth. There is a 1.6x increase in the Cu/Rb ratio between the lowest and highest values over the depth of the core possibly related to the decay of organic matter and the release of Cu into the pore waters. In addition it is not uncharacteristic for the stations of Tonne, Nord-Perd and Wiek to cluster on both the concentration and ratio profiles indicating similar geochemical roles for these stations.

Figure 5-23 Normalised ratio and concentration profiles for Al, K, Y, Ce, U, Th, Cr and P which show a relatively constant ratio value for all stations.

The profiles shown in Figure 5-23 are distinguished by concentration profiles that give individual station profiles but upon normalisation with respect to rubidium they all converge at a similar ratio value. This could be used to infer the association of these metals with lithogenic material.

Once again the concentration profiles remain constant down core and hence this seems to corroborate the inference of them not being the result of anthropogenic input.

5.2.4 Biogenic Geochemistry

With respect to the inorganic geochemistry of the stations sampled it can be seen by reference to Figure 4-17 that there is very little inorganic carbon in evidence. The only noticeable concentration are those peaks found at Nord-Perd and the predominantly background concentrations found at Arkona. The inorganic carbon measurement, in many cases, was below detection limits for the majority of the other stations and hence only a short description is warranted here.

Traditionally the elements associated with biogenic geochemistry are Ca (related to calcium carbonate), Si (related to opal in siliceous organisms) and the possible substitutions and incorporation of Sr and Ba into the Ca lattice site on the formation of carbonate. The virtual absence of any siliceous organisms has been discussed in 5.2.1.2 and so only the profiles for Ca, Sr and Ba are given in Figure 5-24.

As can be seen, only Ca and Sr show close association with the inorganic carbon peaks in Figure 4-17 indicating their incorporation into the mussel shells found at these particular horizons in Nord-Perd. The presence of these bands has a pronounced effect on the concentration of these elements elevating the ratios significantly. Apart from the Nord-Perd peak, the ratios and concentrations for Ca and Sr are relatively constant down core. Barium, however, does not show these attributes and on close inspection it may be postulated that Sr shares some of the same affinities of barium relating to their neighbouring group II chemistry.

The average crust and shale Ba/Rb ratio lies at values of 5.55 and 4.28 respectively. In respect to this it can be seen that Arkona lies slightly depleted in Ba whereas Tonne, Nord-Perd and Wiek approximate closely to the values of average crust and may be predominantly of riverine lithogenic origin. The lower ratios found at Arkona may in turn relate to changes in salinity across the region of interest with desorption of barium from the particulate phase across a low salinity front as described by COFFEY *et al*, 1997.

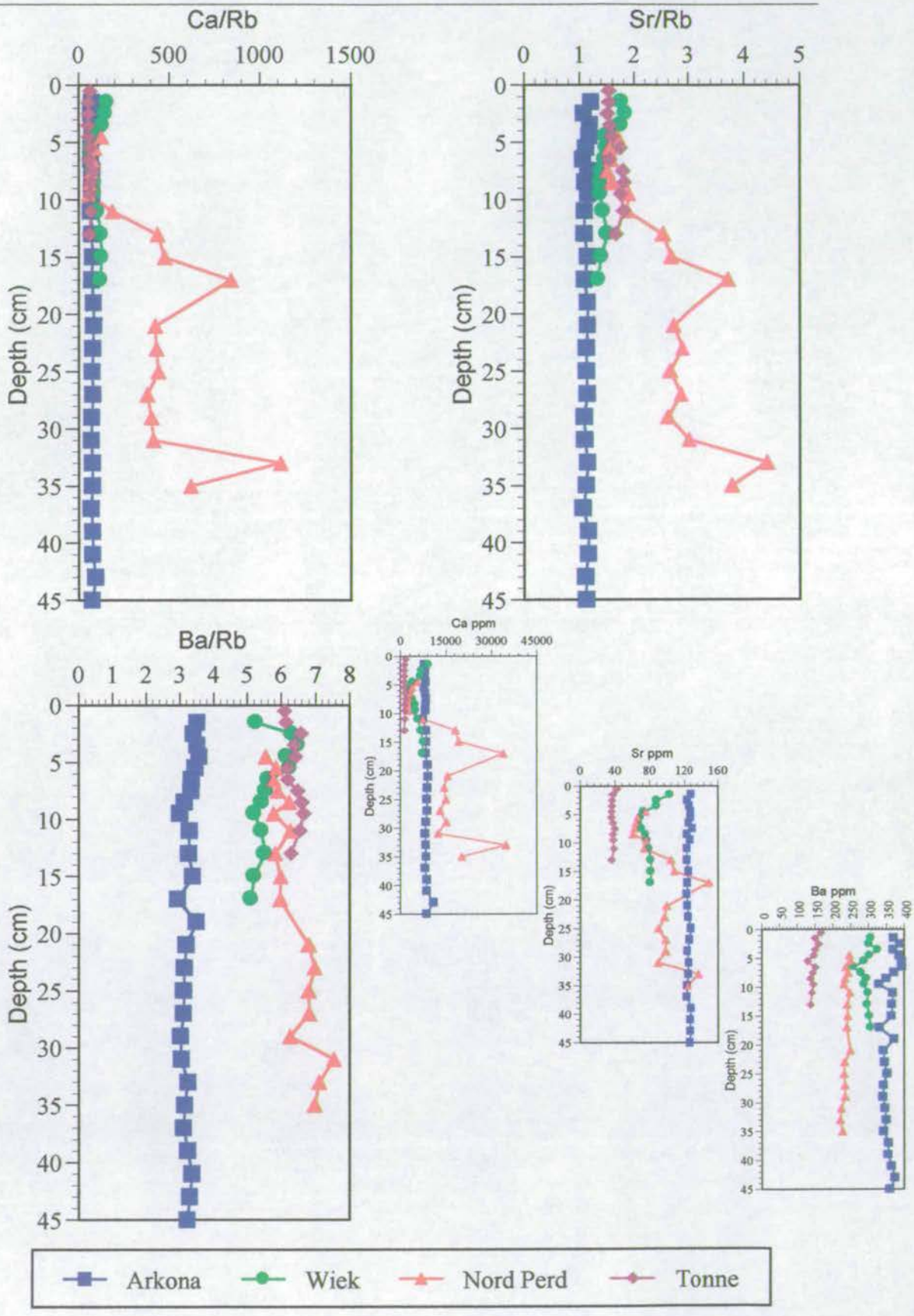

Figure 5-24 Biogenic element profiles for the four Baltic Sea stations

5.2.5 Sediment Core Geochemistry Summary

The initial statistical analysis showed a great deal of statistically significant correlations both between cores and down core. Principal component analysis was then used to try and differentiate the metals into groups of which a summary can be found in 5.1. Elemental profiles were then constructed and the following inferences were made:

- Zirconium acts as a heavy mineral or placer deposit and is most recognisable at Nord-Perd.
- The distribution of silica is predominately controlled by free quartz and the silica associated with aluminosilcates and clay minerals.
- The distribution of Al, K, Mg, Fe and Rb closely approximates to that of average shale especially for the Arkona basin and shows little normalised variation between stations and down core and can therefore be interpreted as being mainly lithogenic in origin and constant in supply.
- In addition Fe and Mg seem to show affiliations for the clay minerals, in particular chlorite along with which there may have been an increase in supply of these clay minerals in the recent past.
- Redox geochemistry shows a classic profile for both Mn and Fe with uptake at depth in the monosulphide and disulphide phase.
- Mo and As show diagenetic features related to the Mn/Fe redox geochemistry and to the possible enrichment of Mo and As as a response to expulsion from the intermediate monosulphide phase.
- Pb, Zn and Sn show significant near surface enrichments which may in part be exacerbated by the redox cycle, however, the onset of enrichment is significantly below the lowest redox boundary and hence is a 'real' anthropogenic affect.
- The peak enrichments are in the order of 2.9 for Pb and Zn and 2.4 for Sn over natural background levels. However, recent values indicate a decrease in the anthropogenic load by approximately 15%.
- The onset of enrichment is at a shallower depth for the shallower stations thus having implications for the rate of sediment accumulation.

- Pb shows a gradual increase throughout the whole of the core which may relate to the major addition of Pb from another source, possibly that of an atmospheric origin.
- In addition Th and U show above average shale and crustal values but are constant down core and hence relate to a naturally-elevated weathering component.
- Cu, Ni, V, Cs, Fe and Mg seem to be associated with the fine-grained component of the sedimentary record and undergo similar geochemical processes within the sediment core.
- In addition copper shows a 1.6x enrichment over the depth of the core and thus can be classed with the anthropogenic group of metals.
- Al, K, Y, Ce, U, Th, Cr and P are predominantly lithogenic in origin and relate to natural weathering processes of crustal material.
- The biogenic elements of Ca and Sr show similar profiles dominated by the shell bands in Nord-Perd.
- Barium meanwhile seems to be strongly affected by a salinity front and becomes depleted at Arkona with respect to average shale and crust.

6.0 Radionuclides in the Southern Baltic Sea Sediment Core

In addition to the collation of trace metal geochemistry data in the sediments, specific radionuclide data was also gathered in order to elucidate and confine some of the processes operating in the Baltic Sea system. The primary purpose of gathering radiochemical data in the sediment core is twofold; the first is to establish a chronology for the core (^{210}Pb) and the second is determine the extent of manmade radionuclide pollution in the sediments by flux and inventory calculations.

Three main isotopes were measured by gamma counting; those of ^{210}Pb, ^{226}Ra and ^{137}Cs. Both ^{210}Pb and ^{226}Ra form part of the ^{238}U decay series as shown in Figure 6-1 and the radiochemistry of these elements along with the manmade ^{137}Cs is well described (MACKENZIE *et al.*, 1979; BROECKER and PENG, 1982; IVANOVICH and HARMON, 1982; CHANTON *et al.*, 1983; SALO *et al.*, 1983; FAURE, 1986; MOLINARI and SNODGRASS, 1990; MOORE *et al.*, 1995).

The following is a brief history of the elemental radiochemistry associated with the ^{238}U decay series and in particular the influences and processes that govern the natural distribution of ^{226}Ra and ^{210}Pb.

6.1 ^{238}U SERIES AND RADIOACTIVE DECAY

There is much literature devoted to the detailed discussion of nuclear and radiochemistry and the process of radioactive decay (KELLER, 1988; FREIDLANDER *et al.*, 1991, CHOPPIN *et al.*, 1996). In basic terms of the ^{238}U decay series there is a relationship between two or more successive nuclei in the series and these are commonly termed parent and daughter nuclide relationships.

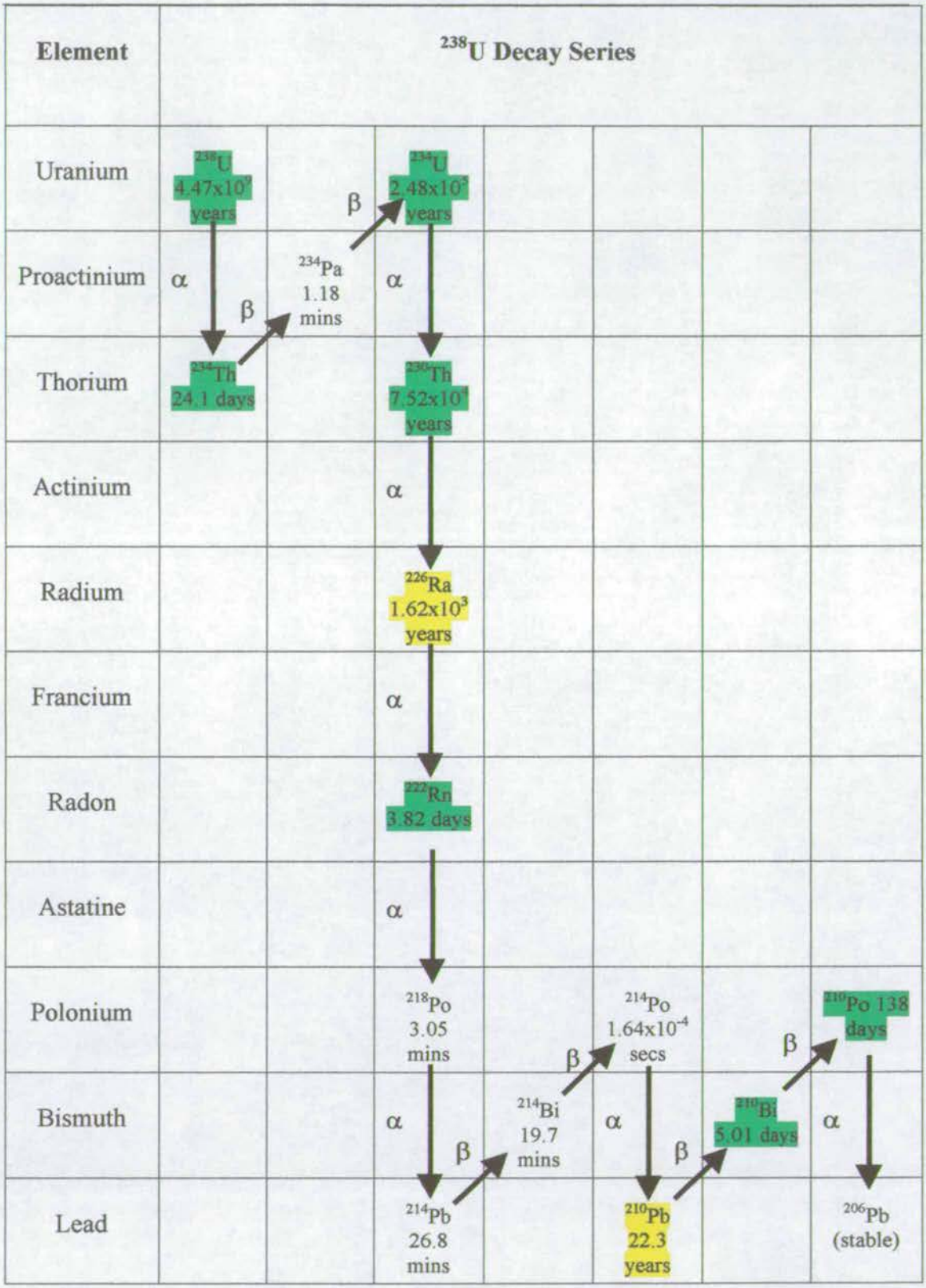

Figure 6-1 The ^{238}U decay series with ^{210}Pb, ^{226}Ra and other nuclides useful in environmental analysis with half lives greater than a day highlighted. (After Molinari and Snodgrass, 1990).

In a closed system the activity of the daughter nuclide will eventually equal that of the parent nuclide due to the balance between radiogenic production and decay. If this particular scenario is achieved then secular equilibrium is said to have been obtained. However, in the natural environment as each element in the decay series has its own individual radiochemistry and affinities then, as expected, they will also have their own specific geochemical behaviour which may in turn lead to fractionation during their appropriation in natural processes. This leads to a degree of disequilibrium depending on the rate of processes separating the two elements and the half-life of the daughter. The systematics of radionuclide decay and ingrowth can be mathematically quantified as shown by the following paragraphs taken from (SHIMMIELD, T., 1993):

The decay of parent nuclide X to from that of a daughter nuclide Y will result in the decay of Y upon separation from X according to the basic decay equation:

Equation 6-1

$$A_{Y(T)} = A_{Y(0)} e^{-\lambda y t}$$

where:

$A_{Y(T)}$ = activity of daughter nuclide at time t

$A_{Y(0)}$ = activity of daughter nuclide at time zero

λ_y = decay constant of daughter nuclide

t = time

If the parent is separated then the daughter activity will grow in and the daughter will in turn also be subject to radioactive decay, Under these conditions the rate of decay of the daughter nuclide can be given by:

Equation 6-2

$$\frac{dN_y}{dt} = -\frac{dN_x}{dt} - \lambda_y N_y = \lambda_x N_x - \lambda_y N_y$$

where N_x and N_y are the numbers of atoms of nuclides X and Y respectively at a given time. As the activity (A) is equal to λN then the two equations above can be combined and differentiating them gives

Equation 6-3

$$N_y = \frac{\lambda_x}{\lambda_y - \lambda_x} N_{x(0)} \left(e^{-\lambda_x t} - e^{-\lambda_y t}\right) + N_{y(0)} e^{-\lambda_y t}$$

where $N_{x(0)}$ and $N_{y(0)}$ are the numbers of atoms of nuclides X and Y present at time zero.

The activity of the daughter nuclide is given by:

Equation 6-4

$$A_y = \frac{\lambda_x}{\lambda_y - \lambda_x} A_{x(0)} \left(e^{-\lambda_x t} - e^{-\lambda_y t}\right)$$

The primary case of interest in this work pertaining to the ingrowth of the daughter activity to that of the parent is that of secular equilibrium in which $(t_{½})_x >> (t_{½})_y$ (X = parent, Y = daughter) and the growth to equilibrium is described by:

Equation 6-5

$$A_y = A_x (1 - e^{-\lambda_y t})$$

and at equilibrium $A_y = A_x$.

6.2 NATURAL RADIONUCLIDES IN THE MARINE ENVIRONMENT

One of the key controls in determining the distribution of radionuclides in the marine environment is the solubility of the radionuclides of interest. The partitioning of the parent/daughter nuclides between the solid and aqueous phase is fundamental to the use of radionuclides as process tracers and is discussed in the following section.

The solubility of the nuclides is largely governed by their interactions with water molecules and other ligands, and the primary governing control on this is their size, charge (oxidation state) and shape. The ionic potential is useful in illustrating the controls on solubility as low values of Z/r (charge/radius) are conducive to simple hydration, high values lead to the formation of soluble oxy-ion complexes but at intermediate values hydrolysis of the nuclide occurs resulting in insoluble ions.

Table 6-1 shows the characteristic properties and typical solubilities of the main relevant components in natural waters for the ^{238}U decay chain.

Table 6-1 Properties of the main components in the ^{238}U decay series, (After Young, 1996 and Molinari and Snodgrass, 1990)

Element	Atomic No.	Group	Electronic Config.	Electro-negativity	Oxidation States (natural H_2O)	Ionic Radii	Ionic Potential (z/R)	Solubility in natural waters
Uranium	92	IIIa	$6p^6 5f^3 6d^1 7s^2$	1.22	4+ 6+	0.93 0.83	4.49 8.22	Insoluble Soluble
Thorium	90	IIIa	$6p^6 6d^2 7s^2$	1.11	4+	0.99	4.25	Insoluble
Radium	88	IIa	$6p^6 7s^2$	0.97	2+	1.52	1.35	Soluble
Radon	86	0	$6p^6$	-	0	-	-	Soluble
Lead	82	IVb	$6p^2$	1.55	2+ 4+	1.32 0.98	5.16	Insoluble

The distribution and behaviour of the principal nuclides outlined above in the natural environment are shown schematically in Figure 6-2 and discussed in the following sections:

6.2.1 Uranium and Thorium

Uranium exists in the natural environment primarily in two oxidation states (IV and VI). The most stable and important oxidation state for the transport of uranium is the VI state which forms soluble anionic uranyl bi and tricarbonate complex ions in seawater $[UO_2(CO_3)_2]^{2-}$ / $[UO_2(CO_3)_3]^{4-}$. This is found uniformly distributed around the worlds oceans behaving as a conservative element normalised to salinity (BROECKER and PENG, 1982; LOFVENDAHL, 1987; NOZAKI, 1991;

ANDERSSON *et al.*, 1995; SKWARZEC, 1997). As the Baltic Sea has a steep salinity gradient then this becomes an important consideration in the dissolved uranium geochemistry of this region. In addition to this simple picture of soluble uranium (VI) geochemistry some uranium may also be removed by adsorption onto Fe / Mn oxyhydroxides and colloids in the estuarine environment (TOOLE *et al.*, 1988; ORLANDI, *et al.*, 1990; SARIN *et al.*, 1990; DEARLOVE, *et al.*, 1991; PORCELLI, *et al.*, 1997) creating localised non-conservative type behaviour.

Thorium, in stark contrast to the mobility of U VI, is insoluble and can therefore only be transported as a detrital weathering product by being absorbed onto particle surfaces or bound in insoluble minerals. (BROECKER and PENG, 1982; SANTSCHI and HONEYMAN, 1989; CHESTER, 1990). Thus, Th IV is only present temporarily in the water column as highly insoluble tetravalent ions and are rapidly scavenged by sinking particulate matter. U IV is generally only present under reducing conditions and is thought to be formed via humate or fulvic uranyl intermediary complexes where upon burial and with the development of reducing conditions the uranous state can be formed (LANGMUIR, 1978; ANDERSON *et al.*, 1989). Thorium, meanwhile, is produced continually from the decay of its uranium VI parents in the water column and is rapidly scavenged by falling marine detritus and colloidal material (BASKARAN *et al.*, 1992; HONEYMAN and SANTSCHI, 1989). Scavenging and particle residence times of ^{234}Th in the Baltic Sea were estimated by KERSTEN *et al.*, 1998. They found that the scavenging residence times were in the order of 1.2-9.7 days for colloidally bound Th and less than 1hr for truly dissolved Th. Residence times for particulate Th were around several days and high thorium removal rates were strongly correlated with an increased suspended particulate matter load but depended also on the depth of water and current velocities.

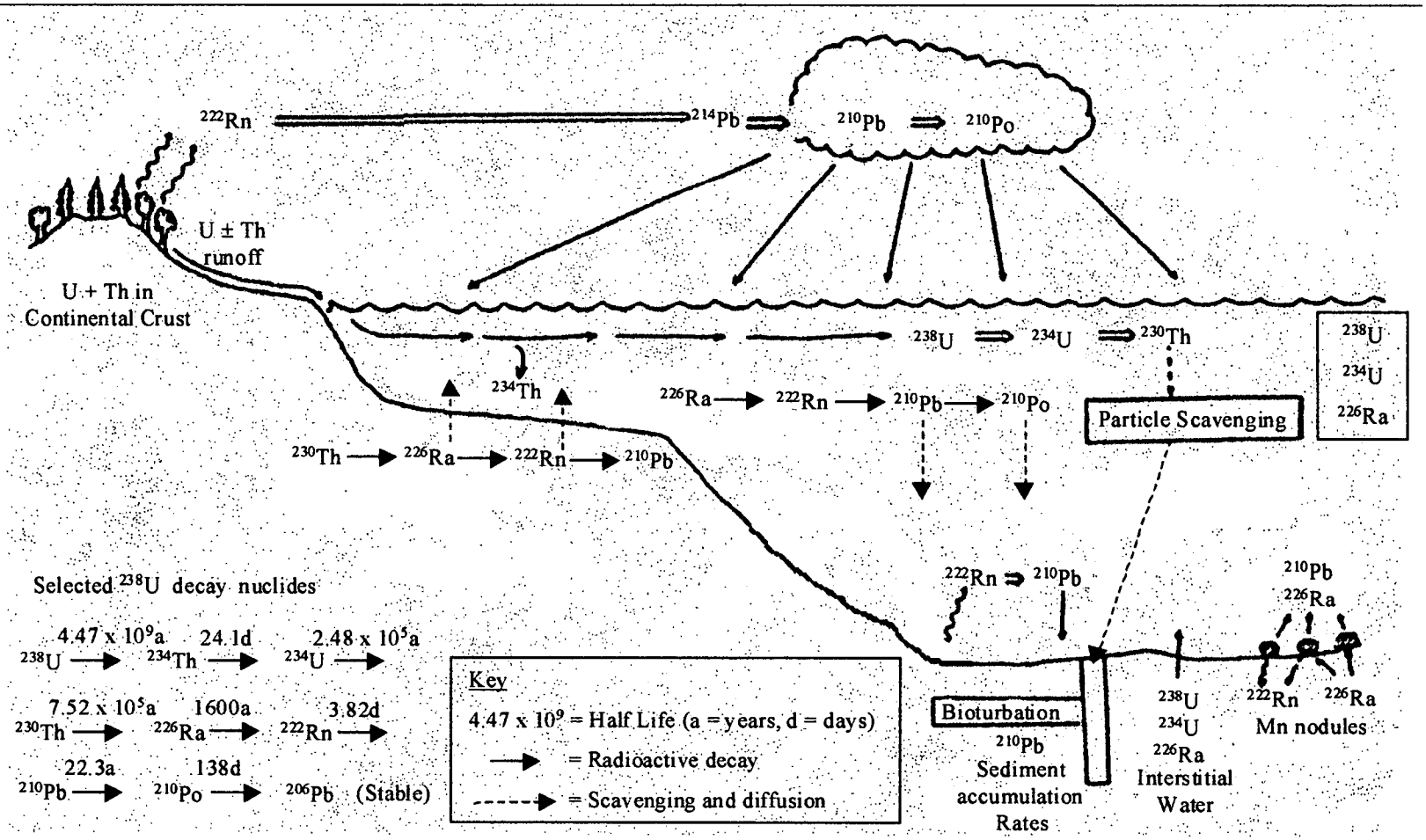

Figure 6-2 Marine environmental geochemistry of selected ^{238}U decay nuclides

Hence, as uranium is generally found in the soluble (VI) form and that upon radioactive decay to its daughter product, thorium, it is rapidly scavenged from the water column thus setting up a disequilibrium in the marine environment. These fundamental attributes and processes are common to the other members of the decay series and govern the distribution and use of radioactive tracers in the marine environment.

6.2.2 Radium and Radon

^{226}Ra is generally found in excess of its parent ^{230}Th in the marine environment, principally due to the greater solubility of radium and the particle reactivity described above. The primary inputs of radium into the marine environment come not only from the decay of thorium in the basinal sediment followed by diffusion into the pore waters and into the overlying bottom water but also from a significant ground and riverine water input. The relative importance of each of these processes varies region by region but they have been extensively described by a number of authors:

- *In the Oceans*: BROECKER *et al.*, 1967; BROECKER *et al.*, 1976; MOORE and SANTSCHI, 1986; CHUNG, 1987; RHEIN *et al.*, 1987; MOORE and DYMOND, 1991;
- *In the Sediments:* MACKENZIE *et al.*, 1979; KADKO, D., 1980; KOWALEWSKA, G., 1986, CLULOW *et al.*, 1998; PARDUE and GUO, 1998;
- *In Groundwater*: JIANG and HOLTZMANN, 1989; BAYES *et al.*, 1996; MOORE, 1996; RAMA and MOORE, 1996; MOORE, 1997.
- *In Rivers and Coastal waters:* KNAUSS *et al.*, 1978; KOWALEWSKA, 1987; SARIN *et al.*, 1990; MOORE *et al.*, 1995; PLATER *et al.*, 1995

Radium exists in the marine environment as a complex chloride but even a small amount of sulphate will lead to its precipitation out of solution and thus care has to be taken in interpreting the radium geochemistry of anoxic bottom waters. Radium

decays to ^{222}Rn which is the only radon isotope which has a sufficient half life to allow significant migration (3.83 days). Radon being a noble gas is free of reaction with other atoms and as it is soluble in seawater offers the possibility of transgressing the sea-air boundary and is regarded by many as being one of the main causes of disequilibrium in the ^{238}U series. In addition to the radon that is produced within the sea there is also a major contribution from terrestrially derived radon which adds to the total atmospheric content.

Hence just as uranium and thorium have different geochemical roles, so do radium and radon in the marine environment. In addition, the governing processes get more complicated as the decay series progresses due to the increasing number of variables.

6.2.3 Lead and Polonium

As radon is a gas and is present in both the hydro and atmosphere then it offers an interesting mix of pathways. ^{222}Rn decays via a series of short-lived intermediates to the three longer-lived nuclides of ^{210}Pb, ^{210}Bi and ^{210}Po. In both the atmosphere and the hydrosphere the decay of ^{222}Rn generates a series of charged decay products which are chemically reactive and eventually become irreversibly associated with aerosols in the atmosphere and particles in the hydrosphere. The aerosols are either washed out as precipitation or fall under the influence of gravity or electrostatic forces (TUREKIAN *et al.*, 1977). Both ^{210}Pb and ^{210}Po are insoluble in the water column and are both particle reactive species. The lead (and polonium) found in the sediment is a product of two main processes. The first is that associated with the in-situ production of lead from radium trapped in detrital minerals in the sediment core, and the second is the lead which is unsupported in the sediment, derived from either the decay of radium in the water column or from the decay of radon in the atmosphere. A summary of these pathways is shown in Figure 6-2. In near shore environments the atmospheric supply of unsupported ^{210}Pb is often predominant whereas, in the deep ocean water column decay of radium takes on a greater role. While ^{210}Pb is closely associated with particles, ^{210}Po is more likely to undergo

recycling as it is more readily adsorbed and released on and from marine plankton than its ^{210}Pb parent (GASCOYNE, 1982).

6.3 MAN-MADE RADIONUCLIDES IN THE MARINE ENVIRONMENT

In addition to the natural radionuclides, man-made radionuclides play an important role as tracers of marine processes and represent an important class of pollutants in the coastal environment (MACKENZIE *et al.*, 1979; KAUTSKY, 1981; SALO *et al.*, 1986; CARLSON and ERLANDSSON, 1991). The primary radionuclide that will be considered here is ^{137}Cs, a fission product and conservative isotope in seawater, as this can be used in a complimentary manner and aid in validating the dates determined by the ^{210}Pb calculations. This is principally due to the very distinct ^{137}Cs input events that have occurred over the last 50 years. Briefly, ^{137}Cs is emitted to the atmosphere solely from anthropogenic activities (nuclear weapon tests, nuclear power and reprocessing plants), the first occurrence of which related to the testing of nuclear weapons with a global fallout maximum in 1963. Thereafter the main source of caesium in the Baltic Sea were releases from the nuclear reprocessing plant in Sellafield, La Hague and the accidental release from the Chernobyl incident which had a measurable effect on ^{137}Cs concentrations in the Baltic Sea. Maximum releases from Sellafield occurred during 1973 and 1975 (Figure 6-3), and were registered in the Baltic some four years after the initial release (Cs acting as a water tracer), (MATTSSON and ERLANDSSON, 1991; CARLSON and HOLM, 1992). In May 1986 fallout from the Russian nuclear reactor at Chernobyl caused a threefold increase in the levels of caesium found in both the sediment and algae of the Swedish sector of the Baltic Sea. The radioactive contamination as a result of this accident has been dominated in the Baltic Sea by the caesium isotopes ^{134}Cs and ^{137}Cs. These isotopes had a typical activity ratio of 0.54 in the water column which could in turn be used to monitor and act as a tracer for the movement of water masses, in particular, the outflow from the Baltic into the Norwegian Sea in the form of the Norwegian Coastal current. However, because the half-life of ^{134}Cs is short at

2.062yrs and thus has decayed over the last ten years, the use of this $^{134/137}Cs$ tracer is no longer viable for the Chernobyl event.

Concerns have additionally been raised about the suitability of ^{137}Cs as a date proxy due to the mobility in terms of a potential downward diffusion of caesium within the sediment. However, according to BERNER, R. A., 1980 diffusion and mixing of ^{137}Cs will not alter the position of a peak maximum generated by a pulsed input but instead will only serve to reduce it in magnitude and to increase its areal distribution within the sediment core. Hence as with ^{210}Pb sediment cores, caesium measurements within a core should be judged with respect to suitability for physical and biological disturbance on a station by station basis.

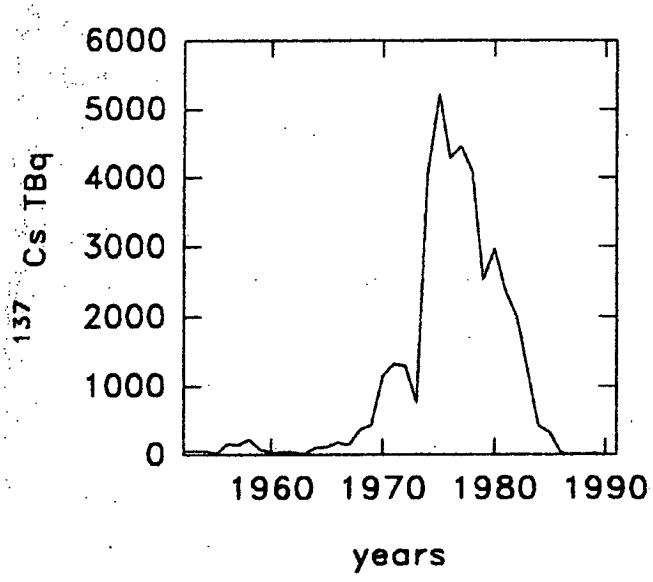

Figure 6-3 Discharge data for ^{137}Cs from BNFL, (Taken from Shimmield, T., 1993)

6.4 LEAD-210 DATING

The isolation of ^{210}Pb from its radon precursor due to the behavioural differences outlined above allows for the use of ^{210}Pb as a dating tool (<150 years, $T_{½}$ = 22.3yrs) in the marine environment. This use of ^{210}Pb as an indicator of sediment

accumulation and sediment mixing processes is well established and has been used for many years (KOIDE, 1973; ROBBINS and EDGINGTON, 1975; CLIFTON and HAMILTON, 1979; CHANTON *et al.*, 1983; SMITH-BRIGGS, 1983; EDGINGTON *et al.*, 1991; THOMSON *et al.*, 1993; KUNZENDORF *et al.*, 1997; MACKENZIE *et al.*, 1998).

A 'text book' theoretical, constant input, ^{210}Pb sediment profile is given in Figure 6-4 showing the near surface mixed layer as a result of physical and biological processes. The intermediate zone of excess ^{210}Pb where as long as the sedimentation rate is constant a first order decay profile will develop and finally at the base the supported ^{210}Pb produced solely by the in situ ^{226}Ra decay.

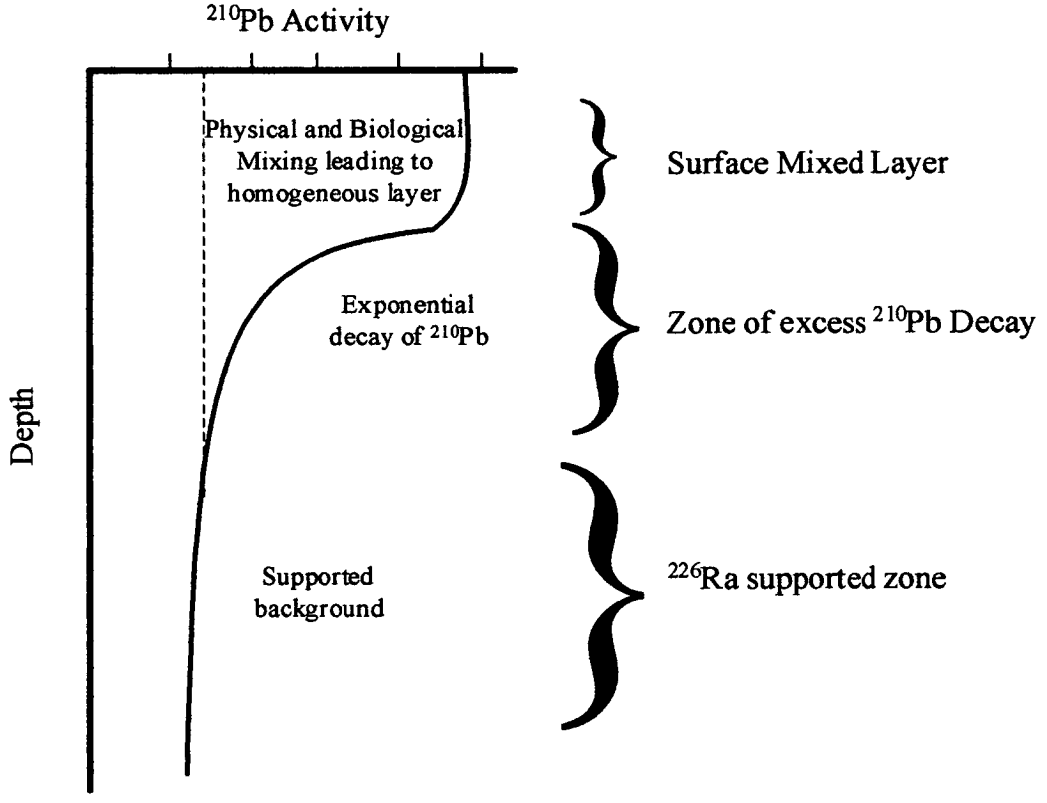

Figure 6-4 Theoretical ^{210}Pb profile for a sediment core

To enable the use of ^{210}Pb in dating a number of assumptions have to be made: The excess ^{210}Pb (i.e. that not supported in the sediment) associated with radioactive

decay, predominantly in the atmosphere, is assumed to have a constant flux to the sediments for a given region. In addition it is also generally assumed that there is no post depositional remobilization of the lead and that the excess ^{210}Pb can be calculated from the ^{226}Ra and the total ^{210}Pb activities of the sediment.

There has however been much debate on the second of these assumptions regarding the mobility of lead in the depositional environment. CARPENTER, *et al.*, 1981; WAN *et al.*, 1987; BENOIT and HEMOND, 1990; BENOIT and HEMOND, 1991; showed that in anoxic bottom waters diffusion of lead into the pore waters associated with iron and manganese cycling occurred which would invalidate this second assumption. Similarly URBAN, *et al.*, 1990 demonstrated that lead mobility in saturated, organic rich peatlands did occur and GUBALA *et al.*, 1990 suggested that the accuracy of ^{210}Pb dating had to be carefully evaluated in low sedimentation-rate environments, especially in those that showed evidence of post depositional movement of iron. MACKENZIE *et al.*, 1997 and 1998 showed that above the water table in the unsaturated zone of peat deposits there was no mobilisation of lead and thus the primary assumption holds true. In contrast to this they found that in zones of saturation lead mobilisation did occur implying that the percolation of groundwater can create post depositional mobility of lead.

However there have been many cases where ^{210}Pb dating have been used successfully based upon known historical trends in industrial output, palynological dates, varve counting and peaks in man-made radionuclides with specific event horizons. In addition SHIMMIELD, T., 1993 advocated no post-depositional migration of lead in the sediment cores from Lochs from the West of Scotland and KUNZENDORF *et al.*, 1997 and PEMPKOWAIK (pers comm) successfully used ^{210}Pb dating, alternatively justified, in the Baltic Sea.

In addition to the lead mobility question, radium is also soluble and as it is known to associate under certain condition with Mn and Fe oxyhydroxides then this could cause problems with the final assumption that excess ^{210}Pb can be calculated from the subtraction of ^{226}Ra from total ^{210}Pb.

In summary the use of ^{210}Pb as a dating tool is heavily dependent upon the region of interest and the environmental variables. If possible, its use as a date proxy should be individually validated for each location by other dating means, with particular attention paid to post depositional diagenesis processes in order to validate the dates.

There are two commonly used methods of determining the sedimentation rate and ages of a sediment core. These are the constant initial concentration method (CIC) and the constant rate of supply (CRS). Both methods are derived from the basic radioactive decay equation:

Equation 6-6

$$A_z = A_0 e^{-\lambda t}$$

where A_z = activity of excess ^{210}Pb at depth z, A_0 = initial activity of excess ^{210}Pb at the surface, λ = ^{210}Pb decay constant, t = time in years

The first method of a constant initial concentration (CIC), (ROBBINS and EDGINGTON, 1975) is calculated by assuming that the downcore excess ^{210}Pb is a function of radioactive decay at a given location in that there is a constant sedimentation rate and hence the difference in sediment age between surface and depth z is given by the transformation of the above equation to:

Equation 6-7

$$\ln A_z = \ln A_0 - \lambda t$$

and as time can be defined as t = M/R, where M = weight of sediment per unit area (g cm^{-2}) and R = the accumulation rate of sediment (g cm^{-2} yr^{-1}) then the equation can be rewritten as:

Equation 6-8

$$\ln A_z = -\left(\frac{\lambda}{R}\right) M + \ln A_0$$

Thus the equation takes on the form of **y = mx + c** and by plotting lnA versus M and calculating the gradient the sedimentation rate can be calculated from R = -(λ/M).

The second model of constant rate of supply (CRS), (APPLEBY and OLDFIELD, 1978; DURHAM and JOSHI, 1980) is used when there is a variable rate of sedimentation and assumes the flux of unsupported ^{210}Pb to the sediment is constant with time at a particular location. Therefore the age (t) of a horizon at depth (z) can be determined from:

Equation 6-9

$$\sum(^{210}Pb\ excess)_z = z_t\left(1 - e^{-\lambda_{210}t}\right)$$

where $\sum(^{210}\text{Pb excess})_z$ = total excess activity of ^{210}Pb from the surface to depth z, Z_t = total excess ^{210}Pb in the core.

In addition to these two models, in response to the mobility of lead in certain environments, an alternative model has been advocated called the advection diffusion equation (ADE) model. Essentially the ADE model can be derived from the CRS model and also shows some commonality with the fundamental equations in both the CIC and CRS models, details of which can be found in SHUKLA, 1996.

6.4.1 ^{210}Pb Dating of the Arkona Basin Sediment Core

The only core which met the conditions for dating was the Arkona Basin sediment core from which the determination of sediment accumulation rates was performed using the constant initial concentration model of dating. This methodology is shown in Figure 6-5 and described below.

Figure 6-5 (A) shows the excess ^{210}Pb profile generated by the subtraction of ^{226}Ra from the total ^{210}Pb activity of the sediment core for each section. The most obvious feature of this core is the section characteristic of a mixed layer penetrating to a depth of 1.85g cm^{-2} (8.5cm) followed by the exponential decay curve down to background values at 5.28g cm^{-2} (21 cm). Data is plotted against g cm^{-2} so as to accommodate for the changes in porosity and compaction that occur down core. Figure 6-5 (B) shows the natural log of these values relating to the first order kinetics of radioactive decay which allows a sediment accumulation rate to be determined. A change in gradient can be seen as a result of this manipulation which may be

indicative of a change in the sedimentation rate over time, or may relate to larger errors associated with the radium contribution at depth which in turn will have a significant impact on the accumulate rate. Hence, these values may be more suspect than the calculations based on the steepest gradient of the curve. To this end a sediment accumulation rate was calculated using the upper four points as shown in figure 6-5 (C) which gave a regression line of almost one and yielded an accumulation rate of 0.0496g cm^{-2} yr^{-1} (linear sedimentation rate of 0.22cm yr^{-1}) over this section of the core. Figure 6-45(D) shows the same calculation but for the lower four points yielding a lower accumulation rate and r value of 0.0288g $cm^{-2}yr^{-1}$ and 0.92, respectively.

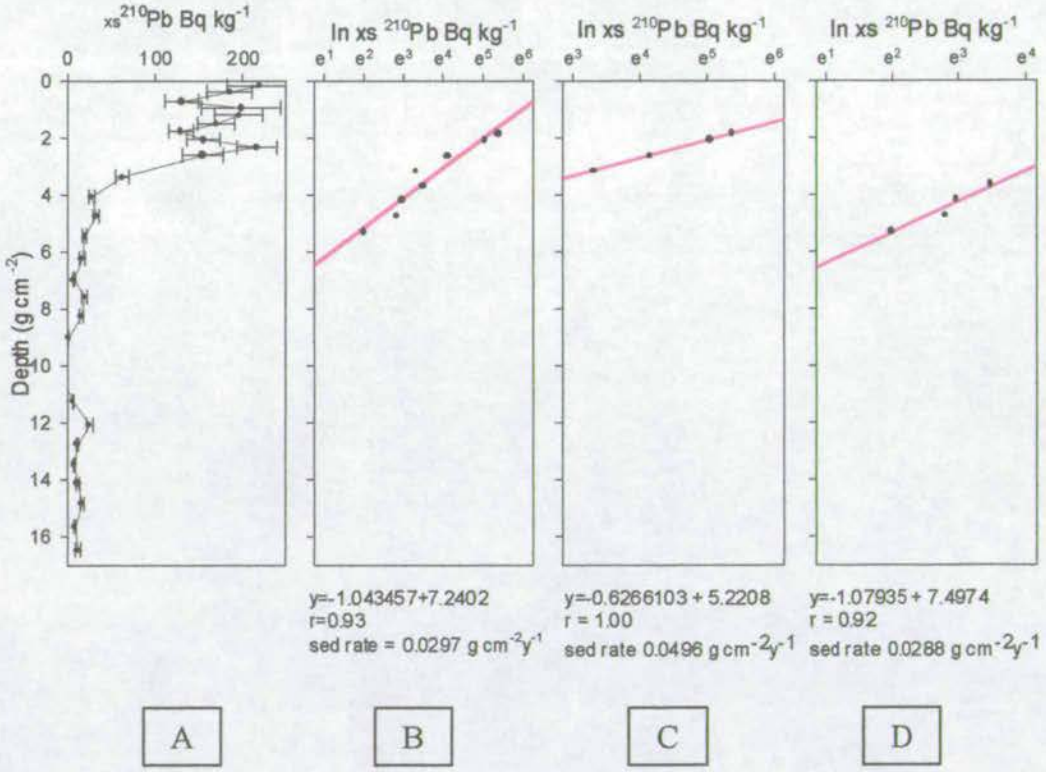

Figure 6-5 Calculation of sedimentation rates by the CIC method.

The mixed layer is problematic when trying to ascertain and account for the historical record of a sediment core. If the sediment accumulation rate of 0.0496g cm^{-2} yr^{-1} is assumed to be true for the whole core then this gives a mixed layer depth equivalent to 37yrs. This means that theoretically it is possible for recent

sedimentation to be immediately mixed down to 8.5 cm thus combining recent sediment with sediment as old as 1959. Hence, traditionally this 37 years is then added to the calculated dates down core so as to account for mixing. However it is unlikely that mixing by both physical and biological means will have remained constant over the period of investigation because of environmental changes over the last century in the Baltic Sea. The change from an oligotrophic water body into one of the most contaminated waterways in the world will almost certainly have had significant effects on the benthos and hence biological reworking over time. In addition physical disturbance by such means as trawling will have changed over time due to the methods used and the intensity of the industry. Indeed the actual cause of mixing cannot be determined with absolute certainty as FLODERUS and PIHL, 1990 suggest that trawling typically disturbs the sediment to depths of 5 to 10cm which is consistent with the 8.5cm depth observed here. However the profile shown in Figure 6-5 (A) seems, currently, to be characteristic of a moderately bioturbated surface (NICKELL, L., pers. comm.) due to the similar surface and bottom mixed layer values (~220Bq Kg^{-1}) and the activity structure in-between. In contrast to this the profile generated solely from the effects of trawling would be expected to have a more constant mixed layer contour. While a bioturbation hypothesis may be consistent from the data presented here the possibility of physical mixing by trawling and then subsequent bioturbation by opportunistic species and bacteria, even in anoxic sediments, superimposed on this profile cannot be ruled out.

The Baltic Sea is also a unique environment in that there are periodic inflow events with periods of stagnation and the development of anoxia in the interim. Due to the decrease in water quality, these periods of stagnation and the development of anoxia have become increasingly commonly in recent times with anoxia not only confined to the deepest parts of the Baltic. Anoxic events are also becoming an increasingly common phenomena in shallower waters such as the Arkona Basin where the effects of hypoxia and anoxia on the macro and meiobenthos are substantial as documented by RADZIEJEWSKA and MASLOWSKI, 1995. The 'normal' environmental gradients in the Baltic Sea characteristically generate a biological system with a high biomass but low biodiversity resulting in a predominance of opportunistic and

environmentally tolerant species. Furthermore in many cases, because of the stressed environment, the growth of many species is also restricted as shown by KUBE *et al.*, 1996a and KUBE *et al.*, 1996b. Hence the Baltic Sea is very transitory in nature over a historical time period in terms of the benthos and bioturbation and is heavily dependant on the hydrodynamics at the time in question. Thus these factors limit the interpretation of the nature of the mixed layer and its role and magnitude over time.

The possibility of a change in the sedimentation rate as suggested by Figure 6-5 (D) needs to be addressed as JONSSON *et al.*, 1990; and KUNZENDORF *et al.*, 1997 have also suggested a recent increase in the sedimentation rate, increasing to 2-3mm yr^{-1} from the 1970's onwards based on varve counting and gamma dating respectively. There are three main reasons given for this increase in sediment accumulation rate. The first relates to increased eutrophication and a related higher primary production over recent times (JONSSON and CARMANN, 1994). The second is based upon the increased preservation of organic matter in the sediment column relating to the increased occurrence and duration of anoxia in the recent past (NEUMANN *et al.*, 1997). Finally, JONSSON *et al.*, 1990 proposes that in situ erosion of shallow water sediments in response to increased recent storminess could be a major source of sediment input to the deep basin. This final suggestion does not seem to be substantiated by this data, as there is no discernible change in grain size down core indicative of a change in input. However, there is an increase in the organic carbon content of the sediments within the mixed layer, possibly indicative of a change in accumulation rate but this cannot be directly dated due to mixing processes (but it does happen to span the inferred period of increase, 1959 to present). The rest of the core below the mixed zone is essentially constant and from the above suggestions this would indicate a constant accumulation rate if there were no change in supply.

In order to validate the hypothesis that an accumulation rate of 0.0496g $cm^{-2}yr^{-1}$ is representative it is possible to use certain events in recent history which can be used to substantiate the data obtained by ^{210}Pb dating. These are primarily in the form of pulsed ^{137}Cs inputs and the historical record associated with variations in stable lead

isotopes. The stable lead isotopes only become useful, however, below the mixed layer due to the continuous nature of the input and thus mixing by physical or biological means will inhibit their use as dating indicators within the mixed layer. Figure 6-6 shows the ^{137}Cs data along with the ^{210}Pb data which is additionally linked with the stable lead isotope data in the following chapter.

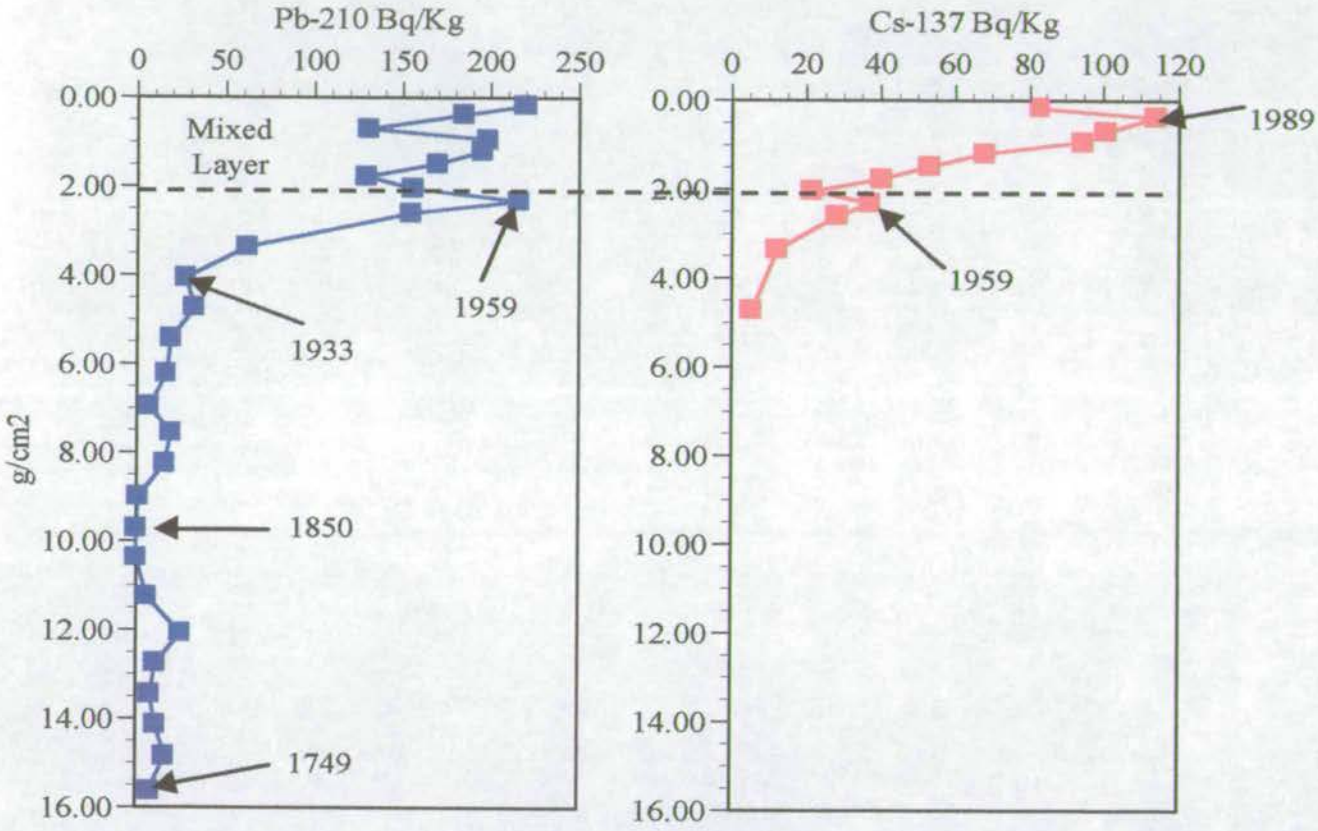

Figure 6-6 Comparative ^{210}Pb and ^{137}Cs profiles for the Arkona Basin

As can be seen from Figure 6-6 the results of the ^{210}Pb dating are relatively close to those of the expected dates for the ^{137}Cs events. The main peak associated with the Chernobyl reactor incident should date at 1986 and the secondary peak should link to the peak in global bomb testing in the early sixties. Although the distribution of ^{137}Cs during the Chernobyl event was uneven as a whole in the Baltic Sea the main peak in caesium was detected only a few weeks after the accident (KNAPINSKA-SKIBA *et al.*, 1994). Thus the ^{137}Cs peak can be considered to have been instantaneous on this scale of dating and thus from the caesium data it seems as though the core is approximately 3 years too young from ^{210}Pb dating. There are two main possibilities for this discrepancy; the first is a result of a decrease in

sedimentation rate over the last decade, however, the evidence from the organic carbon data and other published work suggests that there has been an increase in sedimentation rate during the recent past. Hence, the most likely cause of this discrepancy is due to the loss of the upper fluid core surface (equivalent to 0.6cm) as the dates from a ^{137}Cs deduced accumulation rate (significantly slower) are not compatible with our knowledge of stable lead isotope dates shown in the following chapter. In addition other published work from this region gives linear sedimentation rates comparable with the 2.2mm yr^{-1} obtained from this work (NEUMANN *et al.*, 1996 (2.5mm yr^{-1}); KUNZENDORF *et al.*, 1997 (2-3mm yr^{-1}) and EMEIS *et al.*, 1998 (2.3mm yr^{-1}).

In order to try and determine as to whether there has been a recent change in sediment accumulation rate then the pulsed nature of the ^{137}Cs profile can be used to help us infer possible deviations assuming that the top of the core was lost upon sampling. If the two main peaks are to be placed at 1986 and the early sixties then there must have been a recent change in sedimentation because placing the main peak at 1986 would also shift the lower peak down the equivalent of three years (to older dates). Hence for the data to be consistent with known historical events an increase in the accumulation rate would be postulated as a reason for this discrepancy. As shown earlier, published literature also suggests a recent increase in the accumulation rate and this is corroborated by the increased surficial organic carbon content shown in Figure 4-17 in agreement with the proposed hypotheses. In order to bring both ^{137}Cs inferred dates into line an increase in the sediment accumulation rate from 0.0496g cm^{-2} yr^{-1} to 0.0588g cm^{-2} yr^{-1} (linear accumulation rate change from 0.22cm yr^{-1} to 0.24cm yr^{-1}) commencing from the early sixties would place the ^{137}Cs peaks at their respective known historical ages. It seems likely that both an increase in the organic carbon content relating to higher primary productivity and the preferential conditions for preservation relating to the increased presence of anoxic conditions at depth will have both contributed to this increased rate as opposed to a change in lithogenic input.

Therefore, in summary, a sediment accumulation rate of 0.0496g cm^{-2} yr^{-1} is the best whole core estimate based on the changes and evidence available from the Arkona sediment core which has a mixed surface layer to a depth of 1.85g cm^{-2} yr^{-1} equivalent to a 37 year period. It is probable that the surficial flocculent layer was lost upon sampling and that based upon the above accumulation rate a linear sediment accumulation rate of 0.22cm yr^{-1} is found. In addition to this, a proposed increase in the accumulation rate throughout the mixed layer, based upon the ^{137}Cs data, from the early 1960's is found equivalent to an extra 0.23mm yr^{-1} in terms of linear accumulation rates. As the increase in accumulation rate is only found in the mixed layer then for geochemical inputs that are not of a pulsed nature then the resultant sediment accumulation rate of 0.0496g $cm^{-2}yr^{-1}$ can be applied to other profiles such as stable lead isotope ratios and pollutant metals so as to reconstruct an environmental history for the region. Figure 6-7 summarises this dating excess ^{210}Pb profile with age ranges. The older age is a minimum age based upon no mixing and the upper age takes into account the mixing layer as it is at present.

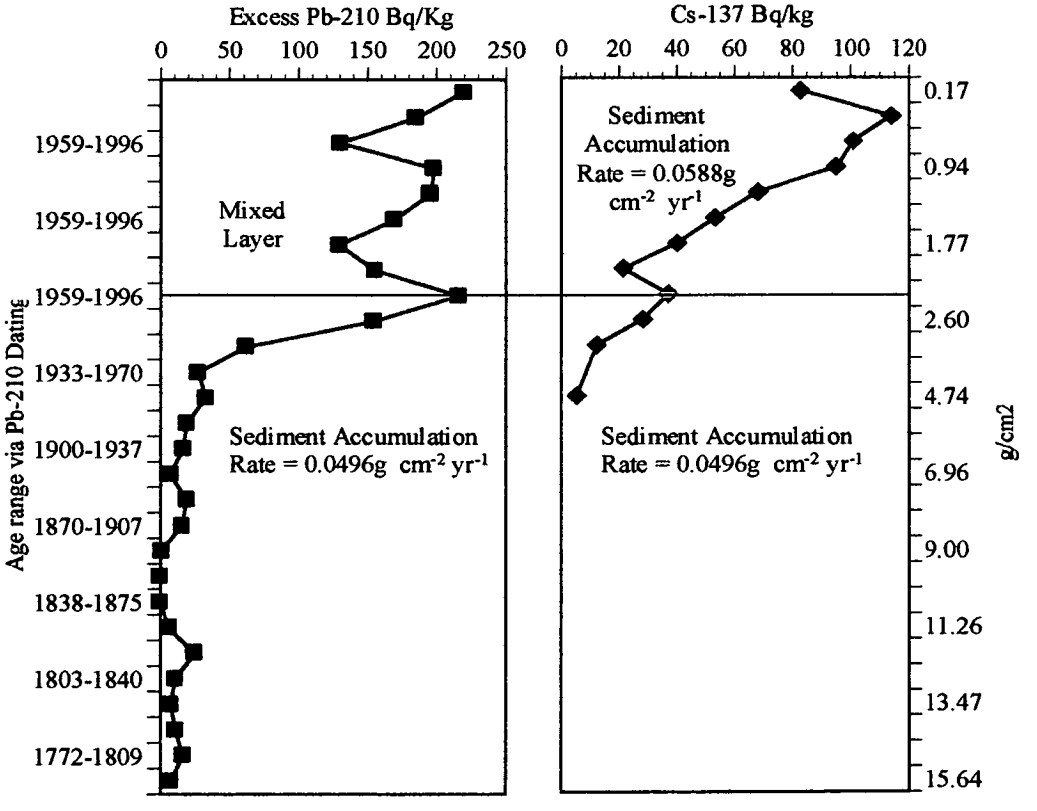

Figure 6-7 Dating summary derived from the excess ^{210}Pb and ^{137}Cs dating method

7.0 Stable Lead Isotope Ratios

7.1 RATIONALE

As lead is one of the metals that shows a significant anthropogenic component it was decided to investigate this further by use of its stable isotopes. The use of stable lead isotopes is twofold; the first is to help elucidate the provenance of the lead input, be it solely natural, related to industrial processes (incineration / metal production) or fuel combustion, and the second is its use as an age proxy for the sediment core knowing something of the history of lead production in the region.

7.2 THEORY OF PROVENANCE DETERMINATION VIA STABLE LEAD ISOTOPES

There are four stable lead isotopes with masses of 204 (1.35%), 206 (25.3%), 207 (21.1%) and 208 (52.2%). A detailed theoretical treatment for the evolution of these isotopes can be found in DOE, 1970 and FAURE, 1986 but in brief ^{204}Pb is non-radiogenic whereas the others represent the stable end members of the ^{238}U, ^{235}U and ^{232}Th decay series respectively as shown in Figure 7-1. As each series has its own individual consolidated half life and decay rate then over time the abundance of the radiogenic lead end members will increase at independent rates throughout the earths history, relative to non- radiogenic ^{204}Pb. For example, the decay rate of ^{238}U to ^{206}Pb is much slower than ^{235}U to ^{207}Pb hence the ratios change continuously over time with the 206/207 Pb ratio decreasing with increasing geological time. The current or modern lead compositions lie within the range $^{206}Pb/^{204}Pb$ = 18.6-19 and $^{207}Pb/^{204}Pb$ = 15.6-15.67 and hence a $^{206}Pb/^{207}Pb$ ratio of 1.20 (STACEY and KRAMERS, 1975). Therefore the decay of any uranium bearing mineral will have two independent radiometric clocks with independently changing Pb ratios at any given time. Thus when a lead ore body containing galena (PbS) is formed then the lead becomes separated from its radioactive parent and holds a isotopic ratio unique

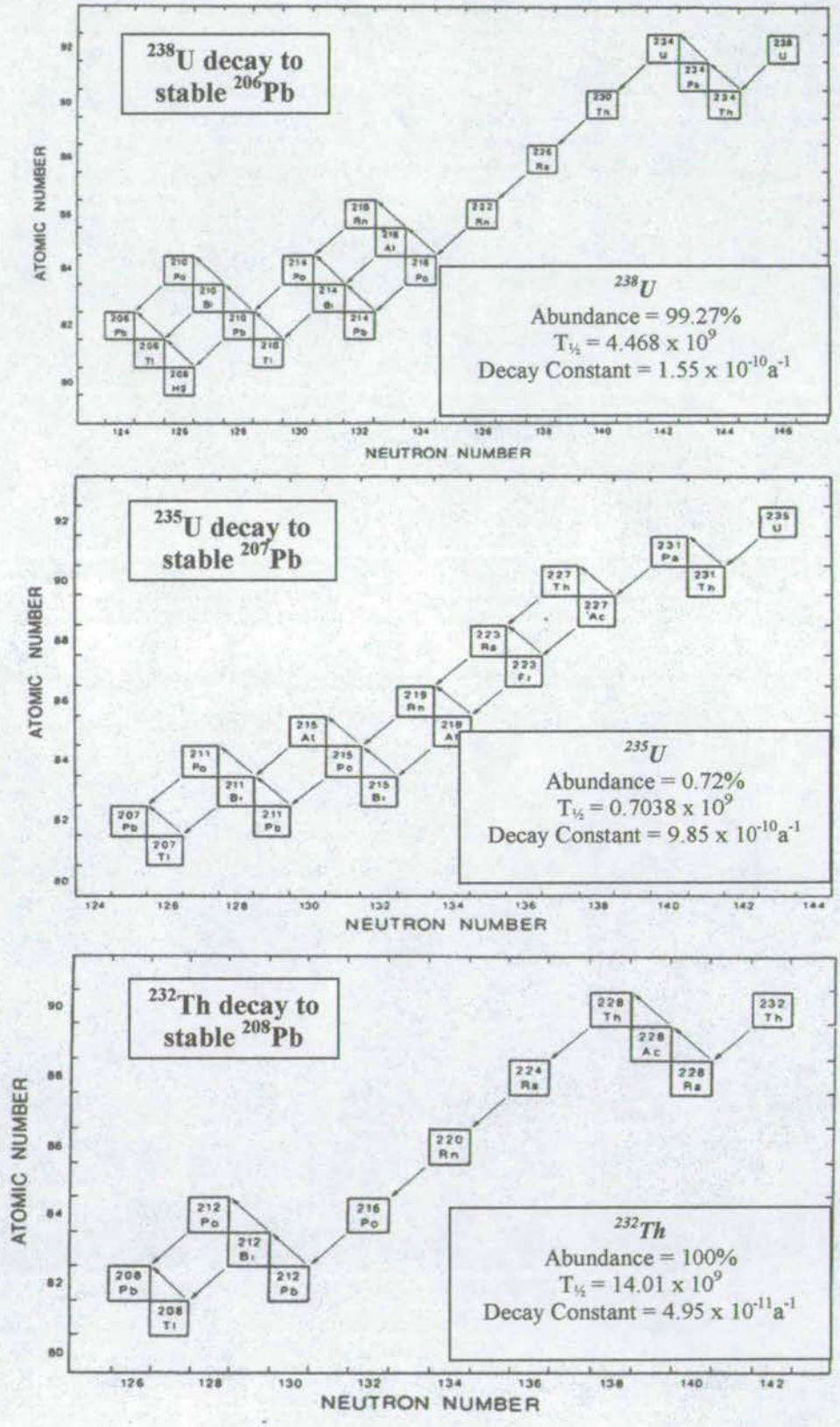

Figure 7-1 ^{238}U, ^{235}U and ^{232}Th decay series to their stable lead isotope end member of ^{206}Pb, ^{207}Pb and ^{208}Pb. (adapted from Faure, 1986)

to that separation event which has a $^{206/207}Pb$ ratio that is usually considerably less than that of recent sediments because the accumulation of ^{206}Pb from ^{238}U decay stops upon formation of the ore but continues in crustal rocks which in turn go on to form the recent sediments.

The relative abundance of the lead isotopes can therefore be used as a geochemical footprint that can be traced back to its provenance if it has been incorporated into a migratory anthropogenic pathway. This is possible because there is no known isotopic fractionation (enrichment and depletion) of modern lead by recent geochemical or biological processes as there is for low mass elements by selective fractionation.

7.2.1 Lead Isotope Ratios as Tracers of Lead Pollution

There are only two main pathways of lead into the Baltic Sea system (aquatic and atmospheric). The aquatic input can be considerably complicated by the set of natural filters and pathways that lead to the depositional environment particularly the transition from riverine through estuarine and finally into a salinity graded sea such as the Baltic. However, the atmospheric inputs are relatively simple and direct as the residence time of lead aerosols is short (1-2 weeks) and because Pb is rapidly scavenged from the marine environment and into the sediment. Hence, there is a relatively short lag time between changes in the lead signature from the burning in one form or another of ores to its incorporation in the sedimentary record.

In contrast to this there are many sources of anthropogenic lead pollution and it would be impossible to categorise them all. However there are three main groups which make identification of the source areas somewhat easier:

- That related to combustion within petrol engines,
- that involved in the processing of industrial and domestic waste by incineration
- and that related to the mining and smelting of ores.

A brief history of industrial lead is given in SHIRAHATA *et al.*, 1980 which clearly shows that anthropogenic lead is not only a recent phenomenon, but can be traced back to ancient Greek and Roman times with the advent of mining and smelting and that the consequences of this ancient anthropogenic activity can even be detected in such remote places as the Greenland ice cap as described by ROSMAN *et al.*, 1995.

The main use of lead isotopes is to discern the changes in lead input over the period extending back to the industrial revolution. Between the industrial revolution and the mid eighties, non-radiogenic lead became increasingly important due to the replacement of coal with oil and the use of Australian and Canadian lead ore in the heavy industries of north-western Europe. Prior to the turn of the century, lead of industrial or coal origin had a typical 206/207 ratio of 1.21. By the end of the 1930's the first signs of significant changes were found relating to a large increase in the atmospheric lead concentrations caused by the lead emissions from automobile exhausts (MUROZUMI *et al.*, 1969). This increase in emissions led to a significant decrease in the ratio signatures pertaining to the use of Australian and Canadian lead ore inputs of Precambrian age for petrol additives (leadtetramethyl and leadtetraethyl) with $^{206/207}$Pb ratios as shown in Table 7-1. These imported ores had considerably different ratios to that of the natural and industrial values of the time. A survey of leaded petrol in Edinburgh by SUGDEN *et al*, 1991 showed that the modern value had a mean ratio of 1.082 ± 0.024 which is manufactured by Associated Octel (AOC) the only alkyl lead manufacturer in Britain. AOC subsidiaries in France, Germany and Italy tend to use a similar ore bodies and ratios and hence the end member lead isotope ratio is very similar for Western Europe.

The introduction and wide spread usage of unleaded petrol in the mid-eighties has had a pronounced affect on the stable lead isotope ratio signature with it reverting closer to natural levels as shown by HOPPER *et al*, 1991; KERSTEN *et al.*, 1991; MIGON *et al.*, 1993; LAKASCHUS, S., 1997 in aerosols SUGDEN *et al.*, 1991; MACKENZIE *et al.*, 1995; WEISS *et al.*, 1999 in ombrotrophic peat bog cores and OHLANDER *et al.*, 1993; VALETTE-SILVER, 1993; GOBEIL *et al.*, 1995; FARMER *et al.*, 1996; FERRAND *et al.*, 1999 in sediment cores.

Table 7-1 $^{206}Pb/^{207}Pb$ ratios for major lead ore bodies used in the manufacture of alkyl lead products in northwestern Europe.

Ore Body	$^{206}Pb/^{207}Pb$ Ratio	Reference:
Mount Isa, Australia	1.04	Sturges and Barrie, 1987
Broken Hill, Australia	1.04	Sturges and Barrie, 1987
New Brunswick, Canada	1.16	Sturges and Barrie, 1987
Sullivan, Canada	1.07	Stukas and Wong, 1981

Although the figures vary, KRUGER, 1996 estimated that since the 1980s more than 75% of the anthropogenic lead emissions were as a result of engine fuel combustion. In contrast to this FARMER *et al.*, 1996 suggested that prior to the 1950s the leaded petrol contribution accounted for only 24-53% of the excess lead deposited and that lead from industrial and domestic activities predominated. Hence, over history there has been a swing in the dominance of various components of the anthropogenic lead contributors and these have been shown to be displayed in the sedimentary record.

7.3 LEAD ISOTOPES AND THE BALTIC SEA

The most obvious control on any atmospheric component of anthropogenic lead pollution and it deposition in the sedimentary record is the wind and its direction. While the above brief history holds true for the majority of north-western Europe, behind the Iron Curtain different ore bodies with very different ratios were being used in their industries. Some east European ore 206/207 ratio values are shown along side 208/207 ratios in Table 7-1. In addition to these ore values HOPPER *et al.*, 1991 published values of 1.174 for the alkyl lead content in Polish petrol. Thus depending upon the predominant wind direction, the nature of the ore and the magnitude of the flux, different ratio signatures could accumulate together thus making the interpretation of a regions history difficult to unravel.

Table 7-2 Lead isotope ratios for ore bodies around central Europe.

Ore Body	Av. $^{206}Pb/^{207}Pb$	Av. $^{208}Pb/^{207}Pb$	Reference:
Eastern Europe	1.193	2.486	Brown, 1962
Poland	1.179	2.469	Russell and Farquhar, 1960
Germany, Austria	1.171	2.457	Doe, 1970
Siberia	1.170	2.459	Brown, 1962
Former USSR (av.)	1.156	2.439	Brown, 1962
Sweden, Finland	1.01	2.3	Brown, 1962

While meteorological observations have been taken since the turn of the century in the southern Baltic Sea region, Figure 7-2 shows actual measurements taken from the Arkona basin site for the period 1980-1992 (SIEGEL *et al.*, 1996). The data is based upon 3 hourly means provided by the German weather service (DWD) from the Arkona weather station. The data is expressed by an east and north component of wind velocity. High frequencies at 0m/s for both the north and east components represent stable and calm conditions.

Figure 7-2 shows that the wind systematics in this region are predominantly controlled by westerly and easterly winds in all seasons. While westerly winds are the predominant wind direction, occurring in a high frequency for all seasons, significant maxima for easterly winds occur mainly in the spring and summer with easterly winds only being predominant in the spring. In addition SIEGEL *et al.*, 1996 report that the direction of westerly winds changes during the year from WNW (290°) in spring over W (270°) in summer to SW (220-230°) in autumn and winter.

These findings have obvious implications for the source regions of anthropogenic lead and its incorporation in the Baltic Sea sediment. In particular a balance has to be struck between the contrasting dominance of the two main wind directions with the important winter period of increased atmospheric aerosols being predominantly from Eastern Europe and Russia. During the rest of the year westerly winds predominate bringing a anthropogenic lead signature from north-western Europe.

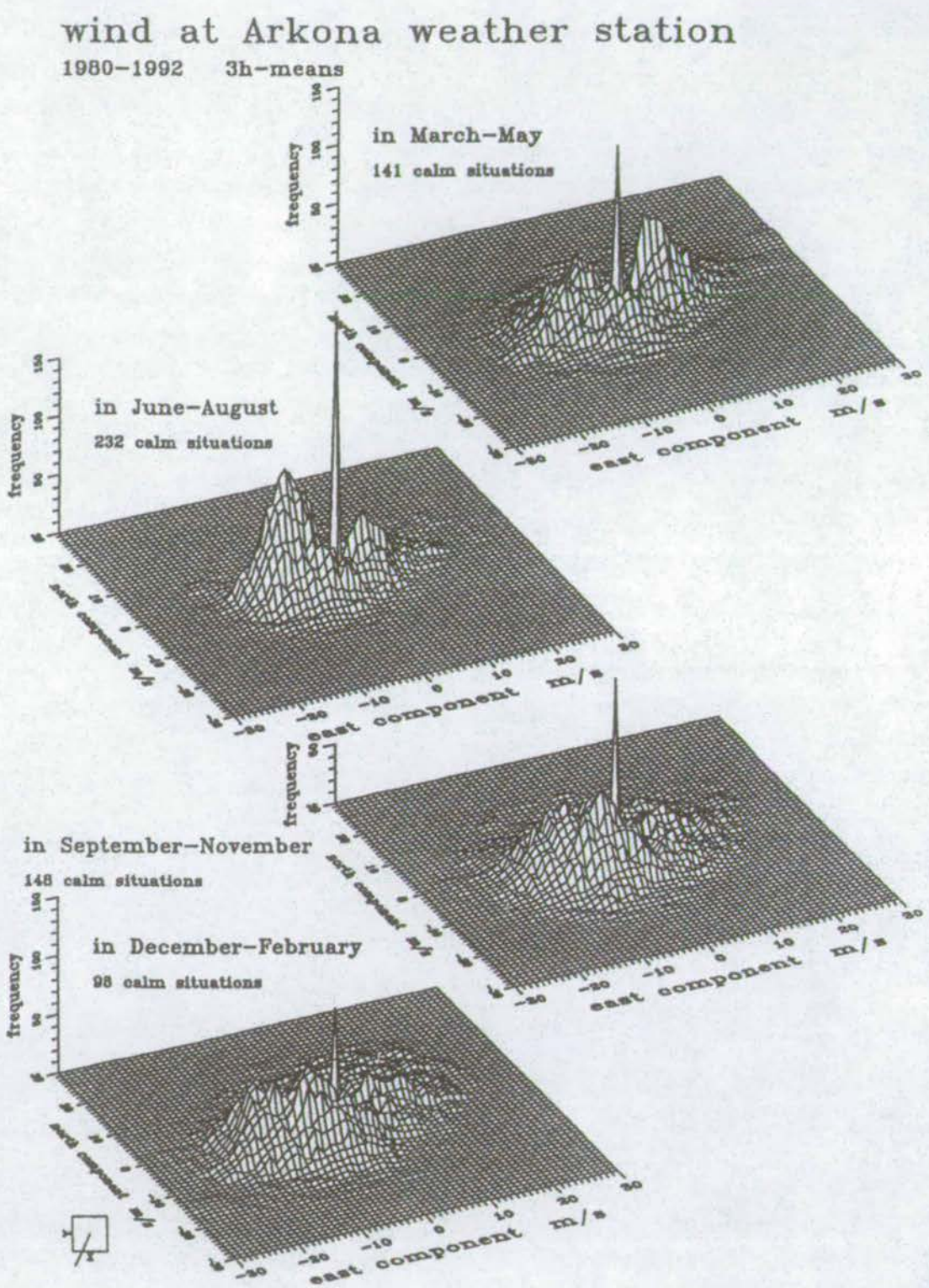

Figure 7-2 Frequency distribution of wind speed and direction at Arkona for the period 1980-1992 (Taken from Siegel *et al.*, 1996).

Thus with respect to the atmospheric aerosol lead isotope content and the importance of wind direction, HOPPER *et al.*, 1991 determined the aerosol lead isotope values for four main source regions around central Europe as shown in Table 7-3

Table 7-3 Characteristic lead isotope signatures for each of the regional source areas as identified by Hopper *et al.*, 1991.

Source Region	Av. $^{206}Pb/^{207}Pb$	Av. $^{208}Pb/^{207}Pb$
Eastern Europe	1.172	2.424
East (USSR, Finland)	1.153	2.428
Northwest (Sweden, Norway)	1.128	2.394
Western Europe	1.142	2.405

7.4 SOUTHERN BALTIC SEA SEDIMENT CORE STABLE LEAD ISOTOPE RESULTS

The ICPMS was optimised for the analysis of lead isotope ratios with 5 repeats for each sample and any result that had errors greater than 2% were rejected, however the accuracy of the ICPMS allowed determinations with the majority of errors less than 1%. The graphs drawn here are therefore without error bars in order to give greater clarity. The results obtained from this study in the southern Baltic Sea are shown in Figure 7-3 and Figure 7-4.

Figure 7-3 shows both the total lead concentrations and the stable lead isotopes for all stations. A striking feature of this figure is the remarkable similarities in value for the stable lead isotopes and the similar trends exhibited down core. Surface ratios are approximately 1.175, which is remarkably close to the value of 1.174 proposed by HOPPER *et al.*, 1991 for the value of Polish petrol, with most station profiles dropping sub-surface before increasing again at depth to values of around 1.24. These profiles are shown in greater detail in Figure 7-4.

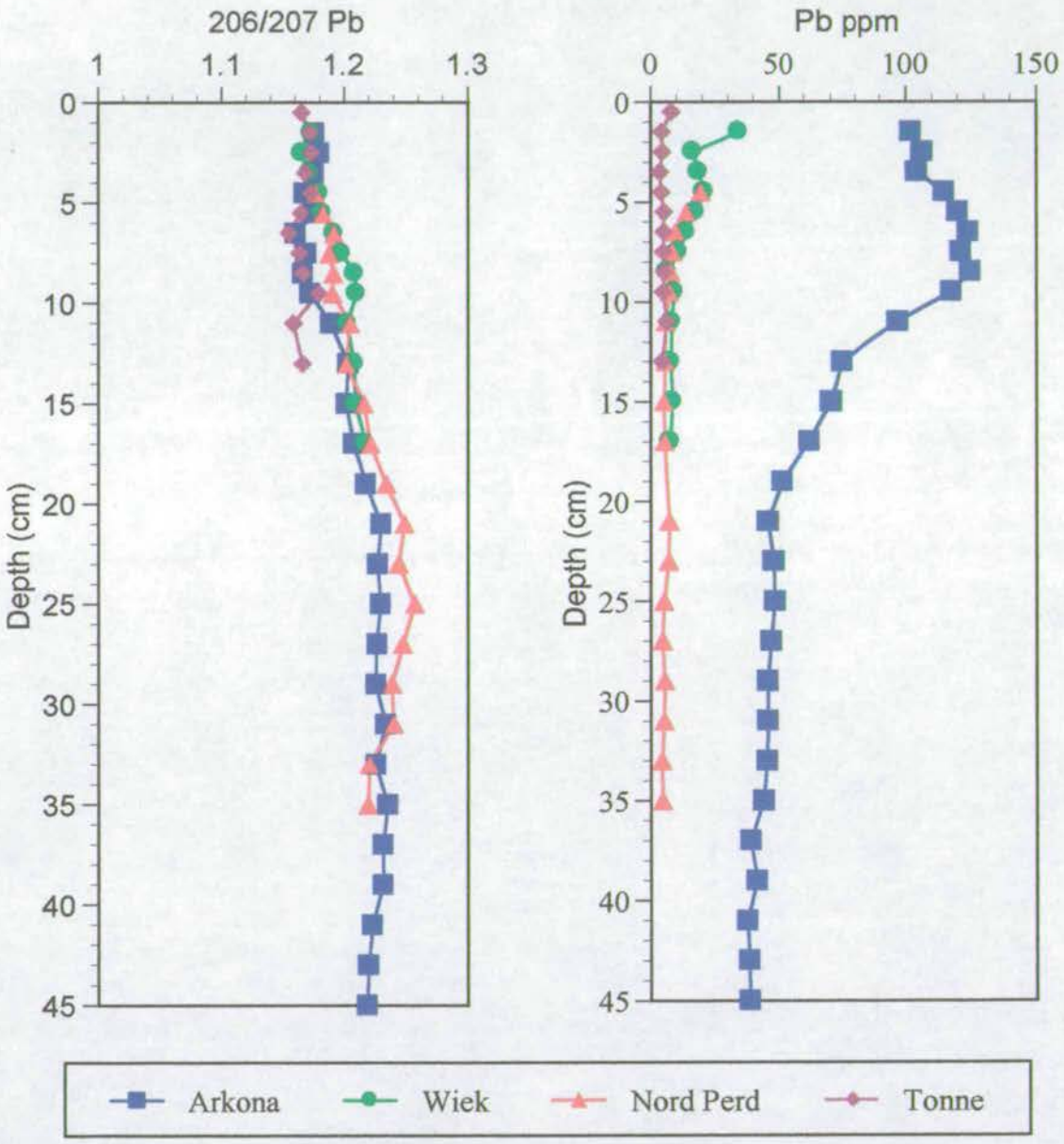

Figure 7-3 Stable lead isotope ratio and lead concentration plot for all four stations

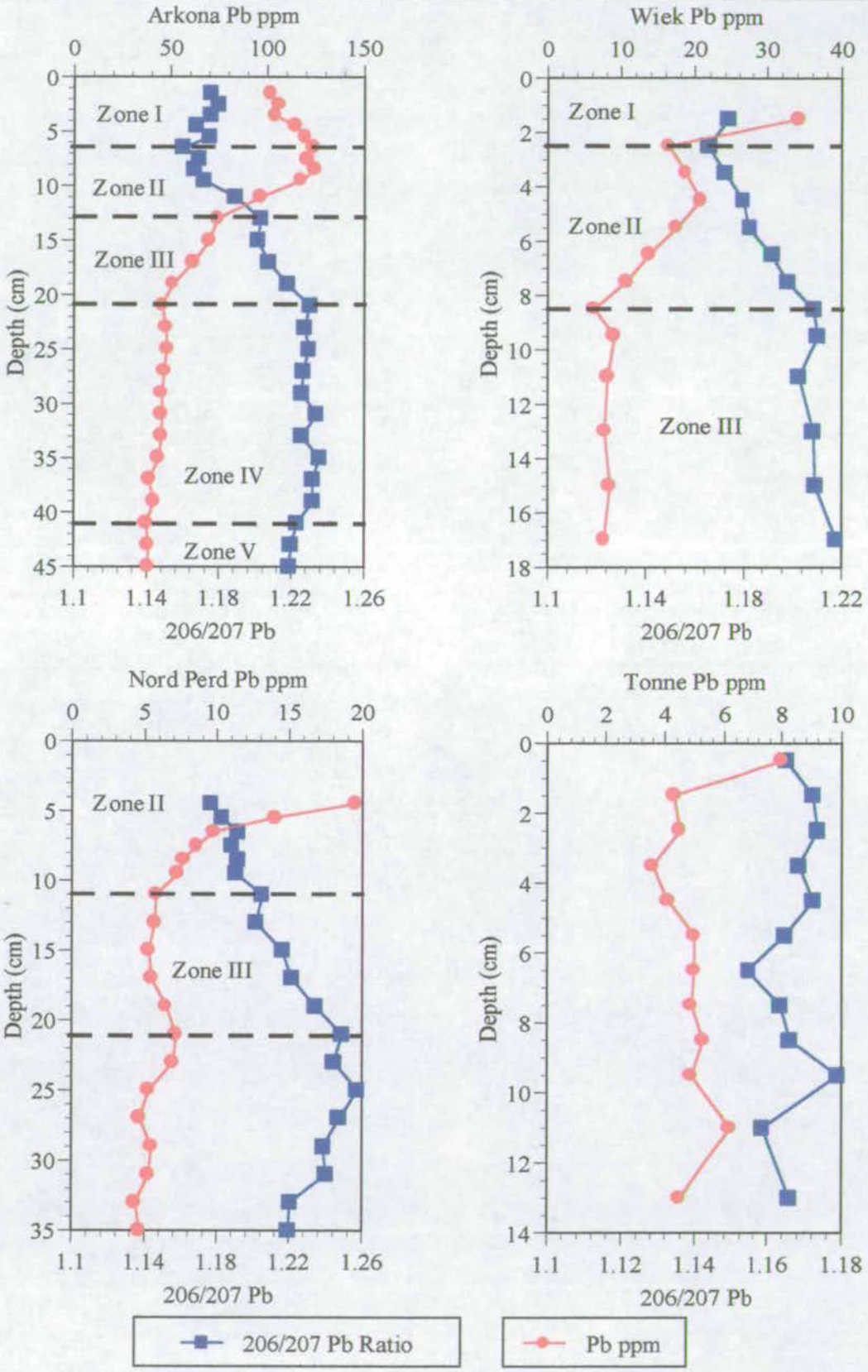

Figure 7-4 Stable lead isotope ratio and lead concentrations for individual stations in the Southern Baltic Sea, NB. Note scale changes.

Figure 7-4 shows the close inverse correlation between total lead concentration and the lead 206/207 ratio. While Arkona shows a 'textbook' profile the three other stations have much lower lead concentrations and thus characteristic zonations as seen in the Arkona profile are not as well developed. However, Wiek and Nord-Perd show very similar trends within the increased error associated with the lower concentrations. Tonne while not displaying a characteristic zonation profile is likely to lie exclusively within Zone I with a profile characteristic of a high energy, non-depositional environment. For completeness the features associated with the Arkona Basin profile as shown in Figure 7-5 will be described.

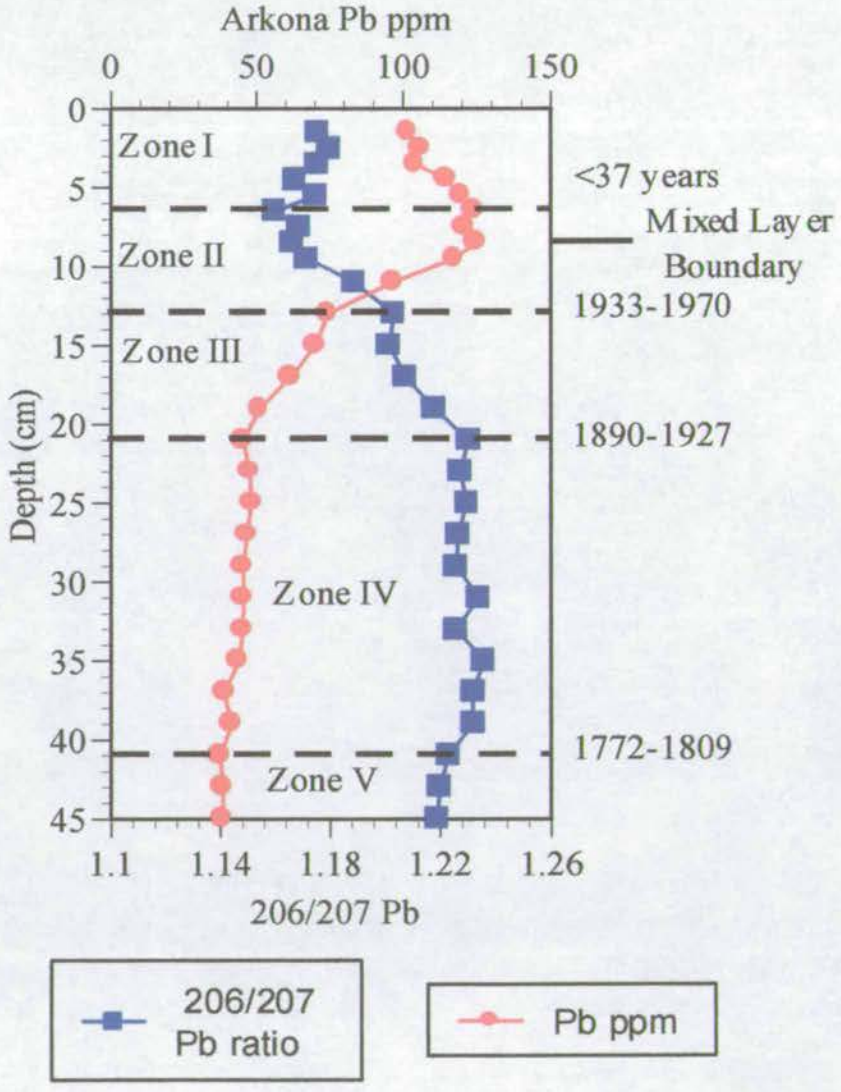

Figure 7-5 Arkona basin stable lead isotope zonations along with inferred dates from ^{210}Pb dating

The profile has been split into five zones for ease of description and is shown along with ^{210}Pb derived dates in Figure 7-5 with which the date ranges proposed have a decreasing confidence with an increase in age. The lowest zone, V extends from the base of the core to 41cm depth and has a 206/207 ratio of approximately 1.22 and a lead concentration of 42 ppm. This zone is as close to the 'natural' background that is possible from this core and probably dates back to pre-modern industrialisation times (late eighteenth century) and consequently is the environmental base line for this area.

Zone IV is characterised by both a stable lead concentration of approximately 45 ppm and a stable 206/207 ratio of 1.23 most probably relating to localised coal and ore development within the immediate vicinity of the Baltic Sea as opposed to the introduction of foreign ores to west and eastern Europe and the onset of mass industrialisation. This period covers over a hundred years in total and relates well to the onset of ship building in Stettin (1750) and the onset of industrialisation in the Silesia region of Poland associated with the coal and metal deposits there (WEIR, 1994). In addition, TUBILCOCK, 1981 wrote of lead smelters in operation in Silesia since 1800 which tie in well with the calculated ^{210}Pb dates.

At 21cm depth a steep decline in the 206/207 ratio is observed concomitant with an abrupt increase in total lead concentration which shallows in gradient towards the surface, characteristic of Zone III. ^{210}Pb dates place the start of zone III around the start of this century which is in good agreement with the introduction of Australian lead ore to western Europe, initially for industrial uses and then subsequently as the main anti-knocking additive in automobile petrol for Western Europe. This zone is most likely to be related to the main heavy industrial period during the early part of this century in which lead ores with a lower 206/207 ratio than that found naturally in the region were used.

Zone II shows the steepest change in gradient towards higher lead concentrations and lower $^{206/207}Pb$ ratios. The start of this main period of decline is dated around 1930, coincidental with the onset of mass car usage and peaks around 1959 plus the mixing

component which the spans the range to present. It is likely that the peak would be envisaged to occur around the 1970's and that the subsequent decline in ratios to occur from around the mid 1980's. However, all these key dates are found within the mixed layer and thus it is not possible to establish a definitive chronology.

Zone I shows the 'recovery' of the 206/207 ratio back towards the natural level and a decreasing lead concentration which continues to the present day. The effects of mixing can be recognised within this zone assuming that a consistent increase in Pb ratios would occur with an increase in the use of unleaded petrol. As an approximate date proxy based upon the stable lead isotopes for Arkona the start of the main decline in stable lead isotope ratios could be estimated at around 1930 with the onset of mass automobile usage which gives a linear core accumulation rate of approximately 0.197cm yr^{-1} which is in good agreement with that of the ^{210}Pb dating method (0.22cm yr^{-1}).

In addition to the stable lead isotope data measured in the sediment core, measurements were also made on the mobile nepheloid layer and sediment trap samples which span the time gap from October 1996 to June 1998 thus giving an evolutionary change in the ratios beyond the scope of the sediment core collected in 1996. As the nepheloid layer 206/207 ratios are a result of mixing over a period of time then the sediment trap ratios are given in Figure 7-6 as these represent the purist indicators of recent trends in the evolution of the stable lead isotopes.

The main features of Figure 7-6 are one of an increasing ratio value throughout the year with ratios approaching 1.19 during the period December to March 1998. The main exception to this is the period of March to June '98 which shows a slight decrease in the ratio which may relate to an increasing dominance of Polish petrol in the system or to a seasonal change in wind direction carrying a lower lead isotope signature from eastern Europe and Russia.

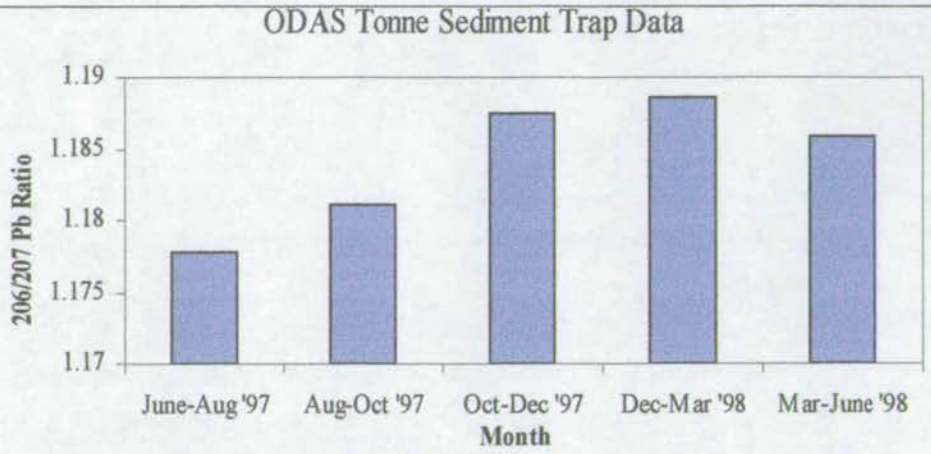

Figure 7-6 Sediment trap stable lead isotope ratio measurements from June '97 to June '98 at ODAS Tonne.

In order to try and unravel the contributory sources to the resultant profile of anthropogenic lead ratio migration, $^{206/207}$Pb was plotted against $^{208/207}$Pb and is shown in Figures 7-7 and 7-8. Figure 7-7 shows data for Arkona, Wiek and Nord-Perd plotted as a function of the zonations previously described in order to see the effect of changing ratios over time. Within Figure 7-7 is an additional figure showing the $^{206/207}$Pb ratio versus concentration in order to aid interpretation. Figure 7-8 shows the same data along with both the regional lead ore and regional atmospheric aerosols ratios from HOPPER *et al.*, 1991 plotted so that comparisons to some of the main sources can be made although, due to the lack of published information, many desirable ratios are unknown.

While the $^{208/207}$Pb ratios cover a small range, as the errors were slightly greater than those of the $^{206/207}$Pb ratios, two general end members can be seen with respect to $^{206/207}$Pb ratios in Figure 7-7. An anthropogenic maximum lying around 1.165 and a natural background ratio of 1.235. Generally Zones I and II lie along a gradient towards the lowest ratios with the natural background ratios lying reasonably consistent around 1.236. The atmospheric aerosol ratio values plotted in Figure 3-8 are from data collected in 1991, thus as current trends of decreasing anthropogenic inputs continue then the ellipses marked will have moved to the right with time. This then places the results obtained within range of the probable current atmospheric aerosol values.

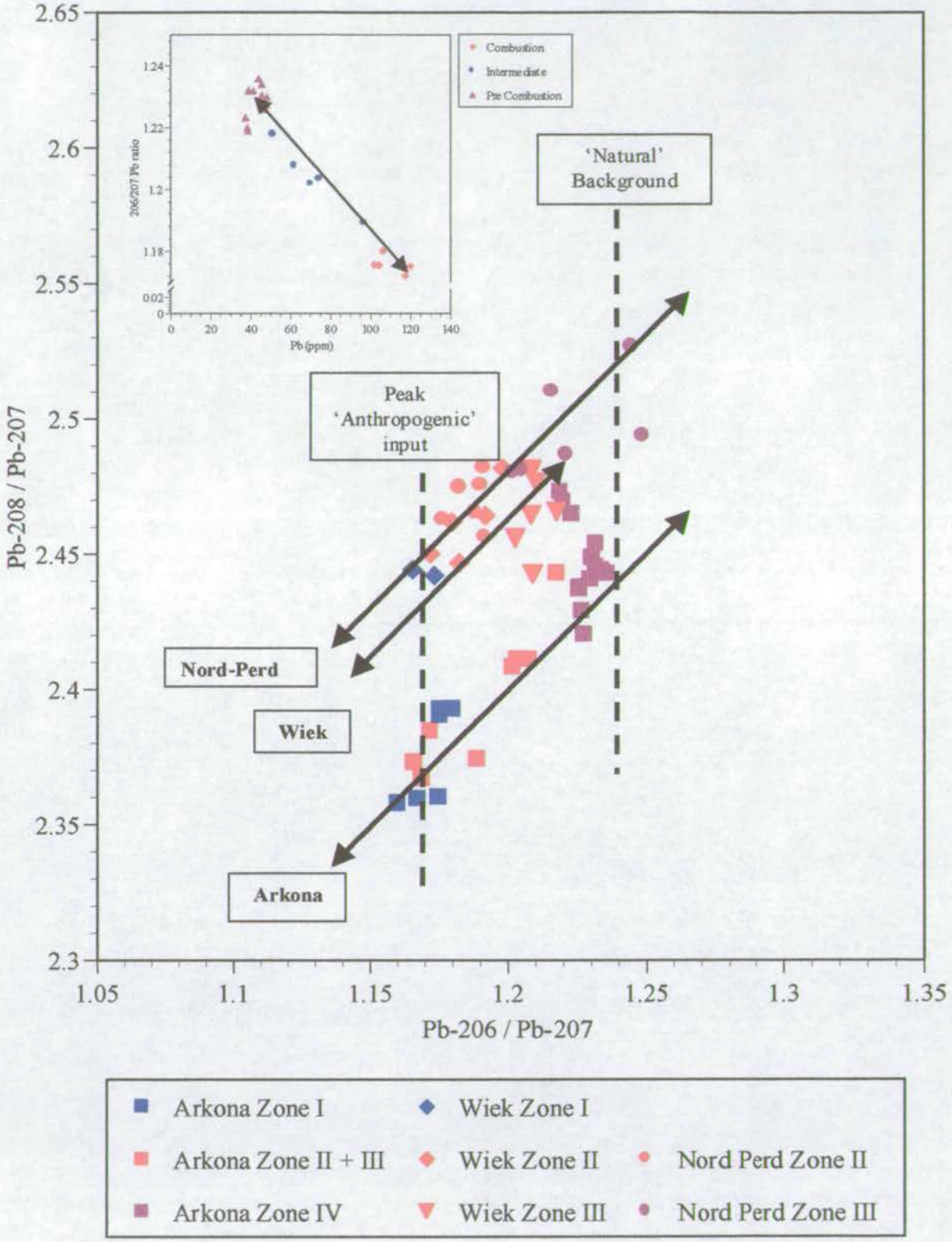

Figure 7-7 Stable isotope ratio plot of the main down core zones for $^{206/207}$Pb Vs. $^{208/207}$Pb.

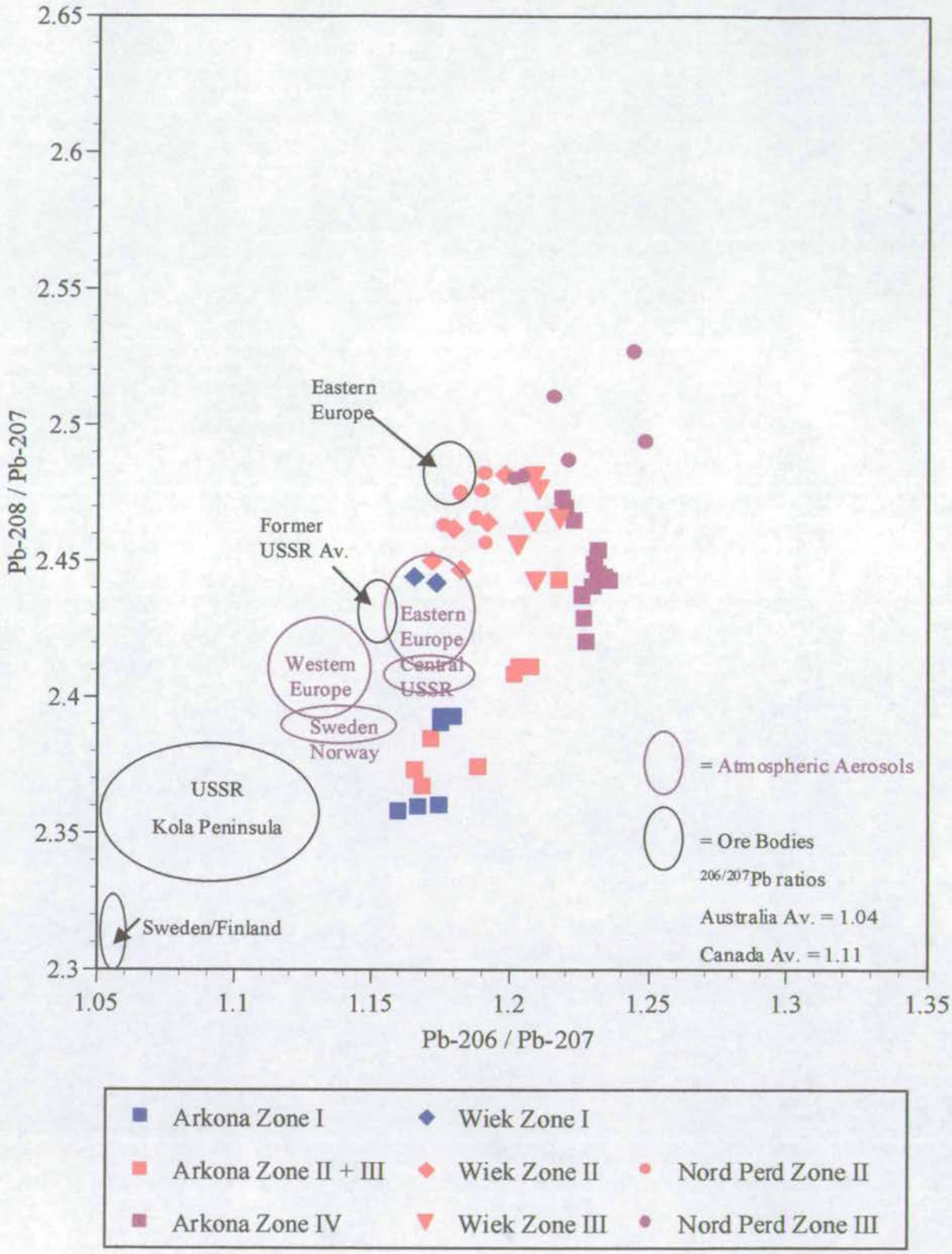

Figure 7-8 Characteristic $^{206/207}$Pb and $^{208/207}$Pb ratios for aerosols and regional ore bodies in central Europe. (After Hopper *et al.*, 1991)

While care must be taken in this complicated system in trying to discern the relative inputs of various contributors to the anthropogenic input (mining, combustion and waste) due to a lack of published data and the critical variations in wind direction it is still possible, via a simplified model, to get a best estimate of the two largest contributors, industry and combustion. A best guess estimate can be made based upon the observation that the average Russian ore approximates close, or greater to, the actual anthropogenically influenced values found. Therefore while there maybe a contribution from this source, the predominant source of pollution is from the lower ratio ore used in Western Europe. ROHDE *et al.*, 1980 showed that for airborne pollutants arriving in the Baltic Sea that the predominant wind direction over the year as a whole was from the West. In order to quantify these inputs of lead to the Baltic Sea system, a first approximation to the proportional contributions can be intimated by using Equation 7-1 taken from FARMER *et al.*, 1996. This equation is used to calculate the $^{206/207}Pb$ ratio of the excess lead (anthropogenic input) and, additionally, by multiplying the excess lead concentration by the accumulation rate determined the excess lead flux. If the same concepts are applied to the Southern Baltic Sea and a background concentration of 40ppm and a $^{206/207}Pb$ ratio of 1.22 is assumed then the results are summarised in Figure 7-9.

Equation 7-1

$$^{206/207}Pb_{excess} = [(Pb_{mease} \times {}^{206/207}Pb_{meas}) - (40 \times 1.22)] / (Pb_{meas} - 15)$$

It is clear that for the majority of the nineteenth century anthropogenic lead fluxes were comparatively low, being less than 5mg m^{-2} yr^{-1}, but towards the start of the twentieth century a steep increase associated with a lowering of the residual $^{206/207}Pb$ ratio occurred. This excess lead flux peaked in the late 1950 and has been sustained at greater than 20mg m^{-2} yr^{-1} for over 40 years. A recent trend towards decreasing lead fluxes (and an increase in the $^{206/207}Pb$ ratios) bodes well for the environment relating mainly to the change from leaded to unleaded petrol over the past 15 years.

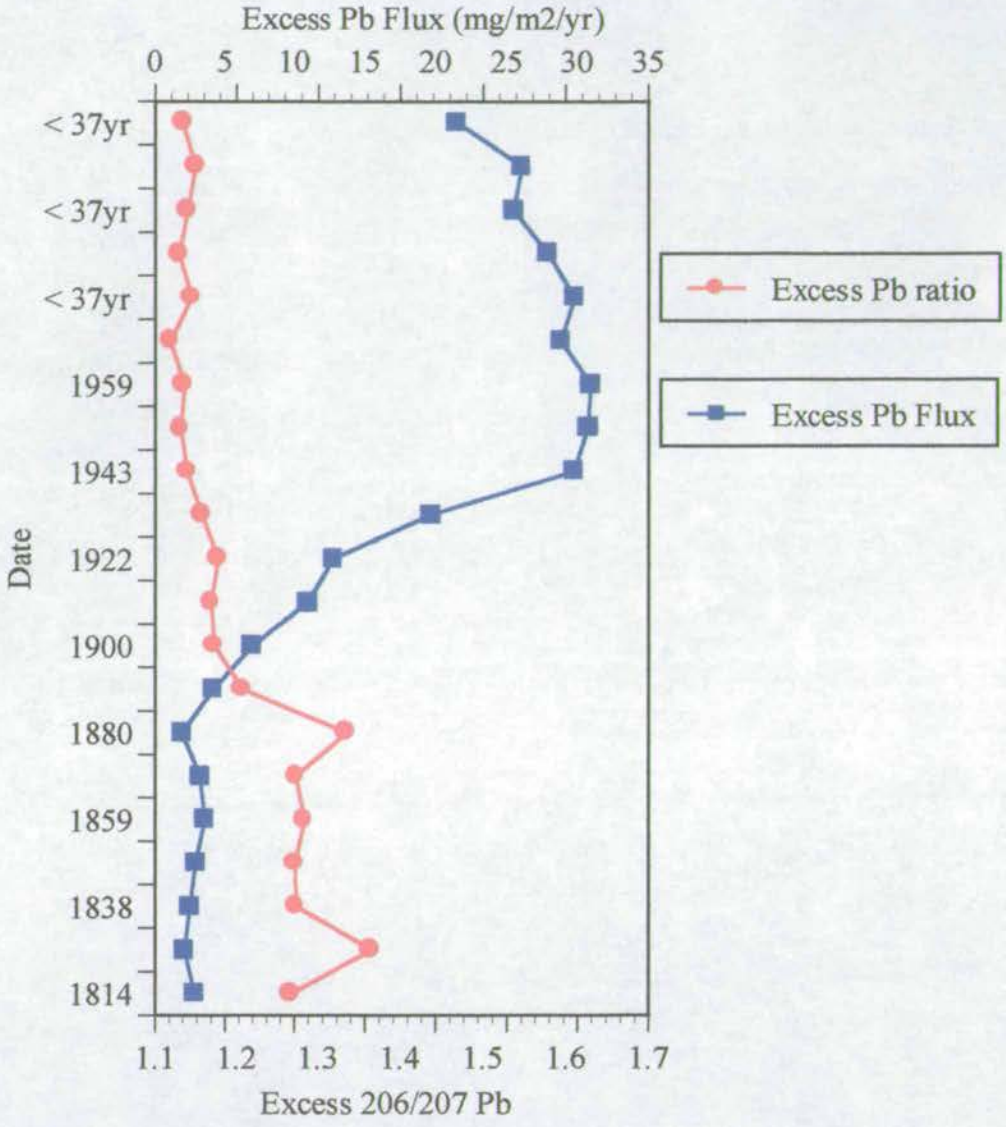

Figure 7-9 Excess (anthropogenic) lead fluxes and associated $^{206/207}$Pb ratios in the Arkona Basin versus ^{210}Pb derived chronology.

FARMER *et al.*, 1996 then used Equation 7-2 to try and determine the relative contribution of petrol to the total lead flux as a function of time. In order to do this a number of assumptions have to be made, which are at best tentative, due to the uncertainties surrounding the value of the $^{206/207}$Pb ratio for petrol in this region of the Baltic Sea and the relative contributions of the anthropogenic input via westerly and easterly winds. A best estimate however based on the predominance of westerly winds can be made by assuming a petrol value close to that characteristic of Western Europe. Direct information about the true $^{206.207}$Pb ratio of petrol from the beginning

of the century is unavailable but measurements by FARMER *et al.*, 1996 of 1.071 ± 0.010 (n = 18) and SUGDEN *et al.*, 1991 of 1.082 ± 0.024 in leaded petrol provide a basis for these calculations. FARMER *et al.*, 1991 suggests an upper limit of 1.12 for petrol derived atmospheric lead so as to take into account the possible usage of imported tetraalkyllead from America during past times. Thus Figure 7-10 details the contributions of industrial and petrol lead to the excess lead flux in the twentieth century for three scenarios all of which take an industrial $^{206/207}Pb$ ratio of 1.236 but are differentiated by $^{206/207}Pb$ ratios of 1.08, 1.10 and 1.12 for petrol.

Equation 7-2

$$Pb_{petrol}\ (\%) = [(1.236 - {}^{206/207}Pb_{excess}) \times 100] / (1.236 - {}^{206/207}Pb_{petrol})$$

The results shown in Figure 7-10 tell of a total excess lead flux (A) which is substantially impacted upon by the introduction of leaded petrol and the increased mobility of the population throughout the twentieth century. Taking a petrol $^{206/207}Pb$ ratio of 1.12 shows that at its peak petrol contributions to the total lead flux approximated to 100% of the total excess lead flux. Based upon historical records and known increases in car usage this peak would be estimated to date sometime during the 1970's. Typically throughout the latter half of the century, however, based upon this ratio scenario petrol has been responsible for roughly 85-90% of the anthropogenic lead flux with only 10-15% coming from industrial sources.

The remaining two scenarios (1.10 and 1.08) while showing the same form of historical variations, detail smaller overall contributions of petrol (70% and 60% respectively over the last 50 years) and a larger industrial component. Thus when combined with the historical fluxes which pre-twentieth century were less than 5mg m^{-2} yr^{-1} then the influence of petrol has had a major effect on the flux of lead deposited in this region of the Baltic Sea with a 600% increase at its peak. Depending on the scenario taken, a petrol ratio value of 1.12 would indicate that the industrial component has remained relatively constant over time during the last 200 years (~ 5mg m^{-2} yr^{-1}). In comparison, with the 1.10 and 1.08 scenarios, industrial

input would have grown to approximately 9 and 12 mg m^{-2} yr^{-1} when compared to pre twentieth century values.

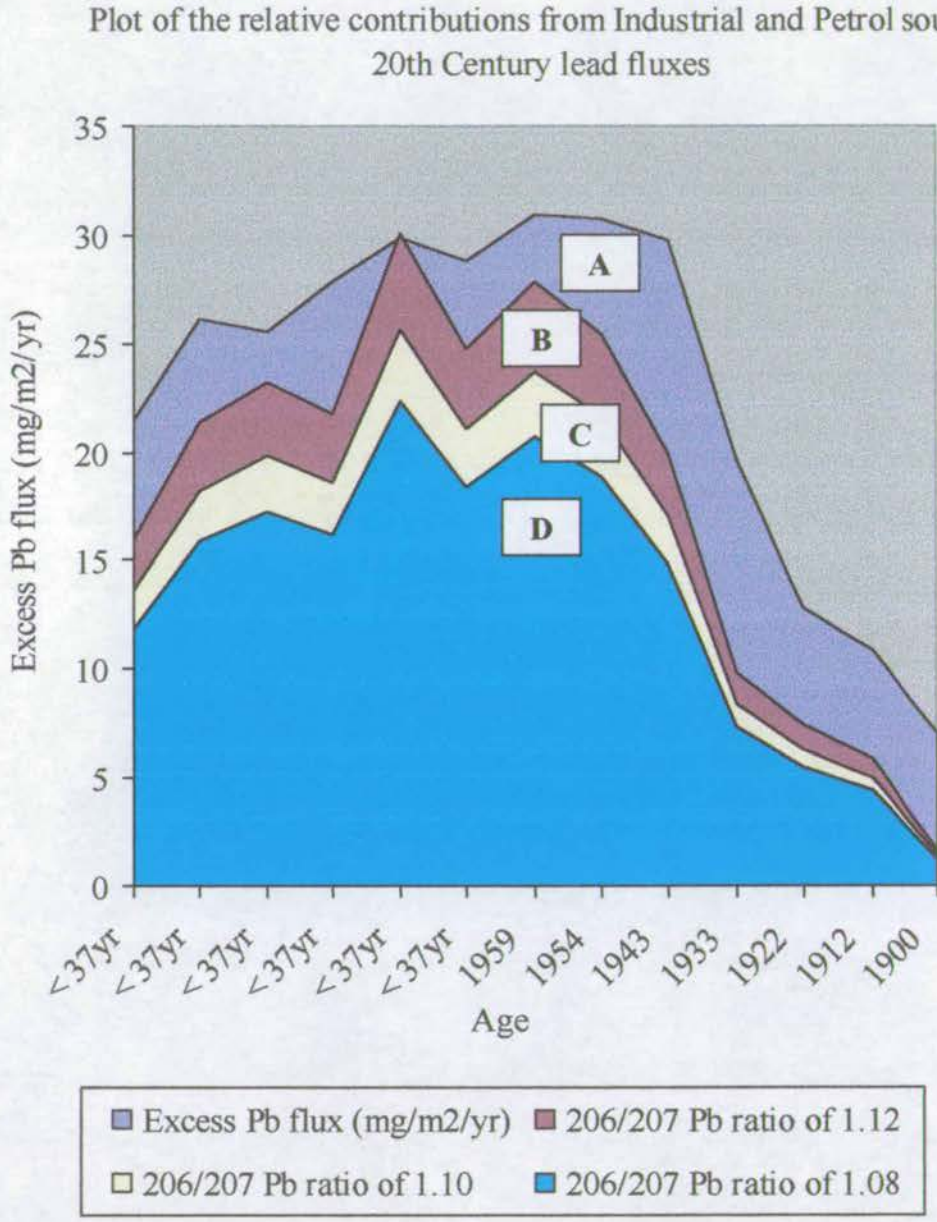

Figure 7-10 The relative contributions of petrol and industrial lead to the excess lead flux in the Arkona Basin based upon a range of petrol lead ratios (1.08, 1.10 and 1.12).

Figure 7-11 is a comparative representation of the Arkona core with that of the other stations and although the lead concentrations are much lower than Arkona and

therefore have a slightly larger error associated with them, essentially the same stable lead isotope patterns can be seen with reference to Wiek and Nörd-Perd. However, the most noticeable difference is that displayed at ODAS Tonne which has a relatively constant, modern signature of 1.167 characteristic of the minimum lead isotope ratio reached in this region of the Baltic Sea. Little deviation from this value is found which has important implications for the sedimentary history of this station because this value shows none of the subsequent increase in ratios estimated to range in age from 1985 to 1996. The most obvious implication of which is that there has been no recent depositional events in the region of ODAS Tonne and that the sediment has been reworked to at least 14cm depth. Additionally, it would seem that both Nord-Perd and Wiek may have had a recent period of non deposition based upon the expected stable lead isotope recovery profile found in Arkona.

Furthermore, Figure 7-11 also has the potential to be used as a dating proxy as the radionuclide profiles found at the shallower stations were not conducive to the determination of down core age horizons by radiometric methods. Time lines, based upon the dating of the Arkona core, are shown in Figure 7-11 for the pronounced stable lead isotope ratio event horizons. These time lines show that on the basis of stable lead isotope relationships that the sediment accumulation rate has been constant over the three deepest station for at least the period from the 1930's to the mid 1980's. The implications of this along with the possible cessation of deposition will be presented in greater detail in the discussion.

Thus the main points from this chapter on stable lead isotopes relate to the simultaneous increase in lead concentrations with a decrease in the stable lead isotope ratio which can be attributed to anthropogenic sources related to the use of lead ore material and in particular during more recent times, that associated with the combustion engine. Significant increases in the fluxes of lead associated with the increased usage of the automobile were found for the mid twentieth century and with the introduction of unleaded petrol a decrease in lead concentrations and a rise in ratio value is found.

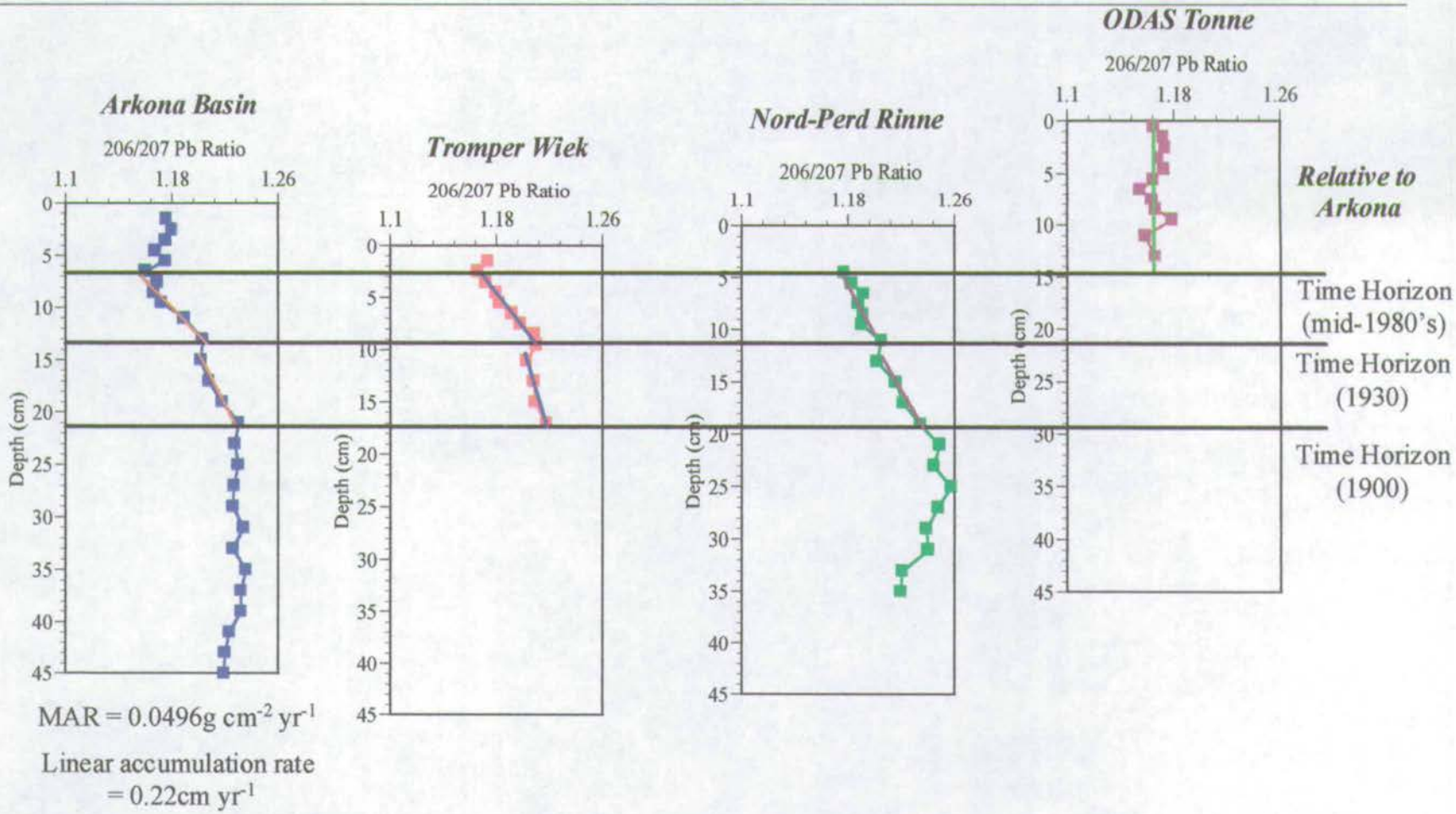

Figure 7-11 BASYS sampling stations stable lead isotope data with event horizons marked for comparison.

8.0 Water Column Geochemistry

8.1 INTRODUCTION

While the geochemistry of a sediment core may be viewed as a historical record of the metal and mineralogical inputs superimposed with diagenetic features, the coastal zone water column represents a much more dynamic and transitory environment in terms of processes and inputs for the majority of elements. The main processes and associations found in the water column are shown in Figure 8-1 and in general shallow water processes are less well understood in contrast to the 'steady state' open ocean. While this is a simplified view of the complex biogeochemical interactions that take place, it serves as a suitable starting point to which detailed information can be added. In this chapter the geochemistry of the water column has been divided into three sections to investigate the main pathways, which are those of:

- The dissolved phase operationally defined as that which passes through a 0.45μm filter (but as recent research has shown may contain a significant colloidal fraction).
- The particulate phase, defined by the retention of particles >0.45μm on a filter commonly divided into organic (bacteria, fungi, phyto and zooplankton, detritus) and inorganic (riverine mineral matter, atmospheric dust etc).
- The mobile nepheloid layer (MNL) or 'fluff' layer, i.e. that relating to the highly mobile, high density and frequently resuspended layer which merges the bottom of the water column with that of the sediment core, containing both organic and inorganic phases.

Before these are considered, the fundamental characteristics of the water column are presented which essentially comprise of the conductivity (salinity), temperature, and density (CTD) measurements for each station. In contrast to the sediment core data, a temporal and spatial distribution of trace metals within the water column were determined in the Baltic Sea. However it must be remembered that the water column

is a highly migratory system and that each survey only provides a snap shot in time and thus careful interpretation of the results should be made.

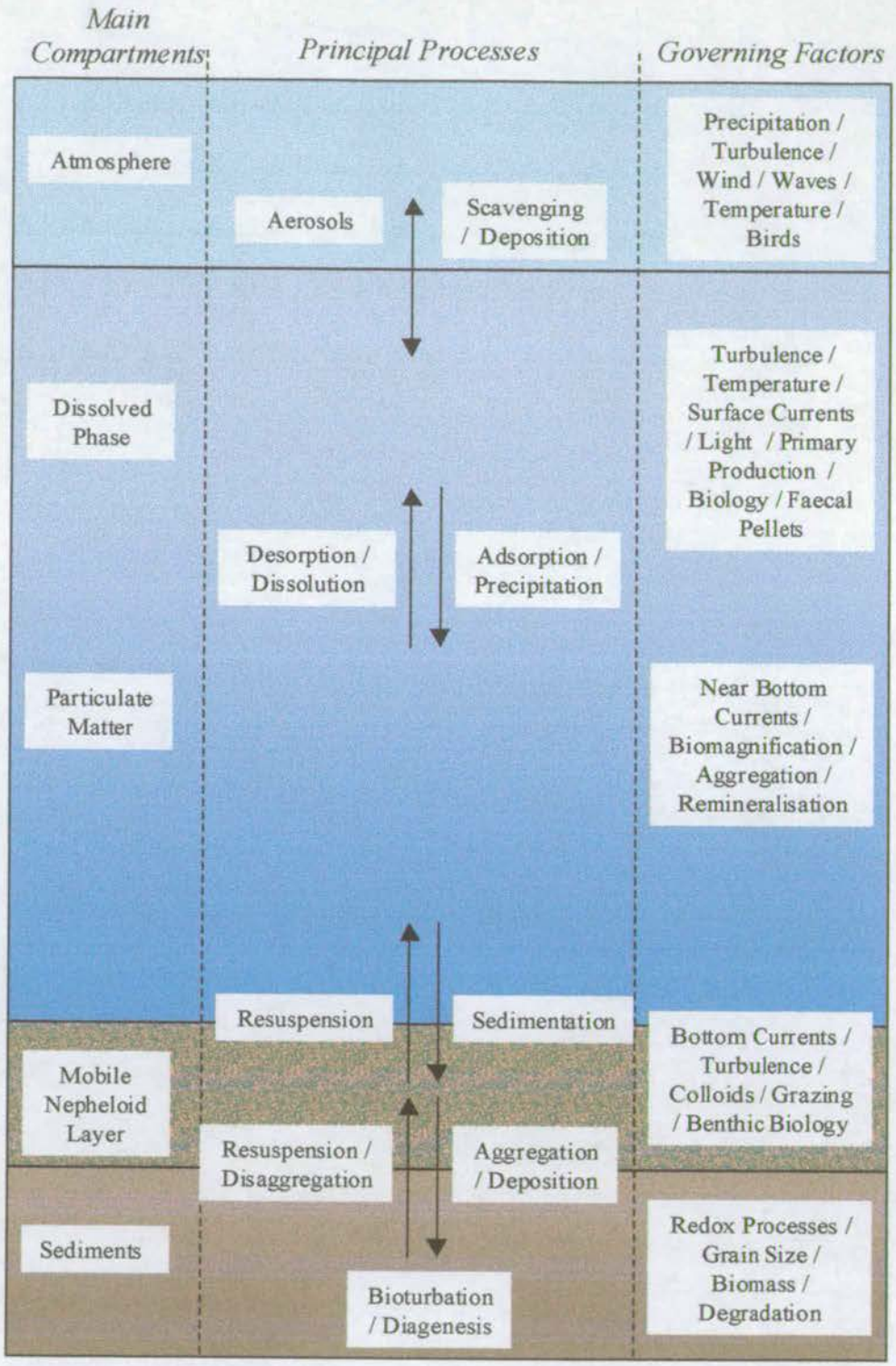

Figure 8-1 Primary controls and processes governing elemental distributions in the water column.

8.2 FUNDAMENTAL PARAMETERS

On each of the research cruises the CTD measurements were taken at each station and the results are displayed below in the form of contour plots. These measurements serve as the primary indicators and controls of the processes that operate throughout the water column. The initial sequence shows a spatial station inter-comparison for each cruise followed by a temporal sequence from October 1996 to December 1997 including CTD data from the Oder Flood which occurred during late July and early August 1997. As a note of caution the contour plots generated can only be used as an aid to interpretation as the contours represent a mathematical best-fit to the point by point data.

Figure 8-2 shows the CTD and oxygen profiles for the first Baltic Sea cruise in October 1996. The temperature profile shows a tongue of cooler water entering from the shallow station and mixing with the warmer, deeper, basinal waters around Wiek. A combined thermo / halo and pycnocline is evident at 35-40m depth for the Arkona station but above this, salinity, density and the oxygen profile are remarkably constant across the whole survey range. The water column is well oxygenated down to 15 meters but at depth oxygen deficiencies become more apparent culminating with sub oxic waters at the base of the Arkona water column. The presence of this low oxygen, near bottom water at Nord-Perd and Wiek as well as Arkona, may in part relate to the presence of an extensive nepheloid layer with the in situ breakdown of the organic constituents of the autumn bloom.

The profiles for March '97 are given in Figure 8-3 and show the coldest temperatures for the whole survey with temperatures just above freezing. Temperature, salinity and hence density all show the influence of fresh surficial river water mixing with the Baltic sea water and protruding as tongue of fresher water. Once again steep gradients in all the parameters can be seen at the deepest station, however in contrast to the October profiles the whole water column is well oxygenated with little biological activity stripping oxygen out of the water column and in addition the cold water temperature increases the solubility of oxygen.

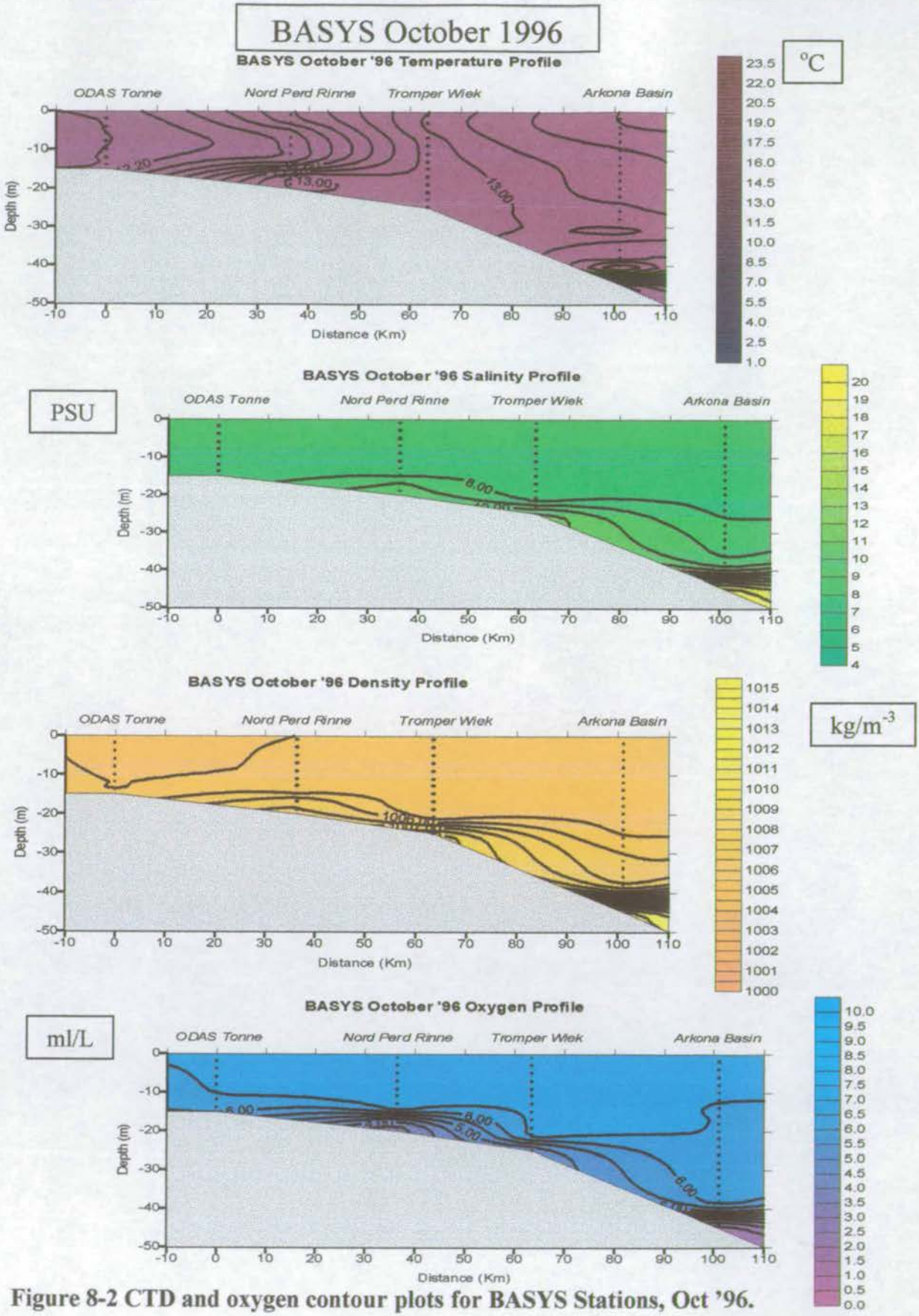

Figure 8-2 CTD and oxygen contour plots for BASYS Stations, Oct '96.

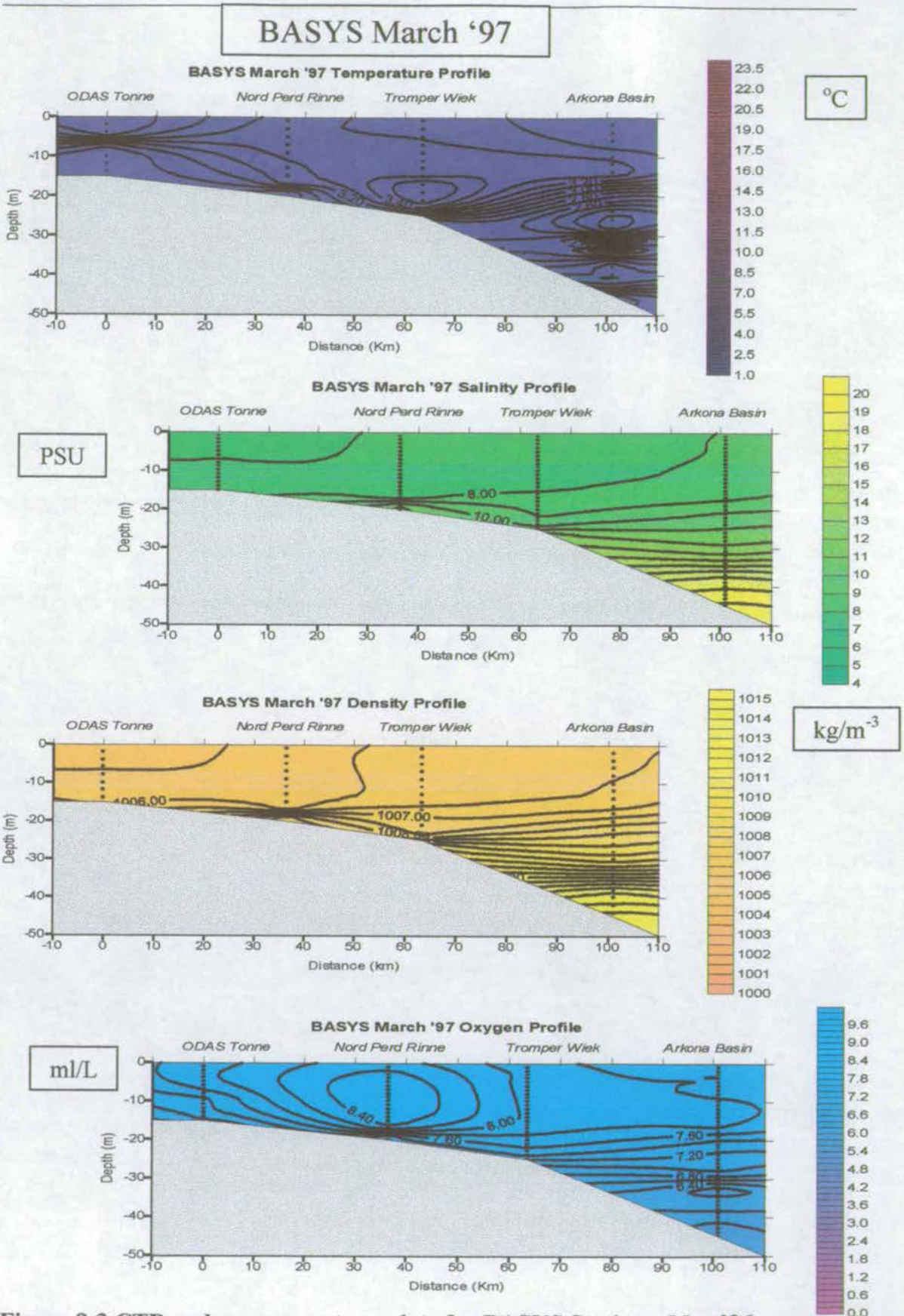

Figure 8-3 CTD and oxygen contour plots for BASYS Stations, Mar '96.

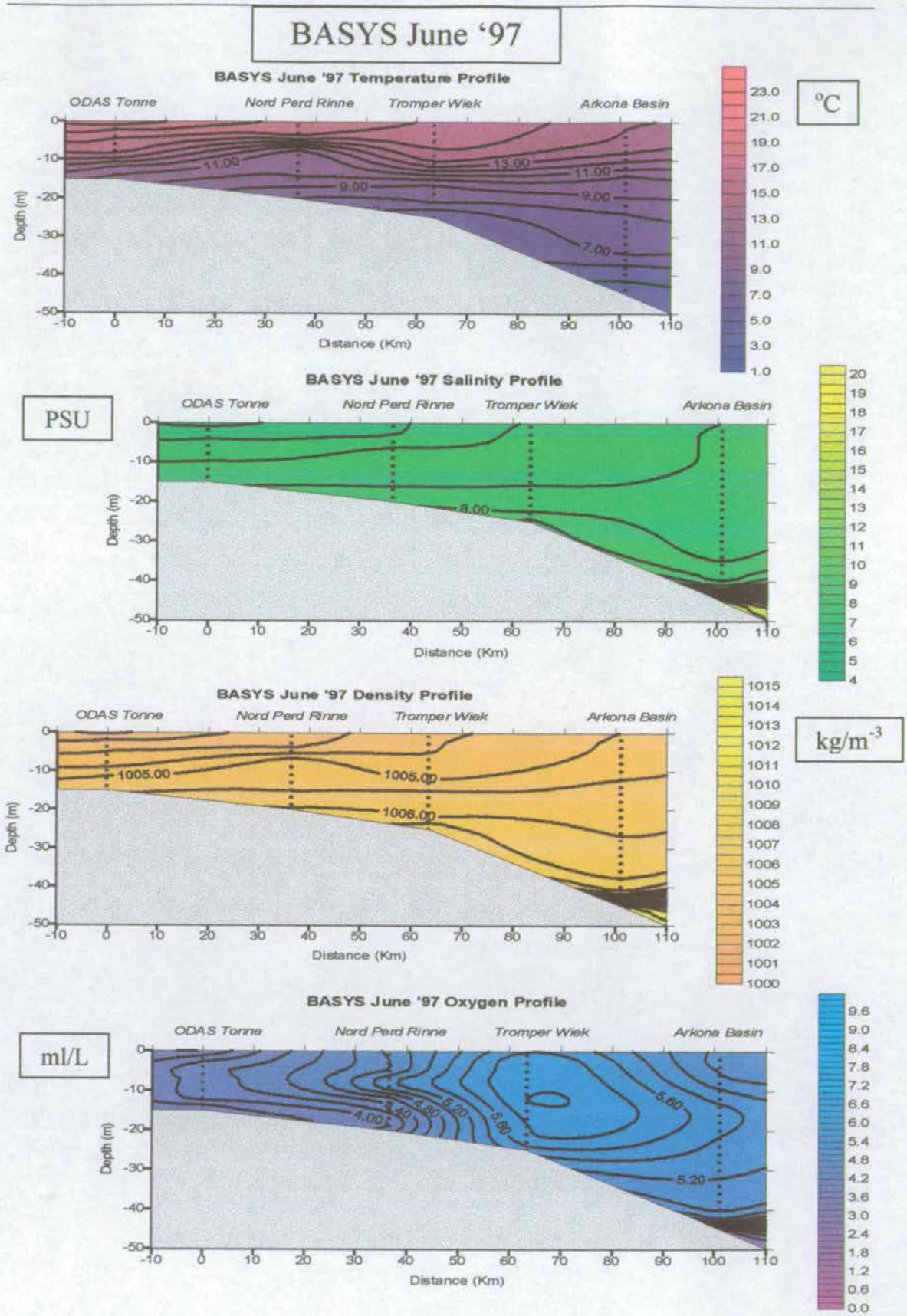

Figure 8-4 CTD and oxygen contour plots for BASYS Stations, June '97.

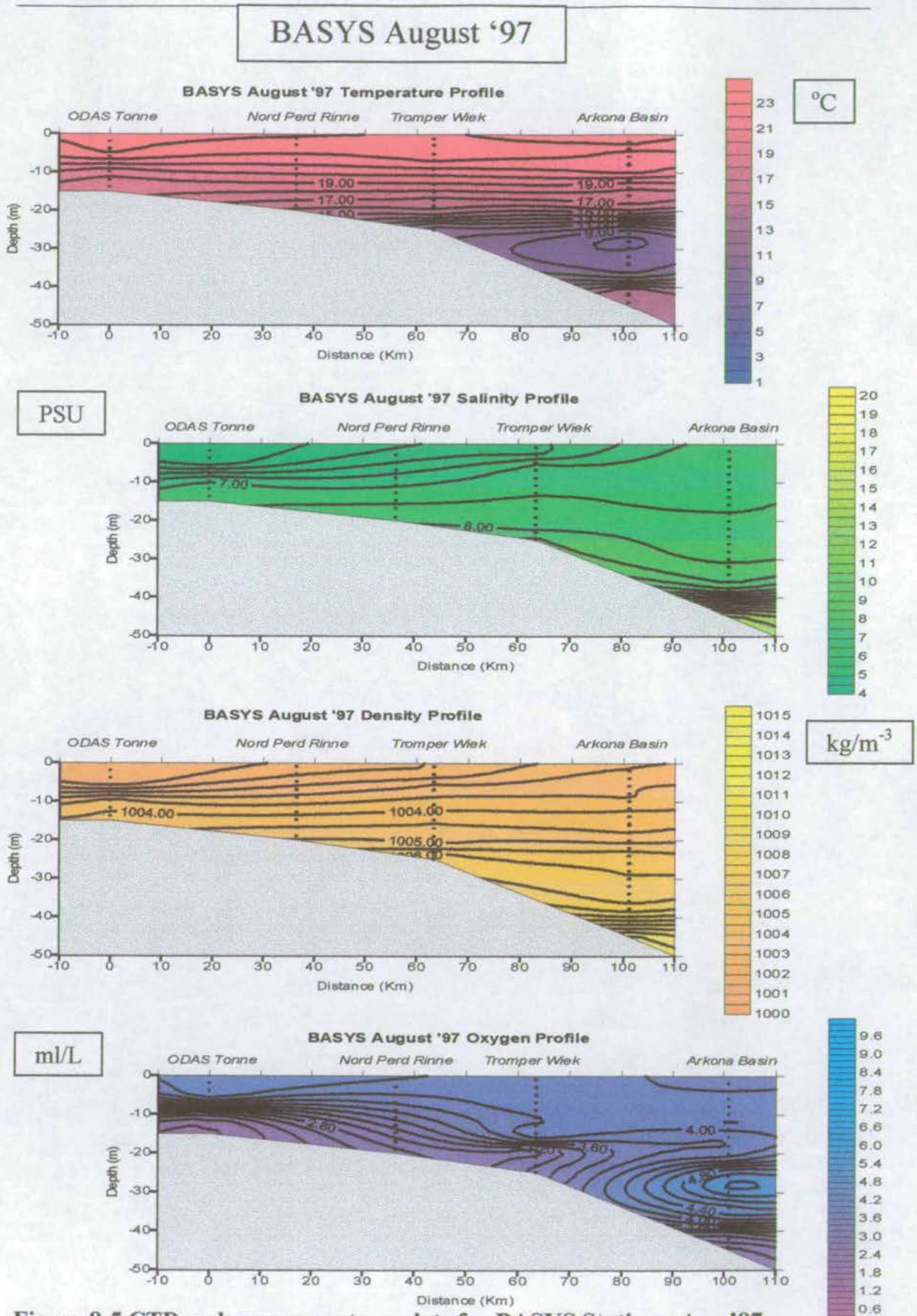

Figure 8-5 CTD and oxygen contour plots for BASYS Stations, Aug '97.

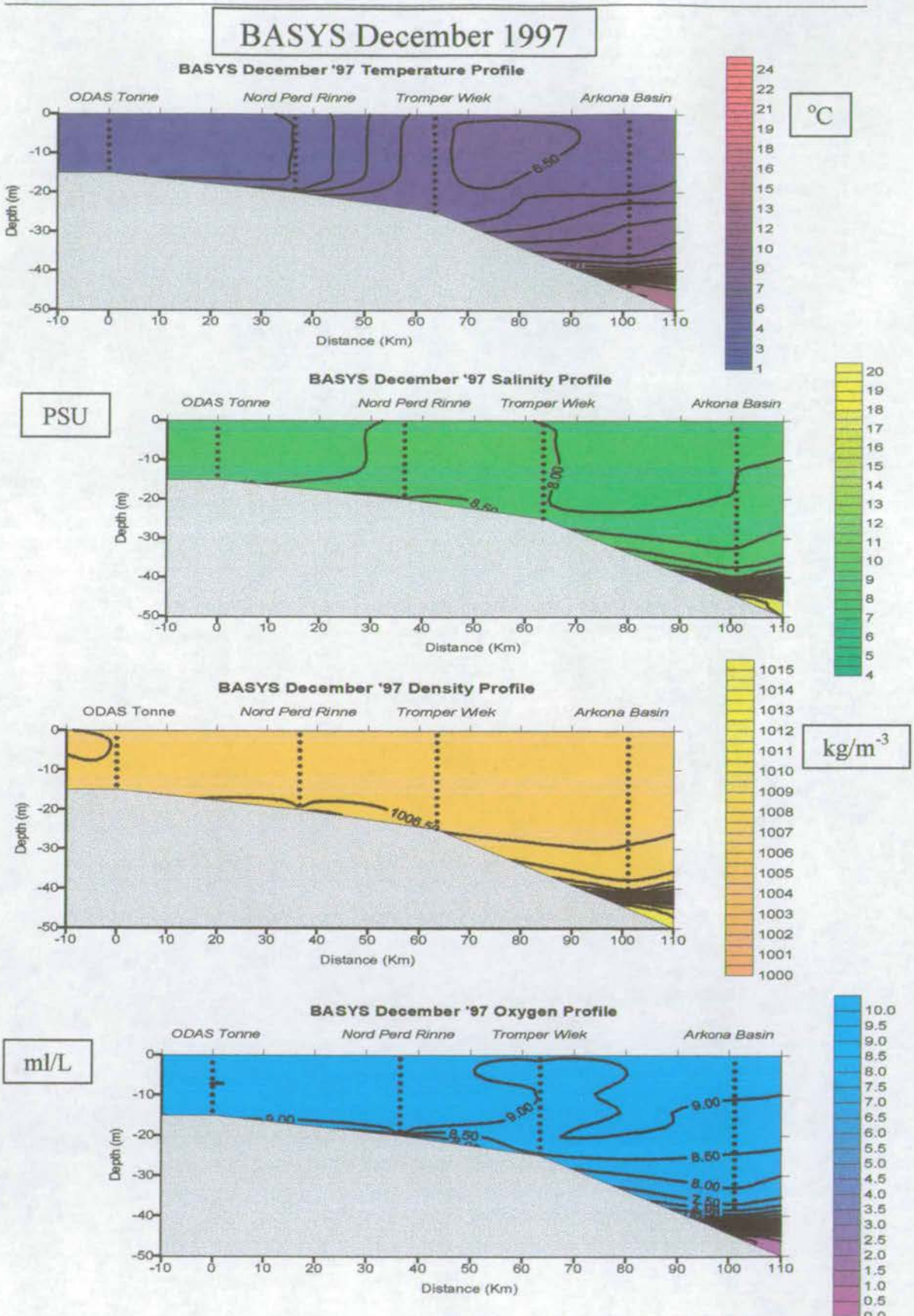

Figure 8-6 CTD and oxygen contour plots for BASYS Stations, Dec '97.

Figure 8-4 shows the presence of a strong thermocline situated at approximately 10m depth. The surface layers are significantly warmer across the whole survey site than the deeper waters. This well developed thermocline seems to be acting as a barrier when the oxygen profile is viewed in conjunction with the temperature profile. The degradation and breakdown products of the biological activity associated with a bloom event seem to be consuming oxygen, particularly at the shallower stations and their depth distribution seems to be limited by the presence of the thermocline. Both salinity and density show similar profiles with a gradient away from the surface shallow water station to the deep basinal waters of Arkona where a halo / pycnocline can be found at depth and where, in addition, the oxygen content below the pycnocline is also limited.

The Oder flood occurred during mid July and lasted for a period of approximately one month. In the closing stages of this flood event an impromptu cruise was organised to capitalise on this unique event. The CTD and oxygen profiles are detailed in Figure 8-5 which shows the thermocline found in June having moved deeper to approximately 20m and also in the same contour plot the presence of a temperature inversion. This is probably due to the presence of a high salinity, high density, relatively warm pocket of water becoming stable at the base of the Arkona water column relative to the overlying slightly less dense colder water. Hence there are two thermoclines present at Arkona. This induced stratification has important consequences for the oxygen distribution with the shallowest thermocline controlling a layer of low oxygen conditions at the three shallowest stations. The cold water lens has a higher oxygen content before returning to low oxygen conditions at the base of Arkona. Surface water values of salinity and density show a common shallowing progression to the distal stations whereas mid water column and deeper show a well developed stratification across all stations.

The profiles for December, shown in Figure 8-6, are those dominated by the input from the river Oder. Both temperature, salinity and density exhibit trends associated with the input of fresh, cold water into the main Baltic sea system. A gradient is well developed through the shallowest three stations whereas the water of the Arkona

basin is more typically stratified. The density profile is remarkably consistent over the majority of the water column and the pycnocline is well developed at depth at the base of the Arkona water column. As before the pycnocline separates high density, high salinity and low oxygen conditions from the lower density overlying waters. In addition the thermocline separates the remnants of the summer's deep, warm and high-density waters from that of the seasonally high and recent surficial fresh water input.

In order to illustrate some of the temporal trends from the survey season, Figure 8-7 and 8-8 show the temperature and density profiles respectively for the 15 months of survey. As the profiles have already been described the annual trends will instead just be clarified. Figure 8-7 shows the typical temperature distribution expected with the warmest surficial temperatures and strongest thermoclines in June and August and the warmest water column temperatures with a corresponding breakdown of the thermocline in October. Conversely, the coldest, whole water column temperatures are found in March which is preceded by the season with the highest runoff and lowest temperatures allowing the water column to cool dramatically. The density profiles serve as an indicator of the cumulative effect of the temperature and salinity profiles. In all of the profiles, irrespective of season, there is a strong trend that tapers away from the shallow, freshwater and low density station, towards the denser, saline waters of the distal station. This increase in density both as a function of depth and also as a function of distance illustrates that the river Oder does have a significant influence upon the hydrography of the region. While the density is generally more homogeneous throughout the water column during the winter months, in the summer intense stratification can be found throughout the water column. However, irrespective of the season there is almost always a pycnocline present at the base of the Arkona water column which has important ramifications for the quality of the water (sub oxic) and the development of anoxia in the sediments at this, the deepest of stations surveyed. In summary strong seasonal trends can be found amongst the fundamental parameters associated with the water column which may have important consequences for the distribution of metals and pollutants in the Southern Baltic Sea.

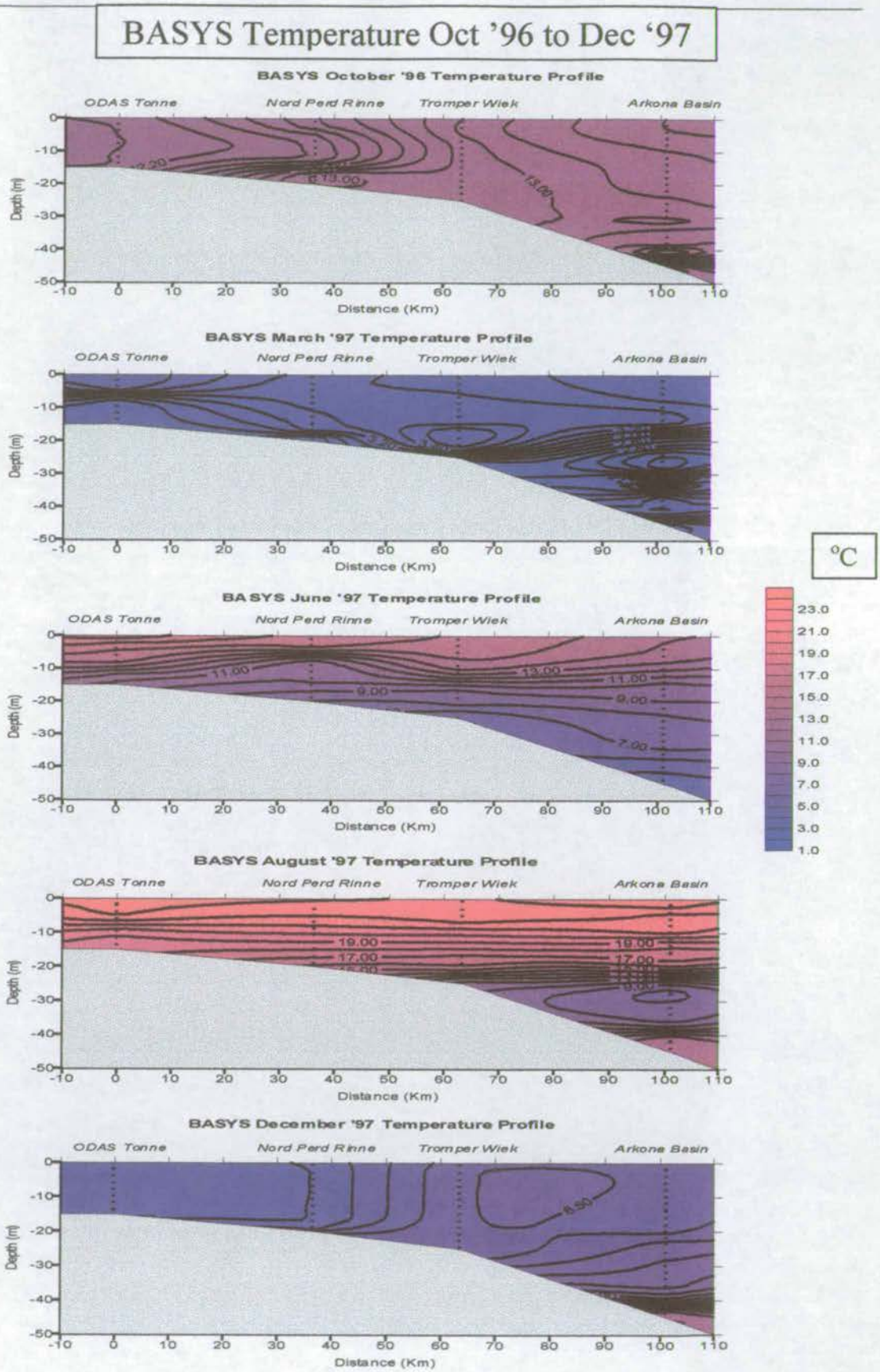

Figure 8-7 Temperature contour plots for BASYS Stations, Oct '96 – Dec '97.

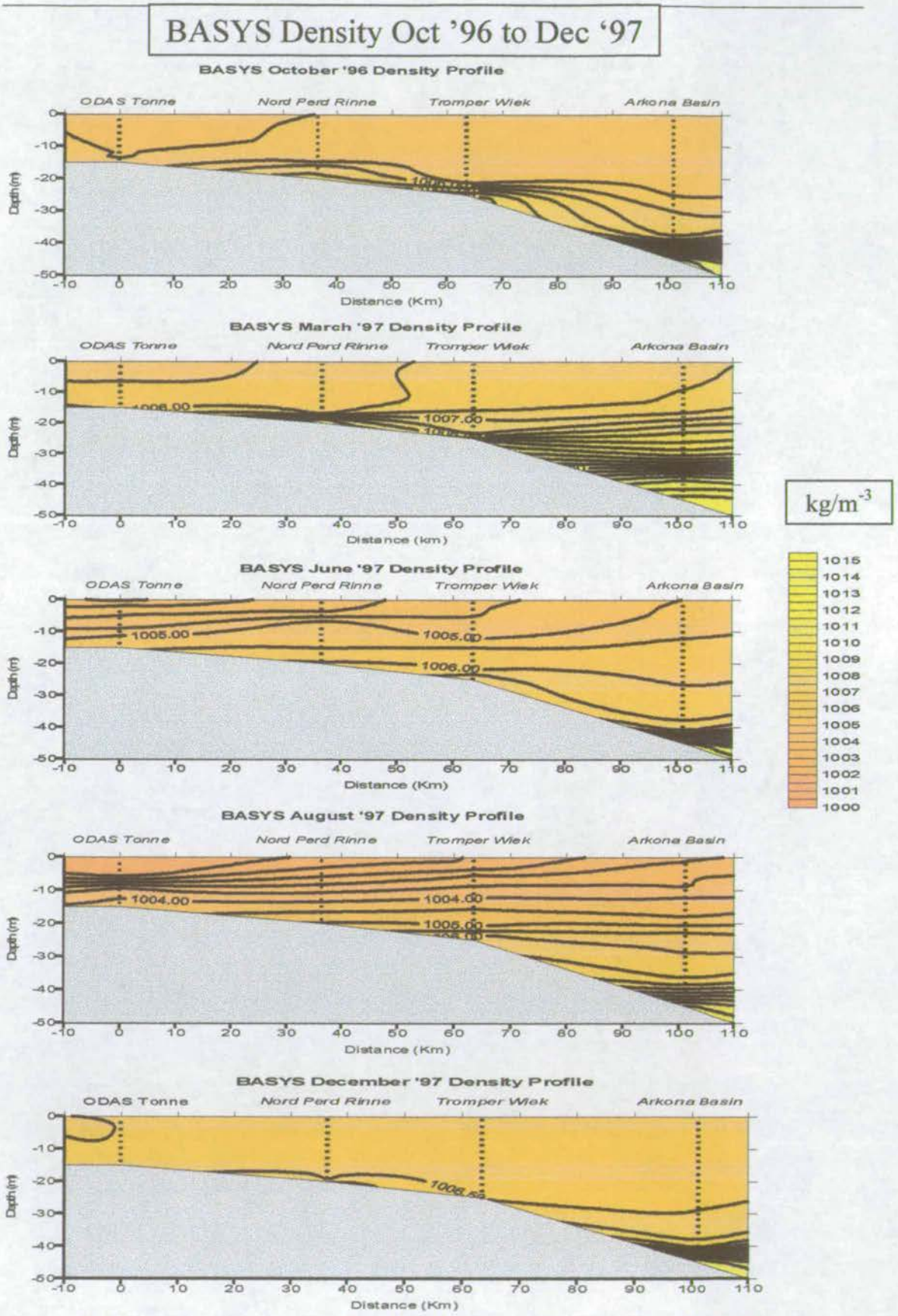

Figure 8-8 Density contour plots for BASYS Stations, Oct '96 – Dec '97.

8.3 DISSOLVED PHASE ASSOCIATIONS

Seawater acquires its trace chemical characteristics from the chemical reactions and desorption / dissolution processes that occur between solids, liquids and gases with which it has come into contact with on its journey through the hydrological cycle as shown in Figure 8-1. As seawater is a highly variable medium for those elements other than the conservative elements, molecular and turbulent diffusion have an important role to play in the distribution of metals and pollutants in the water column irrespective of their initial concentrations (PRANDKE and STIPS, 1992; JANKOWSKI, 1996; ZHOU, 1998). While these processes may be inferred, no direct measurements were taken and hence literature values are used. In addition an important category of dissolved constituent in the seawater that is not covered in this project, but has been the subject of much research, is the nutrient geochemistry which has obvious controls on the biological cycles that take place in the marine environment (RYDBERG *et al.*, 1990; WULFF *et al.*, 1990; NEHRING, 1992; OCHOCKI *et al.*, 1995, PASTUSZAK *et al.*, 1996; VOSS and STRUCK, 1997).

As a note of caution the commonly used division of a 0.45μm filter to differentiate between the particulate and dissolved phase can prove less than satisfactory for certain hydrated forms. In particular, the hydrated forms of iron and manganese tend to coalesce to form colloidal particles which will remain indefinitely in suspension unless they enlarge by a process of aggregation and become large enough to settle out under gravity. Thus trace metal concentrations in the dissolved phase associated with these particles can provide typically spurious results if the colloidal fraction is not considered.

The following statistical analysis, previously described and used to aid in the interpretation of the sediment core, will again be used to determine the initial groupings of the elements analysed. However in contrast to the sediment core, many of the elements were not present in detectable amounts and those that are presented here were, in general, very close to the detection limit. While emphasis may be placed on the general trends care must be taken so as not to over interpret the results as the dissolved phase correlation coefficients are somewhat higher than expected.

8.3.1 BASYS Cruise, Dissolved, October 1996

Table 8-1 Correlation matrix for the multi-element dissolved analysis during the Oct '96 cruise

	Li	Ti	V	Mn	Fe	As	Rb	Sr	Mo	Ba	U
Li	1.00										
Ti	0.74	1.00									
V	0.92	0.59	1.00								
Mn	0.69		0.78	1.00							
Fe	0.93	0.58	0.89	0.70	1.00						
As	0.92	0.71	0.98	0.68	0.89	1.00					
Rb	0.95	0.69	0.92	0.65	0.94	0.93	1.00				
Sr	-0.71	-0.88	-0.58		-0.59	-0.68	-0.70	1.00			
Mo	0.82	0.43	0.86	0.74	0.81	0.81	0.86	-0.46	1.00		
Ba			0.61	0.49	0.49	0.53	0.45		0.52	1.00	
U	0.54		0.54	0.75	0.53	0.42	0.49		0.70		1.00

n = 38, significant at p = 0.01 (>0.418)

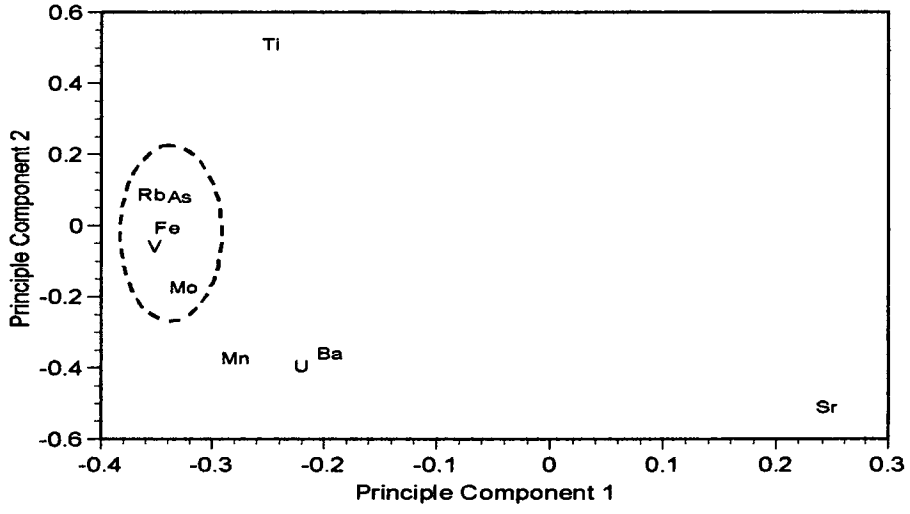

Figure 8-9 PCA for the October '96 dissolved phase, 2 components account for 85% of the variation.

Correlation matrices and principal component analysis on the limited data set show only one major grouping of Rb, As, Fe, V and Mo and, instead, has quite a large spread of the elemental distributions. There are a large amount of significant correlations due to the large data set but low statistically significant threshold values. Manganese shows a limited association with U and Mo, Ti can probably be ignored

due to its extremely low concentrations, whereas Sr was present well within the detectable limits and is quite distinct. The main grouping is primarily composed of lithogenic elements, which may be associated with Fe as the dominant carrier and Sr was demonstrated to be associated with the biogenic phase in the sediment core but care must be taken in the interpretation until the concentration profiles are additionally examined.

8.3.2 BASYS Cruise, Dissolved, March 1997

Table 8-2 Correlation matrix for the multi-element dissolved analysis during the March '97 cruise

	Li	*V*	*Mn*	*Fe*	*As*	*Rb*	*Sr*	*Mo*	*Ba*	*U*
Li	1.00000									
V	0.99999	1.00000								
Mn	0.99989	0.99990	1.00000							
Fe	0.99999	0.99999	0.99989	1.00000						
As	1.00000	0.99999	0.99989	1.00000	1.00000					
Rb	1.00000	1.00000	0.99989	0.99999	1.00000	1.00000				
Sr	0.99974	0.99968	0.99951	0.99975	0.99974	0.99972	1.00000			
Mo	1.00000	0.99999	0.99988	0.99999	1.00000	1.00000	0.99974	1.00000		
Ba	0.99999	0.99997	0.99986	0.99999	0.99999	0.99998	0.99982	0.99999	1.00000	
U	0.99993	0.99995	0.99986	0.99993	0.99993	0.99994	0.99949	0.99994	0.99988	1.00000

n = 38, significant at p = 0.01 (>0.418)

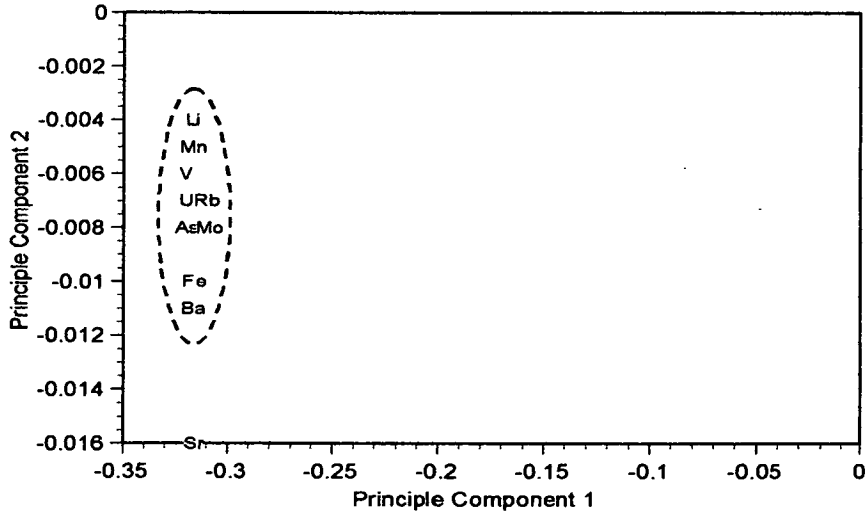

Figure 8-10 PCA for the March '97 dissolved phase, 2 components account for all of the variation.

The results from March are quite unique in that the distribution is almost wholly defined by one principal component and that there is such a strong correlation between all of the elements. Sr once again stands out with Ba as its closest main group relative. Thus, on first inspection of the results there must be a strong, overwhelming factor controlling the elemental distribution. This maybe due to the absence of water column features such as stratification in March but may also be as a result of the concentrated input of seasonal runoff waters which reach a peak during the March and April months. In addition the role of Fe in the well-oxygenated waters as a carrier of these metals must also be considered.

8.3.3 BASYS Cruise, Dissolved, June 1997

Table 8-3 Correlation matrix for the multi-element dissolved analysis during the June '97 cruise

	Li	*Ti*	*V*	*Mn*	*Fe*	*As*	*Rb*	*Sr*	*Mo*	*Ba*	*U*
Li	1.00										
Ti	0.94	1.00									
V	0.93	0.97	1.00								
Mn	0.93	0.92	0.93	1.00							
Fe	0.90	0.92	0.94	0.91	1.00						
As	0.90	0.93	0.95	0.93	0.93	1.00					
Rb	0.94	0.97	0.99	0.95	0.96	0.97	1.00				
Sr	-0.49	-0.45	-0.47	-0.46	-0.43		-0.43	1.00			
Mo	0.79	0.87	0.85	0.74	0.81	0.78	0.84		1.00		
Ba	-0.47	-0.53	-0.54	-0.48	-0.46	-0.55	-0.55		-0.54	1.00	
U	0.75	0.74	0.82	0.80	0.76	0.84	0.82		0.52	-0.48	1.00

n = 38, significant at p = 0.01 (>0.418)

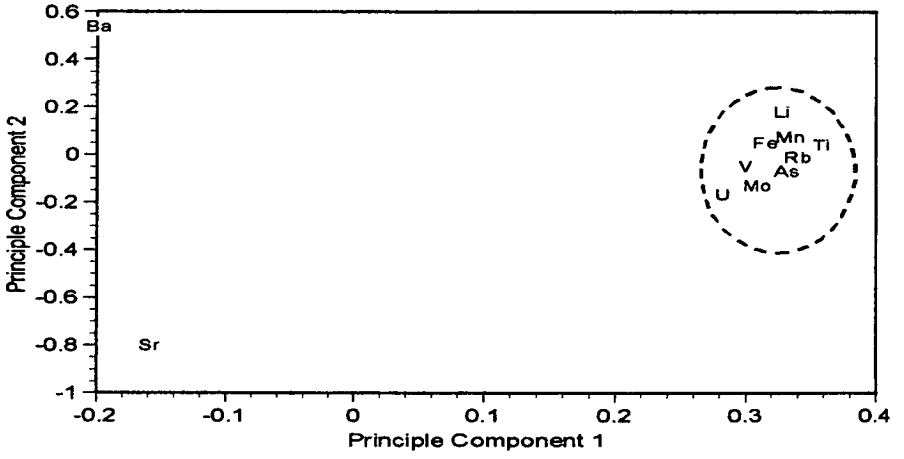

Figure 8-11 PCA for the June '97 dissolved phase, 2 components account for 87% of the variation.

Once again a close distribution is found for the majority of elements with only the elements commonly associated with the biogenic solid phase lying separate, although no significant correlation can be seen between the two of them. The question begs as to whether the same processes governing the groupings in March are still relevant to June. However, in June stratification of the water column is found and in addition biogenic activity in the form of primary production and the advent of the ensuing biological cycle is in motion.

8.3.4 BASYS Cruise, Dissolved, December 1997

Table 8-4 Correlation matrix for the multi-element dissolved analysis during the December '97 cruise

	Li	*Ti*	*V*	*Mn*	*Fe*	*As*	*Rb*	*Sr*	*Ba*	*U*
Li	1.00									
Ti		1.00								
V	0.91	-0.48	1.00							
Mn	0.54		0.51	1.00						
Fe	0.85		0.70	0.59	1.00					
As	0.75	-0.54	0.93		0.47	1.00				
Rb	0.96		0.88	0.66	0.87	0.70	1.00			
Sr	-0.89		-0.75	-0.63	-0.88	-0.51	-0.94	1.00		
Ba	-0.51		-0.59			-0.59	-0.56	0.46	1.00	
U	0.55			0.52	0.69		0.66	-0.75		1.00

n = 10, significant at p = 0.01 (>0.765)

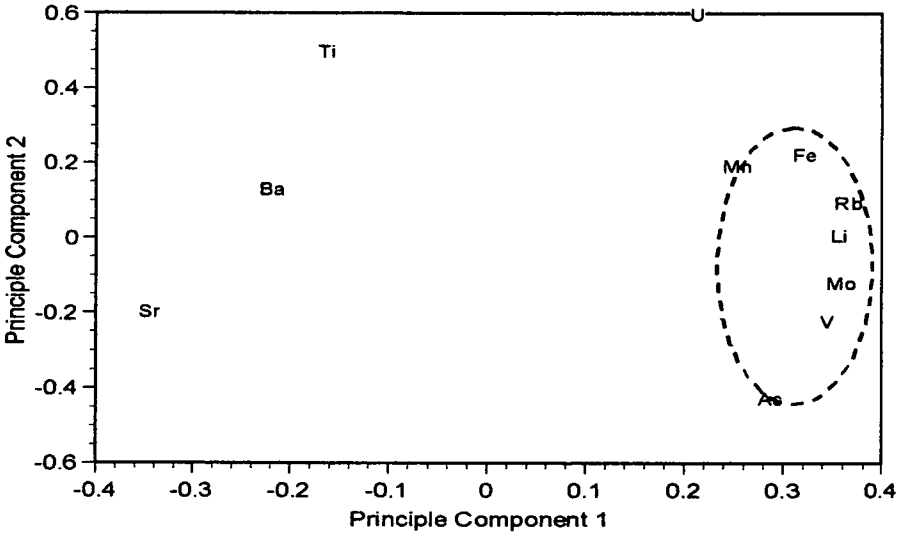

Figure 8-12 PCA for the December '97 dissolved phase, 2 components account for 81% of the variation.

A distribution not too dissimilar from that of the October analysis can be seen during the December cruise. Once again there is a relatively wide distributional spread with much lower correlation matrix values than any other cruise. There is still a vague grouping around Fe primarily consisting of lithogenic elements with the addition of Mn also in close proximity.

8.3.5 Dissolved Phase Statistical Summary

As can be seen the number of elements measured in comparison with all other phase measurements made were relatively few, with these measured often close to detection limits and hence on the edge of reliability. From the results obtained, which only provide a glimpse of the dynamic variability of water column processes, it may be possible to determine some seasonality from the statistical analysis alone. In contrast to the spring and summer values the autumn and winter statistical analysis is much weaker and wide spread. While it is not possible to determine the causes of this from statistics alone a number of possibilities may be postulated. These range from changes in the fundamental characteristics of the water column, association with Fe oxyhydroxides and / or a relation to runoff values for the river Oder entering the Baltic Sea to biogenic controls and degradation processes within the water column. The main control of variability could additionally be the role of the colloidal fraction, which could neatly explain the association with the lithogenic elemental concentrations. However these processes can not be fully evaluated until the elemental concentrations and distributions are likewise considered.

8.4 PARTICULATE PHASE ASSOCIATIONS

The particulate phase plays a vital role in regulating the composition of seawater via the removal of dissolved constituents from solution and vertical and lateral transport to the sediment sink. The particulate phase can be split into two broad categories; that associated with the organic phase and that related to the inorganic fraction. The relative contributions of each fraction depend upon the environmental setting in terms of the dynamics of the region and closeness to land. Ignoring allocthonous terrestrial input, most of the organic input to the marine system stems from the primary production in the surface waters from which grazing and biomagnification occurs throughout the water column. The most common organic particles are composed of bacteria, algal cells, phytoplankton, zooplankton, diatoms and faecal pellets. The inorganic phase, which is the primary phase considered here, consists mainly of terrestrially derived deposits such as clay minerals, primary aluminosilicates and hydrous oxides of Mn and Fe.

Heavy metals that are particle reactive can be incorporated into the particulate matter via a number of mechanisms. Direct precipitation from the water column, adsorption onto clay mineral lattices, aggregation of colloidal material, direct uptake by plankton and retained or excreted in the form of faecal pellets are the main processes. In addition many of the carrier particles can be coated in Fe and Mn oxyhydroxides which often serve as a further carrier phase for metals and pollutants in the marine environment.

Furthermore the speciation of metals also plays an important role in the biogeochemical reactivity of the system as has been seen with the redox processes in the sediment column. This is also an important factor in the water column although in this study speciation investigations were not initiated and hence due consideration must be taken when drawing conclusions from the data.

In addition to the filter collected particulate matter, sediment trap data was also collected at ODAS Tonne as part of the BASYS project and this was analysed for metals and stable lead isotopes, the results of which are given later in this chapter.

8.4.1 BASYS Cruise, Particulate, October 1996

Table 8-5 Correlation matrix for the multi-element particulate analysis during the October '96 cruise

	Li	Ti	V	Mn	Fe	Co	Ni	Cu	Zn	As	Rb	Sr	Y	Zr	Mo	Cd	Sn	Sb	Cs	Ba	Ce	Pb	Th	U
Li	1																							
Ti	1.00	1.00																						
V	1.00	1.00	1.00																					
Mn	0.69	0.68	0.70	1.00																				
Fe	1.00	0.99	0.99	0.69	1.00																			
Co	0.92	0.91	0.93	0.75	0.92	1.00																		
Ni	0.85	0.84	0.87	0.74	0.86	0.93	1.00																	
Cu	0.83	0.83	0.84	0.63	0.84	0.81	0.88	1.00																
Zn	0.88	0.87	0.90	0.77	0.89	0.93	0.98	0.93	1.00															
As	0.99	0.99	0.99	0.72	0.99	0.94	0.90	0.85	0.92	1.00														
Rb	1.00	1.00	1.00	0.68	1.00	0.92	0.85	0.83	0.88	0.99	1.00													
Sr	0.90	0.89	0.92	0.78	0.91	0.93	0.95	0.83	0.94	0.95	0.90	1.00												
Y	1.00	1.00	1.00	0.68	1.00	0.93	0.87	0.85	0.90	0.99	1.00	0.91	1.00											
Zr	0.95	0.94	0.95	0.79	0.96	0.92	0.89	0.83	0.92	0.97	0.94	0.97	0.95	1.00										
Mo	0.95	0.95	0.96	0.74	0.95	0.94	0.94	0.91	0.95	0.97	0.95	0.93	0.96	0.93	1.00									
Cd	0.99	0.98	0.99	0.76	0.99	0.93	0.89	0.86	0.93	0.99	0.99	0.93	0.99	0.97	0.97	1.00								
Sn	0.98	0.98	0.98	0.71	0.99	0.92	0.87	0.86	0.91	0.98	0.98	0.91	0.98	0.96	0.95	0.98	1.00							
Sb	0.99	1.00	0.99	0.66	0.99	0.90	0.83	0.82	0.86	0.98	0.99	0.87	0.99	0.92	0.95	0.98	0.97	1.00						
Cs	1.00	1.00	1.00	0.67	1.00	0.91	0.84	0.83	0.87	0.99	1.00	0.89	1.00	0.94	0.95	0.99	0.98	0.99	1.00					
Ba	1.00	1.00	1.00	0.68	0.99	0.91	0.85	0.83	0.88	0.98	1.00	0.89	1.00	0.93	0.96	0.98	0.97	1.00	0.99	1.00				
Ce	0.99	1.00	0.99	0.67	0.98	0.91	0.84	0.82	0.86	0.98	0.99	0.88	0.99	0.92	0.96	0.97	0.96	1.00	0.99	1.00	1.00			
Pb	1.00	1.00	1.00	0.70	1.00	0.93	0.86	0.85	0.90	0.99	1.00	0.91	1.00	0.95	0.96	0.99	0.98	0.99	1.00	0.99	0.99	1.00		
Th	1.00	1.00	1.00	0.67	1.00	0.91	0.85	0.84	0.88	0.99	1.00	0.89	1.00	0.94	0.96	0.99	0.98	1.00	1.00	1.00	0.99	1.00	1.00	
U	1.00	1.00	0.99	0.67	0.99	0.91	0.83	0.83	0.87	0.98	1.00	0.88	0.99	0.93	0.95	0.98	0.98	0.99	1.00	0.99	0.99	1.00	1.00	1

n = 38, significant at p = 0.01 (>0.418)

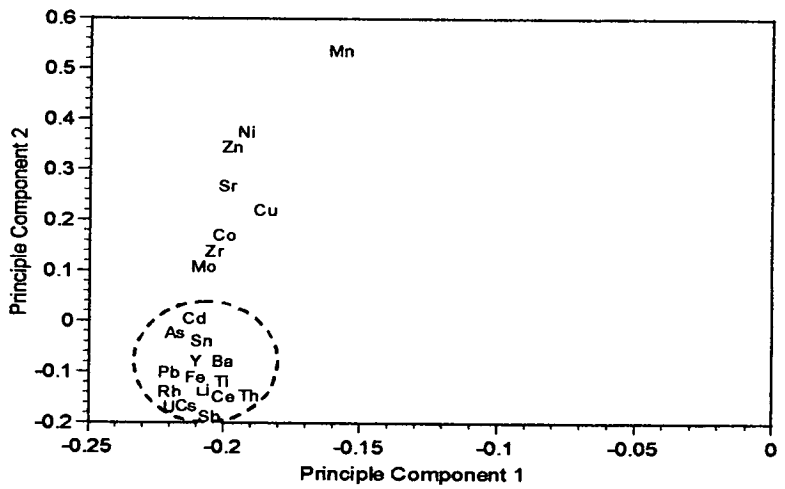

Figure 8-13 PCA for the October '96 particulate phase, 2 components account for 97% of the variation.

8.4.2 BASYS Cruise, Particulate, March 1997

Table 8-6 Correlation matrix for the multi-element particulate analysis during the March '97 cruise.

	Li	Ti	V	Mn	Fe	Co	Ni	Cu	Zn	As	Rb	Sr	Y	Zr	Mo	Cd	Sn	Sb	Cs	Ba	Ce	Pb	Th	U
Li	1.00																							
Ti	0.97	1.00																						
V	0.88	0.97	1.00																					
Mn	0.42			1.00																				
Fe	1.00	0.95	0.86	0.48	1.00																			
Co	0.77	0.74	0.66		0.77	1.00																		
Ni	0.96	0.87	0.74	0.58	0.97	0.75	1.00																	
Cu	0.97	0.88	0.75	0.59	0.98	0.78	0.99	1.00																
Zn	0.95	0.87	0.76	0.61	0.96	0.73	0.97	0.97	1.00															
As	0.99	0.93	0.83	0.51	1.00	0.77	0.98	0.99	0.96	1.00														
Rb	0.99	0.99	0.93		0.99	0.76	0.93	0.94	0.92	0.97	1.00													
Sr	0.96	0.86	0.72	0.61	0.97	0.74	0.99	0.99	0.97	0.98	0.92	1.00												
Y	0.99	0.92	0.81	0.52	1.00	0.77	0.99	0.99	0.97	1.00	0.97	0.99	1.00											
Zr	0.96	1.00	0.98		0.94	0.73	0.85	0.85	0.85	0.92	0.98	0.83	0.91	1.00										
Mo	0.90	0.86	0.77		0.90	0.71	0.92	0.90	0.86	0.90	0.89	0.87	0.90	0.84	1.00									
Cd	0.79	0.61		0.69	0.82	0.63	0.90	0.91	0.85	0.85	0.72	0.92	0.87	0.58	0.76	1.00								
Sn	0.99	0.94	0.83	0.43	0.99	0.76	0.97	0.98	0.95	0.99	0.97	0.97	0.99	0.92	0.90	0.85	1.00							
Sb	0.99	0.93	0.82	0.50	0.99	0.76	0.98	0.98	0.97	0.99	0.97	0.98	0.99	0.91	0.91	0.85	0.99	1.00						
Cs	1.00	0.94	0.84	0.47	1.00	0.77	0.98	0.98	0.95	1.00	0.98	0.97	1.00	0.92	0.91	0.84	1.00	0.99	1.00					
Ba	0.97	1.00	0.97		0.96	0.74	0.88	0.88	0.88	0.94	0.99	0.86	0.93	1.00	0.86	0.62	0.93	0.93	0.94	1.00				
Ce	0.90	0.98	1.00		0.87	0.67	0.76	0.76	0.76	0.84	0.94	0.73	0.83	0.99	0.78	0.44	0.85	0.84	0.85	0.98	1.00			
Pb	0.99	0.93	0.82	0.53	1.00	0.78	0.99	0.99	0.97	1.00	0.97	0.98	1.00	0.91	0.90	0.86	0.99	0.99	1.00	0.93	0.83	1.00		
Th	0.99	0.99	0.93		0.99	0.76	0.93	0.93	0.92	0.97	1.00	0.91	0.97	0.98	0.89	0.71	0.97	0.97	0.98	0.99	0.94	0.97	1.00	
U	0.99	1.00	0.95		0.97	0.75	0.91	0.91	0.90	0.96	1.00	0.89	0.95	0.99	0.88	0.68	0.96	0.95	0.97	1.00	0.96	0.95	1.00	1.00

N = 38, significant at p = 0.01 (>0.418)

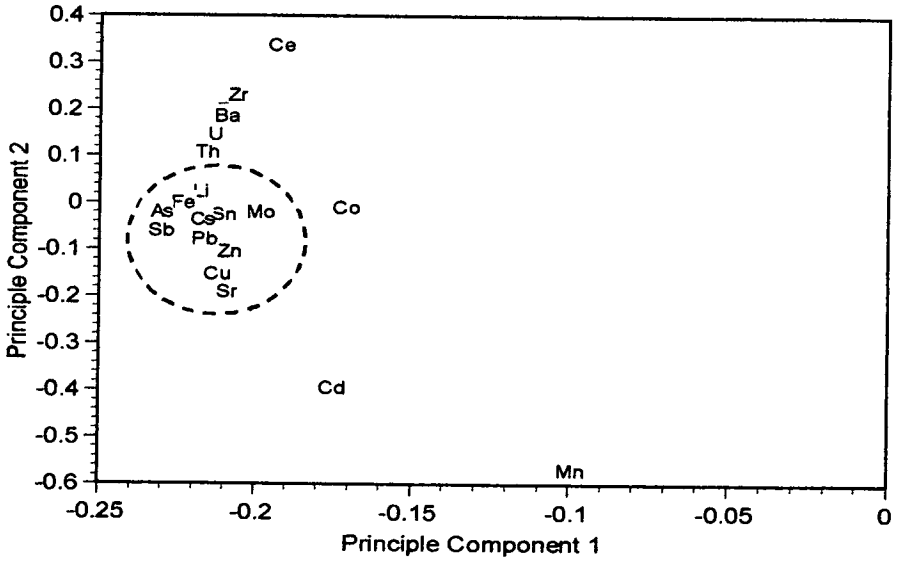

Figure 8-14 PCA for the March '97 particulate phase, 2 components account for 96% of the variation.

8.4.3 BASYS Cruise, Particulate, June 1997

Table 8-7 Correlation matrix for the multi-element particulate analysis during the June '97 cruise.

	Li	Ti	V	Mn	Fe	Co	Ni	Zn	Cu	As	Rb	Sr	Y	Zr	Mo	Cd	Sn	Sb	Cs	Ba	Ce	Pb	Th	U
Li	1.00																							
Ti	0.99	1.00																						
V	0.99	0.99	1.00																					
Mn				1.00																				
Fe	0.98	0.98	0.98		1.00																			
Co	0.76	0.79	0.80		0.79	1.00																		
Ni	0.87	0.90	0.90		0.89	0.80	1.00																	
Zn	0.92	0.93	0.95	0.46	0.94	0.80	0.92	1.00																
Cu	0.97	0.97	0.99		0.98	0.82	0.92	0.97	1.00															
As	0.92	0.95	0.96		0.95	0.80	0.97	0.97	0.96	1.00														
Rb	1.00	0.99	0.99		0.98	0.77	0.87	0.91	0.97	0.92	1.00													
Sr	0.80	0.83	0.82		0.80	0.77	0.94	0.83	0.84	0.90	0.80	1.00												
Y	0.97	0.97	0.97		0.97	0.80	0.90	0.94	0.97	0.95	0.97	0.85	1.00											
Zr	0.94	0.96	0.95		0.95	0.81	0.92	0.91	0.94	0.96	0.94	0.87	0.94	1.00										
Mo	0.77	0.80	0.80		0.78	0.70	0.96	0.82	0.80	0.90	0.77	0.90	0.79	0.85	1.00									
Cd				0.44			0.53	0.52	0.45	0.50		0.46			0.49	1.00								
Sn	0.87	0.87	0.89	0.50	0.85	0.64	0.75	0.88	0.88	0.83	0.86	0.65	0.86	0.78	0.63	0.46	1.00							
Sb	0.85	0.84	0.78		0.77	0.72	0.71	0.66	0.75	0.72	0.86	0.75	0.83	0.79	0.66		0.63	1.00						
Cs	0.87	0.87	0.86		0.85	0.72	0.81	0.82	0.85	0.84	0.88	0.83	0.95	0.84	0.70		0.77	0.87	1.00					
Ba	0.95	0.96	0.96		0.93	0.73	0.90	0.94	0.96	0.94	0.95	0.85	0.96	0.93	0.80	0.46	0.85	0.77	0.87	1.00				
Ce	0.99	1.00	0.99		0.99	0.80	0.90	0.94	0.98	0.95	0.99	0.83	0.98	0.96	0.80		0.86	0.84	0.88	0.95	1.00			
Pb	0.93	0.93	0.95	0.48	0.91	0.74	0.84	0.94	0.93	0.90	0.93	0.74	0.91	0.87	0.73	0.43	0.91	0.71	0.79	0.93	0.93	1.00		
Th	1.00	0.99	0.98		0.97	0.75	0.84	0.90	0.96	0.90	1.00	0.76	0.95	0.93	0.75		0.86	0.84	0.85	0.94	0.99	0.93	1.00	
U	0.96	0.95	0.91		0.88	0.67	0.79	0.80	0.87	0.83	0.96	0.75	0.90	0.87	0.73		0.79	0.92	0.84	0.89	0.94	0.86	0.96	1.00

N = 38, significant at p = 0.01 (>0.418)

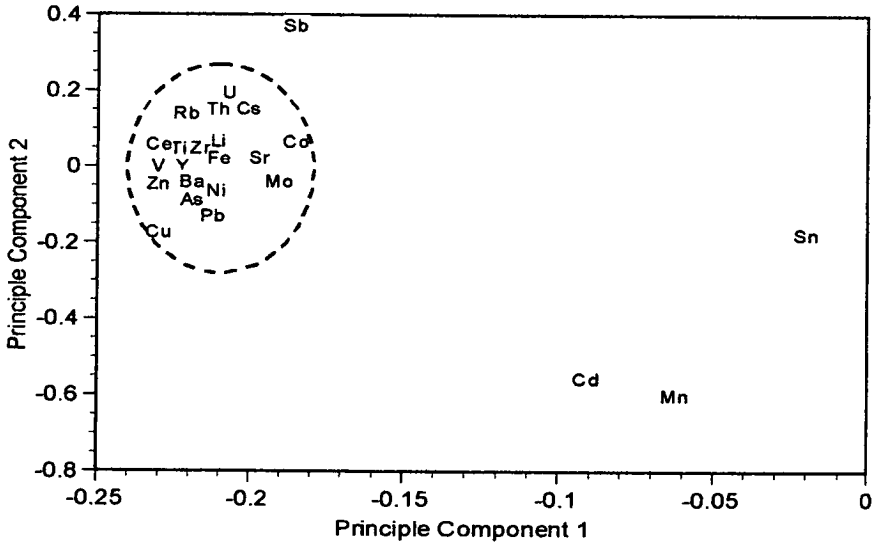

Figure 8-15 PCA for the June '97 particulate phase, 2 components account for 89% of the variation.

8.4.4 BASYS Cruise, Particulate, December 1997

Table 8-8 Correlation matrix for the multi-element particulate analysis during the December '97 cruise.

	Li	Ti	V	Mn	Fe	Co	Ni	Zn	Cu	As	Rb	Sr	Y	Zr	Mo	Cd	Sn	Sb	Cs	Ba	Ce	Pb	Th	U
Li	1.00																							
Ti	0.87	1.00																						
V	0.99	0.87	1.00																					
Mn	0.48	0.62	0.52	1.00																				
Fe	0.99	0.84	0.98		1.00																			
Co	0.69	0.80	0.69	0.80	0.59	1.00																		
Ni	0.69	0.74	0.70	0.69	0.59	0.94	1.00																	
Zn	0.88	0.87	0.90	0.78	0.82	0.90	0.89	1.00																
Cu	0.95	0.88	0.97	0.64	0.93	0.77	0.78	0.95	1.00															
As	0.98	0.81	0.97		0.96	0.65	0.69	0.85	0.94	1.00														
Rb	0.98	0.92	0.99	0.50	0.99	0.67	0.65	0.87	0.95	0.94	1.00													
Sr	0.80	0.71	0.78		0.73	0.67	0.79	0.77	0.81	0.87	0.74	1.00												
Y	0.94	0.89	0.94		0.93	0.63	0.68	0.83	0.92	0.95	0.95	0.84	1.00											
Zr	0.66	0.94	0.67	0.61	0.62	0.76	0.69	0.74	0.71	0.60	0.75	0.57	0.74	1.00										
Mo		0.52		0.61		0.87	0.89	0.69	0.50			0.54		0.51	1.00									
Cd				0.74		0.75	0.80	0.63	0.44					0.43	0.87	1.00								
Sn	0.76	0.90	0.76	0.67	0.68	0.93	0.92	0.89	0.82	0.74	0.76	0.76	0.78	0.87	0.76	0.64	1.00							
Sb		0.61		0.72		0.86	0.77	0.62						0.71	0.79	0.72	0.81	1.00						
Cs	0.58		0.59		0.62				0.55	0.68	0.57	0.64	0.75						1.00					
Ba	0.92	0.98	0.92	0.63	0.89	0.79	0.75	0.90	0.92	0.86	0.95	0.73	0.91	0.89	0.50		0.88	0.54	0.45	1.00				
Ce	0.93	0.98	0.93	0.53	0.92	0.74	0.69	0.86	0.90	0.88	0.97	0.71	0.93	0.87	0.45		0.85	0.49	0.48	0.98	1.00			
Pb	0.98	0.88	0.98	0.62	0.96	0.73	0.69	0.92	0.97	0.93	0.97	0.73	0.91	0.69			0.77		0.49	0.93	0.93	1.00		
Th	0.92	0.98	0.92	0.56	0.91	0.76	0.70	0.87	0.90	0.86	0.96	0.69	0.91	0.88	0.47		0.85	0.51	0.44	0.98	1.00	0.92	1.00	
U	0.97	0.94	0.97	0.52	0.96	0.72	0.68	0.87	0.93	0.92	0.99	0.71	0.93	0.79			0.81		0.50	0.96	0.98	0.96	0.98	1.00

N = 34, significant at p = 0.01 (>0.44)

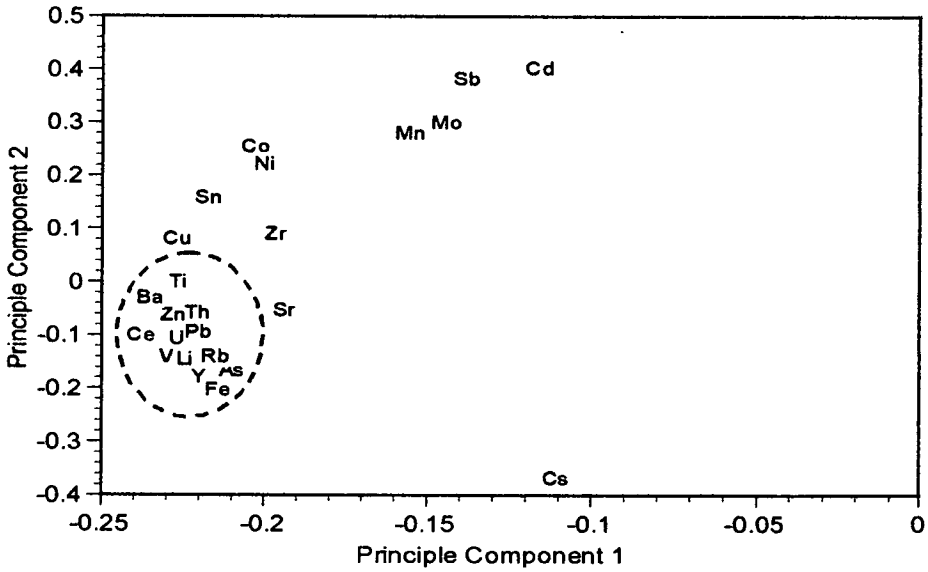

Figure 8-16 PCA for the December '97 particulate phase, 2 components account for 89% of the variation.

8.4.5 Particulate Phase Statistical Summary

It can be seen in contrast to the dissolved phase that many more elements could be analysed in the particulate phase as dilutions due to the salt content of the seawater were not an issue with the digested filters. Furthermore, there was a much greater statistical significance between the elements in general and a very high percentage for the first two components in PCA for all the cruises. The first component is the dominant control in PCA analysis with very few elements deviating from this axis. In common to all four cruises is a cluster of elements that always has Fe present and in contrast Mn is rarely seen in close proximity. The main associations in the principal cluster with Fe do vary over time but common to all are V, As, Y, Pb, Rb, Li, Ti, Th and U. In close proximity or as part of the principal cluster Cs, Cu, Zn, Ni, Ba, Zr and Mo can also typically be found. Mn is conspicuous in its absence from the main groupings and attention will be paid to its concentration profile in the following description.

8.5 MOBILE NEPHELOID LAYER STATISTICS

The nepheloid layer is a highly mobile, turbid region in close proximity to the sea floor where the particle density is high. This region represents the interface between the water column and sediments where repeated processes of deposition and resuspension occur along with the migration of matter from one region to another depending on the bottom current velocities. This region is one of the most dynamic in the marine environment and generally contains a high percentage of refractory elements which are constantly recycled until incorporation into the sediment proper.

Unlike the previous particulate and dissolved phase proper the fluff layer sampling was carried out on a number of cruises from October '96 though to June '98. The results obtained from these investigations are analysed in the same statistical manner as detailed previously and are shown in Table 8-9 and Figure 8-17. PC1 versus PC2 and PC1 versus PC3 are shown so as to provide a more informed overview.

Table 8-9 Correlation matrix for the multi-element analysis of the fluff layer during the period October '96 to June '98.

	Li	Ti	V	Mn	Fe	Co	N	Cu	Zn	As	Rb	Sr	Y	Zr	Sn	Cs	Ba	Ce	Pb	Th	U
Li	1.00																				
Ti	0.77	1.00																			
V	0.93	0.75	1.00																		
Mn				1.00																	
Fe	0.86	0.68	0.96	0.53	1.00																
Co	0.56		0.61		0.60	1.00															
N							1.00														
Cu	0.71		0.74	0.59	0.79	0.50		1.00													
Zn	0.53					0.71	0.52	0.69	1.00												
As	0.84	0.54	0.87	0.68	0.92	0.49		0.80	0.61	1.00											
Rb	0.76	0.82	0.79		0.77	0.51				0.59	1.00										
Sr											0.50	1.00									
Y	0.75	0.66	0.79		0.82			0.54		0.66	0.87	0.72	1.00								
Zr	0.62	0.86	0.57		0.52						0.74		0.70	1.00							
Sn	0.56		0.59		0.65					0.60			0.50		1.00						
Cs	0.87	0.56	0.88		0.82	0.57		0.63		0.74	0.69		0.75			1.00					
Ba	0.66	0.61	0.61		0.59						0.74	0.76	0.86	0.75		0.59	1.00				
Ce	0.54	0.57	0.64		0.70					0.54	0.82	0.76	0.89	0.60		0.58	0.74	1.00			
Pb	0.80	0.53	0.88	0.67	0.94	0.56		0.86	0.61	0.95	0.58		0.64		0.62	0.74		0.50	1.00		
Th	0.65	0.58	0.70		0.75					0.56	0.82	0.77	0.93	0.62		0.72	0.81	0.93	0.54	1.00	
U	0.87	0.91	0.83		0.72	0.56				0.57	0.84		0.74	0.81	0.50	0.75	0.71	0.55	0.57	0.66	1.00

N = 24, significant at p = 0.01 (>0.487)

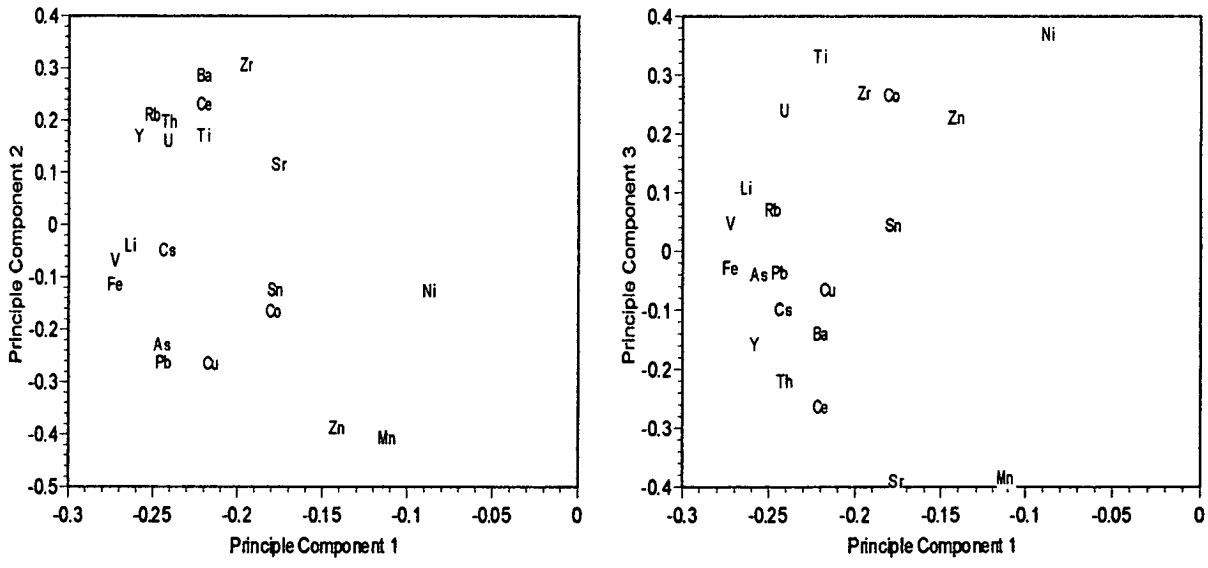

Figure 8-17 PCA for the fluff layer, 3 components account for 80% of the variation.

The significant correlations of the mobile nepheloid layer are much weaker than either the dissolved or particulate phase seen thus far. While Fe can still conceivably be near the centre of the wide distribution found the distribution seems to be moving towards an 'everyman for himself' type of system, one of high independency and one in which common associations break down.

On a statistical basis alone the nepheloid layer seems to lie in-between the highly correlated particulate phase and the slightly less so dissolved phase and the much lower significant correlations of the sediment core. Thus the system seems to diffuse into a more disorderly assemblage as the duration of time in the marine environment increases synchronous with a weakening in the effect of the hydrography.

8.6 SEDIMENT TRAP STATISTICS

Sediment trap deployments were made as part of the BASYS cruise by LUND-HANSEN of Aarhus University, Denmark and samples were taken for metal analysis. The trap was deployed at the shallow station of Tonne for periods of time from June '97 to June '98 and the data obtained is presented here. A description of the sediment trap is given in (LAIMA *et al.*, *In Press*). Sediment traps collect falling material (organic and inorganic) over a set period of time from which fluxes can be calculated. A consideration when using sediment trap data especially in a high energy, shallow water site is that not only sediment falling from the waters surface but also particles that have been resuspended will be collected. In view of this the amount of resuspension can be inferred from the near surface sediment trap accumulation rate and the calculated ^{210}Pb dating from the sediment core.

The statistical analysis of the sediment trap samples analysed is given in Table 8-10 and Figure 8-18.

Table 8-10 Correlation matrix for the multi-element analysis of the Sediment trap material during the period June '97 to June '98.

	Li	Ti	V	Mn	Fe	Co	Ni	Cu	Zn	As	Rb	Sr	Y	Zr	Mo	Cd	Sn	Sb	Cs	Ba	Ce	Pb	Th	U
Li	1.00																							
Ti	0.66	1.00																						
V			1.00																					
Mn				1.00																				
Fe	0.59		0.72		1.00																			
Co						1.00																		
Ni						0.81	1.00																	
Cu					0.69			1.00																
Zn	0.69								1.00															
As	0.73		0.78		0.86					1.00														
Rb	0.82	0.60									1.00													
Sr						0.82	0.62					1.00												
Y	0.75	0.81		0.68							0.84		1.00											
Zr														1.00										
Mo			0.87		0.65					0.61					1.00									
Cd				0.83									0.57			1.00								
Sn			0.85	-0.57	0.60					0.60					0.89		1.00							
Sb			0.58							0.56					0.63		0.58	1.00						
Cs	0.78		0.80		0.77				0.66	0.90	0.58				0.58				1.00					
Ba	0.71								0.61		0.80								0.72	1.00				
Ce	0.69	0.73		0.65							0.84		0.93								1.00			
Pb	0.86	0.70			0.68					0.69	0.65		0.67						0.64		0.65	1.00		
Th	0.92	0.72								0.69	0.77		0.75						0.72	0.65	0.77	0.89	1.00	
U	0.64		0.73		0.81					0.86					0.67		0.66		0.86		0.09	0.62	0.63	1.00

N = 20, significant at p = 0.01 (>0.561)

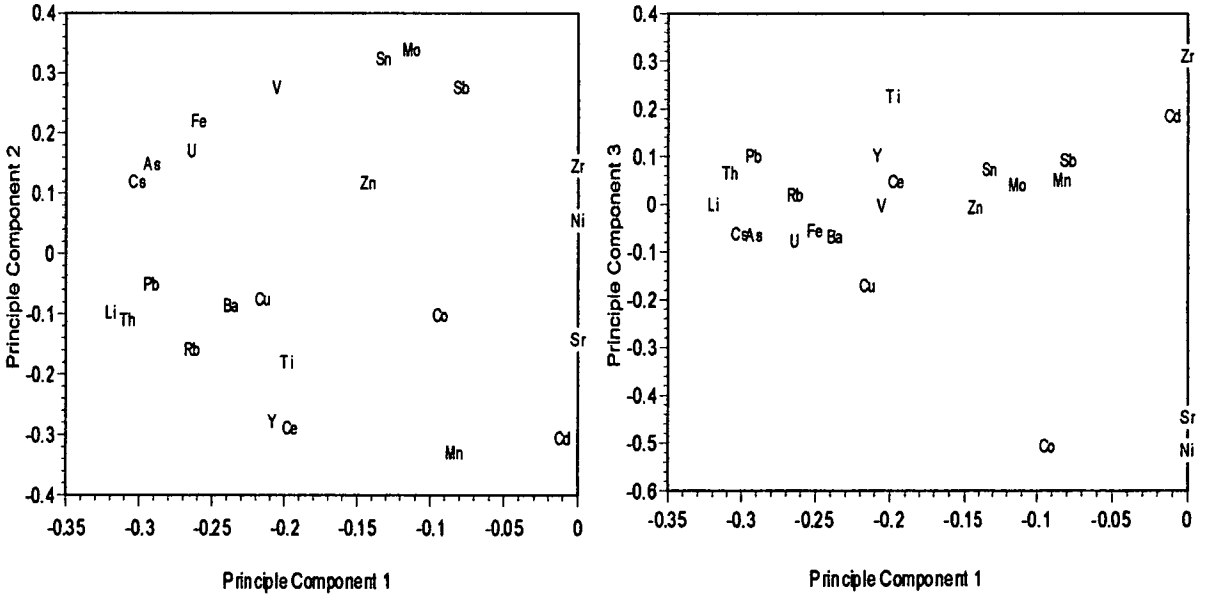

Figure 8-18 PCA for the sediment trap material, 3 components account for 76% of the variation.

The statistical analysis of the sediment trap data provides an interesting spread of data that would not be predicted from that associated solely with the highly correlated water particulate data alone. The data shown above has generally low degrees of correlation for the matrix and the principal component analysis accounts for a relatively lowly 76% for three components. Perhaps the most obvious deduction from this could be the involvement of resuspended material in the sediment traps and / or the involvement of organic material collected in the trap and the resulting micro-environment degradation that would occur over the period of deployment along with the obvious seasonally changing time accumulation period.

8.7 INORGANIC GEOCHEMISTRY OF THE WATER COLUMN

As there have been so many elements analysed and also a reasonably large number of variables to be examined from a temporal and spatial perspective then representative elements are displayed in the coming section which is again divided into four sub sections pertaining to the dissolved, particulate, nepheloid and sediment trap phases. An attempt is made to select the prominent elements from the broad groupings that were defined in the sediment core chapter in an attempt to elucidate the main processes at work throughout the marine system. Furthermore attempts will be made to investigate as to whether any seasonality can be found over the period of study.

The main elements selected in the coming section are Fe, Mn, Pb, Cu, Zn, Sn, Sr and Rb which are shown in order to capture the essence of the main groupings postulated from the sediment core. The following figures are arranged in cruise order (October-March-June and December) with each page comprising of the four stations for each element in terms of the main water column data and additionally supplemented with samples yielded from the BIOPROBE lander. Figures 8-19 to 8-22 and 8-23 to 8-26 display the data obtained for iron in both the particulate and dissolved phase respectively. In comparison to the published data by BRULAND, 1983 for the open ocean the dissolved iron levels are somewhat high and while the blanks were good

other potential contamination problems cannot be addressed until further studies are initiated to establish the true iron content of this estuarine type environment.

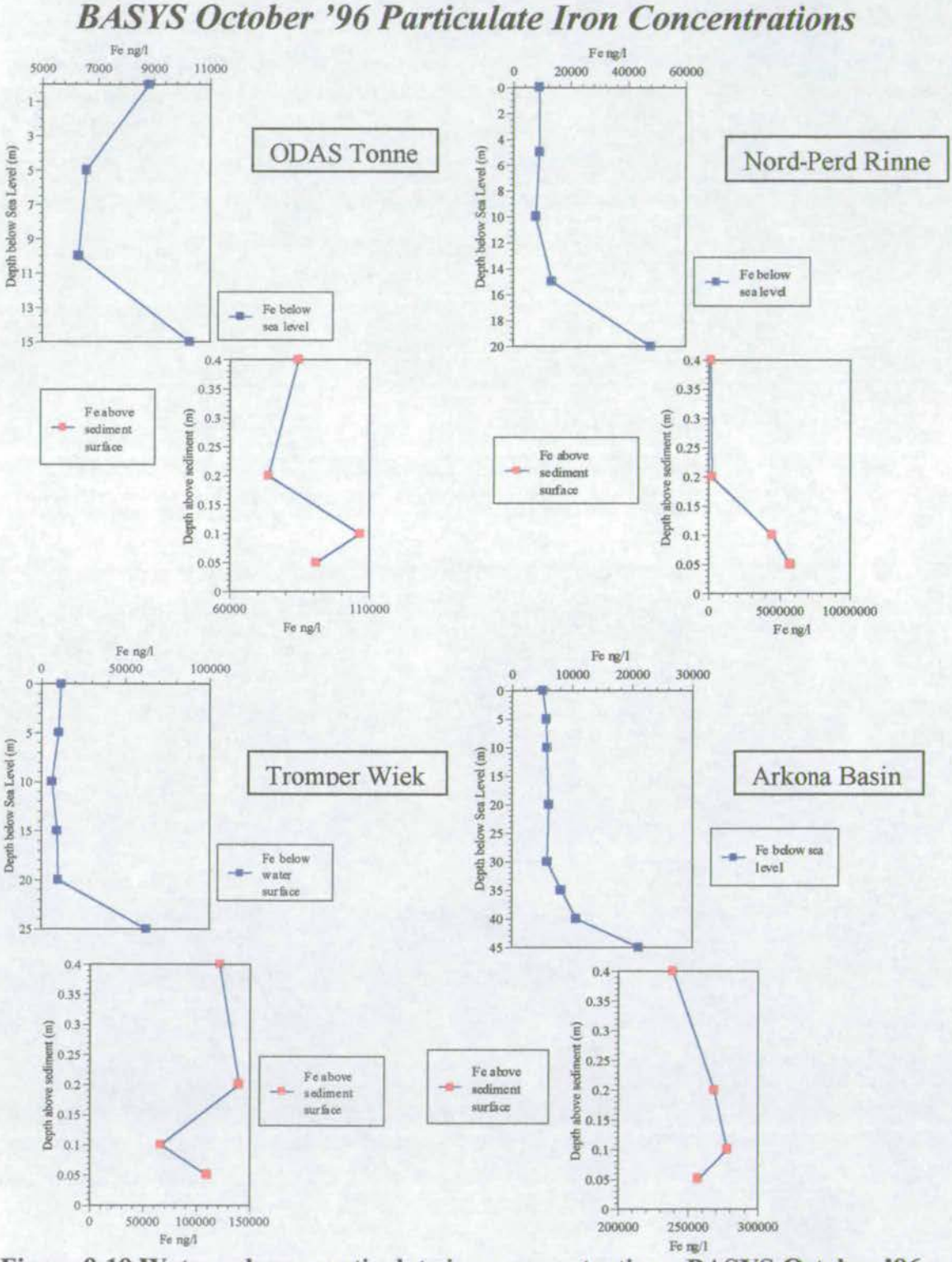

Figure 8-19 Water column particulate iron concentrations, BASYS October '96. Samples marked by the red box are from the bioprobe lander and represent nepheloid layer characteristics.

BASYS March '97 Particulate Iron Concentrations

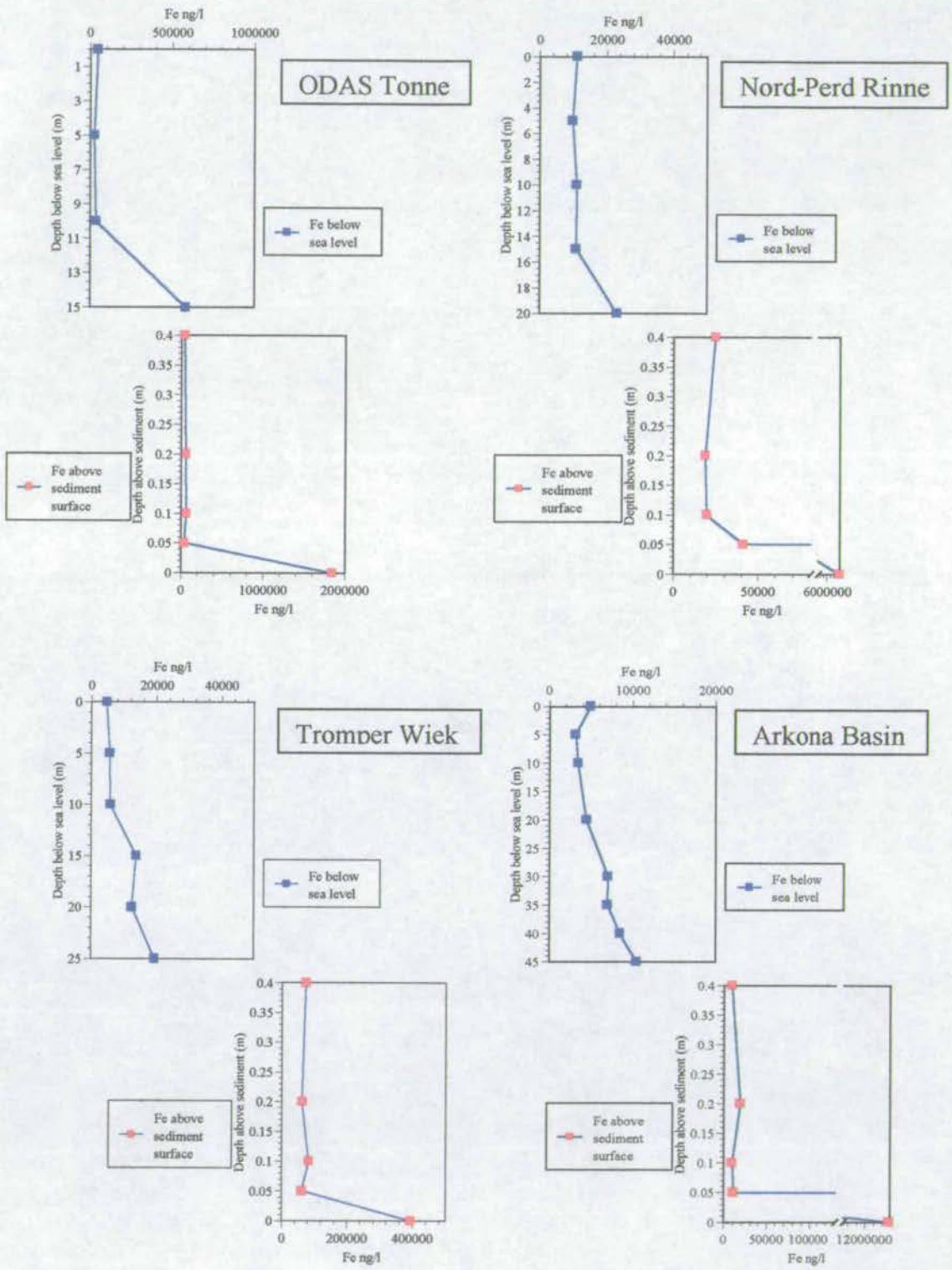

Figure 8-20 Water column particulate iron concentrations, BASYS March '97 . Samples marked by the red box are from the bioprobe lander and represent nepheloid layer characteristics.

BASYS June '97 Particulate Iron Concentrations

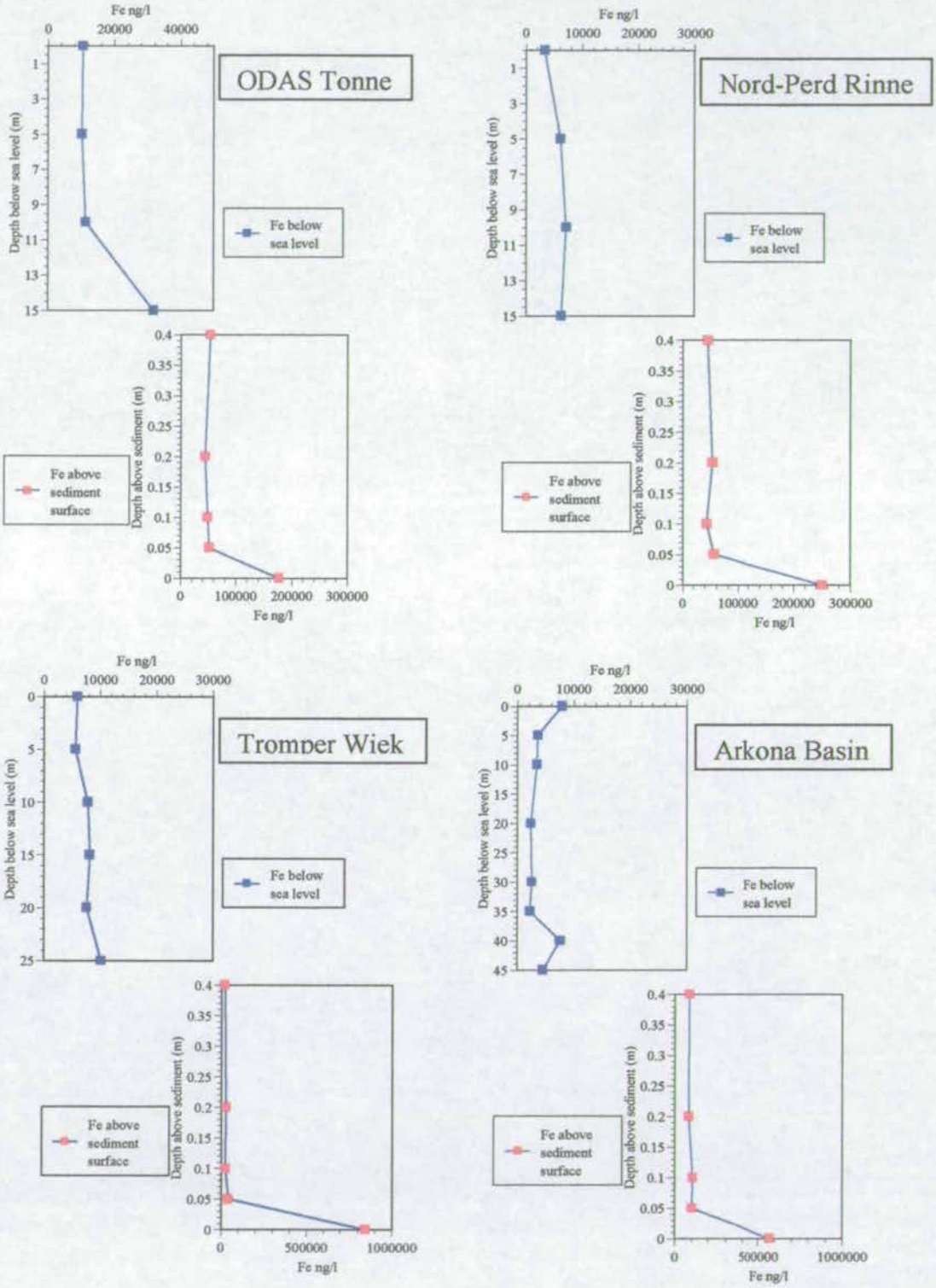

Figure 8-21 Water column particulate iron concentrations, BASYS June '97 . Samples marked by the red box are from the bioprobe lander and represent nepheloid layer characteristics.

BASYS December '97 Particulate Iron Concentrations

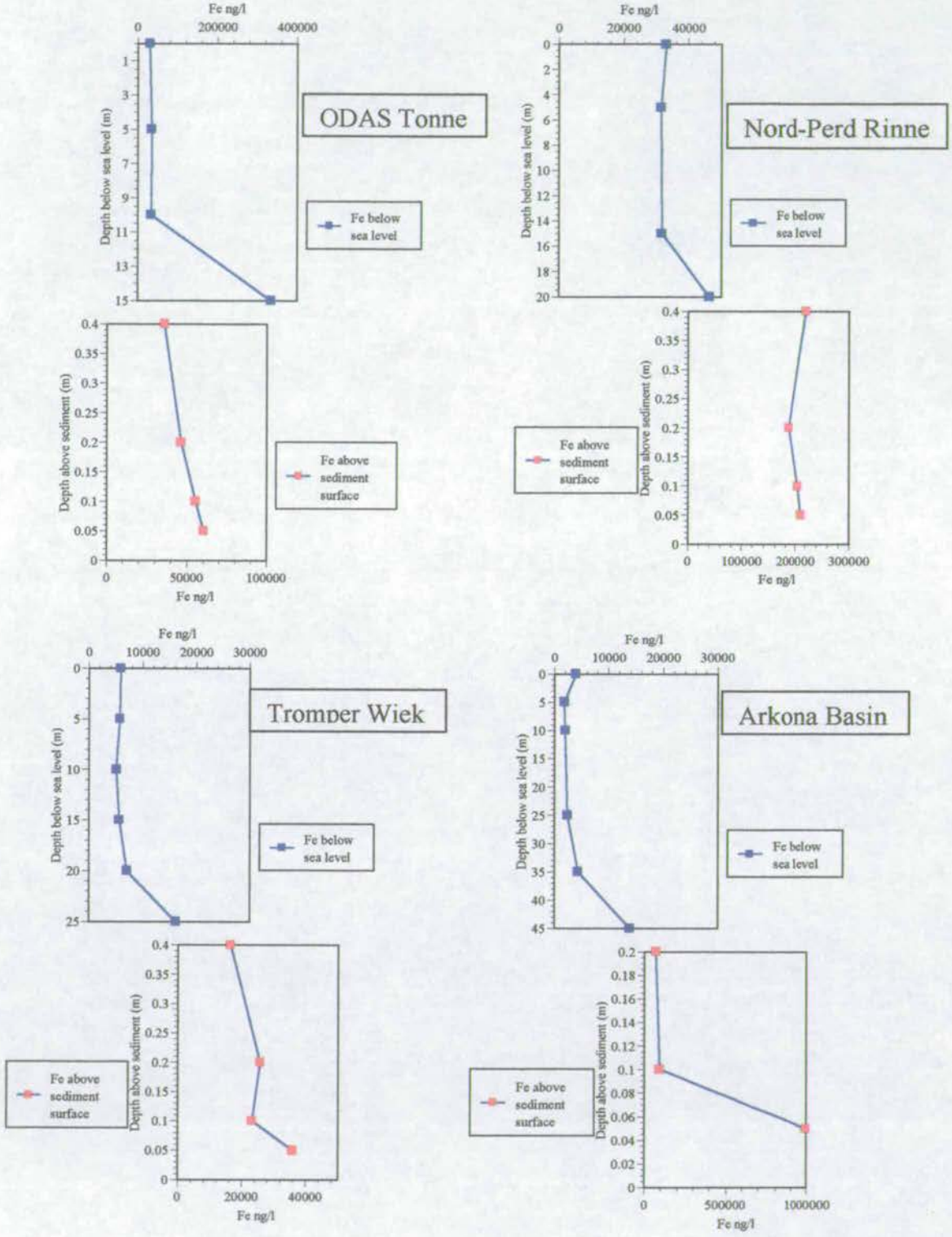

Figure 8-22 Water column particulate iron concentrations, BASYS December '97. Samples marked by the red box are from the bioprobe lander and represent nepheloid layer characteristics.

BASYS October '96 Dissolved Iron Concentrations

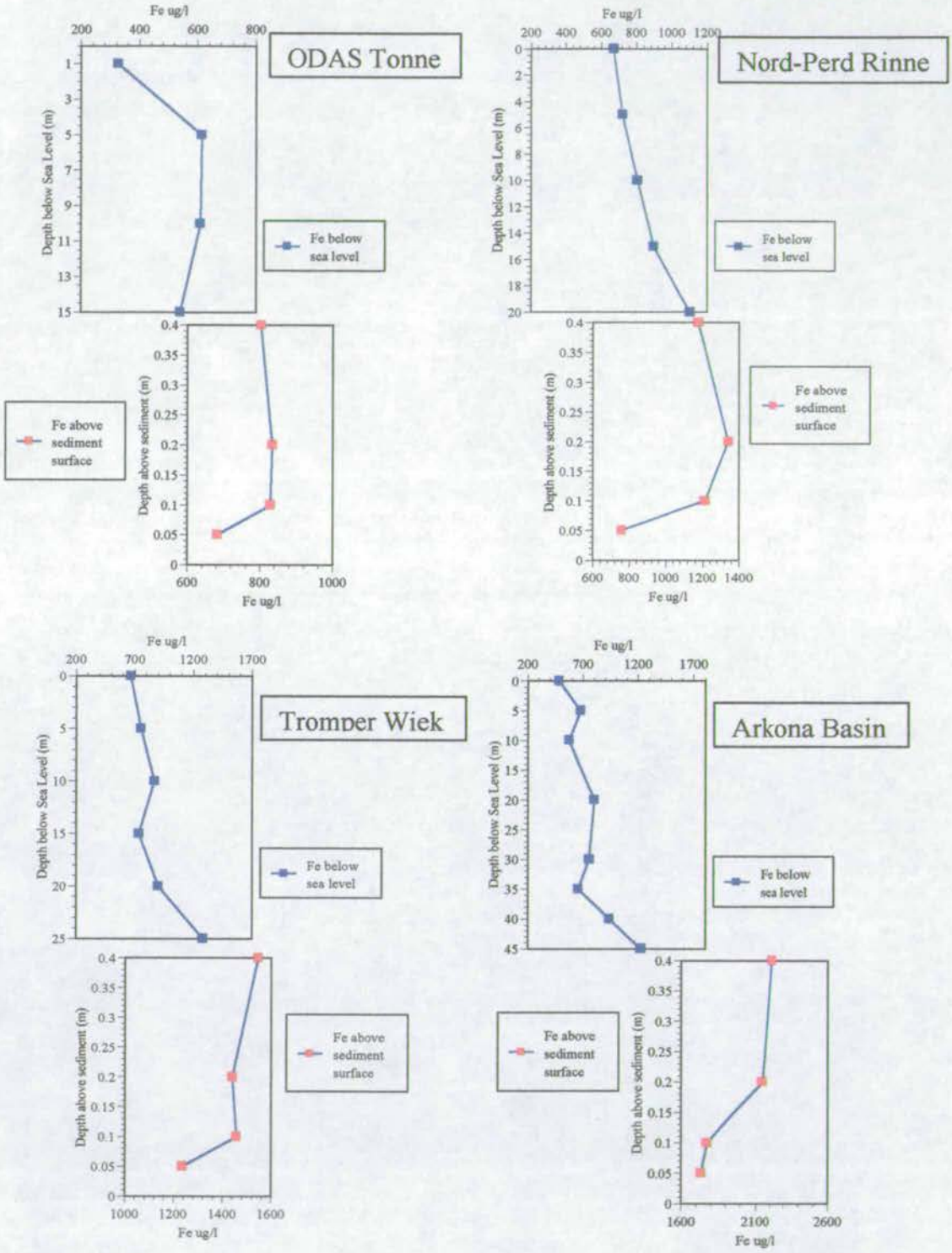

Figure 8-23 Water column dissolved iron concentrations, BASYS October '96. Samples marked by the red box are from the bioprobe lander and represent nepheloid layer characteristics.

BASYS March '97 Dissolved Iron Concentrations

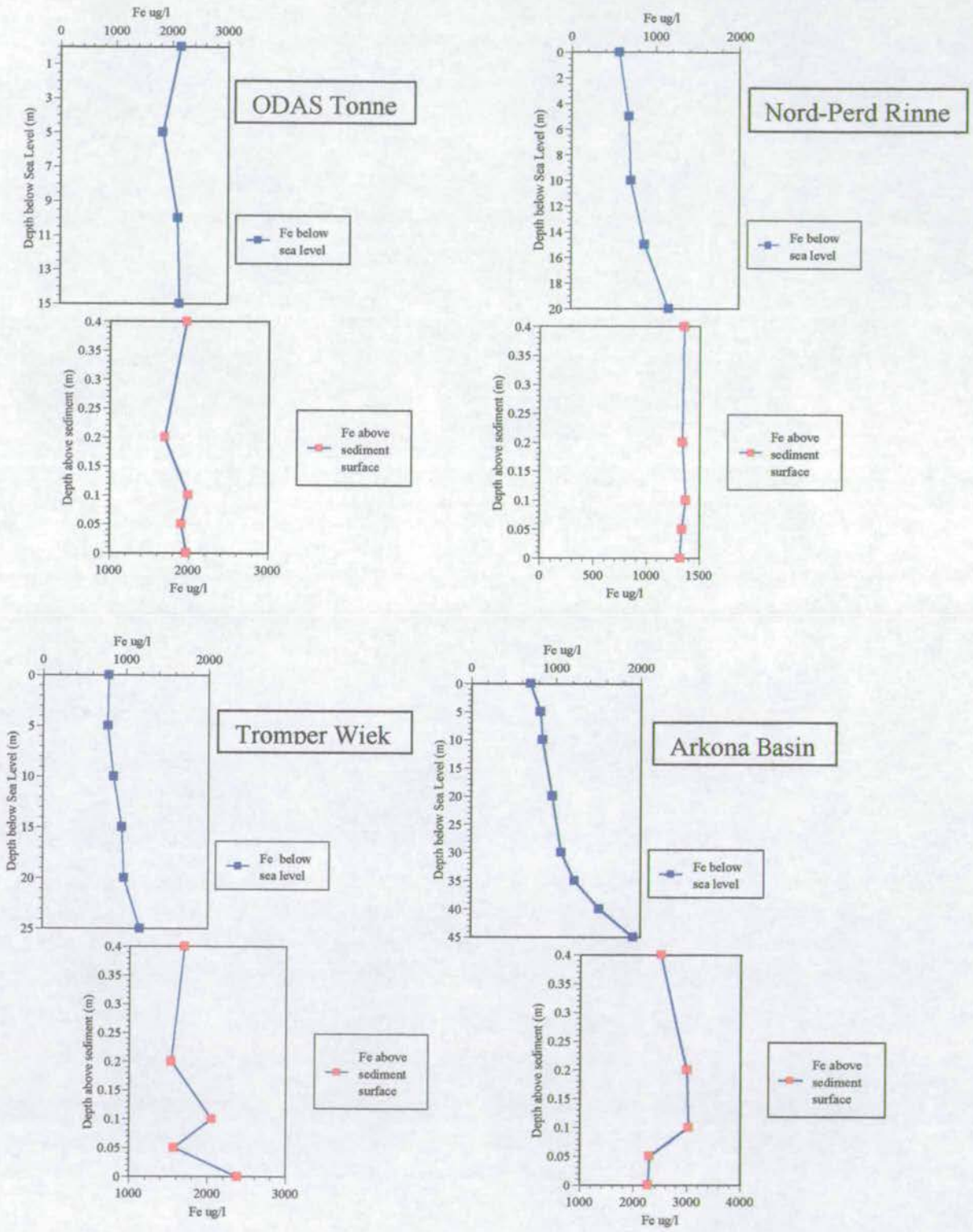

Figure 8-24 Water column dissolved iron concentrations, BASYS March '97 . Samples marked by the red box are from the bioprobe lander and represent nepheloid layer characteristics.

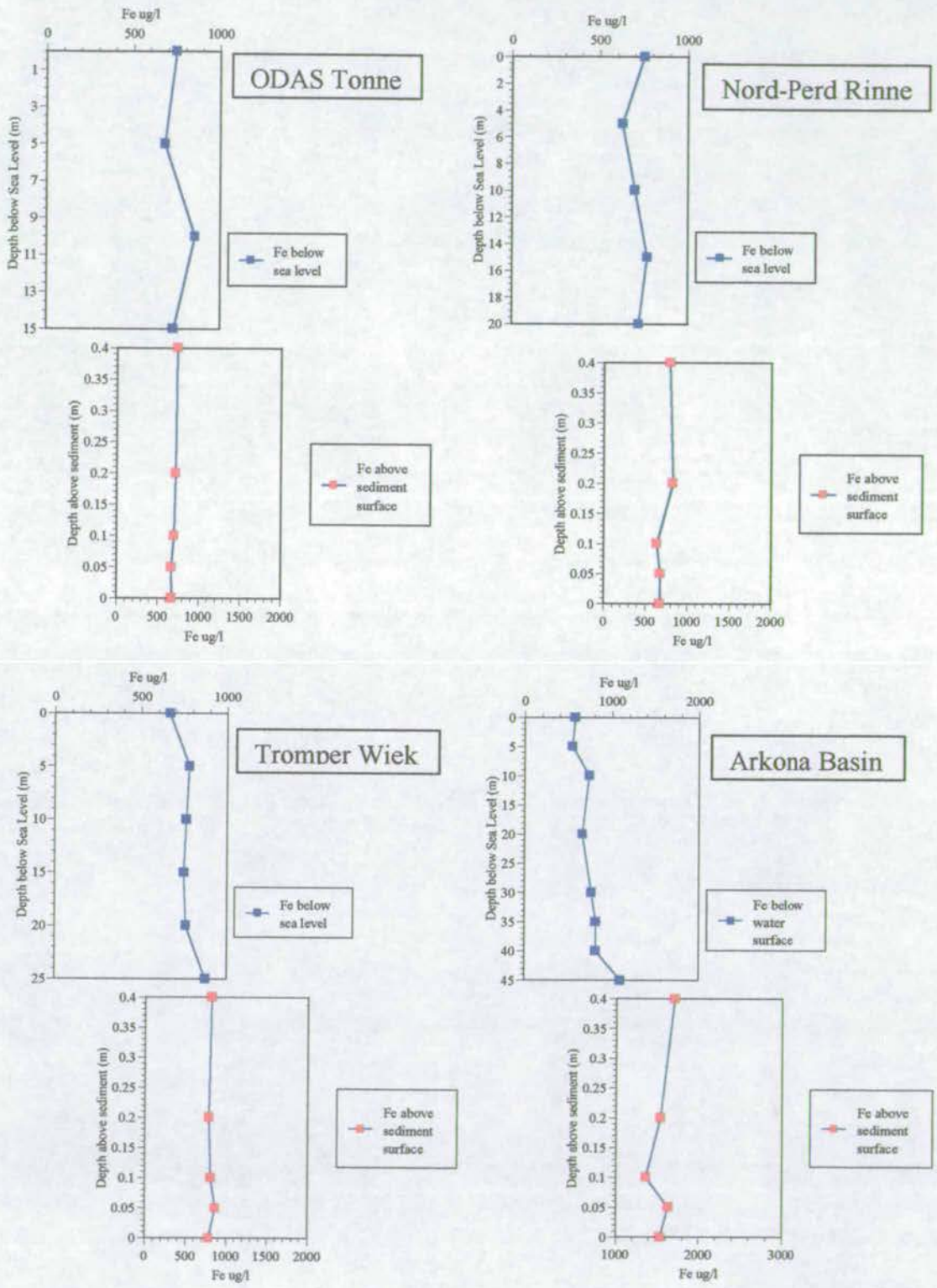

Figure 8-25 Water column dissolved iron concentrations, BASYS June '97. Samples marked by the red box are from the bioprobe lander and represent nepheloid layer characteristics.

BASYS December '97 Dissolved Iron Concentrations

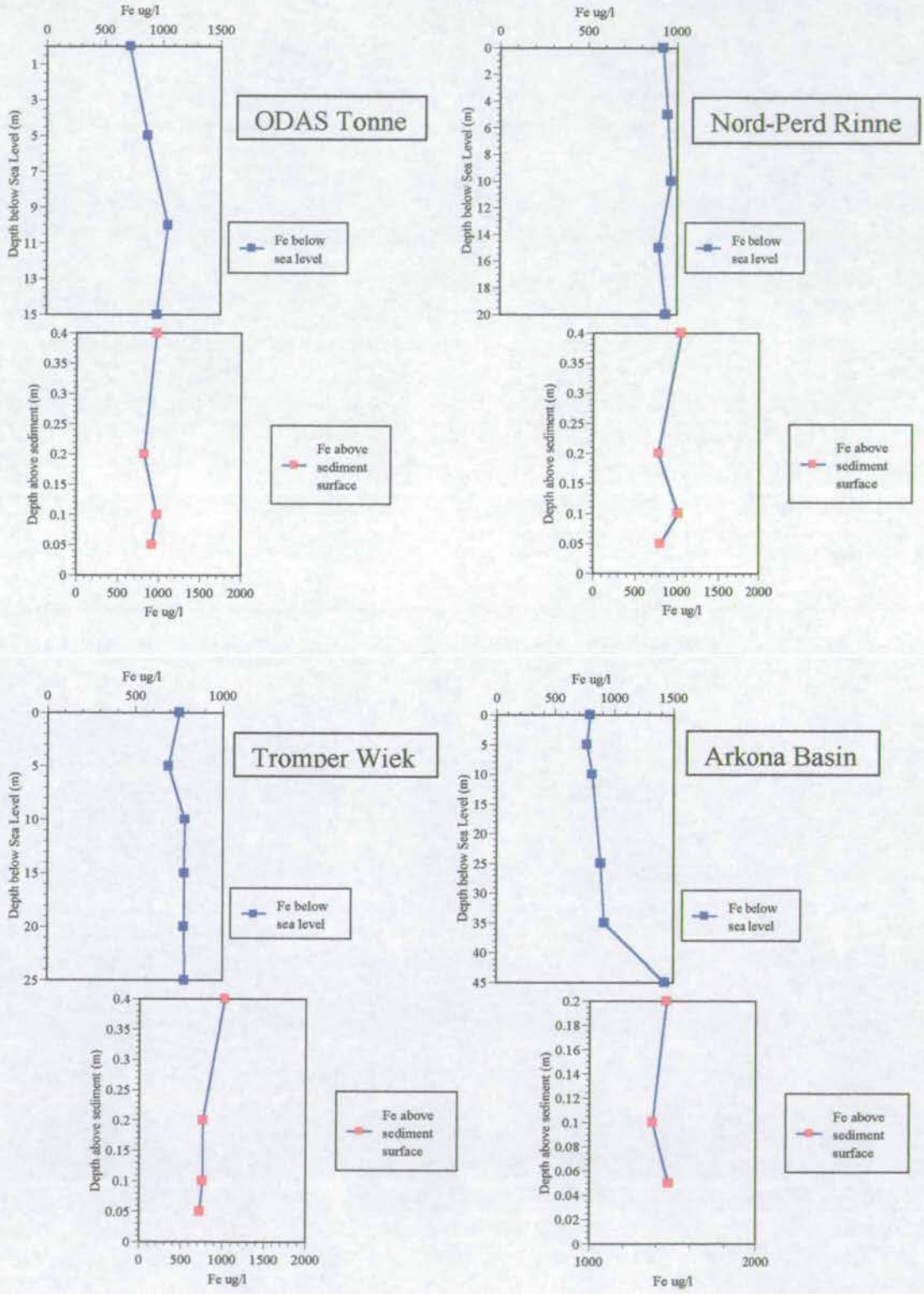

Figure 8-26 Water column dissolved iron concentrations, BASYS December '97. Samples marked by the red box are from the bioprobe lander and represent nepheloid layer characteristics.

8.7.1 Water column Iron concentrations

Figures 8-19 to 8-26 detail the water column distribution of iron for the four cruises through 1996 to 1997. To help summarise the information presented, Table 8-11 shows the variations in iron concentration in terms of the average lander to average water column ratios and Figure 8-27 shows the average water column variations (above resuspension / active bedload, (non-lander)) on a seasonal basis.

Table 8-11 Particulate Iron; Average lander to Average water column ratios

	Particulate Phase			
	October '96	***March '97***	***June '97***	***December '97***
Tonne	11	4*	5	2*
Nord Perd	171†	151†	16	6
Wiek	6	13	25	3
Arkona	30	490‡	44	62
	Dissolved Phase			
Tonne	1.54	0.93	0.93	1.02
Nord Perd	1.39	1.68	1.01	0.97
Wiek	1.66	1.99	1.06	1.08
Arkona	2.57	2.33	2.07	1.28

*value excludes 15m depth for Tonne as the sediment was also sampled at 15m, † these values are suspect and probably relate to a significant proportion of sediment layer sampling for the particulate phase ‡ probable sediment sampling by lander.

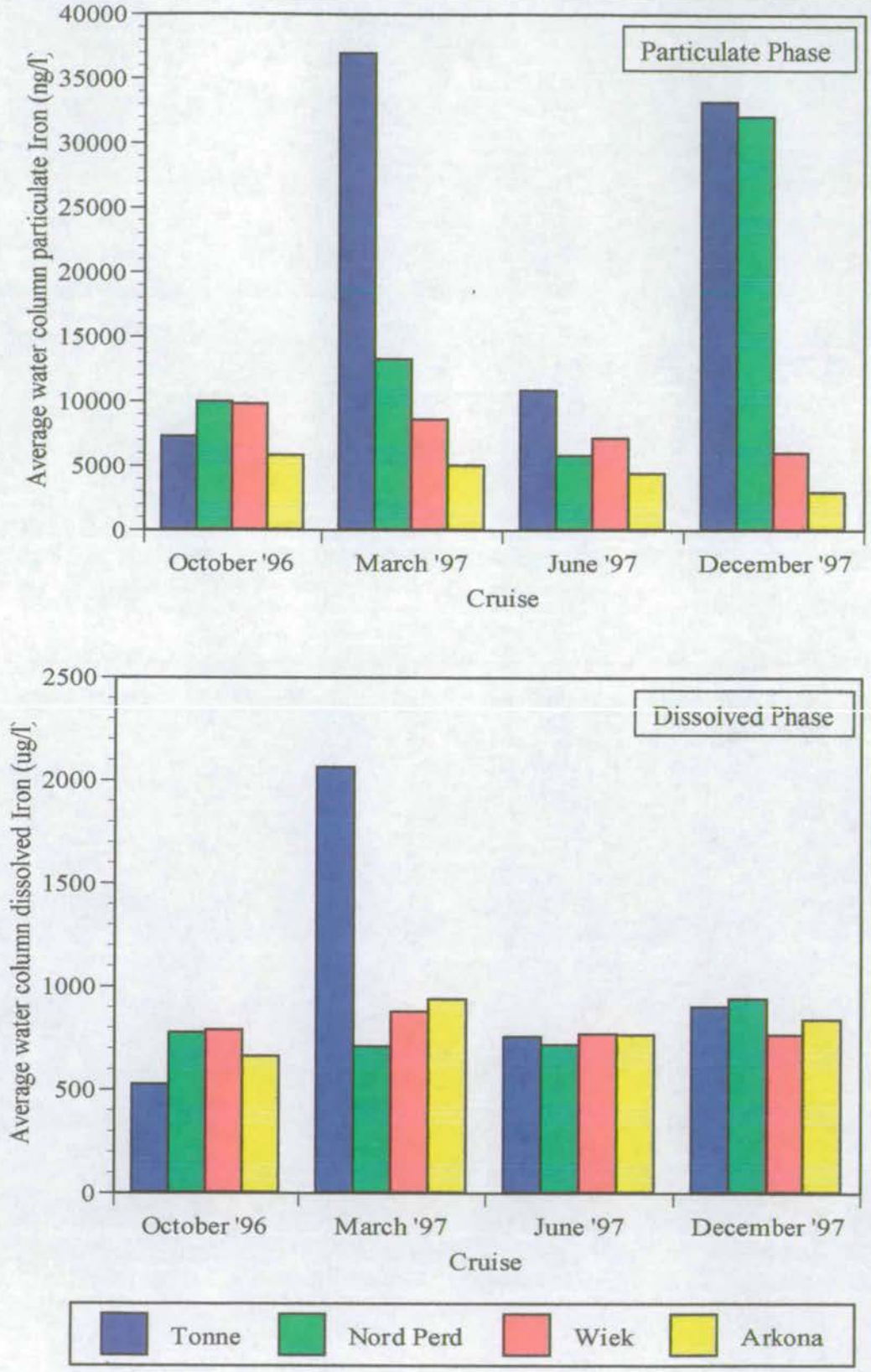

Figure 8-27 Average particulate and dissolved iron concentrations for the Southern Baltic Sea.

Detailed discussion of trends is reserved for the summary after the detailing of further elemental distributions, however the most obvious general trends from Figures 8-19 to 8-26 are that both the particulate and dissolved iron concentrations show a relatively constant down column distribution. This is modified in terms of the particulate matter by the presence of a near bottom resuspended layer or active bedload transport layer which ranges from negligible to 10m above the sediment water interface. June shows the least resuspension (Figure 8-21) possibly relating to calmer weather and wind conditions while October (Figure 8-19) shows the most significant influence of higher near bottom particulate concentrations. Generally, for the particulate matter the lander measurements show a large near bottom increase in the particulate concentrations of iron. In contrast to this, the dissolved phase shows a near consistency over the whole water column but there is evidence of near bottom removal of iron from the water column as displayed most clearly in Figure 8-23.

These traits are reflected in Table 8-11 with the ratio of average lander to average water column concentration for the dissolved phase approximating to unity. Significant variations from unity are shown for the particulate layer which reflect significant particulate concentration enrichments in the near bottom zone as measured by the lander which most probably represents, when coupled with the presence of resuspended matter, the presence of a mobile nepheloid layer. The interesting feature of both the dissolved and particulate phase ratio values are that they all consistently increase at Arkona. This is in part due to the decrease in water column particulate concentrations but also to the much larger lander concentrations at Arkona. This may be a result of the finer grain size and a corresponding increased ease of sampling of the fine, iron rich, sediment at Arkona or as a real increase in fluff layer concentrations.

The main trends displayed in Figure 8-27 are of a general decreasing particulate concentration from Tonne to Arkona which shows little seasonality. The peaks in March and December for Tonne and Nord-Perd, if substantiated by other elemental increases may be as a result of the pulsed nature of the Oder outflow into the Baltic Sea which has recently been described by BESZCYNSKA-MOLLER, 1998.

No seasonality can be detected with reference to the dissolved phase concentrations which are remarkably consistent over the whole period of investigation which is surprising considering the hydrographic gradients from the shallow to the deepest station.

As iron was primarily considered to be an element associated with the lithogenic phase in the sediment core then in order to corroborate the possibility of a similar association in the water column then the data for rubidium was also plotted.

8.7.2 Water column Rubidium concentrations (Lithogenic)

The profiles for both the particulate and dissolved phase of rubidium are shown in Figures 5-28 and 5-29. Instead of showing the full complement of plots these two figures were taken as being representative of the typical rubidium profiles with the main conclusion drawn that they are almost identical in form to the iron concentration profiles. As rubidium was considered to be exclusively resident as a lithophilic element in the sediment core, then their similar behaviour in the water column suggests a strong mineralogical control especially in the particulate phase

BASYS June '97 Particulate Rubidium Concentrations

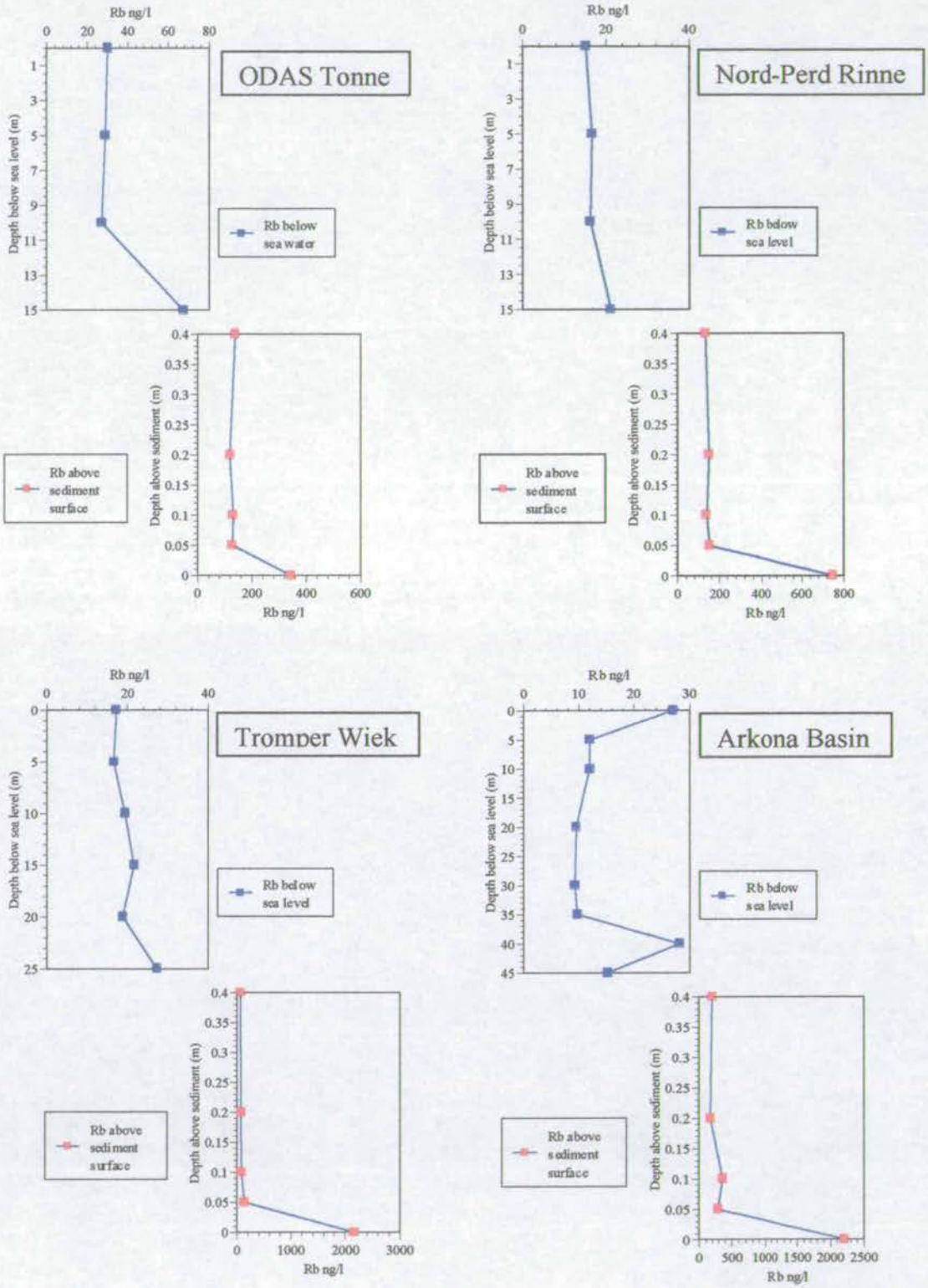

Figure 8-28 Water column particulate rubidium concentrations, BASYS June '97. Samples marked by the red box are from the bioprobe lander and represent nepheloid layer characteristics.

BASYS June '97 Dissolved Rubidium Concentrations

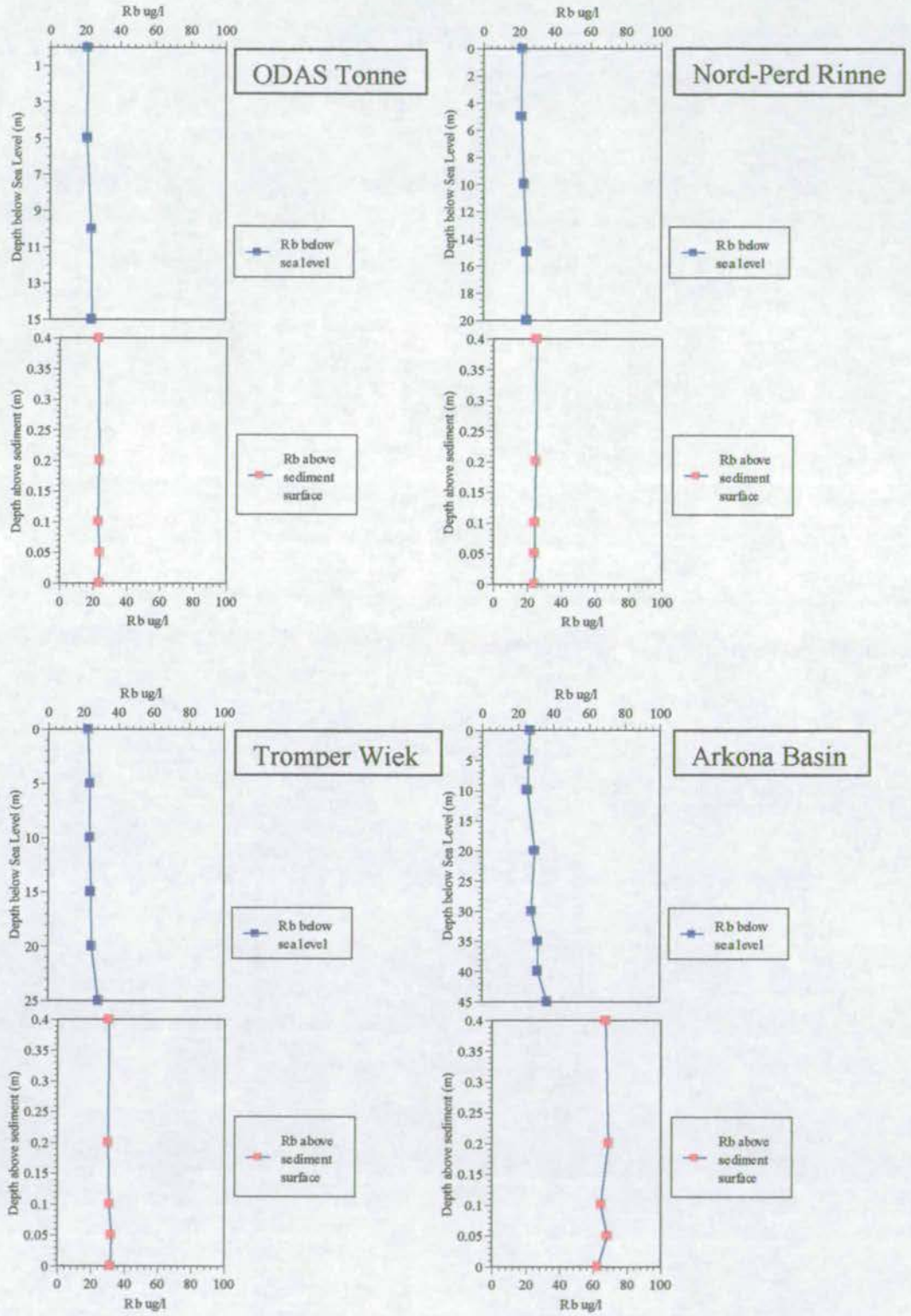

Figure 8-29 Water column dissolved rubidium concentrations, BASYS June '97. Samples marked by the red box are from the bioprobe lander and represent nepheloid layer characteristics.

8.7.3 Water column Lead, Zinc, Tin and Copper concentrations (anthropogenic)

Another important group of elements identified in the sediment core are those related to anthropogenic sources. In the following section Pb, Zn, Sn and Cu are considered with Figures 5-28 to 5-31 showing the distribution of lead for the particulate phase. All these 'anthropogenic' related elements were below the limit of detection in the dissolved phase and hence cannot be considered in this discussion.

Average seasonal concentrations of lead are shown in Figure 8-30 which shows similar trends for lead as those observed for iron for the majority of months, the main exception being June where elevated lead concentrations are found with respect to iron.

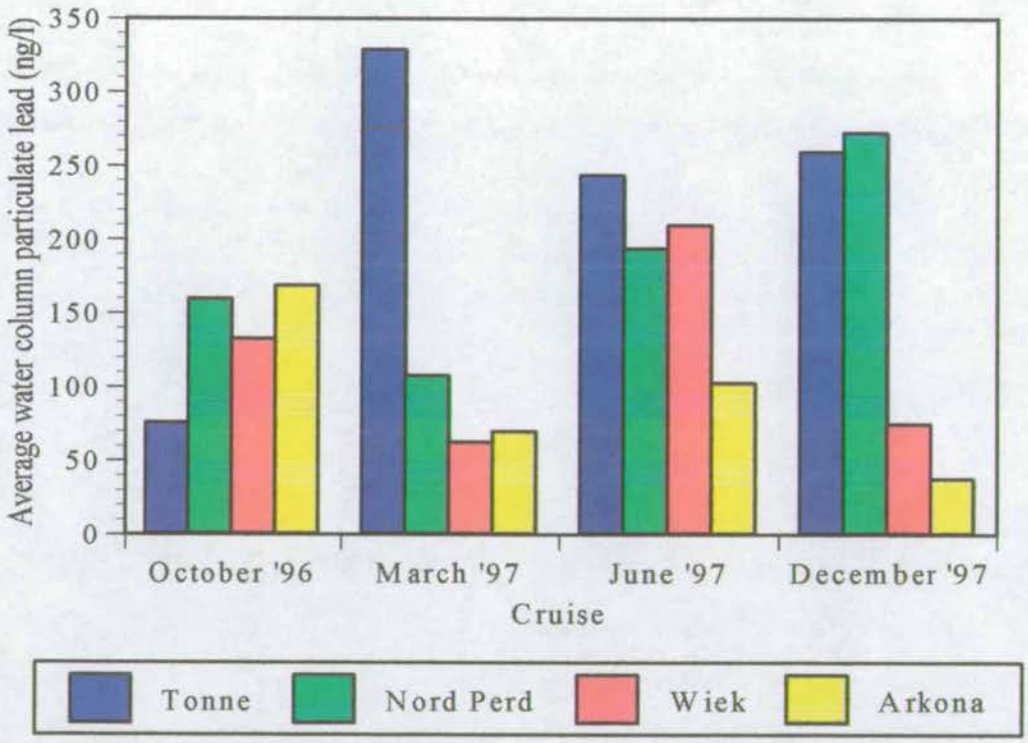

Figure 8-30 Average water column particulate lead in the Southern Baltic Sea

In addition the three peaks at Tonne in March and Tonne plus Nord-Perd in December are evident for the lead concentrations as they were in the iron concentrations providing additional evidence that this is a real feature.

BASYS October '96 Particulate Lead Concentrations

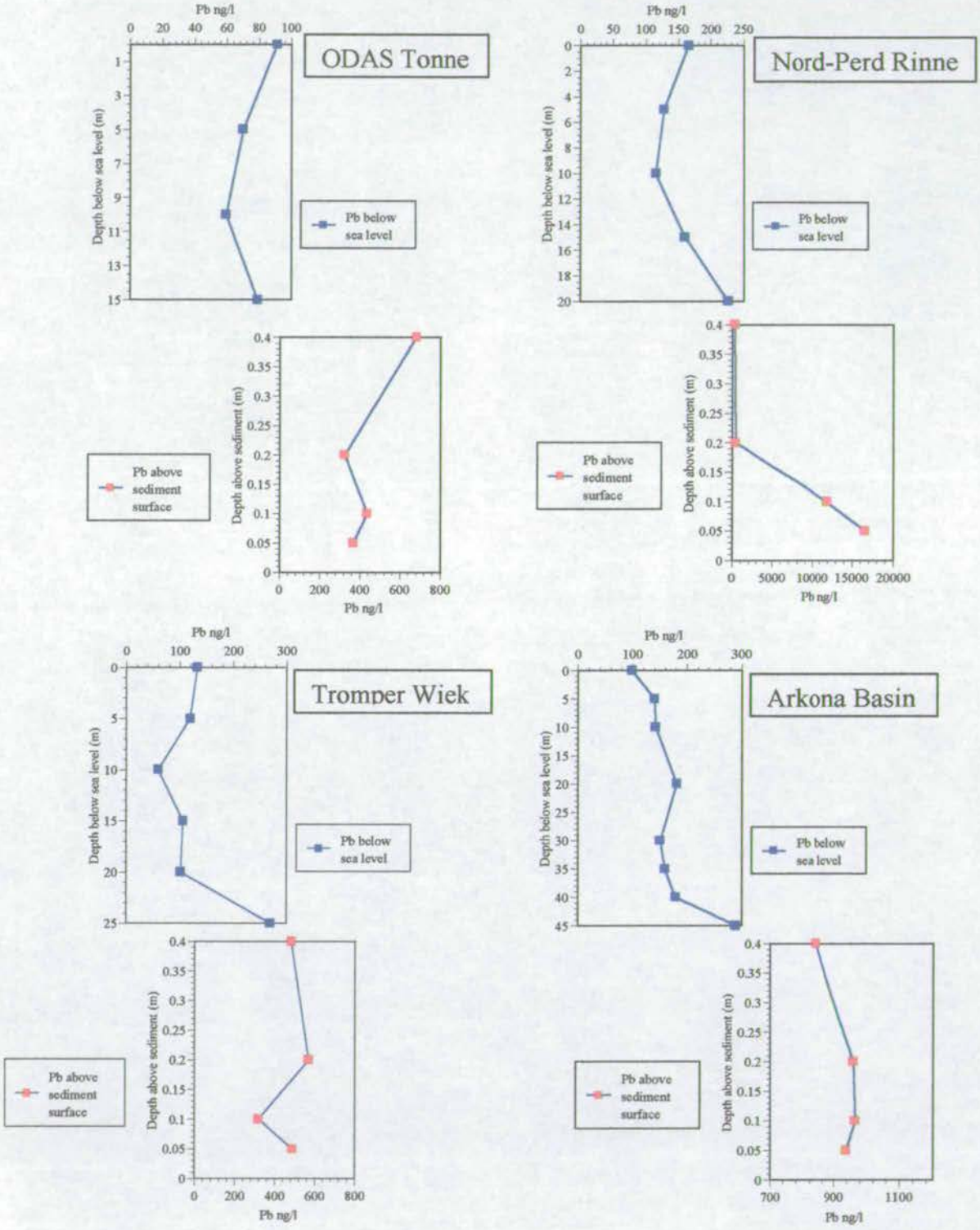

Figure 8-31 Water column particulate lead concentrations, BASYS October '96. Samples marked by the red box are from the bioprobe lander and represent nepheloid layer characteristics.

BASYS March '97 Particulate Lead Concentrations

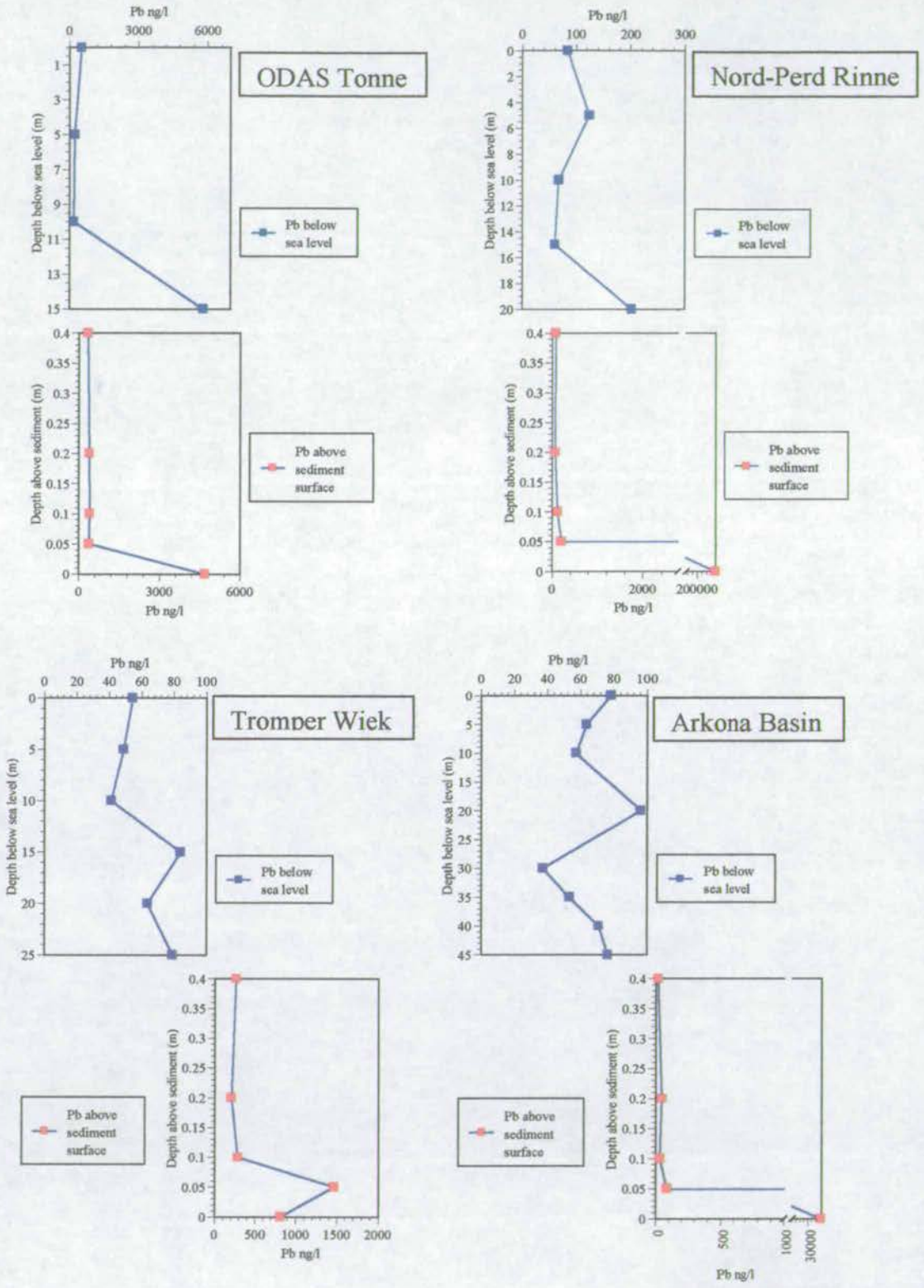

Figure 8-32 Water column particulate lead concentrations, BASYS March'97. Samples marked by the red box are from the bioprobe lander and represent nepheloid layer characteristics.

BASYS June '97 Particulate Lead Concentrations

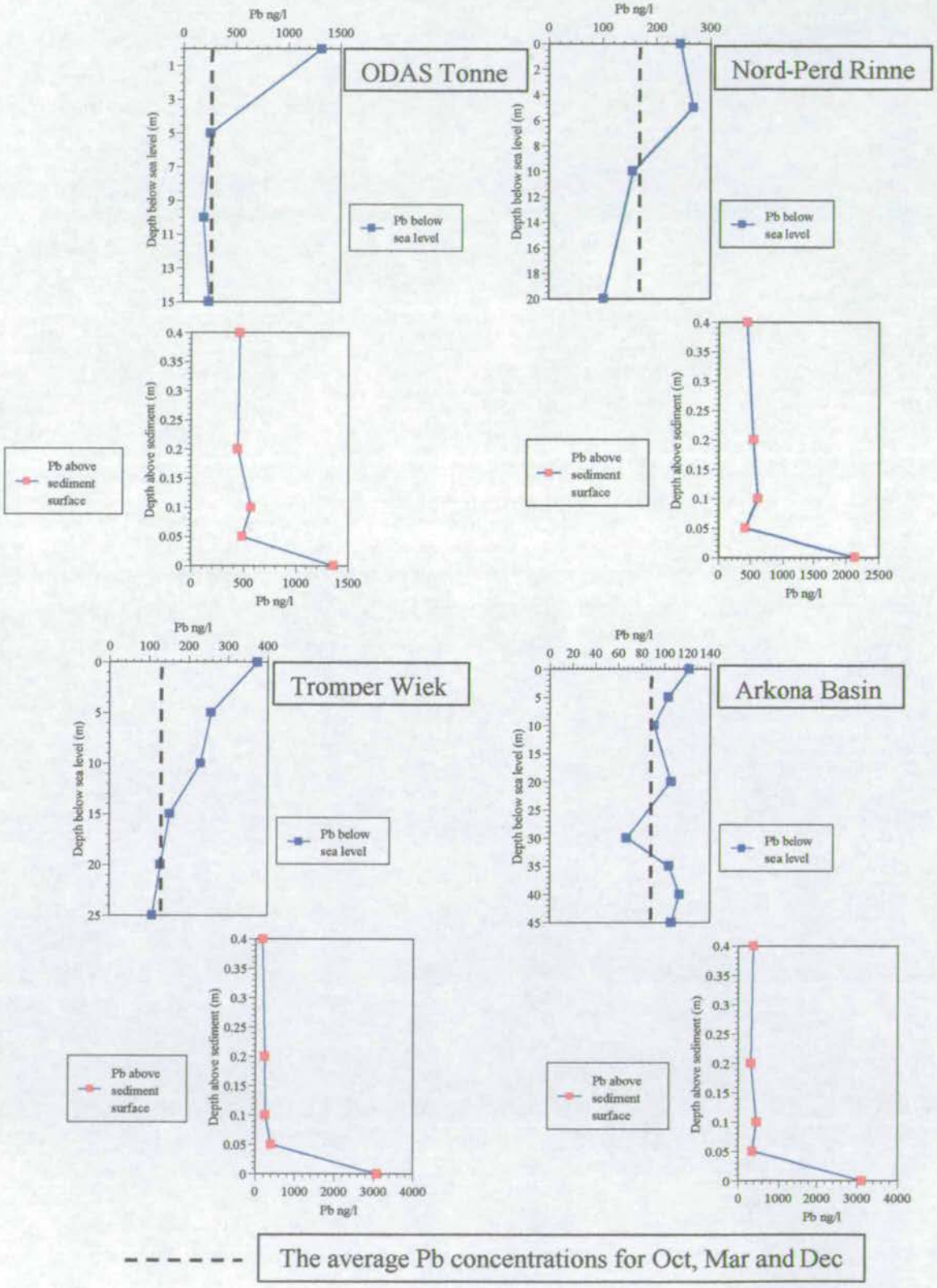

Figure 8-33 Water column particulate lead concentrations, BASYS June '97

BASYS December '97 Particulate Lead Concentrations

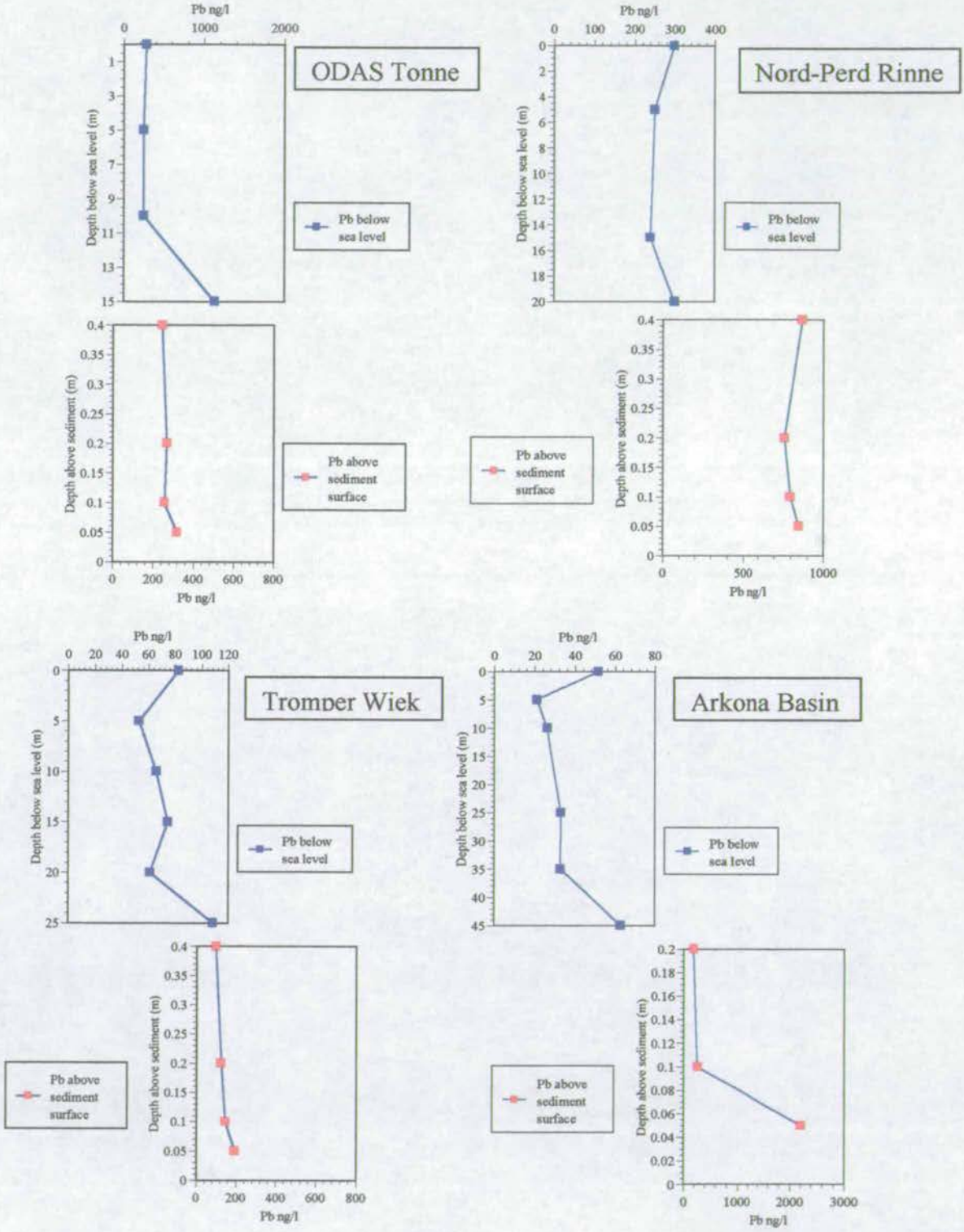

Figure 8-34 Water column particulate lead concentrations, BASYS December '97. Samples marked by the red box are from the bioprobe lander and represent nepheloid layer characteristics.

The profiles generated in Figures 8-31 to 8-34 are remarkably consistent in their overall trend to those displayed in the iron profiles. However, there is some variance in the actual detail of the water column profiles but the main differences are associated with the profiles for June where elevated surface values of lead increase the average value which accounts for the relatively high June concentrations shown in Figure 8-30.

This increased surface concentration may be related to a combination of contributory factors. The most likely possibilities relate the presence of dust, biological activity in the surface waters and its recycling and / or due to the retention of an atmospheric lead component and its enhanced concentration due to the development of a thermoclinic barrier at 5 to 10m depth.

In a similar respect Cu, Sn and Zn also show similar profiles with the same general trends, characteristically in June they show surface enrichment with depletion at depth as shown in Figures 8-35 to 8-37. However in contrast, lead is the only one that shows a substantial increase in concentration against the average for June. Cu, Zn and Sn all show values that lie in close proximity to the averaged values for the period of observation

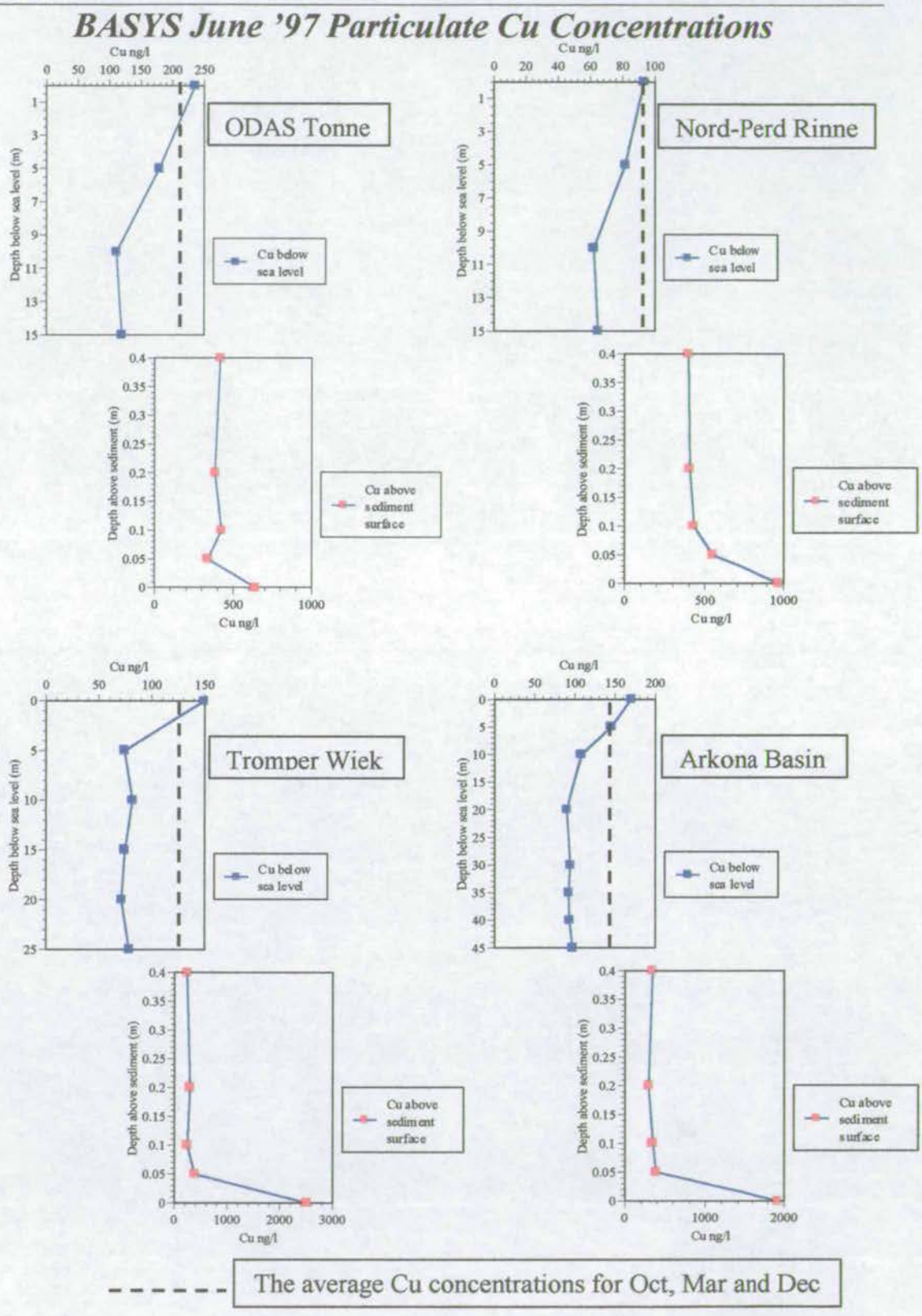

Figure 8-35 Water column particulate copper concentrations, BASYS June '97. Samples marked by the red box are from the bioprobe lander and represent nepheloid layer characteristics.

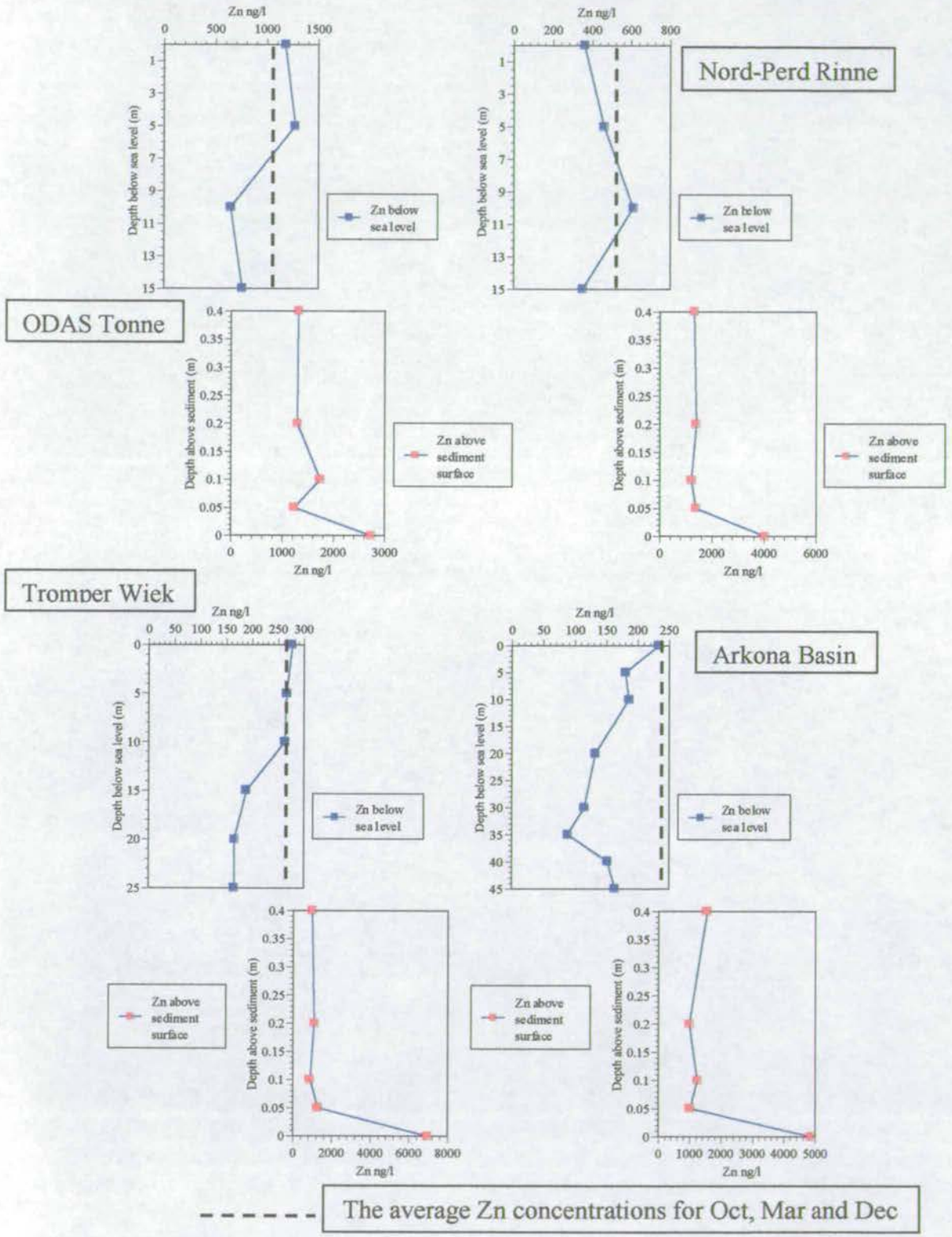

Figure 8-36 Water column zinc concentrations, BASYS June '97. Samples marked by the red box are from the bioprobe lander and represent nepheloid layer characteristics.

BASYS June '97 Particulate Sn Concentrations

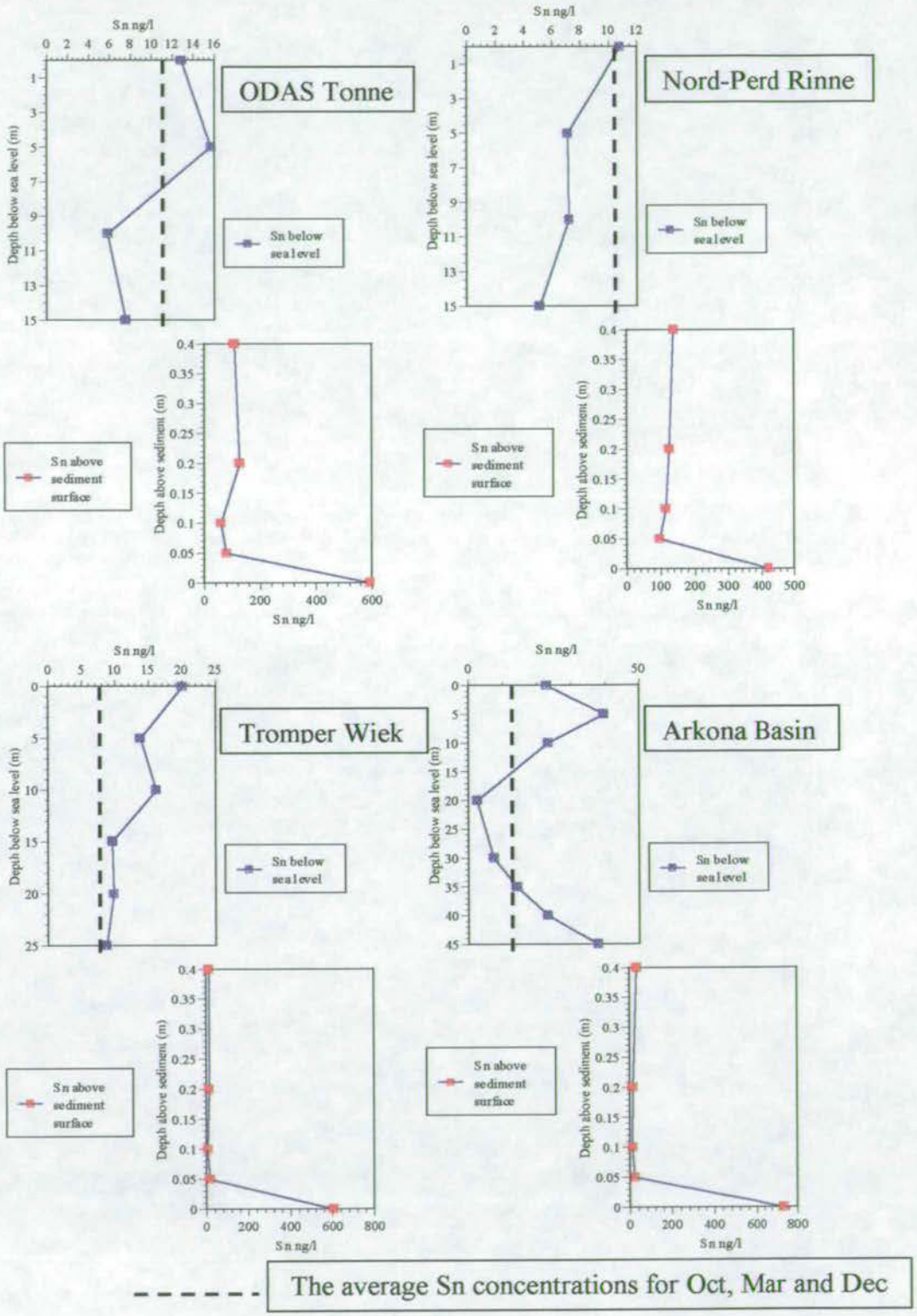

Figure 8-37 Water column particulate tin concentrations, BASYS June '97. Samples marked by the red box are from the bioprobe lander and represent nepheloid layer characteristics.

Two final groups were identified in the sediment core these being those associated with redox processes and the second related to biogenic activity.

8.7.4 Water column Manganese concentrations (redox)

As manganese shows the greatest redox variations Figures 5-38 to 5-41 show the profiles generated for the particulate phase and in addition Figure 5-42 shows a typical profile of dissolved manganese.

The particulate manganese profiles are not dissimilar from the general forms of the rest of the elements studied except for one striking feature of the Arkona profiles for October, March and December that set it apart. While the rest of the elements show a near bottom increase in concentration, manganese in contrast, especially in the October profile has a decreasing near bottom profile possibly relating to sub oxic or reducing conditions in the water column which reduces the manganese from Mn^{4+} to the more soluble Mn^{2+}. This is corroborated by elevated dissolved manganese concentrations in the lander samples, which may indicate reducing conditions close to the sediment-water interface.

In addition the near bottom, dissolved iron profiles shown in Figures 8-23 to 8-26 show removal of iron close to the sediment water interface. This may relate to the increased precipitation at depth on floccs as the salinity gradient is crossed leading to a greater ability for the scavenging of iron from the water column dissolved phase.

The dissolved manganese profile shown in Figure 8-42 reveals the absence of any detectable amounts of manganese in the water column proper with generally low values in the lander samples. Although in the deeper basins where reducing conditions are suspected, greatly elevated levels of manganese can be found.

BASYS October '96 Particulate Mn Concentrations

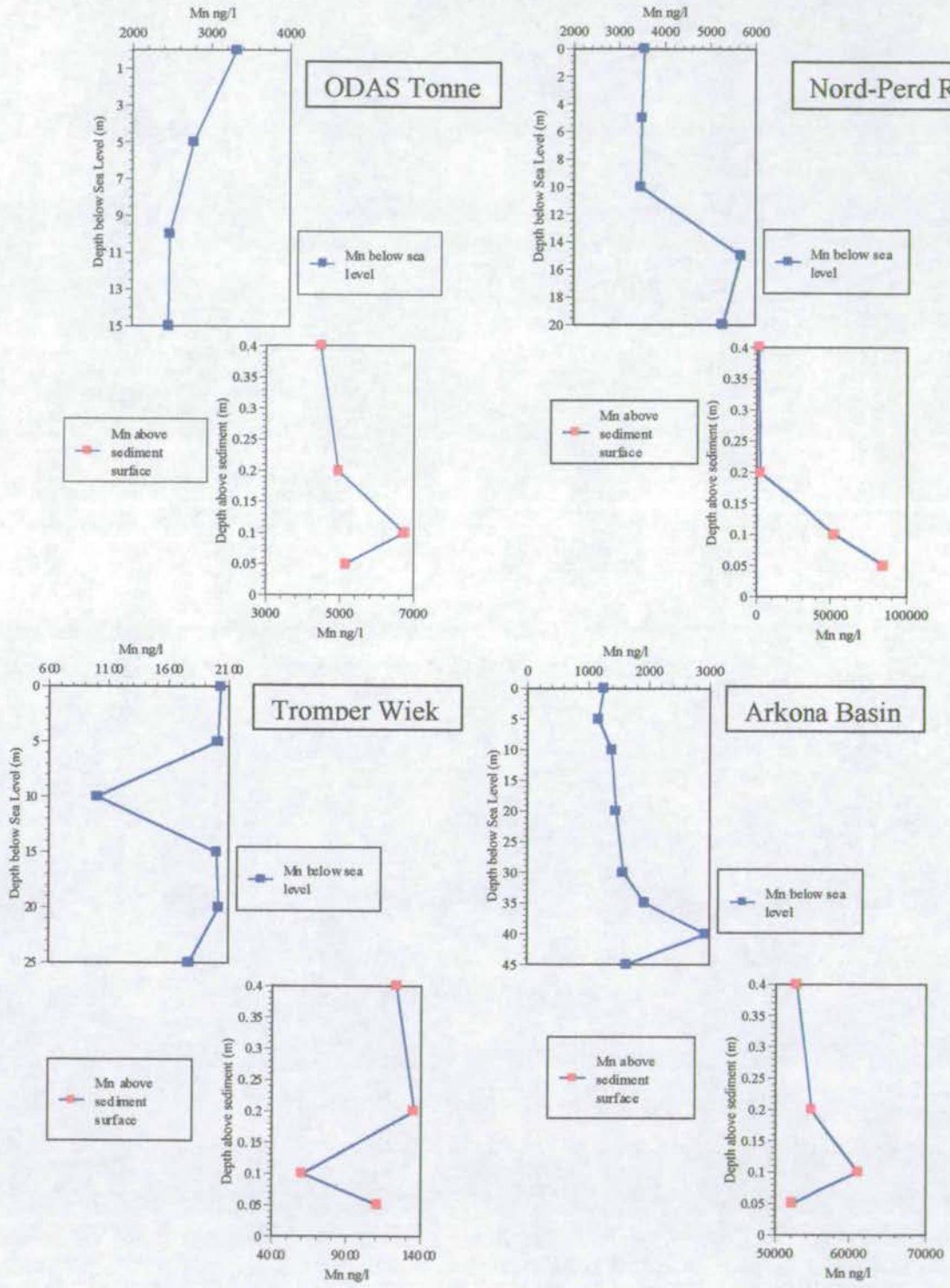

Figure 8-38 Water column particulate manganese concentrations, BASYS October '96 . Samples marked by the red box are from the bioprobe lander and represent nepheloid layer characteristics.

BASYS March '97 Particulate Mn Concentrations

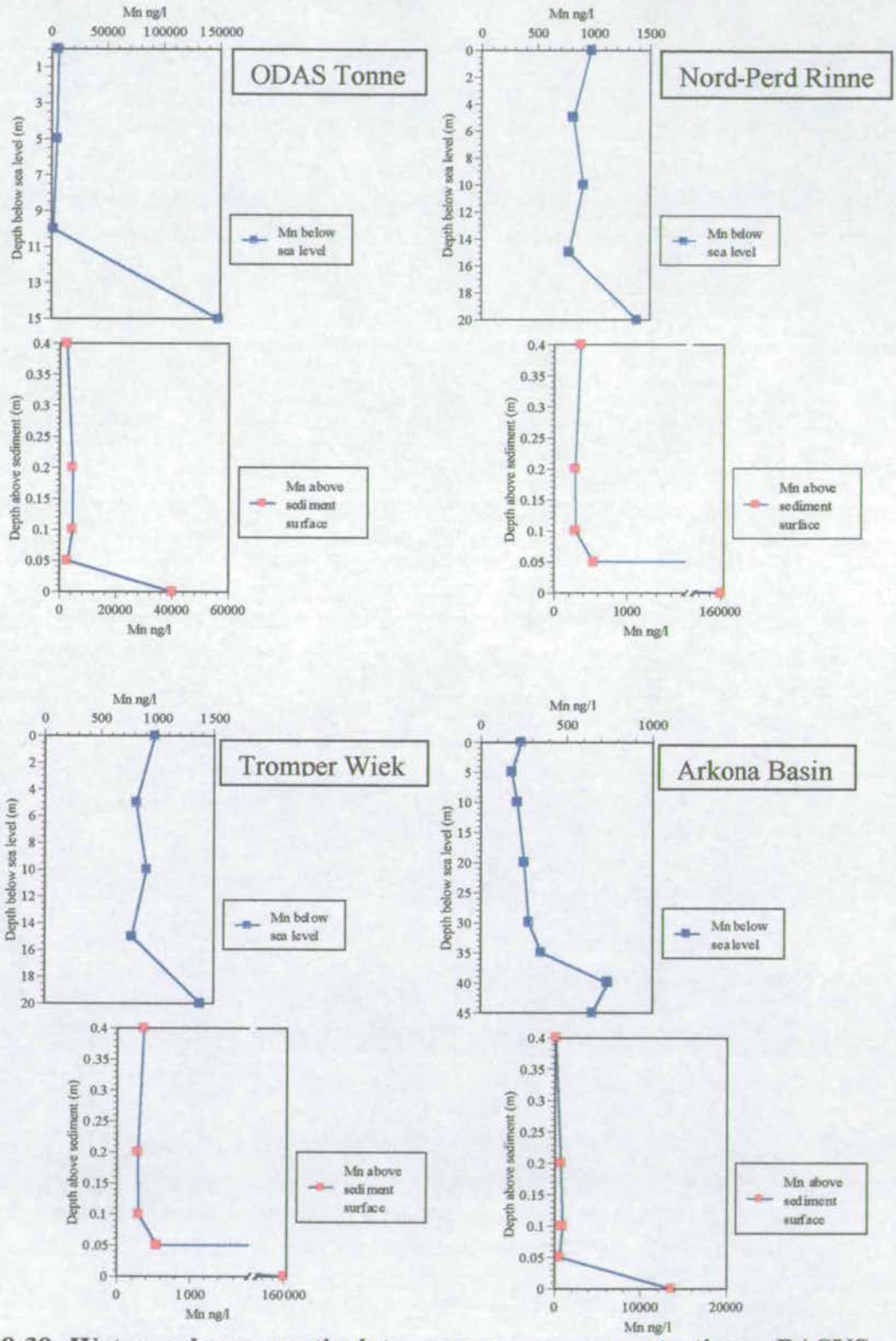

Figure 8-39 Water column particulate manganese concentrations, BASYS March '97. Samples marked by the red box are from the bioprobe lander and represent nepheloid layer characteristics.

BASYS June '97 Particulate Mn Concentrations

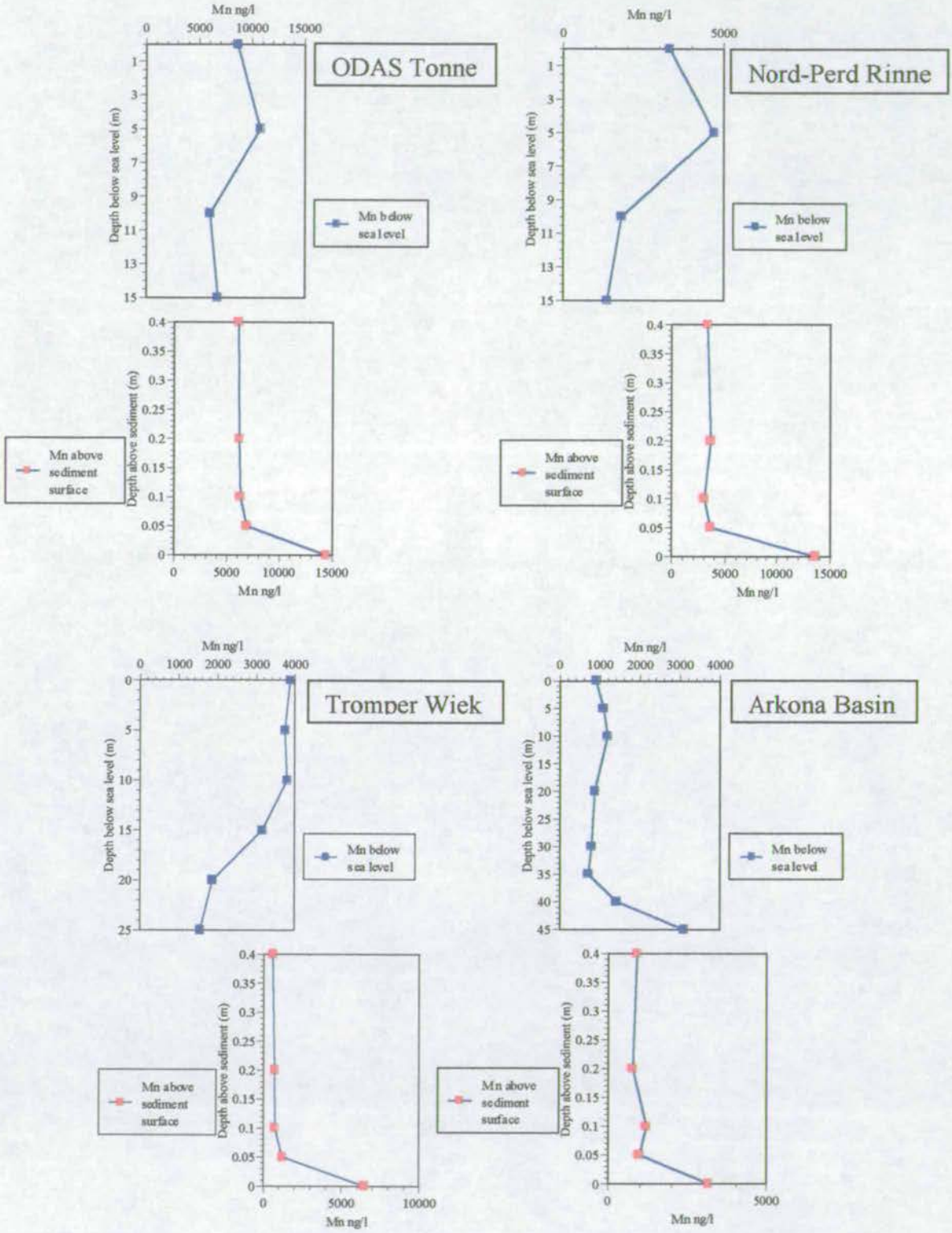

Figure 8-40 Water column particulate manganese concentrations, BASYS June '97. Samples marked by the red box are from the bioprobe lander and represent nepheloid layer characteristics.

BASYS December '97 Particulate Mn Concentrations

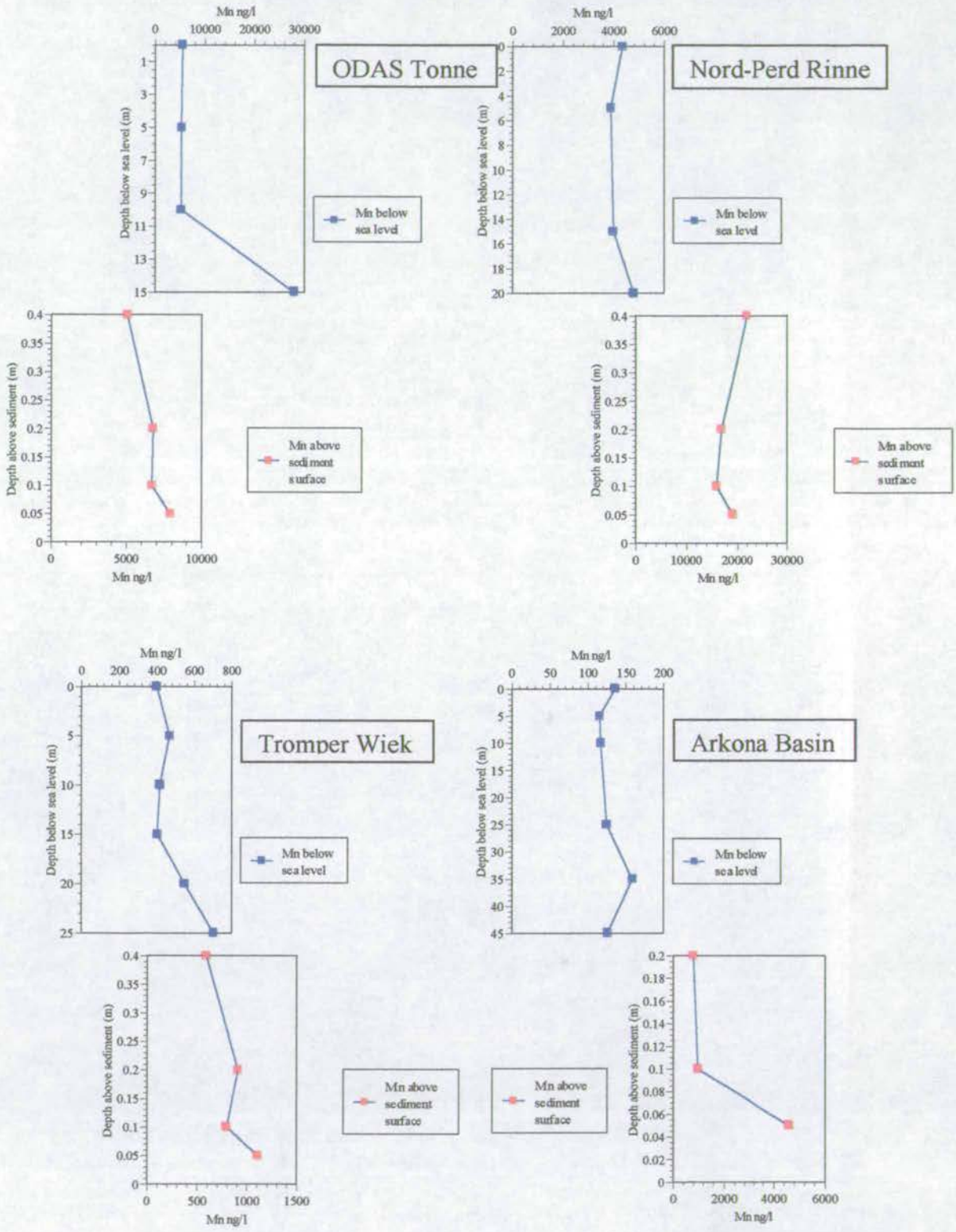

Figure 8-41 Water column particulate manganese concentrations, BASYS December '97. Samples marked by the red box are from the bioprobe lander and represent nepheloid layer characteristics.

BASYS June '97 Dissolved Mn Concentrations

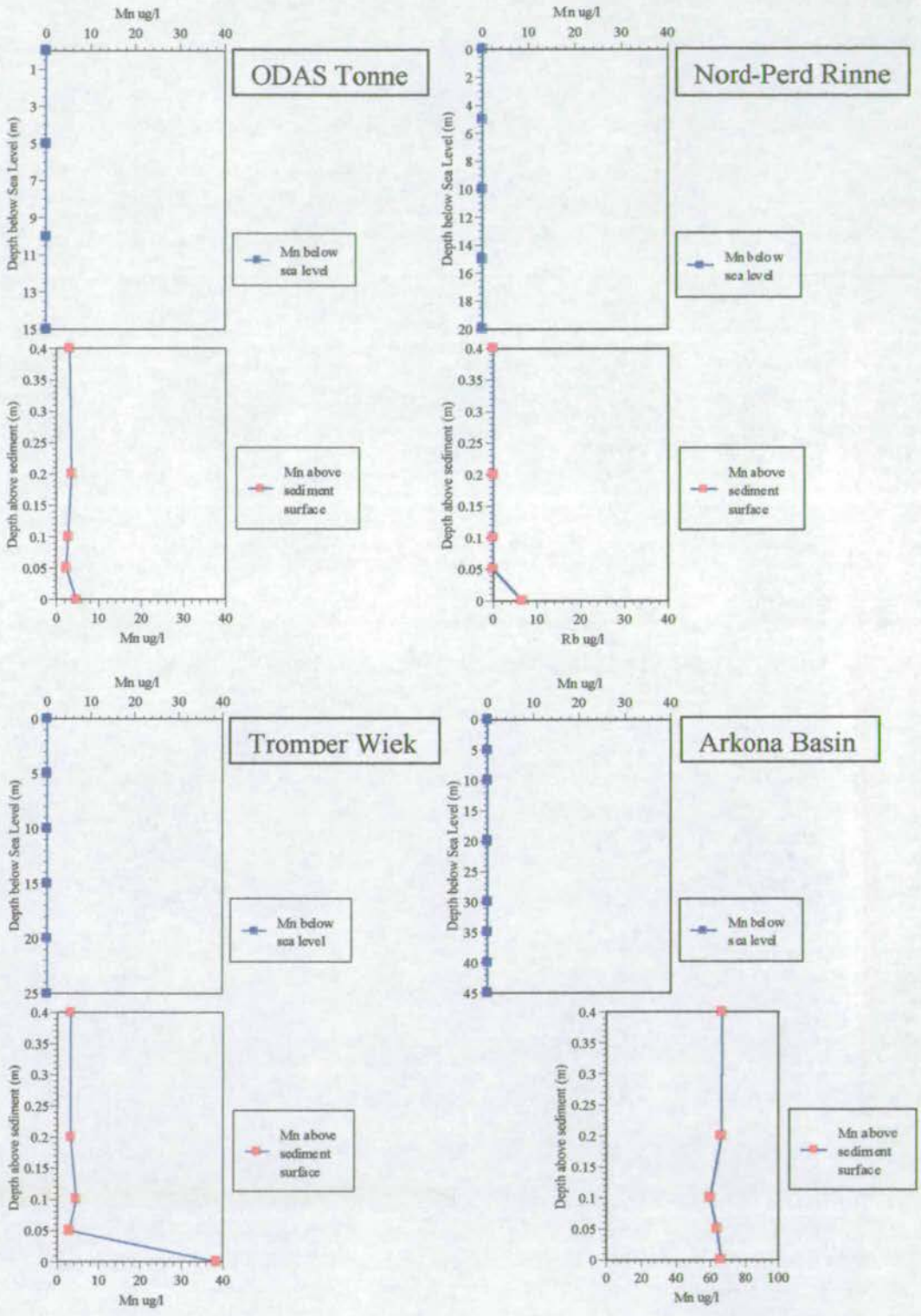

Figure 8-42 Water column dissolved manganese concentrations, BASYS June '97 . Samples marked by the red box are from the bioprobe lander and represent nepheloid layer characteristics.

8.7.5 Water column Strontium concentrations (Biogenic)

In order to complete the elemental categories defined in the sediment core a brief examination of Sr as a representative of the biogenic phase is warranted. The Sr profiles are again relatively similar to those already displayed and show no discriminatory features.

Figure 8-43 below shows the main average seasonal concentrations in strontium for the region of investigation. The main trend that can be seen is that for the majority of stations and seasons there is little variance in the concentration of strontium with the main exception being the two peaks in March and June at Tonne. Generally a concentration trend decreasing from Tonne to Arkona can also be observed over the seasonal periods. These features probably relate to an increase in primary productivity in the shallow water sites which occur most noticeably during the biologically productive months of March and June. For the rest of the stations on a seasonal basis there is however little change and a consistency in strontium concentration can be seen over the whole period.

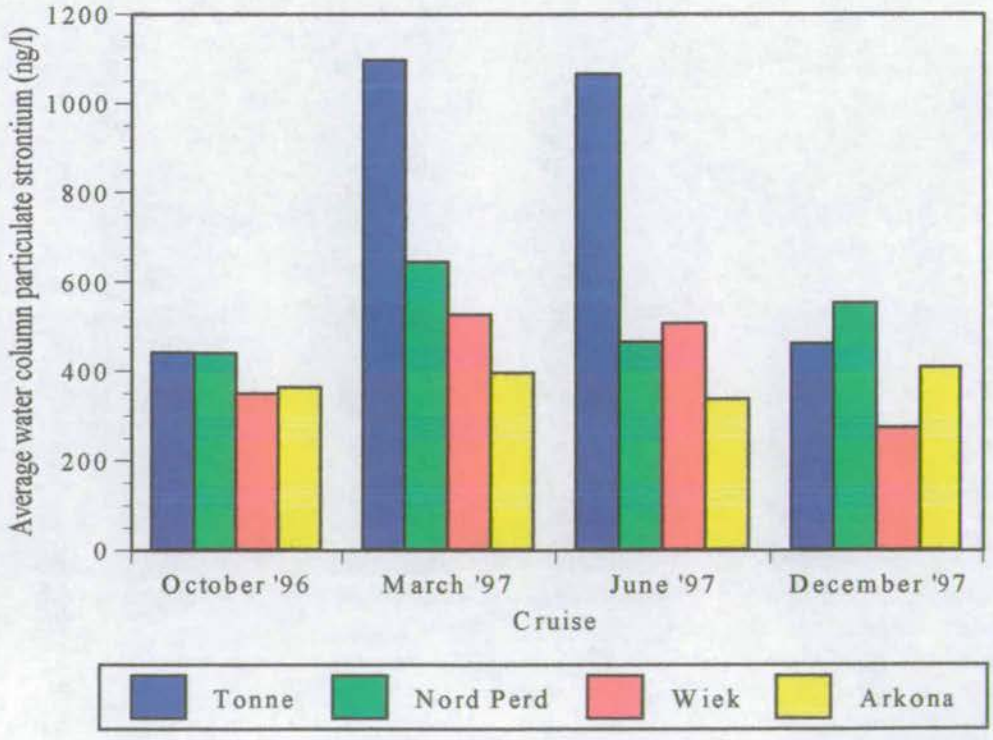

Figure 8-43 Average water column particulate strontium in the Southern Baltic Sea

8.7.6 Normalised metal water column ratios

As ratio values are dependant upon the variation of two elements then they are inherently of greater variability than concentration profiles and hence only general trends can be inferred from the following two figures. Tables 8-44 and 8-45 show a selection of normalised to rubidium metal values, which are shown for each station. Three values are given, the first is an average, above the resuspended layer, water column ratio, the second ratio is at 0.40cm above the sea floor and finally a 0.05cm above the sea floor value. In order that comparisons can be made the average sediment core surface ratio is also noted but care should be taken as only in the case of Tonne is this the 0-1cm slice, both Arkona and Wiek are represented by the 1-2cm slice and the Nord-Perd ratio is taken as the 4-5cm slice. This could have important implications if one element has an exponential type increase in concentration in the near surface layers.

Figure 8-44 shows the rubidium normalised iron ratios for the particulate and dissolved phase over the four months of survey. The results show no definite trends, however, for the particulate phase; Tonne generally has the highest ratios and Arkona generally has the lowest values but there is no consistent pattern to the changes. This is in stark comparison to the sediment core ratios which, conversely, tend to show a definite increase with station depth. Therefore, the water column particulate iron is relatively constant in comparison to the sediment core ratio. This could indicate that the majority of the iron in the system is deposited at Arkona with little being deposited at Tonne. The material incorporated into the sediment core probably undergoes some secondary transformations from the primary water particulate phase possibly as a result of extended transport or diagenesis before it is incorporated in the sediment core. It seems likely that iron in the water column particulate phase goes on to comprise the mobile nepheloid layer whereby it is transported and recycled until final deposition occurs in the Arkona sediment core.

In addition the biologically important months of March and June show ratio values lower than the sediment core ratio for the 0.05cm lander sample whereas in October and December the values are slightly higher than the sediment core values. This may

be used to infer that removal of iron from the water column system occurs during months of high biological productivity and that the sediment core is a product of an averaged ratio over the whole year.

Similarly, the dissolved phase ratios are relatively constant over all the stations and are much lower than the particulate phase. No obvious trends can be seen in this data set including little evidence of any seasonal variations over the period of investigation.

Figure 8-45 shows only particulate ratio data for lead, copper, tin and strontium for in June and December as no dissolved phase data was obtained. The ratios for lead, copper and tin show pronounced variations with the average water column ratios being much greater than the sediment core ratio values. However, these ratios decrease to near unity with the sediment core with decreasing distance above the sediment water interface as shown by the lander measurements.

Strontium does not seem to have any apparent trends which may relate to its close relationship with the biological cycle, in particular the formation of shelly material, and hence takes part in a separate geochemical cycle.

As iron shows a relatively constant ratio value in the particulate and dissolved phase with possible trends of decreasing ratios from Tonne to Arkona a lateral transitional component is proposed as the main transport mechanism. In contrast to this the data for lead, copper and tin shows less of a lateral component as the ratios are strongly consistent over the survey area and instead shows a strong vertical zonation in which the bottom of the water column has a strong relationship with the sediment core surface ratios.

Iron / Rubidum Water Column Ratios

Station and month of observation		Particulate Phase			Dissolved Phase			Sed. Core
		Average water column ratio	0.40m a.s.f.* lander ratio value	0.05m a.s.f* lander ratio value	Average water column ratio	0.40m a.s.f.* lander ratio value	0.05m a.s.f* lander ratio value	Average surface ratio value
October '96	Tonne	420	589	589	19	25	32	89
	Nord-Perd	426	835	232	32	34	23	179
	Wiek	421	482	452	32	34	29	231
	Arkona	346	337	352	26	34	29	319
March '97	*Tonne*	*400*	*465*	*521*	*72*	*78*	*66*	89
	Nord-Perd	*398*	*330*	*379*	*27*	*28*	*29*	179
	Wiek	*394*	*185*	*264*	*32*	*35*	*35*	231
	Arkona	*238*	*168*	*260*	*27*	*28*	*26*	319
June '97	Tonne	398	387	515	34	31	28	89
	Nord-Perd	331	345	335	31	31	28	179
	Wiek	374	347	389	31	27	25	231
	Arkona	279	457	259	25	25	25	319
December '97	*Tonne*	*440*	*391*	*427*	*35*	*39*	*37*	89
	Nord-Perd	*448*	*400*	*400*	*35*	*30*	*26*	179
	Wiek	*395*	*401*	*425*	*29*	*32*	*26*	231
	Arkona	*426*	*570*	*461*	*27*	*20*	*20*	319

Figure 8-44 Iron / Rubidium ratios for the water column particulate and dissolved phases over the period of survey, *a.s.f = above sea floor

		June '97 Particulate Phase				Dec '97 Particulate Phase			
		Tonne ratio	Nord-Perd ratio	Wiek ratio	Arkona ratio	Tonne ratio	Nord-Perd ratio	Wiek ratio	Arkona ratio
Lead	Av. Water column	4	5.5	4.2	8.1	3.6	2.8	5	5.7
	0.4m lander a.s.f.*	2.7	1.8	1.9	1.2	2.6	1.0	2.4	1.5
	0.05m lander a.s.f.*	2.4	0.7	1.9	1.3	2.2	1.6	2.3	1.2
	Av. sed. core surface	0.3	0.4	0.6	1.0	0.3	0.4	0.6	1.0
Copper	*Av. Water column*	*7.2*	*7.5*	*6.1*	*8.1*	*2.7*	*2.7*	*8.4*	*11.1*
	*0.4m lander a.s.f.**	*4.6*	*3.8*	*2.5*	*1.9*	*2.8*	*0.73*	*4.5*	*2.1*
	*0.05m lander a.s.f.**	*4.1*	*0.3*	*2.8*	*1.4*	*2.5*	*1.19*	*4.2*	*0.6*
	Av. sed. core surface	*0.5*	*0.3*	*0.3*	*0.4*	*0.5*	*0.3*	*0.3*	*0.4*
Tin	Av. Water column	0.59	0.31	0.35	0.68	0.08	0.25	0.30	0.71
	0.4m lander a.s.f.*	0.65	0.21	0.13	0.03	0.39	0.14	0.38	0.20
	0.05m lander a.s.f.*	0.21	0.03	0.06	0.05	0.27	0.14	0.33	0.04
	Av. sed. core surface	0.02	0.03	0.03	0.05	0.02	0.03	0.03	0.05
Stromtium	*Av. Water column*	*24*	*19*	*14*	*16*	*6.4*	*7.1*	*18*	*54*
	*0.4m lander a.s.f.**	*31*	*28*	*26*	*12*	*24*	*4.0*	*30*	*34*
	*0.05m lander a.s.f.**	*30*	*1.5*	*2*	*11*	*14*	*6.0*	*26*	*3*
	Av. sed. core surface	*1.5*	*1.5*	*1.5*	*1.3*	*1.5*	*1.5*	*1.5*	*1.3*

Figure 8-45 Selected metal to rubidium ratios for the June and December water column particulate phase, *a.s.f. = above sea floor

8.8 INORGANIC GEOCHEMISTRY OF THE MOBILE NEPHELOID LAYER

Mobile nepheloid layer samples were collected throughout the whole of the BASYS project which ran from October 1996 through to June 1998 by Dr T. Leipe of IOW, Warnemunde. Within this time period the Oder Flood in late July / early August occurred and nepheloid samples were collected on a relevant time scale on both sides of the event so as to provide an insight into this major perturbation of the environmental system. The following section attempts to address the inorganic geochemical changes on both a spatial and temporal time scale over this period. In particular, the same elements (Fe, Mn, Pb, Cu, Zn, Sn, Sr and Rb) as those studied in the sediment core will be used so as to provide a comparison.

8.8.1 Mobile Nepheloid Layer Metal Concentrations

Due to the difficulty in obtaining these samples and ensuring the quality of a wholly nepheloid sample rather than a mixture of sediment surface and nepheloid layer, especially at the deep water stations, then the amount of samples collected (especially at Arkona) was substantially lower than at other stations. The following figures show the concentrations for each station over the period of study followed by a selective metal comparison. Each station is arranged with the elements in groupings of similar concentration values.

Care has to be taken in deciphering any trends from the following data as the mobile nepheloid layer is by definition mobile and hence likely to be very variable in composition. This can be seen where repeated sampling of stations has occurred with widely varying repeat concentrations at Tonne and Wiek for example. However, the main features of Figures 8-46 to 8-49 are that no consistent seasonality can be found in the mobile nepheloid layer with the possible exception of some metal specific seasonality at Nord Perd and Wiek. However, the question as to whether these variations can be interpreted as real or merely coincidental is arguable.

Figure 8-46 shows the mobile nepheloid data for Tonne and while no seasonal trends are apparent it can be seen that in the main the elemental profiles vary considerably. However the group of elements containing Pb, Cu, Sn, Co and As have, in contrast, a relatively constant concentration.

Both Nord-Perd and Wiek (Figures 8-47 and 8-48) are the only stations in which samples were received and which captured a pre and post flood phase. The effect on the October 1997, post flood, mobile nepheloid layer concentrations are striking with a consistent drop in all element concentrations which is deliberated on in the discussion. In addition the data for Nord-Perd and Wiek tend to show more variability in concentration with the elements that were constant at Tonne taking a more month specific value which may suggest a move to seasonality in these mid range basinal environments.

Possible seasonal cyclicity can be seen for caesium at Nord-Perd and Cs plus U and Fe at Wiek as shown in Figure 8-50. In interpreting this possible cyclicity it must be remembered that there is no data for March '98 and that the values for repeated stations are averages. Thus the reliability of this interpretation is open to question and the conclusion that December and October have in general lower concentrations than, especially March and possibly June is very tentative at this stage.

Little information can be derived from the Arkona station due to only three samples being collected but the metal concentrations are of the same order of magnitude as for all the other stations.

However, in general, the mobile nepheloid layer seems to be a variable in composition. Possible seasonal cycles are postulated for the mid water depth basins and the period post Oder flood shows the only definite feature of the whole collection period with a consistent drop in elemental concentrations.

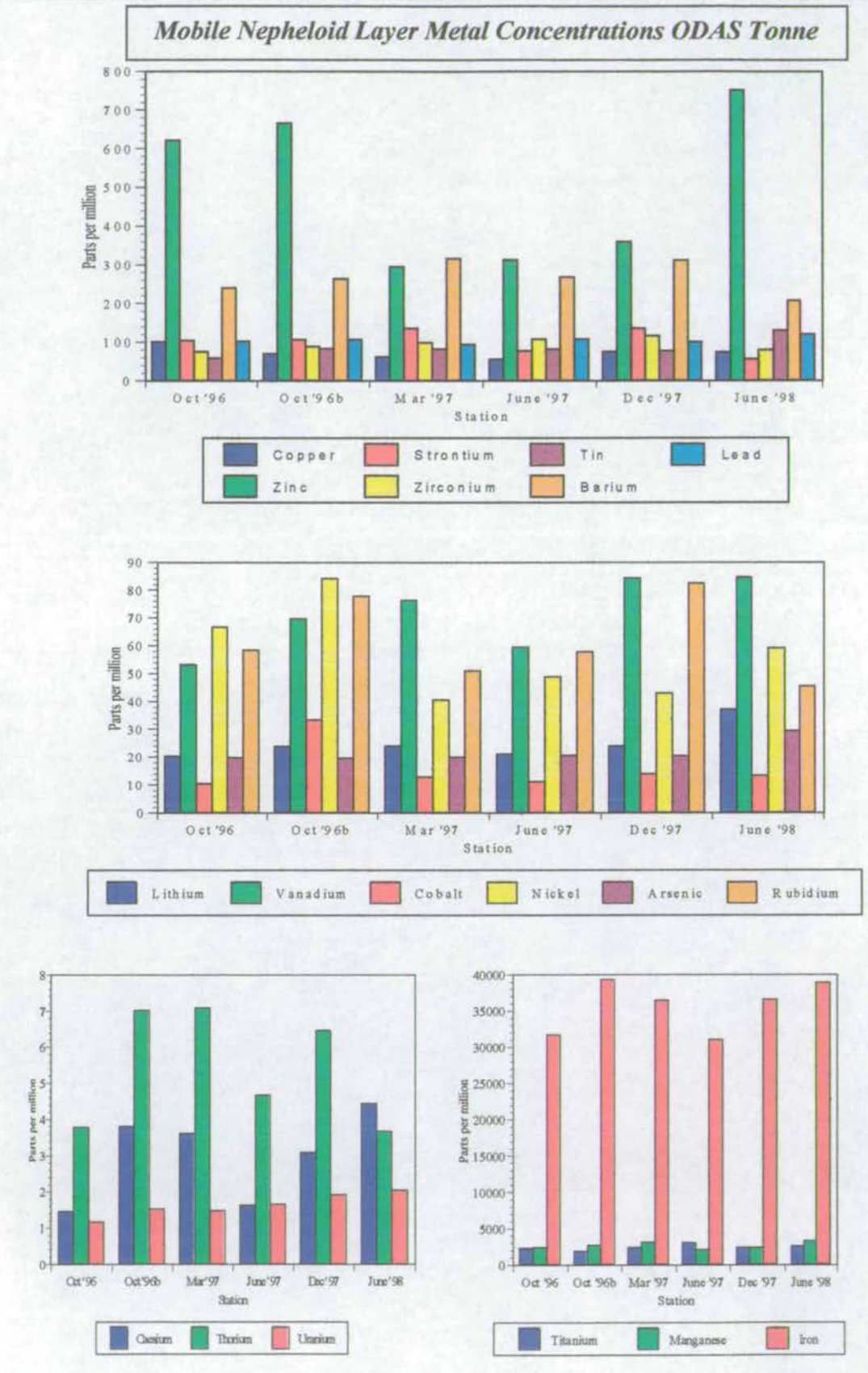

Figure 8-46 Seasonal mobile nepheloid layer metal concentrations at Tonne.

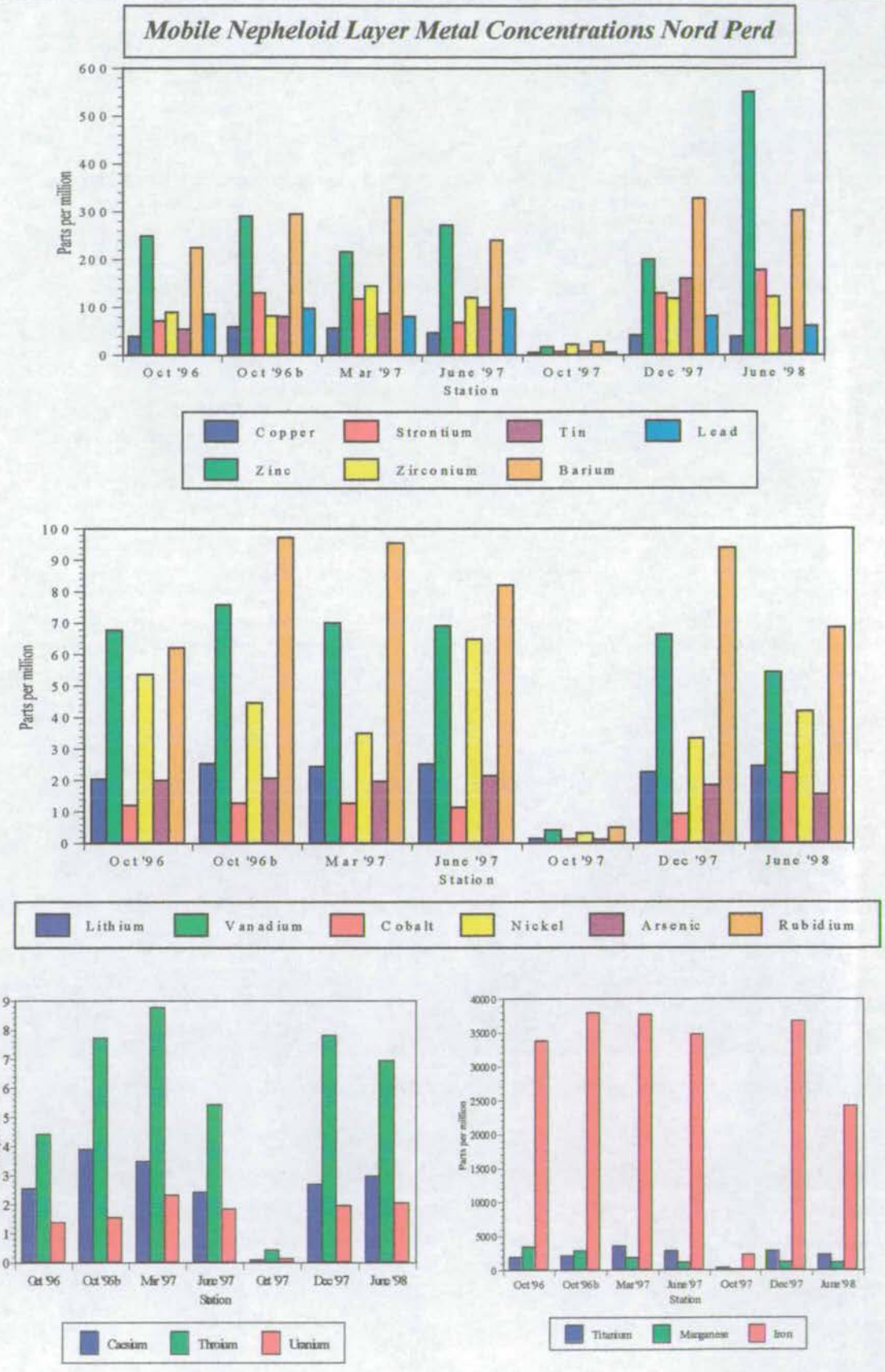

Figure 8-47 Seasonal mobile nepheloid layer metal concentrations at Nord Perd

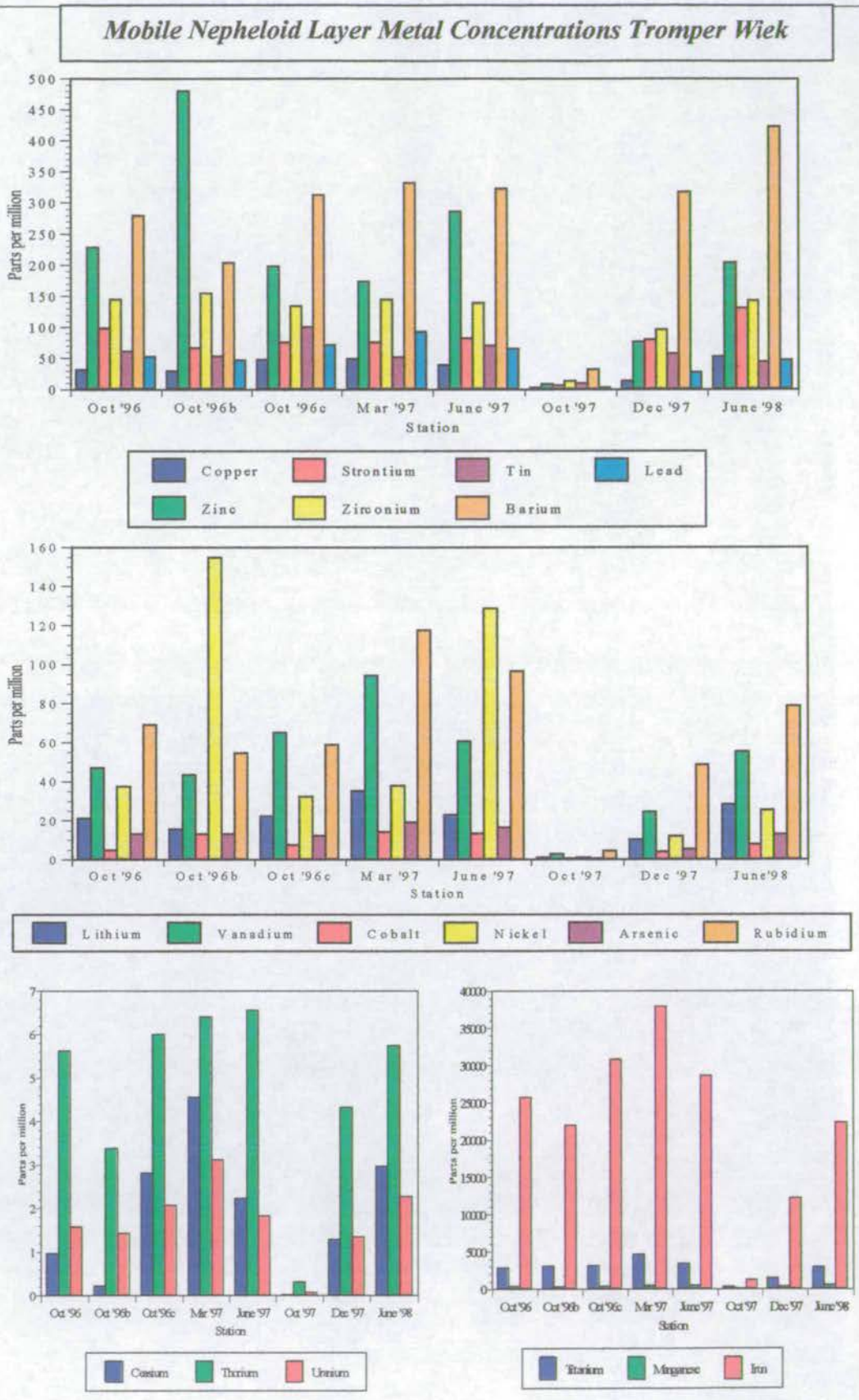

Figure 8-48 Seasonal mobile nepheloid layer metal concentrations at Wiek

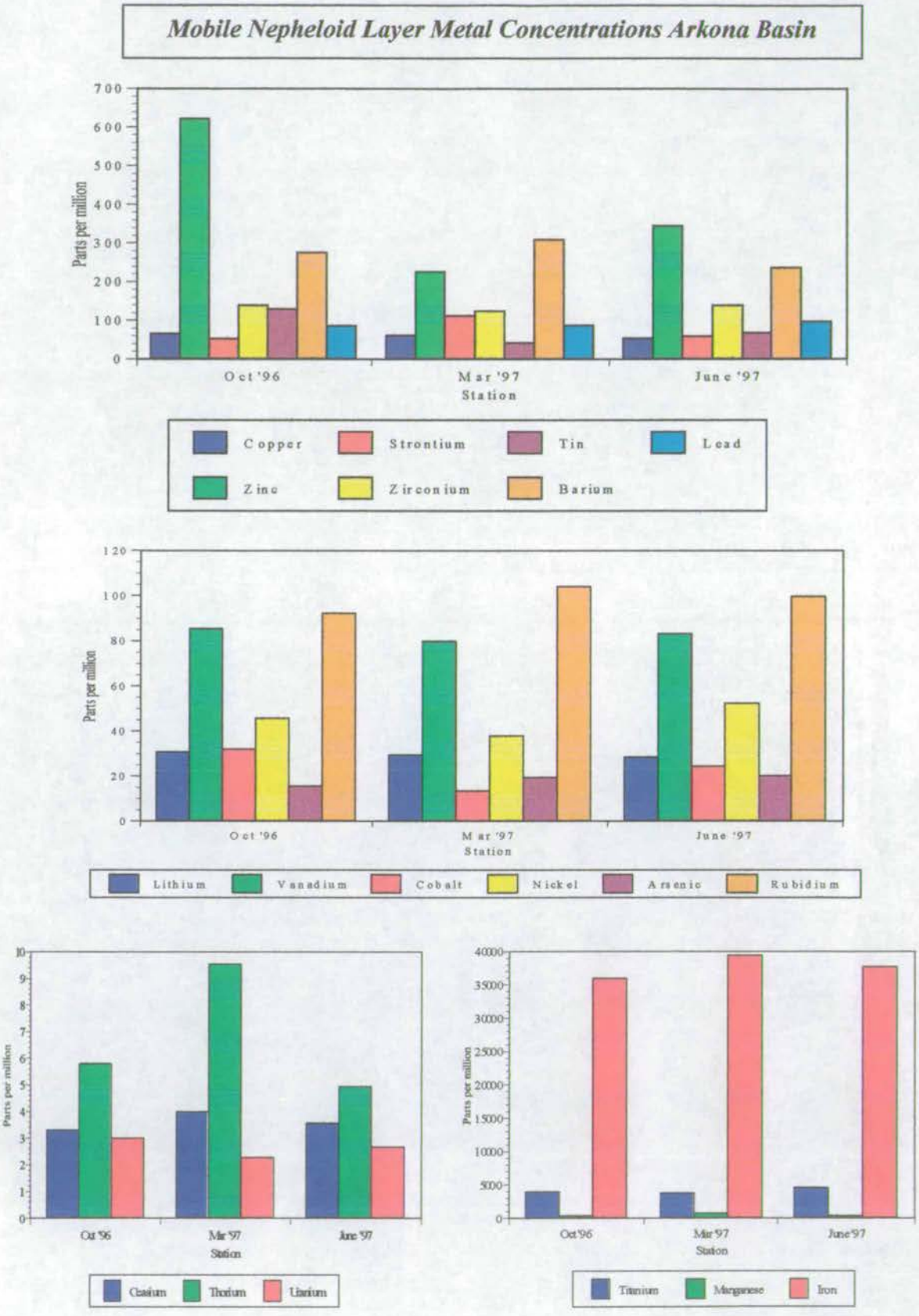

Figure 8-49 Seasonal mobile nepheloid layer metal concentrations at Arkona

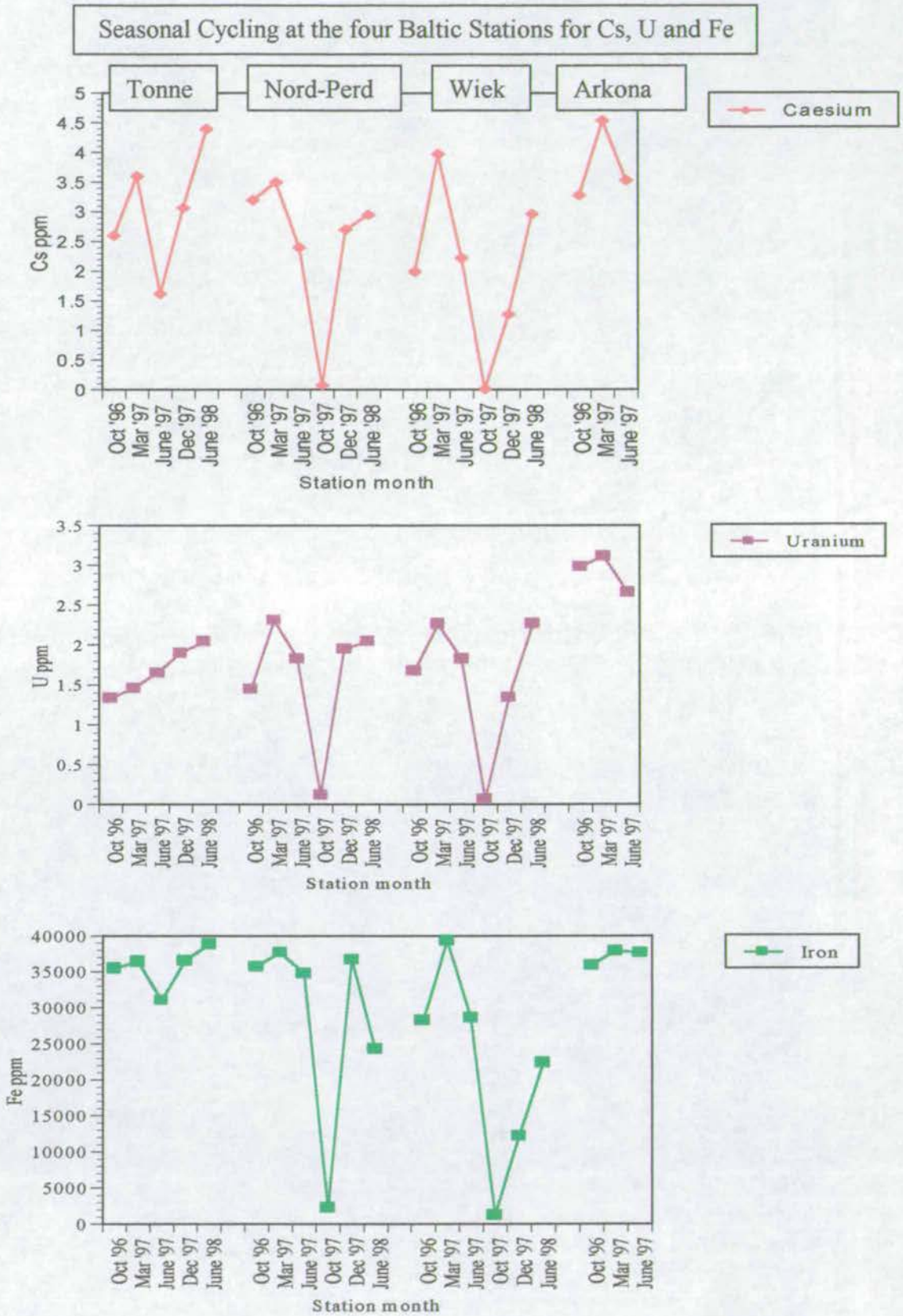

Figure 8-50 Seasonal cycling in the Mobile Nepheloid Layer for Cs, U and Fe.

8.8.2 Comparison of the Mobile Nepheloid Layer with the Sediment Core

A close association between the nepheloid layer and the sediment core would be expected if the hypothesis was consistent that the major contributor to the sediment core was the material donated from the mobile nepheloid layer suspended just above the sediment water interface. While variations in concentrations have been shown in the mobile nepheloid layer it would be expected that if the above hypothesis holds true then an average contribution over the whole year would be the contributing signature to the sediment core. As the core was collected on the first cruise in October then in this investigation only the nepheloid layer samples from the same cruise will be used for comparative matters.

Figure 8-51 shows plots of the normalised elements versus element concentrations and this in addition to Table 8-12 helps to elucidate some of the processes occurring at the crucial sediment/water interface. The most noticeable feature is that all the nepheloid layer samples plot consistently close to the Arkona sediment surface rather than Tonne, Nord Perd or Wiek. A general transition from low concentrations and low ratios at Tonne with increasing concentrations and ratios to Arkona is clearly shown. This implies that the nepheloid layer already has the signature of the Arkona basin at the shallower stations and that the nepheloid layer is modified from even higher concentrations and ratios at Tonne with a gradually decreasing ratio and concentration to Arkona as shown in Table 8-12.

Table 8-12 Ratio comparisons between surface sediment core and mobile nepheloid layer

	Surface Sediment Core ratio (M/Rb)				Average Oct '96 MNL ratio (M/Rb)			
M	Tonne	N. Perd	Wiek	Arkona	Tonne	N. Perd	Wiek	Arkona
Fe	89	179	231	319	523	469	320	390
Pb	0.32	0.42	0.59	0.79	1.55	1.19	0.99	0.92
Cu	0.46	0.36	0.36	0.44	1.3	0.61	0.63	0.69

M = Metal, MNL = Mobile Nepheloid Layer

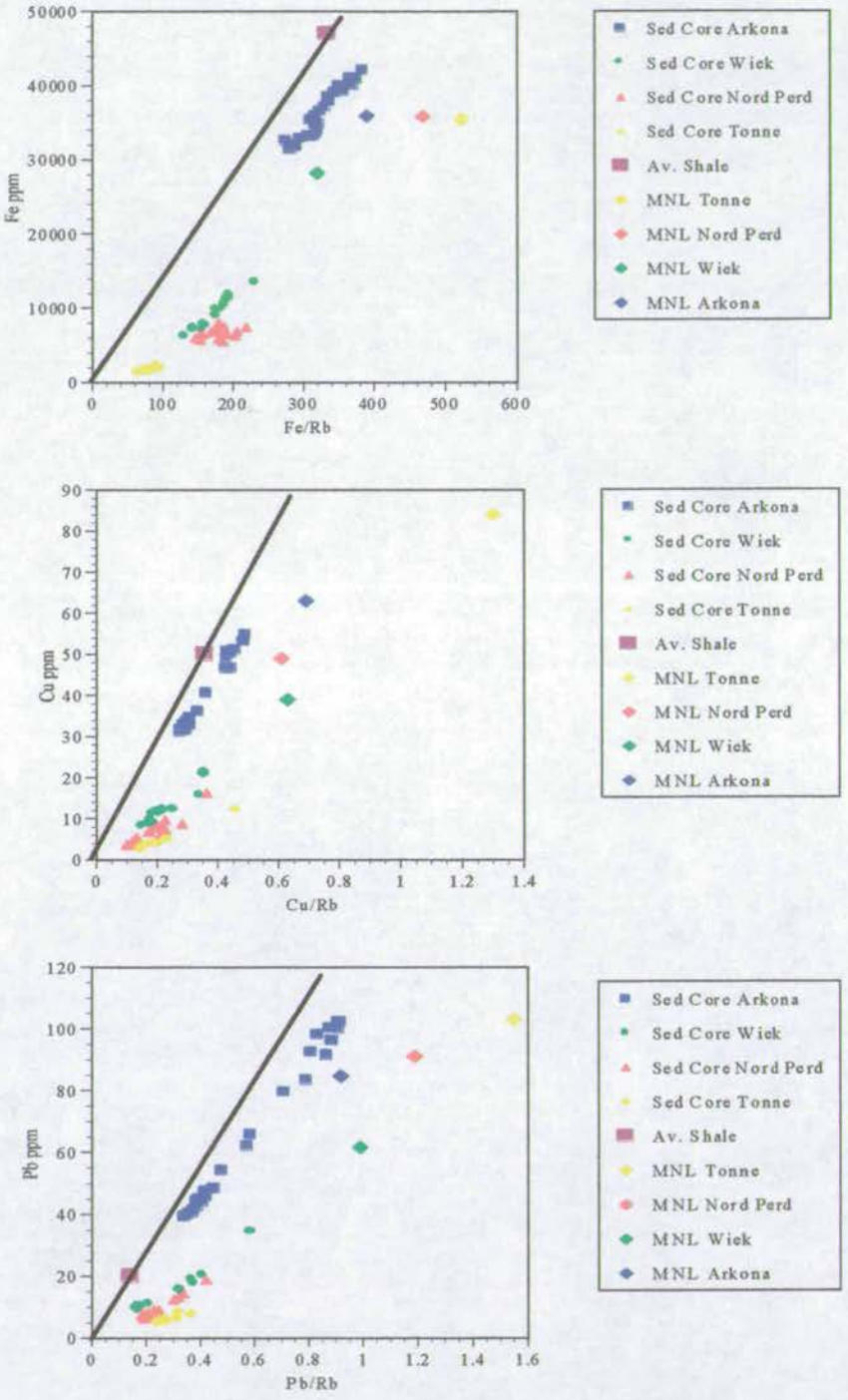

Figure 8-51 Element versus normalised element ratios for Fe, Cu and Pb for the sediment core and mobile nepheloid layer samples. The black line denotes average shale ratio values.

8.9 INORGANIC GEOCHEMISTRY OF THE SEDIMENT TRAP

Lars Christian Lund-Hansen and Mario Laima of Århus University, Denmark, collected sediment trap samples at the shallow water station of ODAS Tonne and both the trap description and fluxes are described in LAIMA *et al.*, (*In press).* A summary of these findings is shown in Table 8-13. Material collected in the sediment traps gives a gross sedimentation rate which is composed of a net sedimentation flux and a resuspended flux. The effect of resuspension can clearly be seen from the data below in which the lower traps at 0.35m above the sea floor have a clear excess of material over the average at greater heights above the sea floor. The time period covered by the deployments also covered the Oder flood event but comparatively low fluxes were found during the period between 11th June and 19th August which may infer that the large amounts of flood related suspended material moved as a surficial layer rather than throughout the water column.

Table 8-13 Vertical sediment fluxes (g m^2 day^{-1}) at various sediment trap heights during three deployment periods at ODAS Tonne in 1997.

Height (m)	11/6-19/8	21/8-14/10	14/10-6/12
1.75	19.6	47.0	46.1
1.40	24.2	52.7	49.5
1.05	30.5	56.7	57.1
0.7	43.3	69.3	65.3
0.35	82.9	114.3	86.6

These sediment trap samples were analysed for their inorganic geochemistry and the results of which are presented here. However, it must be remembered that from the evidence thus far ODAS Tonne is a relatively high energy, shallow water station and that the statistical analysis on these samples showed a relatively low degree of correlation and would probably not rank as a primary site for this type of investigation but unfortunately it is the only trap data that is available.

In addition to the collection of the sediment trap samples Christian Christiansen of the University of Copenhagen also carried out resuspension experiments on sediment cores collected from the stations in which he found that a typical resuspension velocity for this area was 5cm s^{-1} (pers. Comm.). Data from the sediment trap lander showed that the average current speed at 1m above the seabed at ODAS Tonne was 5.2cm s^{-1} during the June-August deployment, 4.7cm s^{-1} during the August-October deployment and 5.4cm s^{-1} during October to December (LAIMA *et al., In Press*). Furthermore, maximum current speeds were 16cm s^{-1} during June to August and 19cm s^{-1} during the following two periods. While at first inspection these values seem to exceed the resuspension threshold it must be remembered that close to the sediment surface there is a drag factor to be accounted for and invariably this leads to lower current velocities. Lund-Hansen (Pers. Comm.) concluded that based solely upon current velocities that the resuspension velocity is seldom reached over the period of investigation. However, there are also two other very important factors influencing resuspension and these are wave induced resuspension (LUND-HANSEN *et al.*, 1997) and the effects of trawling (FLODERUS and PIHL, 1990). Hence it seems likely that in this high energy environment, especially in terms of wave dynamics, that resuspension could be an important process at ODAS Tonne.

Figures 8-52 to 8-57 show details of selected element concentrations and element to rubidium ratios for the sediment trap samples at 0.35, 0.7, 1.05, 1.4 and 1.75 m above the sea floor and in a water column totalling 15m in depth. From the data set there seems to be quite a large variability in the concentrations for certain elements which are not consistent with regards to height above the sea floor, although two geochemical groupings may be identified. The first group contains those elements that increase in height above the sea floor in both concentration and ratios. This group includes Fe, Pb and Cu that are shown in Figures 8-52 to 8-54 and include V, As, Zr, Mo, Sn, Sb, Th and U. Conversely, the second group has higher concentrations and ratios nearest the sea bed and these are shown in Figures 8-55 to 8-57 and include Li, Ti, Mn, Co, Ni, Zn, Rb, Sr, Y, Cs, Ba and Ce. These two broad groups in reality probably generate a continuum from both end members with a middle ground of constancy which is best reflected by Pb, Ba, U and Cs.

The question as to whether these variations are real or just an artefact of the transitory nature of this compartment of the marine environment is disputable.

In order that an approximate comparison can be made between the data measured in the sediment traps with that obtained for the water particulate and fluff layer. Data for December '97 is compared with the sediment trap data for October 14th to December 6th as shown in Table 8-14 below:

Table 8-14 Comparison of sediment trap and water particulate concentrations and ratios (Me/Rb).

Metal	Average Water Part. Conc.	Average Sed. Trap Conc.	Average water. Part Ratio	Average Sed. Trap Ratio
Fe	79127	41382	435	581
Pb	375	86	2.69	1.21
Cu	326	213	2.53	2.98
Zn	1433	421	10.7	5.8
Mn	8846	1318	60.6	18
Ba	1016	294	6.84	4.12

As can be seen from the above table there is quite a difference between the sediment trap data obtained and that of the water particulate phase collected on the December 1997 cruise. In general the concentrations in the particulate phase are much higher than that of the sediment trap and the ratios are generally higher. This could arise from a number of factors amongst the most obvious is that the sediment trap material is collected over a period of time and hence will be a product of the average concentrations over this time, whereas the particulate phase is date and time specific. Material collected in the sediment trap will also be subjected to various diagenetic processes which may serve to alter the concentration of the matter over a period of time. In addition it must be remembered that the comparison is made after a period of major perturbation and one in which the nepheloid layer samples showed very low concentrations in the October samples. However the ratio values between the particulate phase and sediment trap are not too dissimilar for the majority of elements.

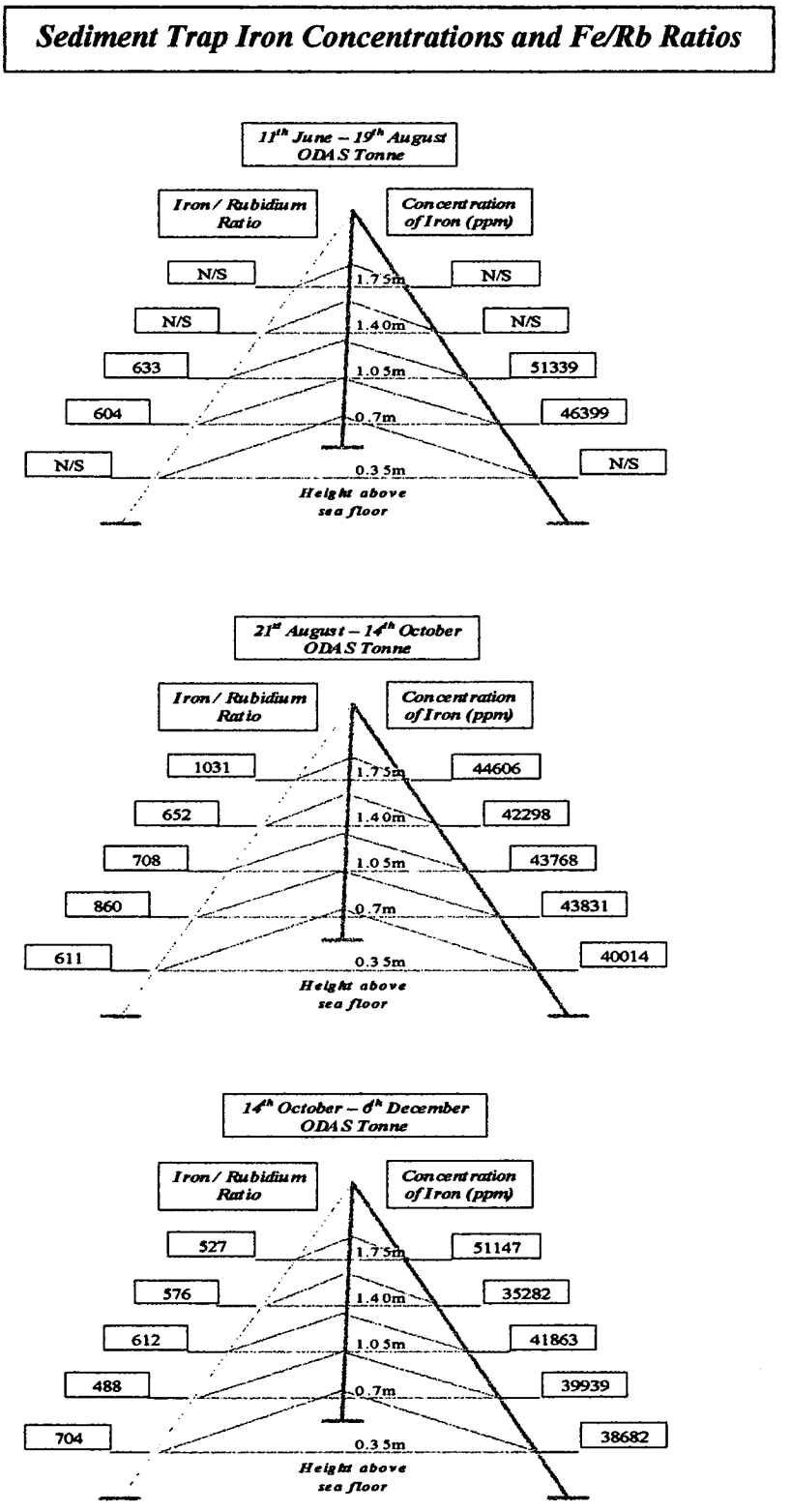

Figure 8-52 Iron concentrations and Fe/Rb ratios in the sediment trap samples (N/S = no sample).

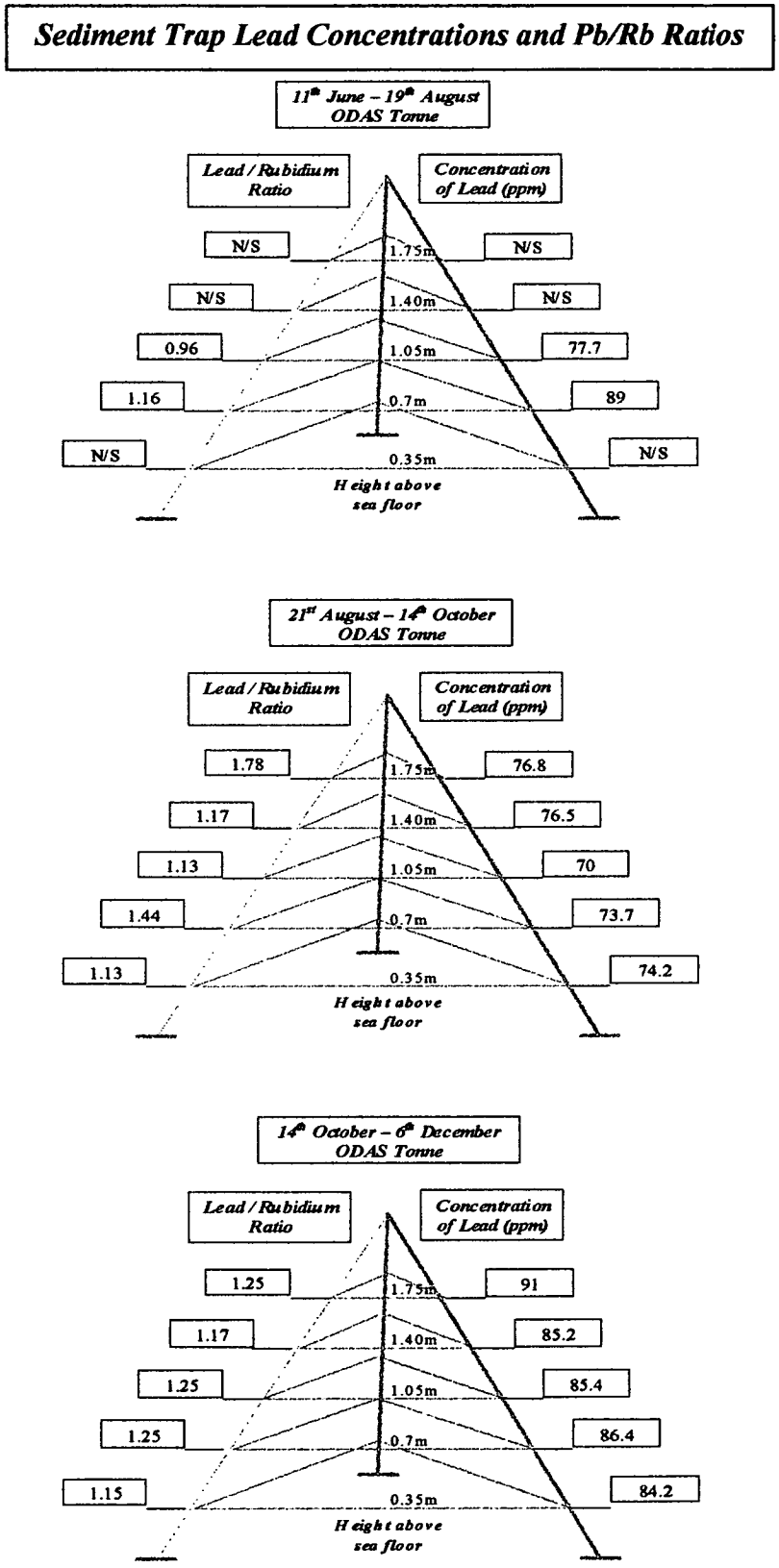

Figure 8-53 Lead concentrations and Pb/Rb ratios in the sediment trap samples (N/S = no sample).

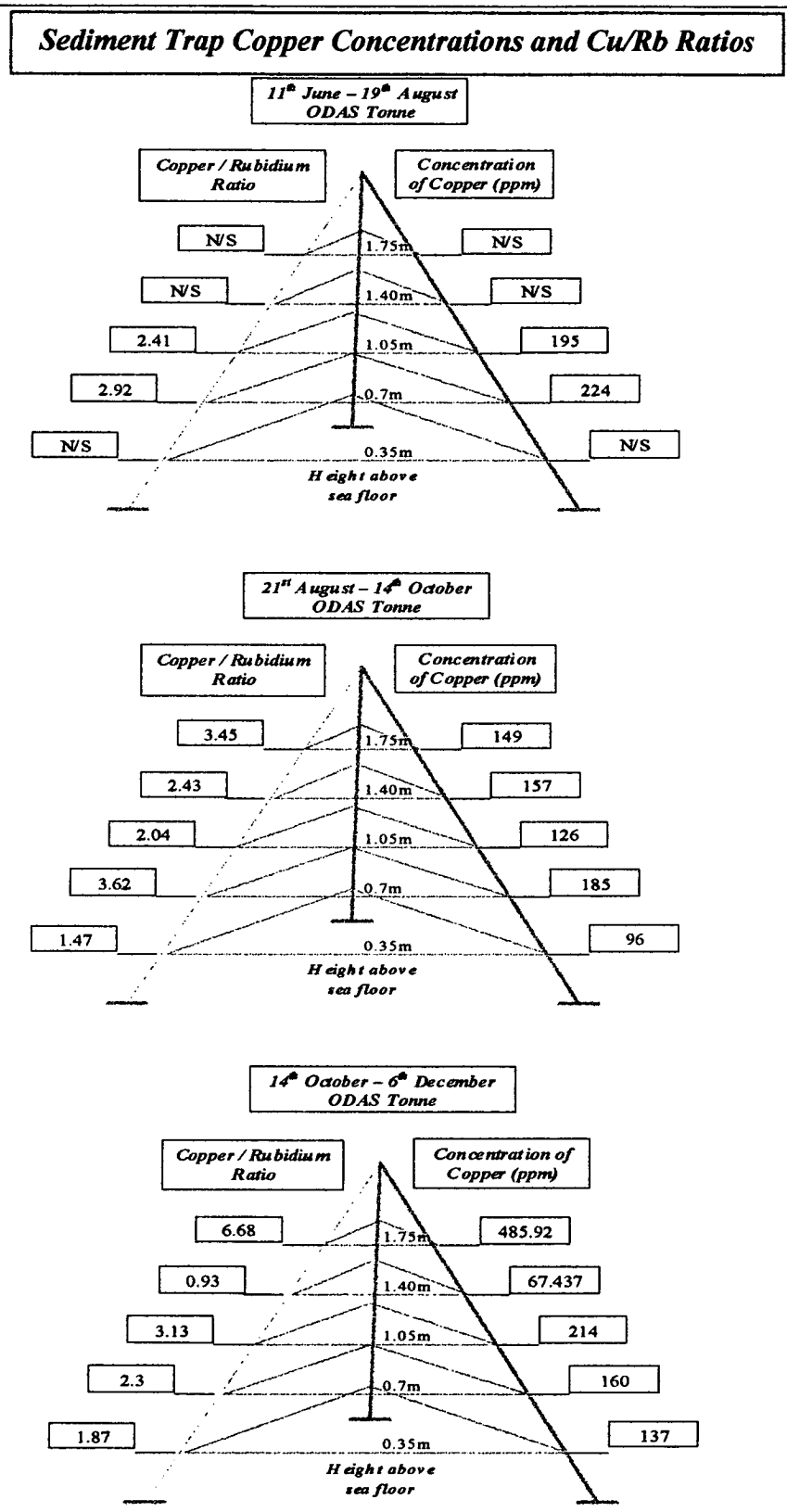

Figure 8-54 Copper concentrations and Cu/Rb ratios in the sediment trap samples (N/S = no sample).

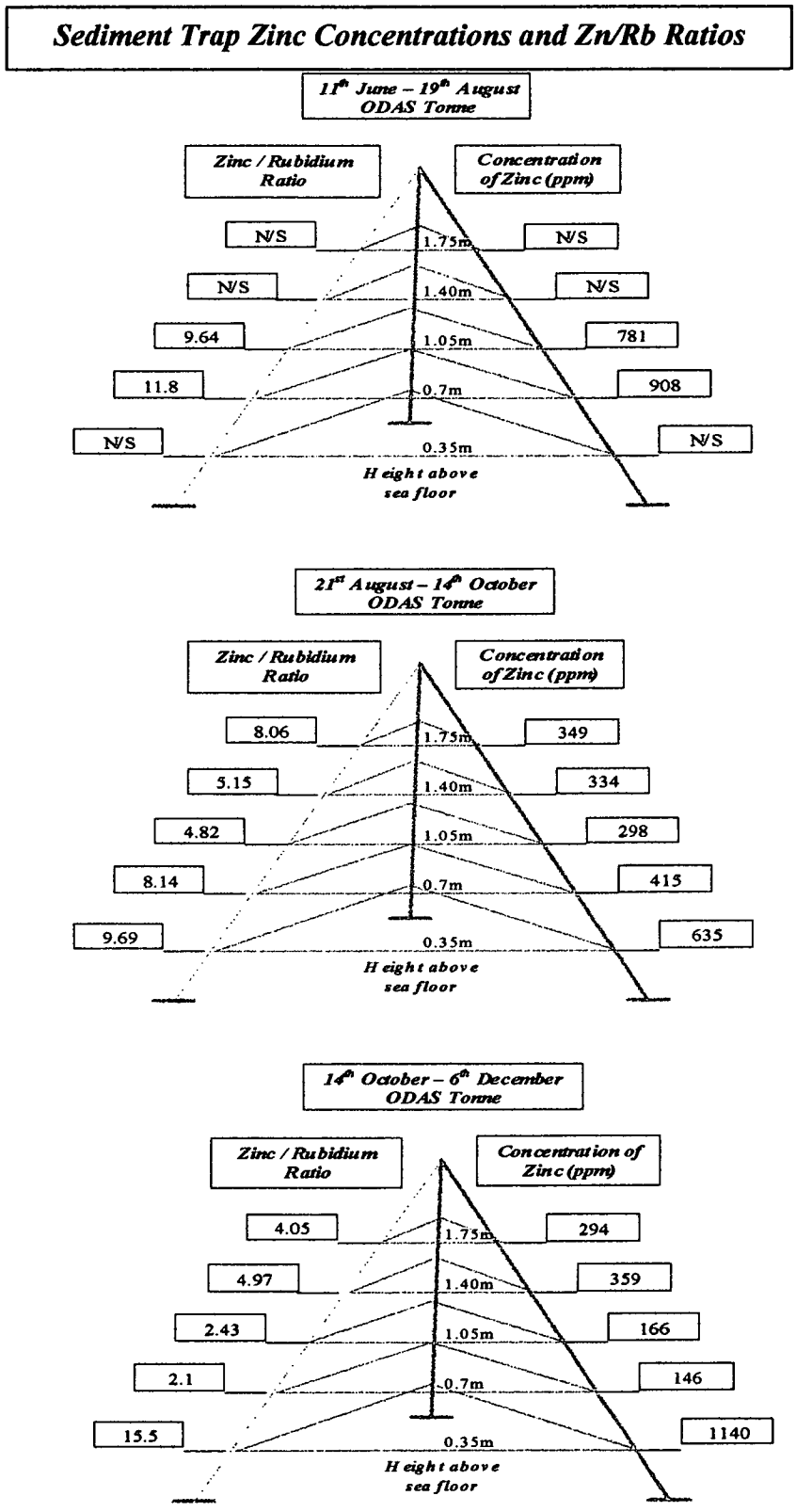

Figure 8-55 Zinc concentrations and Zn/Rb ratios in the sediment trap samples (N/S = no sample).

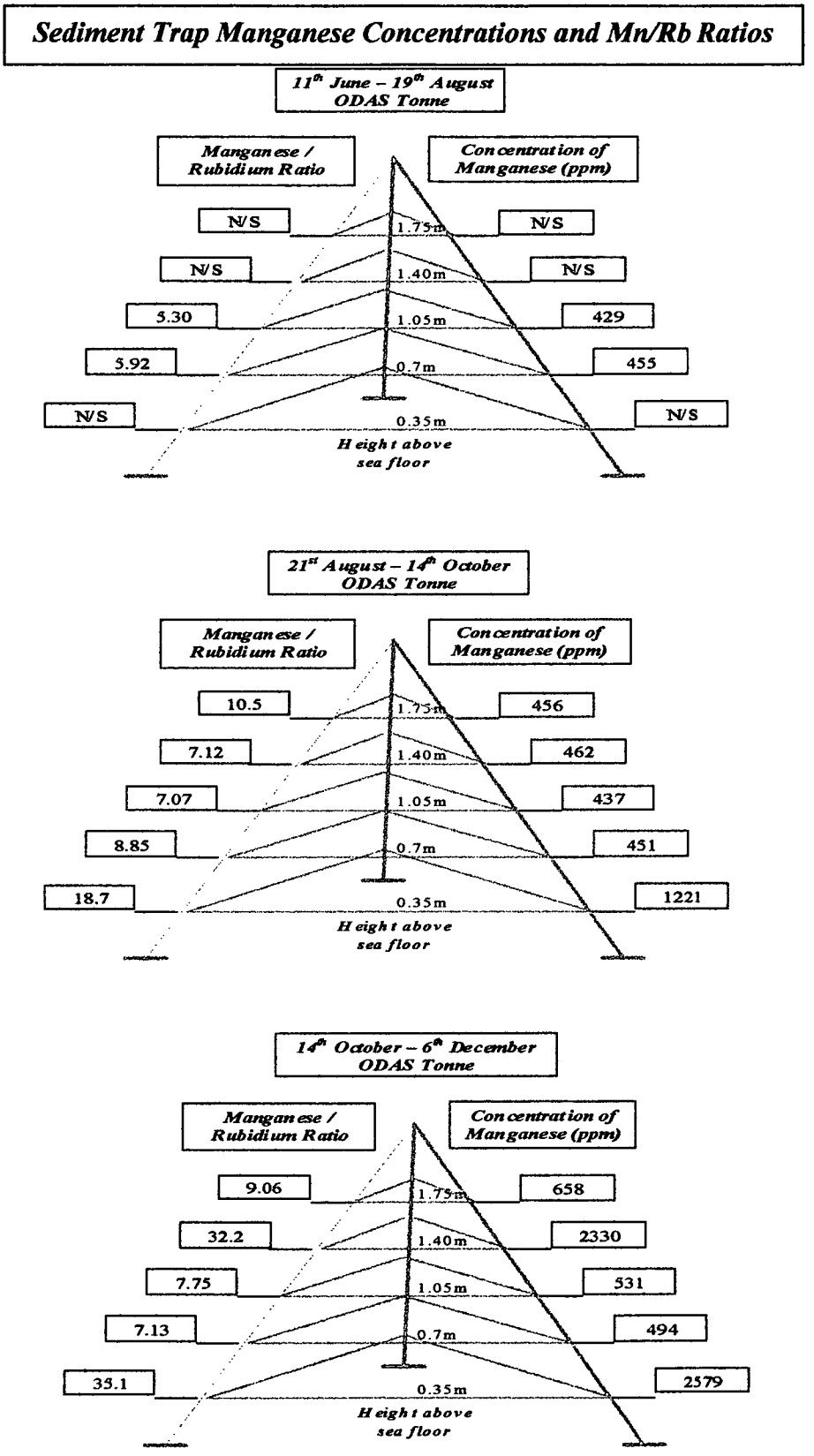

Figure 8-56 Manganese concentrations and Mn/Rb ratios in the sediment trap samples (N/S = no sample).

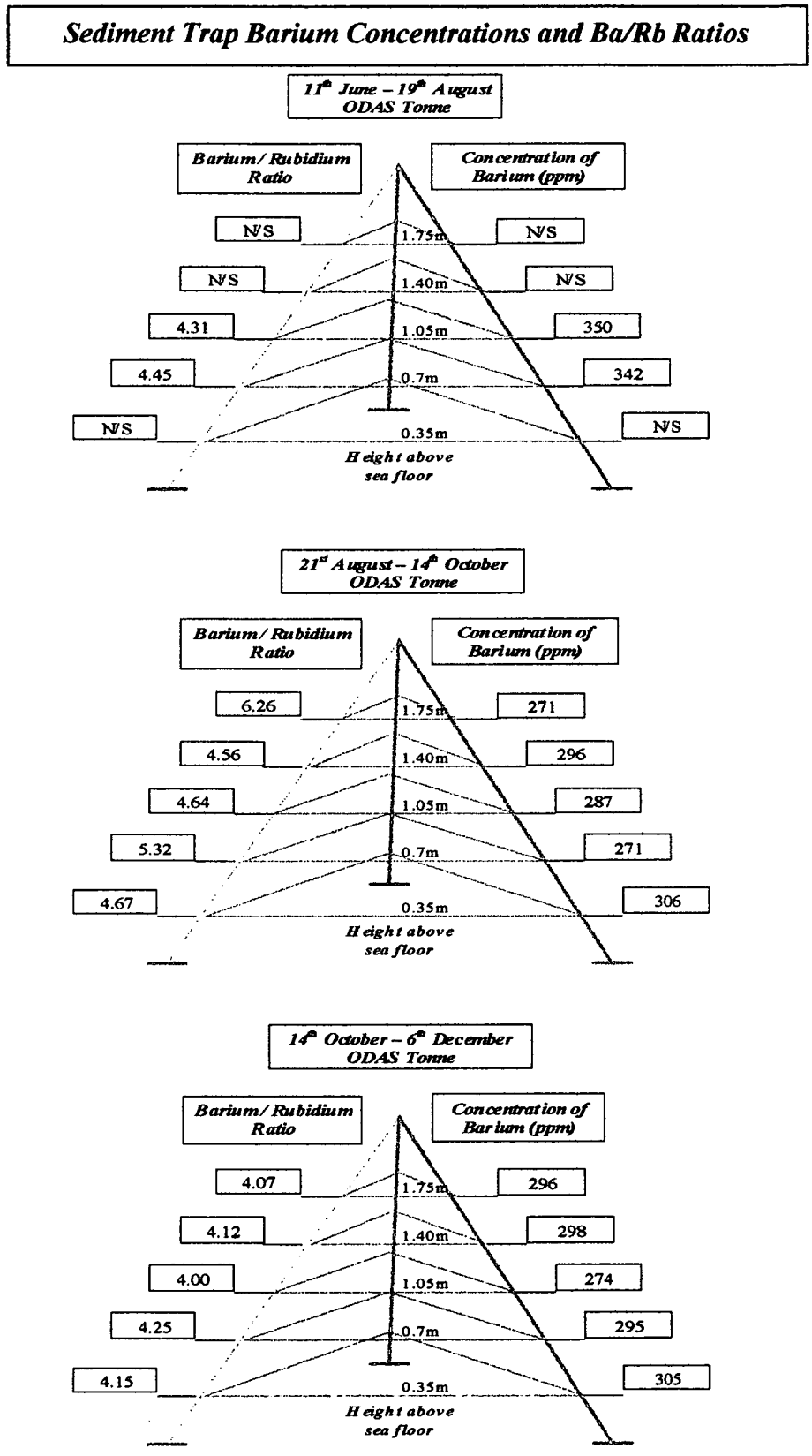

Figure 8-57 Barium concentrations and Ba/Rb ratios in the sediment trap samples (N/S = no sample).

8.10 WATER COLUMN SUMMARY

The water column provides an interesting and varied array of environments in which a whole range of interactive processes occur. While an attempt has been made to elucidate some of these processes this has only been possible on a broad and general scale with detailed element specific interactions not being possible in this study. The following bulleted points summarise the pertinent findings from this section on the geochemistry of the water column and are described for each compartment of the water column system.

8.10.1 Hydrography

- CTD measurements indicate the presence of the expected seasonal variations in temperature and indicate some stratification of the water column with a pycnocline evident, situated close to the sediment water interface, which is most pronounced at Arkona.
- Salinity profiles show a gradational profile with the shallow water station of Tonne being proximal to the River Oder outlet having the lowest salinity and Arkona having the highest salinity.
- In addition to this oxygen measurements show the presence of sub-oxic conditions at depth at the deeper stations which were especially evident in October, June and December.

8.10.2 Particulate Phase

- The particulate phase iron shows a relatively constant down column profile with exponential type increases close to the sediment-water boundary possibly related to an increase in the colloidal fraction.
- The presence of resuspended material can be inferred by the abrupt increases in particulate concentrations that can be found upto 15m above the sea floor at Arkona.

- The particulate phase concentration shows some evidence of the pulsating nature of the discharge of the River Oder into the Southern Baltic Sea especially for the months of March and December.
- The particulate phase profiles for Rb, Pb, Cu, Sn and Zn are remarkably consistent with those of iron.
- The particulate manganese profile acting as a tracer of redox processes, while being generally similar to iron, shows depletion of manganese close to the sediment-water boundary which may relate to reducing conditions at depth in the Arkona Basin.
- Normalised metal particulate ratios show a tentative decrease in ratio values from Tonne to Arkona which could be as a result of the modification of material with an increase in their residence time in the Southern Baltic Sea.
- The data for Pb, Cu and Sn in the particulate phase show a decreasing metal to rubidium ratio with a decreasing distance to the sediment-water interface in which the value approaches near unity with the sediment core ratio.

8.10.3 Dissolved Phase

- As opposed to the particulate profile, iron in the dissolved phase shows a relatively constant profile with possibly some depletion close to the sediment water interface.
- No seasonality could be found with respect to iron in the dissolved phase, which remained relatively constant over the whole period of investigation.
- No dissolved manganese is found in the majority of the water column although the lander profiles do indicate the presence of some manganese at depth. This may be as a result of reducing conditions or as a result of an increase in sub 45um colloidal particles contributing to the manganese concentrations.
- All the elements studied in the dissolved phase generally showed near constant down column concentrations.

8.10.4 Miscellaneous

- In common to both the dissolved and particulate phases, the average lander to average water column, iron to rubidium ratios continually increase from Tonne to Arkona which may relate to increasing scavenging of Iron with respect to Rubidium from the system.
- A predominately lateral transport motion is proposed for iron on the basis of metal to rubidium ratios with a greater vertical component proposed for Pb, Cu and Sn.
- The mobile nepheloid layer proved to be highly variable in nature and no consistent seasonal trends could be determined indicative of a well mixed and resuspended system.
- The first cruise after the August flood event in October showed consistent depleted metal concentrations for all the elements analysed which may be as a result of a lower particulate load due to the previous months particulate explosion.
- A close correlation can be seen between the mobile nepheloid layer at all stations and that of the Arkona Basin inferring that the nepheloid layer is the primary contributor to the Arkona sediment core. A transition from high ratios at the shallow water station decreasing in values to approach unity with the sediment core at Arkona.
- The sediment trap samples show very weak correlations probably as a result of the mix of particulate matter that has accumulated temporally with some degradation as a possible modifying process.
- Sediment trap fluxes are generally in the order of 50 g m^2 day^{-1} and are relatively consistent for the two deployments after the Oder flood event.

9.0 Discussion

Thus far, each major component of the marine system has been viewed on a stand-alone basis with little integration between the various components. While most of the significant findings have been discussed in relevant sections throughout this thesis it still requires one further chapter to inter-link and to put into context on a regional and an environmental scale the main geochemical processes operating throughout this region both spatially and temporally.

9.1 SPATIAL VARIABILITY IN THE SOUTHERN BALTIC SEA

9.1.1 The Southern Baltic Sea Marine Environment

Sediment core and water column sampling were conducted at four stations along a progressively deepening transect in the southern Baltic Sea with the shallowest station being proximal to the main outflow of the river Oder. Therefore with an increase in water depth, hydrographic profiles may be expected to show a decreasing influence of the river Oder. In the following sections each station will be examined as an entity followed by a summary of the environmental system on a spatial scale. As the sediment core was only collected during the October 1996 cruise and in order to compare the data on a spatial basis, only the October data set will be used to provide a consistent data set.

9.1.2 ODAS Tonne

ODAS Tonne is the shallowest of all stations at approximately 15m water depth and is the closest to the Oderhaff lagoon and Swine outflow of the river Oder (Figure 1-3). These sediments are primarily composed of a sandy grain sized material with a predominance of quartz throughout the core and a low total and organic carbon content (Chapter 4). Redox reactions are not observed; both the manganese and iron profiles display little change with depth and are therefore assumed to exist in their oxidative state.

9.1.3 Nord-Perd Rinne

Nord-Perd is found at an intermediate depth of approximately 20m and is characterised by a predominantly sandy matrix with the additional initial occurrence of a significant silt fraction. The mineralogy is again dominated by quartz but with the additional occurrence of hematite and some feldspars (Figure 4-9). Organic carbon contents are again around 1% dry weight but also with high inorganic carbon contents relating to the presence of two shell bands. Iron and manganese profiles show no characteristic diagenetic profiles remaining constant down core.

9.1.4 Tromper Wiek

At 25m depth, Wiek is the deepest of the coastal near shore environments before the depositional basin of Arkona (Figure 1-2). The occurrence of mud as well as a significant proportion of silt is typical of a more distal environment and, as with all the cores, grain size remains relatively constant with depth. With the decrease in grain size comes a more varied mineralogy which includes hematite, mica and feldspars along with a decreasing preponderance of quartz. The first indications of diagenetic change and the presence of sub oxic conditions within the sediment core can be seen in the manganese profile for Wiek.

9.1.5 Arkona Basin

Arkona is the most distal of the sites studied, and at 45m depth, the deepest. This basinal environment has the greatest contribution from the finer grain sizes, particularly silt, and has a varied mineralogy comprising of quartz, associated feldspars, mica and importantly pyrite. Additionally, it is the only station to have a significant organic carbon component of around 5%. The manganese profile best illustrates the redox processes at work in this environment. Clear indications of Mn^{4+} reduction and release of Mn^{2+} are seen indicating a sub oxic environment in the upper 2cm of the core. Furthermore, the presence of pyrite in the deeper regions of the core along with a strong H_2S smell on extraction point to a sulphidic, and hence anoxic, environment at depth.

9.2 SPATIAL VARIABILITY IN METAL DISTRIBUTIONS

The following station-specific metal distributions in Figure 9-1 are based upon the normalised ratios of metals to rubidium, which allow cross-compartment comparisons and inferences to be made. The two principal metals shown are iron and lead as these have been shown to be of contrasting geochemical significance. Iron being primarily of a detrital origin, and lead showing a large anthropogenic input with the most pronounced enrichment in the Arkona Basin core. The values shown in Figure 9-1 are averaged values for each compartment for October '96 apart from the atmospheric and sediment trap component which are derived from external data sets from one year later and are as credited. In addition, concentration data is shown below in Table 9-1 for the sediment core over the same period of time which can aid in the interpretation of the bulk metal environmental impact in the system.

Table 9-1 Average concentration of Iron and Lead in the sediment cores at the survey stations

Sediment Core Concentration	**Iron (ppm)**	**EQS**	**Lead* (ppm)**	**EQS**
ODAS Tonne	1,768	n.v.	5-8	30.2
Nord-Perd Rinne	6,546	n.v.	6-19	30.2
Tromper Wiek	9,700	n.v.	9-35	30.2
Arkona Basin	32,905	n.v.	40-102	30.2

*Pb is shown as a range so as to accommodate the anthropogenic range, EQS = Environmental Quality Standard from Environment Canada. The EQS level indicated of 30.2 is biologically derived and classed at the threshold effects level. Probable effects level is given at 112 ppm for lead. n.v. =No value given for iron in sediments.

Furthermore, Table 9-2 provides comparative data for sediment cores from close and similar geographic environments in order to give a better perspective on the data obtained.

Table 9-2 Comparative values of Iron and Lead from geographically close localities.

All in ppm	Loch Etive*	North Sea†	N. Atlantic§	Atlantic Shelf Edge‡
Iron Concentration	51,400	13,500	15,127	12,200
Lead Concentration	69	18	8	8.7

Data taken from * S. A. Young, 1996, † Langston *et al., 1999* (Dogger Bank), § Baseline Environmental data, Enterprise Oil, Block 154/1, ‡ Unpublished data from the LOIS project

With respect to the sediment core concentrations (Table 9-1) it can be seen that both Tonne and Nord-Perd are relatively unpolluted sites being well below the Canadian environmental quality standard. While a relatively constant concentration gradient is observed for Tonne, Nord-Perd and Wiek there is a marked jump to Arkona in which both iron and lead concentrations increase dramatically. The values for lead are substantially above the environmental standard and define a strong enrichment factor against average shale, unlike iron which is close to unity. These increases are most likely to be predominantly controlled by the distribution and final resting-place of the finer sediment grain sizes and the increase in organic carbon content and associated metals at Arkona. Thus it seems as though the shallower sites, while being proximal to the Oder outlet, represent the cleanest environment in terms of sediment core bulk metal content while in contrast the most distal station of Arkona has the highest concentrations of certain metals within the sediment (Pb, Cu, Zn and Sn).

Figure 9-1 and Table 9-3 detail a number of striking trends particularly with respect to the sediment and mobile nepheloid layer. With an increase in station water depth the sediment core data shows an increasing metal to rubidium ratio whereas the nepheloid layer decreases from Tonne to Arkona reaching a similar ratio value to that of the sediment core at Arkona. Table 9-3 shows enrichment factors for various metals in terms of normalised nepheloid layer to normalised sediment core in which the same transition from shallow to deep stations can be observed for the majority of metals to a near unity value at Arkona.

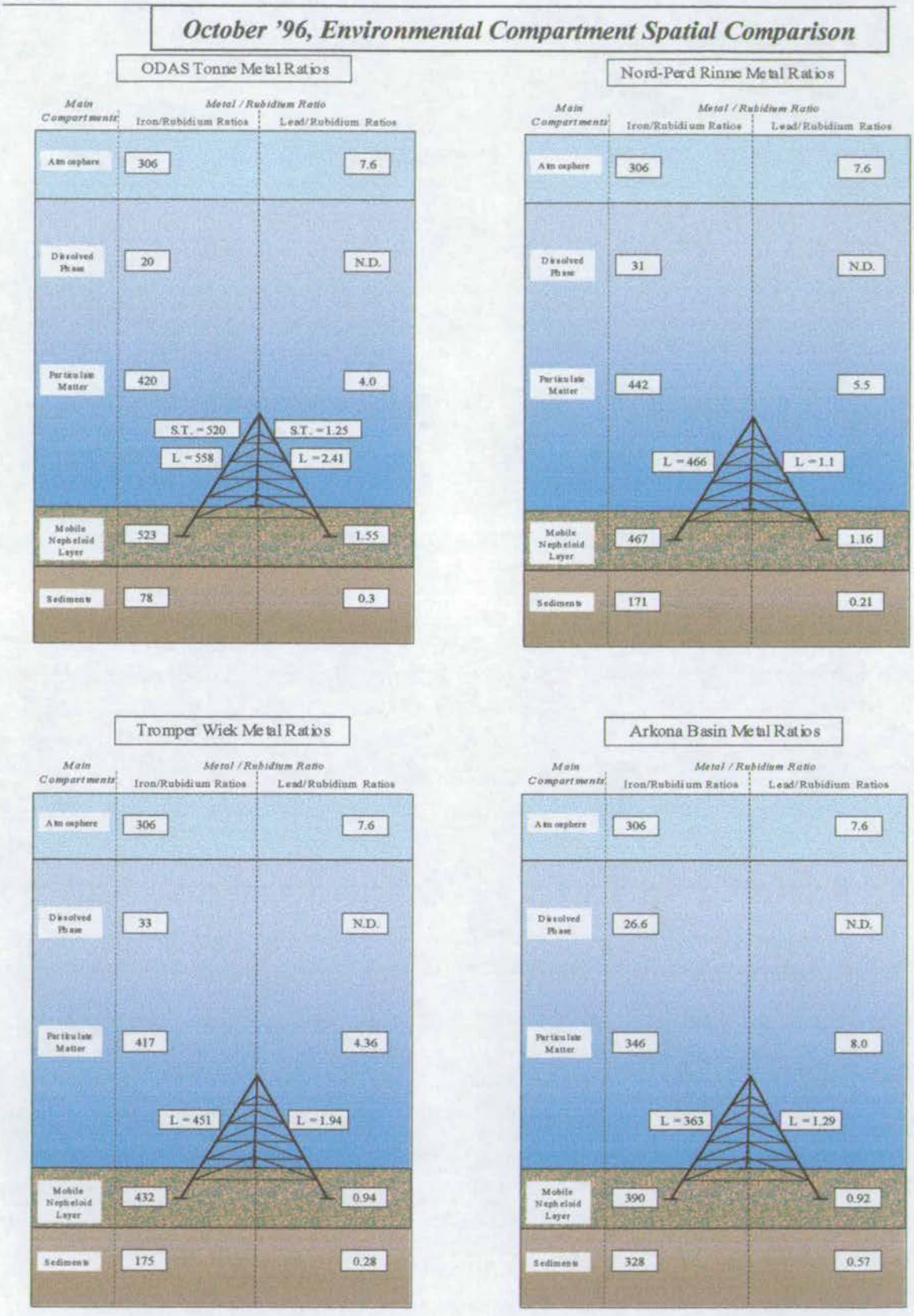

Figure 9-1Spatial variations in metal to rubidium ratios for the study area, Oct '96, Atmospheric ratios courtesy of B. Schneider, IOW for 16/06/97-09/08/97, S.T. = Sediment Trap data from 1 year later, L = averaged Lander ratios,

Table 9-3 Enrichment Factors of the Mobile Nepheloid Layer relative to surface sediment core for the study area, with additionally, the enrichment factor for the Arkona Sediment core relative to average shale for reference.

Metal	E.F. MNL/S.C. Tonne	E.F. MNL/S.C. Nord-Perd	E.F. MNL/S.C. Wiek	E.F. MNL/S.C. Arkona	E.F. Sediment Core / Av. Shale Arkona Basin
Fe	6.55	2.29	1.49	1.14	0.98
Mn	10.2	7.40	2	1.17	0.55
Pb	5.51	2.43	1.27	1.12	4.66
Zn	9.32	3.7	1.96	1.13	2.17
Sn	69.5	52.2	33.4	16.6	0.875
Cu	2.57	1.53	1.44	1.2	0.95
Ni	5.47	2.89	2.53	1.42	0.60
V	5.45	1.78	1.11	0.94	0.95
Cs	6.25	1.67	0.88	0.71	1.04
Ba	0.72	0.68	0.92	0.77	0.76
Th	2.12	0.81	0.80	0.53	1.31
U	1.59	0.70	0.86	0.78	1.56

While the values for the sediment core and nepheloid layer at Arkona maybe similar, it must be remembered that not only does the Arkona Basin cover a relatively large area with ongoing modification processes changing the ratios throughout, but in addition, for some material the Arkona Basin may not be the final resting place. For instance, LARSEN and KOGLER, 1975 detail the presence of a submarine channel between the deepest parts of the Arkona and Bornholm basins through which transfer of material may occur. However, BRAND and SHIMMIELD, 1995 showed by the use of lead and polonium isotopes that the water masses of the two basins were distinct and that there was probably only a small exchange of water between the two basinal environments. It is quite probable however, that the primary transport route for material is in the nepheloid layer which may become entrained in bottom currents

which operate independently of the main water masses throughout the area. Nevertheless, the ratio values at Arkona are sufficiently close as a first approximation to indicate the main modification processes at work. These changes in ratios are shown comparatively as a percentage change in Figure 9-2 which indicates that the biggest percentage change in ratio for the nepheloid layer, for both iron and lead, is that between the two shallowest stations. This may be as a result of dilution by biogenic material associated with the intense shallow water primary productivity or as a result of exchanges between the nepheloid layer and the sediments. Conversely, the biggest percentage changes in the sediment core are between the two deepest stations coincident with a large increase in the presence of fine sediment grain sized material.

Hence, while the sediments of the shallowest station of ODAS Tonne are the cleanest, the mobile nepheloid layer suspended above the surface is the most contaminated compartment in this region of study. Therefore, if as expected, the nepheloid layer is the primary source of metal input into the sediments then it becomes clear that because the nepheloid layer has the elevated metal characteristics at Tonne then physical conditions must hinder the deposition and inclusion of this material into the historical record until it reaches an environment where deposition is conducive and can occur. It is clear that modification of the nepheloid layer occurs throughout the region of study and while the ratio decreases with depth and transport length it seems plausible that a proportion of the nepheloid metal content is lost to the sediments in which the ratio increases with depth. It is interesting to note that the biggest change in the sediment core corresponds to an increase from 2% to over 20% clay content of the sediments at Arkona and that the largest change in the nepheloid layer also corresponds to the first occurrence of clay in the sediment system.

In addition to these lateral modifications two contrasting vertical signatures can be observed with respect to iron and lead. Iron shows no consistent pattern of modification throughout the water column and remains relatively constant in each compartment over the study area. Conversely, lead shows a constantly modified ratio signature, decreasing with depth in the water column. Therefore while iron in

the sediment core seems to be predominantly controlled by lateral transport of the mobile nepheloid layer, lead in contrast seems to be a two component mix of both lateral and vertical transport with obvious connotations for a significant riverine and atmospheric input for this metal. In order to try and quantify the magnitude of each of these inputs a simple mass balance comparison can be made.

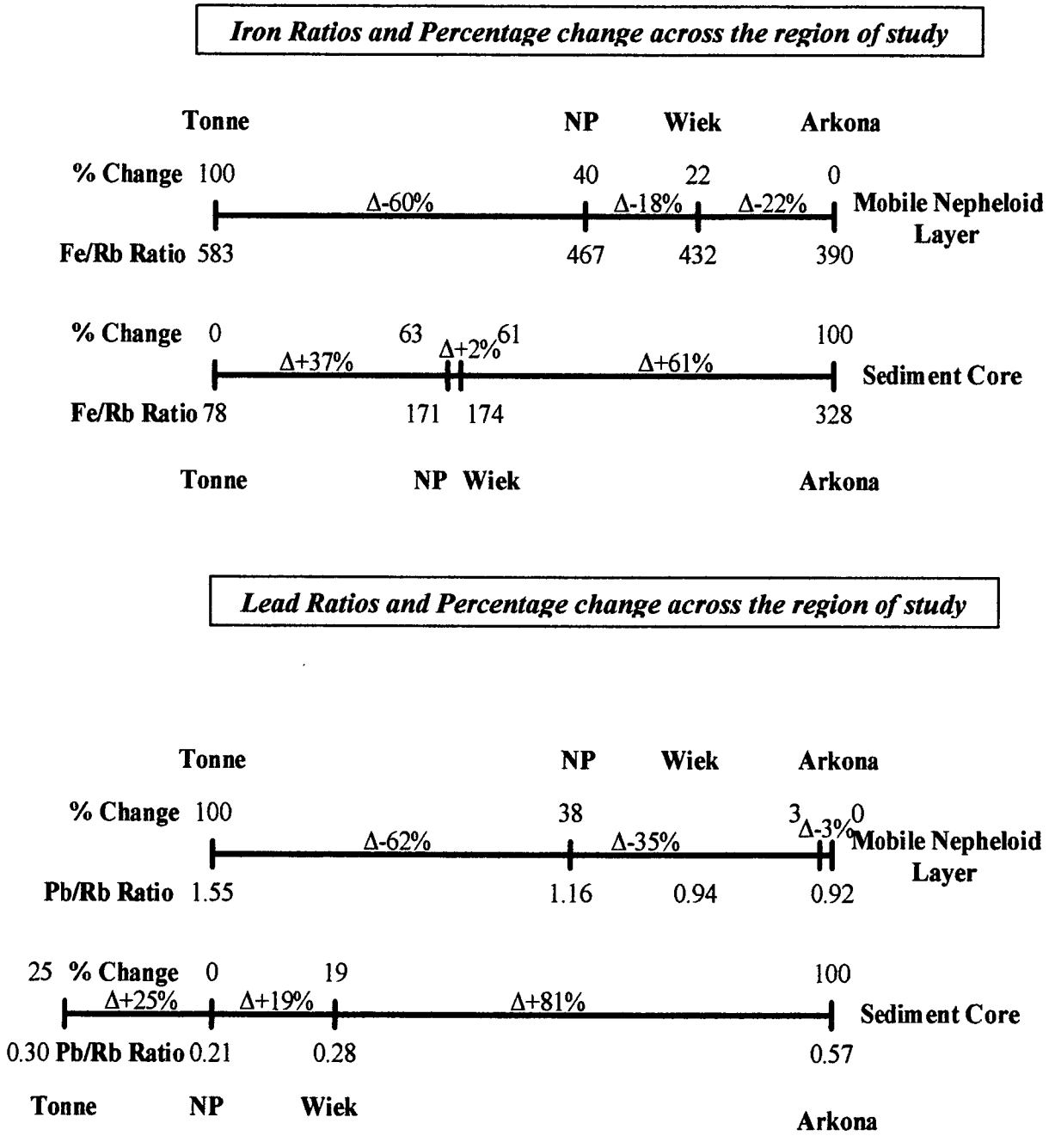

Figure 9-2 Comparative changes in the nepheloid layer and sediment core across the study area.

The HELCOM, 1998 report ascertained that the lead input of the river Oder was in the order of 55t a^{-1} and POHL *et al.*, 1998 found that 90.4 % of the Pb, 79.7% of the Cu and 94.9% of the Zn is retained in the inner lagoons of the Oderhaff and hence only a small net percentage of these metals transported by the Oder ever reaches the Pomeranian Bight. Therefore, if only 9.6% of the lead reaches the Pomeranian Bight then this is equivalent to approximately 5.28 t a^{-1} of which some of the lead will contain atmospheric lead from the catchment. Additionally, SCHNEIDER (pers. comm.) gives values of atmospheric lead input to the Arkona region of the Baltic Sea for the summer of 1997 at 2.9mg m^{-2} yr^{-1}. If the area of the Pomeranian Bight is taken as 5580km^2 and the area of the Arkona Basin at 3876km^2, totalling 9456km^2 then an atmospheric input of 27.42 t a^{-1} can be calculated for this region. Hence the total input of lead to this region is in the order of 32.7 t a^{-1} (excluding that locked away in the Oderhaff lagoon) and of this 16% is from a riverine input and 84% is atmospheric in origin.

Table 9-2 shows iron and lead concentration data from the neighbouring environments of the North Sea and north Atlantic to give some perspective as to the metal concentration in the Baltic Sea. It is quite clear though that Loch Etive on the west coast of Scotland is the closest analogy to this set of data, which probably pertains to the similarities in environment (restricted exchange, brackish water and reducing conditions in the sediment cores) to that of the Baltic Sea, but with a restricted pollutant load.

Thus far, in the context of spatial metal distributions, it seems likely that the main controlling factor in the carrying capacity of the sediment with respect to pollutants is the physical and dynamical regime of each of the stations. While the nepheloid layer at Tonne has the potential to create the most polluted sediment core it is not until the low energy waters and the depth protection from wave induced resuspension that significant deposition occurs at Arkona.

Real time video footage of the sea floor at Tonne displays the dynamical nature of this environment with periods of calm showing nepheloid layer build up on the sheltered sides of sand ripples. In slightly breezier conditions the immediate clearance of any nepheloid layer material was observed leaving a pristine sandy lag deposit. Transport therefore seems to be governed by repeated cycles of deposition and resuspension when the near surface shear stress exceeds critical values as controlled by wind and current induced mechanisms. In addition to the dynamics and mobility of the nepheloid layer the composition of this material is thought to be relatively robust to large variations in composition and instead acts as long term mixer of short term changes in metal concentrations. However, the nepheloid layer does show some ratio changes, particularly for lead, associated with both vertical and lateral biogeochemical transitions and the continual modification occurring as a result of the dynamic conditions of this environment.

JÄHMLICH (pers. comm.) calculated that the theoretical settling velocities of particulate matter in the water column with no flow to be in the order of 20hrs, and that of aggregates to be approximately 5 hours. In addition she calculated the theoretical residence time of particulate matter in the water column to be of the order of 11 to 36 hours which was corroborated by data from SHIMMIELD (pers. comm.) where ^{210}Pb and ^{210}Po data gave particulate residence times of 2 days for Nord-Perd, 5 days for Wiek and 86 days for Arkona.

Sediment trap data from CHRISTIANSEN (pers. comm.) shows that on short-term deployments during calm conditions the rate of sedimentation was of the order <10g m^{-2} day^{-1}. In contrast to this, long term deployments yielded average sedimentation rates of 80-110 g m^{-2} day^{-1} which he attributes to resuspension of particles from the mobile nepheloid layer as the critical threshold for sediment resuspension is seldom reached but the resuspension velocity for the nepheloid layer is frequently exceeded. EMEIS (pers. comm) estimated that the shallow water current speed is above the threshold of nepheloid layer resuspension for more than 50% of the time, and while the specific movement of the nepheloid layer is episodic in nature, the absolute movement may be viewed as almost continuous. Thus the mobility of the nepheloid

layer is considerable and resuspension of this material is some 8-10x greater than the primary sediment fluxes. From the same sedimentation rate experiments Christiansen also concluded that if it was not for resuspension then the water column would empty of suspended matter during calm conditions on a daily basis and that the shallow regions are non-depositional on a time scale longer than weeks and only act as a temporary sedimentary material store.

9.2.1 The importance of the Oderhaff Lagoon on metal distribution in the Southern Baltic Sea

While this study has been primarily concerned with the basins of the southern Baltic Sea and the transitional environments in the Pomeranian Bight it is also necessary to evaluate the environmental loading in this region to consider the environment of the Oderhaff lagoon, and the estuarine-type environment this represents. As already has been intimated by the data from POHL *et al.*, 1998 in the previous section, the Oderhaff lagoon region seems to be of great importance as a filter and depositional area of metals from the river Oder before they enter the Baltic Sea proper. A number of authors have detailed the significant enrichment in heavy metals within the Oderhaff lagoon amongst which LEIPE *et al.*, 1989; NEUMANN *et al.*, 1996; NEUMANN *et al.*, 1998 and POHL *et al.*, 1998 are some of the more recent ones. Typical values for specific metal enrichment factors are given in Table 9-4 which is taken from NEUMANN *et al.*, 1996.

The main inferences from this table are that the Oderhaff lagoon where the freshwater first meets the brackish water of the Baltic in the settling ponds of the haffs and boddens act as filters and depositional zones for the outflowing water and that there is a decrease in the respective enrichment factors from the lagoon out to the Arkona Basin.

Table 9-4Enrichment factors in surficial sediments of the Oderhaff, Achterwasser and Arkona Basin related to the pre-industrial background; taken from NEUMANN *et al.*, 1996.

	Oderhaff	*Achterwasser*	*Arkona Basin*
Co	2.0	1	1
Ni	2.1	1.3	1.4
Cu	4.5	1.8	1.5
Zn	15.0	4.2	2.4
Pb	5.7	2.4	2.4

However the data obtained in this thesis also shows that while the Oderhaff lagoon has the highest enrichment factors, it is not a progressive decrease to Arkona but instead throughout the Pomeranian Bight there is actually an increase in the enrichment factor to Arkona. Thus in terms of metal stress on the environment, the sediments of the Oderhaff and Arkona are among the most polluted with respect to Pb, Cu, Zn and Sn while the shallow sediments of the Pomeranian Bight are among the cleanest.

In addition to these strong regional trends in metal concentration there are some metals which show elevated concentrations towards the sediment surface. Thus as far as the data obtained in this study shows there are two main sources of metal input into this environment; those associated with a minerogenic component and those associated with an anthropogenic component. The main contributors to the anthropogenic component in the Pomeranian Bight and the Arkona Basin are Pb, Cu, Zn and Sn with which a further two component split can be inferred. The relative magnitude of the inputs to the region have already been illustrated with respect to lead with over three quarters derived from atmospheric input and the rest from a riverine source. The close association and characteristics of the other metals above with lead seems to indicate a similar mode of input to the southern Baltic Sea.

The relative contributions of the two minerogenic and anthropogenic components for Pb, Cu, Zn and Sn in terms of fluxes for the Arkona Basin are given in Table 9-5 which shows the relative percentage contribution in parentheses. The results obtained are comparable to those of SZEFER and SKWARZEC, 1988 in terms of fluxes for the neighbouring Gdansk Bay with values of 65, 30 and 150 mg m^{-2} yr^{-1} for Pb, Cu and Zn respectively. Thus while active measures in reducing the pollutant load have been implemented by the Helsinki Commission and that measurable results have been obtained it should be noted that there is still significant scope for improvement in this region. In addition it is also worth noting that spatially, widely ranging variations in concentration within sediment cores to a regionally consistent source (atmospheric) are found and that the easily resuspendable nepheloid layer may represent a greater health hazard than the sediments themselves, particularly, in shallow high energy environments.

Table 9-5 Total (minerogenic + anthropogenic) and anthropogenic flux of Pb, Cu, Zn and Sn (mg m^{-2} yr^{-1}) during the historical peak and currently in surface sediments.

Flux	Pb mg m^{-2} yr^{-1}	Cu mg m^{-2} yr^{-1}	Zn mg m^{-2} yr^{-1}	Sn mg m^{-2} yr^{-1}
Peak Total (whole core)	50.8	27.2	139.7	3.17
Peak Anthropogenic	30.9 (61)	11.0 (40)	93.7 (67)	1.91 (60)
Surface Total	41.4	23.1	108.0	2.61
Surface Anthropogenic	21.5 (42)	6.87 (30)	62.0 (12)	1.35 (51)

Values in parentheses show the percentage of the anthropogenic metals in relation to the total flux.

9.3 TEMPORAL VARIATIONS IN METAL DISTRIBUTION

The cruises were timed so as to ascertain whether there was any marked seasonal variation in concentrations within the various compartments of the marine system studied. The results of these investigations yielded no consistent trends for either the dissolved or particulate phase over the period of study and are instead suggestive of a

well mixed, turbulent system, especially at ODAS Tonne, with a large resuspended component which inhibits and masks any seasonal trends from being displayed. As the period between cruises was approximately 4 months then small scale changes and processes cannot be inferred from this particular system but on a broad scale the primary control seems to be the wind forcing which drives this turbulent hydrodynamic system. In addition the wind direction also influences the direction and route of the outflow from the Oderhaff lagoon and the corresponding pollutant load entering the Arkona Basin system or transportation eastwards towards the Bornholm and Gdansk Basin.

9.4 RADIONUCLIDE AND TRACE METAL INVENTORIES AND FLUXES.

Calculations of the inventories and fluxes of the main isotopes and metals studied in this thesis were determined so as to provide a data set which could be used to show spatial variations in this region of the Baltic Sea.

9.4.1 Radionuclide Inventories and Fluxes

The inventories for ^{210}Pb and ^{137}Cs along with flux calculations for ^{210}Pb at each station are given in Table 9-6. The flux and inventories show a common trend of maximum values at Arkona with decreasing values relating to a shallowing in station water depth as shown in Figure 9-3 which, additionally, are compared with data from SHIMMIELD *et al.*, 1995.

Table 9-6 Radionuclide flux and inventories for the BASYS sampling stations.

Station	^{210}Pb Inventory ($Bq\ m^{-2}$)	Excess ^{210}Pb Inventory ($Bq\ m^{-2}$)	^{210}Pb Flux ($Bq\ m^{-2}yr^{-1}$)	^{137}Cs Inventory $Bq\ m^{-2}$
Arkona Basin	8178 ± 571	5028 ± 703	156.3	1390 ± 132
Tromper Wiek	3742 ± 284	1898 ± 251	59.0	860 ± 67
Nord-Perd	3104 ± 247	487 ± 68	15.1	56 ± 23
ODAS Tonne	525 ± 41	211 ± 31	6.6	257 ± 54

The most noticeable features of both Table 9-6 and Figure 9-3 are the dominance of Arkona in all the inventories in which the sum of all the other stations is less that that of Arkona alone. This suggests that Arkona is acting as a sink for both ^{210}Pb and ^{137}Cs which most likely relates to the association with the fine grained material deposited at Arkona. Figure 9-3 shows the additional data of SHIMMIELD *et al.*, 1995, as an average, in which the data for the Arkona Basin ranged from 7495 to 14191 Bq m^{-2} which over the 5 sampling stations seemed to indicate large spatial variations within the Arkona Basin as a whole. The only exception to these findings is the ^{137}Cs data for Nord-Perd which is significantly lower than the expected trend relating to the presence of a shell band in the uppermost 4cm of the core in which there was no significant sediment that could be analysed and hence added to the inventory for the core.

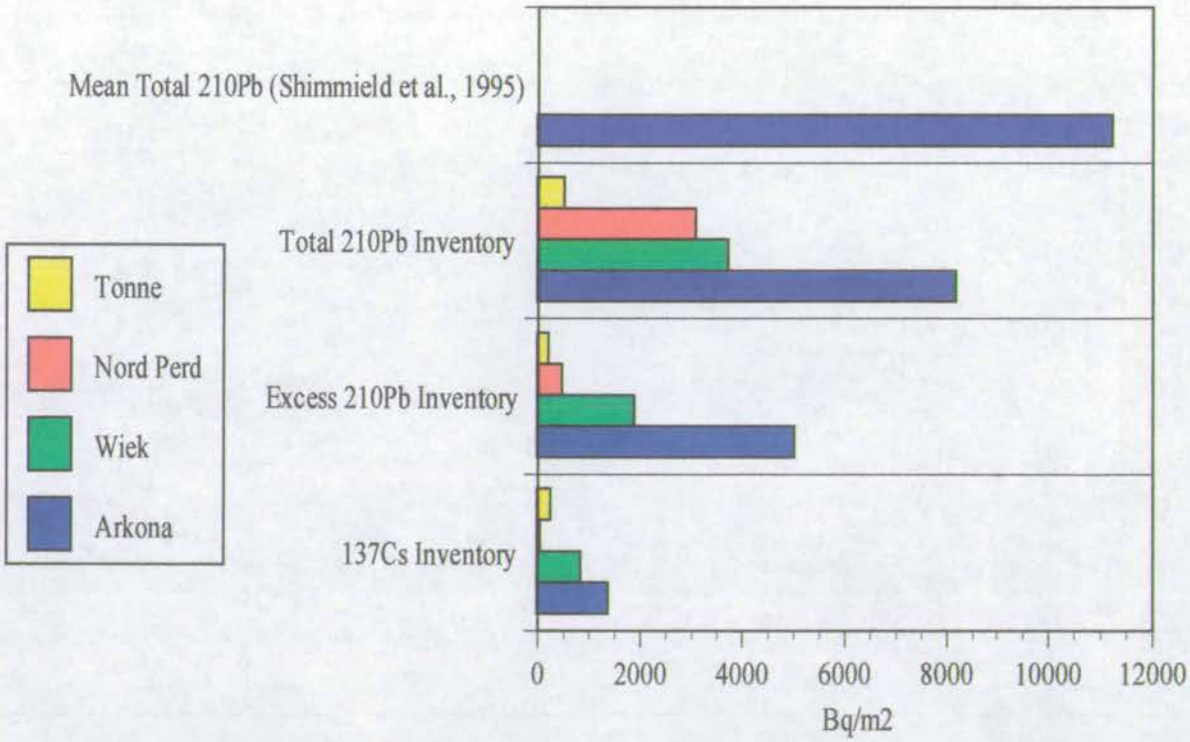

Figure 9-3 Inventories of total ^{210}Pb, excess ^{210}Pb and ^{137}Cs for the BASYS Stations

If the area of the Arkona Basin is assumed to be 3876 km^2 and that the average ^{137}Cs inventory for this region is 1390 Bq m^{-2} then the total activity of this man-made

radionuclide within the Arkona Basin is 5.4 TBq. This is less that 50% of that calculated by SHIMMIELD *et al.*, 1995 (11.8 TBq, sampled 1993) and may relate to the patchy distribution as shown by the comparative ^{210}Pb distribution or may instead be as a result of the removal of caesium from the sediments.

The flux of excess ^{210}Pb is shown in Figure 9-4 along with comparative benchmarks taken from KRISHNASWAMI and LAI, 1978 and BEKS *et al.*, 1998. The data can also be compared to the fluxes given by APPLEBY and OLDFIELD, 1978 of 148 Bq $m^{-2}yr^{-1}$ from a sea loch sediment core in north west Scotland and fluxes of 71.3 to 150 Bq $m^{-2}yr^{-1}$ obtained by SUGDEN, 1993 from Scottish peat cores.

The mean global atmospheric flux given by KRISHNASWAMI and LAI is within error of that measured for the Arkona Basin, however, work in the late 1980's by BEKS *et al.*, 1998 gave revised global estimates in the range of 73 to 110 Bq $m^{-2}yr^{-1}$. In addition BEKS *et al.*, 1998 also calculated the actual ^{210}Pb deposition over the North Sea to be 42 Bq $m^{-2}yr^{-1}$ and also found that inland at Groningen fluxes were higher at 73 Bq $m^{-2}yr^{-1}$. This short scale spatial variability was attributed to the effects of continental ^{222}Rn additions and the number of heavy rain or thunder-storms. Thus for the Southern Baltic sea and the close proximity to land of the survey area, a ^{210}Pb flux value somewhere between 42 and 73 Bq $m^{-2}yr^{-1}$ would be expected. Therefore taking the data of BEKS *et al.*, 1998 into consideration gives a strong indication that the ^{210}Pb found within the sediment is well within the ranges characteristic of a predominantly atmospheric input into the system. While the physical conditions are not conducive to the deposition of lead at the shallower stations it seems as though sediment transport mechanisms, principally related to the mobility of the mobile nepheloid layer, lead to the deposition of lead, associated with the fine grained material, in the Arkona Basin. Thus it seems as though the Arkona Basin acts as a sink for the mainly atmospheric input of lead into this environment which gives rise to enrichment factors in the sediment core significantly above that of average shale.

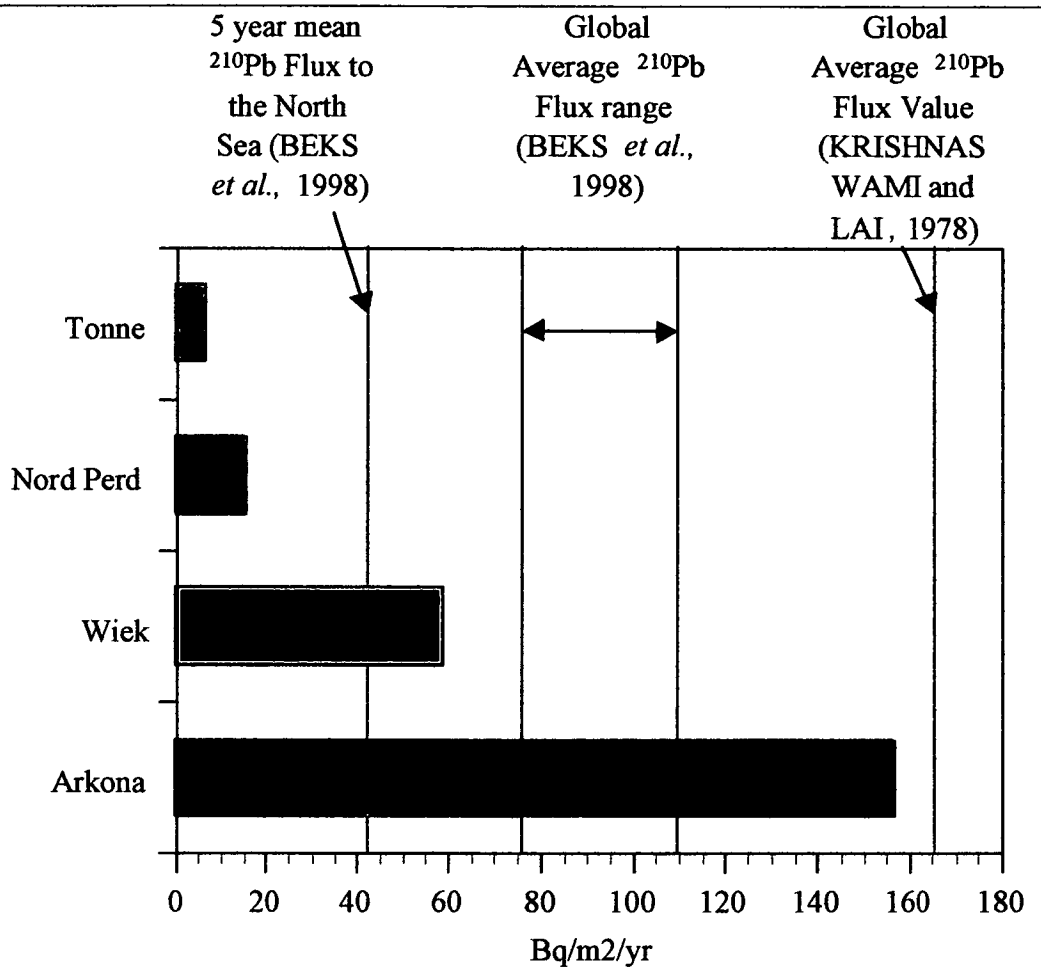

Figure 9-4 Flux of excess ^{210}Pb for the BASYS stations along with the mean global atmospheric flux reference line.

9.4.2 Trace Metal Inventories and Fluxes

In order to compare the following metal inventories the values shown are those defined for the two time spans delineated by the time lines in Figure 9-7. The metals selected are those that displayed the highest enrichment factors over the historical sediment core record and are shown in Table 9-7.

Table 9-7 Metal inventories for Fe, Pb, Cu and Zn at Nord-Perd, Wiek and Arkona for two time ranges (1900-1930 and 1930-1980).

Station	Fe (g m^{-2})		Pb (g m^{-2})		Zn (g m^{-2})		Cu (g m^{-2})	
	1900-1930	*1930-1980*	*1900-1930*	*1930-1980*	*1900-1930*	*1930-1980*	*1900-1930*	*1930-1980*
Nord-Perd	328	363	0.35	0.55	0.77	1.08	0.34	0.36
Wiek	474	366	0.43	0.66	0.29	1.61	0.47	0.48
Arkona	741	686	1.11	1.66	2.24	3.93	0.70	0.87

The main features of Table 9-7 are that the inventories increase in a similar fashion to that shown by the radionuclide data with lower values at the shallower water depth stations increasing to a maximum at Arkona. Additionally there is a strong contrast in the behaviour of iron as opposed to the anthropogenic group of metals as shown in Figure 9-5. Pb, Cu and Zn all show an increase in the metal inventory for the youngest time period whereas iron shows the opposite trend. This pattern of increased anthropogenic metal inventories for the younger time period is expected when reference is made to the fluxes shown in Figure 9-6 which detail peak fluxes during the 1970's and early parts of the 1980's. In the same figure iron shows a small increase with age over the whole of the core and appears to have had a relatively constant input to the Arkona Basin over the last 200 years.

In all the anthropogenic metal profiles a rapid increase since the 1900's is seen after which there has been a steady decrease in the fluxes of these metals to the sediment since the peak flux of the 1970/80's.

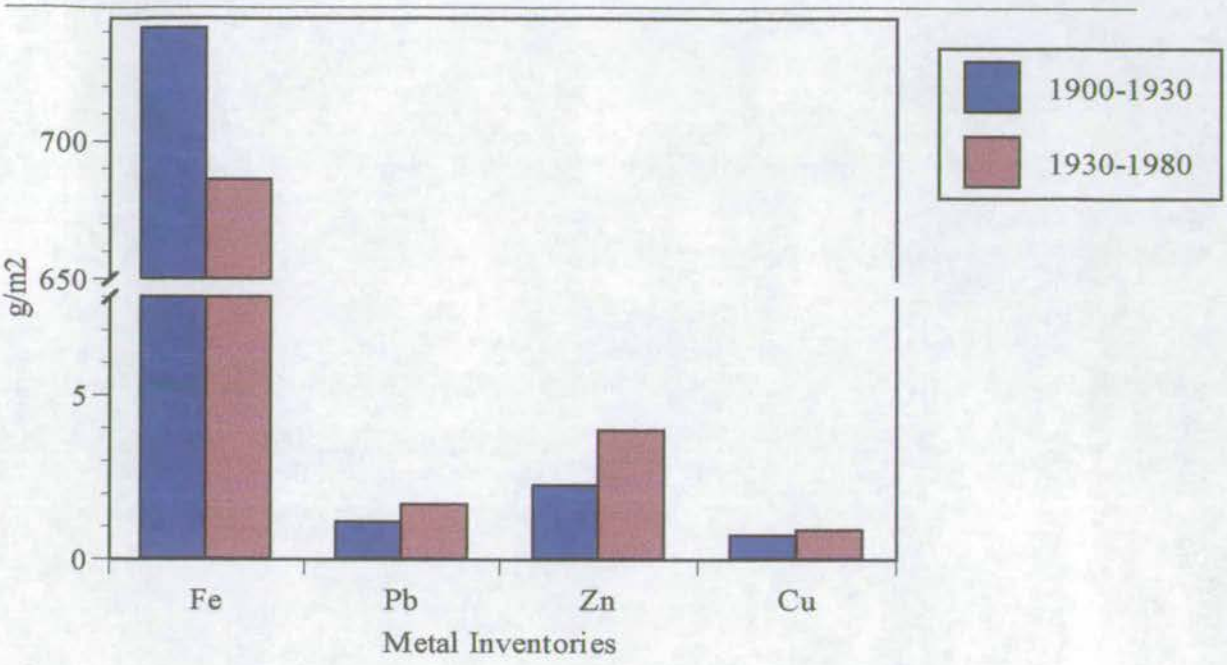

Figure 9-5 Inventories for Fe, Pb, Zn and Cu in the Arkona Basin

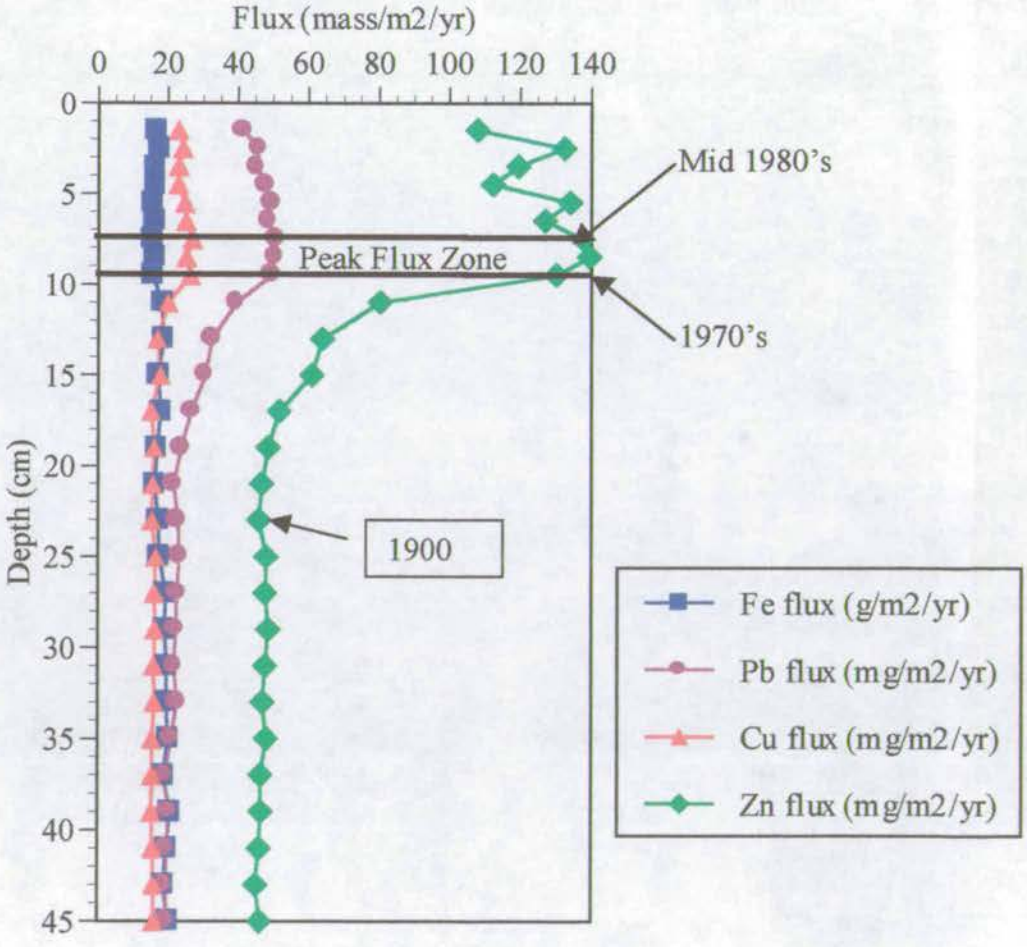

Figure 9-6 Fe, Pb, Cu and Zn fluxes in the Arkona Basin

9.5 STABLE LEAD ISOTOPES AND THEIR APPLICATION AS A DATE AND SEDIMENTATION PROXY INDICATOR

Figure 9-7 shows the stable lead isotope data for all four stations in the Southern Baltic Sea. Key to the interpretation of this data set are the inferences that can be made from the ODAS Tonne core, particularly the near-constant stable lead isotope ratio that is found throughout the whole 14cm of sediment core. This constant ratio has a value which approximates closely to that of 1.167 which is also identical to that of the lowest ratio attained in all of the cores, with which there was good spatial consistency. Therefore, this seems to suggest, as postulated in chapter 7, that there has been no deposition at ODAS Tonne since the mid 1980's as the increasing ratio trends evident in Arkona are not found at Tonne. Furthermore, because the isotope signature is reasonably invariant over the 14cm core depth then the sediment must have been reworked over this depth and retained its signature since circa 1983. If this non-depositional hypothesis is taken a step further then it has important ramifications for the other stations in the survey area. In summary, due to the presence of a consistent minimum stable lead isotope ratio over the 14cm depth range, the interpretation for the Tonne station is one of a high energy, non-depositional environment in which the last lead isotope signature was deposited during the early 1980's.

Bearing this in mind and with reference to Figure 9-7 which shows time horizons delineating important time periods throughout the three deeper stations in terms of the stable lead isotope history, along with peak fluxes for each station, a picture of pre-1980's spatial consistency is found. The stable lead isotope profiles show constant accumulation periods for the events marked and the peak fluxes coincide almost identically across the region. Hence, with the core profiles placed to show this comparison as in Figure 9-7 then certain questions arise as to what has caused these deviations away from what was a spatially consistent sedimenting region to one in which the cessation of deposition seems to have occurred at different time periods across the region of interest.

Taking Tromper Wiek as an example, based on the profile at Arkona, it would be expected to have a much greater isotope ratio bend back post 1980's than is shown in the profile. A simple comparative calculation shows that some 4cm of recent sediment accumulation history is absent from the core. The most obvious explanation for this would be the loss of 4cm of core on sampling which is highly unlikely even in stormy conditions never mind when the core has been carefully collected by trained research divers and so this possibility is ruled out. One possible scenario based upon the evidence from the Tonne core is that there has been a period of recent non-deposition at this station during the last 10 years.

Similarly, if the pattern at Nord-Perd is observed then it could be argued that this core had not actually reached the minimum ratio value of 1.167 and still had a further centimetre of deposition to go to reach this minimum. This site was further complicated by the presence of a thick shell band in which it was not possible to derive any stable lead isotope ratios from the upper 4cm of this core. Thus it is conceivable that there is an additional 4-5cm of recent deposition missing from the Nord-Perd core as well. This 'missing' value could be slightly larger as Nord-Perd seems to have a slightly greater sediment accumulation rate then that proposed for Arkona as the time lines in Figure 9-7 are slightly too narrow for the generalisations made earlier. This additional increase in the sediment accumulation rate is likely to be as a result of the output of the river Peene through Griefswald Bay as shown in Figure 1-3. Therefore if the accumulation rate is slightly greater at Nord-Perd than that of the other stations then the estimated length of time of non deposition will have increased.

As there is a general theme of progressive recent non-deposition occurring throughout this region of interest then this calls into question the Arkona Basin ^{137}Cs peak which dated three years too young at 1989 instead of 1986. This was initially attributed to the loss of the top sediment core on sampling. While this theory is plausible as the sediment lost was equivalent to only 6mm of sedimentation it is also quite plausible that this may instead relate to the progression of a non-depositional regime crossing the Pomeranian Bight and into the Arkona Basin with time.

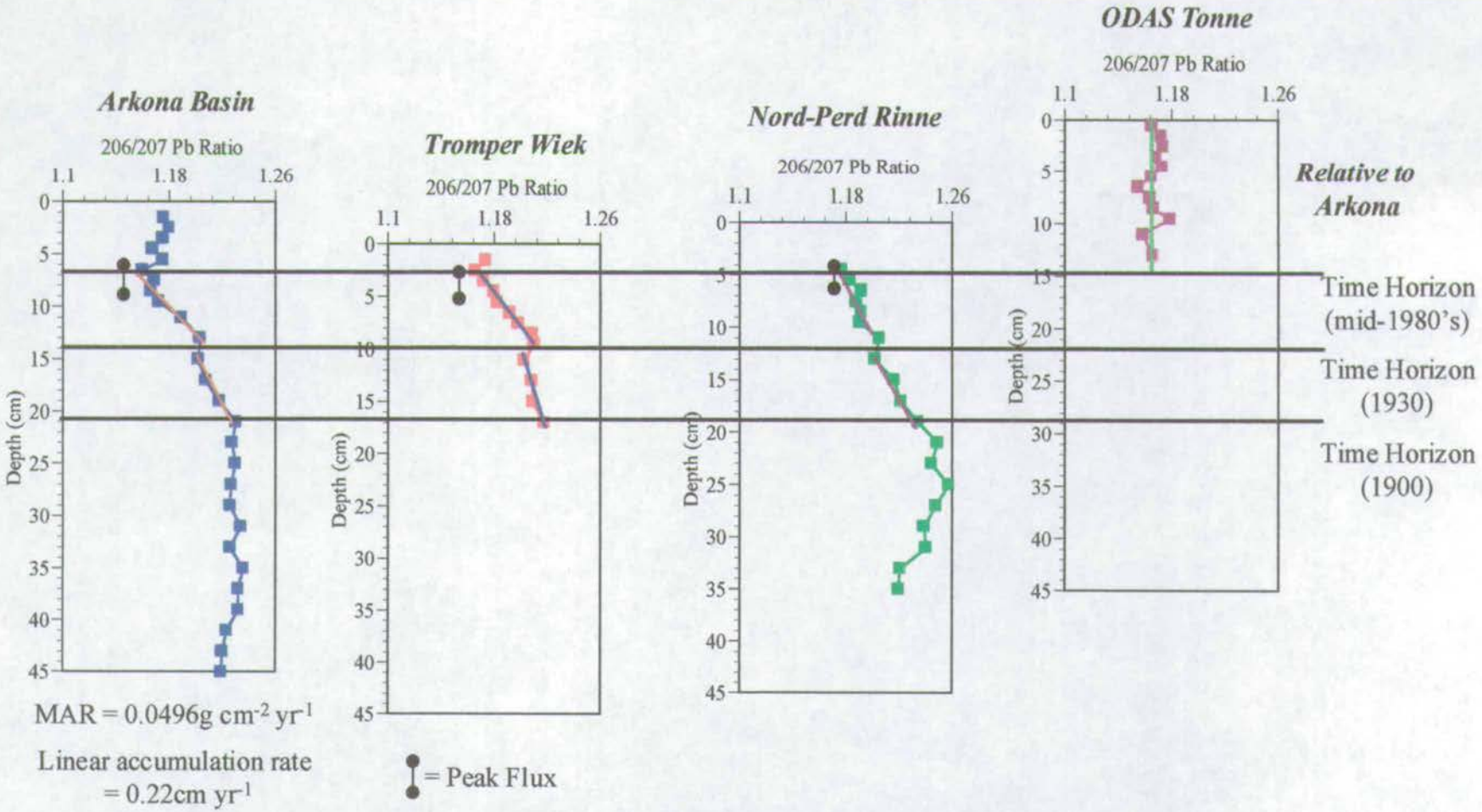

Figure 9-7 Stable lead isotope comparisons for the four sampling stations in the southern Baltic Sea

This hypothesis then throws up the question of what is causing this period of non-deposition and where, if it is not deposited in the Arkona Basin, is the sediment finally being deposited.

While the following is speculative there is sufficient circumstantial evidence in order for it to be proposed as a viable theory to explain this change in depositional history for this region of the southern Baltic Sea.

The onset of this non-depositional history post 1983 coincides with the longest period without an inflow event in the Baltic Sea since records began, lasting nine consecutive seasons from 1983-1992 (the previous longest period being three consecutive seasons in 1927-1930; 1956-1959) as shown in Figure 9-8.

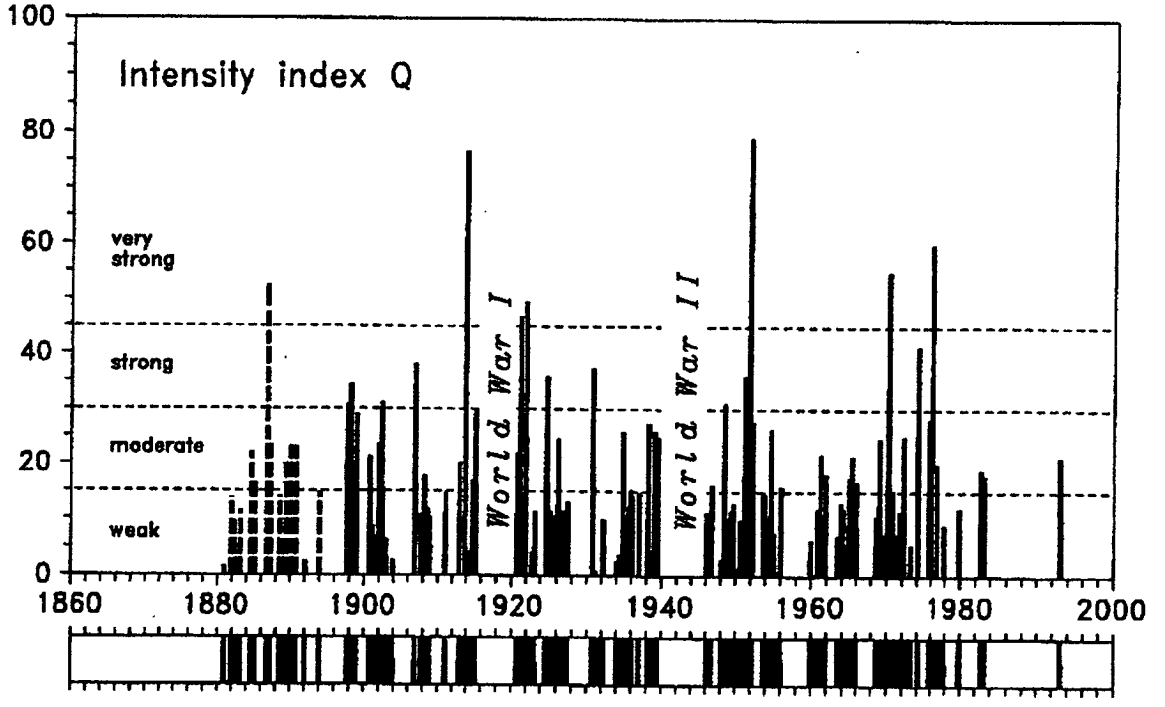

Figure 9-8 Major inflows of highly saline and oxygenated water into the Baltic Sea between 1880 and 1994, (Taken from Matthäus, 1995)

The principal results of an absence in inflow events will be to weaken the salinity structure in the Baltic Sea and to cause increased stagnation in the deep basins. Figure 9-9 shows that during this period of the early to mid 1980's there has been a

significant decrease in the salinity which is also associated with a substantial increase in the river runoff. Additionally, Figure 9-10 shows the seasonal variations in river runoff and mean Baltic sea level. The main consideration to be taken from this figure is that during the period of greatest discharge (from January through to June) the mean Baltic sea level is as much as 20cm below its mean value.

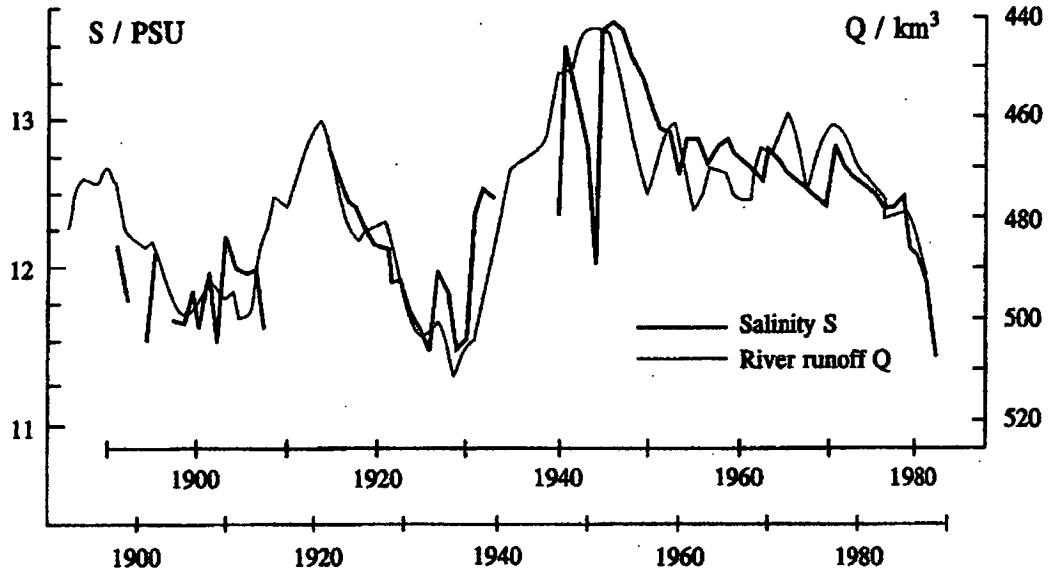

Figure 9-9 Long term variations of river runoff to the Baltic Sea compared to salinity at the 200m level in the Gotland deep. The time axis of the river runoff is shifted forward by six years (according to Launiainen and Vihm, 1990).

Therefore as the peak fluxes are laterally consistent in the sediment cores and the sediment accumulation rate is also spatially consistent pre 1980's, then there has been a major environmental shift in conditions for this region of the Baltic Sea in recent times. It is proposed that these changes are as a result in the paucity of inflow events combined with an increased river discharge at times when the Baltic Sea is below its mean value. The combination of a weaker halocline coupled with an increased river discharge through a lower volume of water and an increase in storminess in recent times (BAERENS and HUPFER, 1995) may have pushed the system beyond a depositional entity and into a primarily depositional role. Periods of quiescence and non-permanent settling are superseded by resuspension and transportation of the mobile nepheloid layer when the bottom velocities exceed 5m s^{-1}.

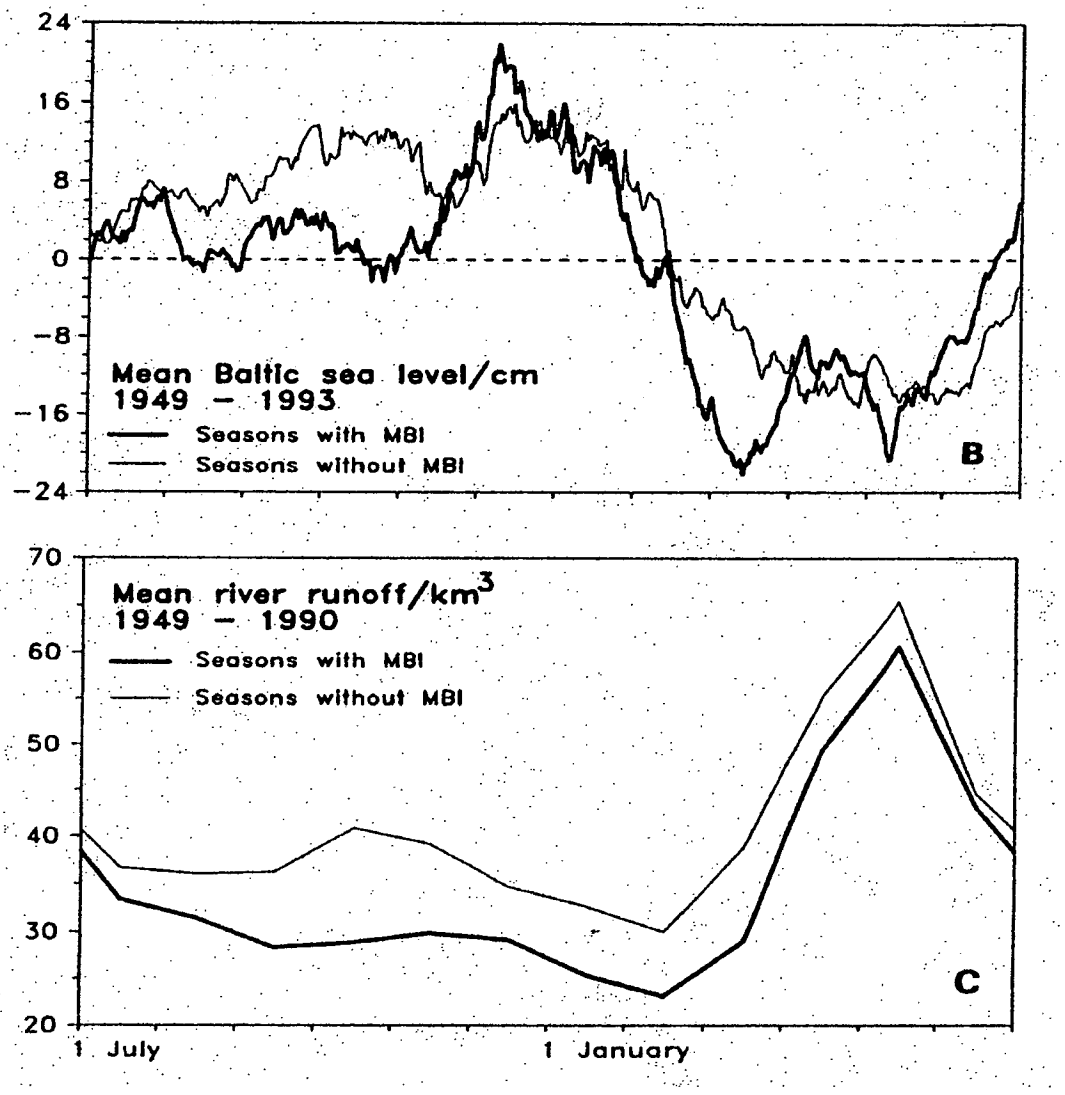

Figure 9-10 Seasonal variations with and without major Baltic inflows (MBI) of (B) Baltic sea level (Lass and, 1994) and (C) river runoff to the Baltic, Taken from Matthäus, 1995.

The extent of this non-depositional environmental change is proposed to have commenced as early as 1983 at ODAS Tonne, having an increasing influence through Nord-Perd and Wiek in the intermediate years and finally affecting Arkona post 1986 with the loss of the equivalent of 3 years sedimentation. However, it is likely that the 1980's were not the beginning of this process because since the 1970's there has been an increase in the sediment accumulation rate. Thus it was only in the 1980's that the threshold of deposition was exceeded and a transportational role was assumed. Additionally it is plausible that these date ranges can be further

constrained as there was the renewal of water via the inflow event of 1993 in which a haloclinic stratification could have been renewed thus acting as a protective barrier to wind and wave induced resuspension.

In order to complete this hypothesis there needs to be an accountable transportational mechanism and final depositional area for the material found within this area. Figure 9-11 details the main circulation pattern in the Baltic Sea in which this passes through the Arkona Basin and onwards through the Bornholm, Gotland, Landsort and finally Karlsö deep. It is therefore proposed that the whole of the study area was non-depositional for 3 years or longer over the recent decade (1983-1993). During these years sediment transport was the main operational process occurring within this region and it is likely that the resultant sediment was transported out of the Arkona Basin and into the Baltic proper with final deposition in one of the Baltic deeps.

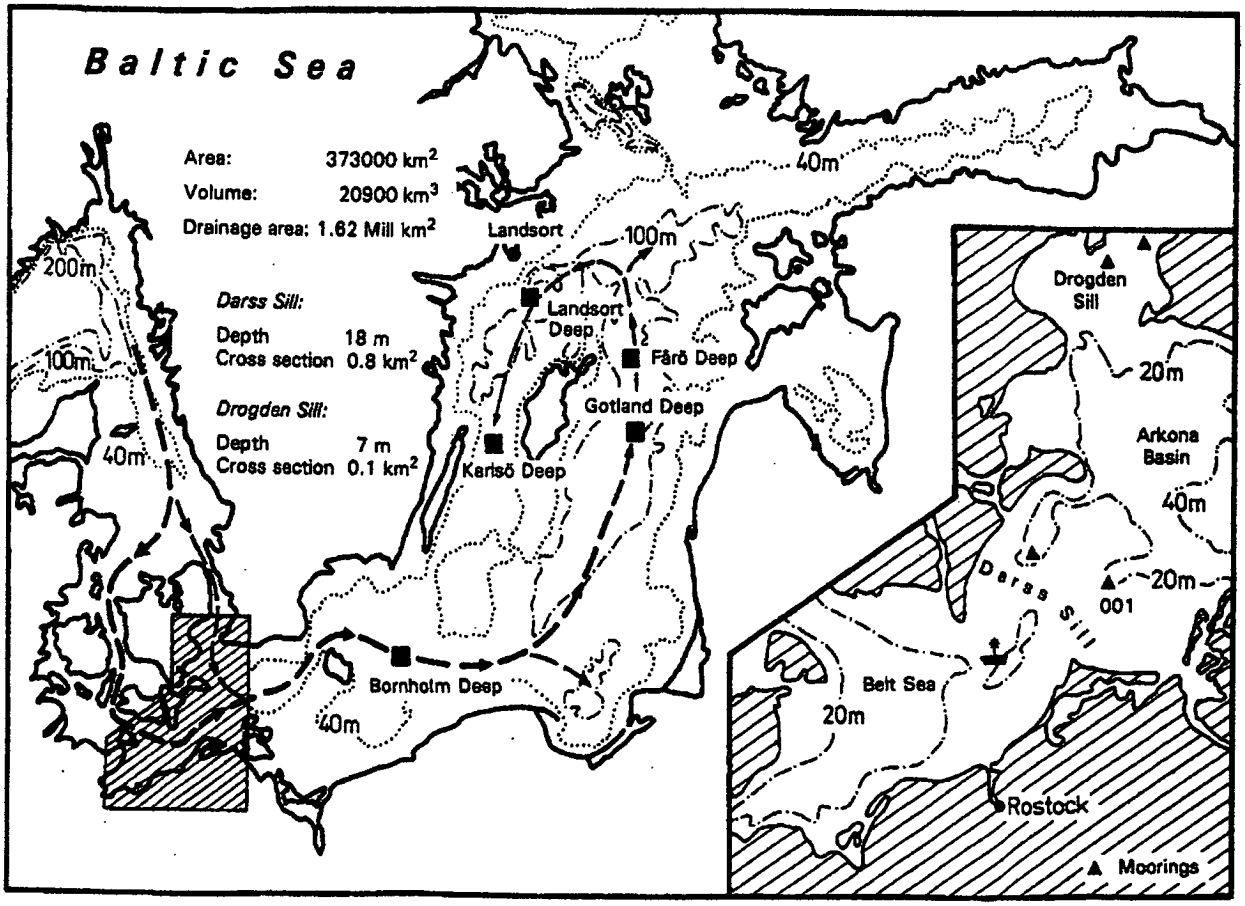

Figure 9-11 The Baltic Sea and transition area with the North Sea indicating major circulation patterns, After Matthäus, 1995.

10.0Conclusions

The main conclusions of this thesis are described, following a spatial pattern out from the lagoonal areas and into the study area proper, and then in an environmental context of the system and the historical changes detailed from the sediment core. The river Oder drains some of the most heavily industrialised regions of Poland, in particular, the economically important coal, Pb, Zn and Cu ores of the Silesia region and has a high pollutant load by the time it has traversed the region collecting hydrological and atmospheric pollutants from within its drainage basin. It has become apparent that the 'boddens' and 'haffs' of the Oderhaff lagoon are a major reservoir for the pollutants transported by the Oder and that they act as a significant filter and accumulator of metals. Additionally, this vast shallow water area also marks the first mixing point of saline with freshwater to produce a brackish salinity front. The river discharge is highly seasonal and peaks in the spring months and the nature of the discharge from the lagoon is via episodic outflows into the Pomeranian Bight.

The region of study follows a progressively deepening transect through the Pomeranian Bight and out into the Arkona Basin. This area has a marked physical gradient with high energy, coarse grain sized sediments at the shallow end of the spectrum at ODAS Tonne, traversing through Nord-Perd and Wiek to Arkona which is a relatively low energy environment comprising of fine silts and clays.

Surface sediment core ratios indicate an increase in the metal to rubidium ratio with the passage into deeper waters whereas, conversely, the mobile nepheloid layer shows the opposite, decreasing from high ratios at Tonne to near unity with the sediment core at Arkona. This modification laterally of the fine-grained and colloidal nepheloid layer into a ratio which approximates closely to that of the sediment core seems to indicate that the nepheloid layer is the primary source of depositional material to the sediment proper.

Fe, Al, Mg, K, Rb, Ti and Zr seem to be primarily of a lithogenic or detrital origin and show little modification vertically through the water column whereas Pb, Cu, Zn and Sn show both lateral and vertical modifications and are proposed to be primarily of an atmospheric anthropogenic origin.

In particular, stable lead isotopes were extensively studied and evidence of increased anthropogenic fluxes as a result of the increased use of the combustion engine were found over the last century. Sediment accumulation rates were estimated to be approximately 0.05g $cm^{-2}yr^{-1}$ although an increase in the sedimentation rate is proposed commencing in the early 1970's. Combined dating and stable lead isotope ratios detail the cessation of deposition throughout the study area. Best estimates place the end of a depositional environment at Tonne during the early 1980's synonymous with the first occurrence of unleaded petrol in the sediment cores and the associated rise in ratio value. During this time the sediment at Tonne was extensively reworked and maintains that low isotope ratio to this day. Nord-Perd, Wiek and Arkona have also become non-depositional since this time with an estimated equivalent of three years deposition missing at the Arkona site.

A further major finding of this thesis is that the Arkona Basin has only been a depositional basin (above average shale) primarily for metals that are of an atmospheric origin, and is not what has traditionally been perceived as the depositional zone for the river Oder. Enrichment factors over average shale in the Arkona Basin are metal specific and associations of lead with Cu, Zn and Sn infer similar introductory routes via the atmosphere to the Baltic. These atmospherically introduced metals have both direct vertical inputs to the region of deposition but are also carried laterally and modified throughout the area of study in the nepheloid layer. Because of the specific enrichment factors and the similarity with average shale for the rest of the metals analysed it is proposed that there is little of the riverine signal in this region of the Baltic Sea. There seems to be two primary pathways for any metals that are transported from the Oderhaff lagoon. The first possibility is that due to the predominance of westerly winds the outflow from the Oderhaff lagoon is transported eastwards along the Polish coast to the Bornholm

Basin or Gdansk Bay and does not actually enter the system studied. Alternatively, the material that is found within the study area prior to the 1980's would have been incorporated to a certain extent within the Arkona Basin. Post 1980's and possibly prior to this, some sediment may have bypassed this region, primarily as a mobile nepheloid layer, and joined the primary current entering the Baltic proper.

The proposed change from a depositional to non depositional environment is thought to have occurred during the 1980's due to the combination of the prolonged pause in inflow events, an increase in the river discharge and storminess, coupled with a lower mean Baltic Sea level. The increased energy of the system coupled with a weakening stratification was initially characterised by increased sedimentation rates until the depositional threshold was passed and a more efficient energy transfer via wind and wave action occurred leading to a change to a more transport orientated system.

Therefore, in summary, the Arkona Basin is not as previously considered a primary depositional site for the pollutant load of the river Oder. Instead it serves primarily as a sink, above average shale, for metals derived from the autochthonous production in the Pomeranian Bight and those of an atmospheric origin, principally Pb, Zn, Cu and Sn. It is perceived that over the last 30 years the main processes at work in this region have changed from one of deposition to that of transportation.

In addition to the above summary the specific findings of this thesis are shown as bullet points below:

- The PERALS methodology was dismissed on grounds of inconsistencies in the standard reproducibility. This was subsequently related to the irregular adsorption of radium onto glassware.
- Rubidium was found to be a suitable normalising agent showing trends indicative of the changes in grain size found across the region of study.
- Carbon and nitrogen ratios indicate a marine based signature for the sedimentary organic matter.

- Manganese is the main redox sensitive element in this region of the Baltic sea and the classic reduction profile is found in the Arkona Basin core. Additionally inferences from the presence of minerals such as pyrite and the smell of hydrogen sulphide indicate anoxia at depth in the core.
- The water column on the whole is well mixed in relation to the dissolved and particulate phase and resuspension effects are clearly observed, upto 15m above the sea floor, especially for the particulate iron phase.
- The only metals to show significant enrichment factors at the Arkona Basin site were Pb, Cu, Zn and Sn which have decreased in value from late 1970's maximums related to a decrease in industrial production and an increase in the use of clean technologies for combustion gases and sewage.
- Sediment accumulation rates were estimated to be approximately 0.05g $cm^{-2}yr^{-1}$ for the period prior to the 1970's
- Dating of the Arkona Basin sediment core yields dates for the onset of industrialisation and is corroborated by the stable lead isotope data revealing the use and end of leaded petrol in combustion engines.
- A marked and substantial ^{137}Cs peak is observed coincident with the Chernobyl event in 1986.
- No seasonality is observed within the region studied and the near constant values of both the down column particulate and dissolved phases indicate a well mixed system.
- The mobile nepheloid layer is shown by association of metal ratios to be the primary transport route of pollutants to the Arkona Basin.

10.1 FUTURE WORK

The main avenues of further research would be to investigate the trace metals and processes associated with the river Oder and the Oderhaff lagoon and to then determine the fate of metals from the outflow of the lagoon. It would be interesting to use event triggered sediment traps both along the Polish coast and throughout the region of study and to couple this with wind data to see if there was a net export of metals in a particular direction. Additionally it would be interesting to compare directly the concentrations of the dissolved, particulate, nepheloid layer and sediment core in order to create a mass balance of the system. Further cruises could also address the question of export out of the Arkona Basin and into the Baltic proper so as to find the final depositional place of these sediments. Finally investigations into the speciation and binding of metals to the inorganic and biogenic components of the nepheloid layer and sediments would give additional information that could be used to infer the primary processes at work in this dynamic region of the marine environment.

11.0Appendices

Appendix A

A.1 Water Column

A.1.1 Density Calculations

The density of seawater was calculated using the temperature (°C) and salinity measurements obtained by the CTD sampler and the polynomial equations given in the international equation of state of seawater, UNESCO, 1983:

$$\rho(S,t,p) = \frac{\rho(S,t,0)}{1-\rho / K(S,t,p)}$$

Where $\rho(S,t,0) = \rho_w + (8.24493 \times 10^{-1} - 4.0899 \times 10^{-3}t + 7.6438 \times 10^{-5}t^2 - 8.2467 \times 10^{-7}t^3 + 5.3875 \times 10^{-9}t^4)S + (-5.72466 \times 10^{-3} + 1.0227 \times 10^{-4}t - 1.6546 \times 10^{-6}t^2)S^{3/2} + 4.8314 \times 10^{-4}S^2$

And ρ_w is the density of Standard Mean Ocean Water (SMOW) taken as pure water reference, is given by

$\rho_w = 999.842594 + 6.793952 \times 10^{-2}t - 9.095290 \times 10^{-3}t^2 + 1.001685 \times 10^{-4}t^3 - 1.120083 \times 10^{-6}t^4 + 6.536332 \times 10^{-9}t^5$

K(S,t,p) is the secant bulk modulus given by

$K(S,t,p) = K(S,t,0) + Ap + Bp^2$

Where

$K(S,t,0) = K_w + (54.6746 - .603459t + 1.09987 \times 10^{-2}t^2 - 6.1670 \times 10^{-5}t^3)S + (7.944 \times 10^{-2} + 1.6483 \times 10^{-2}t - 5.3009 \times 10^{-4}t^2)S^{3/2}$

$$A = A_w + (2.2838 \times 10^{-3} - 1.0981 \times 10^{-5}t - 1.6078 \times 10^{-6}t^2)S + 1.91075 \times 10^{-4}S^{3/2}$$

$$B = B_w + (-9.9348 \times 10^{-7} + 2.0816 \times 10^{-8}t + 9.1697 \times 10^{-10}t^2)S$$

The pure water terms K_w, A_w, and B_w of the secant bulk modulus are given by

$$K_w = 19652.21 + 148.4206t - 2.327105t^2 + 1.360477 \times 10^{-2}t^3 - 5.155288 \times 10^{-5}t^4$$

$$A_w = 3.239908 + 1.43713 \times 10^{-3}t + 1.16092 \times 10^{-4}t^2 - 5.77905 \times 10^{-7}t^3$$

$$B_w = 8.50935 \times 10^{-5} - 6.12293 \times 10^{-6}t + 5.2787 \times 10^{-8}t^2$$

This International Equation of state of Seawater, 1980 is valid for practical salinity from 0 to 42, temperature from –2 to 40°C and applied pressure from 0 to 1000 bar.

A.2 Sediment Collection and Sampling

A.2.1 Sediment processing

The wet sediment samples collected were weighed and then dried in an oven at 60°C for 2-4 days until completely dry. The samples were then reweighed to determine the amount of interstitial pore water relative to the weight of sediment as given by Equation A.2.1.

Equation A.2.1

Water content (wt %) = ((wet wt.- dry wt.) / wet wt.) x 100

In addition the sediment porosity was estimated in accordance with Equation A.2.2 as described by BERNER, 1971.

Equation A.2.2.

Porosity (F) = (water wt. / 1.025) / ((dry wt. / 2.7) + (water wt. / 1.025))

This calculation assumes that all the available pore space is taken up by water and that the mean sea water density is 1.025 g cm^{-3} and the mean solid phase density of the sediment is 2.7 g cm^{-3}.

The determination of the percentage concentrations of various sediment components can be misleading at times, especially if taken as a primary indicator, due to dilution affects and hence variations in the supply and relative importance of these components are best shown normalised to a given indicator such as a lithogenic indicator (Al, Li, Rb) or shown as accumulation rates. In order to calculate the mass accumulation rate and in turn fluxes to the sediment both the linear accumulation rate and the dry bulk density (DBD) of the sediment are required. The dry bulk density is estimated from the wet and dry sediment data using the following equation A.2.3 and uses the same parameters as equation A.2.2.

Equation A.2.3.

DBD (g cm^{-3}) = dry wt. / ((dry wt. / 2.7) + (water wt. / 1.025))

In addition the seawater content of the sediment can also be important in determining the salt content of the sediment pore waters and thus a salt correction factor can be applied to all geochemical data as shown in Equation A.6.4.1, hence increasing their accuracy.

Two sub-samples of the dried sediment were taken for grain size analysis and archiving with the rest being ground to a fine powder in a tungsten-carbide TEMA mill for 45 seconds to ensure homogeneity for later elemental analysis.

A.3 Amberlite Methodology

Chemicals, Reagents and Equipment Required

a) Amberlite XAD-7 macroreticular resin;

b) Potassium Permanganate analar grade; 0.5M DDW Solution

c) Tygon tubing R3603, 19mm Bore and 3.2mm wall;

d) Glass Wool;

e) 25l Carboys with taps

f) Wooden Doweling, 18mm in diameter; and

g) 1l beaker, thermometer, glass rod, porcelain crucibles, furnace and plastic ties

A.3.1 Procedure

1 A 500g batch of Amberlite resin was pre-washed with DDW to remove excess chlorine ions.

2 To the cleaned resin sufficient 0.5M potassium permanganate solution was added to cover the Amberlite.

3 This was then warmed to 70-80°C and left for a period of 2 hours while stirring occasionally.

4 The manganese soaked resin is then rinsed repeatedly with DDW until no further wash out of the excess manganese occurs. At this point the resin is a deep purple-brown colour.

5 Sections of tubing, pre-cut to 30cm lengths are then made into columns by inserting glass wool at one end and then filling the tubing with the resin to a depth of 20cm. The upper end is then closed with glass wool and a wooden doweling stopper.

6 20l seawater samples were filtered and acidified with 10mls of concentrated HCl. The columns were then attached to the carboys by fitting the column to the tap and securing it with plastic ties.

7 The seawater was then allowed to drain under the influence of gravity and any residue was measured so as to correct for the total volume. The samples were then closed at the upper end with doweling and then heat sealed until analysis.

8 On return to the lab the resin was carefully removed in two portions with attention paid to removing all the resin, especially that attached to the glass wool. The first portion (A) consisted of the upper 15cm of resin that was placed in a labelled crucible and the remainder was placed into a second crucible (B).

9 The samples were then left in an 60°C oven so as to remove any excess water present.

10 Samples were then ashed in a vented muffle furnace at an experimentally determined optimum temperature of 300°C for 120 minutes.

11 After cooling, sub-sample A was transferred into a pre-weighed, machined polystyrene pot and weighed to determine the resin weight. This was then made up to the nearest convenient gram by the resin in sub-sample B. Early experiments had determined that all the radium was extracted within the first 12cm of the column and this was reinforced by the findings of GERSHEY and GREEN, 1988 and hence this acted to standardise the calibrations

12 These were then sealed with polystyrene lids, sealed with epoxy resin and left for a period of at least one-month to allow the secular equilibrium of radium and its daughters to ingrow.

13 Standards were made to the gram weights by adding ^{226}Ra spike to distilled water and running it through the columns as described.

14 The samples were then counted for radium on a high purity germanium gamma detector.

A.4. Gamma Ray Spectrometry

Homogenised sediment samples were pressed, under 20 tonnes, into 5g, 10g or 20g pellets (measured to 4 d.p.), depending on sample size, to give a uniform geometry for accurate reproducible comparative counting. The pellets were then placed in polystyrene containers and sealed with quick setting epoxy resin which according to Stewart pers. comm. gave the optimum sealing characteristics and impermeability to the loss of radon-222. The samples were then left for a period of a least one-month so that secular equilibrium between the parent radium-226 and daughter products radon-222 and Bismuth-214 could be reached. The samples were then counted using the gamma emissions of Bismuth-214 at 609KeV (POWERS *et al.* 1980) with which there are no other natural elemental lines of interference. The activity of radium-226 was then back calculated from the activity of its daughter.

A.5 ICPMS Digestion procedures

A.5.1. CEM Microwave digestion summary

Approximately 0.1g (±0.0001 g) of the ground sediment was weighed and transferred into the microwave vessels. To this 5ml of nitric acid, 3ml hydrochloric acid and 3ml hydrofluoric acid were added all of 'Analar' grade. The vessels were then sealed and loaded into the CEM system as per the CEM instruction manual. The microwave program involved a three step heating process from 0°C to 100°C and holding for 5 minutes, a second temperature ramp to 150°C with a hold of 10 minutes and finally a temperature increase to 190°C for 30 minutes followed by a 45 minute cool down period. Each run of twelve consisted of 10 sediment samples, one process blank and one 'in house' sediment standard. On completion of the digestion the samples were transferred into teflon beakers and evaporated to near dryness on a hot plate (125°C) inside a fume cupboard to ensure that all traces of the hydrofluoric acid were removed. The teflon beakers were then rinsed with 2% HNO_3 and left to stand for 10 minutes with the hotplate switched off. The resulting solution was then transferred to a 50ml volumetric flask and taken close to the mark with 2% HNO_3. The flask was then left overnight and filled to the correct mark before being transferred to a 2% HNO_3 pre-rinsed polypropylene bottle.

A.5.2 Filter digestion procedure

The filters containing the particulate phase were placed in teflon beakers and 40ml nitric acid, 5ml hydrochloric acid and 5ml hydrofluoric acid were added. The beakers were then placed with a teflon lid on a hot plate at 150°C and left to reflux for 24 hours. The lids were then removed and the sample was left to evaporate to near dryness. The hot plate was then switched off and 2% HNO_3 was used to rinse the sides of the beaker and also to re-dissolve any salts that may have formed. The resulting solution was transferred to a 50ml volumetric flask and the procedure followed as in A.5.1.

In both the digestion procedures all the equipment underwent a thorough cleaning process involving a first stage wash in 10% Decon and then in an acid-wash

dishwasher at 90°C. The equipment was then placed in a 10% HCl bath and when required taken out rinsed in 2% HNO_3 and then in double distilled water.

A.6 X-Ray Fluorescence

A.6.1. Major element disc preparation

Major element (Si, Al, Fe, Mg, Ca, Na, K, Ti, Mn & P) concentrations were determined by preparing fused, glass discs (45mm diameter) using a similar method to that of NORRISH and HUTTON, 1969 and the full preparation procedure can be found in SHIMMIELD, 1985. In summary, approximately 3g of finely ground sediment was dried overnight at 50°C and of this a 1g quotient was accurately weighed (±0.0001g) into a platinum crucible. To this sediment an ultra pure flux (Spectroflux 105, Johnson Matthey Chemicals Ltd.) was added in a weight ratio of exactly 5:1 (flux:sample). The crucible is then covered with a platinum lid and placed in a muffle furnace at 1200°C for 20 minutes.

The flux consists of a mixture comprising $Li_2B_4O_2$, La_2O_2 and $LiCO_3$ of which the tetraborate helps to dissolve the sample and the lanthinum acts as a heavy absorber of X-rays, thus by way of a fivefold sample dilution, this helps to minimise the matrix affects of different sediment and standard compositions.

The crucible having been withdrawn from the furnace is then allowed to cool on a stainless steel block to room temperature whereby it is then reweighed. Any loss from the total calculated weights, namely from the water absorbed by the flux, is made up by the addition of a small quantity of flux (±0.0002 g). The sample along with the lid is then fused again over a Meker burner for 5 minutes until completely molten. This molten glass is then poured into the centre of a graphite mould situated in a brass sleeve on a hot plate at 220°C. The glass is then pressed into a 1mm thick disk using an aluminium plunger also at 220°C and the left to anneal and cool slowly covered by a Vitreosil crucible to prevent shattering. The discs were prepared in

batches of six and were stored in polythene bags and then placed in a dessicator until analysis.

A.6.2 Minor element disc preparation

The minor elements (Sc, Ba, La, Ce, Nd, Cr, Ni, Cu, Zn, Pb, Th, U, Rb, Sr, Y, Zr, Nb, Mo, I, Br) were determined using pressed powder discs (32mm in diameter). A minimum 3 grams of the ground and dried sediment was placed in a stainless steel sleeve resting on a highly polished tungsten carbide disc which in turn were encapsulated in another larger stainless steel sleeve. A leucite plunger was then inserted into the steel sleeve and using hand pressure a semi-competent disc was formed. The leucite plunger and inner sleeve were then removed and sufficient boric acid was added to cover the sediment disc. A large stainless steel plunger was then lowered onto the powder and compressed using a hydraulic jack to 15 tons for 90 seconds. The pressed discs were then stored in polythene bags within a dessicator to prevent the loss of halogens and salt leaching.

A.6.3 Calibrations, analytical conditions and precision

Calibration of the XRF was accomplished via the use of international and internal rock standards which covered the likely range of elements found in the marine environment. Table A-1 (after MATTHEWSON, 1995) shows the standards used in the XRF Calibration and for all the elements measured the calibration line was found to be linear.

Table A-6.3.1 Standards used in the calibration of the XRF

Ba-1 (I-III)	Ba-2 (I-III)	Ba-3 (I-III)	Ba-4 (I-III)	Ba-5 (I-III)	Ba-6 (I-III)
BRIMO-1 (I-III)	BRIMO-2 (I-III)	BRIMO-3 (I-III)	BRIMO-4 (I-III)	BRIMO-5 (I-III)	BRIMO-6 (I-III)
BRIMO-7 (I-III)					
MAG-1	BCR-1	AGV-1	GA	BR	GH
SY-2	SY-3	JB-1	PCC-1	SGR-1	GSP-1

Ba- and BRIMO- standards are a synthetic dilution series made from AnalaR grade $Ba(IO_3)_2$, $KbrO_3$, $((NH_4)Mo_7)_{24}.H_2O$ and $BaCO_3$.

A.6.4 Salt Corrections

As the sediment contains seawater within its pore spaces an important corrective factor has to be applied in order to adjust for the additional concentrations of Na, Mg, Ca, K, and Br relating to residual sea salt and in turn a dilution factor by these elements has to be accounted for. In order to apply these corrective measures it is assumed that the porewater salinity is constant and normally this value would be taken as that of 'normal' seawater (35.13‰). However, due to the relatively large salinity gradient in the Southern Baltic Sea the following values in Table A.6.4.1 were taken from the bottom water salinity as given by the CTD at each station:

Table A.6.4.1 Bottom water salinities used for the salt correction calculation

Station	Bottom Water Salinity ‰
ODAS Tonne	7.143
Nord Perd Rinne	9.3949
Tromper Wiek	11.7071
Arkona Basin	18.3734

Given the above salinities the salt content of the sediment samples can be calculated using the following equation:

Equation A.6.4.1

Salt content (wt %) = (Salinity % x W)/(100-W)

W = Water content (wet wt %) calculated from the wet and dry sediment weights.

Due to the nature of this equation there will be an exponential increase in salt relative to the sediment with increasing water content and this is exacerbated by the nature of

the Baltic sea sediments as the samples with the highest water content also have the highest salinities. However the individual salt contribution corrections for Na, Mg, Ca, K and Br were calculated using the following equations.

Na_{sed} (wt. %) = Total Na_{sed} (wt. %) – (0.306 x Salt content)
Mg_{sed} (wt. %) = Total Mg_{sed} (wt. %) – (0.037 x Salt content)
Ca_{scd} (wt. %) = Total Ca_{scd} (wt. %) – (0.012 x Salt content)
K_{sed} (wt. %) = Total K_{sed} (wt. %) – (0.011 x Salt content)
Br_{sed} (wt. %) = Total Br_{sed} (ppm) – (19 x Salt content)

Finally all the elements measured were corrected for the dilution effect of the salt content using equation A.6.4.2

Equation A.6.4.2

$Element_{salt\text{-}free} = Element_{measured} \times (100/(100 - \text{Salt content}))$

Where the salt content is from equation A.6.4.1 and the $Element_{measured}$ is from the XRF data or the equations above for Na, Mg, Ca, K and Br.

Appendix B

B.1 Data

The following section lists the salt corrected major and minor elements for the XRF analysis and the results of the ICPMS analysis for major and minor elements along with stable lead isotope data for each station. In addition radionuclide data is shown for the sediment core and nepheloid layer. The data is organised in the following manner:

Station

XRF Sediment core	Major element salt corrected
	Major element to Rubidium ratios
	Trace metal corrected
	Trace metal to Rubidium ratios
ICPMS	Sediment Core
	Normalised sediment core to rubidium ratios

Cruise

	Water Particulate Phase
	Normalised Particulate phase to rubidium ratios
	Water Dissolved Phase
	Normalised Dissolved phase to rubidium ratios
	Mobile Nepheloid Layer
	Normalised Nepheloid layer to rubidium ratios
	Sediment Trap
	Normalised sediment trap to rubidium ratios
	Stable Lead Isotopes
Gamma Ray Spec.	Radionuclides
Miscellaneous	C/N Ratio
	Porosity
	Grain Size

Arkona, XRF major elements, salt corrected, sediment core, Wt. %

	Si	Al	Fe	Na	Mg	Ca	K	Ti	Mn	P
A0-1	24.232	5.822	3.536	3.008	1.358	0.843	1.971	0.436	0.047	0.096
A1-2	24.962	5.968	3.647	2.286	1.368	0.799	2.283	0.394	0.028	0.149
A2-3	26.008	6.305	3.763	1.566	1.342	0.819	2.464	0.415	0.033	0.114
A3-4	25.501	6.229	3.773	2.177	1.388	0.807	2.375	0.404	0.028	0.108
A4-5	26.979	6.542	3.991	1.884	1.475	0.837	2.506	0.416	0.030	0.112
A5-6	26.198	6.431	3.818	1.349	1.327	0.794	2.500	0.415	0.028	0.108
A6-7	25.985	6.342	3.730	1.898	1.367	0.823	2.455	0.416	0.029	0.108
A7-8	26.107	6.323	3.879	1.806	1.352	0.852	2.456	0.417	0.031	0.108
A8-9	25.798	6.254	4.102	1.624	1.351	0.838	2.447	0.408	0.031	0.106
A9-10	25.733	6.327	4.256	1.474	1.346	0.830	2.469	0.413	0.031	0.107
A10-12	26.334	6.411	4.434	1.322	1.306	0.758	2.507	0.421	0.036	0.103
A12-14	26.283	6.322	4.372	1.322	1.254	0.851	2.542	0.434	0.047	0.096
A14-16	26.572	6.449	3.981	1.298	1.283	0.852	2.551	0.442	0.047	0.101
A16-18	26.650	6.366	4.133	1.240	1.327	0.837	2.502	0.428	0.050	0.099
A18-20	26.727	6.324	4.001	1.265	1.366	0.898	2.528	0.426	0.049	0.096
A20-22	27.513	6.261	3.843	1.311	1.344	0.912	2.489	0.428	0.049	0.096
A22-24	28.830	7.009	4.069	1.476	1.578	0.887	2.564	0.426	0.052	0.104
A24-26	26.643	6.542	4.234	1.173	1.423	0.874	2.539	0.427	0.052	0.097
A26-28	27.137	6.657	4.162	1.719	1.475	0.890	2.531	0.424	0.050	0.102
A28-30	26.144	6.394	4.206	1.863	1.375	0.845	2.536	0.429	0.050	0.100
A30-32	26.453	6.468	4.087	1.122	1.389	0.821	2.503	0.430	0.049	0.100
A32-34	26.299	6.371	4.281	1.033	1.327	0.840	2.545	0.427	0.051	0.099
A34-36	26.171	6.322	4.237	1.106	1.366	0.854	2.527	0.424	0.052	0.099
A36-38	26.372	6.412	4.072	1.229	1.374	0.815	2.528	0.425	0.050	0.099
A38-40	26.885	6.572	4.200	1.150	1.451	0.874	2.562	0.430	0.051	0.101
A40-42	26.435	6.332	4.129	1.414	1.365	0.866	2.504	0.422	0.055	0.098
A42-44	32.688	7.954	4.949	1.637	1.826	1.096	3.120	0.514	0.064	0.124
A44-46	25.975	6.376	4.284	1.079	1.398	0.868	2.553	0.417	0.062	0.101
A46-48	25.902	6.329	4.365	1.279	1.401	0.898	2.535	0.414	0.055	0.099

Arkona, XRF major elements to rubidium ratios, sediment core. (x 10^4)

	Si/Rb	Al/Rb	Fe/Rb	Na/Rb	Mg/Rb	Ca/Rb	K/Rb	Ti/Rb	Mn/Rb	P/Rb
A0-1	0.21870	0.05255	0.03192	0.02715	0.01225	0.00760	0.01779	0.00394	0.00042	0.00087
A1-2	0.21650	0.05176	0.03163	0.01982	0.01186	0.00693	0.01980	0.00342	0.00024	0.00129
A2-3	0.21819	0.05289	0.03157	0.01313	0.01126	0.00687	0.02067	0.00348	0.00028	0.00096
A3-4	0.21833	0.05333	0.03231	0.01864	0.01188	0.00691	0.02033	0.00346	0.00024	0.00093
A4-5	0.22691	0.05502	0.03357	0.01584	0.01241	0.00704	0.02107	0.00350	0.00025	0.00094
A5-6	0.20516	0.05036	0.02990	0.01056	0.01039	0.00622	0.01958	0.00325	0.00022	0.00084
A6-7	0.21600	0.05272	0.03100	0.01577	0.01137	0.00684	0.02040	0.00346	0.00024	0.00090
A7-8	0.20819	0.05042	0.03094	0.01440	0.01078	0.00679	0.01959	0.00333	0.00024	0.00086
A8-9	0.22012	0.05336	0.03500	0.01386	0.01153	0.00715	0.02088	0.00348	0.00027	0.00090
A9-10	0.20652	0.05078	0.03415	0.01183	0.01080	0.00666	0.01981	0.00331	0.00025	0.00086
A10-12	0.21603	0.05259	0.03637	0.01084	0.01071	0.00621	0.02057	0.00345	0.00030	0.00085
A12-14	0.21667	0.05212	0.03604	0.01090	0.01034	0.00702	0.02096	0.00358	0.00038	0.00079
A14-16	0.21394	0.05193	0.03205	0.01045	0.01033	0.00686	0.02054	0.00356	0.00038	0.00081
A16-18	0.22025	0.05261	0.03416	0.01025	0.01097	0.00692	0.02068	0.00354	0.00041	0.00082
A18-20	0.21943	0.05192	0.03285	0.01039	0.01121	0.00737	0.02075	0.00349	0.00041	0.00079
A20-22	0.23062	0.05248	0.03221	0.01099	0.01127	0.00764	0.02086	0.00359	0.00041	0.00080
A22-24	0.23554	0.05727	0.03324	0.01206	0.01289	0.00725	0.02095	0.00348	0.00043	0.00085
A24-26	0.20432	0.05017	0.03247	0.00900	0.01091	0.00670	0.01947	0.00327	0.00040	0.00075
A26-28	0.21251	0.05213	0.03259	0.01346	0.01155	0.00697	0.01982	0.00332	0.00039	0.00080
A28-30	0.20932	0.05120	0.03367	0.01491	0.01101	0.00677	0.02030	0.00344	0.00040	0.00080
A30-32	0.21011	0.05137	0.03246	0.00891	0.01103	0.00652	0.01988	0.00342	0.00039	0.00079
A32-34	0.20199	0.04893	0.03288	0.00793	0.01019	0.00645	0.01954	0.00328	0.00039	0.00076
A34-36	0.21277	0.05140	0.03445	0.00899	0.01111	0.00694	0.02055	0.00344	0.00042	0.00080
A36-38	0.21371	0.05196	0.03300	0.00996	0.01114	0.00660	0.02048	0.00344	0.00040	0.00080
A38-40	0.20777	0.05079	0.03246	0.00888	0.01121	0.00675	0.01980	0.00332	0.00039	0.00078
A40-42	0.20947	0.05018	0.03271	0.01120	0.01082	0.00686	0.01984	0.00335	0.00043	0.00078
A42-44	0.25537	0.06214	0.03867	0.01279	0.01426	0.00856	0.02437	0.00401	0.00050	0.00097
A44-46	0.20293	0.04981	0.03347	0.00843	0.01092	0.00678	0.01995	0.00326	0.00048	0.00079
A46-48	0.20525	0.05015	0.03459	0.01013	0.01110	0.00712	0.02009	0.00328	0.00044	0.00079

Arkona, XRF minor elements, corrected, sediment core, Parts per million

	Sc	Ba	V	La	Ce	Nd	Cr	Ni	Cu	Zn
A0-1	8.44	328.58	91.11	32.94	45.45	20.64	81.00	37.11	38.88	159.50
A1-2	11.45	346.72	91.60	37.16	52.77	21.86	85.46	39.14	42.99	165.40
A2-3	9.43	372.54	106.38	40.99	37.20	17.63	96.03	43.25	50.12	171.66
A3-4	11.62	366.45	95.45	39.53	48.66	21.89	83.42	40.26	44.30	173.26
A4-5	15.04	379.43	103.13	32.99	57.58	26.35	86.43	39.74	46.27	192.15
A5-6	16.13	369.82	115.17	42.08	88.91	32.46	87.47	37.63	44.56	225.90
A6-7	14.60	391.27	105.09	40.17	56.74	25.47	88.84	42.24	47.73	216.70
A7-8	10.47	373.75	110.72	40.95	93.72	36.08	88.02	37.95	43.34	230.16
A8-9	13.14	378.71	105.51	42.21	47.07	26.59	89.17	39.21	46.55	201.72
A9-10	14.41	384.23	112.15	45.92	79.40	36.38	88.21	36.38	41.05	214.35
A10-12	15.28	382.81	106.75	45.01	35.72	18.17	90.44	39.95	42.74	174.79
A12-14	14.95	372.04	107.78	40.08	42.47	21.39	85.04	40.39	38.42	134.57
A14-16	14.72	379.77	108.65	37.43	32.76	18.77	89.37	39.60	37.74	123.58
A16-18	12.23	379.20	105.94	45.82	47.68	24.15	88.63	38.87	35.56	117.76
A18-20	16.59	381.64	109.55	39.89	41.43	20.82	89.56	39.68	36.79	98.94
A20-22	12.52	377.04	106.16	42.01	53.39	24.83	84.33	35.49	34.56	95.71
A22-24	13.45	381.76	105.61	42.12	48.68	20.64	88.40	37.53	34.72	99.66
A24-26	11.73	379.96	112.98	47.87	87.96	33.96	98.76	43.30	30.53	106.13
A26-28	13.76	376.49	114.46	42.64	86.00	38.50	88.90	38.19	33.01	106.49
A28-30	15.84	374.14	111.16	49.89	83.73	38.50	90.15	39.95	33.12	102.98
A30-32	14.24	379.28	112.50	47.10	87.23	38.57	89.62	38.99	33.06	105.11
A32-34	12.86	387.67	110.06	44.13	89.69	37.65	86.40	37.75	32.91	103.58
A34-36	12.57	364.73	102.62	40.29	55.43	28.02	87.58	38.64	34.72	96.85
A36-38	12.87	396.56	111.78	41.10	49.92	23.97	86.45	42.14	35.70	97.14
A38-40	11.82	372.53	116.05	40.65	84.94	38.89	90.33	42.31	31.74	103.19
A40-42	12.16	385.34	110.57	47.70	82.93	33.46	86.67	37.93	29.31	98.31
A42-44	11.52	380.78	116.00	45.03	77.50	35.17	86.12	38.39	30.71	100.02
A44-46	13.63	382.26	111.65	42.35	93.89	36.67	93.06	42.66	30.68	101.53
A46-48	11.86	381.24	110.78	43.63	86.54	38.06	86.54	39.40	28.88	99.64

Arkona, XRF minor elements, corrected, sediment core, Parts per million ctd.

	Pb	Th	U	Rb	Sr	Y	Zr	Nb	Mo	I	Br
A0-1	94.86	8.65	5.32	115.51	132.60	28.67	186.29	13.86	1.98	265.31	239.56
A1-2	102.01	8.85	6.25	120.01	128.76	31.23	193.60	14.26	1.87	286.45	214.61
A2-3	106.38	9.12	6.15	122.16	123.91	31.98	200.57	13.84	2.15	276.82	197.60
A3-4	104.37	6.54	7.16	121.18	126.26	31.23	194.43	13.80	1.87	256.16	196.31
A4-5	114.86	8.51	7.57	123.36	128.34	32.58	201.49	14.21	2.91	265.41	183.69
A5-6	120.03	8.48	3.31	132.03	128.20	32.88	212.25	14.58	3.21	275.63	196.79
A6-7	124.14	9.73	5.49	124.56	125.59	32.41	200.45	15.12	2.90	266.09	173.92
A7-8	121.30	8.29	3.11	130.01	130.11	33.38	207.66	13.89	2.18	259.08	194.34
A8-9	124.96	9.00	6.93	121.24	123.31	32.27	193.65	13.86	1.76	256.65	168.54
A9-10	117.64	7.26	3.94	129.15	127.39	33.38	205.95	14.61	2.07	266.49	196.92
A10-12	97.05	9.09	6.30	125.85	123.17	32.52	212.67	14.97	4.03	248.29	175.17
A12-14	74.66	8.10	6.02	125.95	123.15	31.88	208.50	15.06	5.09	235.91	170.74
A14-16	70.40	10.47	8.40	128.77	125.14	32.76	213.99	15.66	3.42	240.22	177.93
A16-18	61.99	9.74	5.70	125.43	123.98	32.55	216.45	15.45	2.70	228.58	185.72
A18-20	51.32	9.79	6.60	125.53	122.95	32.57	216.53	14.33	3.09	212.51	206.79
A20-22	45.73	10.14	6.21	123.44	123.95	33.11	239.32	14.38	3.21	204.76	209.65
A22-24	47.96	9.49	7.19	127.60	124.79	31.48	214.44	15.53	2.92	208.08	199.89
A24-26	48.39	7.17	4.05	135.41	128.25	33.02	224.72	15.89	2.70	213.19	240.89
A26-28	46.98	7.45	2.48	132.16	126.36	33.01	221.67	15.11	2.69	220.23	247.79
A28-30	45.64	6.83	1.66	129.27	123.58	31.15	212.48	14.90	2.59	213.00	249.21
A30-32	45.64	7.90	2.39	130.90	125.49	32.02	218.75	14.87	2.70	219.59	236.06
A32-34	45.46	8.95	2.88	133.92	124.66	31.89	217.13	14.50	2.78	225.26	251.49
A34-36	44.10	8.45	5.46	126.73	123.23	31.53	203.69	15.15	2.37	213.17	237.38
A36-38	39.02	9.55	6.64	128.07	122.98	32.59	206.74	14.63	3.63	217.12	211.84
A38-40	41.48	10.06	2.90	134.20	128.19	32.88	217.79	15.25	3.53	225.67	244.05
A40-42	37.62	6.65	2.70	131.15	126.99	31.59	224.16	14.65	3.12	210.23	238.53
A42-44	38.49	7.78	1.45	132.81	127.20	32.27	216.22	14.84	3.74	221.41	244.28
A44-46	38.63	8.06	2.38	132.21	126.83	32.02	214.42	14.77	3.82	238.90	249.81
A46-48	35.59	8.56	2.37	130.17	126.87	31.87	215.99	14.54	4.33	215.79	246.53

Arkona, XRF minor elements to rubidium ratios, sediment core.

	Sc/Rb	Ba/Rb	V/Rb	La/Rb	Ce/Rb	Nd/Rb	Cr/Rb	Ni/Rb	Cu/Rb	Zn/Rb
A0-1	0.073	2.845	0.789	0.285	0.394	0.179	0.701	0.321	0.337	1.381
A1-2	0.095	2.889	0.763	0.310	0.440	0.182	0.712	0.326	0.358	1.378
A2-3	0.077	3.049	0.871	0.336	0.305	0.144	0.786	0.354	0.410	1.405
A3-4	0.096	3.024	0.788	0.326	0.402	0.181	0.688	0.332	0.366	1.430
A4-5	0.122	3.076	0.836	0.267	0.467	0.214	0.701	0.322	0.375	1.558
A5-6	0.122	2.801	0.872	0.319	0.673	0.246	0.662	0.285	0.338	1.711
A6-7	0.117	3.141	0.844	0.323	0.456	0.204	0.713	0.339	0.383	1.740
A7-8	0.081	2.875	0.852	0.315	0.721	0.278	0.677	0.292	0.333	1.770
A8-9	0.108	3.124	0.870	0.348	0.388	0.219	0.735	0.323	0.384	1.664
A9-10	0.112	2.975	0.868	0.356	0.615	0.282	0.683	0.282	0.318	1.660
A10-12	0.121	3.042	0.848	0.358	0.284	0.144	0.719	0.317	0.340	1.389
A12-14	0.119	2.954	0.856	0.318	0.337	0.170	0.675	0.321	0.305	1.068
A14-16	0.114	2.949	0.844	0.291	0.254	0.146	0.694	0.308	0.293	0.960
A16-18	0.098	3.023	0.845	0.365	0.380	0.193	0.707	0.310	0.283	0.939
A18-20	0.132	3.040	0.873	0.318	0.330	0.166	0.713	0.316	0.293	0.788
A20-22	0.101	3.054	0.860	0.340	0.433	0.201	0.683	0.288	0.280	0.775
A22-24	0.105	2.992	0.828	0.330	0.382	0.162	0.693	0.294	0.272	0.781
A24-26	0.087	2.806	0.834	0.354	0.650	0.251	0.729	0.320	0.225	0.784
A26-28	0.104	2.849	0.866	0.323	0.651	0.291	0.673	0.289	0.250	0.806
A28-30	0.122	2.894	0.860	0.386	0.648	0.298	0.697	0.309	0.256	0.797
A30-32	0.109	2.898	0.859	0.360	0.666	0.295	0.685	0.298	0.253	0.803
A32-34	0.096	2.895	0.822	0.329	0.670	0.281	0.645	0.282	0.246	0.773
A34-36	0.099	2.878	0.810	0.318	0.437	0.221	0.691	0.305	0.274	0.764
A36-38	0.100	3.096	0.873	0.321	0.390	0.187	0.675	0.329	0.279	0.759
A38-40	0.088	2.776	0.865	0.303	0.633	0.290	0.673	0.315	0.236	0.769
A40-42	0.093	2.938	0.843	0.364	0.632	0.255	0.661	0.289	0.223	0.750
A42-44	0.087	2.867	0.873	0.339	0.584	0.265	0.648	0.289	0.231	0.753
A44-46	0.103	2.891	0.845	0.320	0.710	0.277	0.704	0.323	0.232	0.768
A46-48	0.091	2.929	0.851	0.335	0.665	0.292	0.665	0.303	0.222	0.765

Arkona, XRF minor elements to rubidium ratios, sediment core, ctd.

	Pb/Rb	Th/Rb	U/Rb	Sr/Rb	Y/Rb	Zr/Rb	Nb/Rb	Mo/Rb	I/Rb	Br/Rb
A0-1	0.821	0.075	0.046	1.148	0.248	1.613	0.120	0.017	2.297	2.074
A1-2	0.850	0.074	0.052	1.073	0.260	1.613	0.119	0.016	2.387	1.788
A2-3	0.871	0.075	0.050	1.014	0.262	1.642	0.113	0.018	2.266	1.617
A3-4	0.861	0.054	0.059	1.042	0.258	1.604	0.114	0.015	2.114	1.620
A4-5	0.931	0.069	0.061	1.040	0.264	1.633	0.115	0.024	2.151	1.489
A5-6	0.909	0.064	0.025	0.971	0.249	1.608	0.110	0.024	2.088	1.491
A6-7	0.997	0.078	0.044	1.008	0.260	1.609	0.121	0.023	2.136	1.396
A7-8	0.933	0.064	0.024	1.001	0.257	1.597	0.107	0.017	1.993	1.495
A8-9	1.031	0.074	0.057	1.017	0.266	1.597	0.114	0.015	2.117	1.390
A9-10	0.911	0.056	0.030	0.986	0.258	1.595	0.113	0.016	2.063	1.525
A10-12	0.771	0.072	0.050	0.979	0.258	1.690	0.119	0.032	1.973	1.392
A12-14	0.593	0.064	0.048	0.978	0.253	1.655	0.120	0.040	1.873	1.356
A14-16	0.547	0.081	0.065	0.972	0.254	1.662	0.122	0.027	1.866	1.382
A16-18	0.494	0.078	0.045	0.988	0.260	1.726	0.123	0.021	1.822	1.481
A18-20	0.409	0.078	0.053	0.979	0.259	1.725	0.114	0.025	1.693	1.647
A20-22	0.370	0.082	0.050	1.004	0.268	1.939	0.117	0.026	1.659	1.698
A22-24	0.376	0.074	0.056	0.978	0.247	1.681	0.122	0.023	1.631	1.566
A24-26	0.357	0.053	0.030	0.947	0.244	1.660	0.117	0.020	1.574	1.779
A26-28	0.356	0.056	0.019	0.956	0.250	1.677	0.114	0.020	1.666	1.875
A28-30	0.353	0.053	0.013	0.956	0.241	1.644	0.115	0.020	1.648	1.928
A30-32	0.349	0.060	0.018	0.959	0.245	1.671	0.114	0.021	1.678	1.803
A32-34	0.339	0.067	0.022	0.931	0.238	1.621	0.108	0.021	1.682	1.878
A34-36	0.348	0.067	0.043	0.972	0.249	1.607	0.120	0.019	1.682	1.873
A36-38	0.305	0.075	0.052	0.960	0.254	1.614	0.114	0.028	1.695	1.654
A38-40	0.309	0.075	0.022	0.955	0.245	1.623	0.114	0.026	1.682	1.819
A40-42	0.287	0.051	0.021	0.968	0.241	1.709	0.112	0.024	1.603	1.819
A42-44	0.290	0.059	0.011	0.958	0.243	1.628	0.112	0.028	1.667	1.839
A44-46	0.292	0.061	0.018	0.959	0.242	1.622	0.112	0.029	1.807	1.890
A46-48	0.273	0.066	0.018	0.975	0.245	1.659	0.112	0.033	1.658	1.894

Arkona, ICPMS, sediment core, Parts per million.

	Li	Ti	V	Mn	Fe	Co	Ni	Cu	Zn	As
A1-2	39.19	3699	95.81	297.91	33649	21.28	33.17	46.64	217.83	16.30
A2-3	40.94	3680	107.48	316.48	35428	23.71	37.90	49.09	267.24	19.81
A3-4	36.79	3656	98.39	293.21	33234	23.88	34.23	46.66	241.07	19.01
A4-5	38.60	3866	101.43	306.86	33243	16.31	36.54	46.43	226.73	21.14
A5-6	39.56	3844	102.41	292.42	32018	17.88	36.58	50.37	270.41	20.65
A6-7	41.19	3495	109.26	314.00	32473	18.95	37.12	50.80	281.56	19.17
A7-8	38.86	3885	105.66	309.18	31430	18.07	40.67	54.75	277.61	18.41
A8-9	38.54	3758	104.30	309.80	32905	15.23	33.82	51.10	256.27	18.18
A9-10	40.67	4042	102.28	331.82	31758	16.74	36.46	53.35	262.52	20.16
A10-12	35.88	3807	97.39	366.73	37150	15.25	38.55	40.55	162.33	28.32
A12-14	35.83	3478	98.16	436.68	37893	14.38	36.81	34.63	129.20	24.11
A14-16	35.60	3705	95.10	465.68	34806	15.91	39.89	36.08	123.39	17.99
A16-18	37.32	3741	98.44	524.94	36586	13.67	36.21	31.09	104.42	15.27
A18-20	35.79	3435	93.62	533.44	34144	13.79	36.96	32.83	98.20	16.69
A20-22	35.00	3941	101.56	474.79	33122	13.07	35.15	31.72	94.57	16.25
A22-24	35.67	3530	92.88	506.80	34859	13.57	35.79	31.55	92.97	15.82
A24-26	37.97	3886	95.71	497.42	35862	14.68	37.71	33.76	97.08	19.85
A26-28	35.70	3826	100.12	531.27	39239	13.58	38.48	33.15	96.57	15.22
A28-30	37.95	3927	99.39	522.38	39109	14.75	39.90	33.19	98.21	14.43
A30-32	36.51	3951	92.91	510.24	39983	14.21	37.32	32.85	96.58	14.52
A32-34	33.60	3860	91.57	542.04	40058	14.51	38.29	33.02	95.18	17.29
A34-36	34.02	3732	94.36	549.80	40931	14.64	36.87	31.71	97.16	18.19
A36-38	36.34	3823	95.22	533.03	38431	15.97	39.09	31.72	94.04	16.70
A38-40	36.61	3908	96.95	570.63	42105	16.09	38.39	31.48	94.22	16.83
A40-42	32.12	3786	90.16	550.04	40022	14.83	37.23	32.10	93.14	14.90
A42-44	35.45	3596	98.59	540.44	38319	15.28	38.63	32.61	91.33	14.05
A44-46	33.76	3794	95.37	583.09	41056	18.71	38.40	32.80	93.66	19.13

Arkona, ICPMS, sediment core, Parts per million, ctd.

	Rb	Sr	Y	Zr	Sn	Sb	Cs	Ba	Ce	Pb	Th	U
A1-2	105.46	122.56	15.96	125.35	5.26	2.26	5.33	371.31	75.77	83.42	11.19	3.94
A2-3	114.31	118.44	16.80	126.41	5.53	2.06	5.69	389.40	81.15	92.59	12.36	4.31
A3-4	105.41	116.79	16.74	129.00	5.50	2.40	5.58	370.87	76.06	91.43	12.05	4.19
A4-5	108.21	113.94	18.28	134.50	5.82	3.53	5.55	387.61	78.01	96.26	11.49	4.62
A5-6	113.90	116.60	17.90	140.21	6.42	3.45	5.77	394.40	78.61	100.17	12.00	4.68
A6-7	117.70	119.10	16.82	119.78	6.23	3.39	5.70	394.47	79.43	98.18	11.45	4.61
A7-8	111.70	119.55	16.88	129.40	6.38	2.76	5.56	373.06	79.56	102.42	11.59	4.35
A8-9	111.68	121.27	16.75	126.81	6.30	1.75	5.49	351.44	79.20	102.03	10.89	3.80
A9-10	109.76	118.33	17.31	136.59	6.26	1.78	5.60	330.56	80.44	100.06	11.45	3.90
A10-12	112.26	121.13	16.33	136.26	4.57	2.47	5.70	369.43	79.10	79.69	11.11	4.24
A12-14	112.41	114.96	14.96	120.31	3.24	1.82	5.75	367.31	77.82	65.79	12.04	4.38
A14-16	108.17	110.30	16.20	141.37	3.30	3.40	5.89	366.12	79.12	62.06	12.38	4.42
A16-18	112.94	119.86	16.71	127.63	2.85	2.20	5.36	332.17	78.92	54.11	12.25	3.76
A18-20	106.73	111.12	23.33	132.74	2.76	2.23	5.90	372.89	78.47	48.42	13.31	4.38
A20-22	107.55	114.84	23.20	148.94	2.64	1.90	5.49	343.20	78.79	43.96	12.75	4.15
A22-24	110.00	111.34	23.06	140.65	2.73	1.88	5.68	345.75	76.46	46.52	13.29	4.12
A24-26	113.15	114.10	23.95	139.11	2.82	1.12	5.85	353.25	77.34	47.22	13.06	4.24
A26-28	110.05	118.54	23.26	137.36	2.65	2.87	5.73	343.25	77.38	45.92	12.04	4.13
A28-30	113.04	118.17	23.55	135.72	2.77	1.92	5.98	341.97	82.23	45.10	13.89	4.14
A30-32	113.98	117.28	25.04	139.72	2.64	1.76	6.06	347.79	80.42	44.28	13.32	4.42
A32-34	108.15	106.05	24.99	137.97	2.66	1.89	5.96	351.15	80.35	45.76	13.52	4.32
A34-36	109.17	112.20	24.09	139.60	2.66	1.77	5.71	343.98	76.71	42.59	13.49	4.45
A36-38	114.62	115.57	24.81	137.70	2.55	1.37	5.96	357.26	79.93	39.16	13.56	4.69
A38-40	109.74	113.56	25.21	138.43	2.68	1.33	5.83	355.95	79.31	41.25	13.99	4.69
A40-42	108.86	113.66	24.48	137.18	2.68	2.18	5.84	366.10	78.55	40.64	13.77	4.70
A42-44	113.79	111.97	24.73	134.67	2.52	0.68	6.08	375.62	79.71	39.69	13.71	4.75
A44-46	111.95	113.94	25.76	141.93	2.55	0.78	5.82	360.86	78.35	40.38	13.06	4.26

Arkona, ICPMS, Normalised sediment core to rubidium ratios,

	Li/Rb	Ti/Rb	V/Rb	Mn/Rb	Fe/Rb	Co/Rb	Ni/Rb	Cu/Rb	Zn/Rb	As/Rb
A1-2	0.37	35.07	0.91	2.82	319.08	0.20	0.31	0.44	2.07	0.15
A2-3	0.36	32.19	0.94	2.77	309.92	0.21	0.33	0.43	2.34	0.17
A3-4	0.35	34.68	0.93	2.78	315.28	0.23	0.32	0.44	2.29	0.18
A4-5	0.36	35.72	0.94	2.84	307.20	0.15	0.34	0.43	2.10	0.20
A5-6	0.35	33.75	0.90	2.57	281.09	0.16	0.32	0.44	2.37	0.18
A6-7	0.35	29.70	0.93	2.67	275.90	0.16	0.32	0.43	2.39	0.16
A7-8	0.35	34.78	0.95	2.77	281.37	0.16	0.36	0.49	2.49	0.16
A8-9	0.35	33.65	0.93	2.77	294.64	0.14	0.30	0.46	2.29	0.16
A9-10	0.37	36.82	0.93	3.02	289.34	0.15	0.33	0.49	2.39	0.18
A10-12	0.32	33.91	0.87	3.27	330.94	0.14	0.34	0.36	1.45	0.25
A12-14	0.32	30.94	0.87	3.88	337.09	0.13	0.33	0.31	1.15	0.21
A14-16	0.33	34.25	0.88	4.31	321.77	0.15	0.37	0.33	1.14	0.17
A16-18	0.33	33.12	0.87	4.65	323.95	0.12	0.32	0.28	0.92	0.14
A18-20	0.34	32.18	0.88	5.00	319.91	0.13	0.35	0.31	0.92	0.16
A20-22	0.33	36.65	0.94	4.41	307.98	0.12	0.33	0.29	0.88	0.15
A22-24	0.32	32.09	0.84	4.61	316.90	0.12	0.33	0.29	0.85	0.14
A24-26	0.34	34.34	0.85	4.40	316.96	0.13	0.33	0.30	0.86	0.18
A26-28	0.32	34.77	0.91	4.83	356.55	0.12	0.35	0.30	0.88	0.14
A28-30	0.34	34.74	0.88	4.62	345.97	0.13	0.35	0.29	0.87	0.13
A30-32	0.32	34.66	0.82	4.48	350.78	0.12	0.33	0.29	0.85	0.13
A32-34	0.31	35.69	0.85	5.01	370.40	0.13	0.35	0.31	0.88	0.16
A34-36	0.31	34.18	0.86	5.04	374.94	0.13	0.34	0.29	0.89	0.17
A36-38	0.32	33.35	0.83	4.65	335.29	0.14	0.34	0.28	0.82	0.15
A38-40	0.33	35.61	0.88	5.20	383.68	0.15	0.35	0.29	0.86	0.15
A40-42	0.30	34.78	0.83	5.05	367.64	0.14	0.34	0.29	0.86	0.14
A42-44	0.31	31.61	0.87	4.75	336.75	0.13	0.34	0.29	0.80	0.12
A44-46	0.30	33.89	0.85	5.21	366.74	0.17	0.34	0.29	0.84	0.17

Arkona, ICPMS, Normalised sediment core to rubidium ratios, ctd.

	Sr/Rb	Y/Rb	Zr/Rb	Sn/Rb	Sb/Rb	Cs/Rb	Ba/Rb	Ce/Rb	Pb/Rb	Th/Rb	U/Rb
A1-2	1.162	0.151	1.189	0.050	0.021	0.051	3.521	0.719	0.791	0.106	0.037
A2-3	1.036	0.147	1.106	0.048	0.018	0.050	3.406	0.710	0.810	0.108	0.038
A3-4	1.108	0.159	1.224	0.052	0.023	0.053	3.518	0.722	0.867	0.114	0.040
A4-5	1.053	0.169	1.243	0.054	0.033	0.051	3.582	0.721	0.890	0.106	0.043
A5-6	1.024	0.157	1.231	0.056	0.030	0.051	3.463	0.690	0.879	0.105	0.041
A6-7	1.012	0.143	1.018	0.053	0.029	0.048	3.352	0.675	0.834	0.097	0.039
A7-8	1.070	0.151	1.158	0.057	0.025	0.050	3.340	0.712	0.917	0.104	0.039
A8-9	1.086	0.150	1.135	0.056	0.016	0.049	3.147	0.709	0.914	0.098	0.034
A9-10	1.078	0.158	1.244	0.057	0.016	0.051	3.012	0.733	0.912	0.104	0.036
A10-12	1.079	0.145	1.214	0.041	0.022	0.051	3.291	0.705	0.710	0.099	0.038
A12-14	1.023	0.133	1.070	0.029	0.016	0.051	3.268	0.692	0.585	0.107	0.039
A14-16	1.020	0.150	1.307	0.030	0.031	0.054	3.385	0.731	0.574	0.114	0.041
A16-18	1.061	0.148	1.130	0.025	0.020	0.048	2.941	0.699	0.479	0.108	0.033
A18-20	1.041	0.219	1.244	0.026	0.021	0.055	3.494	0.735	0.454	0.125	0.041
A20-22	1.068	0.216	1.385	0.025	0.018	0.051	3.191	0.733	0.409	0.119	0.039
A22-24	1.012	0.210	1.279	0.025	0.017	0.052	3.143	0.695	0.423	0.121	0.037
A24-26	1.008	0.212	1.229	0.025	0.010	0.052	3.122	0.684	0.417	0.115	0.038
A26-28	1.077	0.211	1.248	0.024	0.026	0.052	3.119	0.703	0.417	0.109	0.038
A28-30	1.045	0.208	1.201	0.024	0.017	0.053	3.025	0.727	0.399	0.123	0.037
A30-32	1.029	0.220	1.226	0.023	0.015	0.053	3.051	0.706	0.388	0.117	0.039
A32-34	0.981	0.231	1.276	0.025	0.017	0.055	3.247	0.743	0.423	0.125	0.040
A34-36	1.028	0.221	1.279	0.024	0.016	0.052	3.151	0.703	0.390	0.124	0.041
A36-38	1.008	0.216	1.201	0.022	0.012	0.052	3.117	0.697	0.342	0.118	0.041
A38-40	1.035	0.230	1.261	0.024	0.012	0.053	3.244	0.723	0.376	0.127	0.043
A40-42	1.044	0.225	1.260	0.025	0.020	0.054	3.363	0.722	0.373	0.127	0.043
A42-44	0.984	0.217	1.183	0.022	0.006	0.053	3.301	0.701	0.349	0.121	0.042
A44-46	1.018	0.230	1.268	0.023	0.007	0.052	3.223	0.700	0.361	0.117	0.038

Wiek, XRF major elements, salt corrected, sediment core, Wt. %

	Si	Al	Fe	Na	Mg	Ca	K	Ti	Mn	P
W1-2	36.635	2.920	1.314	0.766	0.456	0.932	1.537	0.220	0.016	0.073
W2-3	40.376	2.424	0.725	0.461	0.238	0.711	1.482	0.186	0.006	0.041
W3-4	40.754	2.378	0.696	0.576	0.243	0.669	1.462	0.199	0.010	0.039
W4-5	41.379	2.350	0.752	0.514	0.238	0.411	1.424	0.196	0.008	0.036
W5-6	42.046	2.173	0.716	0.395	0.174	0.325	1.342	0.178	0.008	0.029
W6-7	41.374	2.173	0.758	0.378	0.192	0.318	1.332	0.177	0.010	0.030
W7-8	40.905	2.366	0.850	0.647	0.245	0.404	1.403	0.182	0.014	0.032
W8-9	40.374	2.559	1.054	0.848	0.303	0.489	1.506	0.198	0.016	0.036
W9-10	39.934	2.591	1.068	0.736	0.351	0.504	1.530	0.205	0.016	0.036
W10-12	39.826	2.559	1.061	0.460	0.345	0.583	1.538	0.205	0.017	0.042
W12-14	40.206	2.542	0.991	0.589	0.334	0.676	1.487	0.209	0.014	0.035
W14-16	39.607	2.666	1.153	0.697	0.381	0.755	1.551	0.215	0.013	0.039
W16-18	38.992	2.745	1.244	0.563	0.424	0.733	1.606	0.221	0.016	0.039

Wiek, XRF major elements, normalised sediment core to rubidium, (x 10^4)

	Si/Rb	Al/Rb	Fe/Rb	Na/Rb	Mg/Rb	Ca/Rb	K/Rb	Ti/Rb	Mn/Rb	P/Rb
W1-2	0.61788	0.04924	0.02209	0.01298	0.00776	0.01568	0.02597	0.00371	0.00034	0.00118
W2-3	0.81576	0.04889	0.01455	0.00929	0.00485	0.01434	0.02990	0.00384	0.00020	0.00081
W3-4	0.81337	0.04750	0.01397	0.01158	0.00479	0.01337	0.02914	0.00399	0.00020	0.00080
W4-5	0.86208	0.04896	0.01563	0.01063	0.00500	0.00854	0.02958	0.00417	0.00021	0.00083
W5-6	0.92418	0.04769	0.01582	0.00857	0.00374	0.00725	0.02945	0.00396	0.00022	0.00066
W6-7	0.90131	0.04728	0.01656	0.00828	0.00414	0.00697	0.02898	0.00392	0.00022	0.00065
W7-8	0.86469	0.05011	0.01797	0.01374	0.00507	0.00846	0.02960	0.00381	0.00021	0.00063
W8-9	0.77042	0.04885	0.02004	0.01622	0.00573	0.00935	0.02882	0.00382	0.00038	0.00076
W9-10	0.74496	0.04832	0.01996	0.01381	0.00653	0.00933	0.02854	0.00373	0.00037	0.00075
W10-12	0.73487	0.04723	0.01956	0.00849	0.00646	0.01070	0.02841	0.00387	0.00037	0.00074
W12-14	0.73915	0.04669	0.01820	0.01085	0.00607	0.01250	0.02739	0.00386	0.00018	0.00074
W14-16	0.54732	0.04935	0.02126	0.01294	0.00702	0.01386	0.02865	0.00407	0.00018	0.00074
W16-18	0.69254	0.04885	0.02202	0.00995	0.00746	0.01297	0.02860	0.00391	0.00036	0.00071

Wiek, XRF minor elements, corrected, sediment core, Parts per million

	Sc	Ba	V	La	Ce	Nd	Cr	Ni	Cu	Zn	Pb
W1-2	4.47	338.48	32.91	20.22	48.35	19.71	42.87	14.83	16.46	80.66	34.34
W2-3	6.34	360.61	23.14	30.39	37.93	10.97	29.58	6.34	7.55	36.52	16.50
W3-4	4.42	361.59	22.16	23.97	40.39	15.68	32.46	8.59	7.49	35.37	18.79
W4-5	5.02	334.57	17.58	22.40	38.07	19.69	31.74	8.34	7.53	38.17	20.89
W5-6	3.91	308.52	20.37	17.66	36.03	19.27	27.80	5.32	4.22	30.91	17.56
W6-7	3.21	289.77	14.86	24.49	36.94	16.26	21.18	5.22	4.10	23.19	13.85
W7-8	3.31	331.37	21.89	27.41	36.55	18.07	25.30	6.93	4.72	16.47	10.74
W8-9	4.72	351.13	24.42	55.17	39.49	20.10	28.54	8.64	8.04	13.27	6.43
W9-10	5.93	335.45	26.63	18.99	40.30	22.01	29.55	9.04	4.82	17.18	9.15
W10-12	5.02	351.93	24.92	25.83	42.81	21.31	27.33	9.04	6.23	17.08	8.24
W12-14	4.72	335.04	27.63	27.83	41.09	20.69	31.34	8.84	6.83	19.29	7.84
W14-16	6.74	330.43	27.14	18.09	43.02	23.92	37.60	10.15	7.64	19.00	8.54
W16-18	6.23	356.77	28.74	20.00	40.30	22.61	35.07	9.95	7.94	19.09	7.74

Wiek, XRF minor elements, corrected, sediment core, Parts per million, ctd.

	Th	U	Rb	Sr	Y	Zr	Nb	Mo	I	Br
W1-2	2.23	0.71	60.24	102.90	16.35	249.59	7.31	0.91	47.54	60.63
W2-3	1.11	1.81	49.80	88.14	12.98	280.11	6.04	0.80	15.39	12.95
W3-4	3.32	1.36	50.34	88.12	14.82	382.44	6.48	1.11	24.62	12.19
W4-5	3.11	0.60	48.21	73.32	15.17	408.59	6.23	1.10	14.97	11.32
W5-6	3.41	2.01	45.67	69.65	13.85	425.75	5.22	1.41	3.41	6.62
W6-7	3.01	1.61	46.07	67.95	13.45	384.93	6.02	1.81	5.12	8.79
W7-8	3.92	0.20	47.50	70.99	14.36	339.00	5.02	1.10	6.13	15.09
W8-9	3.01	1.51	52.66	75.47	15.78	343.89	6.53	2.11	12.66	20.46
W9-10	3.32	1.00	53.87	77.18	17.29	352.44	7.14	1.51	7.64	23.34
W10-12	4.12	0.30	54.47	79.39	16.78	343.79	6.63	1.51	2.01	20.84
W12-14	3.52	0.90	54.65	81.57	16.88	386.67	7.74	2.41	17.08	21.18
W14-16	3.72	0.30	54.38	81.73	16.79	313.24	6.43	1.81	4.83	20.08
W16-18	4.52	0.20	56.58	81.10	16.98	344.51	7.74	2.01	8.64	24.39

Wiek, XRF minor elements, normalised sediment core to rubidium,

	Sc/Rb	Ba/Rb	V/Rb	La/Rb	Ce/Rb	Nd/Rb	Cr/Rb	Ni/Rb	Cu/Rb	Zn/Rb
W1-2	0.074	5.619	0.546	0.336	0.803	0.327	0.712	0.246	0.273	1.339
W2-3	0.127	7.240	0.465	0.610	0.762	0.220	0.594	0.127	0.152	0.733
W3-4	0.088	7.183	0.440	0.476	0.802	0.311	0.645	0.171	0.149	0.703
W4-5	0.104	6.940	0.365	0.465	0.790	0.408	0.658	0.173	0.156	0.792
W5-6	0.086	6.756	0.446	0.387	0.789	0.422	0.609	0.116	0.092	0.677
W6-7	0.070	6.290	0.322	0.532	0.802	0.353	0.460	0.113	0.089	0.503
W7-8	0.070	6.977	0.461	0.577	0.770	0.381	0.533	0.146	0.099	0.347
W8-9	0.090	6.668	0.464	1.048	0.750	0.382	0.542	0.164	0.153	0.252
W9-10	0.110	6.228	0.494	0.353	0.748	0.409	0.549	0.168	0.090	0.319
W10-12	0.092	6.461	0.458	0.474	0.786	0.391	0.502	0.166	0.114	0.314
W12-14	0.086	6.131	0.506	0.509	0.752	0.379	0.574	0.162	0.125	0.353
W14-16	0.124	6.076	0.499	0.333	0.791	0.440	0.691	0.187	0.140	0.349
W16-18	0.110	6.306	0.508	0.353	0.712	0.400	0.620	0.176	0.140	0.337

Wiek, XRF minor elements, normalised sediment core to rubidium, ctd.

	Pb/Rb	Th/Rb	U/Rb	Sr/Rb	Y/Rb	Zr/Rb	Nb/Rb	Mo/Rb	I/Rb	Br/Rb
W1-2	0.570	0.037	0.012	1.708	0.272	4.143	0.121	0.015	0.789	1.006
W2-3	0.331	0.022	0.036	1.770	0.261	5.624	0.121	0.016	0.309	0.260
W3-4	0.373	0.066	0.027	1.750	0.294	7.597	0.129	0.022	0.489	0.242
W4-5	0.433	0.065	0.013	1.521	0.315	8.475	0.129	0.023	0.310	0.235
W5-6	0.385	0.075	0.044	1.525	0.303	9.323	0.114	0.031	0.075	0.145
W6-7	0.301	0.065	0.035	1.475	0.292	8.355	0.131	0.039	0.111	0.191
W7-8	0.226	0.082	0.004	1.495	0.302	7.137	0.106	0.023	0.129	0.318
W8-9	0.122	0.057	0.029	1.433	0.300	6.531	0.124	0.040	0.240	0.388
W9-10	0.170	0.062	0.019	1.433	0.321	6.543	0.132	0.028	0.142	0.433
W10-12	0.151	0.076	0.006	1.458	0.308	6.312	0.122	0.028	0.037	0.383
W12-14	0.143	0.064	0.017	1.493	0.309	7.075	0.142	0.044	0.313	0.388
W14-16	0.157	0.068	0.006	1.503	0.309	5.760	0.118	0.033	0.089	0.369
W16-18	0.137	0.080	0.004	1.433	0.300	6.089	0.137	0.036	0.153	0.431

Wiek, ICPMS, sediment core, Parts per million.

	Li	Ti	V	Mn	Fe	Co	Ni	Cu	Zn	As
W1-2	14.77	1786	37.79	154.56	13533	10.07	18.94	20.95	95.61	7.30
W2-3	7.26	1259	19.77	96.52	6283	3.76	9.32	12.08	40.79	3.29
W3-4	8.76	1766	22.85	116.66	7166	46.00	9.25	8.98	46.65	3.84
W4-5	8.49	1730	21.42	107.89	7782	38.66	9.15	9.00	48.45	4.96
W5-6	7.43	1504	19.25	103.83	7510	40.80	7.17	15.75	47.64	4.72
W6-7	7.99	1139	18.89	104.60	7141	29.92	7.67	8.71	29.13	4.07
W7-8	9.34	1320	22.93	141.88	8970	39.29	8.39	8.68	23.36	4.24
W8-9	11.03	1619	27.24	153.45	9775	45.70	10.33	11.93	25.41	4.94
W9-10	11.15	1591	27.36	157.91	10547	40.59	10.57	9.79	111.33	4.33
W10-12	10.94	1634	28.18	164.69	9873	21.12	9.58	11.48	24.65	4.69
W12-14	10.16	1658	27.00	171.24	9800	15.17	9.97	8.05	20.31	4.43
W14-16	11.37	1690	28.96	176.34	11286	18.65	10.87	11.79	25.02	4.85
W16-18	12.28	1721	31.26	196.57	11661	30.48	11.54	11.21	26.16	5.09

Wiek, ICPMS, sediment core, Parts per million. ctd.

	Rb	Sr	Y	Zr	Sn	Sb	Cs	Ba	Ce	Pb	Th	U
W1-2	58.41	75.06	12.02	99.43	1.86	1.68	1.59	307.29	38.59	34.32	5.86	1.63
W2-3	47.85	61.68	7.42	69.81	0.92	1.52	0.64	302.49	23.32	15.47	2.86	0.61
W3-4	50.34	68.60	11.46	140.04	1.00	1.57	0.21	326.87	33.12	18.75	4.53	1.30
W4-5	49.26	59.20	10.40	134.26	1.25	1.63	0.75	303.75	33.14	20.23	4.79	1.51
W5-6	46.17	54.11	9.40	102.51	0.84	0.99	0.45	288.92	32.20	17.57	4.86	1.26
W6-7	45.98	57.43	8.77	115.07	0.89	1.41	0.93	258.64	30.28	15.26	4.61	1.36
W7-8	50.47	66.46	10.53	111.97	0.75	1.22	0.87	280.35	32.83	10.83	4.62	1.59
W8-9	54.43	74.59	12.10	134.20	0.87	1.49	1.21	295.55	36.42	10.02	5.24	1.92
W9-10	55.52	71.23	11.70	131.41	0.84	1.58	1.30	289.37	34.72	9.96	5.10	1.92
W10-12	55.36	75.23	12.53	144.76	0.86	0.95	1.30	300.12	37.41	9.55	5.18	1.90
W12-14	53.85	75.50	11.50	136.62	0.83	1.36	1.18	297.11	36.55	9.22	5.09	1.79
W14-16	58.24	83.69	12.52	133.63	0.86	1.67	1.34	303.47	36.30	10.02	5.33	1.98
W16-18	60.10	79.89	12.61	128.57	0.95	1.59	1.47	307.45	38.23	9.77	5.73	2.13

Wiek, ICPMS, normalised sediment core to rubidium,

	Li/Rb	Ti/Rb	V/Rb	Mn/Rb	Fe/Rb	Co/Rb	Ni/Rb	Cu/Rb	Zn/Rb	As/Rb
W1-2	0.25	30.58	0.65	2.65	231.69	0.17	0.32	0.36	1.64	0.125
W2-3	0.15	26.30	0.41	2.02	131.28	0.08	0.19	0.25	0.85	0.069
W3-4	0.17	35.08	0.45	2.32	142.35	0.91	0.18	0.18	0.93	0.076
W4-5	0.17	35.13	0.43	2.19	157.98	0.78	0.19	0.18	0.98	0.101
W5-6	0.16	32.58	0.42	2.25	162.64	0.88	0.16	0.34	1.03	0.102
W6-7	0.17	24.78	0.41	2.28	155.32	0.65	0.17	0.19	0.63	0.089
W7-8	0.19	26.16	0.45	2.81	177.72	0.78	0.17	0.17	0.46	0.084
W8-9	0.20	29.75	0.50	2.82	179.60	0.84	0.19	0.22	0.47	0.091
W9-10	0.20	28.66	0.49	2.84	189.97	0.73	0.19	0.18	2.01	0.078
W10-12	0.20	29.52	0.51	2.97	178.33	0.38	0.17	0.21	0.45	0.085
W12-14	0.19	30.78	0.50	3.18	181.99	0.28	0.19	0.15	0.38	0.082
W14-16	0.20	29.01	0.50	3.03	193.76	0.32	0.19	0.20	0.43	0.083
W16-18	0.20	28.64	0.52	3.27	194.04	0.51	0.19	0.19	0.44	0.085

Wiek, ICPMS, normalised sediment core to rubidium, ctd.

	Sr/Rb	Y/Rb	Zr/Rb	Sn/Rb	Sb/Rb	Cs/Rb	Ba/Rb	Ce/Rb	Pb/Rb	Th/Rb	U/Rb
W1-2	1.285	0.206	1.702	0.032	0.029	0.027	5.261	0.661	0.588	0.100	0.028
W2-3	1.289	0.155	1.459	0.019	0.032	0.013	6.321	0.487	0.323	0.060	0.013
W3-4	1.363	0.228	2.782	0.020	0.031	0.004	6.493	0.658	0.372	0.090	0.026
W4-5	1.202	0.211	2.726	0.025	0.033	0.015	6.166	0.673	0.411	0.097	0.031
W5-6	1.172	0.204	2.220	0.018	0.021	0.010	6.257	0.697	0.381	0.105	0.027
W6-7	1.249	0.191	2.503	0.019	0.031	0.020	5.626	0.659	0.332	0.100	0.030
W7-8	1.317	0.209	2.218	0.015	0.024	0.017	5.555	0.650	0.215	0.092	0.032
W8-9	1.371	0.222	2.466	0.016	0.027	0.022	5.430	0.669	0.184	0.096	0.035
W9-10	1.283	0.211	2.367	0.015	0.028	0.023	5.212	0.625	0.179	0.092	0.035
W10-12	1.359	0.226	2.615	0.015	0.017	0.024	5.421	0.676	0.173	0.094	0.034
W12-14	1.402	0.213	2.537	0.015	0.025	0.022	5.517	0.679	0.171	0.094	0.033
W14-16	1.437	0.215	2.294	0.015	0.029	0.023	5.210	0.623	0.172	0.092	0.034
W16-18	1.329	0.210	2.139	0.016	0.027	0.024	5.116	0.636	0.163	0.095	0.035

Nord-Perd, XRF major elements, salt corrected, sediment core, Wt. %

	Si	Al	Fe	Na	Mg	Ca	K	Ti	Mn	P
NP0-1	N.S.	N.S.	N.S.	N.S.	N.S.	N.S.	N.S.	N.S.	N.S.	N.S.
NP1-2	N.S.	N.S.	N.S.	N.S.	N.S.	N.S.	N.S.	N.S.	N.S.	N.S.
NP2-3	N.S.	N.S.	N.S.	N.S.	N.S.	N.S.	N.S.	N.S.	N.S.	N.S.
NP3-4	N.S.	N.S.	N.S.	N.S.	N.S.	N.S.	N.S.	N.S.	N.S.	N.S.
NP4-5	37.644	1.861	0.731	0.513	0.147	0.569	1.087	0.163	0.010	0.025
NP5-6	41.988	1.912	0.674	0.428	0.139	0.383	1.147	0.176	0.015	0.023
NP6-7	42.054	1.853	0.673	0.404	0.129	0.326	1.140	0.171	0.012	0.021
NP7-8	42.400	1.783	0.575	0.555	0.106	0.291	1.113	0.164	0.009	0.021
NP8-9	42.558	1.789	0.568	0.370	0.100	0.240	1.087	0.160	0.009	0.019
NP9-10	42.221	1.842	0.708	0.554	0.123	0.233	1.092	0.167	0.012	0.021
NP10-12	41.820	1.780	0.709	0.428	0.132	0.748	1.082	0.177	0.014	0.023
NP12-14	40.351	1.780	0.723	0.405	0.162	1.817	1.063	0.175	0.013	0.023
NP14-16	40.212	1.796	0.751	0.523	0.162	1.938	1.078	0.191	0.014	0.025
NP16-18	38.729	1.705	0.653	0.447	0.163	3.400	1.032	0.172	0.019	0.024
NP18-20	N.S.	N.S.	N.S.	N.S.	N.S.	N.S.	N.S.	N.S.	N.S.	N.S.
NP20-22	40.718	1.832	0.744	0.491	0.177	1.558	1.107	0.197	0.017	0.025
NP22-24	44.638	1.816	0.687	0.362	0.207	1.451	1.098	0.198	0.015	0.025
NP24-26	40.971	1.810	0.666	0.435	0.177	1.508	1.075	0.209	0.013	0.025
NP26-28	41.095	1.922	0.715	0.451	0.171	1.315	1.092	0.212	0.014	0.025
NP28-30	41.243	1.805	0.666	0.435	0.171	1.522	1.097	0.194	0.017	0.023
NP30-32	40.758	1.826	0.666	0.508	0.189	1.236	1.080	0.192	0.016	0.025
NP32-34	47.538	2.022	0.869	0.480	0.232	3.477	1.210	0.187	0.016	0.043
NP34-36	40.705	1.714	0.638	0.408	0.166	2.031	1.006	0.160	0.014	0.028

N.S. No Sample

Nord-Perd, XRF major elements, normalised sediment core to rubidium ratio, (x 10^4)

	Si/Rb	Al/Rb	Fe/Rb	Na/Rb	Mg/Rb	Ca/Rb	K/Rb	Ti/Rb	Mn/Rb	P/Rb
NP0-1	N.S.	N.S.	N.S.	N.S.	N.S.	N.S.	N.S.	N.S.	N.S.	N.S.
NP1-2	N.S.	N.S.	N.S.	N.S.	N.S.	N.S.	N.S.	N.S.	N.S.	N.S.
NP2-3	N.S.	N.S.	N.S.	N.S.	N.S.	N.S.	N.S.	N.S.	N.S.	N.S.
NP3-4	N.S.	N.S.	N.S.	N.S.	N.S.	N.S.	N.S.	N.S.	N.S.	N.S.
NP4-5	0.87565	0.04329	0.01700	0.01192	0.00342	0.01323	0.02528	0.00380	0.00024	0.00057
NP5-6	1.04106	0.04741	0.01670	0.01061	0.00345	0.00950	0.02843	0.00435	0.00037	0.00056
NP6-7	1.05099	0.04631	0.01683	0.01010	0.00321	0.00815	0.02849	0.00427	0.00029	0.00052
NP7-8	1.10717	0.04657	0.01501	0.01450	0.00276	0.00759	0.02907	0.00428	0.00024	0.00054
NP8-9	1.14120	0.04796	0.01523	0.00993	0.00267	0.00645	0.02916	0.00430	0.00025	0.00052
NP9-10	1.11530	0.04866	0.01871	0.01463	0.00324	0.00616	0.02884	0.00440	0.00033	0.00054
NP10-12	1.11725	0.04755	0.01894	0.01143	0.00353	0.01999	0.02890	0.00472	0.00037	0.00061
NP12-14	1.07483	0.04742	0.01926	0.01080	0.00430	0.04839	0.02832	0.00466	0.00035	0.00062
NP14-16	1.07421	0.04797	0.02006	0.01397	0.00433	0.05178	0.02881	0.00509	0.00037	0.00066
NP16-18	1.07816	0.04747	0.01817	0.01244	0.00453	0.09466	0.02872	0.00479	0.00052	0.00066
NP18-20	N.S.	N.S.	N.S.	N.S.	N.S.	N.S.	N.S.	N.S.	N.S.	N.S.
NP20-22	1.03571	0.04659	0.01891	0.01250	0.00450	0.03963	0.02817	0.00502	0.00043	0.00063
NP22-24	1.17146	0.04765	0.01804	0.00949	0.00544	0.03807	0.02882	0.00519	0.00039	0.00064
NP24-26	1.13491	0.05015	0.01846	0.01205	0.00491	0.04177	0.02978	0.00578	0.00037	0.00068
NP26-28	1.07849	0.05043	0.01877	0.01185	0.00449	0.03450	0.02867	0.00557	0.00037	0.00067
NP28-30	1.10557	0.04839	0.01786	0.01165	0.00458	0.04081	0.02942	0.00520	0.00046	0.00062
NP30-32	1.03944	0.04658	0.01699	0.01295	0.00482	0.03152	0.02754	0.00491	0.00040	0.00065
NP32-34	1.30989	0.05572	0.02396	0.01323	0.00640	0.09581	0.03334	0.00517	0.00045	0.00119
NP34-36	1.13421	0.04777	0.01778	0.01136	0.00463	0.05658	0.02803	0.00447	0.00039	0.00078

N.S. = No Sample

Nord-Perd, XRF minor elements, corrected, sediment core, Parts per million

	Sc	Ba	V	La	Ce	Nd	Cr	Ni	Cu	Zn
NP0-1	N.S.	N.S.	N.S.	N.S.	N.S.	N.S.	N.S.	N.S.	N.S.	N.S.
NP1-2	N.S.	N.S.	N.S.	N.S.	N.S.	N.S.	N.S.	N.S.	N.S.	N.S.
NP2-3	N.S.	N.S.	N.S.	N.S.	N.S.	N.S.	N.S.	N.S.	N.S.	N.S.
NP3-4	N.S.	N.S.	N.S.	N.S.	N.S.	N.S.	N.S.	N.S.	N.S.	N.S.
NP4-5	3.92	292.89	21.09	18.78	41.18	12.76	29.93	7.33	13.56	33.65
NP5-6	2.31	282.03	16.75	15.35	39.53	14.15	20.47	4.72	4.01	22.07
NP6-7	6.52	272.17	13.54	12.74	36.30	12.84	17.75	5.82	3.31	16.65
NP7-8	3.31	271.98	14.44	10.93	38.60	18.85	24.56	5.91	3.41	11.73
NP8-9	1.70	283.80	10.73	15.64	34.49	16.44	23.46	3.31	2.91	8.52
NP9-10	3.76	272.46	15.39	18.65	40.36	18.30	27.93	4.66	6.27	11.23
NP10-12	3.41	280.09	17.16	19.67	37.23	16.76	25.49	3.41	6.32	9.33
NP12-14	4.92	282.97	18.17	17.37	44.27	9.94	31.62	4.72	8.03	10.04
NP14-16	2.91	272.98	19.47	16.86	34.62	12.14	28.50	5.82	8.93	11.04
NP16-18	6.32	273.33	18.56	18.86	34.92	10.74	33.41	6.22	8.93	10.54
NP18-20	N.S.	N.S.	N.S.	N.S.	N.S.	N.S.	N.S.	N.S.	N.S.	N.S.
NP20-22	3.41	289.44	18.45	19.36	44.23	22.47	26.88	5.22	4.71	10.03
NP22-24	6.42	278.07	16.75	22.26	42.22	24.57	22.16	4.61	4.81	10.33
NP24-26	4.51	250.50	14.54	14.64	83.73	20.86	27.58	4.81	4.41	12.94
NP26-28	5.01	253.80	16.04	20.76	41.31	23.26	29.98	4.41	4.11	10.03
NP28-30	2.31	287.20	18.05	30.18	38.01	20.66	26.07	4.71	3.71	9.73
NP30-32	6.82	272.48	14.34	16.65	34.20	18.35	29.78	6.22	4.81	10.73
NP32-34	3.81	259.76	15.74	11.43	35.99	11.33	24.36	6.72	5.61	10.83
NP34-36	1.70	259.24	13.93	62.45	39.50	19.45	27.67	5.81	7.12	9.12

N.S. = No Sample

Nord-Perd, XRF minor elements, corrected, sediment core, Parts per million, ctd.

	Pb	Th	U	Rb	Sr	Y	Zr	Nb	Mo	I	Br
NP0-1	N.S.	N.S.	N.S.	N.S.	N.S.	N.S.	N.S.	N.S.	N.S.	N.S.	N.S.
NP1-2	N.S.	N.S.	N.S.	N.S.	N.S.	N.S.	N.S.	N.S.	N.S.	N.S.	N.S.
NP2-3	N.S.	N.S.	N.S.	N.S.	N.S.	N.S.	N.S.	N.S.	N.S.	N.S.	N.S.
NP3-4	N.S.	N.S.	N.S.	N.S.	N.S.	N.S.	N.S.	N.S.	N.S.	N.S.	N.S.
NP4-5	19.59	2.61	1.71	42.99	75.43	11.35	429.09	4.52	1.21	14.87	19.59
NP5-6	14.05	3.11	1.61	40.33	66.32	11.54	445.36	5.42	0.70	3.91	12.94
NP6-7	9.83	1.91	0.60	40.01	64.48	11.43	409.46	4.81	1.10	10.73	12.33
NP7-8	8.62	2.31	0.10	38.30	62.26	12.23	493.74	5.61	1.10	14.14	9.72
NP8-9	7.72	2.51	0.90	37.29	60.15	12.83	467.25	4.41	1.30	8.50	9.92
NP9-10	7.32	3.31	0.80	37.86	75.91	14.34	561.07	5.52	1.86	7.17	15.34
NP10-12	5.82	2.51	0.20	37.43	73.96	13.65	483.90	5.12	1.61	4.62	14.25
NP12-14	5.72	3.71	1.41	37.54	104.19	13.65	475.09	5.82	1.61	8.83	15.86
NP14-16	5.32	4.01	0.30	37.43	107.99	13.65	489.25	4.82	1.71	9.43	15.35
NP16-18	5.52	2.71	0.60	35.92	149.51	12.64	436.78	4.82	1.91	9.93	18.06
NP18-20	N.S.	N.S.	N.S.	N.S.	N.S.	N.S.	N.S.	N.S.	N.S.	N.S.	N.S.
NP20-22	7.22	4.71	0.10	39.31	99.29	14.74	537.46	5.92	1.60	6.62	17.95
NP22-24	7.02	4.01	0.70	38.11	96.67	14.74	538.38	5.41	2.11	6.62	17.55
NP24-26	5.31	4.71	2.81	36.10	90.05	14.24	535.90	6.82	1.70	2.91	11.73
NP26-28	4.71	3.71	0.30	38.10	98.17	15.74	658.41	6.32	2.21	7.42	18.55
NP28-30	5.52	3.71	0.40	37.30	97.97	15.04	523.27	6.32	1.70	8.93	20.36
NP30-32	5.32	4.81	0.10	39.21	89.45	14.44	539.03	6.32	2.01	4.91	22.16
NP32-34	4.41	2.81	2.51	36.29	137.55	11.83	360.81	5.01	2.41	4.41	21.55
NP34-36	4.71	2.41	0.70	35.89	123.91	13.43	452.62	5.61	2.31	11.83	20.65

N.S. = No Sample

Nord-Perd, XRF minor elements, normalised sediment core to rubidium ratios.

	Sc/Rb	Ba/Rb	V/Rb	La/Rb	Ce/Rb	Nd/Rb	Cr/Rb	Ni/Rb	Cu/Rb	Zn/Rb
NP0-1	N.S.	N.S.	N.S.	N.S.	N.S.	N.S.	N.S.	N.S.	N.S.	N.S.
NP1-2	N.S.	N.S.	N.S.	N.S.	N.S.	N.S.	N.S.	N.S.	N.S.	N.S.
NP2-3	N.S.	N.S.	N.S.	N.S.	N.S.	N.S.	N.S.	N.S.	N.S.	N.S.
NP3-4	N.S.	N.S.	N.S.	N.S.	N.S.	N.S.	N.S.	N.S.	N.S.	N.S.
NP4-5	0.09	6.81	0.49	0.44	0.96	0.30	0.70	0.17	0.32	0.78
NP5-6	0.06	6.99	0.42	0.38	0.98	0.35	0.51	0.12	0.10	0.55
NP6-7	0.16	6.80	0.34	0.32	0.91	0.32	0.44	0.15	0.08	0.42
NP7-8	0.09	7.10	0.38	0.29	1.01	0.49	0.64	0.15	0.09	0.31
NP8-9	0.05	7.61	0.29	0.42	0.92	0.44	0.63	0.09	0.08	0.23
NP9-10	0.10	7.20	0.41	0.49	1.07	0.48	0.74	0.12	0.17	0.30
NP10-12	0.09	7.48	0.46	0.53	0.99	0.45	0.68	0.09	0.17	0.25
NP12-14	0.13	7.54	0.48	0.46	1.18	0.26	0.84	0.13	0.21	0.27
NP14-16	0.08	7.29	0.52	0.45	0.92	0.32	0.76	0.16	0.24	0.29
NP16-18	0.18	7.61	0.52	0.53	0.97	0.30	0.93	0.17	0.25	0.29
NP18-20	N.S.	N.S.	N.S.	N.S.	N.S.	N.S.	N.S.	N.S.	N.S.	N.S.
NP20-22	0.09	7.36	0.47	0.49	1.13	0.57	0.68	0.13	0.12	0.26
NP22-24	0.17	7.30	0.44	0.58	1.11	0.64	0.58	0.12	0.13	0.27
NP24-26	0.13	6.94	0.40	0.41	2.32	0.58	0.76	0.13	0.12	0.36
NP26-28	0.13	6.66	0.42	0.54	1.08	0.61	0.79	0.12	0.11	0.26
NP28-30	0.06	7.70	0.48	0.81	1.02	0.55	0.70	0.13	0.10	0.26
NP30-32	0.17	6.95	0.37	0.42	0.87	0.47	0.76	0.16	0.12	0.27
NP32-34	0.10	7.16	0.43	0.31	0.99	0.31	0.67	0.19	0.15	0.30
NP34-36	0.05	7.22	0.39	1.74	1.10	0.54	0.77	0.16	0.20	0.25

N.S. = No Sample

Nord-Perd, XRF minor elements, normalised sediment core to rubidium ratios, ctd.

	Pb/Rb	Th/Rb	U/Rb	Sr/Rb	Y/Rb	Zr/Rb	Nb/Rb	Mo/Rb	I/Rb	Br/Rb
NP0-1	N.S.	N.S.	N.S.	N.S.	N.S.	N.S.	N.S.	N.S.	N.S.	N.S.
NP1-2	N.S.	N.S.	N.S.	N.S.	N.S.	N.S.	N.S.	N.S.	N.S.	N.S.
NP2-3	N.S.	N.S.	N.S.	N.S.	N.S.	N.S.	N.S.	N.S.	N.S.	N.S.
NP3-4	N.S.	N.S.	N.S.	N.S.	N.S.	N.S.	N.S.	N.S.	N.S.	N.S.
NP4-5	0.456	0.061	0.040	1.755	0.264	9.981	0.105	0.028	0.346	0.456
NP5-6	0.348	0.077	0.040	1.644	0.286	11.042	0.134	0.017	0.097	0.321
NP6-7	0.246	0.048	0.015	1.612	0.286	10.233	0.120	0.028	0.268	0.308
NP7-8	0.225	0.060	0.003	1.626	0.319	12.893	0.147	0.029	0.369	0.254
NP8-9	0.207	0.067	0.024	1.613	0.344	12.530	0.118	0.035	0.228	0.266
NP9-10	0.193	0.087	0.021	2.005	0.379	14.821	0.146	0.049	0.189	0.405
NP10-12	0.155	0.067	0.005	1.976	0.365	12.928	0.137	0.043	0.123	0.381
NP12-14	0.152	0.099	0.037	2.775	0.364	12.655	0.155	0.043	0.235	0.422
NP14-16	0.142	0.107	0.008	2.885	0.365	13.070	0.129	0.046	0.252	0.410
NP16-18	0.154	0.075	0.017	4.162	0.352	12.159	0.134	0.053	0.277	0.503
NP18-20	N.S.	N.S.	N.S.	N.S.	N.S.	N.S.	N.S.	N.S.	N.S.	N.S.
NP20-22	0.184	0.120	0.003	2.526	0.375	13.671	0.151	0.041	0.168	0.457
NP22-24	0.184	0.105	0.018	2.537	0.387	14.129	0.142	0.055	0.174	0.461
NP24-26	0.147	0.131	0.078	2.494	0.394	14.844	0.189	0.047	0.081	0.325
NP26-28	0.124	0.097	0.008	2.576	0.413	17.279	0.166	0.058	0.195	0.487
NP28-30	0.148	0.099	0.011	2.626	0.403	14.027	0.169	0.046	0.239	0.546
NP30-32	0.136	0.123	0.003	2.281	0.368	13.747	0.161	0.051	0.125	0.565
NP32-34	0.122	0.077	0.069	3.790	0.326	9.942	0.138	0.066	0.122	0.594
NP34-36	0.131	0.067	0.020	3.453	0.374	12.612	0.156	0.064	0.330	0.575

N.S. = No Sample

Nord-Perd, ICPMS, sediment core, Parts per million.

	Li	Ti	V	Mn	Fe	Co	Ni	Cu	Zn	As
NP0-1	N.S.	N.S.	N.S.	N.S.	N.S.	N.S.	N.S.	N.S.	N.S.	N.S.
NP1-2	N.S.	N.S.	N.S.	N.S.	N.S.	N.S.	N.S.	N.S.	N.S.	N.S.
NP2-3	N.S.	N.S.	N.S.	N.S.	N.S.	N.S.	N.S.	N.S.	N.S.	N.S.
NP3-4	N.S.	N.S.	N.S.	N.S.	N.S.	N.S.	N.S.	N.S.	N.S.	N.S.
NP4-5	8.59	1907.18	20.71	139.12	8025.64	13.01	8.42	16.26	43.59	4.80
NP5-6	6.58	1885.49	17.35	128.35	6647.57	7.14	6.46	9.66	31.29	3.44
NP6-7	6.33	1726.68	15.93	122.18	6479.22	8.05	5.84	7.18	26.47	3.22
NP7-8	5.82	1752.91	15.75	118.05	6056.05	34.99	5.97	5.46	21.36	2.88
NP8-9	5.22	1606.85	13.40	113.84	5769.84	29.89	5.18	4.50	16.41	2.34
NP9-10	5.58	1466.66	14.68	131.11	7069.45	24.89	6.05	5.29	17.11	2.68
NP10-12	5.21	1701.67	16.08	145.57	6961.40	4.43	6.06	6.81	15.75	3.14
NP12-14	5.73	1870.11	19.80	159.01	7274.46	7.34	4.89	7.92	15.28	4.88
NP14-16	6.23	1911.93	19.30	159.68	7587.08	8.23	5.16	8.09	15.67	3.95
NP16-18	5.71	1822.85	16.60	162.43	6790.59	6.81	7.17	8.71	17.42	2.99
NP18-20	N.S.	N.S.	N.S.	N.S.	N.S.	N.S.	N.S.	N.S.	N.S.	N.S.
NP20-22	5.93	1713.31	19.68	160.93	6925.60	10.17	4.98	3.59	18.74	4.12
NP22-24	6.01	1577.91	19.39	157.39	6898.81	10.86	33.99	4.11	101.75	5.37
NP24-26	6.30	1707.90	19.69	165.38	7470.92	9.44	11.43	7.59	45.71	3.58
NP26-28	5.87	1662.51	18.67	152.02	6546.39	53.04	6.12	3.62	23.14	3.04
NP28-30	5.78	1696.93	18.72	158.58	6976.66	18.71	5.58	4.77	20.15	4.33
NP30-32	5.63	1723.98	16.43	148.28	5532.41	17.65	4.82	6.33	20.85	2.22
NP32-34	5.75	1349.40	17.50	156.67	6302.05	10.77	6.04	8.76	20.66	3.95
NP34-36	5.59	1443.96	16.90	154.84	5875.86	12.02	6.47	7.37	17.13	3.53

N.S. = No Sample

Nord-Perd, ICPMS, sediment core, Parts per million, ctd

	Rb	Sr	Y	Zr	Sn	Sb	Cs	Ba	Ce	Pb	Th	U
NP0-1	N.S.	N.S.	N.S.	N.S.	N.S.	N.S.	N.S.	N.S.	N.S.	N.S.	N.S.	N.S.
NP1-2	N.S.	N.S.	N.S.	N.S.	N.S.	N.S.	N.S.	N.S.	N.S.	N.S.	N.S.	N.S.
NP2-3	N.S.	N.S.	N.S.	N.S.	N.S.	N.S.	N.S.	N.S.	N.S.	N.S.	N.S.	N.S.
NP3-4	N.S.	N.S.	N.S.	N.S.	N.S.	N.S.	N.S.	N.S.	N.S.	N.S.	N.S.	N.S.
NP4-5	44.76	70.21	9.00	138.07	0.94	1.26	0.81	247.98	28.25	18.95	4.67	1.48
NP5-6	42.80	60.36	8.61	141.51	0.65	1.54	0.64	250.53	27.31	14.45	4.08	1.28
NP6-7	41.20	54.41	7.38	122.52	0.54	0.95	0.59	238.04	25.43	13.20	3.85	1.24
NP7-8	41.31	56.79	8.35	137.90	0.44	1.45	0.51	243.67	25.60	12.57	3.73	1.24
NP8-9	37.66	52.78	7.69	123.07	0.35	1.03	0.34	235.02	24.42	9.24	3.88	1.26
NP9-10	40.21	54.65	7.68	88.00	0.38	1.56	0.41	232.03	26.18	8.38	4.21	1.21
NP10-12	39.60	67.21	8.41	134.41	0.36	1.32	0.49	248.64	28.43	9.12	4.23	1.55
NP12-14	41.47	118.38	9.81	156.23	0.37	0.30	0.57	241.39	30.79	7.77	4.50	1.75
NP14-16	40.62	118.72	9.56	119.38	0.33	0.29	0.57	242.88	31.04	7.80	4.94	1.76
NP16-18	40.26	193.24	9.59	113.86	0.32	1.78	0.51	240.17	29.96	7.53	4.43	1.77
NP18-20	N.S.	N.S.	N.S.	N.S.	N.S.	N.S.	N.S.	N.S.	N.S.	N.S.	N.S.	N.S.
NP20-22	36.71	90.78	11.08	168.71	0.40	1.55	0.62	249.62	34.94	7.43	5.55	1.74
NP22-24	33.60	88.63	10.69	143.44	0.34	59.04	0.59	234.30	34.08	6.90	5.68	1.57
NP24-26	34.16	82.97	11.50	174.78	0.32	18.70	0.58	232.36	34.90	7.00	5.75	1.76
NP26-28	34.48	88.01	11.09	164.52	0.37	4.36	0.53	234.95	36.19	6.99	5.93	1.75
NP28-30	37.66	93.39	11.18	169.00	0.39	1.94	0.58	235.98	31.47	7.01	5.43	1.67
NP30-32	29.79	71.05	10.10	174.54	0.32	1.25	0.23	224.99	31.17	7.03	5.01	1.69
NP32-34	31.13	125.51	9.38	41.90	0.19	1.37	0.56	221.39	26.63	6.98	3.97	1.83
NP34-36	32.71	105.99	9.38	75.79	0.18	2.03	0.53	228.31	28.09	6.42	4.36	1.74

N.S. = No Sample

Nord-Perd, ICPMS, normalised sediment core to rubidium ratios,

	Li/Rb	Ti/Rb	V/Rb	Mn/Rb	Fe/Rb	Co/Rb	Ni/Rb	Cu/Rb	Zn/Rb	As/Rb
NP0-1	N.S.	N.S.	N.S.	N.S.	N.S.	N.S.	N.S.	N.S.	N.S.	N.S.
NP1-2	N.S.	N.S.	N.S.	N.S.	N.S.	N.S.	N.S.	N.S.	N.S.	N.S.
NP2-3	N.S.	N.S.	N.S.	N.S.	N.S.	N.S.	N.S.	N.S.	N.S.	N.S.
NP3-4	N.S.	N.S.	N.S.	N.S.	N.S.	N.S.	N.S.	N.S.	N.S.	N.S.
NP4-5	0.19	42.61	0.46	3.11	179.30	0.29	0.19	0.36	0.97	0.107
NP5-6	0.15	44.06	0.41	3.00	155.32	0.17	0.15	0.23	0.73	0.080
NP6-7	0.15	41.91	0.39	2.97	157.25	0.20	0.14	0.17	0.64	0.078
NP7-8	0.14	42.43	0.38	2.86	146.58	0.85	0.14	0.13	0.52	0.070
NP8-9	0.14	42.67	0.36	3.02	153.20	0.79	0.14	0.12	0.44	0.062
NP9-10	0.14	36.48	0.37	3.26	175.83	0.62	0.15	0.13	0.43	0.067
NP10-12	0.13	42.97	0.41	3.68	175.78	0.11	0.15	0.17	0.40	0.079
NP12-14	0.14	45.09	0.48	3.83	175.41	0.18	0.12	0.19	0.37	0.118
NP14-16	0.15	47.07	0.48	3.93	186.79	0.20	0.13	0.20	0.39	0.097
NP16-18	0.14	45.28	0.41	4.03	168.67	0.17	0.18	0.22	0.43	0.074
NP18-20	N.S.	N.S.	N.S.	N.S.	N.S.	N.S.	N.S.	N.S.	N.S.	N.S.
NP20-22	0.16	46.67	0.54	4.38	188.65	0.28	0.14	0.10	0.51	0.112
NP22-24	0.18	46.96	0.58	4.68	205.31	0.32	1.01	0.12	3.03	0.160
NP24-26	0.18	50.00	0.58	4.84	218.70	0.28	0.33	0.22	1.34	0.105
NP26-28	0.17	48.22	0.54	4.41	189.87	1.54	0.18	0.10	0.67	0.088
NP28-30	0.15	45.06	0.50	4.21	185.26	0.50	0.15	0.13	0.54	0.115
NP30-32	0.19	57.87	0.55	4.98	185.70	0.59	0.16	0.21	0.70	0.074
NP32-34	0.18	43.35	0.56	5.03	202.46	0.35	0.19	0.28	0.66	0.127
NP34-36	0.17	44.15	0.52	4.73	179.65	0.37	0.20	0.23	0.52	0.108

N.S. = No Sample

Nord-Perd, ICPMS, normalised sediment core to rubidium ratios, ctd.

	Sr/Rb	Y/Rb	Zr/Rb	Sn/Rb	Sb/Rb	Cs/Rb	Ba/Rb	Ce/Rb	Pb/Rb	Th/Rb	U/Rb
NP0-1	N.S.	N.S.	N.S.	N.S.	N.S.	N.S.	N.S.	N.S.	N.S.	N.S.	N.S.
NP1-2	N.S.	N.S.	N.S.	N.S.	N.S.	N.S.	N.S.	N.S.	N.S.	N.S.	N.S.
NP2-3	N.S.	N.S.	N.S.	N.S.	N.S.	N.S.	N.S.	N.S.	N.S.	N.S.	N.S.
NP3-4	N.S.	N.S.	N.S.	N.S.	N.S.	N.S.	N.S.	N.S.	N.S.	N.S.	N.S.
NP4-5	1.569	0.201	3.085	0.021	0.028	0.018	5.540	0.631	0.423	0.104	0.033
NP5-6	1.410	0.201	3.306	0.015	0.036	0.015	5.854	0.638	0.338	0.095	0.030
NP6-7	1.321	0.179	2.974	0.013	0.023	0.014	5.777	0.617	0.320	0.094	0.030
NP7-8	1.374	0.202	3.338	0.011	0.035	0.012	5.898	0.620	0.304	0.090	0.030
NP8-9	1.401	0.204	3.268	0.009	0.027	0.009	6.240	0.648	0.245	0.103	0.033
NP9-10	1.359	0.191	2.189	0.009	0.039	0.010	5.771	0.651	0.208	0.105	0.030
NP10-12	1.697	0.212	3.394	0.009	0.033	0.012	6.278	0.718	0.230	0.107	0.039
NP12-14	2.855	0.237	3.767	0.009	0.007	0.014	5.821	0.742	0.187	0.109	0.042
NP14-16	2.923	0.235	2.939	0.008	0.007	0.014	5.980	0.764	0.192	0.122	0.043
NP16-18	4.800	0.238	2.828	0.008	0.044	0.013	5.966	0.744	0.187	0.110	0.044
NP18-20	N.S.	N.S.	N.S.	N.S.	N.S.	N.S.	N.S.	N.S.	N.S.	N.S.	N.S.
NP20-22	2.473	0.302	4.596	0.011	0.042	0.017	6.800	0.952	0.203	0.151	0.048
NP22-24	2.638	0.318	4.269	0.010	1.757	0.017	6.973	1.014	0.205	0.169	0.047
NP24-26	2.429	0.337	5.116	0.009	0.547	0.017	6.802	1.022	0.205	0.168	0.051
NP26-28	2.553	0.322	4.772	0.011	0.126	0.015	6.814	1.050	0.203	0.172	0.051
NP28-30	2.480	0.297	4.488	0.010	0.052	0.015	6.266	0.836	0.186	0.144	0.044
NP30-32	2.385	0.339	5.859	0.011	0.042	0.008	7.552	1.046	0.236	0.168	0.057
NP32-34	4.032	0.301	1.346	0.006	0.044	0.018	7.113	0.856	0.224	0.127	0.059
NP34-36	3.241	0.287	2.317	0.005	0.062	0.016	6.980	0.859	0.196	0.133	0.053

N.S. = No Sample

Tonne, XRF major elements, salt corrected, sediment core, Wt. %

	Si	Al	Fe	Na	Mg	Ca	K	Ti	Mn	P
T0-1	43.8380	1.3051	0.3154	0.3143	0.0526	0.1764	0.7023	0.0432	0.0116	0.0210
T1-2	44.4901	1.0814	0.2381	0.2566	0.0434	0.1343	0.6012	0.0630	0.0054	0.0175
T2-3	43.9374	1.0549	0.2241	0.2353	0.0254	0.1343	0.6203	0.0612	0.0008	0.0153
T3-4	44.5310	1.0761	0.2031	0.2500	0.0254	0.1272	0.6261	0.0516	0.0031	0.0140
T4-5	44.5357	1.0814	0.2171	0.2500	0.0254	0.1272	0.6079	0.0576	0.0047	0.0153
T5-6	44.5559	1.0443	0.2031	0.3084	0.0253	0.1343	0.6087	0.0468	0.0031	0.0144
T6-7	44.4561	1.1716	0.1891	0.3509	0.0250	0.1414	0.6569	0.0348	0.0016	0.0140
T7-8	44.4096	1.0868	0.2031	0.3656	0.0371	0.1771	0.6552	0.0414	0.0031	0.0144
T8-9	44.4129	1.0391	0.2101	0.3294	0.0372	0.1414	0.6103	0.0438	0.0016	0.0144
T9-10	44.5160	1.0656	0.2241	0.3515	0.0311	0.1414	0.6128	0.0528	0.0047	0.0140
T10-12	44.5535	1.1240	0.2312	0.2591	0.0307	0.1484	0.6660	0.0546	0.0016	0.0149
T12-14	44.1998	1.1029	0.2172	0.3101	0.0366	0.1341	0.6560	0.0462	0.0016	0.0162

Tonne, XRF major elements, normalised sediment core to rubidium ratios, (x 10^4)

	Si	Al	Fe	Na	Mg	Ca	K	Ti	Mn	P
T0-1	1.62622	0.04841	0.01170	0.01166	0.00195	0.00654	0.02605	0.00160	0.00043	0.00078
T1-2	1.85905	0.04519	0.00995	0.01072	0.00181	0.00561	0.02512	0.00263	0.00023	0.00073
T2-3	1.90786	0.04581	0.00973	0.01022	0.00110	0.00583	0.02694	0.00266	0.00003	0.00066
T3-4	1.94207	0.04693	0.00886	0.01090	0.00111	0.00555	0.02731	0.00225	0.00014	0.00061
T4-5	1.93383	0.04696	0.00943	0.01086	0.00110	0.00552	0.02639	0.00250	0.00020	0.00066
T5-6	1.95161	0.04574	0.00890	0.01351	0.00111	0.00588	0.02666	0.00205	0.00014	0.00063
T6-7	1.81200	0.04776	0.00771	0.01430	0.00102	0.00576	0.02677	0.00142	0.00006	0.00057
T7-8	1.86333	0.04560	0.00852	0.01534	0.00156	0.00743	0.02749	0.00174	0.00013	0.00061
T8-9	1.94526	0.04551	0.00920	0.01443	0.00163	0.00619	0.02673	0.00192	0.00007	0.00063
T9-10	1.91615	0.04587	0.00965	0.01513	0.00134	0.00609	0.02638	0.00227	0.00020	0.00060
T10-12	1.86139	0.04696	0.00966	0.01082	0.00128	0.00620	0.02782	0.00228	0.00006	0.00062
T12-14	1.84656	0.04607	0.00907	0.01296	0.00153	0.00560	0.02740	0.00193	0.00006	0.00068

Tonne, XRF minor elements, corrected, sediment core, Parts per million

	Sc	Ba	V	La	Ce	Nd	Cr	Ni	Cu	Zn
T 0-1	2.405	172.765	5.913	2.104	11.524	N.D.	6.514	2.606	3.608	20.042
T 1-2	N.D.	159.811	4.506	2.904	6.208	N.D.	3.104	1.502	N.D.	14.419
T 2-3	N.D.	153.699	4.806	0.901	20.827	N.D.	4.906	1.902	N.D.	12.817
T 3-4	N.D.	161.509	2.503	N.D.	16.421	N.D.	4.306	1.101	N.D.	10.714
T 4-5	0.200	133.373	5.307	3.404	7.009	N.D.	9.012	2.103	N.D.	13.217
T 5-6	3.304	152.603	4.706	N.D.	14.219	N.D.	3.204	1.100	N.D.	13.117
T 6-7	0.601	162.126	5.908	1.402	7.110	N.D.	1.202	1.903	N.D.	14.120
T 7-8	N.D.	154.817	3.705	N.D.	11.216	N.D.	3.505	2.403	N.D.	14.520
T 8-9	2.003	157.716	3.104	1.001	9.713	N.D.	5.007	1.602	N.D.	14.820
T 9-10	1.302	156.716	5.708	N.D.	15.722	N.D.	4.706	0.601	N.D.	15.021
T 10-12	1.302	149.823	2.404	N.D.	8.212	N.D.	3.305	0.901	N.D.	11.717
T 12-14	0.901	169.958	5.108	1.502	19.630	N.D.	10.416	2.303	N.D.	12.319

Tonne, XRF minor elements, corrected, sediment core, Parts per million, ctd.

	Pb	Th	U	Rb	Sr	Y	Zr	Nb	Mo
T 0-1	8.017	N.D.	N.D.	26.957	42.189	7.416	58.624	0.802	0.601
T 1-2	4.306	N.D.	N.D.	23.932	37.850	7.510	82.309	1.802	0.200
T 2-3	4.506	N.D.	N.D.	23.030	37.048	7.610	80.804	2.203	0.200
T 3-4	3.605	N.D.	N.D.	22.930	37.048	6.809	58.576	1.402	0.401
T 4-5	4.105	N.D.	N.D.	23.030	36.647	7.510	80.604	1.902	0.401
T 5-6	5.007	N.D.	N.D.	22.830	36.348	6.709	51.368	1.402	0.401
T 6-7	5.007	N.D.	N.D.	24.534	37.953	6.409	40.957	1.402	0.200
T 7-8	4.907	N.D.	N.D.	23.833	39.856	6.810	46.966	1.202	0.100
T 8-9	5.307	N.D.	N.D.	22.831	37.952	7.010	53.573	1.602	0.100
T 9-10	4.907	N.D.	N.D.	23.232	38.253	7.010	57.079	1.702	0.200
T10-12	6.209	N.D.	N.D.	23.936	39.058	7.611	75.512	2.003	0.200
T12-14	4.507	N.D.	N.D.	23.936	36.656	7.211	49.075	1.402	0.200

N.D. = Not Detectable

Tonne, XRF minor elements, normalised sediment core to rubidium ratios,

	Sc/Rb	Ba/Rb	V/Rb	La/Rb	Ce/Rb	Nd/Rb	Cr/Rb	Ni/Rb	Cu/Rb
T 0-1	0.089219	6.408922	0.219331	0.078067	0.427509	N.D.	0.241636	0.096654	0.133829
T 1-2	N.D.	6.677824	0.188285	0.121339	0.259414	N.D.	0.129707	0.062762	N.D.
T 2-3	N.D.	6.673913	0.208696	0.03913	0.904348	N.D.	0.213043	0.082609	N.D.
T 3-4	N.D.	7.043668	0.10917	N.D.	0.716157	N.D.	0.187773	0.048035	N.D.
T 4-5	0.008696	5.791304	0.230435	0.147826	0.304348	N.D.	0.391304	0.091304	N.D.
T 5-6	0.144737	6.684211	0.20614	N.D.	0.622807	N.D.	0.140351	N.D.	N.D.
T 6-7	0.02449	6.608163	0.240816	0.057143	0.289796	N.D.	0.04898	0.077551	N.D.
T 7-8	N.D.	6.495798	0.155462	N.D.	0.470588	N.D.	0.147059	0.10084	N.D.
T 8-9	0.087719	6.907895	0.135965	0.04386	0.425439	N.D.	0.219298	0.070175	N.D.
T 9-10	0.056034	6.74569	0.24569	N.D.	0.676724	N.D.	0.202586	0.025862	N.D.
T10-12	0.054393	6.259414	0.100418	N.D.	0.343096	N.D.	0.138075	0.037657	N.D.
T12-14	0.037657	7.100418	0.213389	0.062762	0.820084	N.D.	0.435146	0.096234	N.D.

Tonne, XRF minor elements, normalised sediment core to rubidium ratios, ctd.

	Zn/Rb	Pb/Rb	Th/Rb	U/Rb	Sr/Rb	Y/Rb	Zr/Rb	Nb/Rb	Mo/Rb
T 0-1	0.743	0.297	N.D.	N.D.	1.565	0.275	2.175	0.030	0.022
T 1-2	0.603	0.180	N.D.	N.D.	1.582	0.314	3.439	0.075	0.008
T 2-3	0.557	0.196	N.D.	N.D.	1.609	0.330	3.509	0.096	0.009
T 3-4	0.467	0.157	N.D.	N.D.	1.616	0.297	2.555	0.061	0.017
T 4-5	0.574	0.178	N.D.	N.D.	1.591	0.326	3.500	0.083	0.017
T 5-6	0.575	0.219	N.D.	N.D.	1.592	0.294	2.250	0.061	0.018
T 6-7	0.576	0.204	N.D.	N.D.	1.547	0.261	1.669	0.057	0.008
T 7-8	0.609	0.206	N.D.	N.D.	1.672	0.286	1.971	0.050	0.004
T 8-9	0.649	0.232	N.D.	N.D.	1.662	0.307	2.346	0.070	0.004
T 9-10	0.647	0.211	N.D.	N.D.	1.647	0.302	2.457	0.073	0.009
T10-12	0.490	0.259	N.D.	N.D.	1.632	0.318	3.155	0.084	0.008
T12-14	0.515	0.188	N.D.	N.D.	1.531	0.301	2.050	0.059	0.008

N.D. = Not Detectable

Tonne, ICPMS, sediment core, Parts per million.

	Li	Ti	V	Mn	Fe	Co	Ni	Cu	Zn	As
T0-1	3.41	343.04	6.03	115.53	2441.88	97.09	4.77	12.49	24.09	2.50
T1-2	3.15	511.37	4.48	64.56	1866.39	31.16	4.01	5.48	16.26	1.53
T2-3	2.92	543.24	4.59	51.42	1784.58	15.33	2.24	3.80	13.35	1.42
T3-4	2.98	417.11	3.39	53.86	1665.44	17.10	3.05	4.29	14.39	1.60
T4-5	3.16	486.19	3.81	55.12	1762.87	42.73	2.58	5.30	16.82	1.47
T5-6	2.42	369.59	4.37	43.69	1657.36	11.75	2.24	3.00	12.31	1.42
T6-7	2.45	319.07	3.31	36.74	1529.30	12.87	2.92	3.54	14.29	1.08
T7-8	2.39	311.46	4.18	38.94	1730.52	14.02	2.65	3.12	14.06	1.36
T8-9	2.43	314.78	4.62	33.25	1677.21	13.92	3.07	4.20	14.20	1.62
T9-10	2.76	446.44	4.17	54.34	2068.47	16.50	1.33	3.31	12.54	1.47
T10-12	2.52	372.58	4.88	47.37	1851.64	5.87	1.17	3.32	10.41	1.59
T12-14	2.67	410.46	3.76	54.23	1996.86	6.19	3.52	3.00	11.26	1.28

Tonne, ICPMS, sediment core, Parts per million, ctd,

	Rb	Sr	Y	Zr	Sn	Sb	Cs	Ba	Ce	Pb	Th	U
T0-1	27.40	38.87	2.97	25.02	0.58	1.70	0.22	167.36	10.12	8.72	1.14	0.48
T1-2	24.43	36.34	3.42	31.80	0.38	1.20	0.09	150.16	11.46	5.77	1.11	0.52
T2-3	24.44	36.24	3.09	26.41	0.38	1.00	0.11	160.76	10.38	6.38	1.06	0.51
T3-4	23.70	33.95	2.78	24.34	0.35	1.93	0.07	151.45	9.06	6.19	0.84	0.41
T4-5	22.95	34.54	3.32	29.48	0.36	1.32	0.05	147.29	9.75	6.22	1.15	0.47
T5-6	20.94	31.67	2.27	27.14	0.42	1.27	0.28	129.64	7.95	5.72	0.89	0.39
T6-7	24.51	34.28	2.18	21.86	0.38	1.90	0.30	151.88	7.87	6.20	0.95	0.39
T7-8	22.31	35.21	2.23	17.12	0.41	1.42	0.17	144.58	9.04	6.90	1.11	0.43
T8-9	20.95	32.09	2.18	19.74	0.41	2.01	0.27	138.32	10.26	6.59	1.45	0.42
T9-10	21.95	33.87	2.52	23.99	0.43	0.11	0.26	146.02	8.97	7.96	1.13	0.39
T10-12	21.69	32.60	2.34	19.27	0.39	0.10	0.27	141.95	7.54	5.60	0.97	0.40
T12-14	22.06	32.55	2.98	22.91	0.40	1.58	0.27	138.69	8.93	5.26	1.26	0.44

Tonne, ICPMS, normalised sediment core to rubidium ratios.

	Li/Rb	Ti/Rb	V/Rb	Mn/Rb	Fe/Rb	Co/Rb	Ni/Rb	Cu/Rb	Zn/Rb	As/Rb
T0-1	0.12	12.52	0.22	4.22	89.12	3.54	0.17	0.46	0.88	0.091
T1-2	0.13	20.94	0.18	2.64	76.41	1.28	0.16	0.22	0.67	0.063
T2-3	0.12	22.23	0.19	2.10	73.03	0.63	0.09	0.16	0.55	0.058
T3-4	0.13	17.60	0.14	2.27	70.27	0.72	0.13	0.18	0.61	0.068
T4-5	0.14	21.19	0.17	2.40	76.83	1.86	0.11	0.23	0.73	0.064
T5-6	0.12	17.65	0.21	2.09	79.14	0.56	0.11	0.14	0.59	0.068
T6-7	0.10	13.02	0.13	1.50	62.41	0.53	0.12	0.14	0.58	0.044
T7-8	0.11	13.96	0.19	1.75	77.56	0.63	0.12	0.14	0.63	0.061
T8-9	0.12	15.02	0.22	1.59	80.04	0.66	0.15	0.20	0.68	0.077
T9-10	0.13	20.34	0.19	2.48	94.25	0.75	0.06	0.15	0.57	0.067
T10-12	0.12	17.17	0.22	2.18	85.35	0.27	0.05	0.15	0.48	0.073
T12-14	0.12	18.61	0.17	2.46	90.53	0.28	0.16	0.14	0.51	0.058

Tonne, ICPMS, normalised sediment core to rubidium ratios.

	Sr/Rb	Y/Rb	Zr/Rb	Sn/Rb	Sb/Rb	Cs/Rb	Ba/Rb	Ce/Rb	Pb/Rb	Th/Rb	U/Rb
T0-1	1.419	0.108	0.913	0.021	0.062	0.008	6.108	0.369	0.318	0.042	0.017
T1-2	1.488	0.140	1.302	0.015	0.049	0.004	6.148	0.469	0.236	0.045	0.021
T2-3	1.483	0.127	1.081	0.016	0.041	0.005	6.579	0.425	0.261	0.043	0.021
T3-4	1.433	0.117	1.027	0.015	0.082	0.003	6.390	0.382	0.261	0.036	0.017
T4-5	1.505	0.145	1.285	0.016	0.058	0.002	6.419	0.425	0.271	0.050	0.021
T5-6	1.512	0.108	1.296	0.020	0.061	0.014	6.190	0.380	0.273	0.042	0.018
T6-7	1.399	0.089	0.892	0.015	0.077	0.012	6.198	0.321	0.253	0.039	0.016
T7-8	1.578	0.100	0.767	0.018	0.063	0.007	6.480	0.405	0.309	0.050	0.019
T8-9	1.531	0.104	0.942	0.020	0.096	0.013	6.601	0.490	0.314	0.069	0.020
T9-10	1.543	0.115	1.093	0.020	0.005	0.012	6.653	0.409	0.363	0.051	0.018
T10-12	1.503	0.108	0.888	0.018	0.005	0.012	6.543	0.347	0.258	0.045	0.019
T12-14	1.476	0.135	1.039	0.018	0.071	0.012	6.287	0.405	0.239	0.057	0.020

OCTOBER '96, ICPMS, Water Particulate Phase, ng/l.

	Li	Ti	V	Mn	Fe	Co	Ni	Cu	Zn	As	Rb	Sr	Y	Zr	Mo	Cd	Sn	Sb	Cs	Ba	Ce	Pb	Th	U
Ton 0m	7.00	1012	52.04	3322	8824	85.58	104	146	429	26.98	20.07	427	13.23	66.38	1.37	3.48	5.37	N.D.	N.D.	230	24.11	91.21	6.66	N.D.
Ton 5m	3.34	447	28.87	2780	6580	29.21	105	122	351	20.87	17.46	432	11.56	32.53	1.20	2.75	4.46	N.D.	N.D.	210	22.39	70.03	6.62	N.D.
Ton 10m	2.34	429	15.88	2477	6305	25.80	122	108	312	14.58	14.60	422	11.09	23.75	1.62	2.41	4.60	N.D.	N.D.	143	9.85	59.52	4.43	N.D.
Ton 15m	5.15	773	49.41	2468	10274	52.04	114	106	340	21.80	23.58	481	12.87	52.21	1.88	2.51	36.32	N.D.	N.D.	213	22.74	79.06	6.09	N.D.
Ton L 5cm	3.00	7564	565.38	5163	90997	374.35	1942	632	5105	192.29	154.33	4646	195.55	401.11	39.47	31.67	32.77	N.D.	N.D.	1779	59.92	368.56	78.50	N.D.
Ton L 10cm	4.43	8470	822.98	6765	106638	322.89	2416	673	6874	261.51	211.87	4388	192.38	321.26	51.17	32.99	34.12	N.D.	N.D.	1719	106.90	437.61	80.08	N.D.
Ton L 20cm	5.65	5133	631.47	4965	73894	181.50	1724	527	9112	272.11	134.09	4691	178.55	193.25	15.05	25.77	35.53	N.D.	N.D.	1437	40.45	324.66	73.34	N.D.
Ton L 40cm	0.38	5721	363.96	4476	84501	216.20	2930	661	7618	166.03	143.44	4579	183.09	219.44	92.89	33.32	93.33	N.D.	N.D.	1524	81.38	382.00	72.14	N.D.
NP 0m	3.59	574	56.15	3540	9096	25.34	139	203	559	26.89	21.28	396	13.29	19.18	2.15	3.59	9.87	N.D.	N.D.	163	14.01	165.25	5.35	N.D.
NP 5m	4.08	567	49.40	3490	9150	86.71	179	170	448	27.40	21.69	440	12.67	19.07	3.65	3.85	9.48	N.D.	N.D.	170	14.82	128.26	5.24	N.D.
NP 10m	3.03	450	38.59	3471	7937	64.72	138	131	365	21.67	18.39	396	12.15	15.72	2.30	3.45	7.55	N.D.	N.D.	145	11.07	115.45	4.89	N.D.
NP 15m	7.25	704	58.08	5677	13521	66.91	185	157	400	25.42	29.18	454	14.81	31.51	4.62	4.22	7.39	N.D.	N.D.	190	19.21	160.15	5.80	N.D.
NP 20m	37.36	2879	137.08	5289	47760	42.58	196	200	508	41.11	106.73	510	27.54	82.52	6.54	4.48	15.92	N.D.	2.79	370	69.50	227.03	13.18	1.04
NP L 5cm	8843	995544	21204	85106	5724881	2665	7985	8458	35164	4171	24654	36321	4843	3508	399	417	928	176	1075	101142	24521	16578	2790	842
NP L 10cm	6046	629267	13519	53084	4465583	1926	5586	6374	26450	3053	16866	29863	3278	3158	227	303	754	98	747	57373	12698	11924	1852	561
NP L 20cm	189.32	16748	906.75	2612	234379	232.65	1173	799	4513	404.38	436.66	11897	238.37	1008	25.89	8.03	38.48	N.D.	N.D.	1884	274.80	455.85	35.60	N.D.
NP L 40cm	119.77	3661	1322.35	1539	161383	173.43	2272	736	4722	514.87	193.17	11501	174.90	272.46	46.38	15.91	41.82	N.D.	N.D.	1838	163.86	362.27	19.72	N.D.

N.D. = Not Detectable, Ton = ODAS Tonne, NP = Nord-Perd Rinne, W = Wiek, Ark = Arkona and L = Lander (height above sea floor)

OCTOBER '96, ICPMS, Water Particulate Phase, ng/l, ctd.

	Li	Ti	V	Mn	Fe	Co	Ni	Cu	Zn	As	Rb	Sr	Y	Zr	Mo	Cd	Sn	Sb	Cs	Ba	Ce	Pb	Th	U
W0m	7.02	914	63.89	2031	11902	24.60	261	198	404	24.76	27.94	375	13.12	25.24	8.30	2.19	9.70	N.D.	N.D.	170	18.24	132.77	2.04	N.D.
W5m	5.57	777	44.11	2013	10489	22.73	206	160	360	20.46	24.10	363	12.86	24.58	4.78	2.02	7.72	N.D.	N.D.	150	14.42	119.71	1.43	N.D.
W10m	0.59	526	22.06	1003	6692	11.73	92	79	218	9.18	15.66	180	11.39	14.69	0.63	0.80	3.22	N.D.	N.D.	98	8.95	59.89	0.82	N.D.
W15m	5.57	706	37.24	2000	9691	30.97	153	141	341	21.20	23.74	359	12.49	17.46	2.64	2.27	6.48	N.D.	N.D.	148	15.01	106.35	1.60	N.D.
W20m	5.78	695	45.96	2021	10117	22.34	176	138	356	19.61	24.09	374	12.99	16.36	3.24	3.21	6.48	N.D.	N.D.	156	17.08	102.04	1.43	N.D.
W25m	56.25	4692	158.11	1773	62884	31.04	114	359	508	43.10	156.84	438	35.84	139.68	1.39	1.86	10.63	N.D.	5.75	476	104.14	269.62	14.83	2.65
WL 5cm	64.60	7004	626.32	11107	110190	458.99	1737	698	6848	213.37	243.61	5450	160.94	209.38	24.07	10.96	25.61	N.D.	N.D.	1134	222.73	487.96	7.54	N.D.
WL 10cm	52.65	4068	637.08	6091	67045	342.46	1738	662	3905	210.63	159.71	6225	140.97	153.43	26.12	5.26	25.08	N.D.	N.D.	731	38.66	318.94	N.D.	N.D.
WL 20cm	85.96	8233	533.51	13573	140176	1175.62	2441	878	7955	254.21	304.38	6862	202.70	264.65	58.71	10.42	65.80	N.D.	N.D.	1396	212.36	569.96	6.93	N.D.
WL 40cm	52.87	7020	653.89	12396	122001	206.89	2050	644	5658	258.12	253.00	6669	195.21	224.37	22.77	9.59	32.39	N.D.	N.D.	1225	98.44	481.82	4.61	N.D.
Ark 0m	9.99	466	26.38	1252	5139	101.37	141	106	214	14.48	16.78	237	2.34	13.34	24.45	3.26	22.73	1.76	0.30	128	8.83	98.79	0.66	59.88
Ark 5m	7.90	450	39.32	1166	5746	20.36	192	175	353	18.26	15.43	332	3.28	18.32	5.95	3.80	18.76	0.52	0.18	152	8.92	140.01	0.73	0.42
Ark 10m	8.11	416	20.30	1386	5837	18.28	169	169	369	15.21	15.03	360	3.48	10.97	5.44	3.92	12.29	0.59	0.28	245	10.43	142.28	0.72	0.39
Ark 20m	8.56	399	55.09	1459	6173	30.36	156	162	286	22.11	17.22	347	3.61	9.58	7.65	3.12	11.41	0.52	0.22	147	10.17	181.73	0.76	0.48
Ark 30m	8.50	420	20.81	1577	5937	23.94	140	165	291	10.81	15.80	355	3.64	12.18	5.13	2.72	9.34	0.44	0.27	113	10.71	150.51	0.97	0.49
Ark 35m	11.38	584	34.63	1930	8250	35.26	161	160	298	14.63	29.66	355	5.83	19.51	6.76	2.76	8.66	0.51	0.77	127	17.37	159.56	2.77	0.51
Ark 40m	14.10	816	45.52	2932	10727	20.37	213	182	266	17.58	31.09	403	6.60	22.24	7.75	3.57	9.36	0.81	1.09	141	21.87	179.40	2.86	0.85
Ark 45m	18.04	995	53.87	1638	21142	72.52	120	170	199	44.81	33.00	505	8.19	36.37	5.97	2.16	6.89	1.50	1.14	152	21.50	290.13	2.56	1.13
Ark L 5cm	340.18	24109	926.67	52215	257045	298.79	1811	1385	9860	320.61	728.41	8250	146.67	793.36	42.29	48.39	227.67	1.84	20.45	3339	536.44	939.14	53.52	20.61
Ark L 10cm	352.30	22556	985.09	61165	278366	622.55	1790	1141	8412	340.88	717.04	8210	149.33	710.11	37.96	50.42	33.32	2.44	22.06	2782	450.44	966.29	57.69	20.35
Ark L 20cm	352.38	21862	909.00	54894	268856	420.90	1846	1070	6687	334.48	714.22	8808	144.10	666.27	79.90	50.69	32.37	4.35	21.31	2837	438.21	960.46	57.93	19.10
Ark L 40cm	352.68	21269	1162.57	52774	239028	334.08	1691	975	7138	387.13	708.86	8668	141.74	767.72	37.48	49.56	27.14	1.92	18.99	3257	486.58	839.73	55.85	19.73

N.D. = Not Detectable, Ton = ODAS Tonne, NP = Nord-Perd Rinne, W = Wiek, Ark = Arkona and L = Lander (height above sea floor)

OCTOBER '96, ICPMS, Normalised Water Particulate Phase to Rubidium ratios.

	Li/Rb	Ti/Rb	V/Rb	Mn/Rb	Fe/Rb	Co/Rb	Ni/Rb	Cu/Rb	Zn/Rb	As/Rb	Sr/Rb	Y/Rb	Zr/Rb	Mo/Rb	Cd/Rb	Sn/Rb	Sb/Rb	Cs/Rb	Ba/Rb	Ce/Rb	Pb/Rb	Th/Rb	U/Rb
Ton 0m	0.35	50.41	2.59	165.50	439.60	4.26	5.18	7.29	21.38	1.34	21.29	0.66	3.31	0.07	0.17	0.27	N.D.	N.D.	11.43	1.20	4.54	0.33	N.D.
Ton 5m	0.19	25.58	1.65	159.20	376.82	1.67	6.04	7.01	20.12	1.20	24.72	0.66	1.86	0.07	0.16	0.26	N.D.	N.D.	12.00	1.28	4.01	0.38	N.D.
Ton 10m	0.16	29.38	1.09	169.61	431.80	1.77	8.38	7.40	21.36	1.00	28.89	0.76	1.63	0.11	0.17	0.31	N.D.	N.D.	9.79	0.68	4.08	0.30	N.D.
Ton 15m	0.22	32.78	2.10	104.63	435.64	2.21	4.85	4.50	14.42	0.92	20.40	0.55	2.21	0.08	0.11	1.54	N.D.	N.D.	9.02	0.96	3.35	0.26	N.D.
Ton L 5cm	0.02	49.01	3.66	33.45	589.63	2.43	12.59	4.09	33.08	1.25	30.11	1.27	2.60	0.26	0.21	0.21	N.D.	N.D.	11.53	0.39	2.39	0.51	N.D.
Ton L 10cm	0.02	39.98	3.88	31.93	503.33	1.52	11.41	3.18	32.45	1.23	20.71	0.91	1.52	0.24	0.16	0.16	N.D.	N.D.	8.12	0.50	2.07	0.38	N.D.
Ton L 20cm	0.04	38.28	4.71	37.03	551.09	1.35	12.86	3.93	67.96	2.03	34.98	1.33	1.44	0.11	0.19	0.26	N.D.	N.D.	10.72	0.30	2.42	0.55	N.D.
Ton L 40cm	0.00	39.88	2.54	31.20	589.12	1.51	20.43	4.61	53.11	1.16	31.92	1.28	1.53	0.65	0.23	0.65	N.D.	N.D.	10.62	0.57	2.66	0.50	N.D.
NP 0m	0.17	26.98	2.64	166.40	427.53	1.19	6.55	9.54	26.28	1.26	18.60	0.62	0.90	0.10	0.17	0.46	N.D.	N.D.	7.65	0.66	7.77	0.25	N.D.
NP 5m	0.19	26.15	2.28	160.86	421.74	4.00	8.23	7.85	20.66	1.26	20.29	0.58	0.88	0.17	0.18	0.44	N.D.	N.D.	7.84	0.68	5.91	0.24	N.D.
NP 10m	0.17	24.48	2.10	188.79	431.68	3.52	7.48	7.14	19.85	1.18	21.52	0.66	0.86	0.12	0.19	0.41	N.D.	N.D.	7.90	0.60	6.28	0.27	N.D.
NP 15m	0.25	24.12	1.99	194.58	463.42	2.29	6.35	5.40	13.72	0.87	15.55	0.51	1.08	0.16	0.14	0.25	N.D.	N.D.	6.50	0.66	5.49	0.20	N.D.
NP 20m	0.35	26.97	1.28	49.55	447.47	0.40	1.84	1.87	4.76	0.39	4.78	0.26	0.77	0.06	0.04	0.15	N.D.	0.03	3.46	0.65	2.13	0.12	0.01
NP L 5cm	0.36	40.38	0.86	3.45	232.21	0.11	0.32	0.34	1.43	0.17	1.47	0.20	0.14	0.02	0.02	0.04	0.01	0.04	4.10	0.99	0.67	0.11	0.03
NP L 10cm	0.36	37.31	0.80	3.15	264.76	0.11	0.33	0.38	1.57	0.18	1.76	0.19	0.19	0.01	0.02	0.04	0.01	0.04	3.40	0.75	0.71	0.11	0.03
NP L 20cm	0.43	38.35	2.08	5.98	536.75	0.53	2.69	1.83	10.34	0.93	27.24	0.55	2.31	0.06	0.02	0.09	N.D.	N.D.	4.32	0.63	1.04	0.08	N.D.
NP L 40cm	0.62	18.95	6.85	7.97	835.45	0.90	11.76	3.81	24.45	2.67	59.54	0.91	1.41	0.24	0.08	0.22	N.D.	N.D.	9.51	0.85	1.88	0.10	N.D.

N.D. = Not Detectable, Ton = ODAS Tonne, NP = Nord-Perd Rinne, W = Wiek, Ark = Arkona and L = Lander (height above sea floor)

OCTOBER '96, ICPMS, Normalised Water Particulate Phase to Rubidium ratios, ctd.

	Li/Rb	Ti/Rb	V/Rb	Mn/Rb	Fe/Rb	Co/Rb	Ni/Rb	Cu/Rb	Zn/Rb	As/Rb	Sr/Rb	Y/Rb	Zr/Rb	Mo/Rb	Cd/Rb	Sn/Rb	Sb/Rb	Cs/Rb	Ba/Rb	Ce/Rb	Pb/Rb	Th/Rb	U/Rb
W 0m	0.25	32.69	2.29	72.70	425.95	0.88	9.34	7.10	14.45	0.89	13.41	0.47	0.90	0.30	0.08	0.35	N.D.	N.D.	6.08	0.65	4.75	0.07	N.D.
W 5m	0.23	32.23	1.83	83.54	435.23	0.94	8.54	6.63	14.93	0.85	15.06	0.53	1.02	0.20	0.08	0.32	N.D.	N.D.	6.23	0.60	4.97	0.06	N.D.
W 10m	0.04	33.57	1.41	64.08	421.04	0.75	5.90	5.03	13.92	0.59	11.49	0.73	0.94	0.04	0.05	0.21	N.D.	N.D.	6.24	0.57	3.83	0.05	N.D.
W 15m	0.23	29.71	1.57	84.24	403.92	1.30	6.46	5.94	14.36	0.89	15.12	0.53	0.74	0.11	0.10	0.27	N.D.	N.D.	6.25	0.63	4.48	0.07	N.D.
W 20m	0.24	28.86	1.91	83.90	420.06	0.93	7.29	5.75	14.78	0.81	15.53	0.54	0.68	0.13	0.13	0.27	N.D.	N.D.	6.46	0.71	4.24	0.06	N.D.
W 25m	0.36	29.92	1.01	11.30	400.95	0.20	0.73	2.29	3.24	0.27	2.79	0.23	0.89	0.01	0.01	0.07	N.D.	0.04	3.04	0.66	1.72	0.09	0.02
W L 5cm	0.27	28.75	2.57	45.59	452.32	1.88	7.13	2.87	28.11	0.88	22.37	0.66	0.86	0.10	0.04	0.11	N.D.	N.D.	4.66	0.91	2.00	0.03	N.D.
W L 10cm	0.33	25.47	3.99	38.14	419.80	2.14	10.88	4.14	24.45	1.32	38.98	0.88	0.96	0.16	0.03	0.16	N.D.	N.D.	4.58	0.24	2.00	N.D.	N.D.
W L 20cm	0.28	27.05	1.75	44.59	460.53	3.86	8.02	2.88	26.13	0.84	22.54	0.67	0.87	0.19	0.03	0.22	N.D.	N.D.	4.59	0.70	1.87	0.02	N.D.
W L 40cm	0.21	27.75	2.58	49.00	482.22	0.82	8.10	2.55	22.36	1.02	26.36	0.77	0.89	0.09	0.04	0.13	N.D.	N.D.	4.84	0.39	1.90	0.02	N.D.
Ark 0m	0.60	27.79	1.57	74.59	306.19	6.04	8.42	6.33	12.75	0.86	14.13	0.14	0.79	1.46	0.19	1.35	0.11	0.02	7.65	0.53	5.89	0.04	3.57
Ark 5m	0.51	29.18	2.55	75.59	372.42	1.32	12.45	11.35	22.91	1.18	21.49	0.21	1.19	0.39	0.25	1.22	0.03	0.01	9.84	0.58	9.07	0.05	0.03
Ark 10m	0.54	27.68	1.35	92.16	388.22	1.22	11.22	11.26	24.55	1.01	23.98	0.23	0.73	0.36	0.26	0.82	0.04	0.02	16.29	0.69	9.46	0.05	0.03
Ark 20m	0.50	23.17	3.20	84.74	358.54	1.76	9.07	9.39	16.60	1.28	20.14	0.21	0.56	0.44	0.18	0.66	0.03	0.01	8.56	0.59	10.56	0.04	0.03
Ark 30m	0.54	26.56	1.32	99.82	375.72	1.52	8.88	10.42	18.41	0.68	22.44	0.23	0.77	0.32	0.17	0.59	0.03	0.02	7.14	0.68	9.53	0.06	0.03
Ark 35m	0.38	19.71	1.17	65.07	278.20	1.19	5.43	5.41	10.03	0.49	11.97	0.20	0.66	0.23	0.09	0.29	0.02	0.03	4.27	0.59	5.38	0.09	0.02
Ark 40m	0.45	26.26	1.46	94.31	344.99	0.66	6.86	5.86	8.57	0.57	12.97	0.21	0.72	0.25	0.11	0.30	0.03	0.03	4.54	0.70	5.77	0.09	0.03
Ark 45m	0.55	30.14	1.63	49.63	640.70	2.20	3.62	5.15	6.04	1.36	15.30	0.25	1.10	0.18	0.07	0.21	0.05	0.03	4.61	0.65	8.79	0.08	0.03
Ark L 5cm	0.47	33.10	1.27	71.68	352.89	0.41	2.49	1.90	13.54	0.44	11.33	0.20	1.09	0.06	0.07	0.31	0.00	0.03	4.58	0.74	1.29	0.07	0.03
Ark L 10cm	0.49	31.46	1.37	85.30	388.22	0.87	2.50	1.59	11.73	0.48	11.45	0.21	0.99	0.05	0.07	0.05	0.00	0.03	3.88	0.63	1.35	0.08	0.03
Ark L 20cm	0.49	30.61	1.27	76.86	376.43	0.59	2.58	1.50	9.36	0.47	12.33	0.20	0.93	0.11	0.07	0.05	0.01	0.03	3.97	0.61	1.34	0.08	0.03
Ark L 40cm	0.50	30.00	1.64	74.45	337.20	0.47	2.38	1.38	10.07	0.55	12.23	0.20	1.08	0.05	0.07	0.04	0.00	0.03	4.60	0.69	1.18	0.08	0.03

N.D. = Not Detectable, Ton = ODAS Tonne, NP = Nord-Perd Rinne, W = Wiek, Ark = Arkona and L = Lander (height above sea floor)

March '97, ICPMS, Water Particulate Phase, ng/l.

	Li	Ti	V	Mn	Fe	Co	Ni	Cu	Zn	As	Rb	Sr	Y	Zr	Mo	Cd	Sn	Sb	Cs	Ba	Ce	Pb	Th	U
Ton 0m	28.46	3555	99.29	6052	46789	68.44	2372.16	547.89	2261.97	62.28	147.78	1420.45	27.28	125.20	545.16	18.37	26.22	15.50	3.50	1191.48	85.64	531.43	11.07	1.55
Ton 5m	19.52	1542	68.26	4842	26348	34.10	313.17	231.21	1498.55	51.87	75.61	1347.55	18.41	50.55	31.59	10.12	10.54	5.73	2.54	650.03	33.11	247.55	1.83	1.62
Ton 10m	19.02	1613	51.75	1778	37592	38.69	192.13	140.54	784.90	21.54	71.67	517.17	15.87	54.04	10.61	3.52	9.18	6.35	2.66	497.60	45.20	205.49	1.49	1.00
Ton 15m	1598	143320	4260	148952	1844480	742	3283	3831	19205	1113	4461	10113	861	4526	96	62	292	62	187	19768	3056	5825	412	94
Ton L Fluff	487	26130	1584	40256	584209	244	1496	1340	7736	486	1120	4232	317	837	29	33	131	5	16	3408	736	4701	92	2
Ton L 5cm	35.11	3072	165.65	2885	41976	111.51	884.12	703.01	16440	44.35	80.55	2671.07	98.74	66.31	13.61	1.09	475.44	53.04	N.D.	1005.25	62.63	385.79	N.D.	N.D.
Ton L 10cm	54.83	5955	210.71	4695	64045	186.53	888.20	687.24	7702.79	49.83	141.90	2838.01	106.37	172.28	10.47	1.65	167.80	5.12	N.D.	1256.64	43.84	410.33	N.D.	N.D.
Ton L 20cm	41.66	3923	263.81	4685	60015	160.33	1303.09	759.52	6046.43	72.24	125.56	2824.81	95.34	126.87	123.75	1.20	110.09	3.25	N.D.	1322.17	8.68	398.33	N.D.	N.D.
Ton L 40cm	33.74	2675	133.64	2643	40571	100.92	1017.96	653.62	5985.35	48.72	87.22	2639.55	94.41	50.81	17.58	0.28	134.81	2.15	N.D.	822.48	27.51	341.77	N.D.	N.D.
NP 0m	9.51	736	35.45	979	11165	18.94	192.73	120.10	666.93	35.21	26.02	851.96	11.14	22.82	9.36	5.66	6.67	1.12	0.69	595.18	13.87	83.97	1.72	0.81
NP 5m	8.65	651	30.55	817	9822	59.94	110.57	83.47	588.98	23.87	24.44	697.11	10.59	20.84	3.24	3.94	6.91	0.13	0.59	471.35	13.91	124.21	1.69	0.49
NP 10m	7.59	605	36.25	908	11092	13.45	164.48	104.42	620.25	33.96	23.15	591.88	10.40	18.14	10.77	4.44	6.68	1.06	0.60	497.41	11.33	67.73	1.55	0.50
NP 15m	11.45	766	41.02	780	10934	11.69	103.25	90.60	427.50	16.87	29.50	431.77	11.27	21.76	3.40	0.79	2.80	5.32	0.89	148.45	13.91	60.79	1.82	0.59
NP 20m	27.79	1804	81.37	1387	23096	20.10	128.56	87.94	378.28	24.94	73.25	645.76	19.90	65.76	3.45	0.06	4.21	6.38	2.64	328.38	41.05	202.53	3.25	1.55
NP L Fluff	9602	481620	1836	160075	8110100	3667	17188	19245	51135	5161	21354	54726	4875	15356	856	1667	23811	325	1266	48012	11319	27077	2129	558
NP L 5cm	141.91	5555	415.18	552	41205	260.22	1269.35	769.16	1106.99	155.41	177.22	4322.26	10.76	261.69	71.38	9.76	110.86	5.52	N.D.	714.97	50.67	210.39	N.D.	N.D.
NP L 10cm	62.25	2507	255.12	298	19921	112.09	739.33	499.98	499.95	90.72	76.79	1995.70	4.14	119.31	44.59	4.04	25.00	3.49	N.D.	341.40	17.43	121.42	N.D.	N.D.
NP L 20cm	58.61	2388	221.63	293	18974	106.50	767.46	453.41	3816.75	81.14	79.47	1922.76	5.61	164.42	58.59	3.08	20.59	2.16	N.D.	444.36	32.64	68.85	N.D.	N.D.
NP L 40cm	62.44	1988	180.04	367	24958	72.97	1535.88	435.18	451.43	71.12	75.44	2135.04	3.70	106.79	101.24	5.11	73.89	3.88	N.D.	334.87	23.74	80.65	N.D.	N.D.

N.D. = Not Detectable, Ton = ODAS Tonne, NP = Nord-Perd Rinne, W = Wiek, Ark = Arkona, L = Lander (height above sea floor), Fluff = Mobile Nepheloid Layer

March '97, ICPMS, Water Particulate Phase, ng/l, ctd

	Li	Ti	V	Mn	Fe	Co	Ni	Cu	Zn	As	Rb	Sr	Y	Zr	Mo	Cd	Sn	Sb	Cs	Ba	Ce	Pb	Th	U
W 0m	8.20	286	26.48	604.23	4780	11.08	86.20	72.82	323.66	27.47	11.38	445.39	1.73	20.16	4.22	3.20	2.54	0.71	N.D.	459.36	5.30	54.46	N.D.	N.D.
W 5m	9.30	346	21.44	471.09	5662	10.59	83.10	75.89	291.96	22.82	15.79	435.28	2.43	13.50	4.25	2.94	3.04	1.80	N.D.	448.21	7.49	48.93	0.40	N.D.
W 10m	9.65	379	24.51	511.88	5911	9.33	90.98	78.69	293.55	20.92	17.27	457.37	2.48	15.34	5.61	3.82	2.39	1.02	N.D.	457.17	14.84	41.37	0.55	N.D.
W 15m	20.83	839	55.79	1252	13808	21.06	174.75	171.48	636.55	42.14	38.48	889.31	6.20	39.64	11.65	6.03	4.59	1.99	N.D.	674.26	18.12	84.29	1.54	N.D.
W 20m	14.63	735	42.07	546.91	12525	12.34	88.41	75.55	234.01	21.84	29.08	437.96	5.94	25.71	6.16	1.81	2.87	1.29	0.63	165.70	15.15	63.71	1.69	N.D.
W 25m	21.66	1146	60.22	725.50	19510	15.66	96.21	86.19	308.41	26.64	42.87	484.31	9.76	38.31	8.47	1.51	4.30	1.56	1.18	200.58	24.47	79.29	3.42	1.04
W L Fluff	536.48	39873	1631	1611	393981	436.63	1681	2048	5048.40	260.75	1879	48282	157.58	1643	414.01	69.16	754	23.76	106	3992.63	486.61	815.88	169	54.90
W L 5cm	100.62	14045	380.76	628.06	62180	5467	640	1473	1805.20	115.90	369.29	231.48	60.71	671.48	95.64	14.14	36.96	N.D.	9.02	1532.72	173.31	1470	27.78	10.41
W L 10cm	124.26	14549	419.14	766.09	83945	339.39	1128	909	1635.74	107.81	416.99	61.69	63.10	723.96	116.73	14.46	44.39	0.86	14.73	1433.41	195.57	290.57	35.79	18.17
W L 20cm	98.34	10676	291.16	721.70	63172	185.21	1241	1083	905.79	86.90	312.88	19.55	47.58	562.58	103.66	14.25	34.39	2.42	7.93	1292.17	149.75	211.40	21.42	9.95
W L 40cm	128.84	13540	477.65	891.48	73516	163.00	772.87	733.31	900.95	182.71	396.80	13.62	53.90	598.57	94.34	16.79	46.29	0.38	11.74	1447.00	154.45	268.30	21.92	13.10
Ark 0m	6.44	313	12.52	234.30	4886	19.12	121.11	150.75	426.72	24.71	25.44	375.02	14.92	17.92	6.73	4.06	4.14	1.41	11.83	249.67	12.93	78.32	1.46	N.D.
Ark 5m	4.01	178	28.21	181.05	3154	7.55	85.24	125.71	337.17	39.07	13.34	395.88	11.92	9.27	4.62	3.35	4.58	0.51	11.21	239.28	8.15	63.80	N.D.	N.D.
Ark 10m	5.03	252	25.15	213.87	3456	13.27	86.87	124.35	527.60	30.01	15.51	435.59	12.20	11.87	3.84	4.12	4.42	1.27	11.31	266.45	8.47	57.46	N.D.	N.D.
Ark 20m	4.70	286	25.15	253.59	4475	539.99	118.00	252.01	702.96	23.60	17.57	353.39	12.79	12.86	7.17	2.55	4.48	0.54	11.58	183.72	9.20	96.48	N.D.	N.D.
Ark 30m	5.86	347	20.33	282.32	7032	29.03	109.70	135.96	1280.50	14.17	21.03	285.29	12.98	13.35	7.16	1.48	2.93	0.54	11.30	106.87	13.89	37.47	N.D.	N.D.
Ark 35m	8.38	585	29.82	355.03	6977	21.09	90.20	150.64	329.09	17.66	30.47	310.33	14.68	20.64	4.45	2.13	4.71	3.10	11.98	121.98	16.62	53.28	N.D.	N.D.
Ark 40m	10.73	813	34.33	740.59	8484	17.87	79.32	116.63	242.73	17.39	36.75	375.57	15.64	23.41	4.56	3.15	4.26	1.43	12.25	158.58	21.32	71.06	0.27	N.D.
Ark 45m	17.24	876	50.50	653.33	10491	74.45	65.94	115.39	245.29	22.53	50.43	622.32	16.76	30.19	3.24	1.65	4.66	0.68	12.29	160.79	28.92	76.53	1.42	N.D.
Ark L Fluff	17214	2.E+06	58379	13617	1.E+07	5770	18665	20909	61940	7310	50424	54874	6502	70075	1272	749	34473	456	1861	175940	2.E+05	36644	5162	1565
Ark L 5cm	23.88	2126	56.49	157.20	12336	18.55	349.14	130.59	151.17	30.25	81.96	1595.81	34.92	122.40	40.78	1.27	6.45	N.D.	31.13	363.07	30.92	33.23	N.D.	N.D.
Ark L 10cm	197.47	25803	628.22	952.10	9552	66.50	657.44	262.23	462.84	120.58	695.34	1975.96	93.42	1033	218.83	2.91	33.17	11.45	49.85	2669.50	N.D.	86.75	74.69	13.79
Ark L 20cm	112.97	17143	360.78	747.71	18662	37.82	532.53	182.96	268.61	70.61	379.12	1030.68	52.95	601.63	139.62	1.65	19.59	4.10	25.99	1492.43	N.D.	48.38	37.23	9.61
Ark L 40cm	15.35	424	57.32	141.41	9113	17.37	565.74	96.96	135.65	23.69	20.56	768.82	15.36	20.94	76.21	0.89	5.91	N.D.	15.13	60.25	N.D.	20.04	N.D.	N.D.

N.D. = Not Detectable, Ton = ODAS Tonne, NP = Nord-Perd Rinne, W = Wiek, Ark = Arkona, L = Lander (height above sea floor),

Fluff = Mobile Nepheloid Layer

March '97, ICPMS, Normalised Water Particulate Phase to Rubidium ratios

	Li/Rb	Ti/Rb	V/Rb	Mn/Rb	Fe/Rb	Co/Rb	Ni/Rb	Cu/Rb	Zn/Rb	As/Rb	Sr/Rb	Y/Rb	Zr/Rb	Mo/Rb	Cd/Rb	Sn/Rb	Sb/Rb	Cs/Rb	Ba/Rb	Ce/Rb	Pb/Rb	Th/Rb	U/Rb
Ton 0m	0.193	24.05	0.672	40.96	317	0.463	16.052	3.707	15.306	0.421	9.612	0.185	0.847	3.689	0.124	0.177	0.105	0.024	8.062	0.579	3.596	0.075	0.010
Ton 5m	0.258	20.39	0.903	64.03	348	0.451	4.142	3.058	19.819	0.686	17.822	0.243	0.669	0.418	0.134	0.139	0.076	0.034	8.597	0.438	3.274	0.024	0.021
Ton 10m	0.265	22.50	0.722	24.81	525	0.540	2.681	1.961	10.952	0.301	7.216	0.221	0.754	0.148	0.049	0.128	0.089	0.037	6.943	0.631	2.867	0.021	0.014
Ton 15m	0.358	32.13	0.955	33.39	413	0.166	0.736	0.859	4.305	0.249	2.267	0.193	1.015	0.022	0.014	0.066	0.014	0.042	4.431	0.685	1.306	0.092	0.021
Ton L Fluff	0.435	23.33	1.414	35.94	522	0.217	1.336	1.197	6.907	0.434	3.778	0.283	0.747	0.025	0.029	0.117	0.004	0.014	3.043	0.657	4.197	0.082	0.002
Ton L 5cm	0.436	38.14	2.057	35.81	521	1.384	10.976	8.728	204.10	0.551	33.161	1.226	0.823	0.169	N.D.	5.902	0.658	N.D.	12.480	0.778	4.789	N.D.	N.D.
Ton L 10cm	0.386	41.96	1.485	33.08	451	1.315	6.259	4.843	54.283	0.351	20.000	0.750	1.214	0.074	N.D.	1.183	0.036	N.D.	8.856	0.309	2.892	N.D.	N.D.
Ton L 20cm	0.332	31.24	2.101	37.32	478	1.277	10.378	6.049	48.156	0.575	22.498	0.759	1.010	0.986	N.D.	0.877	0.024	N.D.	10.530	0.069	3.172	N.D.	N.D.
Ton L 40cm	0.387	30.67	1.532	30.30	465	1.157	11.671	7.494	68.623	0.569	30.263	1.082	0.583	0.202	0.003	1.546	0.025	N.D.	9.430	0.315	3.918	N.D.	N.D.
NP 0m	0.365	28.29	1.362	37.64	429	0.728	7.409	4.616	25.636	1.353	32.749	0.428	0.877	0.360	0.218	0.256	0.038	0.026	22.878	0.533	3.228	0.066	0.031
NP 5m	0.354	26.65	1.250	33.41	402	2.453	4.525	3.416	24.102	0.977	28.526	0.433	0.853	0.133	0.161	0.283	0.005	0.024	19.288	0.569	5.083	0.069	0.020
NP 10m	0.328	26.14	1.565	39.22	479	0.581	7.104	4.510	26.787	1.467	25.562	0.449	0.783	0.465	0.192	0.288	0.046	0.026	21.482	0.489	2.925	0.067	0.021
NP 15m	0.388	25.98	1.391	26.45	371	0.396	3.500	3.071	14.491	0.572	14.636	0.382	0.737	0.115	0.027	0.095	0.169	0.030	5.032	0.472	2.060	0.062	0.020
NP 20m	0.379	24.62	1.111	18.93	315	0.274	1.755	1.201	5.164	0.340	8.816	0.272	0.898	0.047	N.D.	0.058	0.082	0.036	4.483	0.560	2.765	0.044	0.021
NP L Fluff	0.450	22.55	0.086	7.50	380	0.172	0.805	0.901	2.395	0.242	2.563	0.228	0.719	0.040	0.078	1.115	0.015	0.059	2.248	0.530	1.268	0.100	0.026
NP L 5cm	0.801	31.34	2.343	3.12	233	1.468	7.163	4.340	6.247	0.877	24.390	0.061	1.477	0.403	0.055	0.626	0.031	N.D.	4.034	0.286	1.187	N.D.	N.D.
NP L 10cm	0.811	32.65	3.323	3.88	259	1.460	9.628	6.511	6.511	1.181	25.990	0.054	1.554	0.581	0.053	0.326	0.045	N.D.	4.446	0.227	1.581	N.D.	N.D.
NP L 20cm	0.737	30.05	2.789	3.69	239	1.340	9.657	5.706	48.028	1.021	24.195	0.071	2.069	0.737	0.039	0.259	0.027	N.D.	5.592	0.411	0.866	N.D.	N.D.
NP L 40cm	0.828	26.36	2.387	4.86	331	0.967	20.359	5.769	5.984	0.943	28.302	0.049	1.416	1.342	0.068	0.979	0.051	N.D.	4.439	0.315	1.069	N.D.	N.D.

N.D. = Not Detectable, Ton = ODAS Tonne, NP = Nord-Perd Rinne, W = Wiek, Ark = Arkona, L = Lander (height above sea floor), Fluff = Mobile Nepheloid Layer

March '97, ICPMS, Normalised Water Particulate Phase to Rubidium ratios, ctd.

	Li/Rb	Ti/Rb	V/Rb	Mn/Rb	Fe/Rb	Co/Rb	Ni/Rb	Cu/Rb	Zn/Rb	As/Rb	Sr/Rb	Y/Rb	Zr/Rb	Mo/Rb	Cd/Rb	Sn/Rb	Sb/Rb	Cs/Rb	Ba/Rb	Ce/Rb	Pb/Rb	Th/Rb	U/Rb
W 0m	0.721	25.11	2.326	53.08	420	0.974	7.572	6.397	28.430	2.413	39.123	0.152	1.771	0.371	0.281	0.223	0.062	N.D.	40.350	0.466	4.784	N.D.	N.D.
W 5m	0.589	21.94	1.358	29.84	359	0.671	5.263	4.806	18.491	1.445	27.567	0.154	0.855	0.269	0.186	0.193	0.114	N.D.	28.386	0.474	3.099	0.025	N.D.
W 10m	0.559	21.96	1.419	29.64	342	0.540	5.269	4.557	16.999	1.211	26.486	0.143	0.888	0.325	0.221	0.138	0.059	N.D.	26.474	0.859	2.396	0.032	N.D.
W 15m	0.541	21.79	1.450	32.55	359	0.547	4.541	4.456	16.542	1.095	23.111	0.161	1.030	0.303	0.157	0.119	0.052	N.D.	17.522	0.471	2.191	0.040	N.D.
W 20m	0.503	25.28	1.447	18.81	431	0.424	3.040	2.598	8.046	0.751	15.059	0.204	0.884	0.212	0.062	0.099	0.044	0.022	5.697	0.521	2.191	0.058	N.D.
W 25m	0.505	26.74	1.405	16.92	455	0.365	2.244	2.011	7.195	0.621	11.298	0.228	0.894	0.198	0.035	0.100	0.036	0.027	4.679	0.571	1.850	0.080	0.024
W L Fluff	0.286	21.22	0.868	0.86	210	0.232	0.894	1.090	2.687	0.139	25.695	0.084	0.875	0.220	0.037	0.401	0.013	0.057	2.125	0.259	0.434	0.090	0.029
W L 5cm	0.272	38.03	1.031	1.70	168	14.803	1.733	3.989	4.888	0.314	0.627	0.164	1.818	0.259	0.038	0.100	N.D.	0.024	4.150	0.469	3.982	0.075	0.028
W L 10cm	0.298	34.89	1.005	1.84	201	0.814	2.704	2.180	3.923	0.259	0.148	0.151	1.736	0.280	0.035	0.106	0.002	0.035	3.437	0.469	0.697	0.086	0.044
W L 20cm	0.314	34.12	0.931	2.31	202	0.592	3.966	3.460	2.895	0.278	0.062	0.152	1.798	0.331	0.046	0.110	0.008	0.025	4.130	0.479	0.676	0.068	0.032
W L 40cm	0.325	34.12	1.204	2.25	185	0.411	1.948	1.848	2.271	0.460	0.034	0.136	1.508	0.238	0.042	0.117	0.001	0.030	3.647	0.389	0.676	0.055	0.033
Ark 0m	0.253	12.29	0.492	9.21	192	0.751	4.760	5.925	16.771	0.971	14.739	0.587	0.704	0.264	0.159	0.163	0.055	0.465	9.813	0.508	3.078	0.057	N.D.
Ark 5m	0.301	13.32	2.115	13.57	237	0.566	6.391	9.425	25.279	2.929	29.681	0.894	0.695	0.346	0.251	0.343	0.039	0.840	17.940	0.611	4.783	N.D.	N.D.
Ark 10m	0.324	16.26	1.621	13.79	223	0.855	5.600	8.017	34.015	1.935	28.083	0.786	0.765	0.248	0.265	0.285	0.082	0.729	17.178	0.546	3.705	N.D.	N.D.
Ark 20m	0.268	16.28	1.431	14.43	255	30.726	6.714	14.340	40.000	1.343	20.109	0.728	0.731	0.408	0.145	0.255	0.031	0.659	10.454	0.524	5.490	N.D.	N.D.
Ark 30m	0.279	16.49	0.967	13.43	334	1.381	5.217	6.466	60.903	0.674	13.569	0.617	0.635	0.340	0.071	0.139	0.026	0.537	5.083	0.661	1.782	N.D.	N.D.
Ark 35m	0.275	19.20	0.979	11.65	229	0.692	2.960	4.944	10.801	0.580	10.186	0.482	0.677	0.146	0.070	0.154	0.102	0.393	4.004	0.545	1.749	N.D.	N.D.
Ark 40m	0.292	22.13	0.934	20.15	231	0.486	2.158	3.174	6.605	0.473	10.220	0.426	0.637	0.124	0.086	0.116	0.039	0.333	4.315	0.580	1.934	0.007	N.D.
Ark 45m	0.342	17.38	1.001	12.95	208	1.476	1.307	2.288	4.864	0.447	12.340	0.332	0.599	0.064	0.033	0.092	0.014	0.244	3.188	0.573	1.517	0.028	N.D.
Ark L Fluff	0.341	35.94	1.158	0.27	260	0.114	0.370	0.415	1.228	0.145	1.088	0.129	1.390	0.025	0.015	0.684	0.009	0.037	3.489	3.718	0.727	0.102	0.031
Ark L 5cm	0.291	25.94	0.689	1.92	151	0.226	4.260	1.593	1.844	0.369	19.471	0.426	1.493	0.498	0.015	0.079	0.028	0.380	4.430	0.377	0.405	N.D.	N.D.
Ark L 10cm	0.284	37.11	0.903	1.37	14	0.096	0.946	0.377	0.666	0.173	2.842	0.134	1.486	0.315	0.004	0.048	0.016	0.072	3.839	N.D.	0.125	0.107	0.020
Ark L 20cm	0.298	45.22	0.952	1.97	49	0.100	1.405	0.483	0.709	0.186	2.719	0.140	1.587	0.368	0.004	0.052	0.011	0.069	3.937	N.D.	0.128	0.098	0.025
Ark L 40cm	0.747	20.61	2.788	6.88	443	0.845	27.517	4.716	6.598	1.152	37.395	0.747	1.018	3.707	0.044	0.288	0.066	0.736	2.930	N.D.	0.975	N.D.	N.D.

N.D. = Not Detectable, Ton = ODAS Tonne, NP = Nord-Perd Rinne, W = Wiek, Ark = Arkona, L = Lander (height above sea floor), Fluff = Mobile Nepheloid Layer

June '97, ICPMS, Water Particulate Phase, ng/l.

	Li	Ti	V	Mn	Fe	Co	Ni	Zn	Cu	As	Rb	Sr	Y	Zr	Mo	Cd	Sn	Sb	Cs	Ba	Ce	Pb	Th	U
Ton 0m	13.52	642	106.91	8646	10621	67.99	323.7	1181	235.8	70.31	30.23	1129	27.85	29.58	13.35	7.57	12.94	1.20	24.94	839	18.83	264	0.06	N.D.
Ton 5m	13.36	543	82.33	10809	10334	27.98	204.2	1274	179.2	64.53	29.17	1132	30.14	24.40	6.30	6.16	15.73	N.D.	26.94	830	19.58	261	N.D.	N.D.
Ton 10m	8.66	564	42.61	6042	11439	13.80	114.2	647	111.4	32.93	27.33	902	28.91	22.73	4.29	2.20	5.90	N.D.	25.73	657	21.79	197	0.14	N.D.
Ton 15m	26.75	1855	83.24	6770	31920	19.89	124.0	760	119.7	36.51	67.62	1097	36.30	55.55	4.41	1.89	7.62	N.D.	27.81	580	44.60	248	4.34	N.D.
Ton L Fluff	140.4	7821	566.83	14448	177801	100.6	643.4	2737	641.2	213.0	344.6	1451	173.5	263.0	25.37	26.81	595	N.D.	128	1127	216	1363	25.87	N.D.
Ton L 5cm	52.57	3146	193.59	6934	52569	25.66	544.4	1240	340.8	103.1	129.2	1648	97.41	102.8	34.94	48.79	81.39	N.D.	84.87	1349	75.29	489	3.48	N.D.
Ton L 10cm	53.09	2986	208.11	6315	49298	26.12	602.5	1751	426.2	114.3	132.2	1723	99.15	130.5	36.81	27.20	61.88	N.D.	84.91	1491	111	574	10.28	N.D.
Ton L 20cm	53.11	2770	171.91	6208	44933	28.26	520.8	1302	385.5	98.53	119.8	1647	85.79	111.2	30.94	33.62	130	N.D.	74.63	1366	99.37	446	2.75	N.D.
Ton L 40cm	55.69	2934	306.96	6110	53851	24.49	655.1	1314	418.5	157.9	139.0	1914	109.7	108.1	43.64	54.47	111	N.D.	98.58	1587	90.20	463	1.92	N.D.
NP 0m	7.11	254	26.84	3325	3402	17.83	86.8	361	93.21	25.09	15.23	473	15.44	20.20	3.87	5.97	10.86	0.25	13.44	124	12.53	244	0.07	N.D.
NP 5m	6.45	336	28.20	4705	6126	16.72	92.6	461	81.82	26.13	16.76	624	15.57	18.95	3.07	7.00	7.16	0.65	13.34	318	14.45	269	0.28	N.D.
NP 10m	6.32	326	30.50	1823	7171	11.62	77.6	611	62.20	23.50	16.33	398	15.38	17.31	2.79	2.51	7.26	0.27	13.12	222	14.55	156	0.28	N.D.
NP 15m	7.72	451	33.57	1370	6315	6.87	69.4	353	64.70	22.39	21.21	363	15.01	19.23	3.21	1.74	5.17	N.D.	12.63	174	12.58	103	0.67	N.D.
NP 20m	N.D.	N.D.	N.D.	N.D.	N.D.	N.D.	N.D.	N.D.	N.D.	N.D.	N.D.	N.D.	N.D.	N.D.	N.D.	N.D.	N.D.	N.D.	N.D.	N.D.	N.D.	N.D.	N.D.	N.D.
NP L Fluff	311.4	17206	1032	13627	250785	160.8	1626	4041	974.5	383.3	748.6	2266	190.7	592.9	173	87.60	422	0.17	44.60	2530	463	2144	78.47	19.62
NP L 5cm	74.90	3881	320.75	3642	56292	87.87	1065	1406	551.0	150.0	150.8	2392	34.87	146.4	121	44.19	98.86	N.D.	5.98	1084	113	424	7.46	0.95
NP L 10cm	74.31	3289	330.63	3085	43466	123.7	660.8	1236	431.5	139.7	136.4	2434	31.10	112.6	55.26	67.34	118	N.D.	4.76	876	67.40	616	5.67	N.D.
NP L 20cm	72.70	3776	252.82	3679	53542	81.62	1002	1408	404.3	126.4	148.9	2312	35.44	145.5	80.10	69.59	128	N.D.	5.77	985	89.26	548	8.59	1.59
NP L 40cm	67.79	3491	236.02	3361	45101	72.99	727.1	1336	396.3	117.8	130.9	2242	31.44	119.7	48.38	66.93	141	N.D.	4.43	901	72.84	453	5.21	0.12

N.D. = Not Detectable, Ton = ODAS Tonne, NP = Nord-Perd Rinne, W = Wiek, Ark = Arkona, L = Lander (height above sea floor), Fluff = Mobile Nepheloid Laye

June '97, ICPMS, Water Particulate Phase, ng/l, ctd.

	Li	Ti	V	Mn	Fe	Co	Ni	Zn	Cu	As	Rb	Sr	Y	Zr	Mo	Cd	Sn	Sb	Cs	Ba	Ce	Pb	Th	U
W 0m	9.70	461	27.51	3885	6005	21.72	80.6	277	149.2	25.90	17.33	517	4.93	16.59	4.21	5.97	20.19	N.D.	0.38	186	13.85	374	0.86	0.13
W 5m	9.59	331	25.85	3753	5650	18.89	77.6	267	74.60	17.86	16.75	553	4.69	19.03	3.53	5.09	13.94	N.D.	0.40	179	13.26	257	0.72	0.01
W 10m	9.71	459	24.21	3812	7877	16.54	75.9	264	82.13	17.00	19.54	439	5.56	19.82	3.22	4.37	16.28	N.D.	0.61	171	14.48	231	1.21	0.16
W 15m	10.60	477	32.67	3164	8251	14.99	86.1	189	74.77	18.50	21.80	406	6.39	18.20	4.03	3.44	9.73	N.D.	0.75	244	13.82	153	1.27	0.19
W 20m	9.50	423	24.36	1877	7700	14.29	66.8	166	71.76	17.03	19.00	517	5.70	16.33	4.81	3.10	9.92	N.D.	0.59	256	11.86	130	1.05	0.04
W 25m	12.46	615	44.54	1566	10272	17.71	96.2	166	78.86	25.51	27.43	601	6.95	20.98	15.09	3.03	8.83	0.24	0.99	269	18.67	109	1.82	0.34
W L Fluff	862.2	39556	2342	6510	845089	482.0	3096	6970	2516	707.3	2168	5636	535.8	1468	238.8	47.24	607.2	17.0	263.0	4984	1145	3087	200.6	38.98
W L 5cm	30.61	4154	204.75	1243	42899	407.1	593.1	1312	388.3	112.2	142.4	2079	95.54	273.6	30.67	17.66	20.58	9.47	74.73	663	125.1	404	0.84	N.D.
W L 10cm	16.87	1907	131.58	749	25844	76.08	577.6	899	248.6	106.2	84.43	2139	77.48	161.3	43.71	3.37	9.29	2.08	72.81	431	79.12	257	N.D.	N.D.
W L 20cm	6.82	1605	141.96	732	28735	171.7	749.9	1110	303.6	87.46	76.27	1898	78.06	85.58	69.58	10.22	16.27	2.15	72.72	357	83.77	246	N.D.	N.D.
W L 40cm	5.25	1816	169.89	599	21989	82.47	517.7	992	245.9	97.21	69.12	2012	75.60	89.55	34.19	7.79	15.27	N.D.	72.36	463	88.23	186	N.D.	N.D.
Ark 0m	7.20	796	30.36	901	7970	14.99	80.2	233	169.9	16.02	27.15	370	15.03	25.36	2.42	8.38	23.05	0.94	11.79	256	24.88	122	2.53	1.22
Ark 5m	1.33	287	19.93	1088	3687	11.73	75.3	181	145.6	17.33	12.06	355	12.07	13.40	1.83	9.39	39.90	0.84	10.68	215	13.37	103	0.68	0.53
Ark 10m	0.98	288	25.62	1187	3516	11.40	74.2	186	108.1	21.39	12.08	350	12.16	10.76	2.68	9.10	23.43	0.67	10.71	223	13.66	91	0.71	0.57
Ark 20m	0.45	189	18.88	866	2436	10.30	55.9	132	90.05	17.34	9.59	330	11.56	7.50	0.49	0.77	2.70	0.62	10.61	191	11.55	106	0.47	0.61
Ark 30m	0.39	208	12.90	793	2615	23.60	54.5	115	94.40	10.08	9.37	296	11.58	9.23	0.45	2.79	7.60	0.83	10.64	204	15.37	67	0.37	0.56
Ark 35m	0.37	166	20.14	714	2308	8.39	48.3	89	92.27	12.54	9.77	323	11.74	27.61	0.91	3.35	14.40	0.65	10.84	167	14.43	104	0.50	0.49
Ark 40m	7.82	645	39.13	1421	7677	15.91	62.6	152	93.51	25.30	28.30	348	14.96	19.52	0.67	4.25	23.37	0.94	11.37	205	26.88	113	2.39	0.91
Ark 45m	3.13	286	26.01	3109	4606	15.72	60.3	164	97.49	19.28	15.28	323	12.66	8.73	2.02	3.35	38.04	0.92	11.05	165	14.79	106	0.81	0.60
Ark L Fluff	874.3	38010	2032	3140	573155	320.5	2203	4848	1922	477.8	2210	5268	501.7	1063	177.0	13.44	735.4	34.8	336.0	4957	1042	3122	204.0	64.74
Ark L 5cm	117.1	8806	332.70	985	105173	72.66	577.1	1028	389.0	190.7	292.3	2974	115.0	353.9	45.27	10.48	25.63	7.10	97.62	1165	202.9	364	21.45	10.59
Ark L 10cm	136.3	9177	332.08	1193	108866	92.24	1368	1253	350.8	238.3	364.4	3903	123.7	719.3	170.0	11.06	14.89	8.76	97.98	1629	207.1	469	23.03	11.32
Ark L 20cm	82.18	3729	210.81	775	85444	62.62	1069	1002	297.0	174.4	171.3	2585	98.34	113.8	118.5	8.97	17.02	7.46	94.73	643	143.6	326	11.17	6.11
Ark L 40cm	90.59	3869	219.38	908	90615	120.2	1180	1553	344.0	173.9	198.3	2669	100.2	164.0	146.4	14.37	36.03	8.01	96.01	653	155.5	387	13.53	6.66

N.D. = Not Detectable, Ton = ODAS Tonne, NP = Nord-Perd Rinne, W = Wiek, Ark = Arkona, L = Lander (height above sea floor),

Fluff = Mobile Nepheloid Layer

June '97, ICPMS, Normalised Water Particulate Phase to Rubidium ratios.

	Li/Rb	Ti/Rb	V/Rb	Mn/Rb	Fe/Rb	Co/Rb	Ni/Rb	Cu/Rb	Zn/Rb	As/Rb	Sr/Rb	Y/Rb	Zr/Rb	Mo/Rb	Cd/Rb	Sn/Rb	Sb/Rb	Cs/Rb	Ba/Rb	Ce/Rb	Pb/Rb	Th/Rb	U/Rb
Ton 0m	0.447	21.239	3.537	286.0	351.3	2.249	10.706	39.081	7.801	2.326	37.339	0.921	0.979	0.442	0.250	0.428	0.040	0.825	27.752	0.623	8.739	0.002	N.D.
Ton 5m	0.458	18.599	2.823	370.6	354.3	0.959	7.000	43.691	6.143	2.212	38.802	1.033	0.837	0.216	0.211	0.539	N.D.	0.924	28.453	0.671	8.946	N.D.	N.D.
Ton 10m	0.317	20.647	1.559	221.0	418.5	0.505	4.177	23.689	4.076	1.205	33.004	1.058	0.832	0.157	0.080	0.216	N.D.	0.941	24.037	0.797	7.209	0.005	N.D.
Ton 15m	0.396	27.428	1.231	100.1	472.0	0.294	1.834	11.239	1.770	0.540	16.218	0.537	0.822	0.065	0.028	0.113	N.D.	0.411	8.580	0.660	3.670	0.064	N.D.
Ton L Fluff	0.407	22.694	1.645	41.9	515.9	0.292	1.867	7.942	1.860	0.618	4.211	0.503	0.763	0.074	0.078	1.726	N.D.	0.372	3.272	0.626	3.956	0.075	N.D.
Ton L 5cm	0.407	24.344	1.498	53.7	406.8	0.199	4.213	9.595	2.637	0.798	12.756	0.754	0.796	0.270	0.378	0.630	N.D.	0.657	10.438	0.583	3.787	0.027	N.D.
Ton L 10cm	0.402	22.595	1.575	47.8	373.0	0.198	4.559	13.249	3.225	0.864	13.036	0.750	0.988	0.278	0.206	0.468	N.D.	0.642	11.280	0.842	4.344	0.078	N.D.
Ton L 20cm	0.444	23.134	1.436	51.8	375.2	0.236	4.349	10.868	3.219	0.823	13.755	0.716	0.929	0.258	0.281	1.083	N.D.	0.623	11.405	0.830	3.724	0.023	N.D.
Ton L 40cm	0.401	21.116	2.209	44.0	387.5	0.176	4.714	9.456	3.012	1.136	13.773	0.789	0.778	0.314	0.392	0.797	N.D.	0.709	11.417	0.649	3.329	0.014	N.D.
NP 0m	0.467	16.675	1.762	218.3	223.3	1.170	5.699	23.715	6.118	1.647	31.060	1.013	1.326	0.254	0.392	0.713	0.017	0.882	8.127	0.822	16.036	0.005	N.D.
NP 5m	0.385	20.066	1.682	280.7	365.5	0.997	5.521	27.494	4.881	1.559	37.210	0.929	1.131	0.183	0.418	0.427	0.039	0.796	18.990	0.862	16.054	0.017	N.D.
NP 10m	0.387	19.972	1.868	111.6	439.2	0.712	4.750	37.395	3.809	1.439	24.353	0.942	1.060	0.171	0.154	0.444	0.017	0.804	13.598	0.891	9.539	0.017	N.D.
NP 15m	0.364	21.258	1.583	64.6	297.7	0.324	3.273	16.623	3.050	1.055	17.106	0.708	0.907	0.151	0.082	0.244	N.D.	0.595	8.191	0.593	4.848	0.031	N.D.
NP 20m	N.D.	N.D.	N.D.	N.D.	N.D.	N.D.	N.D.	N.D.	N.D.	N.D.	N.D.	N.D.	N.D.	N.D.	N.D.	N.D.	N.D.	N.D.	N.D.	N.D.	N.D.	N.D.	N.D.
NP L Fluff	0.416	22.984	1.378	18.2	335.0	0.215	2.172	5.398	1.302	0.512	3.026	0.255	0.792	0.231	0.117	0.563	N.D.	0.060	3.379	0.618	2.863	0.105	0.026
NP L 5cm	0.497	25.735	2.127	24.1	373.2	0.583	7.060	9.319	3.653	0.994	15.858	0.231	0.971	0.800	0.293	0.655	N.D.	0.040	7.187	0.751	2.811	0.049	0.006
NP L 10cm	0.545	24.103	2.423	22.6	318.6	0.907	4.843	9.058	3.162	1.024	17.835	0.228	0.825	0.405	0.494	0.862	N.D.	0.035	6.421	0.494	4.516	0.042	N.D.
NP L 20cm	0.488	25.367	1.698	24.7	359.7	0.548	6.731	9.459	2.716	0.849	15.532	0.238	0.978	0.538	0.467	0.859	N.D.	0.039	6.618	0.600	3.684	0.058	0.011
NP L 40cm	0.518	26.671	1.803	25.7	344.6	0.558	5.555	10.210	3.027	0.900	17.131	0.240	0.914	0.370	0.511	1.081	N.D.	0.034	6.887	0.556	3.458	0.040	0.001

N.D. = Not Detectable, Ton = ODAS Tonne, NP = Nord-Perd Rinne, W = Wiek, Ark = Arkona, L = Lander (height above sea floor), Fluff = Mobile Nepheloid Layer

June '97, ICPMS, Normalised Water Particulate Phase to Rubidium ratios, ctd.

	Li/Rb	Ti/Rb	V/Rb	Mn/Rb	Fe/Rb	Co/Rb	Ni/Rb	Cu/Rb	Zn/Rb	As/Rb	Sr/Rb	Y/Rb	Zr/Rb	Mo/Rb	Cd/Rb	Sn/Rb	Sb/Rb	Cs/Rb	Ba/Rb	Ce/Rb	Pb/Rb	Th/Rb	U/Rb
W 0m	0.560	26.588	1.587	224.1	346.4	1.253	4.651	16.004	8.610	1.494	29.831	0.284	0.957	0.243	0.344	1.165	N.D.	0.022	10.734	0.799	21.602	0.050	0.007
W 5m	0.572	19.748	1.543	224.1	337.3	1.128	4.635	15.920	4.454	1.067	33.032	0.280	1.136	0.211	0.304	0.832	N.D.	0.024	10.685	0.792	15.345	0.043	0.001
W 10m	0.497	23.489	1.239	195.1	403.1	0.846	3.884	13.501	4.203	0.870	22.469	0.285	1.014	0.165	0.223	0.833	N.D.	0.031	8.768	0.741	11.819	0.062	0.008
W 15m	0.486	21.892	1.498	145.1	378.4	0.687	3.949	8.669	3.429	0.849	18.640	0.293	0.835	0.185	0.158	0.446	N.D.	0.034	11.205	0.634	7.017	0.058	0.009
W 20m	0.500	22.254	1.282	98.8	405.3	0.752	3.517	8.749	3.777	0.897	27.216	0.300	0.859	0.253	0.163	0.522	N.D.	0.031	13.454	0.624	6.840	0.055	0.002
W 25m	0.454	22.433	1.624	57.1	374.5	0.646	3.508	6.039	2.875	0.930	21.921	0.253	0.765	0.550	0.110	0.322	0.009	0.036	9.791	0.681	3.974	0.066	0.013
W L Fluff	0.398	18.248	1.080	3.0	389.9	0.222	1.428	3.216	1.161	0.326	2.600	0.247	0.677	0.110	0.022	0.280	0.008	0.121	2.299	0.528	1.424	0.093	0.018
W L 5cm	0.215	29.164	1.438	8.7	301.2	2.858	4.164	9.215	2.727	0.788	14.594	0.671	1.921	0.215	0.124	0.145	0.066	0.525	4.656	0.879	2.834	0.006	N.D.
W L 10cm	0.200	22.582	1.559	8.9	306.1	0.901	6.841	10.644	2.945	1.257	25.341	0.918	1.910	0.518	0.040	0.110	0.025	0.862	5.101	0.937	3.046	N.D.	N.D.
W L 20cm	0.089	21.037	1.861	9.6	376.7	2.251	9.832	14.559	3.980	1.147	24.880	1.023	1.122	0.912	0.134	0.213	0.028	0.953	4.683	1.098	3.221	N.D.	N.D.
W L 40cm	0.076	26.265	2.458	8.7	318.1	1.193	7.490	14.358	3.557	1.406	29.108	1.094	1.295	0.495	0.113	0.221	N.D.	1.047	6.701	1.276	2.695	N.D.	N.D.
Ark 0m	0.265	29.318	1.118	33.2	293.5	0.552	2.953	8.588	6.259	0.590	13.641	0.554	0.934	0.089	0.309	0.849	0.035	0.434	9.440	0.916	4.479	0.093	0.045
Ark 5m	0.110	23.810	1.653	90.2	305.8	0.973	6.246	14.973	12.078	1.437	29.449	1.001	1.112	0.152	0.779	3.309	0.069	0.886	17.795	1.109	8.580	0.057	0.044
Ark 10m	0.081	23.880	2.121	98.3	291.1	0.943	6.141	15.408	8.952	1.770	28.997	1.006	0.891	0.221	0.754	1.939	0.055	0.887	18.429	1.131	7.559	0.059	0.047
Ark 20m	0.047	19.701	1.969	90.3	254.0	1.074	5.831	13.797	9.389	1.808	34.363	1.205	0.782	0.051	0.080	0.282	0.065	1.106	19.921	1.204	11.057	0.049	0.063
Ark 30m	0.042	22.189	1.377	84.7	279.1	2.519	5.812	12.296	10.075	1.075	31.566	1.236	0.985	0.049	0.298	0.811	0.089	1.135	21.762	1.640	7.159	0.040	0.060
Ark 35m	0.037	17.036	2.062	73.1	236.3	0.858	4.948	9.113	9.445	1.284	33.111	1.202	2.826	0.093	0.342	1.474	0.066	1.109	17.116	1.477	10.684	0.051	0.050
Ark 40m	0.276	22.803	1.383	50.2	271.3	0.562	2.211	5.369	3.304	0.894	12.288	0.529	0.690	0.024	0.150	0.826	0.033	0.402	7.241	0.950	4.004	0.084	0.032
Ark 45m	0.205	18.747	1.703	203.5	301.5	1.029	3.944	10.717	6.382	1.262	21.134	0.828	0.572	0.132	0.219	2.490	0.060	0.723	10.784	0.968	6.967	0.053	0.039
Ark L Fluff	0.396	17.200	0.919	1.4	259.4	0.145	0.997	2.194	0.870	0.216	2.384	0.227	0.481	0.080	0.006	0.333	0.016	0.152	2.243	0.471	1.413	0.092	0.029
Ark L 5cm	0.400	30.123	1.138	3.4	359.8	0.249	1.974	3.518	1.331	0.652	10.174	0.393	1.211	0.155	0.036	0.088	0.024	0.334	3.984	0.694	1.245	0.073	0.036
Ark L 10cm	0.374	25.186	0.911	3.3	298.8	0.253	3.755	3.438	0.963	0.654	10.713	0.339	1.974	0.466	0.030	0.041	0.024	0.269	4.470	0.568	1.286	0.063	0.031
Ark L 20cm	0.480	21.769	1.231	4.5	498.8	0.366	6.240	5.849	1.734	1.018	15.092	0.574	0.664	0.692	0.052	0.099	0.044	0.553	3.756	0.838	1.906	0.065	0.036
Ark L 40cm	0.457	19.510	1.106	4.6	456.9	0.606	5.949	7.829	1.735	0.877	13.457	0.505	0.827	0.738	0.072	0.182	0.040	0.484	3.295	0.784	1.949	0.068	0.034

N.D. = Not Detectable, Ton = ODAS Tonne, NP = Nord-Perd Rinne, W = Wiek, Ark = Arkona, L = Lander (height above sea floor),

Fluff = Mobile Nepheloid Layer

December '97, ICPMS, Water Particulate Phase, ng/l.

	Li	Ti	V	Mn	Fe	Co	Ni	Zn	Cu	As	Rb	Sr	Y	Zr	Mo	Cd	Sn	Sb	Cs	Ba	Ce	Pb	Th	U
Ton 0m	24.32	2436	97.1	5569	30154	24.63	124.5	683	210.4	45.5	77.5	472	39.23	72.2	1.38	2.96	7.49	N.D.	33.5	536	65.6	280.7	N.D.	N.D.
Ton 5m	23.50	2320	94.4	5350	35207	22.14	119.8	652	201.4	43.8	73.1	464	39.45	59.5	1.01	3.19	6.70	N.D.	34.4	525	69.5	249.1	N.D.	N.D.
Ton 10m	23.04	2446	97.7	5307	34101	22.22	111.5	637	195.2	43.6	70.2	444	38.12	109.0	0.89	2.85	6.05	N.D.	32.5	540	63.4	248.3	N.D.	N.D.
Ton 15m	256.1	22174	824.4	28000	334825	140.8	539.8	3229	754.7	240.8	827.3	1759	148.5	926.8	23.05	24.91	29.2	N.D.	49.5	3234	406.7	1132	74.04	18.42
Ton L 5cm	80.36	10460	189.1	7934	60650	185.9	693.7	1849	291.2	124.4	142.0	1976	54.76	286.4	119.1	22.14	39.7	3.68	2.2	883	209.4	320.0	41.28	6.04
Ton L 10cm	74.58	6163	198.9	6730	55594	124.6	914.8	1448	310.3	107.3	119.1	2075	34.68	278.9	116.4	42.87	39.3	3.32	0.8	883	77.3	258.5	6.60	3.24
Ton L 20cm	72.84	3943	189.2	6790	46461	167.6	668.1	1483	382.9	108.9	107.4	2018	31.57	121.3	65.05	20.02	41.7	2.68	0.6	768	57.4	270.0	6.90	2.72
Ton L 40cm	68.14	2148	232.2	5084	36025	122.6	736.3	1485	264.5	122.1	92.1	2202	25.15	75.3	76.70	18.95	36.1	2.45	0.8	762	60.4	246.2	3.26	1.83
NP 0m	34.39	2208	111.5	4351	32965	32.51	113.6	529	207.2	46.9	71.4	497	21.65	71.5	6.00	5.32	14.9	1.28	3.0	361	50.8	298.1	7.37	2.17
NP 5m	34.11	2118	91.1	3900	31443	25.74	110.1	499	178.5	40.1	67.2	525	21.57	71.5	4.88	3.91	14.7	1.13	2.7	331	47.4	251.2	7.39	2.09
NP 10m	N.D.	N.D.	N.D.	N.D.	N.D.	N.D.	N.D.	N.D.	N.D.	N.D.	N.D.	N.D.	N.D.	N.D.	N.D.	N.D.	N.D.	N.D.	N.D.	N.D.	N.D.	N.D.	N.D.	N.D.
NP 15m	34.13	2590	99.7	3997	31703	28.33	114.3	505	196.4	63.3	72.1	519	23.30	120.8	5.20	4.19	26.6	1.33	3.2	359	51.4	240.0	7.22	2.25
NP 20m	48.40	3437	140.9	4798	46553	34.98	143.0	683	275.1	77.5	109.6	661	34.17	150.3	5.57	5.54	29.4	1.56	5.5	500	83.5	299.9	12.47	3.81
NP L 5cm	252.2	17980	658.3	19161	211793	302.8	1171	3209	630.5	303.9	530.0	3162	165.6	828.3	110.5	26.43	76.9	10.7	21.9	2606	395.3	849.0	57.07	15.89
NP L 10cm	227.5	20862	636.3	15983	205024	226.3	944.6	3223	552.9	253.1	487.5	3163	155.7	821.5	82.81	26.70	59.2	6.62	17.5	2112	342.6	797.8	50.62	15.18
NP L 20cm	209.5	19166	544.0	16948	187614	178.5	726.3	2252	519.8	218.1	432.3	3201	142.7	719.9	49.52	22.24	48.5	6.11	15.1	1808	359.9	763.3	49.06	14.59
NP L 40cm	238.6	61188	648.4	21870	221603	344.1	1238	3284	657.0	218.8	889.8	3586	267.3	4450	110.5	30.75	124	14.4	20.6	5735	1059	869.9	159.7	30.04

N.D. = Not Detectable, Ton = ODAS Tonne, NP = Nord-Perd Rinne, W = Wiek, Ark = Arkona, L = Lander (height above sea floor), Fluff = Mobile Nepheloid Layer

December '97, ICPMS, Water Particulate Phase, ng/l, ctd.

	Li	Ti	V	Mn	Fe	Co	Ni	Zn	Cu	As	Rb	Sr	Y	Zr	Mo	Cd	Sn	Sb	Cs	Ba	Ce	Pb	Th	U
W 0m	5.88	571	36.6	401	5918	12.88	63.9	352	142.6	24.5	18.0	265	17.50	22.8	1.96	2.58	6.13	N.D.	19.5	142	18.6	82.6	N.D.	N.D.
W 5m	0.69	418	19.2	469	5777	5.31	161.5	273	126.1	12.4	9.2	217	30.90	14.1	1.63	0.36	2.70	N.D.	37.9	118	5.3	52.9	N.D.	N.D.
W 10m	6.51	434	24.2	418	5135	9.38	62.3	250	127.2	30.7	14.5	275	17.33	15.1	1.39	2.81	5.81	N.D.	20.2	103	7.2	66.1	N.D.	N.D.
W 15m	5.91	445	20.6	405	5676	14.96	75.0	256	127.4	31.6	14.3	273	16.49	17.0	3.41	3.38	6.12	N.D.	18.9	290	7.4	74.7	N.D.	N.D.
W 20m	7.69	727	34.2	549	7140	9.63	65.7	271	147.9	40.4	21.2	276	17.89	21.7	1.31	2.07	5.22	N.D.	19.5	140	11.8	61.4	N.D.	N.D.
W 25m	17.46	1313	52.0	703	16228	15.07	89.7	300	201.5	40.5	47.9	336	23.60	53.1	2.07	3.66	6.46	N.D.	22.1	198	28.1	108.6	N.D.	N.D.
W L 5cm	34.15	3057	192.9	1111	35921	18.89	456.4	1382	363.0	136.0	84.7	2238	139.0	275.8	7.43	10.42	28.5	N.D.	166.5	504	36.6	194.7	N.D.	N.D.
W L 10cm	31.33	1731	218.1	799	23291	15.76	338.8	657	197.1	116.4	65.2	2128	113.5	115.3	9.21	8.23	20.6	N.D.	138.3	383	5.7	147.8	N.D.	N.D.
W L 20cm	25.98	1888	107.7	912	25792	22.12	442.5	642	315.0	70.3	63.6	1950	113.9	106.1	18.19	9.07	19.3	N.D.	138.7	404	11.1	125.9	N.D.	N.D.
W L 40cm	20.25	1569	76.0	594	16546	4.74	243.0	511	186.6	53.5	41.3	1243	77.59	113.6	7.13	7.52	15.8	N.D.	92.4	403	26.5	99.1	N.D.	N.D.
Ark 0m	7.58	331	21.2	136	3929	15.68	77.7	148	104.8	33.3	9.1	416	19.27	27.9	3.98	N.D.	3.96	N.D.	15.9	109	14.7	51.7	N.D.	N.D.
Ark 5m	3.01	176	28.8	116	1824	10.09	58.5	159	55.3	16.9	4.6	328	14.42	17.1	2.61	N.D.	4.77	N.D.	15.9	55	N.D.	21.1	N.D.	N.D.
Ark 10m	3.28	158	19.3	117	2009	5.62	53.6	209	58.1	14.4	4.7	409	14.69	37.8	3.66	N.D.	4.56	N.D.	15.9	74	N.D.	26.3	N.D.	N.D.
Ark 25m	2.96	167	15.0	125	2416	5.24	63.0	160	58.1	12.8	5.1	323	14.66	28.7	4.06	N.D.	6.02	N.D.	15.9	798	N.D.	33.1	N.D.	N.D.
Ark 35m	4.88	284	25.2	159	4337	7.03	62.2	125	58.7	16.4	10.9	307	15.40	30.9	3.12	N.D.	4.85	N.D.	16.1	67	1.0	32.9	N.D.	N.D.
Ark 45m	14.15	414	38.2	126	13903	4.17	61.9	120	85.2	35.4	22.0	660	16.32	31.2	3.81	N.D.	5.07	N.D.	16.3	92	4.4	62.9	0.26	N.D.
Ark L 5cm	808.4	62378	2026	4614	997684	226.1	1023	4609	1311	853.2	2163	6592	559.1	2343	41.43	N.D.	94.8	N.D.	289.8	7075	1555	2211	221.8	62.22
Ark L 10cm	121.4	5694	239.1	987	95925	29.12	411.1	915	359.9	215.1	216.4	4602	122.8	162.0	18.79	N.D.	19.3	N.D.	114.9	996	95.6	269.6	7.89	0.15
Ark L 20cm	95.29	2617	211.6	792	72771	68.19	386.0	769	270.1	221.1	127.5	4396	110.7	89.5	21.68	N.D.	25.2	N.D.	112.3	577	23.4	194.3	0.22	N.D.

N.D. = Not Detectable, Ton = ODAS Tonne, NP = Nord-Perd Rinne, W = Wiek, Ark = Arkona, L = Lander (height above sea floor), Fluff = Mobile Nepheloid Layer

December '97, ICPMS, Normalised Water Particulate Phase to Rubidium ratios.

	Li/Rb	Ti/Rb	V/Rb	Mn/Rb	Fe/Rb	Co/Rb	Ni/Rb	Cu/Rb	Zn/Rb	As/Rb	Sr/Rb	Y/Rb	Zr/Rb	Mo/Rb	Cd/Rb	Sn/Rb	Sb/Rb	Cs/Rb	Ba/Rb	Ce/Rb	Pb/Rb	Th/Rb	U/Rb
Ton 0m	0.314	31.446	1.253	71.890	389	0.318	1.607	8.823	2.717	0.588	6.099	0.506	0.933	0.018	0.038	0.097	N.D.	0.433	6.916	0.847	3.623	N.D.	N.D.
Ton 5m	0.321	31.729	1.292	73.185	482	0.303	1.639	8.916	2.755	0.599	6.353	0.540	0.813	0.014	0.044	0.092	N.D.	0.470	7.177	0.950	3.408	N.D.	N.D.
Ton 10m	0.328	34.866	1.393	75.656	486	0.317	1.589	9.084	2.783	0.622	6.323	0.543	1.554	0.013	0.041	0.086	N.D.	0.464	7.693	0.903	3.540	N.D.	N.D.
Ton 15m	0.310	26.803	0.996	33.846	405	0.170	0.653	3.903	0.912	0.291	2.126	0.180	1.120	0.028	0.030	0.035	N.D.	0.060	3.909	0.492	1.368	0.089	0.022
Ton L 5cm	0.566	73.650	1.331	55.864	427	1.309	4.884	13.015	2.050	0.876	13.916	0.386	2.017	0.839	0.156	0.280	0.026	0.015	6.216	1.474	2.253	0.291	0.043
Ton L 10cm	0.626	51.740	1.670	56.497	467	1.046	7.679	12.153	2.605	0.901	17.418	0.291	2.341	0.977	0.360	0.330	0.028	0.007	7.412	0.649	2.170	0.055	0.027
Ton L 20cm	0.678	36.694	1.761	63.191	432	1.560	6.218	13.804	3.564	1.014	18.779	0.294	1.129	0.605	0.186	0.388	0.025	0.005	7.152	0.535	2.513	0.064	0.025
Ton L 40cm	0.740	23.322	2.521	55.198	391	1.331	7.994	16.123	2.872	1.325	23.912	0.273	0.818	0.833	0.206	0.391	0.027	0.008	8.274	0.656	2.673	0.035	0.020
NP 0m	0.481	30.902	1.560	60.897	461	0.455	1.589	7.405	2.900	0.657	6.961	0.303	1.001	0.084	0.074	0.208	0.018	0.042	5.058	0.711	4.173	0.103	0.030
NP 5m	0.508	31.536	1.356	58.057	468	0.383	1.638	7.426	2.657	0.597	7.813	0.321	1.064	0.073	0.058	0.219	0.017	0.040	4.930	0.706	3.740	0.110	0.031
NP 10m	N.D.	N.D.	N.D.	N.D.	N.D.	N.D.	N.D.	N.D.	N.D.	N.D.	N.D.	N.D.	N.D.	N.D.	N.D.	N.D.	N.D.	N.D.	N.D.	N.D.	N.D.	N.D.	N.D.
NP 15m	0.473	35.926	1.383	55.446	440	0.393	1.585	7.005	2.725	0.878	7.204	0.323	1.676	0.072	0.058	0.370	0.019	0.044	4.985	0.713	3.330	0.100	0.031
NP 20m	0.442	31.368	1.286	43.796	425	0.319	1.305	6.231	2.511	0.707	6.036	0.312	1.372	0.051	0.051	0.268	0.014	0.050	4.568	0.762	2.738	0.114	0.035
NP L 5cm	0.476	33.922	1.242	36.150	400	0.571	2.208	6.054	1.190	0.573	5.965	0.312	1.563	0.208	0.050	0.145	0.020	0.041	4.917	0.746	1.602	0.108	0.030
NP L 10cm	0.467	42.793	1.305	32.786	421	0.464	1.938	6.611	1.134	0.519	6.488	0.319	1.685	0.170	0.055	0.121	0.014	0.036	4.332	0.703	1.637	0.104	0.031
NP L 20cm	0.485	44.336	1.258	39.205	434	0.413	1.680	5.208	1.202	0.505	7.405	0.330	1.665	0.115	0.051	0.112	0.014	0.035	4.182	0.833	1.766	0.113	0.034
NP L 40cm	0.268	68.764	0.729	24.579	249	0.387	1.391	3.691	0.738	0.246	4.030	0.300	5.001	0.124	0.035	0.139	0.016	0.023	6.445	1.190	0.978	0.179	0.034

N.D. = Not Detectable, Ton = ODAS Tonne, NP = Nord-Perd Rinne, W = Wiek, Ark = Arkona, L = Lander (height above sea floor), Fluff = Mobile Nepheloid Layer

December '97, ICPMS, Normalised Water Particulate Phase to Rubidium ratios, ctd.

	Li/Rb	Ti/Rb	V/Rb	Mn/Rb	Fe/Rb	Co/Rb	Ni/Rb	Cu/Rb	Zn/Rb	As/Rb	Sr/Rb	Y/Rb	Zr/Rb	Mo/Rb	Cd/Rb	Sn/Rb	Sb/Rb	Cs/Rb	Ba/Rb	Ce/Rb	Pb/Rb	Th/Rb	U/Rb
W0m	0.326	31.679	2.028	22.233	328	0.714	3.544	19.515	7.905	1.357	14.702	0.970	1.265	0.109	0.143	0.340	N.D.	1.080	7.852	1.032	4.580	N.D.	N.D.
W5m	0.075	45.236	2.075	50.747	625	0.574	17.471	29.567	13.645	1.341	23.461	3.342	1.524	0.176	0.039	0.292	N.D.	4.096	12.769	0.574	5.722	N.D.	N.D.
W10m	0.447	29.809	1.665	28.756	353	0.645	4.283	17.195	8.740	2.111	18.927	1.191	1.037	0.095	0.193	0.400	N.D.	1.386	7.108	0.496	4.545	N.D.	N.D.
W15m	0.413	31.101	1.439	28.288	397	1.045	5.244	17.888	8.903	2.210	19.048	1.152	1.191	0.238	0.236	0.428	N.D.	1.322	20.267	0.518	5.220	N.D.	N.D.
W20m	0.363	34.309	1.615	25.919	337	0.455	3.102	12.775	6.981	1.909	13.044	0.844	1.023	0.062	0.098	0.246	N.D.	0.919	6.607	0.558	2.896	N.D.	N.D.
W25m	0.365	27.434	1.086	14.679	339	0.315	1.873	6.271	4.209	0.847	7.017	0.493	1.109	0.043	0.076	0.135	N.D.	0.461	4.136	0.586	2.269	N.D.	N.D.
WL 5cm	0.403	36.095	2.277	13.111	424	0.223	5.388	16.322	4.286	1.606	26.417	1.641	3.256	0.088	0.123	0.337	N.D.	1.966	5.956	0.432	2.299	N.D.	N.D.
WL 10cm	0.480	26.535	3.343	12.242	357	0.242	5.193	10.070	3.021	1.784	32.612	1.740	1.767	0.141	0.126	0.316	N.D.	2.120	5.871	0.087	2.265	N.D.	N.D.
WL 20cm	0.408	29.680	1.693	14.336	405	0.348	6.955	10.089	4.950	1.105	30.649	1.791	1.667	0.286	0.143	0.303	N.D.	2.181	6.358	0.175	1.978	N.D.	N.D.
WL 40cm	0.491	38.024	1.840	14.385	401	0.115	5.887	12.377	4.520	1.297	30.105	1.880	2.753	0.173	0.182	0.382	N.D.	2.238	9.761	0.642	2.401	N.D.	N.D.
Ark 0m	0.836	36.483	2.340	15.023	433	1.730	8.578	16.352	11.566	3.673	45.948	2.127	3.078	0.439	N.D.	0.437	N.D.	1.756	12.007	1.617	5.700	N.D.	N.D.
Ark 5m	0.656	38.352	6.281	25.274	398	2.200	12.756	34.616	12.065	3.680	71.587	3.144	3.730	0.569	N.D.	1.040	N.D.	3.459	11.970	N.D.	4.599	N.D.	N.D.
Ark 10m	0.699	33.753	4.126	25.036	429	1.200	11.455	44.655	12.403	3.080	87.328	3.137	8.067	0.783	N.D.	0.974	N.D.	3.389	15.769	N.D.	5.615	N.D.	N.D.
Ark 25m	0.580	32.669	2.942	24.551	474	1.027	12.350	31.327	11.384	2.507	63.240	2.874	5.623	0.795	N.D.	1.180	N.D.	3.117	156.52	N.D.	6.487	N.D.	N.D.
Ark 35m	0.449	26.062	2.315	14.587	398	0.646	5.712	11.465	5.394	1.502	28.236	1.415	2.837	0.286	N.D.	0.446	N.D.	1.477	6.195	0.089	3.025	N.D.	N.D.
Ark 45m	0.644	18.848	1.740	5.753	633	0.190	2.818	5.458	3.880	1.611	30.031	0.743	1.421	0.174	N.D.	0.231	N.D.	0.740	4.199	0.199	2.864	0.012	N.D.
Ark L 5cm	0.374	28.833	0.936	2.133	461	0.105	0.473	2.130	0.606	0.394	3.047	0.258	1.083	0.019	N.D.	0.044	N.D.	0.134	3.270	0.719	1.022	0.103	0.029
Ark L 10cm	0.561	26.319	1.105	4.563	443	0.135	1.900	4.227	1.664	0.994	21.270	0.567	0.749	0.087	N.D.	0.089	N.D.	0.531	4.605	0.442	1.246	0.036	0.001
Ark L 20cm	0.747	20.530	1.660	6.215	571	0.535	3.028	6.035	2.119	1.735	34.483	0.868	0.702	0.170	N.D.	0.198	N.D.	0.881	4.524	0.183	1.524	0.002	N.D.

N.D. = Not Detectable, Ton = ODAS Tonne, NP = Nord-Perd Rinne, W = Wiek, Ark = Arkona, L = Lander (height above sea floor), Fluff = Mobile Nepheloid Layer

OCTOBER '96, ICPMS, Water Dissolved Phase, ug dm^{-3}.

	Li	Ti	V	Mn	Fe	As	Rb	Sr	Mo	Ba	U
Ton 0m	28.26	0.23	4.37	N.D.	327.24	5.28	27.36	1949.33	2.86	23.27	1.57
Ton 5m	23.38	1.24	4.32	N.D	614.60	6.89	27.73	1955.29	2.57	24.16	1.36
Ton 10m	20.19	0.61	4.37	N.D.	609.95	7.58	26.31	1867.21	2.62	22.74	1.43
Ton 15m	20.95	1.60	5.05	N.D.	541.75	7.29	27.66	1887.82	2.67	24.48	1.59
Ton L 5cm	33.93	2.74	11.85	N.D.	683.46	12.59	27.20	1595.40	2.83	2410.11	1.38
Ton L 10cm	32.17	2.94	11.70	N.D	829.76	13.41	25.36	1448.82	2.40	610.43	1.59
Ton L 20cm	26.60	5.48	14.95	N.D.	834.57	16.06	27.78	1575.34	2.30	2919.62	1.40
Ton L 40cm	36.46	4.05	12.86	N.D.	803.02	13.03	26.51	1531.52	2.74	176.99	1.57
NP 0m	28.00	N.D.	2.27	N.D	671.89	3.05	23.80	1662.39	2.94	23.94	2.71
NP 5m	29.11	N.D	1.94	N.D.	722.79	3.17	23.63	1724.34	2.70	23.35	2.60
NP 10m	28.08	N.D.	2.83	N.D.	806.93	4.23	24.70	1755.18	2.63	24.13	2.23
NP 15m	31.10	N.D.	4.91	10.14	897.79	5.62	26.64	1855.33	3.02	23.62	2.05
NP 20m	37.15	N.D.	6.23	100.92	1105.29	6.59	32.71	2022.49	3.46	23.41	2.45
NP L 5cm	39.35	N.D.	25.55	118.82	760.20	16.03	31.93	1831.33	3.67	1001.84	2.57
NP L 10cm	44.56	N.D	29.01	126.22	1212.54	17.43	34.93	1948.35	3.89	6168.80	2.78
NP L 20cm	46.74	N.D.	23.83	130.98	1344.18	15.49	36.57	2050.78	3.99	1456.68	2.68
NP L 40cm	45.89	N.D.	25.99	129.58	1176.80	18.13	33.70	1850.26	3.64	338.50	2.63

N.D. = Not Detectable, Ton = ODAS Tonne, NP = Nord-Perd Rinne, W = Wiek, Ark = Arkona, L = Lander (height above sea floor), Fluff = Mobile Nepheloid Layer

OCTOBER '96, ICPMS, Water Dissolved Phase, ug dm^{-3}, ctd.

	Li	Ti	V	Mn	Fe	As	Rb	Sr	Mo	Ba	U
W 0m	27.86	N.D.	2.28	N.D.	666.56	3.08	25.15	1733.33	1.75	22.88	1.66
W 5m	26.17	N.D	2.26	N.D.	754.05	2.91	24.00	1757.32	1.26	21.79	1.68
W 10m	28.43	N.D.	2.27	N.D	870.44	3.77	24.39	1749.31	2.07	23.41	1.51
W 15m	28.74	N.D.	0.47	N.D.	737.53	4.31	25.11	1786.04	1.63	22.92	1.43
W 20m	26.83	N.D.	1.73	N.D.	903.75	3.10	24.51	1754.12	1.28	21.87	1.43
W 25m	37.61	N.D	6.11	5.57	1285.57	7.75	37.65	1997.56	2.81	22.03	1.81
W L 5cm	46.30	N.D.	25.36	48.38	1237.42	20.45	42.71	1607.86	3.87	5630.31	2.01
W L 10cm	44.35	N.D	30.18	50.94	1458.56	23.19	43.83	1938.60	4.00	4786.95	2.14
W L 20cm	47.24	N.D.	31.16	52.37	1442.06	24.55	47.38	728.10	3.81	2631.34	2.14
W L 40cm	48.69	N.D.	32.39	55.39	1547.26	23.18	44.86	1483.37	4.31	1635.90	1.83
Ark 0m	25.95	6.99	4.94	N.D.	484.30	7.35	22.82	1286.38	1.77	20.97	1.55
Ark 5m	29.60	8.34	4.78	N.D	681.52	8.23	23.90	1375.62	1.98	22.49	1.50
Ark 10m	24.22	6.93	3.20	N.D.	575.56	7.57	21.93	1302.76	1.57	22.29	1.30
Ark 20m	30.46	9.02	5.85	N.D.	802.69	8.75	25.50	1400.95	2.14	23.06	1.52
Ark 30m	30.35	8.34	5.79	N.D.	757.96	8.80	26.73	1387.63	2.32	21.45	1.65
Ark 35m	32.54	9.21	6.67	N.D	660.61	8.90	28.88	1390.25	2.42	21.77	1.71
Ark 40m	36.68	10.08	9.05	N.D.	938.56	10.23	33.22	627.13	3.03	21.89	1.71
Ark 45m	54.35	13.40	13.15	N.D.	1227.01	12.40	46.94	345.70	4.36	22.20	2.26
Ark L 5cm	66.16	18.63	40.10	90.24	1732.27	38.00	58.60	395.65	4.38	429.35	2.52
Ark L 10cm	74.44	20.99	47.37	93.82	1771.09	38.29	62.82	408.05	4.67	1389.32	2.56
Ark L 20cm	85.62	23.39	51.60	102.52	2146.33	43.74	64.90	327.46	5.22	2754.67	2.19
Ark L 40cm	94.80	24.32	50.68	107.58	2215.47	42.50	65.31	317.76	4.39	2484.08	2.29

N.D. = Not Detectable, Ton = ODAS Tonne, NP = Nord-Perd Rinne, W = Wiek, Ark = Arkona, L = Lander (height above sea floor), Fluff = Mobile Nepheloid Layer

October '96, ICPMS, Normalised Water Dissolved Phase to Rubidium ratios.

	Li/Rb	Ti/Rb	V/Rb	Mn/Rb	Fe/Rb	As/Rb	Sr/Rb	Mo/Rb	Ba/Rb	U/Rb
Ton 0m	1.033	0.009	0.160	N.D.	11.960	0.193	71.241	0.105	0.850	0.057
Ton 5m	0.843	0.045	0.156	N.D	22.164	0.249	70.514	0.093	0.871	0.049
Ton 10m	0.767	0.023	0.166	N.D.	23.185	0.288	70.976	0.100	0.864	0.054
Ton 15m	0.758	0.058	0.183	N.D	19.589	0.264	68.260	0.096	0.885	0.058
Ton L 5cm	1.247	0.101	0.436	N.D.	25.129	0.463	58.660	0.104	88.615	0.051
Ton L 10cm	1.269	0.116	0.461	N.D.	32.724	0.529	57.138	0.095	24.074	0.053
Ton L 20cm	0.957	0.197	0.538	N.D.	30.038	0.578	56.700	0.083	105.084	0.050
Ton L 40cm	1.375	0.153	0.485	N.D.	30.295	0.492	57.778	0.103	6.677	0.059
NP 0m	1.176	N.D.	0.095	N.D	28.230	0.128	69.848	0.124	1.006	0.114
NP 5m	1.232	N.D	0.082	N.D.	30.583	0.134	72.962	0.114	0.988	0.110
NP 10m	1.137	N.D.	0.114	N.D.	32.669	0.171	71.059	0.106	0.977	0.090
NP 15m	1.167	N.D.	0.184	0.381	33.701	0.211	69.646	0.113	0.887	0.077
NP 20m	1.136	N.D.	0.191	3.085	33.788	0.201	61.826	0.106	0.716	0.075
NP L 5cm	1.232	N.D.	0.800	3.721	23.808	0.502	57.354	0.115	31.376	0.081
NP L 10cm	1.276	N.D	0.830	3.614	34.714	0.499	55.779	0.111	176.607	0.080
NP L 20cm	1.278	N.D.	0.652	3.582	36.756	0.424	56.077	0.109	39.832	0.073
NP L 40cm	1.362	N.D.	0.771	3.845	34.922	0.538	54.908	0.108	10.045	0.078

	Li/Rb	Ti/Rb	V/Rb	Mn/Rb	Fe/Rb	As/Rb	Sr/Rb	Mo/Rb	Ba/Rb	U/Rb
W 0m	1.108	N.D.	0.091	N.D.	26.499	0.123	68.908	0.070	0.910	0.066
W 5m	1.090	N.D.	0.094	N.D.	31.420	0.121	73.224	0.052	0.908	0.070
W 10m	1.166	N.D	0.093	N.D	35.695	0.154	71.737	0.085	0.960	0.062
W 15m	1.144	N.D.	0.019	N.D.	29.367	0.172	71.117	0.065	0.913	0.057
W 20m	1.095	N.D.	0.071	N.D.	36.868	0.127	71.558	0.052	0.892	0.058
W 25m	0.999	N.D.	0.162	0.148	34.149	0.206	53.062	0.075	0.585	0.048
WL 5cm	1.084	N.D.	0.594	1.133	28.972	0.479	37.645	0.091	131.824	0.047
WL 10cm	1.012	N.D	0.689	1.162	33.277	0.529	44.229	0.091	109.215	0.049
WL 20cm	0.997	N.D.	0.658	1.105	30.434	0.518	15.366	0.080	55.534	0.045
WL 40cm	1.085	N.D.	0.722	1.235	34.493	0.517	33.068	0.096	36.469	0.041
Ark 0m	1.137	0.306	0.216	N.D.	21.225	0.322	56.376	0.078	0.919	0.068
Ark 5m	1.238	0.349	0.200	N.D.	28.511	0.344	57.548	0.083	0.941	0.063
Ark 10m	1.104	0.316	0.146	N.D.	26.242	0.345	59.398	0.072	1.016	0.059
Ark 20m	1.194	0.354	0.229	N.D.	31.475	0.343	54.934	0.084	0.904	0.060
Ark 30m	1.135	0.312	0.217	N.D.	28.355	0.329	51.911	0.087	0.803	0.062
Ark 35m	1.127	0.319	0.231	N.D	22.873	0.308	48.136	0.084	0.754	0.059
Ark 40m	1.104	0.304	0.272	N.D.	28.255	0.308	18.880	0.091	0.659	0.051
Ark 45m	1.158	0.286	0.280	N.D.	26.142	0.264	7.365	0.093	0.473	0.048
Ark L 5cm	1.129	0.318	0.684	1.540	29.558	0.648	6.751	0.075	7.326	0.043
Ark L 10cm	1.185	0.334	0.754	1.493	28.194	0.609	6.496	0.074	22.116	0.041
Ark L 20cm	1.319	0.360	0.795	1.580	33.071	0.674	5.046	0.080	42.444	0.034
Ark L 40cm	1.451	0.372	0.776	1.647	33.920	0.651	4.865	0.067	38.033	0.035

N.D. = Not Detectable, Ton = ODAS Tonne, NP = Nord-Perd Rinne, W = Wiek, Ark = Arkona, L = Lander (height above sea floor), Fluff = Mobile Nepheloid Layer

March '97, ICPMS, Water Dissolved Phase, ug dm^{-3}.

	Li	V	Mn	Fe	As	Rb	Sr	Mo	Ba	U
Ton 0m	38.036	8.254	N.D.	2155.3	10.732	27.223	1755.6	2.097	32.044	1.256
Ton 5m	34.615	6.820	N.D.	1835.2	12.506	28.007	1842.3	1.890	31.451	1.288
Ton 10m	34.385	7.723	N.D.	2107.7	10.989	28.681	1736.0	1.974	27.034	1.378
Ton 15m	37.281	7.242	N.D.	2142.9	11.459	29.676	1411.0	1.696	25.783	1.264
Ton L Fluff	36.384	6.615	N.D.	1973.5	12.374	29.982	1793.1	1.739	23.786	1.208
Ton L 5cm	32.210	7.307	N.D.	1910.0	12.849	28.989	1729.6	1.491	26.996	1.158
Ton L 10cm	33.615	7.218	N.D.	1993.9	12.175	28.569	1809.0	2.025	24.909	1.175
Ton L 20cm	33.474	8.198	N.D.	1698.0	12.057	29.065	1771.7	2.003	26.651	1.322
Ton L 40cm	32.160	6.559	N.D.	1969.4	11.915	25.322	1791.8	1.863	25.861	1.236
NP 0m	44.443	3.931	0.231	566.0	3.711	24.385	1915.8	1.011	23.503	0.903
NP 5m	42.042	3.874	0.601	684.4	4.658	24.750	1933.8	0.887	21.935	0.992
NP 10m	38.877	4.098	0.227	710.1	4.712	25.625	1975.9	0.994	23.341	0.980
NP 15m	45.591	5.620	0.055	871.2	6.977	31.142	2182.9	3.256	21.522	1.140
NP 20m	58.644	8.559	2.713	1165.4	9.969	44.185	533.0	3.565	20.077	1.511
NP L Fluff	56.833	9.251	2.680	1323.0	12.195	45.642	589.2	2.969	20.068	1.541
NP L 5cm	59.075	15.886	3.766	1339.9	14.714	46.037	625.3	3.483	25.731	1.422
NP L 10cm	54.350	23.082	4.827	1373.6	24.339	46.968	678.3	3.847	22.030	1.578
NP L 20cm	55.907	19.558	4.985	1343.3	18.636	47.677	565.0	4.909	19.889	1.507
NP L 40cm	56.423	17.645	4.654	1358.0	19.577	48.200	566.5	3.218	21.378	1.524

N.D. = Not Detectable, Ton = ODAS Tonne, NP = Nord-Perd Rinne, W = Wiek, Ark = Arkona, L = Lander (height above sea floor), Fluff = Mobile Nepheloid Layer

March '97, ICPMS, Water Dissolved Phase, ug dm^{-3}, ctd.

	Li	V	Mn	Fe	As	Rb	Sr	Mo	Ba	U
W 0m	30.286	10.570	4.898	795.3	7.975	25.083	1917.7	0.843	23.272	0.834
W 5m	28.115	8.211	N.D.	785.6	8.671	24.942	1965.4	0.601	20.954	0.649
W 10m	29.639	7.629	N.D.	856.9	9.437	27.169	2078.6	0.504	20.729	0.576
W 15m	34.013	9.435	N.D.	959.0	8.848	29.419	2106.1	0.813	21.205	0.680
W 20m	40.156	9.725	0.316	984.2	8.479	32.126	2081.3	1.279	21.593	0.734
W 25m	41.359	11.046	3.798	1180.3	10.523	35.409	1453.2	1.408	19.602	0.862
W L Fluff	51.510	17.679	62.043	2381.1	14.512	45.103	363.8	1.177	21.793	1.197
W L 5cm	50.793	21.202	7.720	1577.5	17.791	45.285	162.0	1.909	20.924	1.195
W L 10cm	54.268	18.849	16.149	2055.6	15.896	47.099	51.5	1.495	20.365	1.238
W L 20cm	55.002	21.568	8.533	1538.2	18.861	48.054	163.3	1.392	19.187	1.257
W L 40cm	55.765	20.661	9.939	1701.2	17.633	47.948	73.9	2.325	19.426	1.221
Ark 0m	34.138	11.771	N.D.	703.5	8.187	28.699	2086.6	2.429	19.850	0.803
Ark 5m	30.534	9.905	N.D.	820.2	10.261	29.405	2180.7	2.288	21.745	0.848
Ark 10m	30.300	9.394	N.D.	844.2	9.257	28.284	2205.5	2.203	20.739	0.801
Ark 20m	37.567	13.957	N.D.	960.3	11.533	33.469	2130.4	3.162	20.337	0.899
Ark 30m	43.491	14.039	N.D.	1065.2	12.531	40.947	546.0	4.209	19.898	1.262
Ark 35m	47.239	17.723	N.D.	1226.0	13.878	44.881	314.9	4.008	19.071	1.367
Ark 40m	61.181	21.031	N.D.	1514.9	16.110	56.108	47.9	3.816	19.246	1.703
Ark 45m	79.987	26.527	3.945	1919.5	20.737	74.256	N.D.	6.119	18.825	2.302
Ark L Fluff	89.239	31.333	38.919	2275.6	23.085	87.716	N.D.	7.692	19.676	3.859
Ark L 5cm	91.177	38.027	8.339	2301.6	27.763	90.060	N.D.	8.051	16.968	3.477
Ark L 10cm	95.775	45.369	11.835	3033.6	30.079	89.696	N.D.	7.068	18.525	3.173
Ark L 20cm	98.701	38.560	8.628	3000.9	25.949	90.603	N.D.	6.070	16.425	2.553
Ark L 40cm	95.324	42.394	18.877	2511.2	28.866	87.970	N.D.	7.322	15.526	2.774

N.D. = Not Detectable, Ton = ODAS Tonne, NP = Nord-Perd Rinne, W = Wiek, Ark = Arkona, L = Lander (height above sea floor), Fluff = Mobile Nepheloid Layer

March '97, ICPMS, Normalised Water Dissolved Phase to Rubidium ratios.

	Li/Rb	V/Rb	Mn/Rb	Fe/Rb	As/Rb	Sr/Rb	Mo/Rb	Ba/Rb	U/Rb
Ton 0m	1.397	0.303	N.D.	79.171	0.394	64.489	0.077	1.177	0.046
Ton 5m	1.236	0.244	N.D.	65.525	0.447	65.778	0.067	1.123	0.046
Ton 10m	1.199	0.269	N.D.	73.487	0.383	60.530	0.069	0.943	0.048
Ton 15m	1.256	0.244	N.D.	72.212	0.386	47.549	0.057	0.869	0.043
Ton L Fluff	1.214	0.221	N.D.	65.822	0.413	59.805	0.058	0.793	0.040
Ton L 5cm	1.111	0.252	N.D.	65.888	0.443	59.664	0.051	0.931	0.040
Ton L 10cm	1.177	0.253	N.D.	69.794	0.426	63.320	0.071	0.872	0.041
Ton L 20cm	1.152	0.282	N.D.	58.422	0.415	60.957	0.069	0.917	0.045
Ton L 40cm	1.270	0.259	N.D.	77.775	0.471	70.761	0.074	1.021	0.049
NP 0m	1.823	0.161	0.009	23.212	0.152	78.564	0.041	0.964	0.037
NP 5m	1.699	0.157	0.024	27.654	0.188	78.134	0.036	0.886	0.040
NP 10m	1.517	0.160	0.009	27.710	0.184	77.110	0.039	0.911	0.038
NP 15m	1.464	0.180	0.002	27.976	0.224	70.096	0.105	0.691	0.037
NP 20m	1.327	0.194	0.061	26.376	0.226	12.062	0.081	0.454	0.034
NP L Fluff	1.245	0.203	0.059	28.986	0.267	12.908	0.065	0.440	0.034
NP L 5cm	1.283	0.345	0.082	29.106	0.320	13.582	0.076	0.559	0.031
NP L 10cm	1.157	0.491	0.103	29.246	0.518	14.442	0.082	0.469	0.034
NP L 20cm	1.173	0.410	0.105	28.174	0.391	11.850	0.103	0.417	0.032
NP L 40cm	1.171	0.366	0.097	28.174	0.406	11.753	0.067	0.444	0.032

	Li/Rb	V/Rb	Mn/Rb	Fe/Rb	As/Rb	Sr/Rb	Mo/Rb	Ba/Rb	U/Rb
W 0m	1.207	0.421	0.195	31.707	0.318	76.454	0.034	0.928	0.033
W 5m	1.127	0.329	N.D.	31.496	0.348	78.797	0.024	0.840	0.026
W 10m	1.091	0.281	N.D.	31.540	0.347	76.507	0.019	0.763	0.021
W 15m	1.156	0.321	N.D.	32.599	0.301	71.590	0.028	0.721	0.023
W 20m	1.250	0.303	0.010	30.634	0.264	64.786	0.040	0.672	0.023
W 25m	1.168	0.312	0.107	33.332	0.297	41.041	0.040	0.554	0.024
W L Fluff	1.142	0.392	1.376	52.793	0.322	8.065	0.026	0.483	0.027
W L 5cm	1.122	0.468	0.170	34.834	0.393	3.577	0.042	0.462	0.026
W L 10cm	1.152	0.400	0.343	43.644	0.338	1.093	0.032	0.432	0.026
W L 20cm	1.145	0.449	0.178	32.010	0.392	3.398	0.029	0.399	0.026
W L 40cm	1.163	0.431	0.207	35.479	0.368	1.541	0.048	0.405	0.025
Ark 0m	1.190	0.410	N.D.	24.512	0.285	72.706	0.085	0.692	0.028
Ark 5m	1.038	0.337	N.D.	27.892	0.349	74.161	0.078	0.739	0.029
Ark 10m	1.071	0.332	N.D.	29.849	0.327	77.976	0.078	0.733	0.028
Ark 20m	1.122	0.417	N.D.	28.693	0.345	63.652	0.094	0.608	0.027
Ark 30m	1.062	0.343	N.D.	26.015	0.306	13.335	0.103	0.486	0.031
Ark 35m	1.053	0.395	N.D.	27.317	0.309	7.017	0.089	0.425	0.030
Ark 40m	1.090	0.375	N.D.	26.999	0.287	0.854	0.068	0.343	0.030
Ark 45m	1.077	0.357	0.053	25.850	0.279	N.D.	0.082	0.254	0.031
Ark L Fluff	1.017	0.357	0.444	25.942	0.263	N.D.	0.088	0.224	0.044
Ark L 5cm	1.012	0.422	0.093	25.556	0.308	N.D.	0.089	0.188	0.039
Ark L 10cm	1.068	0.506	0.132	33.820	0.335	N.D.	0.079	0.207	0.035
Ark L 20cm	1.089	0.426	0.095	33.121	0.286	N.D.	0.067	0.181	0.028
Ark L 40cm	1.084	0.482	0.215	28.546	0.328	N.D.	0.083	0.176	0.032

N.D. = Not Detectable, Ton = ODAS Tonne, NP = Nord-Perd Rinne, W = Wiek, Ark = Arkona, L = Lander (height above sea floor), Fluff = Mobile Nepheloid Layer

June '97, ICPMS, Water Dissolved Phase, ug dm^{-3}.

	Li	Ti	V	Mn	Fe	As	Rb	Sr	Mo	Ba	U
Ton 0m	27.808	N.D.	1.518	N.D.	747.95	4.542	21.362	1741.46	N.D.	25.694	0.661
Ton 5m	26.108	N.D.	1.152	N.D.	682.61	4.998	21.134	1761.90	N.D.	26.517	0.501
Ton 10m	28.826	N.D.	1.527	N.D.	855.68	6.261	23.604	1880.95	N.D.	23.510	0.537
Ton 15m	29.282	N.D.	1.298	N.D.	734.44	5.878	23.989	1888.03	N.D.	23.600	0.468
Ton L Fluff	28.212	N.D.	1.441	4.779	675.43	6.300	23.850	1906.69	N.D.	23.946	0.468
Ton L 5cm	28.963	N.D.	1.407	2.421	671.99	5.806	24.164	1889.36	N.D.	23.954	0.464
Ton L 10cm	27.915	N.D.	1.899	2.855	704.51	5.816	23.544	1888.00	N.D.	23.595	0.537
Ton L 20cm	28.577	N.D.	1.414	3.673	721.74	5.995	23.907	1925.99	N.D.	24.422	0.369
Ton L 40cm	29.022	N.D.	1.587	3.141	738.69	6.012	23.355	1837.13	N.D.	23.913	0.405
NP 0m	28.239	N.D.	1.003	N.D.	753.23	5.117	21.795	1782.38	N.D.	24.820	0.533
NP 5m	27.108	N.D.	0.692	N.D.	627.57	4.701	21.403	1725.59	N.D.	25.256	0.374
NP 10m	26.527	N.D.	0.796	N.D.	699.39	5.542	22.749	1818.25	N.D.	24.234	0.402
NP 15m	28.253	N.D.	1.753	N.D.	771.96	5.591	24.451	1886.90	N.D.	20.970	0.182
NP 20m	29.008	N.D.	2.108	N.D.	723.22	5.749	24.280	1941.37	N.D.	20.957	0.212
NP L Fluff	27.178	N.D.	2.219	6.679	677.18	5.706	24.170	1879.36	3.388	21.440	0.071
NP L 5cm	26.764	N.D.	1.850	N.D.	682.49	4.558	24.392	1906.52	1.461	21.262	0.027
NP L 10cm	27.076	N.D.	1.043	N.D.	640.33	4.678	24.451	1917.51	1.498	21.093	0.035
NP L 20cm	25.885	N.D.	1.270	N.D.	829.46	5.910	24.967	1910.53	1.422	22.393	0.004
NP L 40cm	27.617	N.D.	2.031	N.D.	792.73	4.985	25.721	1979.12	1.580	22.440	0.049

N.D. = Not Detectable, Ton = ODAS Tonne, NP = Nord-Perd Rinne, W = Wiek, Ark = Arkona, L = Lander (height above sea floor), Fluff = Mobile Nepheloid Layer

June '97, ICPMS, Water Dissolved Phase, ug dm^{-3}, ctd.

	Li	Ti	V	Mn	Fe	As	Rb	Sr	Mo	Ba	U
W 0m	25.238	N.D.	1.125	N.D.	667.49	5.032	22.812	1794.87	1.497	23.472	0.053
W 5m	27.558	N.D.	1.478	N.D.	780.90	5.453	23.940	1868.92.	1.542	24.508	0.046
W 10m	26.139	N.D.	0.966	N.D.	763.16	4.281	23.757	1854.92	2.912	23.659	0.007
W 15m	27.540	N.D.	2.254	N.D.	749.67	5.197	24.476	1899.07	1.378	22.216	0.027
W 20m	28.892	N.D.	2.598	N.D.	761.63	4.891	24.855	1897.45	1.703	20.065	0.129
W 25m	32.696	N.D.	3.908	N.D.	876.38	4.640	28.793	1840.57	1.856	31.884	0.121
W L Fluff	30.066	N.D.	5.355	38.558	790.75	8.064	32.112	2061.35	N.D.	22.090	1.477
W L 5cm	28.034	N.D.	3.816	3.064	869.58	8.213	32.400	2163.14	N.D.	21.836	1.024
W L 10cm	28.957	N.D.	4.901	4.692	815.93	8.690	31.237	2079.22	N.D.	22.571	1.343
W L 20cm	29.228	N.D.	3.578	3.348	791.83	7.993	30.474	1975.94	N.D.	20.619	1.365
W L 40cm	28.181	N.D.	2.990	3.310	821.45	7.963	30.802	1955.51	N.D.	20.869	1.153
Ark 0m	44.072	2.498	3.467	N.D.	574.15	4.475	26.828	2049.34	2.522	19.990	0.625
Ark 5m	31.735	1.341	3.309	N.D.	543.29	4.480	25.962	1994.72	2.143	22.976	0.630
Ark 10m	25.371	0.132	3.020	N.D.	739.64	4.968	25.315	1968.07	2.361	20.279	0.663
Ark 20m	25.503	2.192	3.338	N.D.	661.27	6.331	29.396	2099.13	2.524	22.782	0.516
Ark 30m	23.414	1.769	2.559	N.D.	766.01	6.368	27.575	2073.63	2.362	20.858	0.597
Ark 35m	25.241	2.314	5.128	N.D.	818.11	5.787	31.228	2143.90	2.776	22.128	0.531
Ark 40m	24.003	4.459	5.566	N.D.	817.78	7.779	31.098	2145.81	2.758	21.119	0.613
Ark 45m	32.466	2.522	6.919	N.D.	1097.90	10.258	36.587	2495.56	5.736	20.170	0.996
Ark L Fluff	60.239	11.243	12.954	66.676	1542.18	17.855	62.878	2739.53	6.193	20.508	1.879
Ark L 5cm	64.092	13.266	17.770	66.524	1636.63	19.868	68.553	1194.38	7.602	19.136	1.584
Ark L 10cm	59.471	12.402	17.356	59.962	1371.99	20.432	64.784	1466.65	6.413	18.545	1.658
Ark L 20cm	62.591	10.835	16.462	63.914	1545.78	17.355	69.223	974.45	6.719	18.969	1.879
Ark L 40cm	63.718	13.498	19.432	66.091	1709.15	15.747	67.532	906.66	6.085	19.039	1.888

N.D. = Not Detectable, Ton = ODAS Tonne, NP = Nord-Perd Rinne, W = Wiek, Ark = Arkona, L = Lander (height above sea floor), Fluff = Mobile Nepheloid Layer

June '97, ICPMS, Normalised Water Dissolved Phase to Rubidium ratios.

	Li/Rb	Ti/Rb	V/Rb	Mn/Rb	Fe/Rb	As/Rb	Sr/Rb	Mo/Rb	Ba/Rb	U/Rb
Ton 0m	1.302	N.D.	0.071	N.D.	35.01	0.213	81.52	N.D.	1.203	0.031
Ton 5m	1.235	N.D.	0.055	N.D.	32.30	0.236	83.37	N.D.	1.255	0.024
Ton 10m	1.221	N.D.	0.065	N.D.	36.25	0.265	79.69	N.D.	0.996	0.023
Ton 15m	1.221	N.D.	0.054	N.D.	30.62	0.245	78.71	N.D.	0.984	0.019
Ton L Fluff	1.183	N.D.	0.060	0.200	28.32	0.264	79.95	N.D.	1.004	0.020
Ton L 5cm	1.199	N.D.	0.058	0.100	27.81	0.240	78.19	N.D.	0.991	0.019
Ton L 10cm	1.186	N.D.	0.081	0.121	29.92	0.247	80.19	N.D.	1.002	0.023
Ton L 20cm	1.195	N.D.	0.059	0.154	30.19	0.251	80.56	N.D.	1.022	0.015
Ton L 40cm	1.243	N.D.	0.068	0.134	31.63	0.257	78.66	N.D.	1.024	0.017
NP 0m	1.296	N.D.	0.046	N.D.	34.56	0.235	81.78	N.D.	1.139	0.024
NP 5m	1.267	N.D.	0.032	N.D.	29.32	0.220	80.62	N.D.	1.180	0.017
NP 10m	1.166	N.D.	0.035	N.D.	30.74	0.244	79.93	N.D.	1.065	0.018
NP 15m	1.156	N.D.	0.072	N.D.	31.57	0.229	77.17	N.D.	0.858	0.007
NP 20m	1.195	N.D.	0.087	N.D.	29.79	0.237	79.96	N.D.	0.863	0.009
NP L Fluff	1.124	N.D.	0.092	0.276	28.02	0.236	77.76	0.140	0.887	0.003
NP L 5cm	1.097	N.D.	0.076	N.D.	27.98	0.187	78.16	0.060	0.872	0.001
NP L 10cm	1.107	N.D.	0.043	N.D.	26.19	0.191	78.42	0.061	0.863	0.001
NP L 20cm	1.037	N.D.	0.051	N.D.	33.22	0.237	76.52	0.057	0.897	0.000
NP L 40cm	1.074	N.D.	0.079	N.D.	30.82	0.194	76.94	0.061	0.872	0.002

	Li/Rb	Ti/Rb	V/Rb	Mn/Rb	Fe/Rb	As/Rb	Sr/Rb	Mo/Rb	Ba/Rb	U/Rb
W 0m	1.106	N.D.	0.049	N.D.	29.26	0.221	78.68	0.066	1.029	0.002
W 5m	1.151	N.D.	0.062	N.D.	32.62	0.228	78.07	0.064	1.024	0.002
W 10m	1.100	N.D.	0.041	N.D.	32.12	0.180	78.08	0.123	0.996	0.000
W 15m	1.125	N.D.	0.092	N.D.	30.63	0.212	77.59	0.056	0.908	0.001
W 20m	1.162	N.D.	0.105	N.D.	30.64	0.197	76.34	0.069	0.807	0.005
W 25m	1.136	N.D.	0.136	N.D.	30.44	0.161	63.92	0.064	1.107	0.004
WL Fluff	0.936	N.D.	0.167	1.201	24.62	0.251	64.19	N.D.	0.688	0.046
WL 5cm	0.865	N.D.	0.118	0.095	26.84	0.253	66.76	N.D.	0.674	0.032
WL 10cm	0.927	N.D.	0.157	0.150	26.12	0.278	66.56	N.D.	0.723	0.043
WL 20cm	0.959	N.D.	0.117	0.110	25.98	0.262	64.84	N.D.	0.677	0.045
WL 40cm	0.915	N.D.	0.097	0.107	26.67	0.259	63.49	N.D.	0.678	0.037
Ark 0m	1.643	0.093	0.129	N.D.	21.40	0.167	76.39	0.094	0.745	0.023
Ark 5m	1.222	0.052	0.127	N.D.	20.93	0.173	76.83	0.083	0.885	0.024
Ark 10m	1.002	0.005	0.119	N.D.	29.22	0.196	77.74	0.093	0.801	0.026
Ark 20m	0.868	0.075	0.114	N.D.	22.50	0.215	71.41	0.086	0.775	0.018
Ark 30m	0.849	0.064	0.093	N.D.	27.78	0.231	75.20	0.086	0.756	0.022
Ark 35m	0.808	0.074	0.164	N.D.	26.20	0.185	68.65	0.089	0.709	0.017
Ark 40m	0.772	0.143	0.179	N.D.	26.30	0.250	69.00	0.089	0.679	0.020
Ark 45m	0.887	0.069	0.189	N.D.	30.01	0.280	68.21	0.157	0.551	0.027
Ark L Fluff	0.958	0.179	0.206	1.060	24.53	0.284	43.57	0.098	0.326	0.030
Ark L 5cm	0.935	0.194	0.259	0.970	23.87	0.290	17.42	0.111	0.279	0.023
Ark L 10cm	0.918	0.191	0.268	0.926	21.18	0.315	22.64	0.099	0.286	0.026
Ark L 20cm	0.904	0.157	0.238	0.923	22.33	0.251	14.08	0.097	0.274	0.027
Ark L 40cm	0.944	0.200	0.288	0.979	25.31	0.233	13.43	0.090	0.282	0.028

N.D. = Not Detectable, Ton = ODAS Tonne, NP = Nord-Perd Rinne, W = Wiek, Ark = Arkona, L = Lander (height above sea floor), Fluff = Mobile Nepheloid Layer

December '97, ICPMS, Water Dissolved Phase, ug dm^{-3}.

	Li	Ti	V	Mn	Fe	As	Rb	Sr	Ba	U
Ton 0m	31.713	1.114	2.605	N.D.	718.87	4.424	25.174	1985.48	26.527	1.661
Ton 5m	26.689	1.101	1.617	N.D.	871.93	3.188	25.204	1919.79	25.025	1.498
Ton 10m	29.772	0.745	2.059	N.D.	1049.25	3.063	27.122	1992.15	25.804	1.566
Ton 15m	27.739	1.242	2.403	N.D.	955.22	3.289	24.524	1925.04	24.523	1.531
Ton L 5cm	29.050	2.525	2.180	N.D.	920.29	2.783	24.481	1878.58	25.528	1.491
Ton L 10cm	31.156	0.215	2.292	N.D.	980.15	3.402	24.824	1926.66	25.556	1.618
Ton L 20cm	28.778	2.409	1.596	N.D.	823.74	4.042	25.087	1881.88	25.352	1.519
Ton L 40cm	30.430	2.783	2.941	N.D.	974.07	3.637	24.847	1933.80	25.538	1.509
NP 0m	28.958	3.212	2.834	N.D.	924.73	3.398	27.211	1967.00	23.655	1.589
NP 5m	30.787	3.006	3.354	N.D.	948.45	3.544	26.987	1997.12	22.495	1.612
NP 10m	29.620	2.331	2.268	N.D.	968.26	3.675	25.130	1871.10	23.177	1.491
NP 15m	29.360	3.753	3.178	N.D.	900.76	4.000	26.293	1947.26	22.446	1.389
NP 20m	29.502	3.064	2.164	N.D.	940.41	2.913	26.701	1975.57	23.272	1.502
NP L 5cm	32.496	2.858	5.670	3.940	806.34	6.990	33.162	1996.29	20.735	1.785
NP L 10cm	32.331	3.789	4.371	2.542	1010.19	7.013	32.242	2145.52	22.058	1.685
NP L 20cm	37.631	6.171	5.687	2.979	785.30	8.003	33.731	2226.12	22.833	1.548
NP L 40cm	35.699	4.022	6.086	4.619	1043.53	8.116	33.788	2119.11	21.556	1.656

N.D. = Not Detectable, Ton = ODAS Tonne, NP = Nord-Perd Rinne, W = Wiek, Ark = Arkona, L = Lander (height above sea floor), Fluff = Mobile Nepheloid Layer

December '97, ICPMS, Water Dissolved Phase, ug dm^{-3}, ctd.

	Li	Ti	V	Mn	Fe	As	Rb	Sr	Ba	U
W 0m	27.237	2.557	3.796	N.D.	752.81	5.270	25.770	2039.94	18.974	1.503
W 5m	27.565	2.333	2.311	N.D.	690.62	5.244	24.997	1955.41	18.880	1.477
W 10m	29.728	3.637	3.431	N.D.	785.26	5.832	26.801	2027.22	19.855	1.527
W 15m	27.100	1.141	2.915	N.D.	782.54	5.531	25.436	1992.37	19.146	1.514
W 20m	28.309	2.621	3.500	N.D.	781.20	5.411	27.046	2083.05	20.130	1.344
W 25m	30.130	4.285	5.252	N.D.	784.53	5.516	26.689	2009.26	20.195	1.479
W L 5cm	32.124	N.D.	9.415	N.D.	730.80	11.491	28.021	2151.22	25.207	0.944
W L 10cm	30.046	N.D.	6.915	N.D.	765.61	12.014	27.251	2120.73	21.221	0.783
W L 20cm	32.257	N.D.	9.648	N.D.	768.75	12.444	28.407	2118.71	21.264	0.699
W L 40cm	32.572	N.D.	9.260	N.D.	1027.33	12.572	28.345	2145.74	21.788	0.783
Ark 0m	33.699	N.D.	5.763	N.D.	793.62	8.439	28.130	2036.58	20.688	0.672
Ark 5m	32.454	N.D.	5.980	N.D.	767.55	9.727	27.939	2138.49	20.992	0.702
Ark 10m	34.524	N.D.	6.160	N.D.	814.16	8.402	28.057	2150.49	21.869	0.766
Ark 25m	35.944	N.D.	6.860	N.D.	887.22	9.989	29.672	2136.45	21.424	0.885
Ark 35m	37.121	N.D.	6.912	N.D.	918.17	9.715	33.247	2178.98	22.235	0.877
Ark 45m	64.999	N.D.	17.127	N.D.	1432.77	15.830	68.576	490.64	18.627	2.083
Ark L 5cm	55.182	N.D.	14.892	80.951	1471.94	12.864	74.991	491.07	18.618	2.475
Ark L 10cm	55.499	N.D.	15.840	16.399	1378.81	13.845	78.526	579.83	18.397	2.409
Ark L 20cm	61.586	N.D.	14.934	15.043	1458.99	13.958	74.351	531.76	17.930	2.389

N.D. = Not Detectable, Ton = ODAS Tonne, NP = Nord-Perd Rinne, W = Wiek, Ark = Arkona, L = Lander (height above sea floor), Fluff = Mobile Nepheloid Layer

December '97, ICPMS, Normalised Water Dissolved Phase to Rubidium ratios.

	Li/Rb	Ti/Rb	V/Rb	Mn/Rb	Fe/Rb	As/Rb	Sr/Rb	Ba/Rb	U/Rb
Ton 0m	1.260	0.044	0.103	N.D.	28.557	0.176	78.872	1.054	0.066
Ton 5m	1.059	0.044	0.064	N.D.	34.595	0.126	76.170	0.993	0.059
Ton 10m	1.098	0.027	0.076	N.D.	38.686	0.113	73.451	0.951	0.058
Ton 15m	1.131	0.051	0.098	N.D.	38.951	0.134	78.498	1.000	0.062
Ton L 5cm	1.187	0.103	0.089	N.D.	37.592	0.114	76.736	1.043	0.061
Ton L 10cm	1.255	0.009	0.092	N.D.	39.484	0.137	77.612	1.029	0.065
Ton L 20cm	1.147	0.096	0.064	N.D.	32.836	0.161	75.015	1.011	0.061
Ton L 40cm	1.225	0.112	0.118	N.D.	39.203	0.146	77.828	1.028	0.061
NP 0m	1.064	0.118	0.104	N.D.	33.984	0.125	72.287	0.869	0.058
NP 5m	1.141	0.111	0.124	N.D.	35.145	0.131	74.004	0.834	0.060
NP 10m	1.179	0.093	0.090	N.D.	38.530	0.146	74.457	0.922	0.059
NP 15m	1.117	0.143	0.121	N.D.	34.259	0.152	74.060	0.854	0.053
NP 20m	1.105	0.115	0.081	N.D.	35.221	0.109	73.990	0.872	0.056
NP L 5cm	0.980	0.086	0.171	0.119	24.315	0.211	60.198	0.625	0.054
NP L 10cm	1.003	0.118	0.136	0.079	31.331	0.218	66.544	0.684	0.052
NP L 20cm	1.116	0.183	0.169	0.088	23.281	0.237	65.996	0.677	0.046
NP L 40cm	1.057	0.119	0.180	0.137	30.885	0.240	62.718	0.638	0.049

	Li/Rb	Ti/Rb	V/Rb	Mn/Rb	Fe/Rb	As/Rb	Sr/Rb	Ba/Rb	U/Rb
W 0m	1.057	0.099	0.147	N.D.	29.213	0.205	79.161	0.736	0.058
W 5m	1.103	0.093	0.092	N.D.	27.628	0.210	78.226	0.755	0.059
W 10m	1.109	0.136	0.128	N.D.	29.299	0.218	75.640	0.741	0.057
W 15m	1.065	0.045	0.115	N.D.	30.765	0.217	78.328	0.753	0.060
W 20m	1.047	0.097	0.129	N.D.	28.884	0.200	77.018	0.744	0.050
W 25m	1.129	0.161	0.197	N.D.	29.395	0.207	75.285	0.757	0.055
WL 5cm	1.146	N.D.	0.336	N.D.	26.080	0.410	76.770	0.900	0.034
WL 10cm	1.103	N.D.	0.254	N.D.	28.095	0.441	77.821	0.779	0.029
WL 20cm	1.136	N.D.	0.340	N.D.	27.061	0.438	74.583	0.749	0.025
WL 40cm	1.149	N.D.	0.327	N.D.	36.243	0.444	75.700	0.769	0.028
Ark 0m	1.198	N.D.	0.205	N.D.	28.213	0.300	72.399	0.735	0.024
Ark 5m	1.162	N.D.	0.214	N.D.	27.472	0.348	76.542	0.751	0.025
Ark 10m	1.230	N.D.	0.220	N.D.	29.018	0.299	76.648	0.779	0.027
Ark 25m	1.211	N.D.	0.231	N.D.	29.901	0.337	72.002	0.722	0.030
Ark 35m	1.117	N.D.	0.208	N.D.	27.617	0.292	65.539	0.669	0.026
Ark 45m	0.948	N.D.	0.250	N.D.	20.893	0.231	7.155	0.272	0.030
Ark L 5cm	0.736	N.D.	0.199	1.079	19.628	0.172	6.548	0.248	0.033
Ark L 10cm	0.707	N.D.	0.202	0.209	17.559	0.176	7.384	0.234	0.031
Ark L 20cm	0.828	N.D.	0.201	0.202	19.623	0.188	7.152	0.241	0.032

N.D. = Not Detectable, Ton = ODAS Tonne, NP = Nord-Perd Rinne, W = Wiek, Ark = Arkona, L = Lander (height above sea floor), Fluff = Mobile Nepheloid Layer

Mobile Nepheloid Layer, ICPMS, Multi-element analysis, Parts per million.

	Li	Ti	V	Mn	Fe	Co	Ni	Cu	Zn	As
Ton Oct '96	20.06	2150	53.06	2362	31648	10.22	66.62	100.00	620.27	19.71
Ton Oct '96	23.73	1790	69.60	2617	39254	33.20	84.05	68.29	665.07	19.61
Ton Mar '97	23.80	2350	76.14	3077	36403	12.79	40.34	61.02	292.93	19.88
Ton June '97	20.92	3024	59.30	2027	31017	10.99	48.65	53.77	311.34	20.52
Ton Dec '97	23.92	2327	84.20	2352	36544	13.88	42.80	74.24	357.73	20.26
Ton June '98	37.01	2500	84.34	3208	38849	13.16	59.07	72.87	750.81	29.28
NP Oct '96	20.26	1893	67.62	3417	33743	11.99	53.54	38.74	248.54	19.88
NP Oct '96	25.24	2039	75.66	2839	37897	12.67	44.55	58.62	289.60	20.54
NP Mar '97	24.23	3508	69.90	1834	37699	12.67	34.86	55.62	214.99	19.61
NP June '97	24.98	2810	69.00	1122	34739	11.31	64.75	45.67	270.66	21.29
NP Oct '97	1.31	318	4.01	77	2251	1.17	3.00	3.90	16.50	1.07
NP Dec '97	22.42	2811	66.27	1145	36700	9.23	33.27	40.44	199.04	18.32
NP June '98	24.42	2232	54.28	1108	24262	22.22	41.87	37.65	549.39	15.33
W Oct '96	20.84	2762	46.90	310	25679	4.73	37.33	30.70	227.85	12.93
W Oct '96	15.43	3019	43.14	279	21886	13.01	154.57	29.14	478.97	12.90
W Oct '96	21.99	3086	64.77	330	30712	7.40	32.01	47.28	197.68	12.11
W Mar '97	29.15	3701	79.52	660	39322	13.27	37.74	59.85	224.75	19.33
W June '97	22.64	3389	60.51	423	28575	13.12	128.43	38.78	285.38	16.32
W Oct '97	0.79	209	2.67	22	1189	0.33	0.95	1.92	7.59	0.44
W Dec '97	10.05	1414	24.22	332	12181	3.84	11.72	12.72	75.66	5.20
W June '98	28.02	2914	54.99	470	22345	7.56	25.18	52.33	203.15	12.74
Ark Oct '96	30.48	3856	85.33	305	35908	31.76	45.47	63.78	620.32	15.32
Ark Mar '97	34.91	4624	94.06	404	37881	13.98	37.66	48.51	173.04	18.84
Ark June '97	28.27	4452	83.05	324	37626	24.32	52.21	51.95	342.84	20.06

Ton = ODAS Tonne, NP = Nord-Perd Rinne, W = Wiek, Ark = Arkona,

Mobile Nepheloid Layer, ICPMS, Multi-element analysis, Parts per million, ctd.

	Rb	Sr	Y	Zr	Sn	Cs	Ba	Ce	Pb	Th	U
Ton Oct '96	58.29	102.65	10.26	74.47	57.09	1.44	238.69	32.25	101.16	3.77	1.15
Ton Oct '96	77.77	105.08	13.87	86.93	82.23	3.79	262.75	36.96	105.06	7.00	1.51
Ton Mar '97	50.84	134.21	14.05	97.30	81.14	3.60	314.41	49.25	93.55	7.07	1.46
Ton June '97	57.61	76.80	9.82	106.66	80.47	1.62	266.71	32.60	106.14	4.66	1.65
Ton Dec '97	82.42	134.20	15.11	115.64	76.09	3.07	310.46	50.20	99.68	6.44	1.90
Ton June '98	45.34	55.41	10.80	78.39	128.20	4.42	205.77	13.57	118.82	3.66	2.04
NP Oct '96	62.03	70.71	11.89	88.57	54.19	2.53	224.24	35.65	85.03	4.40	1.36
NP Oct '96	97.03	129.09	15.72	81.86	80.35	3.87	293.91	54.85	97.22	7.72	1.53
NP Mar '97	95.29	117.22	16.11	144.26	85.95	3.46	329.45	61.25	80.13	8.77	2.31
NP June '97	81.96	67.15	12.64	119.16	99.20	2.40	239.59	36.86	96.01	5.42	1.83
NP Oct '97	4.84	5.81	1.25	21.81	6.57	0.07	26.79	2.70	4.30	0.42	0.12
NP Dec '97	93.89	128.49	15.33	117.79	159.18	2.67	326.29	57.17	81.13	7.79	1.95
NP June '98	68.50	177.10	13.18	121.40	55.01	2.95	301.48	43.82	60.06	6.93	2.04
W Oct '96	68.89	97.69	14.38	144.22	60.47	0.95	279.19	41.83	52.19	5.61	1.56
W Oct '96	54.30	66.28	7.54	154.19	52.60	0.22	202.81	28.28	46.79	3.37	1.41
W Oct '96	58.72	75.42	13.03	133.48	99.90	2.81	311.94	32.97	71.04	5.99	2.06
W Mar '97	103.98	111.23	16.73	122.68	40.81	3.97	307.79	64.67	86.12	9.53	2.26
W June '97	96.41	81.40	14.48	138.81	69.99	2.22	322.36	45.73	64.55	6.55	1.82
W Oct '97	4.29	5.67	0.83	13.00	9.41	0.01	31.78	2.10	2.41	0.30	0.06
W Dec '97	48.44	79.73	12.00	95.90	57.33	1.27	316.89	25.65	26.88	4.31	1.34
W June '98	78.47	129.92	12.57	142.27	43.44	2.96	422.51	33.67	46.80	5.74	2.26
Ark Oct '96	92.10	51.31	12.18	137.98	127.91	3.28	273.81	26.03	84.72	5.77	2.98
Ark Mar '97	117.19	75.23	14.82	144.39	51.15	4.54	332.02	48.69	92.23	6.39	3.11
Ark June '97	99.61	57.95	14.33	137.46	65.99	3.53	235.60	38.29	96.20	4.92	2.66

Ton = ODAS Tonne, NP = Nord-Perd Rinne, W = Wiek, Ark = Arkona,

Mobile Nepheloid Layer, ICPMS, normalised multi-element analysis to rubidium ratios.

	Li/Rb	Ti/Rb	V/Rb	Mn/Rb	Fe/Rb	Co/Rb	Ni/Rb	Cu/Rb	Zn/Rb	As/Rb
Ton Oct '96	0.344	36.887	0.910	40.519	542.959	0.175	1.143	1.716	10.642	0.338
Ton Oct '96	0.305	23.012	0.895	33.655	504.748	0.427	1.081	0.878	8.552	0.252
Ton Mar '97	0.468	46.228	1.498	60.527	716.055	0.252	0.793	1.200	5.762	0.391
Ton June '97	0.363	52.495	1.029	35.187	538.412	0.191	0.845	0.933	5.404	0.356
Ton Dec '97	0.290	28.234	1.022	28.538	443.381	0.168	0.519	0.901	4.340	0.246
Ton June '98	0.816	55.145	1.860	70.754	856.900	0.290	1.303	1.607	16.561	0.646
NP Oct '96	0.327	30.516	1.090	55.084	544.028	0.193	0.863	0.625	4.007	0.321
NP Oct '96	0.260	21.014	0.780	29.262	390.554	0.131	0.459	0.604	2.985	0.212
NP Mar '97	0.254	36.808	0.734	19.248	395.619	0.133	0.366	0.584	2.256	0.206
NP June '97	0.305	34.281	0.842	13.690	423.848	0.138	0.790	0.557	3.302	0.260
NP Oct '97	0.270	65.696	0.829	15.819	464.897	0.243	0.620	0.807	3.408	0.221
NP Dec '97	0.239	29.939	0.706	12.194	390.869	0.098	0.354	0.431	2.120	0.195
NP June '98	0.357	32.581	0.792	16.180	354.165	0.324	0.611	0.550	8.020	0.224
W Oct '96	0.303	40.093	0.681	4.505	372.755	0.069	0.542	0.446	3.307	0.188
W Oct '96	0.284	55.600	0.794	5.145	403.028	0.240	2.846	0.537	8.820	0.238
W Oct '96	0.375	52.556	1.103	5.619	522.998	0.126	0.545	0.805	3.366	0.206
W Mar '97	0.280	35.593	0.765	6.350	378.185	0.128	0.363	0.576	2.162	0.186
W June '97	0.235	35.151	0.628	4.385	296.376	0.136	1.332	0.402	2.960	0.169
W Oct '97	0.184	48.597	0.622	5.038	276.916	0.078	0.221	0.446	1.767	0.103
W Dec '97	0.207	29.193	0.500	6.853	251.437	0.079	0.242	0.263	1.562	0.107
W June '98	0.357	37.141	0.701	5.985	284.776	0.096	0.321	0.667	2.589	0.162
Ark Oct '96	0.331	41.871	0.927	3.315	389.889	0.345	0.494	0.693	6.735	0.166
Ark Mar '97	0.298	39.460	0.803	3.450	323.236	0.119	0.321	0.414	1.477	0.161
Ark June '97	0.284	44.699	0.834	3.253	377.745	0.244	0.524	0.522	3.442	0.201

Ton = ODAS Tonne, NP = Nord-Perd Rinne, W = Wiek, Ark = Arkona,

Mobile Nepheloid Layer, ICPMS, normalised multi-element analysis to rubidium ratios, ctd.

	Sr/Rb	Y/Rb	Zr/Rb	Sn/Rb	Cs/Rb	Ba/Rb	Ce/Rb	Pb/Rb	Th/Rb	U/Rb
Ton Oct '96	1.761	0.176	1.278	0.979	0.025	4.095	0.553	1.736	0.065	0.020
Ton Oct '96	1.351	0.178	1.118	1.057	0.049	3.379	0.475	1.351	0.090	0.019
Ton Mar '97	2.640	0.276	1.914	1.596	0.071	6.184	0.969	1.840	0.139	0.029
Ton June '97	1.333	0.170	1.851	1.397	0.028	4.630	0.566	1.842	0.081	0.029
Ton Dec '97	1.628	0.183	1.403	0.923	0.037	3.767	0.609	1.209	0.078	0.023
Ton June '98	1.222	0.238	1.729	2.828	0.097	4.539	0.299	2.621	0.081	0.045
NP Oct '96	1.140	0.192	1.428	0.874	0.041	3.615	0.575	1.371	0.071	0.022
NP Oct '96	1.330	0.162	0.844	0.828	0.040	3.029	0.565	1.002	0.080	0.016
NP Mar '97	1.230	0.169	1.514	0.902	0.036	3.457	0.643	0.841	0.092	0.024
NP June '97	0.819	0.154	1.454	1.210	0.029	2.923	0.450	1.171	0.066	0.022
NP Oct '97	1.199	0.259	4.506	1.358	0.015	5.535	0.557	0.889	0.086	0.024
NP Dec '97	1.369	0.163	1.255	1.695	0.028	3.475	0.609	0.864	0.083	0.021
NP June '98	2.585	0.192	1.772	0.803	0.043	4.401	0.640	0.877	0.101	0.030
W Oct '96	1.418	0.209	2.094	0.878	0.014	4.053	0.607	0.758	0.081	0.023
W Oct '96	1.220	0.139	2.839	0.969	0.004	3.735	0.521	0.862	0.062	0.026
W Oct '96	1.284	0.222	2.273	1.701	0.048	5.312	0.561	1.210	0.102	0.035
W Mar '97	1.070	0.161	1.180	0.392	0.038	2.960	0.622	0.828	0.092	0.022
W June '97	0.844	0.150	1.440	0.726	0.023	3.343	0.474	0.669	0.068	0.019
W Oct '97	1.320	0.193	3.027	2.191	0.003	7.400	0.490	0.561	0.071	0.013
W Dec '97	1.646	0.248	1.980	1.184	0.026	6.541	0.529	0.555	0.089	0.028
W June '98	1.656	0.160	1.813	0.554	0.038	5.385	0.429	0.596	0.073	0.029
Ark Oct '96	0.557	0.132	1.498	1.389	0.036	2.973	0.283	0.920	0.063	0.032
Ark Mar '97	0.642	0.126	1.232	0.436	0.039	2.833	0.415	0.787	0.055	0.027
Ark June '97	0.582	0.144	1.380	0.663	0.035	2.365	0.384	0.966	0.049	0.027

Ton = ODAS Tonne, NP = Nord-Perd Rinne, W = Wiek, Ark = Arkona,

Sediment Trap, ICPMS, Multi-element analysis, Parts per million.

	Li	Ti	V	Mn	Fe	Co	Ni	Cu	Zn	As
J-A 97 3	30.371	2649.5	287.0	429.5	51339	13.871	400.8	195.0	780.9	36.528
J-A 97 4	29.188	2570.3	205.5	455.0	46399	12.161	310.4	224.3	908.0	34.081
A-O 97 5	25.907	2446.2	86.3	1221.1	40014	27.936	1339.8	96.1	634.5	26.636
A-O 97 4	22.813	2390.0	156.6	451.3	43831	8.944	290.9	184.7	415.3	26.370
A-O 97 3	20.775	2428.0	160.3	437.2	43768	8.683	321.3	126.3	297.9	23.628
A-O 97 2	22.697	2353.8	164.5	461.9	42298	9.607	309.6	157.7	334.0	28.626
A-O 97 1	21.606	2443.7	131.9	455.9	44606	9.090	306.0	149.2	348.9	27.191
O-D 97 5	29.466	2966.6	65.8	2578.9	38682	13.334	163.3	137.2	1139.9	26.497
O-D 97 4	26.385	2704.4	164.9	494.3	39939	10.351	346.3	159.8	145.6	22.471
O-D 97 3	24.716	2915.9	140.0	530.6	41863	10.555	362.3	213.8	166.1	29.903
O-D 97 2	27.138	3044.0	55.7	2330.9	35282	11.466	33.3	67.4	359.2	22.909
O-D 97 1	26.055	2939.6	88.3	657.8	51147	13.099	518.8	485.9	294.2	23.061
M-J 98 5	21.369	2199.9	63.4	921.9	24831	8.373	42.8	66.6	305.9	15.025
M-J 98 4	20.643	3039.3	56.2	908.2	25004	8.181	43.3	49.7	256.6	13.098
D-M 98 5	15.421	1955.0	58.8	387.0	24963	10.086	560.6	88.3	150.5	12.989
D-M 98 4	18.636	2238.5	88.6	363.2	32324	7.974	365.8	143.7	126.5	16.188
D-M 98 3	18.068	2282.8	71.8	573.2	33478	14.906	912.5	98.9	180.4	16.723
D-M 98 2	23.079	2737.9	149.2	438.7	45261	10.656	415.6	156.1	152.9	28.864
D-M 98 1	27.627	2915.9	74.2	1882.0	36410	10.783	40.0	68.5	335.6	23.115

J = June, A = August, O = October, D = December, M= March, 1 = top sediment trap and 5 = bottom sediment trap

Sediment Trap, ICPMS, Multi-element analysis, Parts per million, ctd.

	Rb	Sr	Y	Zr	Mo	Cd	Sn	Sb	Cs	Ba	Ce	Pb	Th	U
J-A 97 3	81.041	55.418	16.909	131.077	1106.5	N.D.	57.433	1.630	5.681	349.653	46.218	77.736	8.014	2.837
J-A 97 4	76.832	62.741	17.694	109.977	593.0	N.D.	67.871	0.660	5.675	341.896	50.418	89.012	8.554	2.809
A-O 97 5	65.470	198.244	15.110	36.719	78.2	N.D.	4.891	0.416	3.517	305.643	49.479	74.210	7.341	2.436
A-O 97 4	50.986	58.458	10.953	134.972	1009.6	N.D.	51.965	1.989	3.377	271.458	35.755	73.717	6.257	2.581
A-O 97 3	61.797	50.831	11.979	117.839	915.2	N.D.	54.252	1.546	3.408	286.676	44.230	70.012	6.932	2.496
A-O 97 2	64.913	54.506	13.686	26.716	600.2	N.D.	20.437	1.465	3.522	296.035	47.643	76.520	7.484	2.548
A-O 97 1	43.279	47.454	10.821	138.425	812.0	N.D.	48.814	2.296	3.329	270.943	35.045	76.841	7.065	2.585
O-D 97 5	73.414	69.191	20.450	33.902	151.3	1.247	3.983	N.D.	3.227	305.164	54.825	84.264	8.103	2.193
O-D 97 4	69.352	68.462	16.799	62.992	575.1	0.639	34.581	0.770	3.136	294.790	51.613	86.418	7.797	2.173
O-D 97 3	68.423	64.435	17.429	139.692	317.6	0.224	30.502	4.088	3.061	273.504	48.891	85.410	7.342	2.185
O-D 97 2	72.282	93.380	20.376	138.131	1.4	1.434	7.722	N.D.	3.075	297.865	55.359	85.224	8.346	2.009
O-D 97 1	72.634	79.889	19.553	120.095	87.3	N.D.	9.383	0.235	3.062	295.518	53.372	91.001	7.688	2.144
M-J 98 5	62.553	92.061	15.186	84.544	1.7	0.323	6.905	N.D.	2.021	306.617	47.220	67.792	6.427	1.429
M-J 98 4	60.663	82.226	16.332	133.099	1.6	0.510	6.505	0.243	1.891	290.045	48.287	61.413	6.712	1.749
D-M 98 5	52.117	61.197	11.311	93.705	136.8	0.335	10.894	N.D.	1.400	275.296	38.832	44.837	5.335	1.116
D-M 98 4	57.839	60.621	12.433	100.512	288.4	N.D.	22.582	0.571	2.022	281.450	38.364	59.581	5.300	1.389
D-M 98 3	56.873	68.911	14.284	93.980	178.2	0.703	15.687	0.059	2.060	285.638	42.405	59.141	5.903	1.524
D-M 98 2	67.532	63.788	15.120	116.713	592.6	0.024	27.292	1.888	2.961	300.958	47.694	79.817	7.388	1.853
D-M 98 1	74.794	36.061	19.412	92.791	0.9	1.085	5.461	N.D.	3.485	327.543	56.973	86.243	8.221	1.870

N.D. = Not Detectable, J = June, A = August, O = October, D = December, M= March, 1 = top sediment trap and 5 = bottom sediment trap

Sediment Trap, ICPMS, normalised multi-element analysis to rubidium ratios

	Li/Rb	Ti/Rb	V/Rb	Mn/Rb	Fe/Rb	Co/Rb	Ni/Rb	Cu/Rb	Zn/Rb	As/Rb
J-A 97 3	0.375	32.694	3.541	5.299	633.49	0.171	4.945	2.407	9.636	0.451
J-A 97 4	0.380	33.454	2.675	5.922	603.91	0.158	4.040	2.920	11.818	0.444
A-O 97 5	0.396	37.364	1.318	18.652	611.19	0.427	20.465	1.468	9.692	0.407
A-O 97 4	0.447	46.877	3.071	8.851	859.67	0.175	5.705	3.623	8.145	0.517
A-O 97 3	0.336	39.290	2.594	7.075	708.26	0.141	5.200	2.045	4.820	0.382
A-O 97 2	0.350	36.261	2.534	7.116	651.61	0.148	4.770	2.429	5.145	0.441
A-O 97 1	0.499	56.463	3.047	10.533	1030.66	0.210	7.070	3.447	8.062	0.628
O-D 97 5	0.401	40.409	0.897	35.129	526.90	0.182	2.225	1.868	15.527	0.361
O-D 97 4	0.380	38.996	2.378	7.128	575.89	0.149	4.993	2.304	2.100	0.324
O-D 97 3	0.361	42.615	2.047	7.754	611.82	0.154	5.295	3.125	2.427	0.437
O-D 97 2	0.375	42.112	0.771	32.247	488.12	0.159	0.461	0.933	4.969	0.317
O-D 97 1	0.359	40.472	1.215	9.056	704.17	0.180	7.142	6.690	4.051	0.317
M-J 98 5	0.342	35.169	1.013	14.739	396.96	0.134	0.684	1.065	4.890	0.240
M-J 98 4	0.340	50.101	0.927	14.972	412.18	0.135	0.714	0.819	4.229	0.216
D-M 98 5	0.296	37.512	1.129	7.425	478.97	0.194	10.756	1.694	2.888	0.249
D-M 98 4	0.322	38.703	1.531	6.279	558.86	0.138	6.325	2.484	2.187	0.280
D-M 98 3	0.318	40.139	1.263	10.079	588.65	0.262	16.045	1.739	3.171	0.294
D-M 98 2	0.342	40.542	2.209	6.496	670.22	0.158	6.153	2.311	2.265	0.427
D-M 98 1	0.369	38.985	0.992	25.162	486.80	0.144	0.535	0.916	4.487	0.309

J = June, A = August, O = October, D = December, M= March, 1 = top sediment trap and 5 = bottom sediment trap

Sediment Trap, ICPMS, normalised multi-element analysis to rubidium ratios, ctd.

	Sr/Rb	Y/Rb	Zr/Rb	Mo/Rb	Cd/Rb	Sn/Rb	Sb/Rb	Cs/Rb	Ba/Rb	Ce/Rb	Pb/Rb	Th/Rb	U/Rb
J-A 97 3	0.684	0.209	1.617	13.654	N.D.	0.709	0.020	0.070	4.315	0.570	0.959	0.099	0.035
J-A 97 4	0.817	0.230	1.431	7.718	N.D.	0.883	0.009	0.074	4.450	0.656	1.159	0.111	0.037
A-O 97 5	3.028	0.231	0.561	1.195	N.D.	0.075	0.006	0.054	4.668	0.756	1.134	0.112	0.037
A-O 97 4	1.147	0.215	2.647	19.801	N.D.	1.019	0.039	0.066	5.324	0.701	1.446	0.123	0.051
A-O 97 3	0.823	0.194	1.907	14.810	N.D.	0.878	0.025	0.055	4.639	0.716	1.133	0.112	0.040
A-O 97 2	0.840	0.211	0.412	9.246	N.D.	0.315	0.023	0.054	4.560	0.734	1.179	0.115	0.039
A-O 97 1	1.096	0.250	3.198	18.761	N.D.	1.128	0.053	0.077	6.260	0.810	1.775	0.163	0.060
O-D 97 5	0.942	0.279	0.462	2.061	0.017	0.054	N.D.	0.044	4.157	0.747	1.148	0.110	0.030
O-D 97 4	0.987	0.242	0.908	8.293	0.009	0.499	0.011	0.045	4.251	0.744	1.246	0.112	0.031
O-D 97 3	0.942	0.255	2.042	4.642	0.003	0.446	0.060	0.045	3.997	0.715	1.248	0.107	0.032
O-D 97 2	1.292	0.282	1.911	0.019	0.020	0.107	N.D.	0.043	4.121	0.766	1.179	0.115	0.028
O-D 97 1	1.100	0.269	1.653	1.202	N.D.	0.129	0.003	0.042	4.069	0.735	1.253	0.106	0.030
M-J 98 5	1.472	0.243	1.352	0.028	0.005	0.110	N.D.	0.032	4.902	0.755	1.084	0.103	0.023
M-J 98 4	1.355	0.269	2.194	0.027	0.008	0.107	0.004	0.031	4.781	0.796	1.012	0.111	0.029
D-M 98 5	1.174	0.217	1.798	2.625	0.006	0.209	N.D.	0.027	5.282	0.745	0.860	0.102	0.021
D-M 98 4	1.048	0.215	1.738	4.987	N.D.	0.390	0.010	0.035	4.866	0.663	1.030	0.092	0.024
D-M 98 3	1.212	0.251	1.652	3.133	0.012	0.276	0.001	0.036	5.022	0.746	1.040	0.104	0.027
D-M 98 2	0.945	0.224	1.728	8.775	0.000	0.404	0.028	0.044	4.457	0.706	1.182	0.109	0.027
D-M 98 1	0.482	0.260	1.241	0.013	0.015	0.073	N.D.	0.047	4.379	0.762	1.153	0.110	0.025

N.D. = Not Detectable, J = June, A = August, O = October, D = December, M= March, 1 = top sediment trap and 5 = bottom sediment trap

Stable Lead Isotopes, Sediment Core ICPMS analysis, $^{206/207}Pb$ and $^{208/207}Pb$ ratios

	206/207 Ratio	S.D. +/-	208/207 Ratio	S.D. +/-
Ark 1-2	1.175674	0.006253	2.392694	0.009778
Ark 2-3	1.180128	0.004201	2.392715	0.022778
Ark 3-4	1.175537	0.009396	2.390229	0.009583
Ark 4-5	1.167564	0.010814	2.359540	0.016789
Ark 5-6	1.175183	0.024093	2.361277	0.021851
Ark 6-7	1.160223	0.015535	2.358476	0.015825
Ark 7-8	1.169015	0.014583	2.367178	0.017076
Ark 8-9	1.166362	0.010576	2.373344	0.013021
Ark 9-10	1.172062	0.020825	2.384520	0.020103
Ark 10-12	1.189179	0.008741	2.374219	0.020113
Ark 12-14	1.203443	0.004473	2.410875	0.016987
Ark 14-16	1.201893	0.010130	2.408195	0.011849
Ark 16-18	1.207784	0.006474	2.410833	0.027613
Ark 18-20	1.217934	0.005618	2.442869	0.017405
Ark 20-22	1.230429	0.008083	2.448723	0.017610
Ark 22-24	1.227579	0.009519	2.420119	0.018821
Ark 24-26	1.229864	0.009845	2.440614	0.027529
Ark 26-28	1.226865	0.004934	2.428660	0.013292
Ark 28-30	1.226083	0.009896	2.436955	0.015057
Ark 30-32	1.234120	0.006919	2.443839	0.028247
Ark 32-34	1.226076	0.009847	2.437603	0.007632
Ark 34-36	1.235831	0.006285	2.442645	0.016026
Ark 36-38	1.232005	0.008085	2.445233	0.013780
Ark 38-40	1.232007	0.005508	2.453884	0.020621
Ark 40-42	1.223320	0.002392	2.464686	0.012674
Ark 42-44	1.220106	0.004232	2.469375	0.005774
Ark 44-46	1.219027	0.005729	2.472916	0.014001

	206/207 Ratios	S.D. +/-	208/207 Ratio	S.D. +/-
Wiek 1-2	1.173531	0.007387	2.442058	0.007015
Wiek 2-3	1.165641	0.006256	2.444224	0.010786
Wiek 3-4	1.172020	0.009387	2.450093	0.011521
Wiek 4-5	1.179851	0.004956	2.461678	0.020214
Wiek 5-6	1.182522	0.004338	2.446687	0.022217
Wiek 6-7	1.191896	0.007078	2.464251	0.013864
Wiek 7-8	1.198202	0.011642	2.481702	0.019366
Wiek 8-9	1.208757	0.004137	2.480971	0.013634
Wiek 9-10	1.210436	0.011950	2.476258	0.007709
Wiek 10-12	1.202869	0.014948	2.455767	0.019579
Wiek 12-14	1.208600	0.008297	2.464264	0.018398
Wiek 14-16	1.209291	0.006856	2.442420	0.013976
Wiek 16-18	1.217806	0.009262	2.465443	0.020387

Stable Lead Isotopes, Sediment Core ICPMS analysis, $^{206/207}Pb$ and $^{208/207}Pb$ ratios, ctd.

	206/207 Ratio	S.D. +/-	208/207 Ratio	S.D. +/-
NP 4-5	1.176916	0.011408	2.462500	0.030698
NP 5-6	1.182862	0.009289	2.474552	0.023270
NP 6-7	1.191763	0.012077	2.456262	0.010154
NP 7-8	1.188270	0.004200	2.465263	0.012526
NP 8-9	1.191564	0.004447	2.481738	0.016326
NP 9-10	1.190434	0.005182	2.475309	0.024852
NP 10-12	1.205197	0.008218	2.480963	0.011497
NP 12-14	1.201847	0.008404	2.479971	0.016383
NP 14-16	1.216313	0.007844	2.510001	0.020125
NP 16-18	1.221534	0.017276	2.486696	0.016058
NP 20-22	1.249146	0.016553	2.493466	0.028794
NP 22-24	1.244712	0.010811	2.526651	0.011183
NP 24-26	1.257641	0.016313	2.583042	0.014713
NP 26-28	1.247728	0.003571	2.572227	0.020141
NP 28-30	1.239162	0.005124	2.517205	0.036167
NP 30-32	1.240412	0.003627	2.516176	0.015359
NP 32-34	1.220722	0.007461	2.475733	0.005163
NP 34-36	1.219670	0.004039	2.487695	0.006015

	206/207 Ratio	S.D. +/-	208/207 Ratio	S.D. +/-
Ton 0-1	1.165269	0.002659	2.424983	0.009409
Ton 1-2	1.172311	0.001523	2.437406	0.008995
Ton 2-3	1.173564	0.003059	2.423223	0.007166
Ton 3-4	1.168555	0.006974	2.419753	0.004791
Ton 4-5	1.172539	0.003540	2.424975	0.007342
Ton 5-6	1.164822	0.003280	2.408517	0.006719
Ton 6-7	1.154752	0.002172	2.411724	0.003881
Ton 7-8	1.163699	0.002489	2.424513	0.004910
Ton 8-9	1.166304	0.006412	2.440639	0.003797
Ton 9-10	1.179106	0.003444	2.428437	0.005278
Ton 10-12	1.158810	0.002685	2.405518	0.008645
Ton 12-14	1.166020	0.002072	2.421865	0.008544

Stable Lead Isotopes, Mobile Nepheloid Layer ICPMS analysis, $^{206/207}Pb$ and $^{208/207}Pb$ ratios.

	206/207 Ratio	S.D. +/-	208/207 Ratio	S.D. +/-
Ton Oct '96	1.17985	0.01019	2.46794	0.02436
Ton Oct '96	1.16746	0.00459	2.46924	0.01168
NP Oct '96	1.18303	0.00973	2.47702	0.01317
NP Oct '96	1.17009	0.01170	2.42869	0.01228
W Oct '96	1.17586	0.01961	2.45366	0.02005
W Oct '96	1.17161	0.00896	2.45311	0.02198
W Oct '96	1.17938	0.00575	2.45823	0.02062
Ark Oct '96	1.17790	0.00841	2.47640	0.02684
Ton 03/97	1.18480	0.01575	2.44973	0.01449
NP Mar '97	1.17607	0.01042	2.42535	0.03260
W Mar '97	1.19880	0.00509	2.45961	0.03379
Ark Mar '97	1.18432	0.00547	2.42600	0.01649
Ton June '97	1.18126	0.01104	2.43680	0.01462
NP June '97	1.19203	0.01197	2.45243	0.01907
W June '97	1.18861	0.00967	2.46147	0.02172
Ark June '97	1.18755	0.00879	2.43631	0.02778
NP Oct '97	1.18860	0.01059	2.43143	0.00809
W Oct '97	1.18543	0.02103	2.43997	0.00369
Ton Dec '97	1.17716	0.01255	2.43877	0.02731
NP Dec '97	1.17680	0.00635	2.43508	0.00366
W Dec'97	1.17650	0.02148	2.45047	0.02360
Ton Mar '98	1.18108	0.00485	2.45931	0.02631
Ton June '98	1.17400	0.00251	2.45825	0.01472
NP June '98	1.17051	0.00585	2.43504	0.01294
W June '98	1.18229	0.00550	2.43752	0.02014

Stable Lead Isotopes, Sediment Trap ICPMS analysis, $^{206/207}Pb$ and $^{208/207}Pb$ ratios.

	206/207 Ratio	S.D. +/-	208/207 Ratio	S.D. +/-
J-A 97 3	1.18253	0.01027	2.45122	0.01577
J-A 97 4	1.17316	0.00400	2.44865	0.02359
A-O 97 5	1.18413	0.00583	2.45179	0.01613
A-O 97 4	1.16705	0.00830	2.45478	0.00749
A-O 97 3	1.17873	0.00872	2.46353	0.01676
A-O 97 2	1.19153	0.01405	2.46103	0.01922
A-O 97 1	1.18444	0.00427	2.45064	0.01291
O-D 97 5	1.19030	0.00680	2.46160	0.01012
O-D 97 4	1.18860	0.00631	2.45572	0.01800
O-D 97 3	1.19117	0.00485	2.46919	0.01753
O-D 97 2	1.18538	0.01016	2.46329	0.00881
O-D 97 1	1.18183	0.00999	2.46811	0.01271
M-J 98 5	1.18641	0.00920	2.47702	0.01254
M-J 98 4	1.18536	0.00738	2.46988	0.01761
D-M 98 5	1.19669	0.00286	2.45904	0.01429
D-M 98 4	1.19016	0.00533	2.45284	0.01324
D-M 98 3	1.18975	0.01304	2.45340	0.00515
D-M 98 2	1.18849	0.02643	2.49934	0.03209
D-M 98 1	1.17765	0.01706	2.47639	0.04768

J = June, A = August, O = October, D = December, M= March, 1 = top sediment trap and 5 = bottom sediment trap

Radionuclide Data, Gamma Ray Spectrometry, ^{226}Ra.

Core Depth (cm)	Arkona Ra (Bq/Kg)	Bq/Kg Error (+/-)	Wiek Ra (Bq/Kg)	Bq/Kg Error (+/-)	Nord Perd Ra (Bq/Kg)	Bq/Kg Error (+/-)	Tonne Ra (Bq/Kg)	Bq/Kg Error (+/-)
0.5	26.059	0.130					8.182	1.006
1.5	40.771	0.612	27.114	0.166			8.269	1.045
2.5	39.989	1.000	14.111	0.141			5.761	0.471
3.5	32.446	1.136	12.185	0.138			10.074	1.774
4.5	38.956	1.753	19.705	0.345	17.457	2.049	8.861	1.235
5.5	44.322	2.438	27.386	0.668	14.549	1.609	11.994	1.144
6.5	35.441	2.304	20.595	0.474	20.136	2.374	9.775	1.193
7.5	27.880	2.091	31.469	0.658	11.657	1.382	11.275	1.115
8.5	29.175	2.480	21.829	0.541	18.369	1.504	11.800	1.791
9.5	33.263	3.160	23.370	0.738	14.025	1.502	8.237	0.900
11	28.370	3.121	22.659	0.707	18.069	1.618	11.026	1.643
13	26.195	3.405	23.267	0.792	20.247	2.291	6.269	0.995
15	23.387	3.508	21.890	0.768	18.585	1.927		
17	35.052	5.959	25.157	1.499	21.500	2.495		
19	19.684	3.740			N.S.	N.S.		
21	34.666	7.280			25.283	2.559		
23	21.098	4.852			28.930	2.888		
25	24.718	6.179			21.026	1.831		
27	26.159	7.063			22.826	2.198		
29	26.844	7.785			15.094	1.398		
31	26.859	8.326			23.546	2.345		
33	28.817	9.509			17.483	1.731		
35	23.801	8.330			20.600	1.941		
37	31.572	11.682						
39	31.641	12.340						
41	20.698	8.486						
43	27.694	11.908						
45	30.513	13.731						
47	24.068	11.312						
49	29.236	14.326						

N.S. = No Sample

Radionuclide Data, Gamma Ray Spectrometry, ^{210}Pb.

Core Depth (cm)	Arkona Pb (Bq/Kg)	Bq/Kg Error (+/-)	Wiek Pb (Bq/Kg)	Bq/Kg Error (+/-)	Nord Perd Pb (Bq/Kg)	Bq/Kg Error (+/-)	Tonne Pb (Bq/Kg)	Bq/Kg Error (+/-)
0.5	237.060	1.185					21.303	1.507
1.5	218.316	3.275	27.114	0.888			3.382	0.326
2.5	165.377	4.134	14.111	0.583			9.025	0.485
3.5	222.721	7.795	12.185	0.950			14.638	1.259
4.5	226.484	10.192	19.705	2.008	39.200	3.314	1.976	0.157
5.5	207.265	11.400	27.386	3.122	45.984	3.998	8.411	0.575
6.5	159.748	10.384	20.595	2.139	26.147	1.930	1.751	0.134
7.5	176.827	13.262	31.469	4.173	19.493	1.551	2.903	0.208
8.5	236.513	20.104	21.829	4.388	17.931	1.158	1.417	0.117
9.5	181.604	17.252	23.370	4.032	0.804	0.067	19.418	1.744
11	88.184	9.700	22.659	2.198	9.214	0.607	2.238	0.172
13	52.695	6.850	23.267	1.594	7.349	0.753		
15	54.744	8.212	21.890	1.798	9.457	0.654		
17	53.649	9.120	25.157	2.294	15.710	1.431		
19	35.715	6.786			N.S.	N.S.		
21	41.550	8.726			15.835	1.163		
23	39.569	9.101			28.971	2.202		
25	39.985	9.996			18.119	1.624		
27	27.172	7.336			24.252	1.906		
29	18.948	5.495			20.680	1.803		
31	20.602	6.387			2.420	0.205		
33	34.605	11.419			21.640	0.385		
35	47.969	16.789			13.832	1.355		
37	42.153	15.596						
39	39.138	15.264						
41	31.422	12.883						
43	43.516	18.712						
45	37.980	17.091						
47	3.250	1.528						
49	40.463	19.827						

N.S. = No Sample

Radionuclide Data, Gamma Ray Spectrometry, Excess ^{210}Pb.

Core Deptr (cm)	Arkona XS Pb (Bq/Kg)	Bq/Kg Erro (+/-)	Wiek XS Pb (Bq/Kg)	Bq/Kg Erro (+/-)	Nord Perd XS Pb (Bq/Kg)	Bq/Kg Erro (+/-)	Tonne Xs Pb (Bq/Kg)	Bq/Kg Erro (+/-)
0.5	220.084	17.097					13.720	14.186
1.5	185.219	13.959	166.505	14.708			-5.111	15.899
2.5	130.819	14.835	71.726	11.907			3.419	9.788
3.5	198.533	22.938	70.149	12.131			4.780	19.595
4.5	195.717	14.155	71.724	13.354	22.735	14.464	-7.229	16.052
5.5	170.087	12.600	-1.507	12.219	32.878	14.057	-3.761	11.734
6.5	129.801	10.717	-18.188	15.659	6.331	13.910	-8.449	14.407
7.5	155.557	12.138	-7.157	12.860	8.211	14.280	-8.814	12.209
8.5	216.614	10.570	3.357	12.808	-0.459	10.428	-13.917	17.291
9.5	155.004	15.078	-2.670	12.426	-13.858	13.563	11.776	14.141
11	62.506	12.467	4.665	12.976	-9.329	11.120	-13.888	16.774
13	27.698	12.404	-0.030	11.942	-13.521	15.261	-22.942	20.957
15	32.779	10.660	2.835	12.827	-9.619	12.460		
17	19.442	13.171	16.287	14.380	-6.070	14.755		
19	16.790	17.784						
21	7.211	13.024			-9.905	12.505		
23	19.362	16.363			0.043	12.546		
25	15.996	13.809			-3.053	12.498		
27	1.071	14.130			1.505	12.429		
29	-8.350	13.843			5.901	12.723		
31	-6.571	10.224			-22.311	13.084		
33	6.119	9.679			4.390	11.864		
35	25.385	14.964			-7.146	13.590		
37	11.120	12.637						
39	7.918	13.574						
41	11.343	18.196						
43	16.587	12.532						
45	7.898	14.273						
47	-22.014	13.755						
49	11.871	11.760						

Radionuclide Data, Gamma Ray Spectrometry, ^{137}Cs.

Core Depth (cm)	Arkona Cs (Bq/Kg)	Bq/Kg Error (+/-)	Wiek Cs (Bq/Kg)	Bq/Kg Error (+/-)	Nord Perd Cs (Bq/Kg)	Bq/Kg Error (+/-)	Tonne Cs (Bq/Kg)	Bq/Kg Error (+/-)
0.5	83.138	6.578					11.717	1.417
1.5	114.413	9.043	90.977	6.784				
2.5	101.132	7.824	34.905	1.816			4.213	0.842
3.5	95.216	7.335	31.793	1.881			8.273	1.812
4.5	68.296	7.015	27.928	2.125	4.795	2.339	4.289	2.049
5.5	53.486	4.666	12.471	1.681	5.304	1.845	5.646	1.096
6.5	40.274	3.020					6.484	1.160
7.5	21.671	3.364						
8.5	37.241	3.748						
9.5	28.516	3.551	2.464	1.047				
11	12.414	2.171						
13								
15	5.564	1.250						

Carbon and Nitrogen Ratios, Total Carbon and Nitrogen

Core Depth	Arkona		Wiek		Nord Perd		Tonne	
(cm)	% Total C	% Total N	% Total C	% Total N	% Total C	% Total N	% Total C	% Total N
0.5							0.293	0.036
1.5	6.047	0.700	2.231	0.242			0.073	0.014
2.5	5.955	0.673	0.791	0.089			0.055	0.012
3.5	5.691	0.641	0.995	0.104			0.039	0.003
4.5	5.582	0.628	0.881	0.097	0.870	0.092	0.074	0.010
5.5	5.657	0.637	0.608	0.063	0.525	0.060	0.055	0.006
6.5	5.555	0.613	0.616	0.061	0.464	0.050	0.068	0.011
7.5	5.707	0.630	0.743	0.074	0.355	0.039	0.087	0.014
8.5	6.053	0.626	0.968	0.094	0.311	0.033	0.066	0.014
9.5	5.777	0.632	0.991	0.096	0.420	0.046	0.061	0.012
11	5.374	0.599	0.945	0.089	0.605	0.051	0.052	0.012
13	5.238	0.585	0.952	0.077	0.984	0.058	0.043	0.007
15	N.S.	N.S.	1.015	0.088	1.000	0.056		
17	5.205	0.592	1.118	0.099	1.416	0.054		
19	5.192	0.583			N.S.	N.S.		
21	5.089	0.575			0.820	0.048		
23	5.195	0.591			0.752	0.045		
25	5.403	0.582			0.730	0.046		
27	5.456	0.605			0.847	0.042		
29	5.526	0.624			0.788	0.046		
31	5.600	0.627			0.702	0.047		
33	5.689	0.626			1.344	0.052		
35	5.688	0.619			1.015	0.044		
37	5.520	0.607						
39	5.411	0.607						
41	5.605	0.608						
43	5.841	0.624						
45	5.859	0.650						

N.S. = No Sample

Carbon and Nitrogen Ratios, Organic Carbon and Nitrogen

Core Depth	Arkona		Wiek		Nord Perd		Tonne	
(cm)	% 'Org' C	% 'Org' N	% Org C	% 'Org' N	% Org C	% 'Org' N	% Org C	% 'Org' N
0.5							0.577	0.073
1.5	5.985	0.702	1.759	0.219			0.405	0.053
2.5	5.942	0.597	1.225	0.161			0.390	0.055
3.5	5.336	0.543	1.147	0.141			0.317	0.044
4.5	5.315	0.509	1.076	0.130	1.060	0.129	0.314	0.042
5.5	5.366	0.526	0.799	0.095	0.838	0.106	0.313	0.043
6.5	5.128	0.467	0.871	0.100	0.745	0.089	0.434	0.061
7.5	5.524	0.505	0.982	0.113	0.680	0.082	0.372	0.053
8.5	5.179	0.420	1.087	0.121	0.589	0.072	0.405	0.056
9.5	4.624	0.423	1.136	0.128	0.724	0.089	0.401	0.054
11	5.650	0.495	1.097	0.127	0.677	0.081	0.387	0.054
13	4.105	0.351	0.968	0.103	0.831	0.105	0.392	0.055
15	4.333	0.360	1.090	0.122	0.695	0.083		
17	5.304	0.473	1.195	0.130	0.534	0.063		
19	3.940	0.347			N.S.	N.S.		
21	4.780	0.451			0.856	0.095		
23	4.472	0.398			0.723	0.087		
25	4.339	0.339			0.719	0.091		
27	5.248	0.511			0.705	0.072		
29	4.095	0.401			0.669	0.078		
31	5.334	0.497			0.669	0.076		
33	4.507	0.440			0.779	0.075		
35	6.161	0.592			0.761	0.092		
37	3.943	0.392						
39	4.719	0.475						
41	4.812	0.480						
43	5.682	0.553						
45	5.786	0.582						

N.S. = No Sample

Wet Weight % and Porosity,

Core Depth	Arkona		Wiek		Nord Perd		Torne	
(cm)	Wet Weight (%)	Porosity (F)	Wet Weight (%)	Porosity (F)	Wet Weight (%)	Porosity (F)	Wet Weight (%)	Porosity (F)
0.5	84.884	0.946					24.835	0.778
1.5	81.609	0.935	68.585	0.893			17.183	0.761
2.5	73.665	0.909	39.281	0.813	37.943	0.809	16.650	0.760
3.5	80.380	0.931	32.325	0.795	72.265	0.905	16.686	0.760
4.5	78.438	0.924	30.006	0.790	60.318	0.869	16.731	0.760
5.5	75.497	0.915	25.604	0.780	35.942	0.804	17.050	0.761
6.5	76.699	0.919	25.879	0.780	28.463	0.786	17.720	0.762
7.5	76.534	0.918	28.550	0.787	25.691	0.780	17.866	0.762
8.5	76.708	0.919	32.544	0.795	23.255	0.774	17.594	0.762
9.5	77.024	0.920	32.650	0.795	22.804	0.773	17.676	0.762
11	69.641	0.897	31.128	0.793	25.055	0.779	18.027	0.763
13	72.003	0.904	29.672	0.789	28.605	0.787	18.366	0.763
15	72.500	0.905	32.508	0.795	30.216	0.791		
17	72.301	0.905	32.685	0.795	29.022	0.788		
19	68.577	0.893			27.769	0.785		
21	70.789	0.900			N.S.	N.S.		
23	74.860	0.913			24.719	0.778		
25	72.498	0.905			23.691	0.775		
27	70.245	0.899			24.148	0.776		
29	70.835	0.900			23.665	0.775		
31	73.283	0.908			24.090	0.776		
33	66.233	0.886			24.403	0.777		
35	68.247	0.892			22.186	0.772		
37	72.108	0.904			21.683	0.771		
39	71.528	0.902						
41	72.831	0.907						
43	71.613	0.903						
45	68.917	0.894						
47	68.077	0.892						

N.S. = No Sample

Sediment Core Grain Size Analysis, (um)

Core Depth	Arkona (um)			Wick (um)			Nord Pend (um)			Torre (um)		
(cm)	Sand>63	Silt (2-63)	Clay (<2)	Sand>63	Silt (2-63)	Clay (<2)	Sand>63	Silt (2-63)	Clay (<2)	Sand>63	Silt (2-63)	Clay (<2)
0.5	3.39	76.57	20.04							97.04	2.95	0.01
1.5	6.74	75.59	17.67	64.24	32.61	3.15				98.59	1.41	0.00
2.5	4.40	75.12	20.48	67.40	29.85	2.75				99.05	0.95	0.00
3.5	2.81	76.82	20.37	63.90	32.68	3.42				99.31	0.69	0.00
4.5	6.96	79.25	13.79	62.80	33.59	3.61	82.56	14.02	3.42	99.29	0.71	0.00
5.5	4.05	79.02	16.93	65.80	30.44	3.76	83.76	13.59	2.65	99.36	0.64	0.00
6.5	3.88	79.99	16.13	68.70	28.06	3.24	83.41	14.24	2.35	99.39	0.61	0.00
7.5	1.49	77.11	21.40	77.33	20.13	2.54	82.40	15.26	2.34	99.47	0.53	0.00
8.5	6.58	76.14	17.28	66.40	30.13	3.47	83.24	14.60	2.16	99.53	0.47	0.00
9.5	5.82	76.92	17.26	64.20	32.11	3.69	84.23	13.48	2.29	99.46	0.54	0.00
11	8.24	76.30	15.46	63.80	33.47	4.01	83.55	13.83	2.62	99.68	0.32	0.00
13	2.58	78.46	18.96	59.70	36.25	4.05	84.96	12.56	2.48	99.84	0.16	0.00
15	5.09	80.04	14.87	61.10	35.16	3.74	82.26	15.44	2.30			
17	6.33	76.69	16.98	56.81	39.38	3.81	83.95	14.81	1.24			
19	3.91	82.50	13.59				NS	NS	NS			
21	4.45	76.76	18.83				82.34	15.73	1.93			
23	3.32	86.20	10.48				82.04	15.85	2.11			
25	0.61	78.67	20.72				81.89	15.72	2.39			
27	1.77	76.87	21.36				83.16	15.17	1.67			
29	1.10	77.03	21.87				82.95	14.82	2.23			
31	2.68	76.21	21.11				81.64	15.68	2.68			
33	4.17	77.23	18.60				83.21	15.21	1.58			
35	0.89	77.94	21.17				82.43	15.34	2.23			
37	1.96	76.12	21.92									
39	4.28	80.72	15.00									
41	5.06	83.88	11.06									
43	0.85	76.58	22.57									
45	1.33	75.35	23.32									
47	2.61	78.60	18.79									
49	1.99	76.89	21.12									

N.S. = No Sample

12.0Bibliography

ACKERMANN, F., 1980, A procedure for correcting the grain size effect in heavy metal analyses of estuarine and coastal sediments, *Environmental Technology Letters*, **1**, pp518-527

ADAMS, F. and DAMS, R., 1970, *Applied Gamma Ray Spectrometry.* Oxford, Pergamon Press, 751p

ALONGI, D. M., BOYLE, S. G., TIRENDI, F. and PAYN, C., 1996, Composition and behaviour of trace metals in Post-oxic sediments of the Gulf of Papua, Papua New Guinea, *Estuarine, Coastal and Shelf Science,* **42**, pp 197-211.

ALVARADO, J. S., ORLANDINI, K. A. and ERICKSON, M. D., 1995, Rapid Determination of Radium isotopes by alpha spectrometry. *Journal of Radioanalytical and Nuclear Chemistry-Articles,* **194**, pp 163-172, (1995).

AMES, L. L., MCGARRAH, J. E., WALKER, B. A. and SALTER, P.F., 1983, Uranium and Radium sorption on amorphous ferric oxyhydroxide. *Chemical Geology,* **40,** pp 135-148 (1983).

ANDERSSON, P. S., WASSERBURG, G. J., CHEN, J. H., PAPANASTASSIOU, D. A. and INGRI, J., 1995, ^{238}U-^{234Th} and ^{232}Th-^{230Th} in the Baltic Sea and river water, *Earth and Planetary Science Letters*, **130**, pp 217-234

ANDERSON, R. F., FLEISHER, M. Q. and LEHURAY, A. P., 1989, Concentration, oxidation state, and particulate flux of uranium in the Black Sea, *Geochimica et Cosmochimica Acta,* **53**, 9, pp 2215-2224.

APPLEBY, P. G. and OLDFIELD, F., 1978, The calculation of lead-210 dates assuming a constant rate of supply of unsupported ^{210}Pb to the sediment, *Catena*, **5**, pp 1-8.

BALZER, W., 1982, On the distribution of iron and manganese at the sediment/water interface: thermodynamic versus kinetic control, *Geochimica et Cosmochimica Acta,* **46**, pp 1153-1161.

BALZER, W., 1984, Organic matter degradation and biogenic cycling in a nearshore sediment (Kiel Bight), *Limnology and Oceanography*, **29**, 6, pp 1231-1246.

BAERENS, C. and HUPFER, P., 1995, On the frequency of storm surges at the German Baltic Coast, *Proceedings of the 19th Conference of Baltic Oceanographers*, Sopot, **1**, pp 311-316.

BASKARAN, M, MURPHY, D. J., SANTSCHI, P. H., ORR, J. C. and SCHINK, D. R., 1993, A method for rapid in situ extraction and laboratory determination of Th, Pb and Ra isotopes from large volumes of seawater. *Deep Sea Research I,* **40**, pp 849-865.

BASKARAN, M., SANTSCHI, P. H., BENOIT, G. and HONEYMAN, B. D., 1992, Scavenging of thorium isotopes by colloids in seawater of the Gulf of Mexico, *Geochimica et Cosmochimica Acta,* **56**, pp 3375-3388.

BAYES, J. C., GOMEZ, E., GARCIAS, F., CASAS, F. and CERDA, V., 1996, Radium Determination in Mineral Waters, *Applied Radiation and Isotopes,* **47**, pp 849-853.

BEKS, J. P., EISMA, D., VAN DER PLICHT, J., 1998, A record of atmospheric ^{210}Pb deposition in the Netherlands, *The Science of the Total Environment,* **222**, pp 35-44.

BELMANS, F., VAN GRIEKEN, R. and BRÜGMANN, L., 1993, Geochemical characterisation of recent sediments in the Baltic Sea by bulk and electron microprobe analysis, *Marine Chemistry,* **42**, pp223-236

BELZUNCE SEGARRA, M. J., GÖRLICH, K. and HELIOS-RYBICKA, E., 1987, Heavy metals in surface sediments of the Baltic Sea: sequential extraction. *Proceedings of the 15th conference of the Baltic Oceanographers Copenhagen,* **1**, pp 85-103.

BELZUNCE SEGARRA, M. J., GÖRLICH, K. and HELIOS-RYBICKA, E., 1989, Spatial and stratigraphic controls over chemical speciation of heavy metals in the Baltic Sea muds, *Proceedings of the 16th Conference of the Baltic Oceanographers,* Institute fur Meerskunde, Kiel, **1**, pp 163-175.

BENES, P., 1990, Speciation Procedures, *IAEA Technical Report Series,* **No. 310,** Vol. 3, pp273-299

BENEŠ, P., OBDRZALEK, M. and CEJCHANOVA, M., 1982, The physiochemical forms of traces of radium in aqueous solutions containing chlorides, sulphates and carbonates, *Radiochemical and Radioanalytical Letters,* **50**, 4, pp227-242.

BENOIT, G. and HEMOND, H. F., 1988, Improved methods for the measurement of ^{210}Po, ^{210}Pb, and ^{226}Ra, *Limnology and. Oceanography,* **33**, pp1618-1622.

BENOIT, G. and HEMOND, H. F., 1990, ^{210}Po and ^{210}Pb Remobilization from Lake sediments in relation to Iron and Manganese Cycling, *Environmental Science and Technology Letters,* **24**, pp 1224-1234.

BENOIT, G. and HEMOND, H. F., 1991 Evidence for diffusive redistribution of ^{210}Pb in lake sediments, *Geochimica et Cosmochimica Acta,* **55**, pp 1963-1975.

BERNER, R. A., 1970, Sedimentary pyrite formation, *American Journal of Science*, **268**, pp 1-23.

BERNER, R. A., 1971, *Principles of Chemical Sedimentology*, McGraw Hill, New York, 240pp.

BERNER, R. A., 1980, *Early Diagenesis – A Theoretical Approach.* Princeton Univ. Press, Princeton, 241pp.

BERTINE, K. K., 1972, The deposition of molybdenum in anoxic waters, *Marine Chemistry*, **1**, pp 43-53.

BESZCYZNSKA. –MOLLER, A., 1998, Transport of the Odra river waters and circulation patterns in the Pomeranian Bight, In:, *The changing coastal oceans: From assessment to prediction, Baltic Sea Science Conference Abstracts*, pp 40.

BLACKBURN, R. and AL-MASRI, M. S., 1994, Determination of Uranium by Liquid Scintillation and Cerenkov Counting, *Analyst*, **119**, pp 465-468.

BLAND, C. J., 1990, Methods for measuring radium isotopes: Alpha Particle Spectrometry, *IAEA Technical Report Series*, **No. 310, Vol. 1**, pp173-187.

BLAZHCHISHIN, A. I., 1982c, Main chemical constituents of the sediments of the Baltic Sea, In: *Geology of the Baltic Sea*, (Eds. Emelyanov, E. M. and Gudelis, V. K.), Wydawnictwo Geologiczne, Warsaw, pp 257-290.

BOBERTZ, B., 1996, Untersuchungen der regionalen Verteilung granulometrischer Eigenschaften der Oberflachenseimente der Pommernbucht mit geostatisttischen Verfahren und ihre genetische Interpretation, University Greifswald, 53pp.

BORDOVSKIY, O. K., 1965, Sources of organic matter in marine basins, *Marine Geology*, **3**, p 5-31.

BORG, H. and JONSSONS, P., 1996, Large scale metal distributions in Baltic Sea sediments, *Marine Pollution Bulletin*, **32**, 1 pp 8-21.

BOSTROM, K., BURMAN, J. –O., and INGRI, J., 1983, A geochemical mass balance for the Baltic, *Environmental Biogeochemistry Ecology Bulletin*, **35**, pp 39-58.

BRAND, T. and SHIMMIELD, G. B., 1995, Project Oder-Interim report, *EC Environment programme PL-910398*, Bruxelles, pp 1-68.

BRASSARD, P., KRAMER, J. R., MCANDREW, J and MUELLER, E., 1994, Metal – sediment interaction during resuspension, *Hydrobiologia*, **284**, pp 101-112.

BROWN, J. S., 1962, Ore leads and isotopes, *Economic Geology*, **57**, pp 673-720.

BROECKER, W. S., GODDARD, J and SARMIENTO, J. L., 1976, The distribution of ^{226}Ra in the Atlantic Ocean, *Earth and Planetary Science Letters,* **32**, pp 220-235.

BROECKER, W. S., LI, Y. H., CROMWELL, J., 1967, Radium-226 and Radon-222: Concentration in Atlantic and Pacific Oceans, *Science,* **158**, pp 1307-1310.

BROECKER, W. S. and PENG, T. H., 1982, Tracers in the sea, Lamont-Doherty Geological Observatory, Columbia University, New York, 13pp.

BRÜGMANN, L., 1992, Review of methods for the determination of contaminants in sediments, In '*ICES Cooperative research report: Review of Contaminants in Baltic Sediments*, **180**, pp43-68.

BRUGMANN, L., HALLBERG, R., LARSSON, C. and LOFFLER, A., 1997, Changing redox conditions in the Baltic Sea deep basins: Impacts on the concentration and speciation of trace metals, *Ambio*, **26**, 2, pp 107 – 112.

BRÜGMANN, L and LANGE, D., 1990, Metal distribution in Sediments of the Baltic Sea, *Limnologica (Berlin)*, **20**, 1, pp15-28.

BRÜGMANN, L., LANGE, D. and LEIPE, T., 1992, Western Baltic Sea, *ICES Co-operative research report: Review of Contaminants in Baltic Sediments*, **180**,pp16-24

BRULAND, K.W., 1983, In: Chemical Oceanography, **8**, Eds. Riley J.P. and Chester R., Academic Press, Orlando, pp 172-173

BRUMSACK, H. J., and GIESKES, J. M., 1983, Interstitial water trace metal chemistry of laminated sediments from the Gulf of California, Mexico, *Marine Chemistry,* **14**, pp 89-106.

BURNETT, W. C. and TAI, W., 1992, Determination of Radium in natural waters by alpha liquid scintillation. *Analytical Chemistry,* **64**, pp1691-1697.

BUTTS, J., TODD, J. F., LERCHE, I., MOORE, W. S. and MOORE, D., 1988, A simplified Method for 226Ra Determinations in Natural Waters. *Marine Chemistry,* **25**, pp 349-357.

CADIEUX, J. R., 1990, Evaluation of a photoelectron-rejecting alpha liquid-scintillation spectrometer for the measurement of alpha emitting radionuclides. *Nuclear Instruments and Methods in Physics Research,* **A299**, pp 119-122.

CADIEUX, J. R., CLARK, S., FJELD, R. A., REBOUL, S. and SOWDER, A., 1994, Measurement of actinides in environmental samples by photon-electron rejecting alpha liquid scintillation. *Nuclear Instruments and Methods in Physics Research,* **A353**, pp 534-538.

CANET, A. and JACQUEMIN, R., 1990, The Environmental Behaviour of Radium, *IAEA Tech. Rep. Series,* **No. 320, Vol. 1.**, pp189-204.

CARLSON, L. and ERLANDSSON, 1991, Seasonal variation of Radionuclides in *Fucus vesiculosus* L. from the Oresund, Southern Sweden, *Environmental Pollution*, **73**, pp 53-70.

CARLSON, L. and HOLM, E., 1992, Radioactivity in *Fucus vesiculosus* L. from the Baltic Sea following the Chernobyl accident, *Journal of Environmental Radioactivity*, **15**, pp 231-248.

CARMAN, R. and RAHM, L., 1997, Early diagenesis and chemical characteristics of interstitial water and sediments in the deep deposition bottoms of the Baltic proper, *Journal of Sea Research*, **37**, 1-2, pp 25-47.

CARPENTER, R., BENNET, J. T. and PETERSON, M. L., 1981, ^{210}Pb activities in and fluxes to sediments of the Washington continental slope and shelf, *Geochimica et Cosmochimica Acta*, **45**, pp 1155-1172.

CASE, G. N. and MCDOWELL, W. J., 1990, Separation of radium and its determination by photoelectron-rejection alpha liquid scintillation spectrometry. *Journal of Radioactivity and Radiochemistry*, **1**, pp 4-28.

CHANTON, J. P., MARTENS, C. S. and KIPPHUT, G. W., 1983, Lead-210 sediment geochronology in a changing coastal environment, *Geochimica et Cosmochimica Acta*, **47**, pp 1791-1804.

CHAU, N. D., NIEWODNICZANSKI, J., DORDA, J., OCHONSKI, A., CHRUSIEL, E. and TOMZA, I., 1997, Determination of radium isotopes in mine waters through alpha- and beta- activities measured by liquid scintillation spectrometry, *Journal of Radioanalytical and Nuclear Chemistry*, **222**, pp 69-74.

CHESTER, R. and ASTON, S. R., 1976, The geochemistry of deep-sea sediments, in *Chemical Oceanography, vol. 6*, eds. J. P. Riley and R. Chester, Academic Press, London, p 281-390.

CHESTER, R., 1990, Marine Geochemistry, Unwin Hyman, London.

CHOPPIN, G., LILJENZIN, J. O. and RYDBERG, J., 1995, *Radiochemistry and Nuclear Chemistry*, 2nd Edition, Ed Butterworth-Heinemann, Oxford, pp 198-237.

CHRISTIANSEN, C. and EMELYANOV, E., 1995, Nutrients and organic matter in southern Kattegat- Western Baltic Sea sediments: Effects of resuspension, *Danish Journal of Geography*, **95**, pp 19-27.

CHUNG, Y. 1987, ^{226}Ra in the western Indian Ocean, *Earth and Planetary Science Letters*, **85**, pp 11-27.

CLIFFORD, D. A. and HIGGINS, E.A, 1992, Measurement of 226Ra and 228Ra in water by gamma ray counting after preconcentration on ion exchange resin. *Health Physics*, **62**, pp 413-421.

CLULOW, F. V., DAVE, N. K., LIM, T. P. and AVADHANULA, R., 1998, Radium-226 in water, sediments, and fish from lakes near the city of Elliot Lake, Ontario, Canada, *Environmental Pollution*, **99**, 1, pp 13-28.

COFFEY, M., DEHAIRS, F., COLLETTE, O., LUTHER, G., CHURCH, T. and JICKELLS, T., 1997, The behaviour of dissolved barium in estuaries, *Estuarine, Coastal and Shelf Science*, **45**, pp 113-121.

CONTRERAS, R., FOGG, T. R., CHASTEEN, N. D., GAUDETTE, H. E. and LYONS, W. M. B., 1978, Molybdenum in pore waters of anoxic marine sediments by electron paramagnetic resonance spectroscopy, *Marine Chemistry*, **6**, pp 365-373.

CORL, W. E., 1991, Comparison of microwave versus hot-plate dissolution techniques determining lead in paint chips. *Spectroscopy*, **5**, 4.

CRUSIUS, J., CALVERT, S., PEDERSEN, T. and SAGE, D., 1996, Rhenium and molybdenum enrichments in sediments as indicators of oxic, suboxic and sulfidic conditions of deposition, *Earth and Planetary Science Letters*, **145**, pp 65-78.

CURRIE, L. A., 1968, Limits for qualitative detection and quantitative determination, *Analytical Chemistry*, **40**, 586pp.

CURIE, M., CURIE, P., BEMONT, G., 1898, Another new radioactive element. *Comptes Rendus*, **127**, p.1215-1217.

CURIE, M., 1903, Radioactive Substances, Greenwood Press, Westport, Connecticut (1961, translation of her 1903 doctoral thesis from the French).

CURTIS, C. D. and SPEARS, D. A., 1968, Mineral stability fields in marine depositional waters, *Economic Geology*, **63**, pp 257-70.

DATE, A. and GREY, A., 1987, Applications of Inductively Coupled Plasma Mass Spectrometry. Blackie, 248pp

DAVIS, J. C., HARFF, J., LEMKE, W., OLEA, R. A., TAUBER, F. and BOHLING, G., 1996, Analysis of Baltic Sedimentary Facies by Regionalized Classification. *Geowissenschaften*, **14**, pp 67-72

DAVISON, W., 1985, Conceptual models for transport at the redox boundary, In *Chemical processes in lakes*, Ed W. Stumm, John Wiley and Sons, pp 31-53.

DEARLOVE, J. L. P., LONGWORTH, G., IVANOVICH, M., KIM, J. L., DELAKOWITZ, B. and ZEH, P., 1991, Study of groundwater colloids and their

geochemical interactions with natural radionuclides in Gorleben aquifer systems, *Radiochimica Acta*, **52/53**, pp 83-89.

DE GROOT, A. J., ZSCHUPPE, K. H. and SALOMONS, W., 1982, Standardisation of methods for heavy metal analysis in sediments, *Hydrobiologia*, **92**, pp 689-695.

DEEVEY, E. S. Jr, 1973, Sulfur, nitrogen and carbon in the biosphere. In *Carbon and the Biosphere*, (Eds. Woodwell, G. M. and Peacan, E. V.), USAEC, Washington, D.C., pp 182-190.

DELWICHE, C. C. and LIKENS, G. E., 1977, Biological response to fossil fuel combustion products, In: *Global Chemical Cycles and Their Alterations by Man*, (ed. Stumm. W.), Dahlem Konferenzen, Berlin, pp 73-88.

DIN, Z. B., 1992, Use of Aluminium to normalize heavy metal data from estuarine and coastal sediments of Straits of Melaka, *Marine Pollution Bulletin*, **24**, 10, pp484-491.

DOE, B. R., 1970, Lead Isotopes, In: Minerals, Rocks and Inorganic Materials: Monograph Series of Theoretical and Experimental Studies 3, Eds W. Von Engelhardt, T. T. Hahn, R. Roy and J. W. Winchester, Springer-Verlag Berlin.

DURHAM, R. W. and JOSHI, S. R., 1980, Recent sedimentation rates, ^{210}Pb fluxes, and particle settling velocities in Lake Huron, Laurentian Great Lakes, *Chemical Geology*, **31**, pp 53-66.

DYRSSEN, D., 1985, Metal complex formation in sulphidic seawater, *Marine Chemistry*, **15**, pp 285-293.

DZIUNIKOWSKI, B. 1989, Energy dispersive X-ray fluorescence analysis. In Comprehensive Analytical Chemistry, Ed. SVEHLA, G., Elsevier.

EDENBORN, H. M., BELZILE, N., MUCCI, A., LEBEL, J. and SILVERBERG, N., 1986, Observations on the diagenetic behaviour of arsenic in a deep coastal sediment, *Biogeochemistry*, **2**, pp 359-376.

EDGINGTON, D. N., KLUMP, J. V., ROBBINS, J. A., KUSNER, Y. S., PAMPURA, V. D. and SANDIMIROV, I. V., 1991, Sedimentation rates, residence times and radionuclide inventories in Lake Baikal from ^{137}Cs and ^{210}Pb in sediment cores, *Nature*, **350**, pp 601-604.

ELLIOT, J. C., 1984, Effect of vial composition and diameter on determination of efficiency, background, and quench curves in liquid scintillation counting, *Analytical Chemistry*, **56**, pp758-761.

EMERSON, S. R., 1995 Organic carbon preservation in marine sediments. In: *The Carbon Cycle and Atmospheric CO_2: Natural variations Archean to Present*, (Eds.

Sundquist, E. T. and Broecker, W. S.), American Geophysical Union, Washington D.C., pp 78-87.

EMERSON, S. R. and HUESTED, S. S., 1991, Ocean anoxia and the concentrations of molybdenum and vanadium in seawater, *Marine Chemistry*, **34**, pp 177-196.

EVANS, E. H. and GIGLIO, J. J., 1993, Interferences in Inductively Coupled Plasma Mass Spectrometry: A Review, *Journal of Analytical Atomic Spectrometry*, **8**, pp 1-18.

FARMER, J. G., EADES, L. J., MACKENZIE, A. B., KIRIKA, A. and BAILEY-WATTS, T. E., 1996, Stable lead isotope record of lead pollution in Loch Lomond Sediments since 1630 A.D., *Environmental Science and Technology Letters*, **30**, pp 3080-3083.

FAURE, G., 1986, Principles of Isotope Geology, Second edition, John Wiley & Sons, New York, pp 285-286.

FERRAND, J. L., HAMELIN, B. and MONACO, A., 1999, Isotopic tracing of anthropogenic Pb inventories and sedimentary fluxes in the Gulf of Lions (NW Mediterranean sea), *Continental Shelf Research*, **19**, pp 23-47.

FISENNE, I. and KELLER, H. W., 1985, The EML Pulse Ionisation Chamber Systems for Rn-222 Measurements, *Report EML-437*, Environmental Measurements Laboratory, United States Department of Energy, New York.

FLODERUS, S. and PIHL, S., 1990, Resuspension in the Kattegat: Impact of variation in wind climate and fishery, *Estuarine, Coastal and Shelf Science*, **31**, pp 487-498.

FRANCOIS, R., 1988, A study on the regulation of the concentrations of some trace metals (Rb, Sr, Zn, Pb, Cu, V, Cr, Ni, Mn and Mo) in Saanich inlet sediments, British Columbia, Canada, *Marine Geology*, **83**, pp 285-308.

FRIEDLANDER, G., KENNEDY, J. W., MACIAS, E. S. and MILLER, J. M., 1981, *Nuclear and Radiochemistry*, 3rd Edition, Ed John Wiley, New York, 684p.

FROELICH, P. N., KLINKHAMMER, G. P., BENDER, M. L., LUEDTKE, N. A., HEATH, G. R., HAMMOND, D., HARTMANN, B. and MAYNARD, V., 1979, Early oxidation of organic matter in pelagic sediments of the eastern equatorial Atlantic: suboxic diagensis, *Geochimica et Cosmochimica Acta*, **43**, pp 1075-1090.

GAGNON, C., MUCCI, A. and PELLETIER, E., 1995, Anomalous accumulation of acid-volatile sulphides (AVS) in a coastal marine sediment, Saguenay Fjord, Canada, *Geochimica et Cosmochimica Acta*, **59**, 13, pp 2663-2675.

GARBE-SCHÖNBERG, C-D., 1993, Simultaneous determination of thirty seven trace elements in twenty eight international rock standards by ICP-MS, *Geostandards Newsletter*, **17**, 1, pp 81-97

GASCOYNE, M., 1982, Geochemistry of the actinides and their daughters, In: *Uranium Series Disequilibrium: Application to Environmental Problems*, Eds. M. Ivanovich and R. S. Harmon, Oxford Science publications, p 54.

GERSHEY, R. M. and BOYLE, D. E., 1987, Radionuclide extraction columns-1. Documentation of their performance in the extraction of radium from fresh and seawater. In *The Chemistry of Infiltrex Columns*, AXYS Environmental Systems report, Seastar Instruments Ltd, Sydney, 29pp.

GERSHEY, R. M. and GREEN, D. R., 1988, Sorbents for the extraction of radionuclides from natural waters, In *Radionuclides: A tool for oceanography*, Eds. GUARY, J. C, GUEGUENIAT, P. and PENTREATH, R. J., Elsevier, pp 92-100.

GILMAN, L. B. and ENGELHART, W. G., 1989, Atomic Spectroscopy Advances – Recent advances in Microwave sample preparation, *Spectroscopy*, **4**, 8.

GILSON, G. R., DOUGLAS, D. J., FULFORD, J. E. HALLIGAN, K. W. and TANNER, S. D., 1988, Nonspectroscopic interelement interferences in inductively coupled plasma mass spectrometry, *Analytical chemistry*, **60**, pp 1472-1474.

GINGELE, F. X. and LEIPE, T., Clay mineral assemblages in the western Baltic Sea: recent distribution and relation to sedimentary units. *Marine Geology*, **140**, pp 97-115.

GLASBY, G. P., EMELYANOV, E. M., ZHAMOIDA, V. A., BATURIN, G. N., LEIPE, T., BAHLO, R. and BONACKER, P., 1997, In: Manganese Mineralization: Geochemistry and Mineralogy of Terrestrial and Marine Deposits, Eds. Nicholson, K., Hein, J. R., Buhn, B. and Dasgupta, S., Geological Society Special Publication, **119**, pp 213-237.

GOBEIL, C., JOHNSON, W. K., MACDONALD, R. W. and WONG, C. S., 1995, Sources and Burden of Lead in St. Lawrence Estuary Sediments: Isotopic Evidence, *Environmental Science and Technology Letters*, **29**, pp 193-201.

GODOY, J. M., 1990, Methods for measuring radium isotopes: Coincidence Methods, In *The Environmental Behaviour of Radium, IAEA Technical Report Series*, **No. 310**, Vol. 1, pp 223-227.

GODOY, J. M., 1990, Methods for measuring radium isotopes: Gross Alpha and Beta Counting, In *The Environmental Behaviour of Radium, IAEA Technical Report Series*, **No. 310**, Vol. 1, pp 205-211.

GODOY, J. M., LAURIA, D. C., LUIZA, M., GODOY, D. P. and CUNHA, R. P., 1994, Development of a sequential method for the determination of ^{238}U, ^{234}U, ^{232}Th,

^{230}Th, ^{228}Th, ^{228}Ra, ^{226}Ra and ^{210}Pb in Environmental Samples. *Journal of Radioanalytical and Nuclear Chemistry,* **182**, No. 1, pp 165-169.

GOLDBERG, E. D., 1954, Marine Geochemistry: Chemical scavengers of the sea, *Journal of Geology,* **62**, pp249-255.

GOLDIN, A. S., 1961, Determination of dissolved radium, *Analytical Chemistry,* **33**, pp406-409.

GORLICH, K., GORLICH, E. and STOCH, L., 1978, Iron in the Baltic Sea clay sediments, *Mineralogia Polonica,* **9**, 1, pp 63-78.

GUBALA, C. P., ENGSTROM, D. R. and WHITE, J. R., Effects of Iron cycling on ^{210}Pb dating of sediments in an Adirondack Lake, USA, *Canadian Journal of Fisheries and Aquatic Science,* **47**, pp 1821-1829.

HALLBERG, R. O., 1979, Heavy metals in the sediments of the Gulf of Bothnia, *Ambio,* **20**, pp 309-316.

HASSLEROT, T. B., 1972, Mercury in fish, water and bottom sediments. Investigations made by the research laboratory 1966-1970, *Swedish Environment Protection Board,* **239**, pp 781.

HELCOM, 1988, Guidelines for the Baltic Monitoring Programme for the third stage, *Baltic Sea Environment Proceedings,* **27B**, part A, Introductory Chapters, pp 1-49; part B, Physical and chemical determinants in sea water, pp 1-60.

HELCOM, 1993, The Baltic Sea joint comprehensive environmental action programme, *Baltic Sea Environment Proceedings,* **49**, pp 1-58.

HELCOM, 1996, Third periodic assessment of the state of the marine environment of the Baltic Sea, 1989 – 1993, Background document, *Baltic Sea Environment Proceedings,* **64B**, pp 1-252.

HELCOM, 1998, The third pollution load compilation, *Baltic Sea Environment Proceedings,* **70**.

HELIOS RYBICKA, E., 1992, Heavy metal partitioning in polluted river and sea sediments: clay minerals effects, *Mineralogica et Petrographica Acta,* **XXXV-A**, pp 297-305.

HELIOS RYBICKA, E., 1993, Phase specific bonding of heavy metals in sediments of the Vistula River, Poland, *Applied Geochemistry,* **2**, pp 45-48.

HELIOS RYBICKA, E., 1996, Impact of mining and metallurgical industries on the environment in Poland, *Applied Geochemistry,* **11**, pp 3-9.

HELZ, G. R., MILLER, C. V., CHARNOCK, J. M., MOSSELMANS, J. F. W., PATTRICK, R. A. D., GARNER, C. D. and VAUGHAN, D. J., 1996, Mechanism of molybdenum removal from the sea and its concentration in black shales: EXAFS evidence, *Geochimica et Cosmochimica Acta,* **60**, 19, pp 3631- 3642.

HERITAGE LABORATORIES INCORPORATED, 1994, Application Note #1: Radium (^{226}Ra) by PERALS®, Romeoville, Illinois.

HELLMAN, H., 1983, Grain size distributions and organic trace substances in fluvial sediments and soils, *Analytical Chemistry*, **316**, pp 286-289.

HEWITT, A. and REYNOLDS, C., 1990, Dissolution of metals from soils and sediments with a microwave-nitric acid digestion technique, *Atomic Spectroscopy*, **11**, pp187-192.

HOLLAND, G. and EATON, A. N., 1993, Applications of plasma source mass spectrometry II, *The Royal Society of Chemistry Special Publication No. 124*, Bookcraft.

HONEYMAN, B. D. and SANTSCHI, P. H., 1989, A Brownian-pumping model for oceanic trace metal scavenging: evidence from thorium isotopes, *Journal of Marine Research,* **47**, pp 951-992.

HOPPER, J. F., ROSS, H. B., STURGES, W. T. and BARRIE, L. A., 1991, Regional source discrimination of atmospheric aerosols in Europe using the isotopic composition of lead, *Tellus*, **43B**, pp 45-60.

HORROCKS, D. L., 1964, Alpha particle energy resolution in liquid scintillators, *Review of Scientific Instruments*, **35**, No. 3, pp 334-340

HORROCKS, D. L., 1970, Pulse shape discrimination with organic scintillators, *Applied Spectroscopy*, **24**, 4, pp397-405

HORROCKS, D. L., 1974, *Applications of Liquid Scintillation Counting*, New York, Academic Press, 340p

HUERTA-DIAZ, M. A. and MORSE, J. A., 1992, Pyritization of trace metals in anoxic marine sediments, *Geochimica et Cosmochimica Acta,* **56**, 7, pp 2681-2702.

HUNG, J., 1995, Terrigenous inputs and accumulation of trace metals in the south-eastern Taiwan strait, *Chemistry and Ecology*, **10**, pp 33-46

HUNTLEY, D. J., NISSEN, M. K., THOMSON, J. and CALVERT, S. E., 1986, An improved alpha scintillation counting method for determination of Th, Ra-226, Th-230 excess and Pa-231 excess in marine sediments. *Canadian Journal of Earth Science*, **23**, pp 959-966.

IGNATIUS, H., AXBERG, S., NIEMISTO, L. and WINTERHALTER, B., 1981, Quaternary geology of the Baltic Sea, In *The Baltic Sea*, Ed A. Voipio, Elsevier, Amsterdam, pp 54-104.

IVANOVICH, M. and HARMON, R. S., 1982, Uranium Series Disequilibrium: Applications to Environmental Problems, Clarendon Press, Oxford.

JAHNKE, R. A., EMERSON, S. R. and MURRAY, J. W., 1982B, A model of oxygen reduction, denitrification and organic matter mineralization in marine sediments, *Limnology and Oceanography*, **27**, pp 610-623.

JANKOWSKI, A., 1996, Vertical water circulation in the southern Baltic and its environmental implications, *Oceanologia*, **38**, 4, pp 485-503.

JARVIS. K. E., GRAY A. L, HOUK, R. S., et al, 1992, Handbook of inductively coupled plasma mass spectrometry, Blackie, Glasgow and London

JAWOROWSKI, Z., 1990, Sources and the Global Cycle of Radium, Chapter 2-2, *Technical Report Series, IAEA*, **310 Vol. 1**, p 129-142

JIANG, H. and HOLTZMAN, R. B., 1989, Simultaneous determination of 224Ra, 226Ra and 228Ra in large volumes of well waters, *Health Physics*, **37**, No.1, pp167-168.

JOHNSTON, A. and MARTIN, P., 1997, Rapid Analysis of ^{226}Ra in waters by γ-Ray Spectrometry, *Applied Radiation and Isotopes*, **48**, No. 5, pp 631-638.

JONSSON, P., CARMAN, R. and WULFF, F., 1990, Laminated sediments in the Baltic – A tool for evaluating nutrient mass balances, *Ambio*, **19**, pp 152-158.

JONSSON, P. and CARMAN, R., 1994, Changes in deposition of organic matter and nutrients in the Baltic Sea during the twentieth century, *Marine Pollution Bulletin*, **28**, 7, pp 417-426.

KADKO, D., 1980, ^{230Th}, ^{226}Ra, and ^{222}Rn in abyssal sediments, *Earth and Planetary Science Letters*, **49**, pp 360-380.

KAUTSKY, H., 1981, Radiological investigations in the Western Baltic Sea including Kattegat during the years 1975-1980, *Deutsch Hydrograpische Zeitschrift*, **34**, 4, pp 125-149.

KELLER, C., 1988, Radiochemistry, Ellis Horwood Ltd, Chichester.

KERSTEN, M., FORSTNER, U., KRAUSE, P., KRIEWS, M., DANNECKER, W., GARBE-SCHONBERG, C. D., HOCK, M., TERZENBACH, U. and GRASSL, H., 1991, Pollution source reconnaissance using stable lead isotope ratios ($^{206/207}$Pb), In: Heavy metals in the environment, Ed J. Vernet,

KERSTEN, M., THOMSEN, S., PRIEBSCH, W. and GARBE-SCHONBERG, C. – D., 1998, Scavenging and particle residence times determined from $^{234}Th/^{238}U$ disequilbria in the coastal waters of Mecklenburg Bight, *Applied Geochemistry*, **13**, pp 339-347.

KEY, R. M., BREWER, R. L., STOCKWELL, N. L., GUINASSO, N. L. and SCHINK, D. R., 1979, Some improved techniques for measuring Radon and Radium in Marine Sediments and in seawater. *Marine Chemistry*, **7**, pp 251-264.

KING, P., KENNEDY, H., NEWTON, P. P., JICKELLS, T. D., BRAND, T., CALVERT, S., CAUWET, G., ETCHEBER, H., HEAD, B., KHRIPOUNOFF, A., MANIGHETTI, B. and MIQUEL, J. C., 1998, Analysis of total and organic carbon and total nitrogen in settling oceanic particles and a marine sediment: an interlaboratory comparison. *Marine Chemistry*, **60**, pp 203-216

KINGSTON, H. M. and JASSIE, L. B., 1988, Introduction to microwave sample preparation: Theory and practice, American Chemical Society, Washington.

KINGSTON, H. M. and WALTER, P. J., 1992, Microwave assisted acid digestion of siliceous and organically based matrices, *Draft Method 3052*, Chemistry department, Duquesne University, Pittsburgh, USA.

KNAUSS, K. G., KU, T. –L., MOORE, W. S., 1978, Radium and thorium isotopes in the surface waters of the east Pacific and coastal southern California, *Earth and Planetary Science Letters*, **39**, pp 235-249.

KOIDE, M., BRULAND, K. W. and GOLDBERG, E. D., 1973, Th-228/Th-232 and Pb-210 geochronologies in marine and lake sediments, *Geochimica et Cosmochimca Acta*, **37**, pp 1171-1187.

KOULOURIS, G., 1996, Sorption and distribution of ^{226}Ra in an electrolytic manganese dioxide column in the presence of other ions, *Journal of Radioanalytical Nuclear Chemistry, Letters*, **212**, pp 131-141.

KOWALEWSKA, G., 1986, Radium-226 in water and sediments of the Southern Baltic Sea, *Oceanologia*, **23**, pp65-76.

KOWALEWSKA, G., 1987, Vistula river flux of ^{226}Ra to the Gulf of Gdansk, In: *15th International Conference of the Baltic Oceanographers*, **1**, Copenhagen, pp 304-315.

KNAPINSKA-SKIBA, D., BOJANOWSKI, R. and RADECKI, Z., 1994, Sorption and release of radiocaesium from particulate matter of the Baltic coastal zone, *Netherlands Journal of Aquatic Ecology*, **28**, pp 413-419.

KNAPINSKA-SKIBA, D., BOJANOWSKI, R., RADECKI, Z and LOTOCKA, M., 1995, The biological and physio-chemical uptake of radiocaesium by particulate

matter of natural origin (Baltic Sea), *Netherlands Journal of Aquatic Ecology*, **29**, 3-4, pp283-290.

KREMLING, K., 1983, The behaviour of Zn, Cd, Cu, Ni, Co, Fe and Mn in anoxic Baltic waters, *Marine Chemistry*, **13**, pp 87-108.

KRISHNASWAMI, S. and LAL, D., 1978, Radionuclide limnochronology, In: *Lakes, Chemistry Geology and Physics*, 153, Lerman, A. (ed.), Springer-Verlag, New York.

KRISHNASWAMI, S., LAL, D., SOMAYAJULU, B. L. K., DIXON, F. S., STONECIPHER, S. A. and CRAIG, H., 1972, Silcon, Radium, Thorium and Lead in Seawater: in-situ extraction by synthetic fibre. *Earth and Planetary Science Letters*, **16**, pp 84-90.

KRUGER, O., 1996, Atmospheric deposition of heavy metals to North European marginal seas: scenarios and trend for lead, *GeoJournal*, **39**, 2, pp 117-131.

KUBE, J., PETERS, C. and POWILLEIT, M., 1996a, Spatial variation in growth of *Macoma balthica* and *Mya arenaria* (Mollusca, Bivalvia) in relation to environmental gradients in the Pomeranian Bay (Southern Baltic Sea), *Archive of Fisheries and Marine Research*, **44**, 1/2, pp 81-93.

KUBE, J., POWILLEIT, M. and WARZOCHA, J., 1996b, The importance of hydrodynamic processes and food availability for the structure of macrofauna assemblages in the Pomeranian Bay (Southern Baltic Sea), *Archive of Hydrobiology*, **138**, pp 213-228.

KUNZENDORF, H., EMEIS, K. –C., CHRISTIANSEN, C., 1997, Sedimentation in the central Baltic Sea as viewed by non-destructive Pb-210 dating, In: Proceedings of 'Challenges to Chemical Geology', Carlsbad

LAKASCHUS, S., 1997, Konzentrationen und Depositionen atmospharischer Spurenmetalle en der Kustenstation Arkona, *Meereswissenschaftliche Berichte*, **26**, Institut fur Ostseeforschung Warnemunde

LALLY, A. E. and GLOVER, K. M., 1984, Source preparation in alpha spectrometry, *Nuclear Instruments and Methods in Physics Research*, **223**, pp259-265.

LANGMUIR, D., 1978, Uranium solution-mineral equilibria at low temperatures with applications to sedimentary ore deposits, *Geochimica et Cosmochimca Acta*, **42**, pp 547-569.

LANGSTON, W. J., BURT, G. R. and POPE, N. D., 1999, Bioavailability of metals in sediments of the Dogger Bank (Central North Sea): A Mesocosm Study, *Estuarine, Coastal and Shelf Science*, **48**, pp 519-540.

LAPP, B. and BALZER, W., 1993, Early diagenesis of trace metals used as an indicator of past productivity changes in coastal sediments, *Geochimica et Cosmochimica Acta*, **57**, pp 4639 – 4652.

LARSEN, B. and KOGLER, F. –C., 1975, A submarine channel between the deepest parts of the Arkona and the Bornholm Basins in the Baltic Sea, *Deutsche Hydrographische Zeitschrift*, **28**, 6, pp 274-276.

LARSSON, U., ELMGREN, R. and WULFF, F., 1985, Eutrophication and the Baltic Sea: Causes and consequences, *Ambio*, **1**, pp 9-14.

LASS, H. U. and MATTHAUS, W., 1994, On the forcing of salt water inflows into the Baltic Sea, *Proceedings of the 19th conference of Baltic Oceanographers*, Sopot, **I**, pp 192-211.

LAUNIANINEN, J. and VIHMA, T., 1990, Meteorological, ice and water exchange conditions, In; Second periodic assessment of the state of the marine environment of the Baltic Sea, 1984-1988; Background document, *Baltic Sea Environment Proceedings*, **35B**, pp 22-33.

LEIPE, T., BRUGMANN, L. and BITTNER, U., 1989, On the distribution of heavy metals in recent brackish water sediments of estuaries of the G.D.R., *Chemie der Erde*, **49**, pp 21-38.

LI, Y. H., 1981, Ultimate removal mechanisms of elements from the ocean, *Geochimica et Cosmochimica Acta*, **45**, pp 1659-1664.

LI, Y. H., KU, T. L., MATHIEU, G. G. and WOLGEMUTH, K., 1973, Barium in the Antarctic Ocean and implications regarding the marine geochemistry of Ba and ^{226}Ra, *Earth and Planetary Science Letters*, **19**, pp352-358.

LOFVENDAHL R., 1987, Dissolved uranium in the Baltic Sea, *Marine Chemistry*, **21**, pp 213-227.

LOHRING, L. J., 1991, Normalisation of heavy-metal data from estuarine and coastal sediments, *ICES Journal of Marine Science*, **48**, pp 101-115.

LOUMA, S. N. and BRYAN, G. W., 1981, A statistical assessment of the form of trace metals in oxidised estuarine sediments employing chemical extractants. *Science of the Total Environment*, **17**, pp165-196.

LOYD, D. H. and DRAKE, E. N., 1989, An Alternative method for Ra determinations in water. *Health Physics*, **57**, pp 71-77.

LU, C. S. and CHEN, K. Y., 1977, Migration of trace metals in interfaces of seawater and polluted surficial sediments, *Environmental Science and Technology*, **11**, pp 174-182.

LUCAS, H.F. and MARKUN, F., 1992, The determination of ^{226}Ra and ^{228}Ra in water and solids by the least squares gamma spectrometric method, *Journal of Environmental Radioactivity*, **15**, pp1-18.

LUCAS, H. F., MARKUN, F. and BOULENGER, R., 1990, The Environmental Behaviour of Radium, *IAEA Technical Report Series*, **310, Vol. 1**, pp149-171.

LUND-HANSEN, L. C., VALEUR, J., PEJRUP, M. and JENSEN, A., 1997, Sediment fluxes, Re-suspension and accumulation rates at two wind exposed coastal sites and in a sheltered bay, *Estuarine, Coastal and Shelf Science*, **44**, pp 521-531.

LUTHER, G. W., III, 1991, Pyrite synthesis via polysulphide compounds, *Geochimica et Cosmochimica Acta*, **55**, pp 2839-2849.

MACKENZIE, A. B., 1991, Radiochemical Methods in Instrumental Analysis of Pollutants, Ed HEWITT, C. N., Elsevier, New York, 367pp.

MACKENZIE, A. B., BAXTER, M. S., MCKINLEY, I. G., SWAN, D. S. and JACK, W., 1979, The Determination of ^{134}Cs, ^{137}Cs, ^{210}Pb, ^{226}Ra and ^{228}Ra Concentrations in Nearshore Marine Sediments and Seawater, *Journal of Radioanalytical Chemistry*, **48**, pp29-47.

MACKENZIE, A.B., LOGAN, E., COOK, G. T. and PULFORD, I. D., 1995, Radionuclide and metal distributions in peat deposits in Scotland, *In Proceedings of the 10th International Conference on Heavy Metals in the Environment*, **1**, pp 113-116.

MACKENZIE, A.B., FARMER, J. G. and SUGDEN, C. L., 1997, Isotopic evidence of the relative mobility of lead and radiocaesium in Scottish ombrotrophic peats, *Science of the Total Environment*, **203**, 2, pp 115-127.

MACKENZIE, A.B., LOGAN, E., COOK, G. T. and PULFORD, I. D., 1998, Distributions, inventories and isotopic composition of lead in ^{210}Pb-dated peat cores from contrasting biogeochemical environments: Implications for lead mobility, *The Science of the Total Environment*, **223**, pp 23-35.

MACKENZIE, F. T., 1981, Global carbon cycle: Some minor sinks for CO_2. In: *Flux of Organic Carbon by Rivers to the Sea*, (eds. Likens, G. E., Mackenzie, F. T., Richey, J., Sedwell, J. R. and Turekian, K. K.), USDOE Conference report 8009140, Washington, D. C., pp 360-384.

MACKLIS, R.M., 1993, The Great Radium Scandal. *Scientific American*, **269**, p 78-83.

MALCOLM, S. J., 1985, Early diagenesis of molybdenum in estuarine sediments, *Marine Chemistry*, **16**, pp 213-225

MANHEIM, F. T., 1961, A geochemical profile of the Baltic Sea, *Geochimica et Cosmochimca Acta*, **25**, pp 52-70.

MATHIEU, G. G., BISCAYE, P. E., LUPTON, R. A., and HAMMOND, D.E., 1988, System for measurement of 222Rn at low levels in natural waters, *Health Physics*, **55** No 6, pp 989-992.

MATTHAUS, W., 1995, Natural variability and human impacts reflected in long term changes in the Baltic deep water conditions – a brief review, *Deutsche Hydrographische Zeitschrift*, **47**, pp 47-65.

MATTHAUS, W. and LASS, H. U., 1995, The recent salt inflow into the Baltic Sea, *Journal of Physical Oceanography*, **25**, pp 280-287.

MATTHAUS, W., NEHRING, D., LASS, H. U., NAUSCH, G., NAGEL, K. and SIEGEL, H., 1996, The Baltic Sea in 1996 – Continuation of stagnation and decreasing phosphate concentrations, *Deutsche Hydrographische Zeitschrift*, **48**, 2, pp 161-174.

MATTHEWSON, A. P., 1995, The palaeoclimatology and palaeoceanography of the northwest African margin, *Unpublished PhD Thesis*, University of Edinburgh, pp 227.

MATTSSON, S. and ERLANDSSON, 1991, Variations of the Cs-137 levels in *Fucus* from the Swedish west coast during a 25 year period, In: *The Chernobyl fallout in Sweden: Results from a research programme on environmental radiology*, Swedish radiation protection, Stockholm, pp 143-149.

MCCURDY, D. E. and MELLOR, R. A., 1981, Determination of radium-224, -226 and –228 by coincidence spectrometry, *Analytical Chemistry*, **53**, pp 2212-2216.

MCDOWELL, W. J., 1971, Liquid Scintillation counting techniques for the higher actinides, In *Organic Scintillators and Liquid Scintillation Counting*, Eds HORROCKS, D. L. and PENG, C.T., Academic Press, New York, pp 937-950.

MCDOWELL, W. J., 1986, Alpha counting and spectrometry using liquid scintillation methods. *National Academy of Sciences-National Research Council: Nuclear Science Series, Radiochemistry Techniques.* Office of Scientific and Technical Information, U.S. Department of Energy, Oak Ridge, Tennessee: 108p.

MCDOWELL, W. J., ARNDSTEN, B. A. and CASE, G. N., 1989, The synergistic solvent extraction of Radium from alkaline nitrate media by dicyclohexano-21-crown-8 combined with 2-methyl-2-heptyl nonanoic acid equilibrium reactions and metal ion competition. *Solvent extraction and ion exchange*, **7** (3), pp 377-393.

MCDOWELL, W. J., FARRAR, D. T., and BILLINGS, M. R., 1979, Plutonium and uranium determinations in environmental samples; Combined solvent extraction-liquid scintillation method, *Talanta*, **21**, pp 1231-1245.

MCDOWELL, W. J. and MCDOWELL, B. L., 1992, The Growth of a Radioanalytical Method: Alpha Liquid Scintillation Spectrometry, In *Liquid Scintillation Spectrometry*, Eds NOAKES, J. E., SCHONHOFER, F. and POLACH, H. A., Radiocarbon 1993, pp 193-200.

MCDOWELL, W. J. and MCDOWELL, B. L., 1994, *Liquid Scintillation Alpha Spectrometry*, CRC Press, Boca Raton, Florida.

MCKEE, B.A, DEMASTER, D. J. and NITTROUER, C. A., 1986, Temporal variability in the partitioning of thorium between dissolved and particulate phases on the Amazon shelf: implications for the scavenging of particle-reactive species, *Continental Shelf Research*, **6**, pp 87-106.

MCINTYRE, R. S. C., GREGOIRE, D. C. and CHAKRABARTI, C. L., 1997, Vaporisation of Radium and Other Alkaline Earth Elements in Electrothermal Vaporisation Inductively Couple Plasma Mass Spectrometry, *Journal of Analytical Atomic Spectrometry*, **12**, pp 547-551.

MCNEIL, G. W. and SHIMMIELD, G. B., 1991, Diagenetic controls on uranium, molybdenum and vanadium enrichment in organic rich marine shelf sediments, In: *Heavy Metals in the Environment*, **1**, Conference proceedings, Edinburgh.

MELVASALO, T. (ed.), 1981, Assessment of the effects of pollution on the natural resources of the Baltic Sea, 1980, *Baltic Sea Environment Proceedings*, **5B**, pp 1-426.

MICHEL, J., MOORE, W. S. and KING, P. J., 1981, γ-ray spectrometry for determination of radium-228 and radium-226 in natural waters, *Analytical. Chemistry*, **53**, pp1885-1889.

MIDDLEBURG, J. J., 1991, Organic carbon, sulphur, and iron in recent semi-euxinic sediments of Kau Bay, Indonesia, *Geochimica, et Cosmochimica Acta*, **55**, pp 815-828.

MIGON, C., ALLEMAN, L., LEBLOND, N. and NICOLAS, E., 1993, Evolution of atmospheric lead over the north-western Mediterranean between 1986 and 1992, *Atmospheric Environment*, **27A**, 14, pp 2161-2167.

MOLINARI, J. and SNODGRASS, W. J., 1990, The chemistry and radiochemistry of radium and other elements of the uranium and thorium natural decay series, In: *The Environmental Behaviour of Radium*, IAEA technical report series No. 310, 1 pp 11-56.

MOORE, W. S., 1969, Measurement of Ra228 and Th228 in Sea Water. *Journal of Geophysical Research*, **74**, pp 694-704.

MOORE, W. S., 1972, Radium: element and geochemistry, *The Encyclopedia of Geochemistry and Environmental Sciences,* Encyclopedia of Earth Sciences Series, **IVA**, Van Nostrand Reinhold, Princeton, NJ, and New York, pp 1006-1007.

MOORE, W. S., 1996, Large groundwater inputs to coastal waters revealed by ^{226}Ra enrichments, *Nature*, **380**, pp 612-614.

MOORE, W. S., ASTWOOD, H. and LINDSTROM, C., 1995, Radium isotopes in coastal waters on the Amazon shelf, *Geochimica et Cosmochimica Acta,* **59,** No. 20, pp4285-4298.

MOORE, W. S. and COOK, L. M., 1974, Radium removal from drinking water, *Nature,* **253**, pp262-263.

MOORE, W. S. and DYMOND, J., 1991, Fluxes of ^{226}Ra and barium in the Pacific Ocean: The importance of boundary processes, *Earth and Planetary Science Letters,* **107**, pp55-68.

MOORE, W. S. and REID, D. F., 1973, Extraction of Radium from Natural Waters Using Manganese-Impregnated Acrylic Fibres. *Journal of Geophysical Research,* **78**, pp 8880-8885.

MOORE, W. S. and SANTSCHI, P. H., Ra-228 in the deep Indian Ocean, *Deep-Sea Research,* **33**, 1, pp 107-120.

MORSE, J. W. and ARAKAKI, T., 1993, Adsorption and coprecipitation of divalent metals with mackinawite (FeS), *Geochimcia et Cosmochimica Acta,* **57**, 15, pp 3635-3640.

MUROZUMI, M., CHOW, T. J. and PATERSON C. C., 1969, Chemical concentrations of pollutant lead aerosols, terrestrial dusts and sea salts in Greenland and Antarctic snow strata, *Geochimica et Cosmochimica Acta*, **33**, pp 1247-1294.

MÜLLER, A., 1975, Diagenese stickdstoffhaltiger organischer Substanzen in oxischen und anoxischen marinen Sedimenten, Meteor Forschungsergeb., Reihe C 22, pp1-60.

MÜLLER, A. and MATHESIUS, U., 1999, The palaeoenvironments of coastal lagoons in the southern Baltic Sea, I. The application of sedimentary C_{org}/N ratios as source indicators of organic matter, *Palaeogeography, palaeoclimatology, palaeoecology,* **145**, pp 1-16

MÜLLER, G., DOMINIK, J., REUTHER, R., MALISCH, R., SCHULTE, E., ACKER, L. and IRION, G., 1980, Sedimentary record of environmental pollution in the Western Baltic Sea. *Naturwissenschaft*, **67**, 595-600.

MULLER, P. J., 1977, C/N ratios in Pacific deep sea sediments: Effect of inorganic ammonium and organic nitrogen compounds sorbed by clays, *Geochimica et Cosmochimica Acta,* **41**, pp 765-776.

MURRAY, R. W. and LEINEN, M., 1996, Scavenged excess aluminium and its relationship to bulk titanium in biogenic sediment from the central equatorial Pacific Ocean, *Geochimica et Cosmochimica Acta*, **60**, 20, pp3869-3878.

NAKAI, N., 1986, Palaeoenvironmental features of Lake Biwa deduced from carbon isotope compositions and organic C/N ratios of the upper 800m sample of 1,400 cored column, *Proceedings of the Japenese Academy*, **62B**, 8, 279-282.

NEHRING, D., 1992, Eutrophication in the Baltic Sea, *Science of the Total Environmnent*, Supplement 1992, Elsevier Science, pp 673-682.

NEHRING, D., AERTEBERG, G., ALENIUS, P., ASTOK, V., TROSZINSKA, A., YURKOBSKI, P. & A. K., 1987, In: First periodic assessment of the state of the marine environment of the Baltic sea area, 1980-1985; Background Document, *Baltic Sea Environmental Proceedings*, Ed. J. Lassig, **17B**, pp 35-81.

NEHRING, D., MATTHAUS, W., LASS H. –U., NAUSCH, G. and NAGEL, K., 1996, The Baltic Sea in 1995 – Beginning of a new stagnation period in its central deep waters and decreasing nutrient load in its surface layer, *Marine Science Reports*, **228**, Baltic Sea Research Institute, pp 319-327.

NEUMANN, T., CHRISTIANSEN, C., CLASEN, S., EMEIS, K. –C. and KUNZENDORF, H., 1997, Geochemical records of salt-water inflow into the deep basins of the Baltic Sea, *Continental Shelf Research,* **17**, pp 95-115.

NEUMANN, T., LEIPE, T., BRAND, T. and SHIMMIELD, G., 1996, Accumulation of Heavy Metals in the Oder Estuary and its Off-shore Basins, *Chemie der Erde*, **56**, pp 207-222.

NEUMANN, T., LEIPE, T. and SHIMMIELD, G., 1998, Heavy metal enrichment in surficial sediments in the Oder river discharge area: source or sink for heavy metals?, *Applied Geochemistry*, **13**, pp 329-337.

NIESE, S., 1994, γ- Spectrometric Determination of Radium in Water Samples Taken from an Uranium Mining Area, *Journal of Analytical Chemistry,* **49**, pp 124-126

NORRISH, K., and HUTTON, J. T., 1969, An accurate X-ray spectrographic method for the analysis of a wide range of geological samples, *Geochimica et Cosmochimica Acta,* **33**, pp 431-453.

NOZAKI, Y., 1991, The systematics and kinetics of U/Th decay series nuclides in ocean water, *Reviews in Aquatic Sciences*, **4**, 1, pp 75-105.

OCHOCKI, S., MACKIEWICZ, T., NAKONIECZNY, J. and ZALEWSKI, M., 1995, Primary production, chlorophyll, and qualitative and quantitative composition of phytoplankton in the Pomeranian Bay (Southern Baltic), *Bulletin of the Sea Fisheries Institute*, **3**, 136, pp 33-42.

OHLANDER, B., INGRI, J. and PONTER, C., 1993, Lead isotopes as tracers of lead pollution from various sources: an example from northern Sweden, *Applied Geochemistry*, **2**, pp 67-70.

ORLANDINI, K. A., PENROSE, W. A., HARVEY, B. R., LOVETT, M. B. and FINDLAY, M. W., 1990, Colloidal behaviour of actinides in an oligotrophic lake, *Environmental Science and Technology Letters*, **24**, pp 228-234.

PARDUE, J. H. and GUO, T. Z., Biogeochemistry of ^{226}Ra in contaminated bottom sediments and oilfield waste pits, *Journal of Environmental Radioactivity*, **39**, 3, pp 239-253.

PASTUSZAK, M. NAGEL, K and NAUSCH, G., 1996, Variability in nutrient distribution in the Pomeranian Bay in September 1993, *Oceanologia*, **38**, 2, pp 195-225.

PATES, J. M., 1995, The use of alpha/beta liquid scintillation spectrometry in marine tracer studies, *unpublished PhD thesis*, University of Glasgow.

PATIENCE, R. L., CLAYTON, C. J., KEARSLEY, A. T., ROWLAND, S. J., BISHOP, A. N., REES, A.W.G., BIBBY, K. G. and HOPPERS, A. C., 1990, 'An integrated biochemical, geochemical and sedimentological study of organic diagenesis in sediments from ODP, Leg 112, *Initial report, ODP*, **112B**, pp 135-153.

PEDERSEN, T. F., 1979, The geochemistry of the Panama Basin, Eastern Equatorial Pacific Ocean, PhD thesis, University of Edinburgh, 235 pp.

PLATER, A. J., IVANOVICH, M. and DUGDALE, R. E., 1995, ^{226}Ra contents and ^{228}Ra/^{226}Ra activity ratios of the Fenland rivers and The Wash, eastern England: spatial and seasonal trends, *Chemical Geology (Isotope Geoscience Section)*, **119**, pp 275-292.

PRANDKE, H. and STIPS, A., 1992, A model of Baltic thermocline turbulence patches, deduced from experimental investigations, *Continental Shelf Research*, **12**, 5/6, pp 643-659.

POHL, C and HENNINGS, U., 1999, The effect of redox processes on the partitioning of Cd, Pb, Cu and Mn between dissolved and particulate phases in the Baltic Sea., *Marine Chemistry*, **65**, pp 41-53.

POHL, C., HENNINGS, U., PETERSOHN, I, and SIEGEL, H., 1998, Trace metal budget, transport, modification and sink in the transition area between the Oder and Peene Rivers and the southern Pomeranian Bight, *Marine Pollution Bulletin*, **36**, 8, pp 598-616.

PORCELLI, D., ANDERSSON, P. S., WASSERBURG, G. J., INGRI, J. and BASKARAN, M., 1997, The importance of colloids and mires for the transport of uranium isotopes through the Kalix river watershed and Baltic Sea., *Geochimca et Cosmochimica Acta*, **61**, 19, pp 4095-4113.

POPPITI, J. A., 1994, Practical techniques for laboratory analysis, CRC press, Florida.

POWERS, R. P., TURNAGE, N.E. and KANIPE, L. G., 1980, Determination of radium-226 in environmental samples, *Natural Radiation Environment III (Proc. Int. Conf. Houston)(GESELL, T. F. and LOWDER, W. M., Eds)*, **1**, CONF-780422, Technical Information Centre, United States Department of Energy, Oak Ridge, TN, pp640-660.

PUSEY, W.A., 1911, The biological effects of radium, *Science*, **XXXIII**, p 1001-1005.

RADZIEJEWSKA, T. and MASLOWSKI, J., 1995, Macro- and meiobenthos of the Arkona Basin (western Baltic Sea): differential recovery following hypoxic events, *Proceedings of the 30th European Marine Biological Symposium*, Southampton, pp 251-262.

RAMA and MOORE, W. S., 1996, Using the radium quartet for evaluating groundwater input and water exchange in salt marshes, *Geochimica et Cosmochimica Acta*, **60**, 23, pp 4645-4652,

RANKAMA, K. and SAHAMA, T. G., 1950, *Geochemistry*, University of Chicago Press, 912pp.

REDFIELD, A. C., KETCHUM, B. H. and RICHARD, F. A., 1963, The influence of organisms on the composition of sea water. In: *The Sea*, **2**, pp 26-77 (ed. Hill, M. N.), John Wiley and Sons, New York.

REIMERS, C. E. and SUESS, E., 1983, The partitioning of organic carbon fluxes and sedimentary organic matter decomposition rates in the ocean, *Marine Chemistry*, **13**, pp 141-168.

RHEIN, M., CHAN, L. H., ROETHER, W. and SCHLOSSER, P., 1987, ^{226}Ra and Ba in Northeast Atlantic Deep Water, *Deep Sea Research*, **34**, 9, pp 1541-1564.

RHEINHAMMER, G., 1995, In: Meereskunde der Ostsee, Ed D. Nehring, Springer, Berlin, pp 338.

RIDDLE, C., VANDER VOET, A. and DOHERTY, W., 1988, Rock analysis using inductively coupled plasma mass spectrometry: a review, *Geostandards Newsletter*, **12**, 1, pp203-234

RIDGEWAY, I. M. and PRICE, N. B., 1987, Geochemical associations and post-depositional mobility of heavy metals in coastal sediments: Loch Etive, Scotland, *Marine Chemistry*, **21**, pp 229 – 248.

ROBBINS, J. A. and EDGINGTON, D. N., 1975, Determination of recent sedimentation rates in Lake Michigan using Pb-210 and Cs-137, *Geochimica et Cosmochimica Acta*, **39**, pp 285-304.

RHODE, H., SODERLUND, R. and EKSTEDT, J., 1980, Deposition of airborne pollutants on the Baltic, *Ambio Special Publication*, **9**, pp 168-173.

ROSMAN, K. J. R., CHISHOLM, W., HONG, S., BOUTRON, C. F. and CANDELONE, J. P., 1995, Lead isotope record in ancient Greenland ice, In *Heavy Metals in the Environment*, Conference proceedings, 1, Hamburg.

RUSSELL, R. D. and FARQUHAR, R. M., 1960, *Lead isotopes in geology*, Wiley and Sons, New York.

RYDBERG, L., EDLER, L., FLODERUS, S. and GRANELI, W., 1990, Interaction between supply of nutrients, primary production , sedimentation and oxygen consumption in SE Kattegat, *Ambio*, **19**, 3, pp 134-141.

SAARINEN, L. and SUSKI, J., 1992, Determination of uranium series radionuclides Pa-231 and Ra-226 by liquid scintillation counting, *Report YJT-92-20*, Nuclear Waste Commission of Finnish Power Companies, Helsinki.

SALO, A., SAXEN, R. and PUHAKAINEN, M., 1984, Transport of airborne ^{90}Sr and ^{137}Cs deposited in the basins of the five largest rivers in Finland, *Aqua Fennica*, **14**, 1, pp 21-31.

SALO, A., TUOMAINEN, K. and VOIPIO, A., 1986, Inventories of some long-lived radionuclides in the Baltic Sea, *The Science of the Total Environment*, **54**, pp 247-260.

SALOMONS, W. and FORTSNER, U., 1980, Trace metal analysis on polluted sediments, Part II, Evaluation of environmental impact, *Environment and Technology Letters*, **1**, pp 506-517.

SALONEN, V-P., GRONLUND, T., ITKONEN, A., STURM, M. and VUORINEN, I., 1995, Geochemical record on early diagenesis of recent Baltic Sea sediments, *Marine Geology*, **129**, pp 101-109.

SANTSCHI, P. H., HÖHENER, P., BENOIT, G. and BRINK, M. B., 1990, Chemical processes at the sediment-water interface, *Marine Chemistry*, **30**, pp 269-315.

SANTSCHI, P. H. and HONEYMAN, B. D., 1989, Radionuclides in Aquatic Environments, *Radiation and Physical Chemistry*, **34**, 2, pp 213-240.

SARIN, M. M., KRISHNASWAMI, S., SOMAYAJULU, B. L. K. and MOORE, W. S., 1990, Chemistry of uranium, thorium and radium isotopes in the Ganga-Brahmaputra river system: Weathering processes and fluxes to the Bay of Bengal, *Geochimica et Cosmochimca Acta*, **54**, pp 1387-1396.

SCHLOSSER, P., RHEIN, W., ROETHER and KROMER, 1984, High precision measurement of oceanic 226Ra, *Marine Chemistry*, **15**, pp 203-216.

SCHNEIDER, B and WEILER, K., 1984, A quick grain size correction procedure for trace metal contents of sediments, *Environmental Technology Letters*, **5**, pp 245-256.

SCHROPP, S. J. and WINDOM, H. L., 1988 (Eds.), A guide to the interpretation of metal concentrations in estuarine sediments, Florida Department of Environmental Regulation.

SEIGEL, H., GERTH, M. and SCHMIDT, T., 1996, Water exchange in the Pomeranian Bight investigated by satellite data and shipborne measurements, *Continental Shelf Research*, **16**, 14, pp 1793-1817.

SEKI, H., SKELDING, J. and PARSONS, T. R., 1968, Observations on the decomposition of a marine sediment, *Limnology and Oceanography*, **13**, pp 440-447.

SHIMMIELD. G. B., 1985, The geochemistry and mineralogy of Pacific sediments, Baja California, *unpublished PhD thesis*, pp 200-206.

SHIMMIELD, G. B., (Ed.), 1995, *Oder Project Final Report*, **PL 910398**, EC Environment Program.

SHIMMIELD, G. B. and PEDERSON T.F., 1990, The geochemistry of reactive trace metals and halogens in hemipelagic continental margin sediments, *Review of Aquatic Sciences*, **3**, pp 255-279.

SHIMMIELD, G. B. and PRICE, N. B., The behaviour of molybdenum and manganese during early sediment diagenesis – offshore Baja California, Mexico, *Marine Chemistry*, **19**, pp 261 – 280.

SHIMMIELD, G. B, RITCHIE, G. D. and FILEMAN, T. W., 1995, The impact of marginal ice zone processes on the distribution of ^{210}Pb, ^{210}Po and ^{234}Th and implications for new production in the Bellingshausen Sea, Antarctica, *Deep Sea Research II*, **42**, pp 1313-1335.

SHIMMIELD, T. M., 1993, A study of radionuclides, lead and lead isotopes ratios in some Scottish sea-lochs. Unpublished PhD thesis, University of Edinburgh.

SHIRAHATA, H., ELIAS, R. W. and PATTERSON, C. C., 1980, Chronological variations in concentrations and isotopic compositions of anthropogenic atmospheric lead in sediments of a remote subalpine pond, *Geochimica et Cosmochimca Acta*, **44**, pp 149-162.

SHUKLA, B. S., 1996, Sedimentation rate through environmental radioactivity (software), Pt 1, 210Pb dating of sediments, In: *Environmental Research and Publications Inc*, Ontario, Canada.

SIEGEL, H., GERTH. M. and SCHMIDT, T., 1996, Water exchange in the Pomeranian Bight investigated by satellite data and shipborne measurements, *Continental Shelf Research*, **16**, 14, pp 1793-1817.

SLAWYK, G., COLLOS, Y., MINAS, M. and GRALL, J. R., 1978, On the relationship between carbon to nitrogen composition ratios of the particulate matter and growth rate of marine phytoplankton from the northwest African upwelling, *Journal of Experimental Marine Biology and Ecology*, **33**, pp 119-131.

SKWARZEC, B., 1997, Polonium, Uranium and Plutonium in the Southern Baltic Sea, *Ambio*, **26**, 2, pp 113-117

SLOMP, C. P., MALSCHAERT, J. F. P., LOHSE, L. and VAN RAAPHORST, 1997, Iron and manganese cycling in different sedimentary environments of the North Sea continental margin, *Continental Shelf Research*, **17**, 9, pp 1083-1117.

SOMOGYI, G., 1990, Methods for measuring radium isotopes: Track Detection, In *The Environmental Behaviour of Radium, IAEA Technical Report Series*, **No. 310**, Vol. 1, pp 229-255.

SMITH-BRIGGS, J. L., 1983, A combined trace metal/radionuclide study of the Clyde Sea area, PhD thesis, University of Glasgow, pp 23-26.

STACEY, J. and KRAMERS, J., 1975, Approximation of terrestrial lead isotope evolution by a two stage model, *Earth and Planetary Science Letters*, **26**, pp 207-221.

STARIK, I. E. and GUREVICH, A. M., 1937, Translation, Trav, Inst. Etat radium, USSR, **3**, 241pp.

STUKAS, V. J. and WONG, C. S., 1981, Stable lead isotopes as a tracer in coastal waters, *Science*, **211**, pp 1424-1427.

STUMM, W. and MORGAN, J. J., 1981, Aquatic chemistry, New York, Wiley.

STURGES, W. T. and BARRIE, L. A., 1987, Lead 206/207 isotope ratios in the atmosphere of North America as tracers of US and Canadian emissions, *Nature*, **329**, pp 144-146.

STURQEON, R., 1988, Acid digestions of marine samples for trace element analysis using microwave heating, *Analyst*, **113**, pp 204-211.

SUESS, E. and ERLENKEUSER, H., 1975, History of metal pollution and carbon input in Baltic Sea sediments, *Meyniana*, **27**, pp63-75

SUGDEN, G. L., 1993, Isotopic studies of the environmental chemistry of lead, Unpublished PhD thesis, University of Edinburgh.

SUGDEN, C. L., FARMER, J. G. and MACKENZIE, A. B., 1991, Lead and $^{206}Pb/^{207}Pb$ profiles in ^{210}Pb-dated ombrotrophic peat cores from Scotland, *Proceedings of the 8th International Conference on Heavy Metals in the Environment*, **1**, pp 90-93.

SZEFER, P., 1990, Mass-balance of metals and identification of their sources in both river and fallout fluxes near Gdansk bay, Baltic Sea., *The Science of the Total Environment*, **95**, pp131-139.

SZEFER, P., GLASBY, G. P., PEMPKOWIAK, J. and KALISZAN, R., Extraction studies of heavy metal pollutants in surficial sediments from the southern Baltic Sea off Poland, *Chemical Geology*, **120**, pp 111-126.

SZEFER, P., KUSAK, A., SZEFER, K., GLASBY, G. P., JANKOWSKA, H., WOLOWICZ, M. and ALI, A. A., 1998, Evaluation of the anthropogenic influx of metallic pollutants into Puck Bay, southern Baltic, *Applied Geochemistry*, **13**, pp 293-304.

SZEFER, P. and SKWARZEC, B., 1988, Distribution and possible sources of some elements in the sediment cores of the Southern Baltic, *Marine Chemistry*, **23**, pp 109-129.

SZEFER, P., SZEFER, K., GLASBY, G., PEMPKOWAIK, J., KALISZAN, R., 1996, Heavy-metal pollution in surficial sediments from the southern Baltic Sea off Poland, *Journal of Environmental Science and Health*, **A31**, 10, pp 2723-2754.

TAI, W. C., 1991, PERALS Spectrometry: A New Method for Measurement of Radium in Natural Waters. MSc Thesis, Florida State University.

THAMDRUP, B., FOSSING, H. and JORGENSEN, B. B., 1994, Manganese, iron, and sulfur cycling in a coastal marine sediment, Aarhus Bay, Denmark, *Geochimica et Cosmochimica Acta*, **58**, pp 5115-5129.

THOMSON, J., COLLEY, S., ANDERSON, R., COOK, G. T. and MACKENZIE, A. B., 1993, ^{210}Pb in the sediments and water column of the Northeast Atlantic from 47 to 59°N along 20°W, *Earth and Planetary Science Letters*, **115**, pp 75-87.

THORNGATE, J. H. and CHRISTIAN, D. J., 1977, Optimisation of the detector and associated electronics used for high-resolution liquid-scintillation alpha spectroscopy, *Health Physics*, **33**, pp 443-448.

TOOLE, J. THOMSON, J. and BAXTER, M. S., 1988, Some aspects of the marine geochemistry of Uranium, In: *Radionuclides: A tool for Oceanography*, Eds: J. C. Guary, P. Guegueniat and R. J. Pentreath, Elsevier Science, pp 183-194.

TOTLAND, M., JARVIS, I. and JARVIS, K. M., 1992, An assessment of dissolution techniques for analysis of geological samples by plasma spectrometry, *Chemical Geology*, **95**, pp 35-62.

TOWLER, P. H., SMITH, J. D. and DIXON, D. R., 1996, Magnetic recovery of radium, lead and polonium from seawater samples after preconcentration on a magnetic adsorbent of manganese dioxide coated magnetite. *Analytica Chimica Acta*, **328**, pp 53-59.

TUBILCOCK, C., 1981, The industrialisation of the continental powers 1780-1914, Longmans, pp 495.

TUREKIAN, K. K., NOZAKI, Y. and BENNINGER, L. K., 1977, Geochemistry of atmospheric radon and radon products, *Annual Review of Earth and Planet Science*, **5**, pp 227-255.

TUREKIAN, K. K. and WEDEPOHL, K. H., 1961, Distribution of the elements in some major units of the Earth's crust, *Geological Society of America Bulletin*, **72**, pp 175-192.

UNESCO, 1981, The international equation of state of seawater, 1980, *Unesco Technical Paper of Marine Science*, **38**, Paris, Unesco.

URBAN, N. R., EISENREICH, S. J., GRIGAL, D. F. and SCHURR, K. T., 1990, Mobility and diagenesis of Pb and ^{210}Pb in peat, *Geochimica et Cosmochimica Acta*, **54**, pp 3329-3346.

VALETTE-SILVER, N. J., 1993, The use of Sediment Cores to Reconstruct Historical Trends in Contamination of Estuarine and Coastal Sediments, *Estuaries*, **16**, 3B, pp 577-588.

VAN CAPPELLEN, P. and WANG, Y., 1996, Cycling of iron and manganese in surface sediments: A general theory for the coupled transport and reaction of carbon, oxygen, nitrogen, sulfur, iron and manganese, *American Journal of Science*, **296**, pp 197-243.

VERARDO, D. J., FROELICH, P. N. and MCINTYRE, A., 1990, Determination of organic carbon and nitrogen in marine sediments using the Carlo Erba NA-1500 Analyser, *Deep Sea Research*, **37**, 1, pp 157-165.

VOIPIO, A., 1981, The Baltic Sea, Elsevier Oceanography series, **30**, Amsterdam.

VOLTZ, R., LOPES DA SILVA, J., LAUSTRIAT, G. and COCHE, A. 1966, Influence of the nature of ionising particles on the specific luminescence of organic scintillators, *Journal of Chemical Physics*, **45**, pp 3306-3311.

VOSS, M. and STRUCK, U., 1997, Stable nitrogen and carbon isotopes as indicator of eutrophication of the Oder river (Baltic Sea), *Marine Chemistry*, **59**, pp 35-49.

WAN, G.J, SANTSCHI, P. H., STURM, M., FARRENKOTHEN, K., LUECK, A., WERTH, E. and SCHULER, C., 1987, Natural (^{210}Pb, ^{7}Be) and fallout (^{137}Cs, ^{239,240}Pu, ^{90}Sr) radionuclides as geochemical tracers of sedimentation in Greifensee, Switzerland, *Chemical Geology*, **63**, pp 181-196.

WEIR, F. E., 1994, A study of lead and lead isotope ratios in the Oder river estuary and the Southern Baltic Sea, Unpublished MSc thesis, University of Manchester, pp 24.

WEISS, D., SHOTYK, W., APPLEBY, P. G., KRAMERS, J. D. and CHEBURKIN, A. K., 1999, Atmospheric Pb deposition since the industrial revolution recorded by five Swiss peat profiles: Enrichment factors, fluxes, isotopic composition and sources, *Environmental Science and Technology Letters*, **33**, pp 1340-1352.

WILSON, T. R. S., THOMPSON, J., COLLEY, S., HYDES, D. J. and HIGGS, N. C., Early organic diagenesis: the significance of progressive subsurface oxidation fronts in pelagic sediments, *Geochimica et Cosmochimica Acta*, **49**, pp 811-822.

WULFF, F., STIGEBRANDT, A. and RAHM, L., 1990, Nutrient dynamics of the Baltic Sea, *Ambio*, **19**, 3, pp 126-133.

YANG, D., ZHU, Y. and MOBIUS, S., 1991, Rapid method of alpha counting with extractive scintillator and pulse shape analysis, *Journal of Radioanalytical and Nuclear Chemistry, Articles*, **147**, 1, pp177-189

YOUNG, S. A., 1996, A radionuclide tracer study of heavy metal cycling in Loch Etive, Scotland, *Unpublished PhD thesis*, University of Edinburgh.

ZHOU, M., 1998, Influence of bottom stress on the two-layer flow induced by gravity currents in estuaries, *Estuarine, Coastal and Shelf Science*, **46**, pp 811-825.

ZIKOVSKY, L., 1991, Determination of 226Ra in water with a proportional counter. *Journal of Radioanalytical Nuclear Chemistry, Letters*, **153**, pp 165-170.